CCMT

CENTER FOR COMPRESSIBLE MULTIPHASE TURBULENCE

Multiphase Physics Deep-dive Workshop

October 6-7, 2016

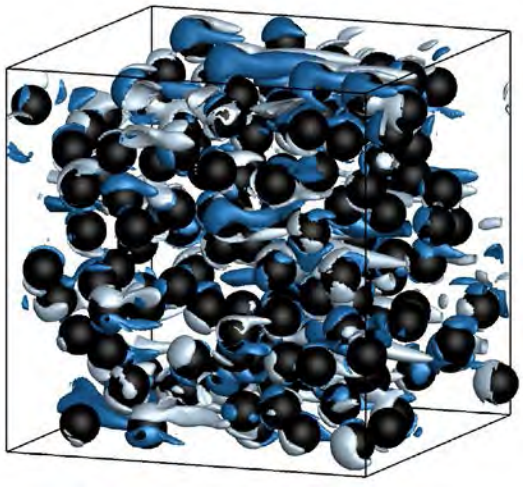

UF UNIVERSITY of FLORIDA

UF UNIVERSITY of FLORIDA CENTER FOR COMPRESSIBLE MULTIPHASE TURBULENCE

Multiphase Physics Deep-dive Workshop

October 6-7, 2016 Attendee List

Georges Akki	gakiki@ufl.edu	University of Florida
Subramanian Annamalai	subbu.ase@ufl.edu	University of Florida
Marco Arienti	marient@sandia.gov	Sandia
S. Balachandar	bala1s@ufl.edu	University of Florida
Ankur Bordoloi	ankur@lanl.gov	LANL
Alexander Brown	albrown@sandia.gov	Sandia
Jesse Capecelatro	jcaps@umich.edu	University of Michigan
Seungwhan Chung	schung58@illinois.edu	University of Illinois
Paul Crittenden	pcritte@ufl.edu	University of Florida
William Dai	dai@lanl.gov	LANL
Angela Diggs	angela.diggs.1@us.af.mil	Eglin AFB
Timothy Dunn	dunn13@llnl.gov	LLNL
Brad Durant	neoncrash@ufl.edu	University of Florida
John Eaton	eatonj@stanford.edu	Stanford University
Mahdi Esmaily	mesmaily@stanford.edu	Stanford University
Giselle Fernandez	giselllefernandez@ufl.edu	University of Florida
Marianne Francois	mmfran@lanl.gov	LANL
Joshua Garno	jgarno@ufl.edu	University of Florida
Jason Hackl	jason.hackl@ufl.edu	University of Florida
Alan Harrison	alanh@lanl.gov	LANL
Jeremy Horwitz	horwitz1@stanford.edu	Stanford University
Kyle Hughes	kylethughes89@ufl.edu	University of Florida
Thomas Jackson	tlj@ufl.edu	University of Florida
Rahul Koneru	rahul.koneru@ufl.edu	University of Florida
Allen Kuhl	kuhl2@llnl.gov	LLNL
Ali Mani	alimani@stanford.edu	Stanford University
Yash Mehta	ymehta@ufl.edu	University of Florida
Chandler Moore	wcm0015@tigermail.auburn.edu	University of Florida
Brandon Morgan	morgan65@llnl.gov	LLNL
Balu Nadiga	balu@lanl.gov	LANL
Fady Najjar	najjar2@llnl.gov	LLNL
Brandon Osborne	bosborne3@ufl.edu	University of Florida
Fred Ouellet	f.ouellet@ufl.edu	University of Florida
John Parra-Alvarez	jcparraa@gmail.com	University of Utah
Katherine Prestridge	kpp@lanl.gov	LANL
Bertrand Rollin	bertrandrollin@gmail.com	Embry-Riddle
Kevin Ruggirello	kruggir@sandia.gov	Sandia

Center for Compressible Multiphase Turbulence

Kambiz Salari	salari1@llnl.gov	LLNL
Shane Schumacher	scschum@sandia.gov	Sandia
Philip Smith	philip.smith@utah.edu	University of Utah
Sean Smith	sean.t.smith@utah.edu	University of Utah
Prashanth Sridharan	shan1130@ufl.edu	University of Florida
Jeff St. Clair	jeff.stclair@navy.mil	University of Florida
Cameron Stewart	csstewart10@ufl.edu	University of Florida
Jeremy Thornock	jthornock@gmail.com	University of Utah
Gretar Tryggvason	gtryggva@nd.edu	University of Notre Dame
Markus Uhlmann	markus.uhlmann@kit.edu	Karlsuhe Institute of Tech.
Laura Villafane	lvillafa@stanford.edu	Stanford University
Robert Voigt	rvoigt@krellinst.org	ASC AST
Seng Keat Yeoh	syeoh2@illinois.edu	XPACC University of Illinois
Duan Zhang	dzhang@lanl.gov	LANL
Ju Zhang	jzhang@fit.edu	Florida Institute of Technology

UF UNIVERSITY of FLORIDA

Center for Compressible Multi-Phase Turbulence

1180 Center Drive
P.O. Box 116135
Gainesville, FL 32611
Phone: (352)294-2829
Fax: (352) 846-1196

Agenda Multiphase Physics Deep-Dive, October 6-7, 2016
St. Petersburg Marriott Clearwater,

12600 Roosevelt Blvd, North St. Petersburg, FL 33716, Phone: 727-572-7800

Thursday Oct 6th, 2016

7:30 – 8:30	Breakfast (Provided)	
8:30 – 8:45	Welcome (S. Balachandar)	
8:45 – 10:15	Overviews	
	Gretar Tryggvason	Challenges and opportunities in fully resolved simulations of multi fluid flows
	Ali Mani	Overview of computational modeling at Stanford PSAAP: particle-laden flows subject to radiative heating
	Kambiz Salari	Research activities for energetic dispersal of particles
10:15 – 10:30	Coffee	
10:30 – 12:00	Overviews	
	Alex Brown	Multiphase Methods for Modeling Fire Environments
	Phil Smith	Multi-phase flow modeling at Utah PSAAP – predictivity in application
	S. Balachandar	Overview of multiphase flow computational strategy at UF PSAAP
12:00 – 12:15	Further Discussion	
12:15 – 1:30	Lunch (Provided)	
1:30 – 3:00	Macroscale	
	Duan Zhang:	Equations and Closures for Deformation and Flow of Continuous and Disperse Materials
	Allen Khul	3-Phase Model of Explosion Fields
	Marco Arienti	Multiphase Flow Simulation Strategies at the CRF

UF UNIVERSITY of FLORIDA

3:00 – 3:15 Coffee

3:15 – 5:15 Microscale

Jeremy Horwitz	Point-particle modeling for two-way-coupled problems: Challenges, verification, and physics-based improvements
Georges Akiki	Extended point particle model
Jesse Capecelatro	Recent insights on turbulence modeling of strongly-coupled particle-laden flows
Tom Jackson	Microscale simulations of shock particle interaction

6:30 – 9:00 Dinner (Provided – all attendees)

Friday Oct 7th, 2016

7:30 – 8:30 Breakfast (Provided)

8:30 – 10:30 Modeling & numerical methods

Sean Smith	Particle dynamics: coal-specific modeling
A. Subramaniam	Microscale modeling based on Generalized Faxen theorem
Alan Harrison	Modeling of Ejecta Particles in the FLAG Continuum Mechanics Code
Markus Uhlmann	Large scale microscale simulations and modeling opportunities

10:30 – 10:45 Coffee

10:45 – 12:15 Experiments and simulations

Ankur Bordoloi	Experimental measurements of drag on shocked particles
Laura Villafañe	Including real experimental effects in validation of numerical models for confined particle-laden flows
Fady Najjar	Meso-scale Simulations of Shock-Particle Interactions

12:15 – 1:30 Lunch (Provided)

1:30 – 3:00 Meso/macroscale

Mahdi Esmaily	A systematic study of turbophoresis by four-way-coupled simulation of Stokesian particles in channel flow
Balu Nadiga	Bayesian Analysis of Inter-Phase Momentum Transfer in the Dispersed Eulerian Formulation of Multiphase Flow
John Parra-Álvarez	Eulerian Models and Polydispersity Treatment for Dilute Gas-Particle Flows

3:00 – 4:00 Discussion & Closing remarks

PSAAP II: Center for Shock Wave-processing of Advanced Reactive Materials (C-SWARM)

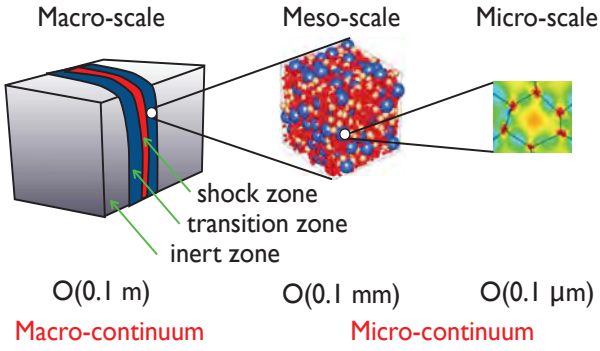

The C-SWARM framework represents a transformative **engineering and science achievement, the ability to synthesize new materials**, that exemplifies what Exascale computing can deliver.

Develop simulations tools that allow prediction of solid-solid transformation, using continuum framework, including chemo-thermo-mechanical behavior

UNIVERSITY OF NOTRE DAME

Challenges and Opportunities in Fully Resolved Simulations of Multi Fluid Flows

Grétar Tryggvason,
University of Notre Dame

Multiphase Physics Deep-Dive
October 6-7, 2016 St. Petersburg Marriott Clearwater

Work supported by NSF & DOE (CASL & PSAAP-II)

UNIVERSITY OF NOTRE DAME

DNS of Multiphase Flows
Numerical Methods

CFD of Multiphase Flows—one slide history

BC: Birkhoff and boundary integral methods for the Rayleigh-Taylor Instability

65’ Harlow and colleagues at Los Alamos: The MAC method

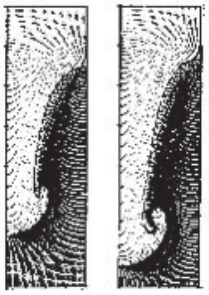

From: B. Daly (1969)

75’ Boundary integral methods for Stokes flow and potential flow

85’ Alternative approaches (body fitted, unstructured, etc.)

95’ Beginning of DNS of multiphase flow. Return of the “one-fluid” approach and development of other techniques

UNIVERSITY OF NOTRE DAME

DNS of Multiphase Flows
Numerical Methods

A number of method have now been developed for incompressible multiphase flows. Many of the difficulties encountered by early methods have been more or less overcome. Those include:

• Artificial fluid motion at high surface tension (parasitic currents), induced by inconsistent numerical approximations.

• Consistent momentum advection near the interface, particularly for large density differences;

• Accurate and robust solution of the pressure equation for large density differences;

• Mass conservation, particularly in the level set method

• Accurate treatment of the viscous stresses.

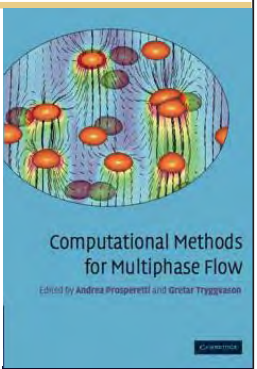

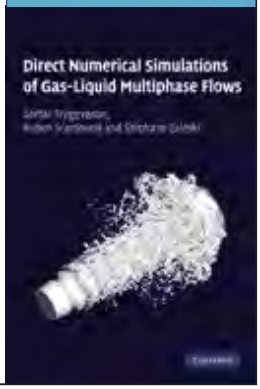

"Simple" Problems

UNIVERSITY OF NOTRE DAME

DNS of Multiphase Flows
Turbulent Multiphased Flows

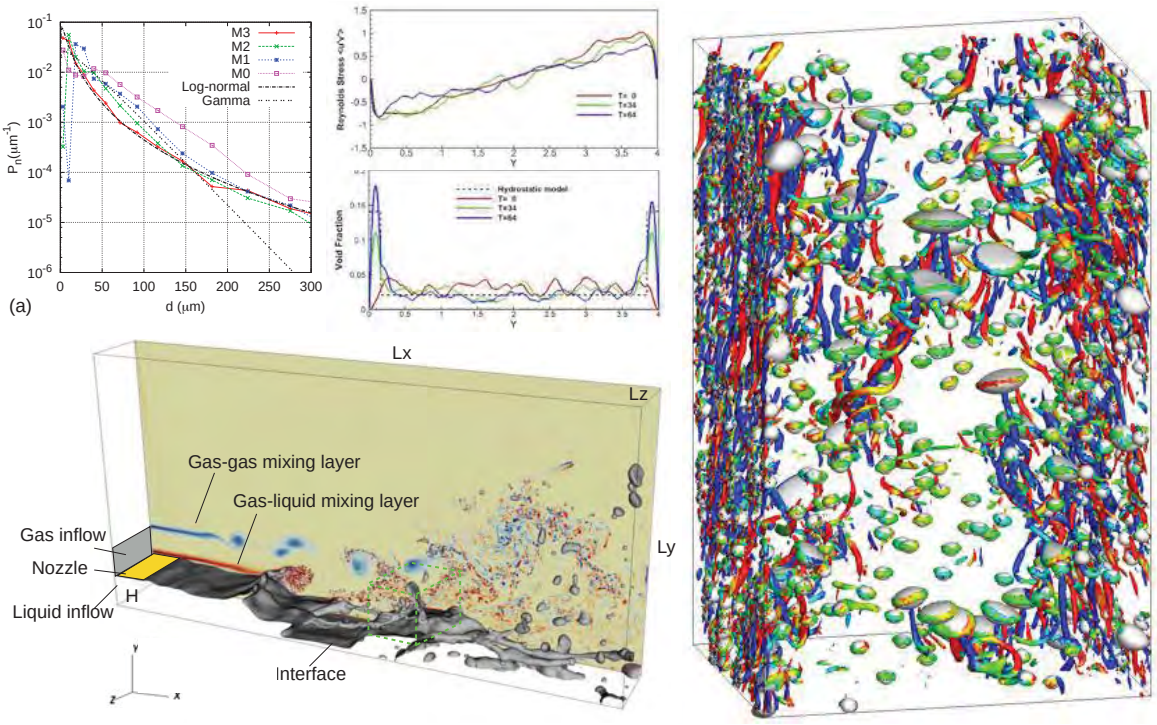

UNIVERSITY OF NOTRE DAME

DNS of Multiphase Flows
Next Challenges

For incompressible two-fluid problems with a clean interface a number of methods now exist that are capable of simulating fairly complex situations, such as hundreds of bubbles in turbulent flows. Thus, current tasks include:

- Extensions to more complex physics. For simple problems this has been done but new physics often includes new scales that are difficult to resolve and the number of studies of very large systems are modest

- Development of multiscale strategies to account for very small scales that appear spontaneously or are imposed by additional physical

- Development of advanced strategies to process the results, including using simulations data to help building reduced order models.

"Complex" Physics

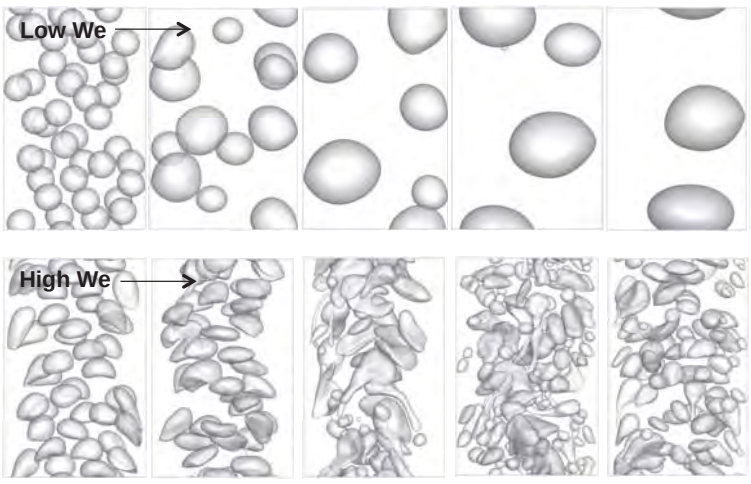

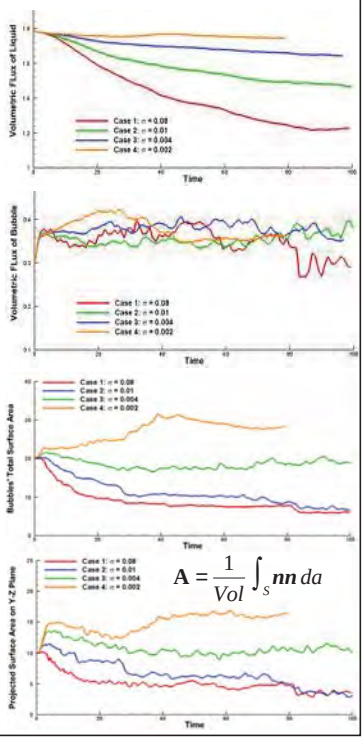

Low We

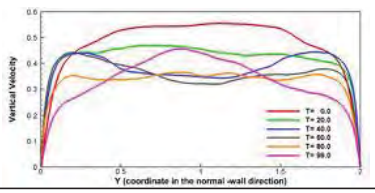

High We

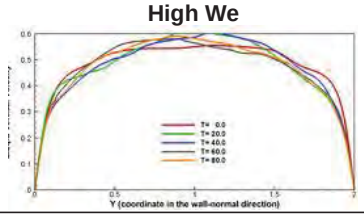

$$\mathbf{A} = \frac{1}{Vol}\int_S \boldsymbol{nn}\, da$$

UNIVERSITY OF NOTRE DAME

DNS of Multiphase Flows
Heat/Mass Transfer & Surfactants

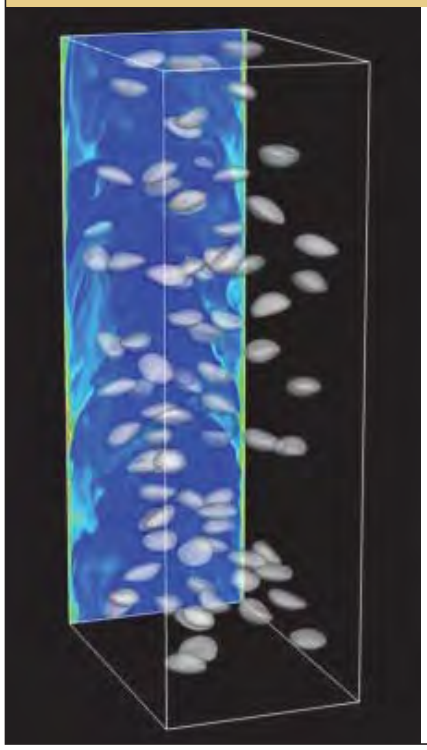

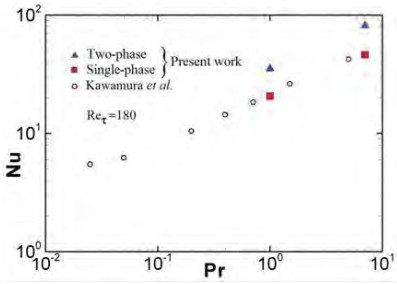

M. Muradoglu and G. Tryggvason. Simulations of Soluble Surfactants in 3D Multiphase Flow. *Journal of Computational Physics,* 274 (2014), 737-757.

S. Dabiri and G. Tryggvason. Heat transfer in turbulent bubbly flow in vertical channels. *Chemical Engineering Science.* 122 (2015), 106-113.

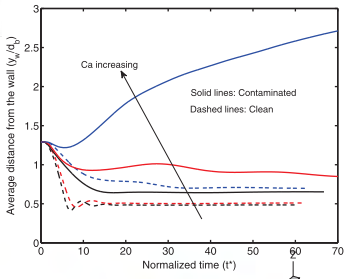

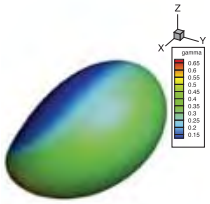

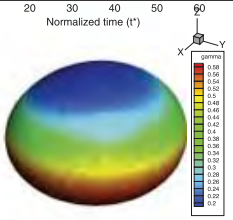

UNIVERSITY OF NOTRE DAME

DNS of Multiphase Flows
Examples

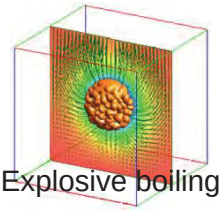

Explosive boiling

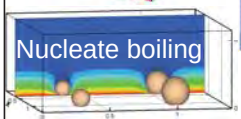

Nucleate boiling

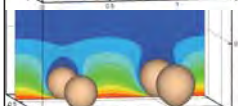

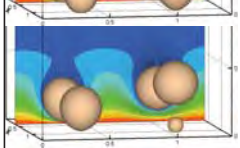

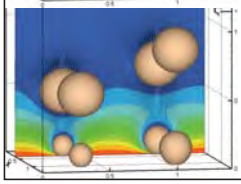

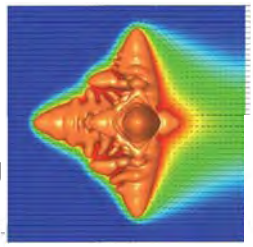

Solidification

EHD of drops

Atomization

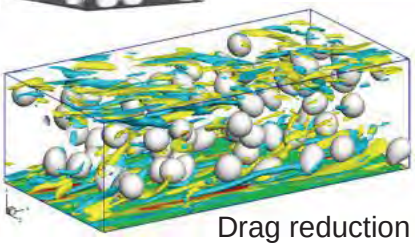

Drag reduction

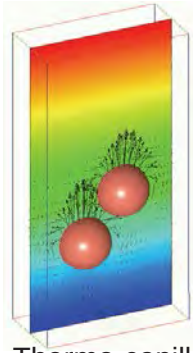

Thermo-capillary migration

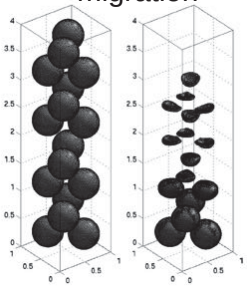

Cavitating bubbles

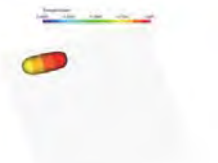

FDM 3D Printing

Rayleigh-Taylor Instability

Multiscale Strategies

Multiscale Issues

Capturing isolated small-scale motion in simulations where the focus is on the larger scales can be done in many ways, such as be various grid refinement techniques (unstructured grids, AMR for Cartesian grids, wavelets, etc.) or reduced order models

However:

At small scales, the effect of surface tension is strong so interface geometries are simple

At small scales the effect of viscosity is strong so the flow is simple

Those are exactly the situation that can be —and have been—handled analytically

Buoyant bubbles in an inclined channel flow

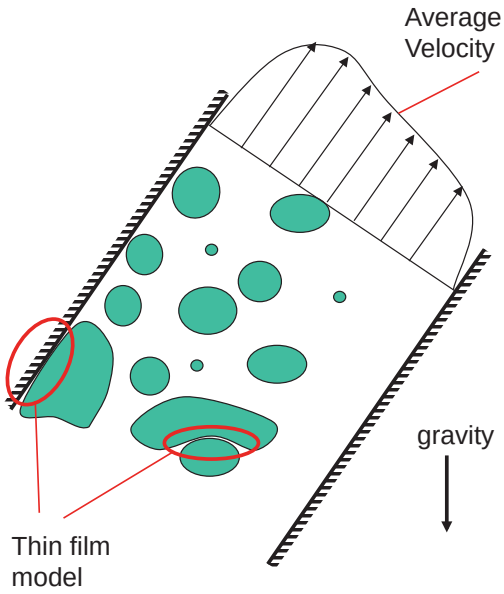

UNIVERSITY OF NOTRE DAME

DNS of Multiphase Flows
Mass Transfer in Gas-Liquid Systems

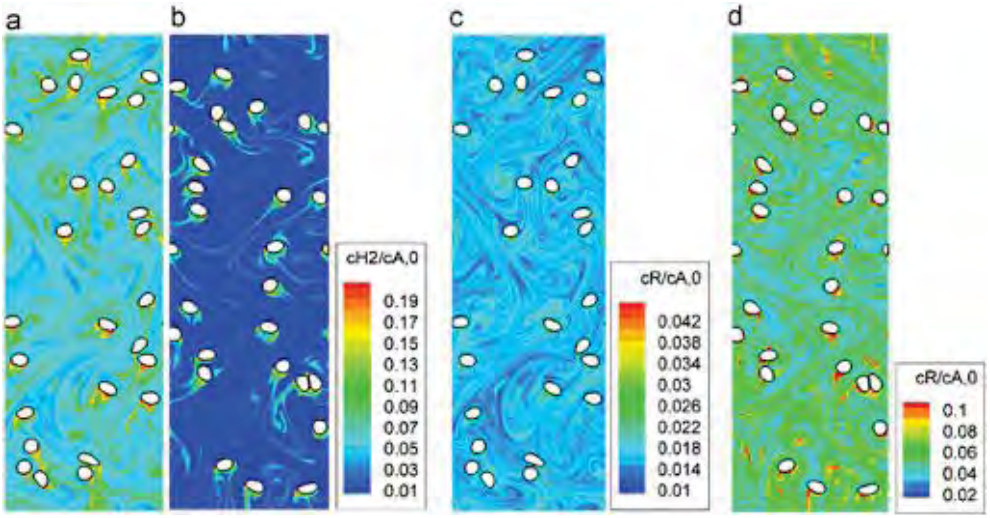

Results from simulations of the of the catalytic hydrogenation of nitroarenes. The hydrogen (frames a and b) and hydroxylamine (frames c and d) concentration profiles are shown for one time for two simulations. In frames a and c the reaction rates are relatively slow, compared with the mass transfer, but in frames b and d the reaction is relatively fast. From Radl, Koynov, Tryggvason, and Khinast (2008).

UNIVERSITY OF NOTRE DAME

DNS of Multiphase Flows
Mass Transfer in Gas-Liquid Systems

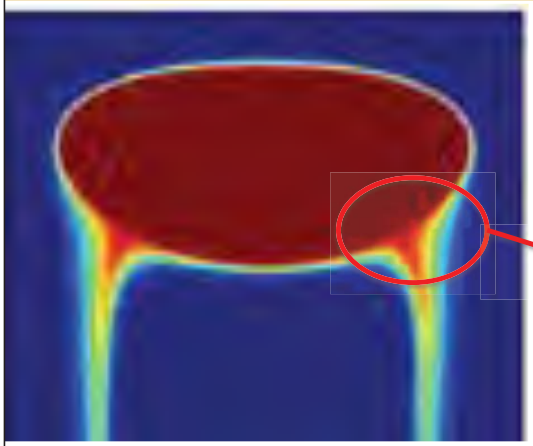

Capturing the mass boundary layer

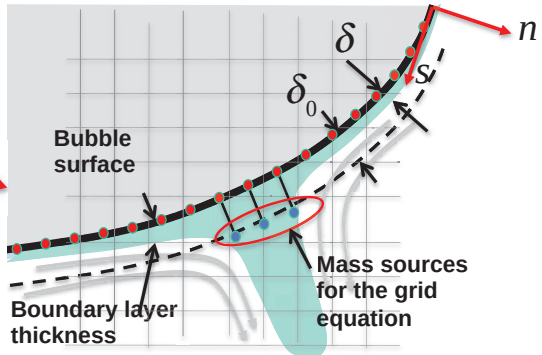

$$\frac{\partial f}{\partial t} = \sigma n \frac{\partial f}{\partial n} + D \frac{\partial^2 f}{\partial n^2}$$

$$M_0 = \int_0^\infty f \, dn$$

$$M_1 = \int_0^\infty n \, f \, dn$$

$$\frac{dM_0}{dt} = -\sigma \left(M_0 - \delta_o f_\delta \right) - D \left. \frac{\partial f}{\partial n} \right|_0$$

$$\frac{dM_1}{dt} = -\sigma \left(2M_1 - \delta_o^2 f_\delta \right) + D \left(f_o - f_\delta \right)$$

B. Aboulhasanzadeh, S. Thomas, M. Taeibi-Rahni, and G. Tryggvason. *Chemical Engineering Science* 75 (2012) 456–467.

UNIVERSITY OF NOTRE DAME

DNS of Multiphase Flows
Mass Transfer in Gas-Liquid Systems

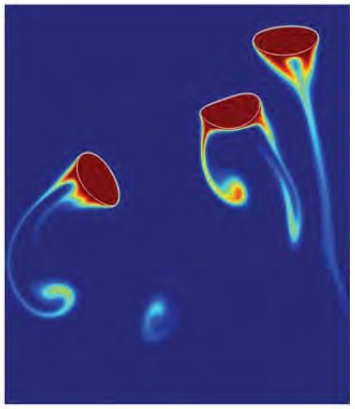

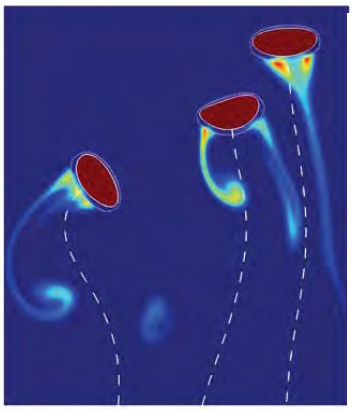

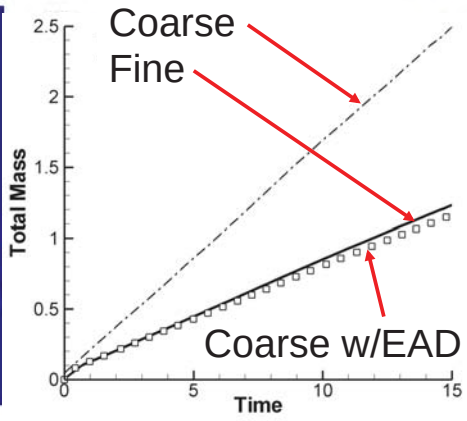

Full Using Model

Re = 60, Sc = 15

Using one moment and a one-parameter profile

$$\frac{dM_0}{dt} = -\sigma\left(M_0 - \delta_o f_\delta\right) - D\left.\frac{\partial f}{\partial n}\right|_0 ; \qquad f(n) = \begin{cases} f_0\left(1 - 2\left(\frac{n}{\delta}\right) + \left(\frac{n}{\delta}\right)^2\right); & n \le \delta_0 \\ 0; & n > \delta \end{cases}$$

UNIVERSITY OF NOTRE DAME

DNS of Multiphase Flows
Capturing the mass boundary layer

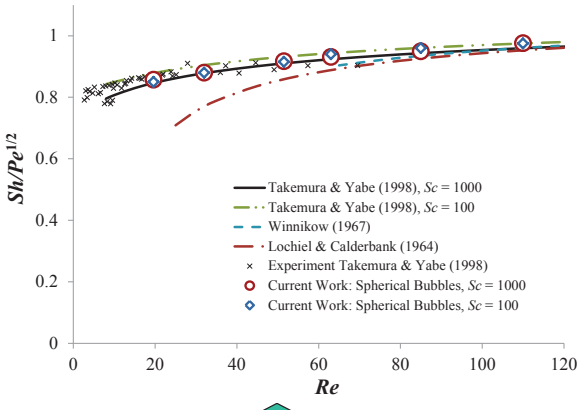

The mass transfer versus Re, for a single bubble in a large domain, along with the predictions of experimental correlations

Comparison with experimental results from A. Tomiyama:
Eo = 24.7
Mo = $10^{-7.78}$ and
Sc= 8260

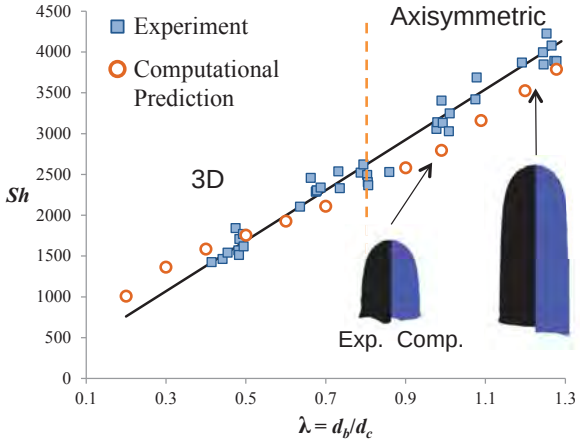

B. Aboulhasanzadeh, S. Hosoda, A. Tomiyama, G. Tryggvason. *Chemical Engineering Science,* 101 (2013), 165-174.

UNIVERSITY OF NOTRE DAME

DNS of Multiphase Flows
Thin films near walls

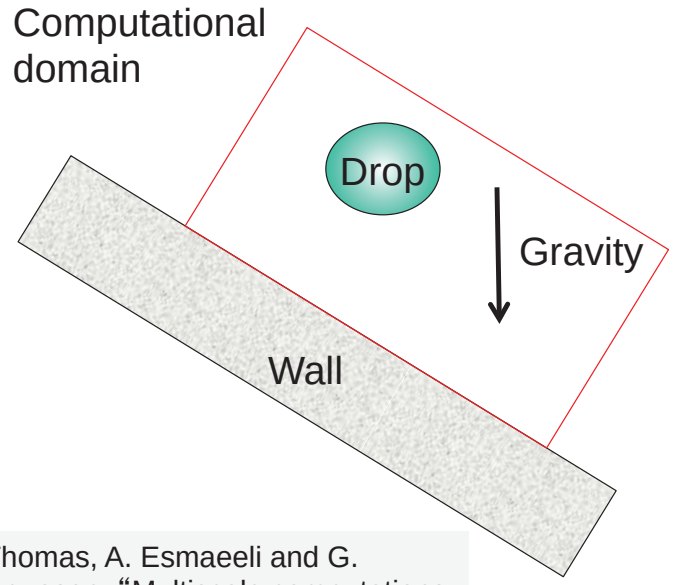

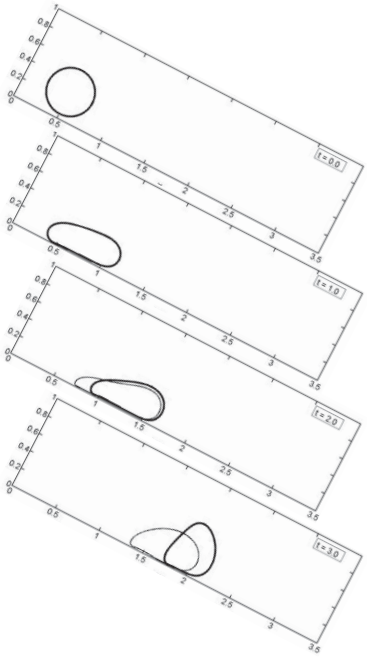

S. Thomas, A. Esmaeeli and G. Tryggvason. "Multiscale computations of thin films in multiphase flows." *Int'l J. Multiphase Flow* 36 (2010), 71-77.

UNIVERSITY OF NOTRE DAME

DNS of Multiphase Flows
Thin films near walls

Film model—linear velocity profile

$$\frac{\partial h}{\partial t}+\frac{1}{2}\frac{\partial}{\partial x}\left(hU_f\right)=0;$$

$$\frac{\partial}{\partial t}\left(hU_f\right)+\frac{2}{3}\frac{\partial}{\partial x}\left(hU_f^2\right)=-\frac{2h}{\rho_o}\left(\frac{dp}{dx}\right)_f,$$

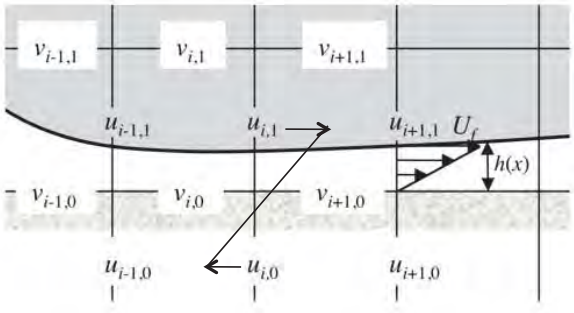

Wall shear and ghost velocity:

$$\tau_f=\mu_o\frac{U_f}{h} \rightarrow u_{i,0}=u_{i,1}-\frac{\tau_f\Delta y}{\mu_d}$$

1. Identify whether a grid points at a wall belong to a film or not.

2. For film wall-points, given h and U_f, find the wall-shear and set the ghost velocities. For points outside the film, use the no-slip boundary condition.

3. Solve the Navier-Stokes equations for the velocity and pressure at the next time step, using the ghost velocities set above.

4. Integrate the thin film equations, using the pressure at the wall as computed by solving the Navier-Stokes equations (step 3).

5. Go back to (1)

UNIVERSITY OF NOTRE DAME

DNS of Multiphase Flows
Thin films near walls

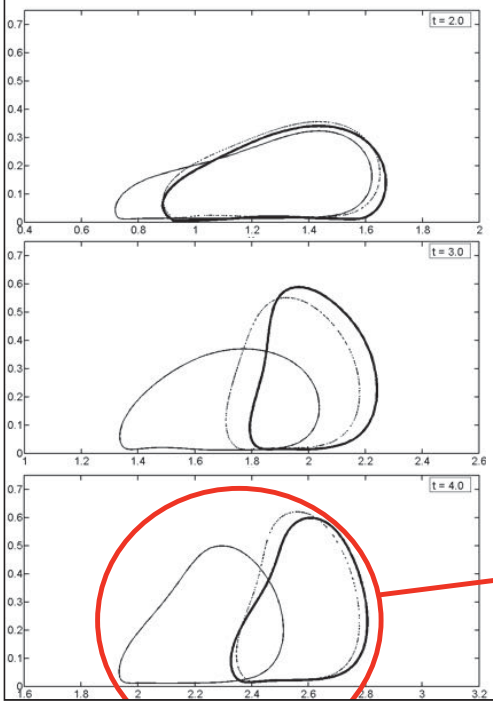

Drop motion on a sloping wall. Impact of fully resolving the film between the drop and the wall

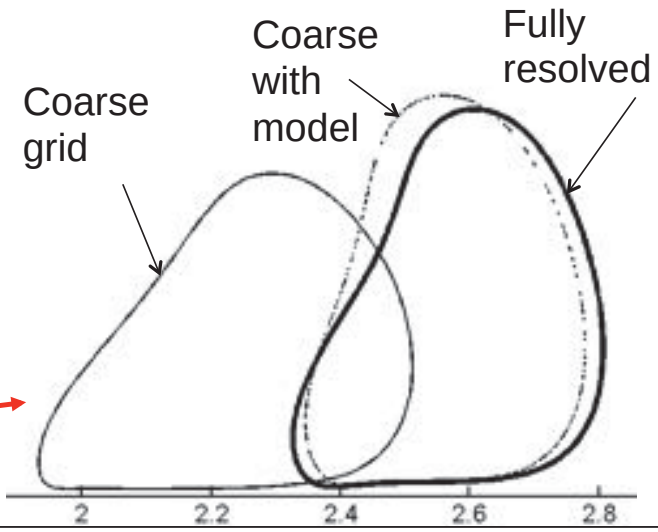

UNIVERSITY OF NOTRE DAME

DNS of Multiphase Flows

"Almost" DNS

• For two-fluid and multi-phase flows the range of scales is sometimes simply too large for everything to be fully resolved, either because of spontaneous generation of small films, ligaments or drops due to collision of fluid masses or topology changes or because of scales introduced by additional physical processes.

• The other reason is that as we consider more complex physics, we are often working with equations that do not fully describe the physics. For surfactants we may be using simplified equations of state and for reactions we may be using a reduced set of equations for the chemistry. So even if the solution is accurate, the physics may not be fully captured.

What to do with the Results

Modeling Challenges and Opportunities:

The enormous of amount of data generated by DNS—and increasingly by experiments—will allow reduced order models that involve large number of variables and complex relationships between the resolve and unresolved variables and are applicable to complex flows

Determining complex nonlinear relationships from massive data involving a range of physical scales using modern statistical learning is becoming easier

Modeling challenges will therefore shift to the development of more sophisticated and comprehensive models, the identification of the appropriate variables, and the incorporation and propagation of physical and model uncertainties

The inclusion of limiting cases, such as where the relationships are known, or the scaling is understood, in fitting is currently difficult but is likely to become increasingly important

UNIVERSITY OF NOTRE DAME

DNS of Multiphase Flows
Closure Terms by Statistical Learning

A simple description of the average flow is derived by integrating the vertical momentum equation and taking the density and viscosity of the gas is zero

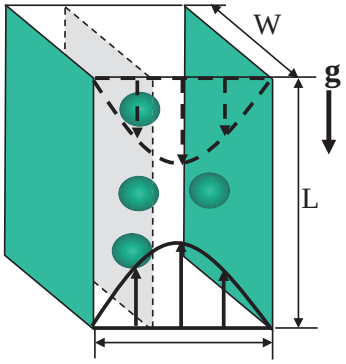

Void fraction and phase averaged velocity

$$\alpha_i = \frac{1}{A_{zy}} \int \chi_i da \qquad < v >= \frac{1}{\alpha_i A_{zy}} \int \chi v da$$

Horizontal flux of bubbles

$$\frac{\partial \alpha_l}{\partial t} + \frac{\partial}{\partial x} F_l = 0. \qquad F_i = \frac{1}{\alpha A_{zy}} \int \chi_i u_i da$$

$$\alpha_b + \alpha_l = 1$$
$$\alpha_b < u >_b + \alpha_l < u >_l = 0$$
$$\alpha_l < u >_l < v >_l = F_l < v >_l$$
$$F_l = \alpha_l < u >_l$$

Averaged vertical momentum of the liquid:

$$\frac{\partial}{\partial t}\alpha_l < v >_l + \frac{\partial}{\partial x} F_l < v >_l =$$
$$-\frac{1}{\rho_l}\frac{dp_o}{dy} - g_y \alpha_l + \nu_l \frac{\partial}{\partial x}\left(\alpha_l \frac{\partial < v >_l}{\partial x}\right)$$
$$-\frac{\nu_l}{L}\frac{\partial}{\partial x}\sum_{int}(v' n_x + u' n_y) - \frac{\partial}{\partial x}\alpha_l < u'v' >_l + \frac{1}{\rho_l}(f_\sigma)_y$$

UNIVERSITY OF NOTRE DAME

DNS of Multiphase Flows
Closure Terms by Statistical Learning

"Closure" variables needed for models of the average flow

Resolved average variables

Quantities summarizing the state of the unresolved flow

F_g	$<u'v'>$	f_σ	α_g	$\frac{\partial \alpha_g}{\partial x}$	$\frac{\partial < v >_l}{\partial x}$	d_w	k_t	ε_t	a	a_{ij}
	Data obtained by averaging the DNS results									

Not include yet

By averaging the DNS results over planes parallel to the walls, we construct the Table above with quantities that are known and unknown in the averaged equations. Using Neural Networks, we fit the data, resulting in:

$$F_b = f_1(\mathbf{x}); \quad <u'v'>= f_2(\mathbf{x}); \quad F_\sigma = f_3(\mathbf{x}); \quad \mathbf{x} = \left(\alpha, \frac{\partial \alpha}{\partial x}, \frac{\partial < v >}{\partial x}, d_w\right)$$

These relationships are used when solving the average equations for the void fraction and the vertical liquid velocity

UNIVERSITY OF NOTRE DAME

DNS of Multiphase Flows
Closure Terms by Statistical Learning

Most recently our emphasize has been neural network as they seem to be giving the most promising results.

$$F_b = f_1(\mathbf{x}); \quad \langle u'v' \rangle = f_2(\mathbf{x}); \quad F_\sigma = f_3(\mathbf{x}); \quad \mathbf{x} = \left(\alpha, \frac{\partial \alpha}{\partial x}, \frac{\partial \langle v \rangle}{\partial x}, d_w\right)$$

A neural network with one hidden layers

m: input variables
n: hidden variables

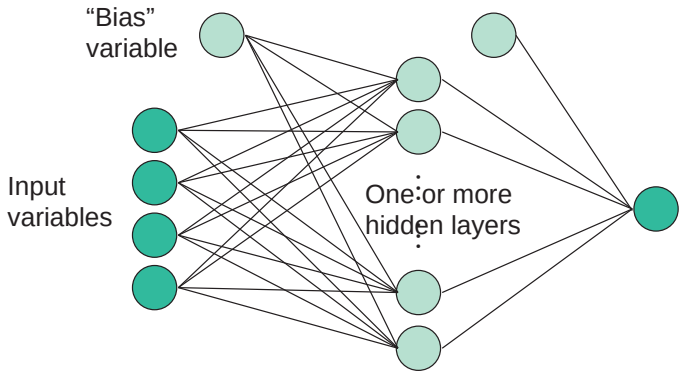

$$f(\mathbf{x}) = b_0 + \sum_{i=1}^{n} b_i h_i(\mathbf{x}); \quad h_i(\mathbf{x}) = s\left(a_{0i} + \sum_{j=1}^{m} x_j a_{j,i}\right); \quad s(u) = \frac{2}{1+e^{-2u}} - 1$$

UNIVERSITY OF NOTRE DAME

DNS of Multiphase Flows
Closure Terms by Statistical Learning

Averaged DNS results and Model predictions using the ANN closure terms at several different times

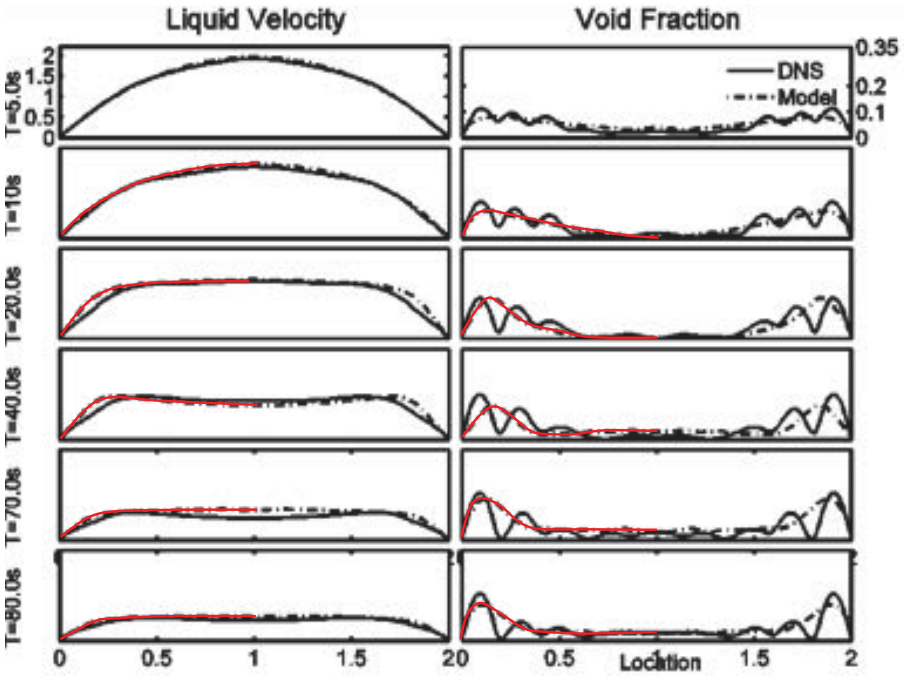

UNIVERSITY OF NOTRE DAME

DNS of Multiphase Flows
Closure Terms by Statistical Learning

The closure relations derived from the upflow cases applied to downflow

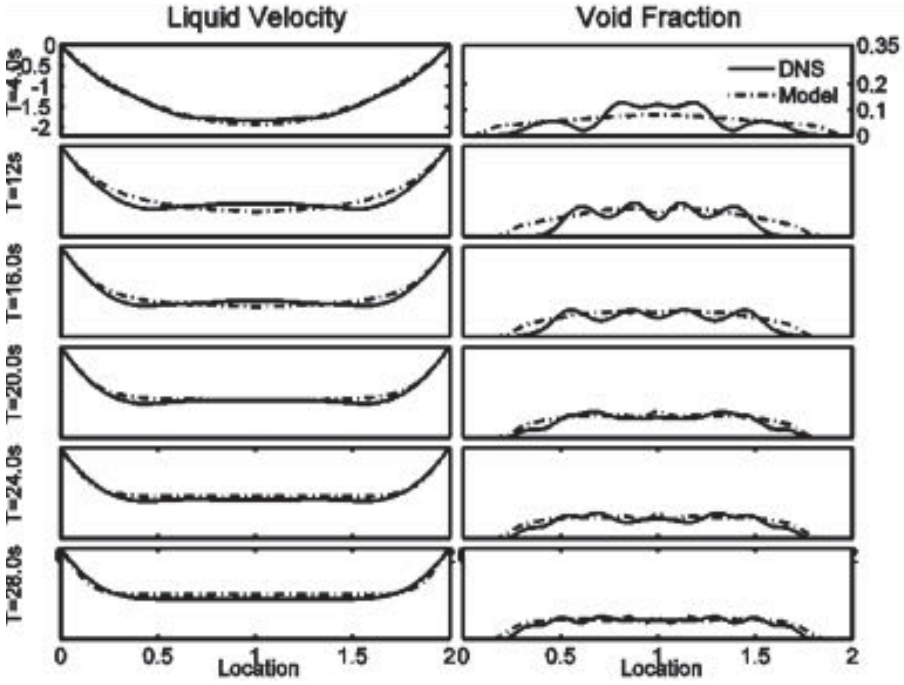

UNIVERSITY OF NOTRE DAME

DNS of Multiphase Flows
Now What?

- DNS of multifluid turbulent flows have been developed to the point that they should be able to help produce new models for "industrial" simulations
- DNS data is putting new demands on the modeling of complex multiphase flows. Currently, such modeling relies of fairly basic ideas, first put forward many years ago. DNS should make much more comprehensive models possible
- DNS needs to be extended to handle flows with more complex topology and those undergoing flow regime transitions
- Complex isothermal flows and flows with phase change and other additional physics, such as mass transfer, need multiscale modeling that must be developed further and put on a rigorous theoretical basis.
- One of the biggest obstacle for more rapid increase in the use of DNS is the high "entry barrier" for new investigators. Many "things" to learn!

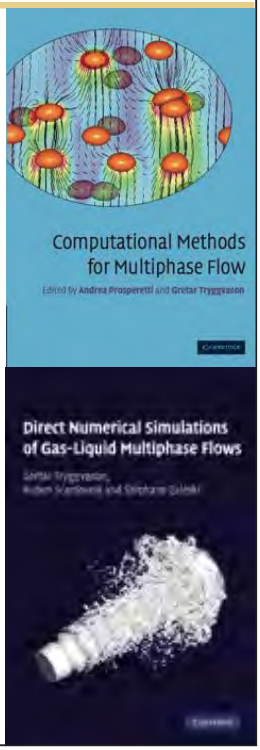

Education

UNIVERSITY OF NOTRE DAME DNS of Multiphase Flows

There is a need for software for a variety of purposes. Those include:

• Codes for education and/or testing of ideas
http://www3.nd.edu/~gtryggva/MultiphaseDNS/index.html

• Large scale “somewhat” general purpose codes that represent close to the state-of-the-art and often can be used as “black-boxes:
http://www.ida.upmc.fr/~zaleski/paris/index.html

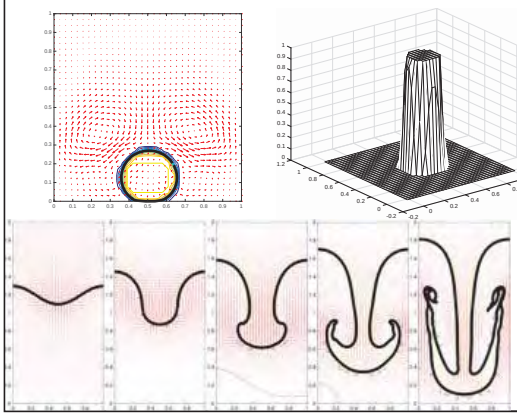

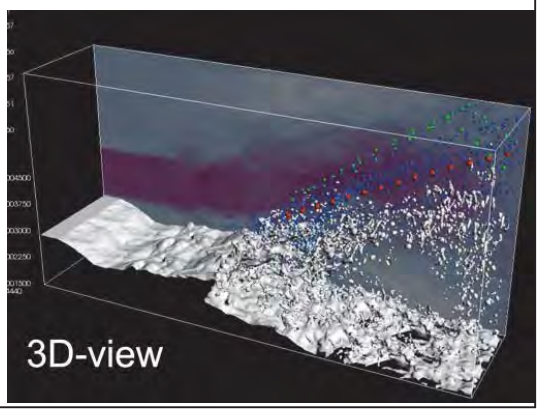

DNS of Multiphase Flows

```
%=================================================================
% CodeC3-frt-st-RK3.m
% A very simple Navier-Stokes solver for a drop falling in a
% rectangular box, using a conservative form of the equations.
% A 3-order explicit projection method and centered in space
% discretizationa are used. The density is advected by a front
% tracking scheme and surface tension and variable viscosity is
% included. This version uses a simple method to create the
% marker function. Last edited 7/6/2016
%=================================================================

Lx=1.0,Ly=1.0,gx=0.0,gy=-100.0; rho1=0.1; rho2=2.0, % Domain size and
m1=0.01; m2=0.1; sigma=10;                          % physical variables
unorth=0;usouth=0;veast=0;vwest=0;time=0.0;
rad=0.15;xc=0.5;yc=0.7;          % Initial drop size and location

%-------------------- Numerical variables ----------------------
nx=32;ny=32;dlt=0.00125;nstep=400; maxit=200;maxError=0.001;beta=1.5; Nf=100;

%-------------------- Zero various arrys -----------------------
u=zeros(nx+1,ny+2);  v=zeros(nx+2,ny+1);  p=zeros(nx+2,ny+2);
ut=zeros(nx+1,ny+2); vt=zeros(nx+2,ny+1); tmp1=zeros(nx+2,ny+2);
uu=zeros(nx+1,ny+1); vv=zeros(nx+1,ny+1); tmp2=zeros(nx+2,ny+2);
fx=zeros(nx+2,ny+2); fy=zeros(nx+2,ny+2); r=zeros(nx+2,ny+2);
r=zeros(nx+2,ny+2);  chi=zeros(nx+2,ny+2);
rn=zeros(nx+2,ny+2);  dl=zeros(nx+2,ny+2);
xf=zeros(1,Nf+2); yf=zeros(1,Nf+2);
uf=zeros(1,Nf+2); vf=zeros(1,Nf+2);
tx=zeros(1,Nf+2); ty=zeros(1,Nf+2);
un=zeros(nx+1,ny+2); vn=zeros(nx+2,ny+1);   % Used for
rn=zeros(nx+2,ny+2); nn=zeros(nx+2,ny+2);   % higher order
xfn=zeros(1,Nf+2); yfn=zeros(1,Nf+2);       % in time

dx=Lx/nx;dy=Ly/ny;                          % Set the grid
for i=1:nx+2; x(i)=dx*(i-1.5);end; for j=1:ny+2; y(j)=dy*(j-1.5);end;

%-------------------- Initial Conditions -----------------------
r=zeros(nx+2,ny+2)+rho1;m=zeros(nx+2,ny+2)+m1; % Set density and viscosity
for i=2:nx+1,for j=2:ny+1;                  % for the domain and the drop
  if((x(i)-xc)^2+(y(j)-yc)^2 <rad^2),r(i,j)=rho2,m(i,j)=m2,chi(i,j)=1.0;end,
end,end

for I=1:Nf+2, xf(I)=xc-rad*sin(2.0*pi*(I-1)/(Nf));     % Initialize
              yf(I)=yc+rad*cos(2.0*pi*(I-1)/(Nf));end   % the Front

hold off,contour(x,y,flipud(rot90(chi))),axis equal,axis([0 Lx 0 Ly]);
hold on;plot(xf(1:Nf),yf(1:Nf),'k','linewidth',3);pause(0.01)

%-------------------- START TIME LOOP --------------------------
for is=1:nstep,is
  un=u; vn=v; rn=r; mn=m; xfn=xf; yfn=yf;  % Higher order
  for substep=1:3                          % in time

%---------------------- Advect the Front -----------------------
 for I=2:Nf+1                    % Interpolate the Front Velocities
    ip=floor(xf(I)/dx)+1; jp=floor((yf(I)+0.5*dy)/dy)+1;
    ax=xf(I)/dx-ip+1;ay=(yf(I)+0.5*dy)/dy-jp+1;
    uf(I)=(1.0-ax)*(1.0-ay)*u(ip,jp)+ax*(1.0-ay)*u(ip+1,jp)+...
          (1.0-ax)*ay*u(ip,jp+1)+ax*ay*u(ip+1,jp+1);



    ip=floor((xf(I)+0.5*dx)/dx)+1; jp=floor(yf(I)/dy)+1;
    ax=(xf(I)+0.5*dx)/dx-ip+1; ay=yf(I)/dy-jp+1;
    vf(I)=(1.0-ax)*(1.0-ay)*v(ip,jp)+ax*(1.0-ay)*v(ip+1,jp)+...
          (1.0-ax)*ay*v(ip,jp+1)+ax*ay*v(ip+1,jp+1);
  end

  for i=2:Nf+1, xf(i)=xf(i)+dt*uf(i); yf(i)=yf(i)+dt*vf(i);end % Move the
 xf(1)=xf(Nf+1);yf(1)=yf(Nf+1);xf(Nf+2)=xf(2);yf(Nf+2)=yf(2); % Front
```

```
%------------- Update the marker function --------------------
  d(2:nx+1,2:ny+1)=2*max(dx,dy); dh=min(dx,dy);

  for I=1:Nf
    nfx=-(yf(I+1)-xf(I));
    nfy=(xf(I+1)-xf(I));  % Normal vector
    ds=sqrt(nfx*nfx+nfy*nfy); nfx=nfx/ds; nfy=nfy/ds;
    xfront=0.5*(xf(I)+xf(I+1)); yfront=0.5*(yf(I)+yf(I+1));
    ip=floor((xfront+0.5*dx)/dx)+1; jp=floor((yfront+0.5*dy)/dy)+1;

    d1=sqrt((xfront-x(ip))^2  +(yfront-y(jp))^2);
    d2=sqrt((xfront-x(ip+1))^2+(yfront-y(jp))^2);
    d3=sqrt((xfront-x(ip+1))^2+(yfront-y(jp+1))^2);
    d4=sqrt((xfront-x(ip))^2  +(yfront-y(jp+1))^2);

    if d1<d(ip,jp), d(ip,jp)=d1;...
     dn1=(x(ip)- xfront)*nfx+(y(jp)- yfront)*nfy;
     chi(ip,jp)=   0.5*(1.0+sign(dn1));
     if abs(dn1)<0.5*dh, chi(ip,jp)=  0.5+(dn1/dh); end;
    end
    if d2<d(ip+1,jp), d(ip+1,jp)=d2;...
     dn2=(x(ip+1)-xfront)*nfx+(y(jp)- yfront)*nfy;
     chi(ip+1,jp)=  0.5*(1.0+sign(dn2));
     if abs(dn2)<0.5*dh, chi(ip+1,jp)=  0.5+(dn2/dh); end;
    end
    if d3<d(ip+1,jp+1), d(ip+1,jp+1)=d3;...
     dn3=(x(ip+1)-xfront)*nfx+(y(jp+1)-yfront)*nfy;
     chi(ip+1,jp+1)=0.5*(1.0+sign(dn3));
     if abs(dn3)<0.5*dh, chi(ip+1,jp+1)=0.5+(dn3/dh); end;
    end
    if d4<d(ip,jp+1), d(ip,jp+1)=d4;...
     dn4=(x(ip)- xfront)*nfx+(y(jp+1)-yfront)*nfy;
     chi(ip,jp+1)=  0.5*(1.0+sign(dn4));
     if abs(dn4)<0.5*dh, chi(ip,jp+1)=  0.5+(dn4/dh); end;
    end
  end

%-------------------- Update the density -----------------------
   ro=r;
   for i=1:nx+2,for j=1:ny+2
    r(i,j)=rho1+(rho2-rho1)*chi(i,j);
   end,end

%--------------------- Find surface tension --------------------
   fx=zeros(nx+2,ny+2);fy=zeros(nx+2,ny+2);  % Set fx & fy to zero
   for I=1:Nf+1,
     ds=sqrt((xf(I+1)-xf(I))^2+(yf(I+1)-yf(I))^2);
     tx(I)=(xf(I+1)-xf(I))/ds;
     ty(I)=(yf(I+1)-yf(I))/ds; % Tangent vectors
   end
   tx(Nf+2)=tx(2);ty(Nf+2)=ty(2);

  for I=2:Nf+1           % Distribute to the fixed grid
     nfx=sigma*(tx(I)-tx(I-1));nfy=sigma*(ty(I)-ty(I-1));

     ip=floor(xf(I)/dx)+1; jp=floor((yf(I)+0.5*dy)/dy)+1;
     ax=xf(I)/dx-ip+1; ay=(yf(I)+0.5*dy)/dy-jp+1;
     fx(ip,jp)    =fx(ip,jp)+(1.0-ax)*(1.0-ay)*nfx/dx/dy;
     fx(ip+1,jp)  =fx(ip+1,jp)+ax*(1.0-ay)*nfx/dx/dy;
     fx(ip,jp+1)  =fx(ip,jp+1)+(1.0-ax)*ay*nfx/dx/dy;
     fx(ip+1,jp+1)=fx(ip+1,jp+1)+ax*ay*nfx/dx/dy;

     ip=floor((xf(I)+0.5*dx)/dx)+1; jp=floor(yf(I)/dy)+1;
     ax=(xf(I)+0.5*dx)/dx-ip+1; ay=yf(I)/dy-jp+1;
     fy(ip,jp)    =fy(ip,jp)+(1.0-ax)*(1.0-ay)*nfy/dx/dy;
     fy(ip+1,jp)  =fy(ip+1,jp)+ax*(1.0-ay)*nfy/dx/dy;
     fy(ip,jp+1)  =fy(ip,jp+1)+(1.0-ax)*ay*nfy/dx/dy;
     fy(ip+1,jp+1)=fy(ip+1,jp+1)+ax*ay*nfy/dx/dy;
   end

   fx(1:nx+2,2)=fx(1:nx+2,2)+fx(1:nx+2,1);          % Correct boundary
   fx(1:nx+2,nx+1)=fx(1:nx+2,nx+1)+fx(1:nx+2,nx+2); % values for the
   fy(2,1:ny+2)=fy(2,1:ny+2)+fy(1,1:ny+2);          % surface force
   fy(nx+1,1:ny+2)=fy(nx+1,1:ny+2)+fy(nx+2,1:ny+2); % on the grid
```

```
%------------ Set tangential velocity at boundaries ----------
  u(1:nx+1,1)=2*usouth-u(1:nx+1,2);u(1:nx+1,ny+2)=2*unorth-u(1:nx+1,ny+1);
  v(1,1:ny+1)=2*vwest-v(2,1:ny+1);v(nx+2,1:ny+1)=2*veast-v(nx+1,1:ny+1);

%--------------- Find the predicted velocities ----------------
  for i=2:nx,for j=2:ny+1     % Temporary u-velocity-advection
    ut(i,j)=(2.0/(r(i+1,j)+r(i,j)))*(0.5*(ro(i+1,j)+ro(i,j))*u(i,j)+ dt*( ...
    -(0.25/dx)*(ro(i+1,j)*(u(i+1,j)+u(i,j))^2-ro(i,j)*(u(i,j)+u(i-1,j))^2)...
    -(0.0625/dy)*( (ro(i,j)+ro(i+1,j)+ro(i,j+1)+ro(i+1,j+1))*          ...
                                  (u(i,j+1)+u(i,j))*(v(i+1,j)+v(i,j))  ...
    -(ro(i,j)+ro(i+1,j)+ro(i+1,j-1)+ro(i,j-1))*(u(i,j                  ...
                                  +u(i,j-1))*(v(i+1,j-1)+v(i,j-1)))   ...
                              + 0.5*(ro(i+1,j)+ro(i,j))*gx + fx(i,j) ) );
  end,end

  for i=2:nx+1,for j=2:ny      % Temporary v-velocity-advection
    vt(i,j)=(2.0/(r(i,j+1)+r(i,j)))*(0.5*(ro(i,j+1)+ro(i,j))*v(i,j)+ dt*( ...
    -(0.0625/dx)*( (ro(i,j+ro(i+1,j)+ro(i+1,j+1)+ro(i,j+1))*          ...
                                  (u(i,j+u(i,j+1))*(v(i,j)+v(i+1,j))  ...
              - (ro(i,j)+ro(i,j+1)+ro(i-1,j+1)+ro(i-1,j))*          ...
                                  (u(i-1,j+1)+u(i-1,j))*(v(i,j)+v(i-1,j)))...
    -(0.25/dy)*(ro(i,j+1)*(v(i,j+1)+v(i,j))^2-ro(i,j)*(v(i,j)+v(i,j-1))^2)...
                              + 0.5*(ro(i,j+1)+ro(i,j))*gy + fy(i,j) ) );
  end,end

  for i=2:nx,for j=2:ny+1     % Temporary u-velocity-viscosity
    ut(i,j)=ut(i,j)+(2.0/(r(i+1,j)+r(i,j)))*dt*(...
          +(1.0/dx)*2.*(m(i+1,j)*(1.0/dx)*(u(i+1,j)-u(i,j)) -     ...
            m(i,j) *(1.0/dx)*(u(i,j)-u(i-1,j)) )                  ...
      +(1.0/dy)*( 0.25*(m(i,j)+m(i+1,j)+m(i+1,j+1)+m(i,j+1))*     ...
        ((1.0/dy)*(v(i,j+1)-v(i,j)) + (1.0/dx)*(v(i+1,j)-v(i,j)) ) -  ...
          0.25*(m(i,j)+m(i+1,j)+m(i-1,j+1)+m(i-1,j))*             ...
        ((1.0/dy)*(u(i-1,j+1)-u(i-1,j))+ (1.0/dx)*(v(i,j)- v(i-1,j)) ) ) ;
  end,end

  for i=2:nx+1,for j=2:ny      % Temporary v-velocity-viscosity
      vt(i,j)=vt(i,j)+(2.0/(r(i,j+1)+r(i,j)))*dt*(...
        +(1.0/x)*( 0.25*(m(i,j+m(i+1,j+m(i+1,j+1)+m(i,j+1))*    ...
        ((1.0/y)*(u(i,j+1)-u(i,j)) + (1.0/x)*(v(i+1,j)-v(i,j)) ) -  ...
          0.25*(m(i,j+m(i,j+1)+m(i-1,j+1)+m(i-1,j))*              ...
        ((1.0/y)*(u(i-1,j+1)-u(-1,j))+ (1.0/x)*(v(i,j)- v(i-1,j)) ) ...
        +(1.0/y)*2.*(m(i,j+1)*(1.0/y)*(v(i,j+1)-v(i,j)) -         ...
            m(i,j) *(1.0/y)*(v(i,j)-v(i,j-1)) ) ) ;
  end,end

%------------------ Solve the Pressure Equation ---------------
  rt=r; lrg=1000;  % Compute source term and the coefficient for p(i,j)
  rt(1:nx+2,1)=lrg;rt(1:nx+2,ny+2)=lrg;
  rt(1,1:ny+2)=lrg;rt(nx+2,1:ny+2)=lrg;

  for i=2:nx+1,for j=2:ny+1
    tmp1(i,j)= (0.5/dt)*( (ut(i,j)-ut(i-1,j))/dx+(vt(i,j)-vt(i,j-1))/dy );
    tmp2(i,j)=1.0/( (1./dx)*(1./dx*(rt(i+1,j)+rt(i,j)))+   ...
                    1./(dx*(rt(i-1,j)+rt(i,j))) )+ ...
              (1./dy)*(1./dy*(rt(i,j+1)+rt(i,j))+   ...
                    1./(dy*(rt(i,j-1)+rt(i,j)) ) );
  end,end

  for it=1:maxit                          % Solve for pressure by SOR
    oldArray=p;
    for i=2:nx+1,for j=2:ny+1
      p(i,j)=(1.0-beta)*p(i,j)+beta* tmp2(i,j)*(      ...
      (1./dx)*( p(i+1,j)/(dx*(rt(i+1,j)+rt(i,j)))+    ...
                p(i-1,j)/(dx*(rt(i-1,j)+rt(i,j))) )+ ...
      (1./dy)*( p(i,j+1)/(dy*(rt(i,j+1)+rt(i,j)))+    ...
                p(i,j-1)/(dy*(rt(i,j-1)+rt(i,j))) - tmp1(i,j));
    end,end
    if max(max(abs(oldArray-p))) <maxError, break, end
  end

  for i=2:nx,for j=2:ny+1   % Correct the u-velocity
    u(i,j)=ut(i,j)-dt*(2.0/dx)*(p(i+1,j)-p(i,j))/(r(i+1,j)+r(i,j));
  end,end

  for i=2:nx+1,for j=2:ny   % Correct the v-velocity
    v(i,j)=vt(i,j)-dt*(2.0/dy)*(p(i,j+1)-p(i,j))/(r(i,j+1)+r(i,j));
  end,end
```

```
    for i=1:nx+2,for j=1:ny+2 % Update the viscosity
      m(i,j)=m1+(m2-m1)*chi(i,j);
    end,end

  if substep==2, % Higher order (RK-3) in time
      u=0.75*un+0.25*u; v=0.75*vn+0.25*v, r=0.75*rn+0.25*r;
      m=0.75*mn+0.25*m; xf=0.75*xfn+0.25*xf; yf=0.75*yfn+0.25*yf;
    elseif substep==3
      u=(1/3)*un+(2/3)*u; v=(1/3)*vn+(2/3)*v, r=(1/3)*rn+(2/3)*r;
      m=(1/3)*mn+(2/3)*m; xf=(1/3)*xfn+(2/3)*xf; yf=(1/3)*yfn+(2/3)*yf;
    end

    end             % End of sub-iteration for RK-3 time integration

%---------------- Add and deleate points in the Front ----------
  xfold=xf;yfold=yf; j=1;
  for I=2:Nf+1
    ds=sqrt( (xfold(I)-xf(j))/dx)^2 + ((yfold(I)-yf(j))/dy)^2);
    if (ds > 0.5)
     j=j+1;xf(j)=0.5*(xfold(I)+xf(j-1));yf(j)=0.5*(yfold(I)+yf(j-1));
     j=j+1;xf(j)=xfold(I);yf(j)=yfold(I);
    elseif (ds < 0.25)
      % DO NOTHING!
    else
     j=j+1;xf(j)=xfold(I);yf(j)=yfold(I);
    end
  end
  Nf=j-1;
  xf(1)=xf(Nf+1);yf(1)=yf(Nf+1);xf(Nf+2)=xf(2);yf(Nf+2)=yf(2);

%----------------- Compute Diagnostic quantitites --------------
  Area(is)=0; CentroidX(is)=0; CentroidY(is)=0; Time(is)=time;

  for j=1:Nf, Area(is)=Area(is)+...
     0.25*((xf(j+1)+xf(j))*(yf(j+1)-yf(j))-(yf(j+1)+yf(j))*(xf(j+1)-xf(j)));
    CentroidX(is)=CentroidX(is)+...
     0.125*((xf(j+1)+xf(j))^2+(yf(j+1)+yf(j))^2)*(yf(j+1)-yf(j));
    CentroidY(is)=CentroidY(is)-...
     0.125*((xf(j+1)+xf(j))^2+(yf(j+1)+yf(j))^2)*(xf(j+1)-xf(j));
  end
  CentroidX(is)=CentroidX(is)/Area(is);CentroidY(is)=CentroidY(is)/Area(is);

%----------------- Plot the results ----------------------------
  time=time+dt                % Plot the results
  uu(1:nx+1,1:ny+1)=0.5*(u(1:nx+1,2:ny+2)+u(1:nx+1,1:ny+1));
  vv(1:nx+1,1:ny+1)=0.5*(v(2:nx+2,1:ny+1)+v(1:nx+1,1:ny+1));
  for i=1:nx+1,xh(i)=dx*(i-1);end;    for j=1:ny+1,yh(j)=dy*(j-1);end
  hold off,contour(x,y,flipud(rot90(r))),axis equal,axis([0 Lx 0 Ly]);
  hold on;quiver(xh,yh,flipud(rot90(uu)),flipud(rot90(vv)),'r');
  plot(xf(1:Nf),yf(1:Nf),'k','linewidth',5);pause(0.01)

end             % End of time step

%------ Extra commands for interactive processing ---------------
% plot(Time,Area,'r','linewidth',2); axis([0 dt*nstep 0 0.1]);
% set(gca,'Fontsize',18, 'LineWidth',2)
% T1=Time;A1=Area;CX1=CentroidX;CY1=CentroidY;
% T2=Time;A2=Area;CX2=CentroidX;CY2=CentroidY;
% figure, mesh(x,y,flipud(rot90(chi)));
```

Full Front Tracking Code 3rd order in time

PSAAP II
Particle-laden Turbulence in a Radiation Environment

Overview of computational modeling at Stanford PSAAP: Particle-laden flows subject to radiative heating

Ali Mani

Multiphase Physics Deep Dive- 2016

Particle-Based Solar Receiver

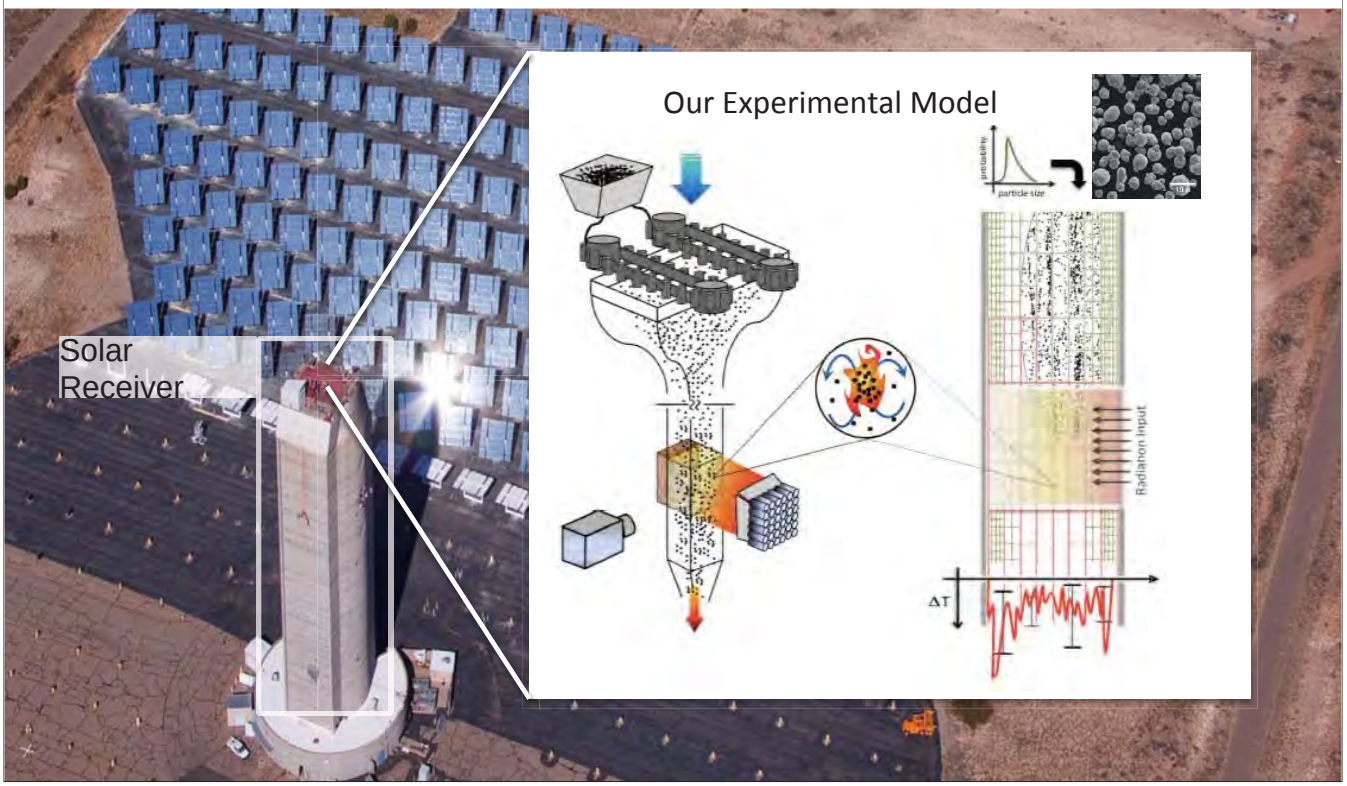

Scientific Challenge

Multiphysics problem involving turbulence, particle transport, and radiation in a tightly coupled environment.

Experiment | Simulations

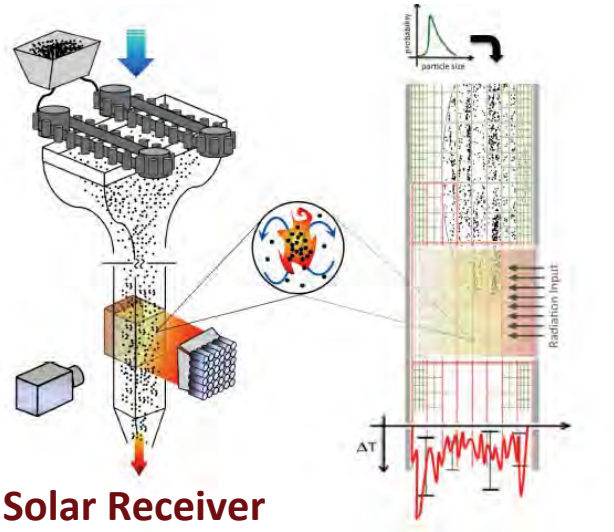

Solar Receiver

- Cold gas-particle mixture enters
- Sunlight is absorbed by particles
- Particle temperature increases
- Air convects energy from particles
- Hot gas-particle mixture exits
- Particles are separated out, hot gas used for energy extraction

Scientific Challenge

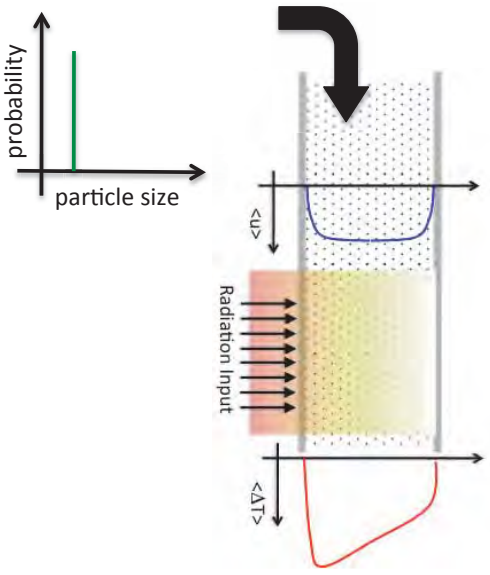

Idealized Scenario
Weak Coupling

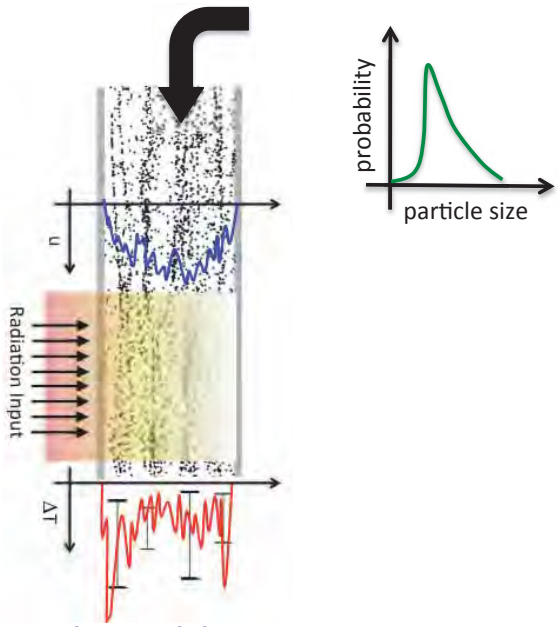

Real-world Scenario
Strong Coupling

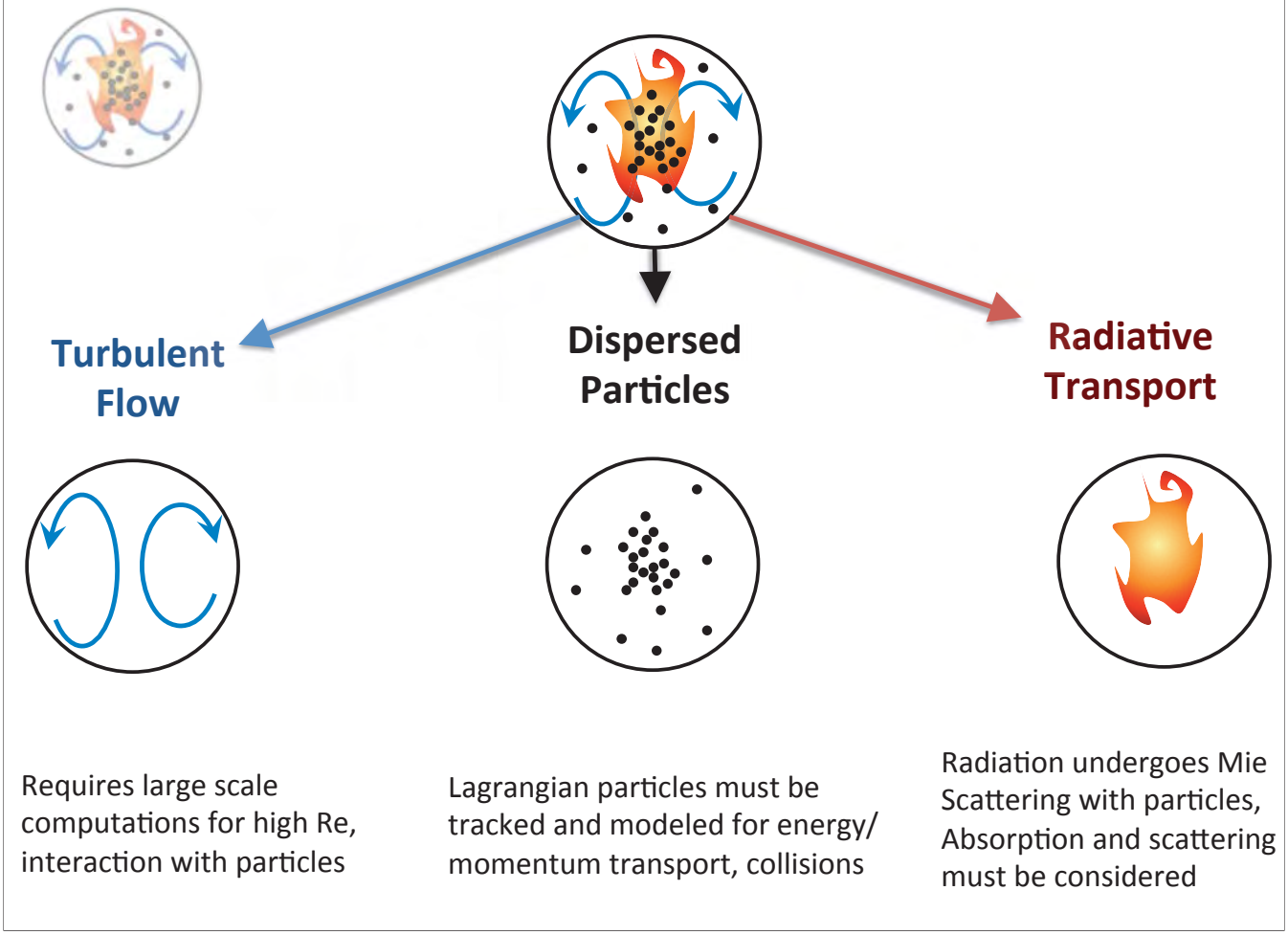
Turbulent Flow
Dispersed Particles
Radiative Transport
Requires large scale computations for high Re, interaction with particles
Lagrangian particles must be tracked and modeled for energy/ momentum transport, collisions
Radiation undergoes Mie Scattering with particles, Absorption and scattering must be considered

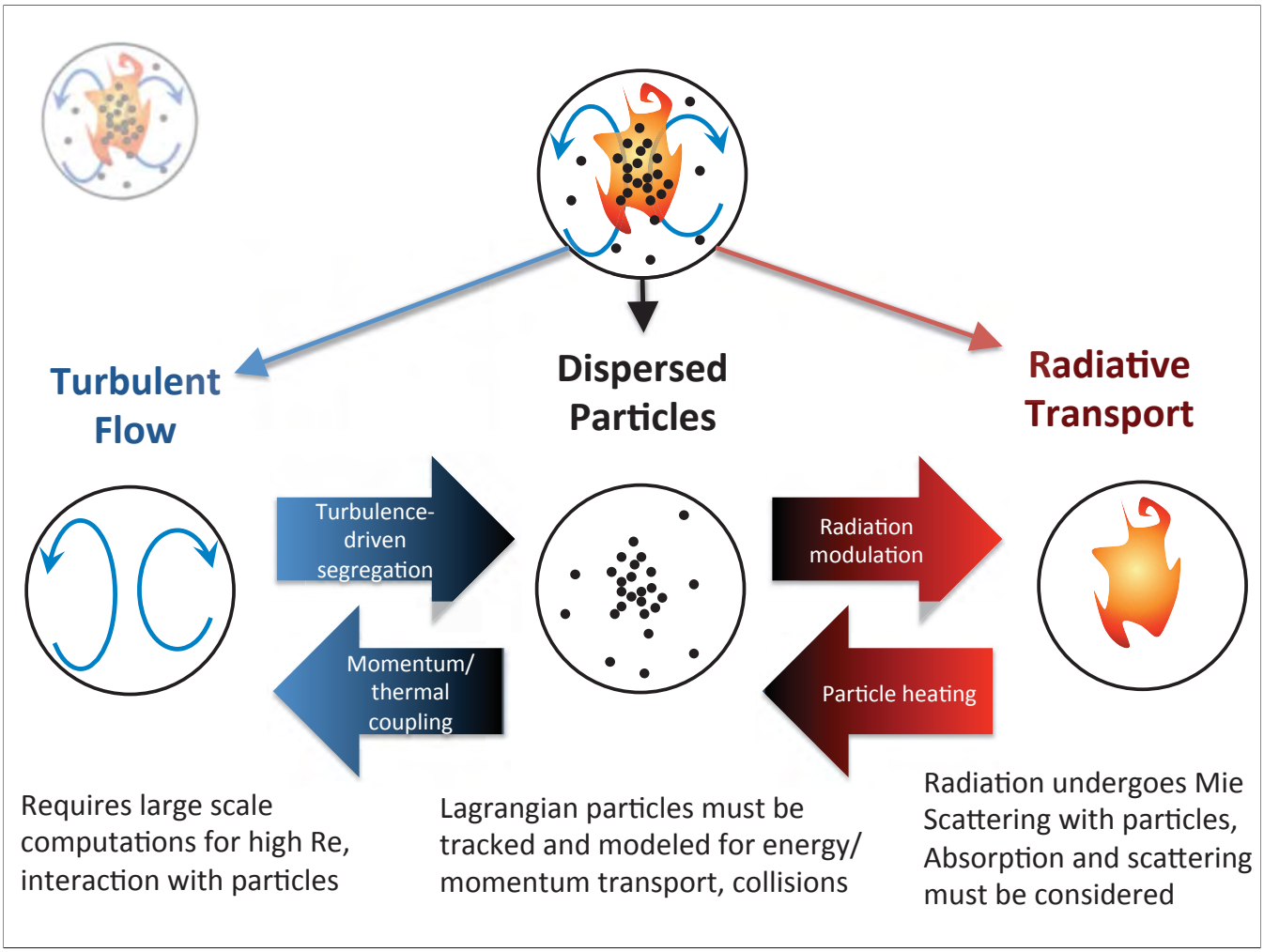
Turbulent Flow
Dispersed Particles
Radiative Transport
Turbulence-driven segregation
Momentum/ thermal coupling
Radiation modulation
Particle heating
Requires large scale computations for high Re, interaction with particles
Lagrangian particles must be tracked and modeled for energy/ momentum transport, collisions
Radiation undergoes Mie Scattering with particles, Absorption and scattering must be considered

Early Demonstrations

Detailed coupling of particle-laden turbulence and radiation

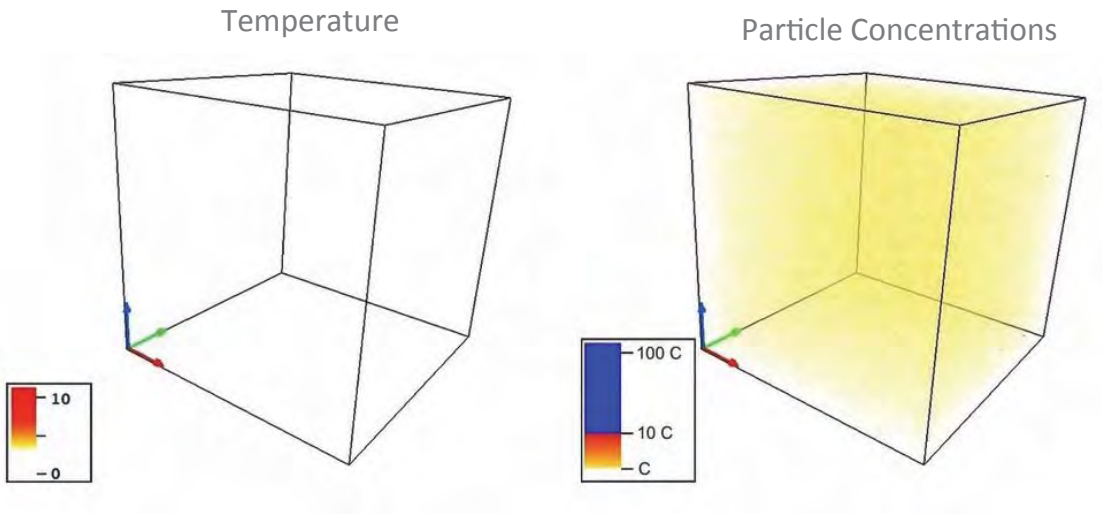

St ~ 1

Ref: Zamansky et al. PoF 26, 071701 (2014)

Stanford PSAAP Regimes and Parameters

- 12 dimensionless parameters describe the full problem
- Typical parameters
  - Re ~ 10^4
  - St ~ 10
  - d_p/η ~ 0.1

Effect of Preferential Concentration on Heat Transfer

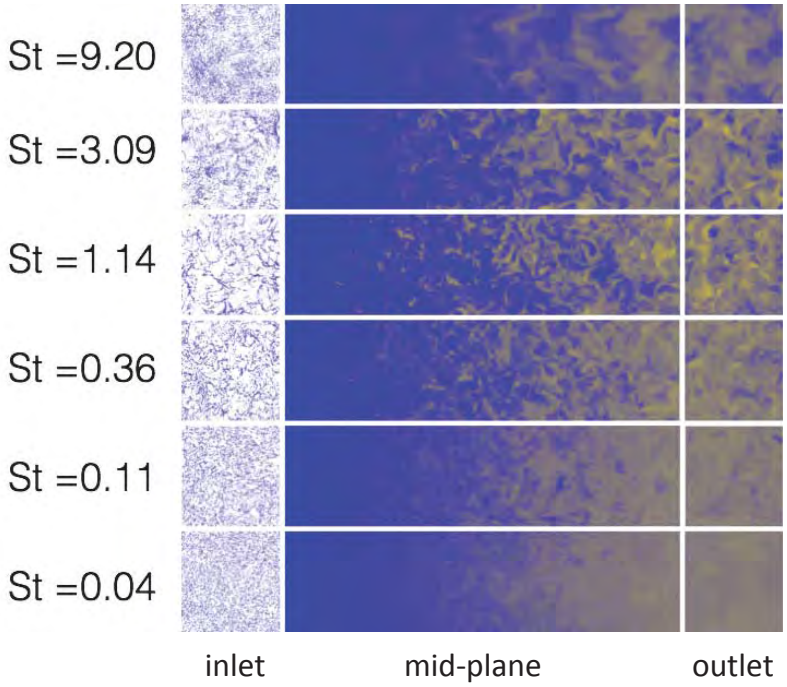

Simulation Framework

SOLEIL-MPI

SOLEIL-X

Legion/Liszt/Terra/Lua

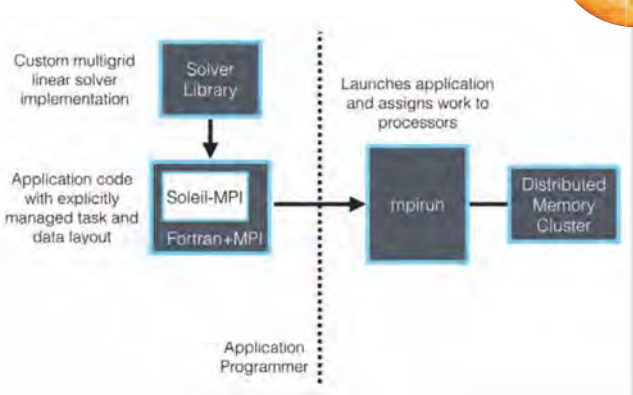

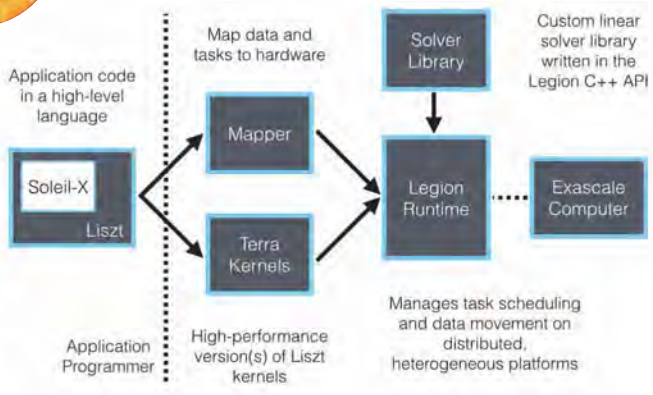

State-of-the-art MPI implementation targeting 100K core clusters

Implementation using data & task based parallelism targeting heterogeneous architectures – includes development of new programming framework

…where are we?

- Physics Models: Demonstrate ability to simulate fully coupled (flow, particle, radiation, heat transfer) system in nominal experimental scenario
- Exascale: Integrate complete software stack (code, compiler, scheduler, libraries)
- Validation: First comparison between experiments and computation
- UQ: Evaluate uncertainties and their effects on key output of interest

Example Simulation

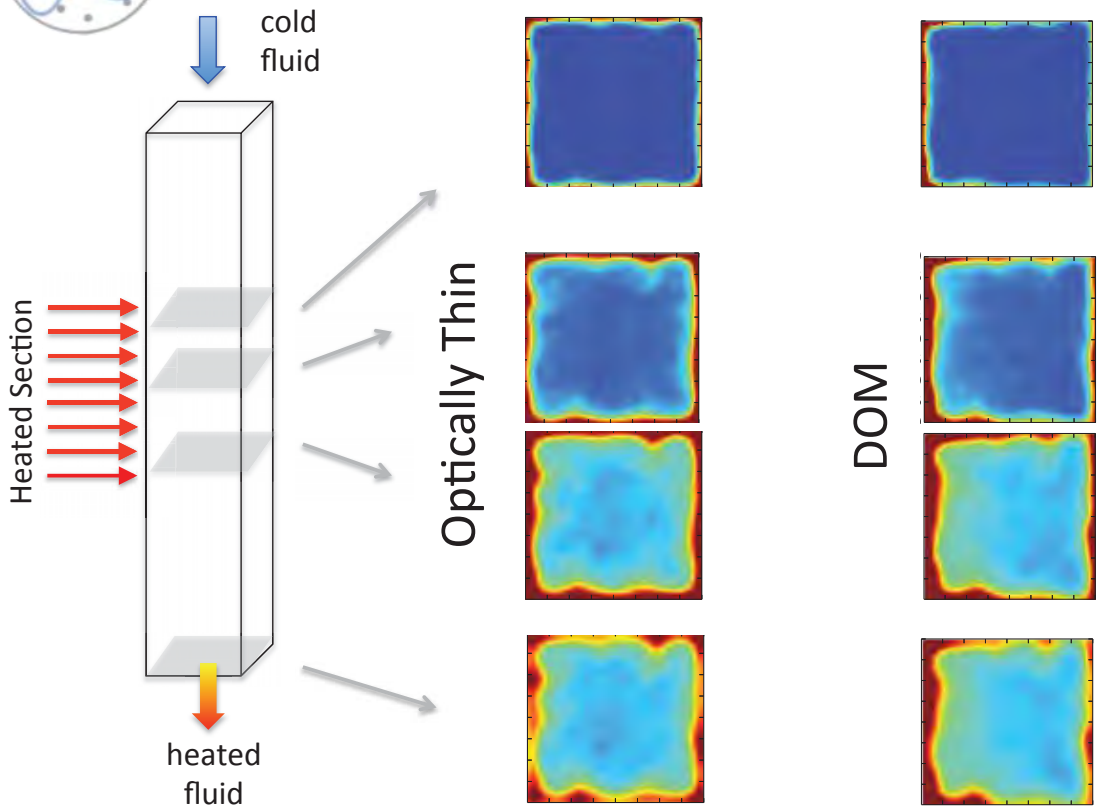

Challenges (multiphase)

- Point particle models
  - Verification → Afternoon talk by J. Horwitz
  - Validation → Experiment/Particle Resolved DNS
- Turbophoresis → Tomorrow talk by M. Moghadam
  - Impact of particle collision model
  - Impact of near wall models
- Poly-dispersity
  - Impact on turbophoresis
  - Impact on heat transfer
- Experimental validation → Tomorrow talk by L. Villafañe
  - Particle concentration
  - Cluster analysis

Challenges (multiphase)

- Point particle models
  - Verification → Afternoon talk by J. Horwitz
  - Validation → Experiment/Particle Resolved DNS
- Turbophoresis → Tomorrow talk by M. Moghadam
  - Impact of particle collision model
  - Impact of near wall models
- Poly-dispersity
  - Impact on turbophoresis
  - Impact on heat transfer
- Experimental validation → Tomorrow talk by L. Villafañe
  - Particle concentration
  - Cluster analysis

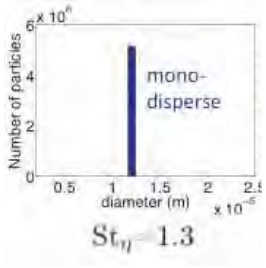

Particle
Inlet Size

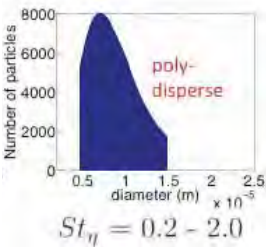

Particle
Inlet Size

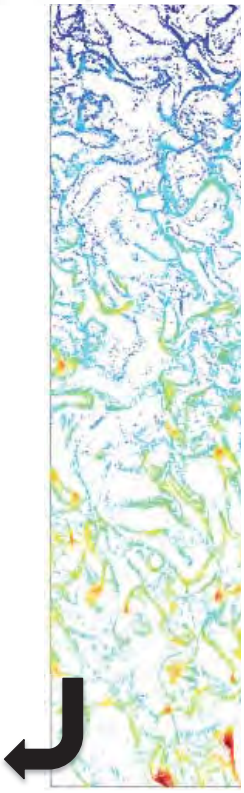

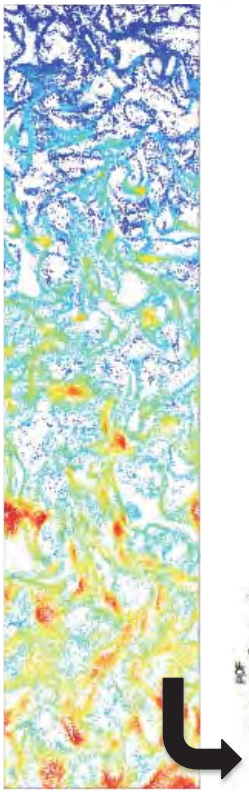

Particle
Exit Temperature

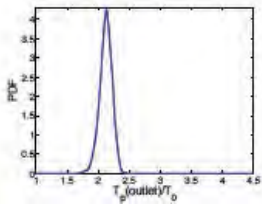

Particle
Exit Temperature

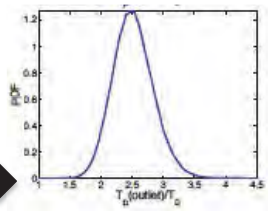

Challenges (heat transfer)

- Lagrangian ←→ Eulerian heat exchange
  - Verification issues
  - Validation
- Radiative heat transfer
  - Particle resolved: expensive but verifiable
  - Eulerian (using homogenization): no verifiable model available

Broader Science Challenges

- LES models
  - Lagrangian particle models
  - Subgrid Heat transfer

- Develop Understanding
  - What is effect of preferential concentration on
    - heat transfer?
    - radiative transfer?
  - Reduced-order models suitable for analysis and design

Publications

Physics:

- "Radiation induces turbulence in particle-laden fluids," Zamansky et al. PoF, 26, 071701 (2014)
- "Settling of heated particles in homogeneous turbulence," Frankel, et al. JFM, 792, 869-893, (2016)
- "Spatially-localized wavelet-based spectral analysis of preferential concentration in particle-laden turbulence," Bassenne, et al. CTR Annual Research Briefs (2015)
- "Polydisperse particles in an irradiated turbulent gas-particle mixture," Rahmani et al. CTR Annual Research Briefs (2015)

Modeling:

- "Particle-laden flows forced by the disperse phase: comparison between Lagrangian and Eulerian simulations ," Vie et al. IJMF, 79, 144-158 (2016)
- "Accurate calculation of Stokes drag for point-particle tracking in two-way coupled flows," Horwitz et al. JCP, 318, 85-109, (2016)
- "A dynamic subgrid-scale model based on differential filters for LES of particle-laden turbulent flows," Park et al. CTR Annual Research Briefs (2015)
- "Parallel variable-density particle-laden turbulence simulation," Pouransari et al. CTR Annual Research Briefs (2015)

Research activities for energetic dispersal of particles

Multiphase physics deep-dive workshop, St. Petersburg, FL

Kambiz Salari

October 6-7, 2016

LLNL-PRES-704180

This work was performed under the auspices of the U.S. Department of Energy by Lawrence Livermore National Laboratory under contract DE-AC52-07NA27344. Lawrence Livermore National Security, LLC

Lawrence Livermore National Laboratory

We rely on high explosives to energetically disperse particles

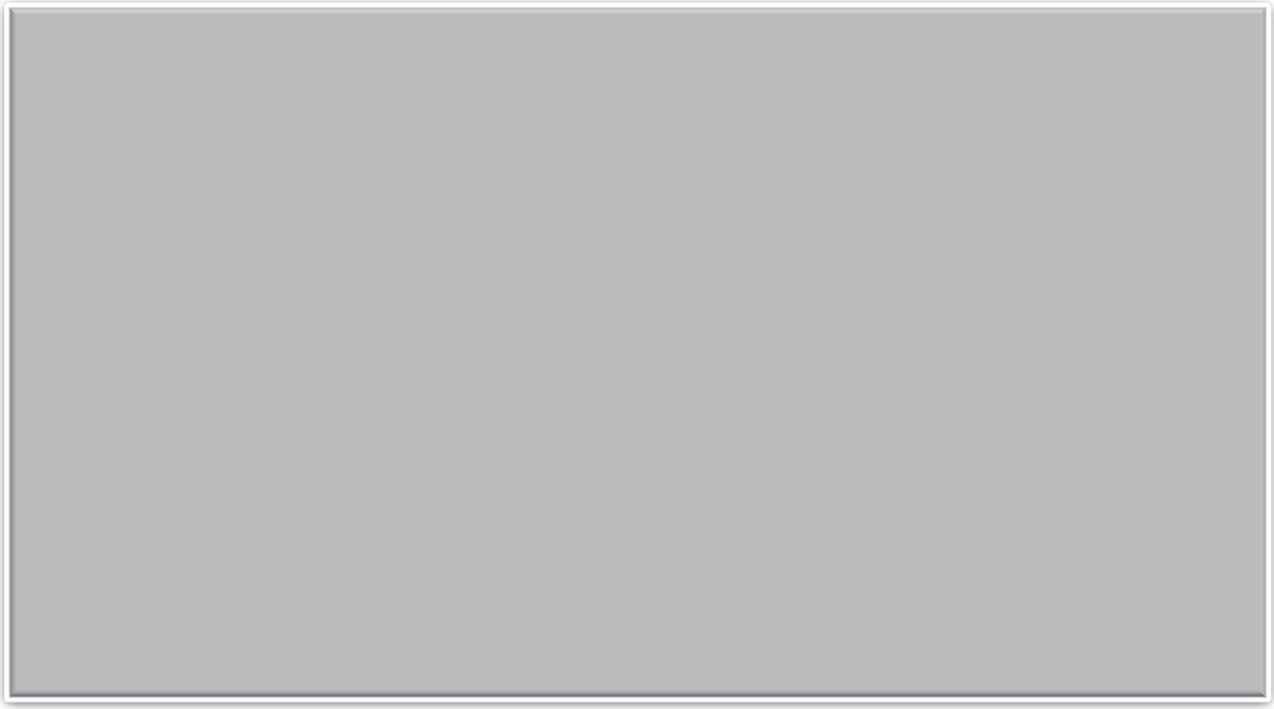

Presence of particles enhances momentum and energy transport

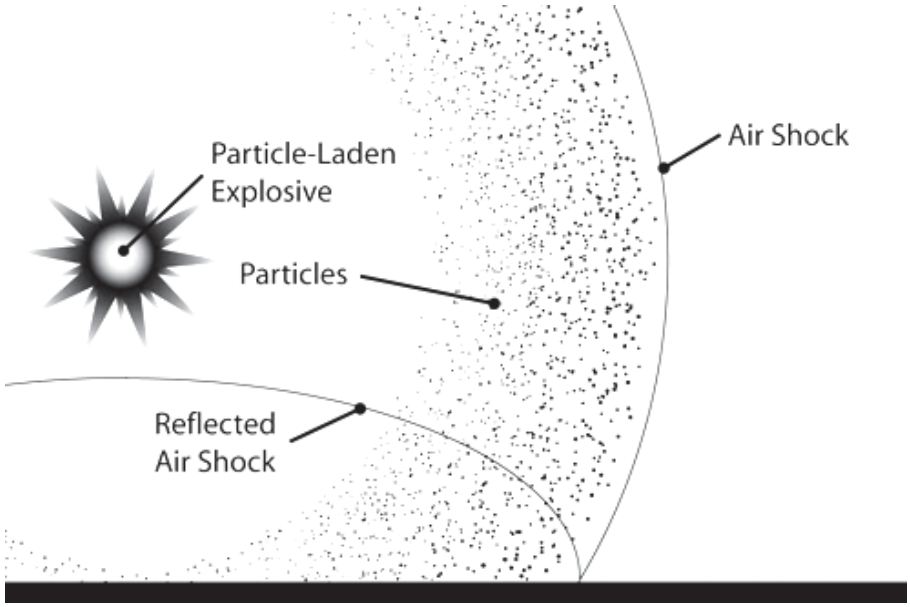

High velocity particles pose a challenge to modeling and simulation

Particle laden flows in shock dominated environment are highly complex

Forces acting on a particle are due to many physical drivers

- Drag, Volumetric, and Pressure gradient
- Shape and surface roughness
- Inviscid and viscous
- Steady and unsteady
- Rotation
- Buoyancy/gravity
- Contact

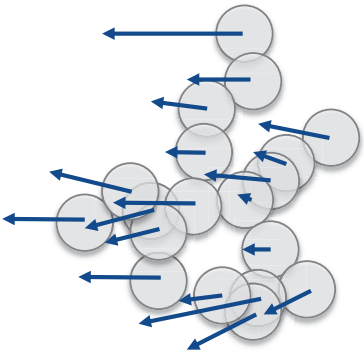

Multiphase particle dispersal process is a multi-physics and multi-scale problem

- Detonics
  - Non-ideal high explosive, particles mixed with HE
  - Inter-particle collision/contact
  - Inter-phase interactions, mass, momentum, and energy
  - Reactive flow
  - Particle surface chemistry
- Transport
  - Particulate plume surface instabilities, particle clustering and jetting
  - Particle drag for dense, dense-dilute transition, and dilute regime
  - Fireball combustion
  - Turbulent mixing
  - Particle surface chemistry
- Characterization of material properties
- Insufficient number of high fidelity experiments for validation and phenomenological study

Standard cylinder test is needed to measure energy release from a non-ideal high explosive

Shimadzu HPV-2 camera,
1 million frame per second

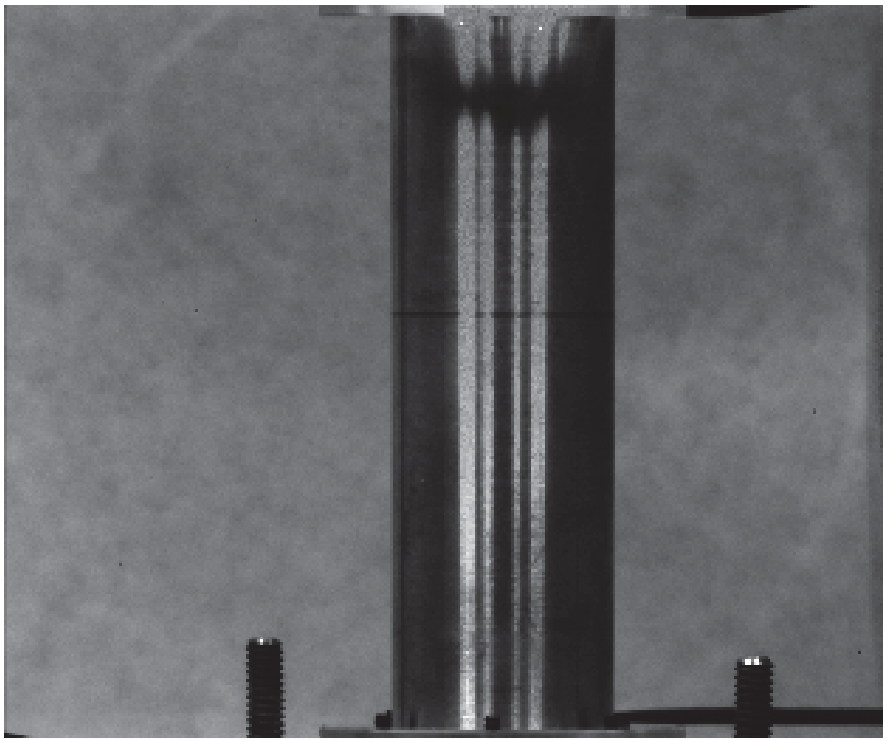

We rely on Mesoscale simulations to gain insight into particle impact on detonation process

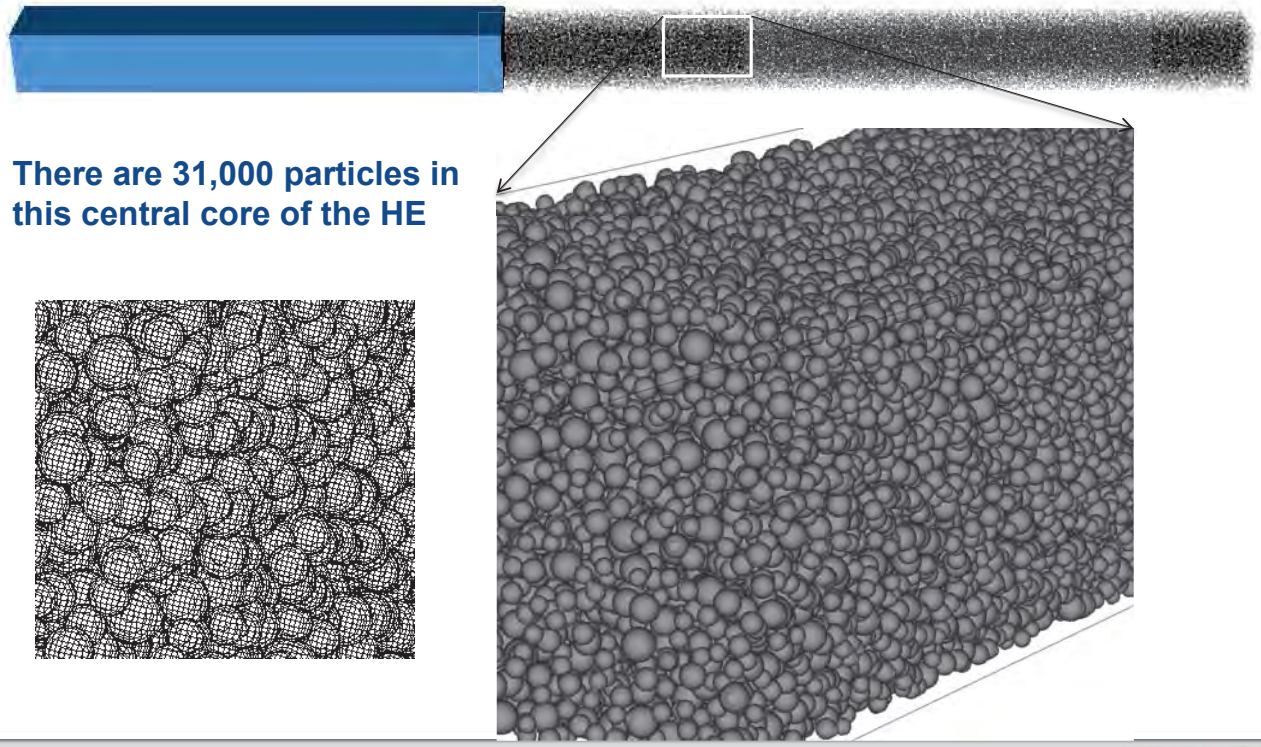

There are 31,000 particles in this central core of the HE

The reaction zone in the presence of particles is wider compared to the parent explosive

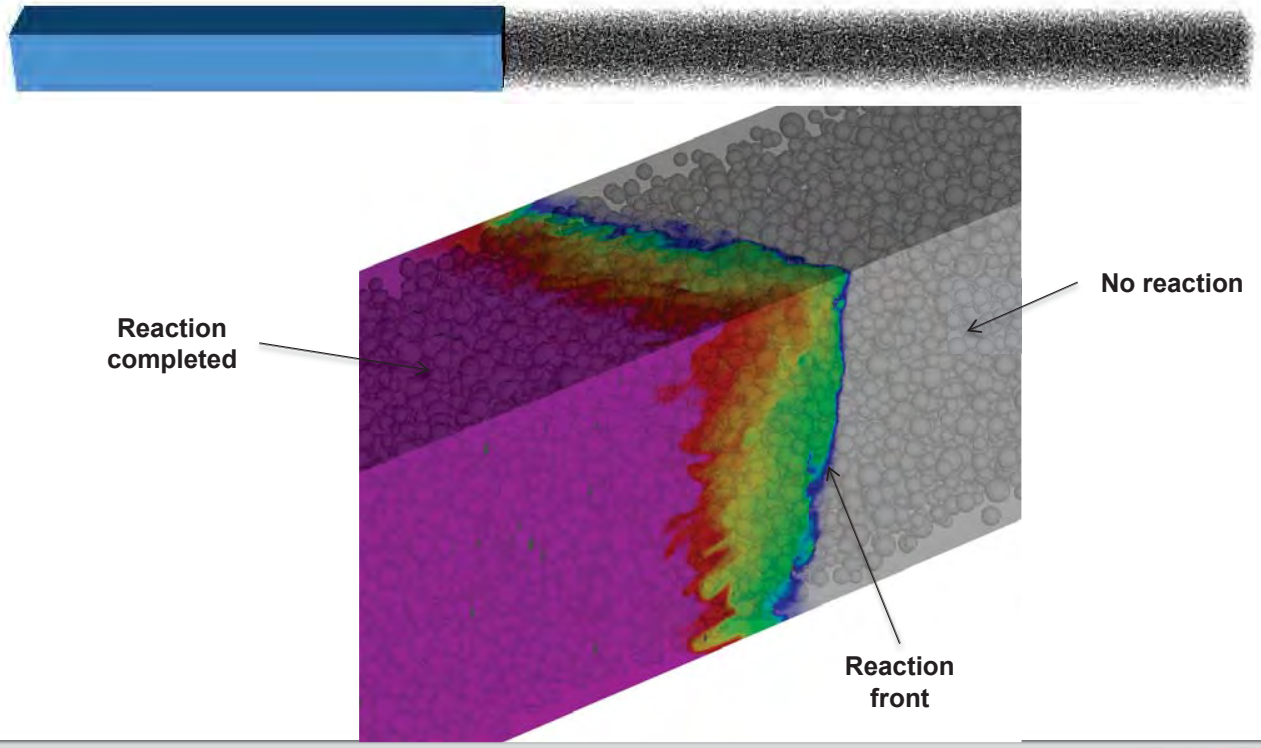

Mesoscale simulations with embedded grid can provide insight into the physics of particle-particle interaction

Problem setup

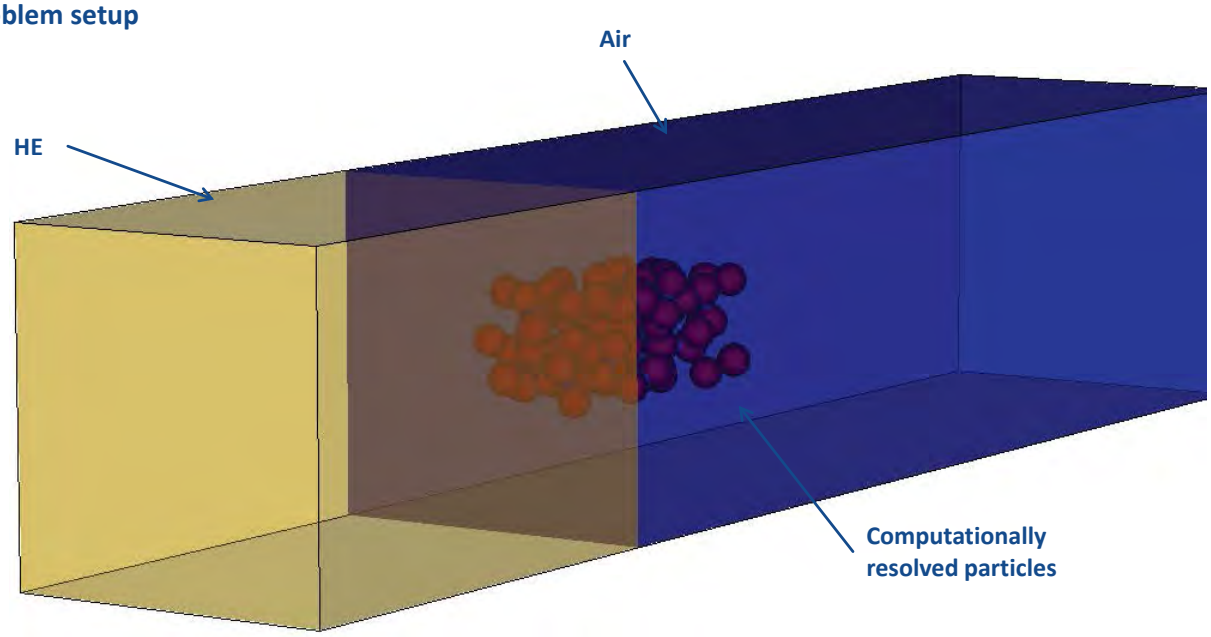

Mesoscale simulations could provide details of particle interactions and transport

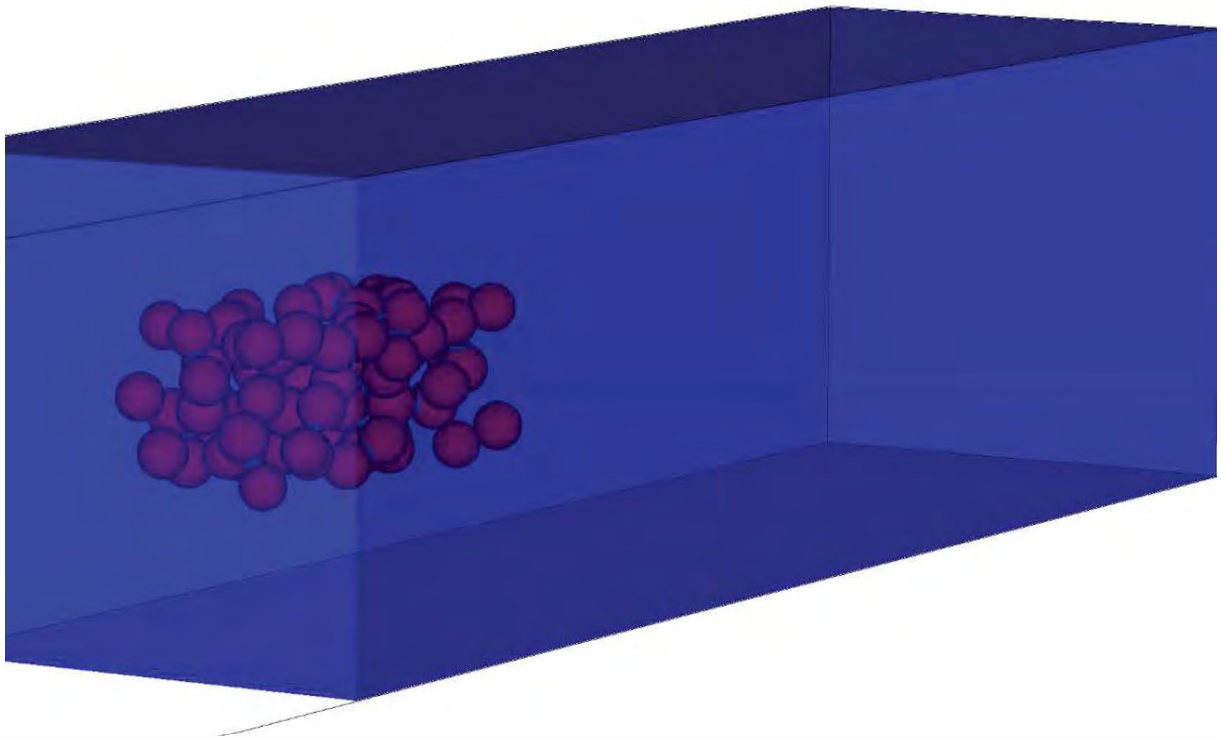

Process of compaction is visible in this simple Mesoscale simulation

Soft and hard contacts are observed in particle dispersal

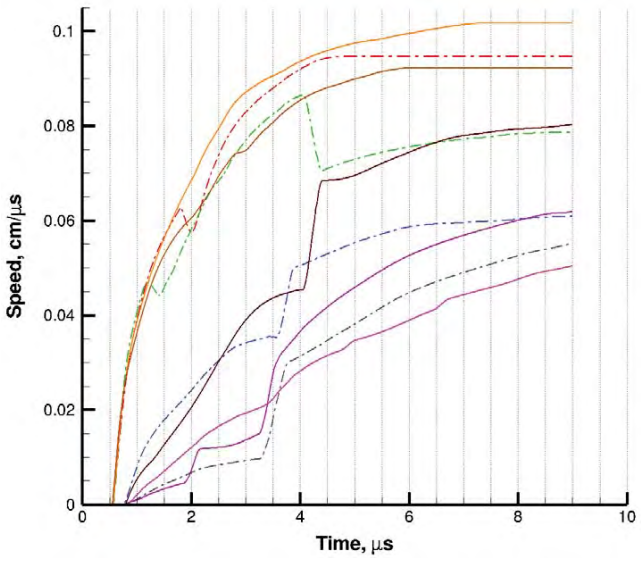

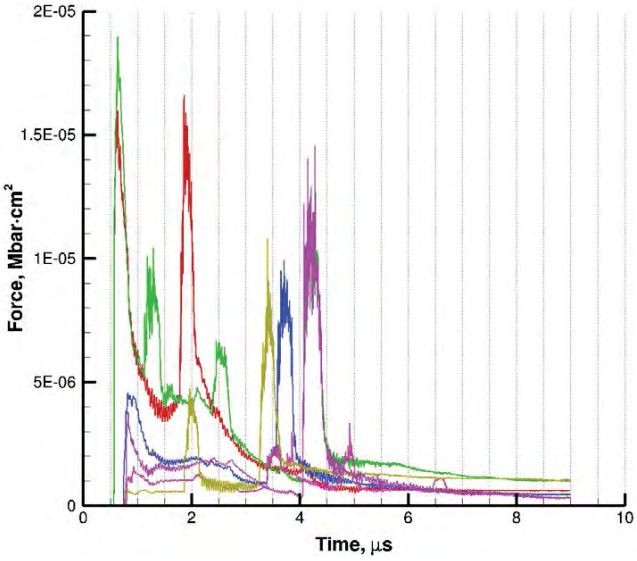

Primary shock slows down as it goes through a particle field

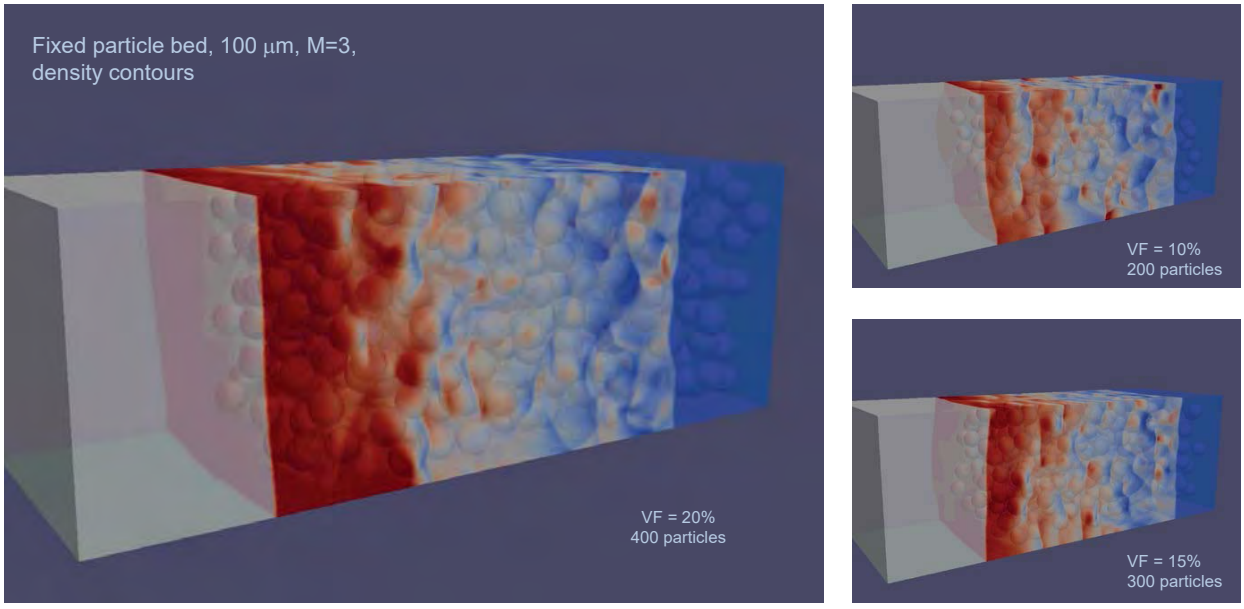

Student Chris Neal from University of Florida – shock particle interaction study using ROCFLU

Reflected shock is more pronounced at higher particle volume fraction – ROCFLU

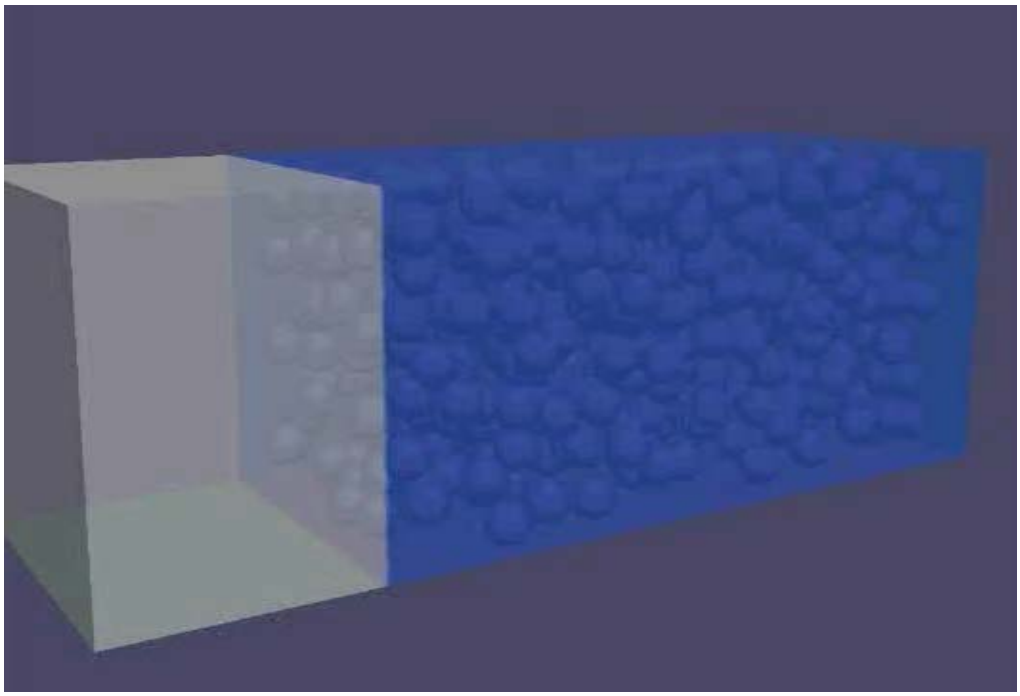

Streamwise particle drag shows noticeable reduction within the particle field

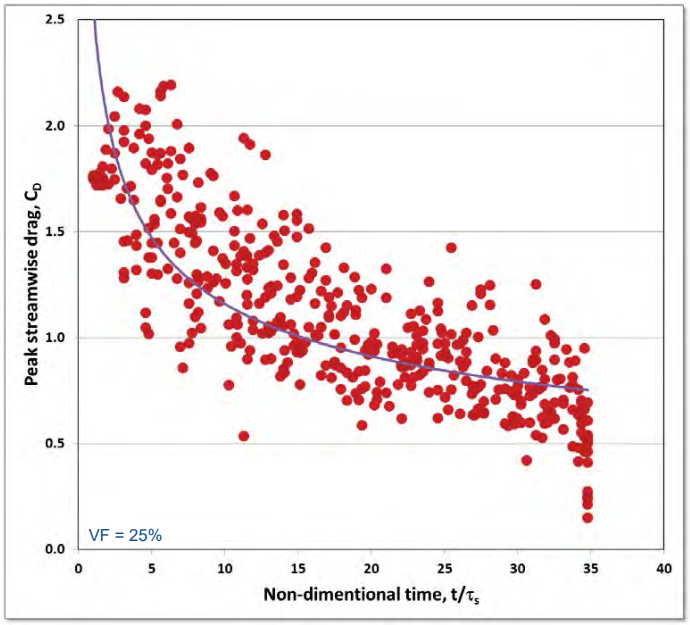

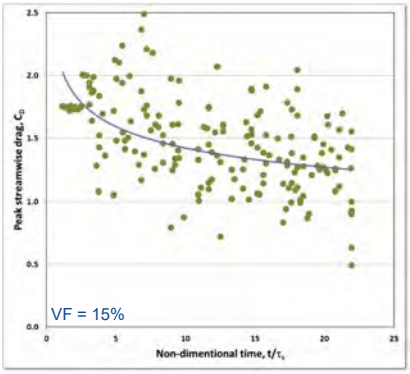

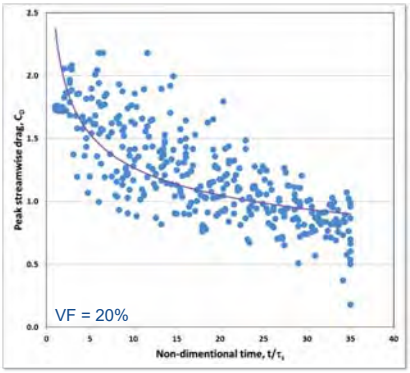

Particle clustering/jetting is a common feature of energetic dispersal

- Particle jets can influence:
  - Turbulent mixing and burning
  - Blast wave propagation
- Particle clustering/jetting can have many physical drivers including instability mechanisms

Spherical dispersal of sand particles

David L. Frost, Yann Grégoire, Sam Goroshin, Fan Zhang, arXiv:1110.3090v1 [physics.flu-dyn]

Fan Zhang demonstrated the presence of particle jets and their correlation with booster case fragments

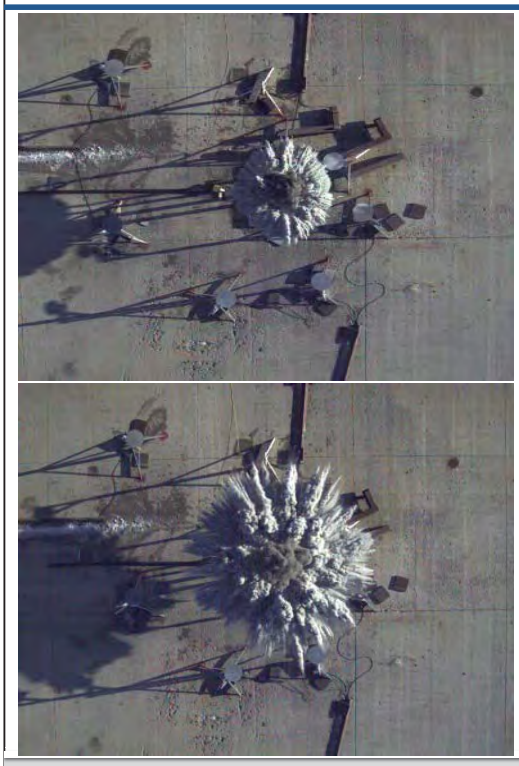

Plenary Talk; 12th Hypervelocity Impact Symposium, Baltimore Sept 16 – 20, 2012

Particulate plume surface instabilities can produce fine clustering/jetting

LLNL activities in energetic release of particles

- LLNL has a long history in designing and testing of charges with particles
- Internally funded experimental campaign to conduct experiments with complex diagnostic to measure gas and particle behavior during detonation and transport, **headed by Ed Kokko**
- 3-Phase model of explosion fields with detailed fireball combustion, **headed by Allen Khul**

SNL and LANL shock tube particle experiments are valuable in evaluation of particle drag in shock dominated conditions

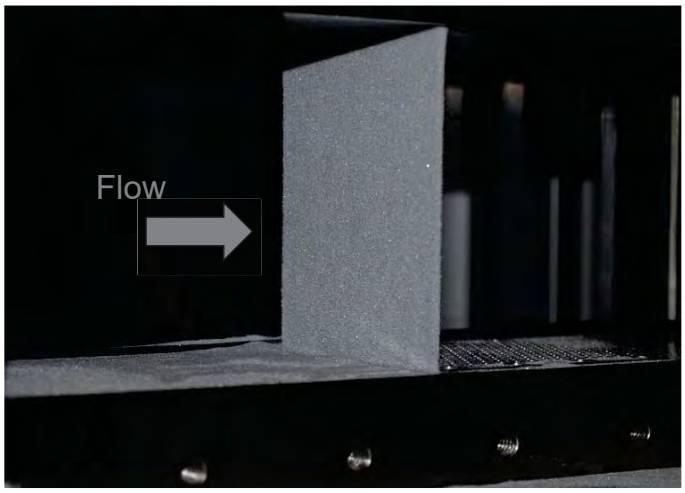

Justin Wagner, SNL

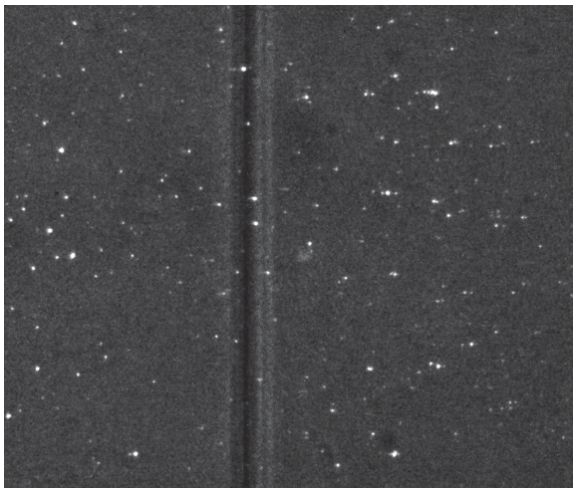

Kathy Prestridge, LANL

Multiphase model can be developed based on the hypothesis of phase separation

- A basic premise of ***two-phase mixture theory is that the mixture can be separated into discrete components***. Each of these components behaves as a single material except when interacting with another component.
- This hypothesis holds if ***the internal state of one phase is not related to the internal state of another phase*** *and the thermodynamic state of a particular phase depends only on the properties of that phase (mass, momentum, energy, and EOS)*
- Each phase mass, momentum, and energy equation contains terms not present in one-phase models that are known as ***phase interaction terms***. These terms model the transfer of mass, momentum, and energy from one phase to another

Akhatov & Vainshtein, 1984, Baer & Nunziato, 1986, Saurel & Abgrall, 1998, Chinnayya, Daniel, and Saurel, 2004, Balakrishnan, Nance, Menon, 2010

We are using Multiphase Discrete Equations Method (DEM)

- Eulerian-Eulerian (DEM-EE): all phases are represented as a continuum
- Eulerian-Lagrangian (DEM-EL): mixed representation. We assume solid particles are represented as a Lagrangian phase

Benefits of DEM approach:

- Each phase has it's own velocity, density, pressure, energy, and equation of State (EOS)
- All phases can be compressible
- Interface quantities can be calculated via a Riemann solve
- DEM allows massively parallel coupling to multi-physics and chemistry

Multiphase theory governing equations

Volume fraction

$$\frac{\partial \alpha_k}{\partial t} + u_i^* \frac{\partial \alpha_k}{\partial x} = \mu(p_1 - p_2)$$

Mass

$$\frac{\partial \alpha_k \rho_k}{\partial t} + \frac{\partial \alpha_k \rho_k u_{k,j}}{\partial x_j} = \dot{m}$$

Mom.

$$\frac{\partial \alpha_k \rho_k u_{k,i}}{\partial t} + \frac{\partial (\alpha_k \rho_k u_{k,i} u_{k,j} + \alpha_k p_k \delta_{ij})}{\partial x_j} = p^* \frac{\partial \alpha_k}{\partial x_j} \delta_{ij} + \dot{m} u_i^* + F_i + \mu p^* (p_1 - p_2)$$

energy

$$\frac{\partial \alpha_k \rho_k E_k}{\partial t} + \frac{\partial \alpha_k (\rho_k E_k + p_k) u_{k,j}}{\partial x_j} = p^* u_j^* \frac{\partial \alpha_k}{\partial x_j} + \dot{m} E_k + F_i u_i^* + Q$$

Equation of state

$$\left(f(E, p, \rho)\right)_K = 0$$

Saturation constraints

$$\sum_{k=1,n} \alpha_k = 1$$

Equations for phase K

Phase exchange terms

Pressure relaxation terms

** Indicates interface quantity*

Saurel & Abgrall, 1998

Modification to governing equations for free lagrangian particles

- Particles are free lagrangian objects
  - $\frac{dm_p}{dt} = \dot{m}$
  - $\frac{dx_{p,i}}{dt} = u_{p,i}$
  - $m_p \frac{du_{p,i}}{dt} = \frac{\pi}{2} r_p^2 C_D \rho_g \left|\vec{u}_g - \vec{u}_p\right| (u_{g,i} - u_{p,i}) - \frac{4}{3} \pi r_p^3 \frac{\partial p_g}{\partial x_i} + m_p A_{c,i} + F_{body}$
  - $m_p C_p \frac{dT_p}{dt} = 2\pi r_p \kappa_g Nu (T_g - T_p)$

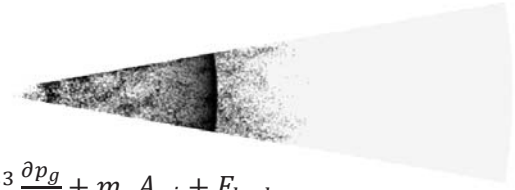

- **DEM-EL volume fractions entirely determined by location of lagrangian particles**
  - $\boldsymbol{\alpha_g = 1 - \alpha_p}$
- **Interface terms handled identically to DEM-EE**
  - **Interface quantities p^* and u^* determined by one-sided Riemann Solve and particle velocities respectively**
- **No pressure relaxation terms**
- Phase exchange terms are calculated as sums of mass, momentum, and energy transfer over all particles

Balakrishnan, Nance, Menon, 2010

DEM-EL computational simulation captures relevant flow features of multiphase blast

Kambiz Salari
Salari1@llnl.gov

Questions?

Exceptional service in the national interest

Sandia National Laboratories

Fire Science & Technology

CCMT Multiphase Deep Dive

October 6-7, 2016, St. Petersburg, FL, USA

Multiphase Methods for Modeling Fire Environments

Alexander L. Brown; albrown@sandia.gov; (505)844-1008
Fire Science and Technology Department

SAND2016-10001 C

U.S. DEPARTMENT OF ENERGY NNSA

Sandia National Laboratories is a multi-program laboratory managed and operated by Sandia Corporation, a wholly owned subsidiary of Lockheed Martin Corporation, for the U.S. Department of Energy's National Nuclear Security Administration under contract DE-AC04-94AL85000.

Outline

Sandia National Laboratories

- Part 1: Drop Break-up and Dense Spray Simulations
  - Why we care?
  - Description of L-J methods
  - Issues with the dense region
  - Test conditions for validating the model
- Part 2: Liquid Pool Fire Modeling
  - Motivating experiment description
  - Modeling approach
  - Preliminary results (verification)
- Summary

Water Slug Impact Experiment

- Tests performed in 2002 provided data for validating liquid spread dynamics for an aluminum tank impacting a concrete slab
- Liquid deposition, particle sizing, and video data
- This is representative of some fireball initiation problems

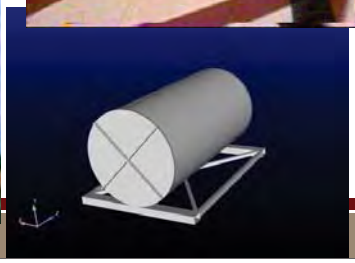

Water Slug Simulations

A coupled capability using SIERRA solid mechanics and fluid mechanics in tandem can simulate fluid behavior beyond just the impact

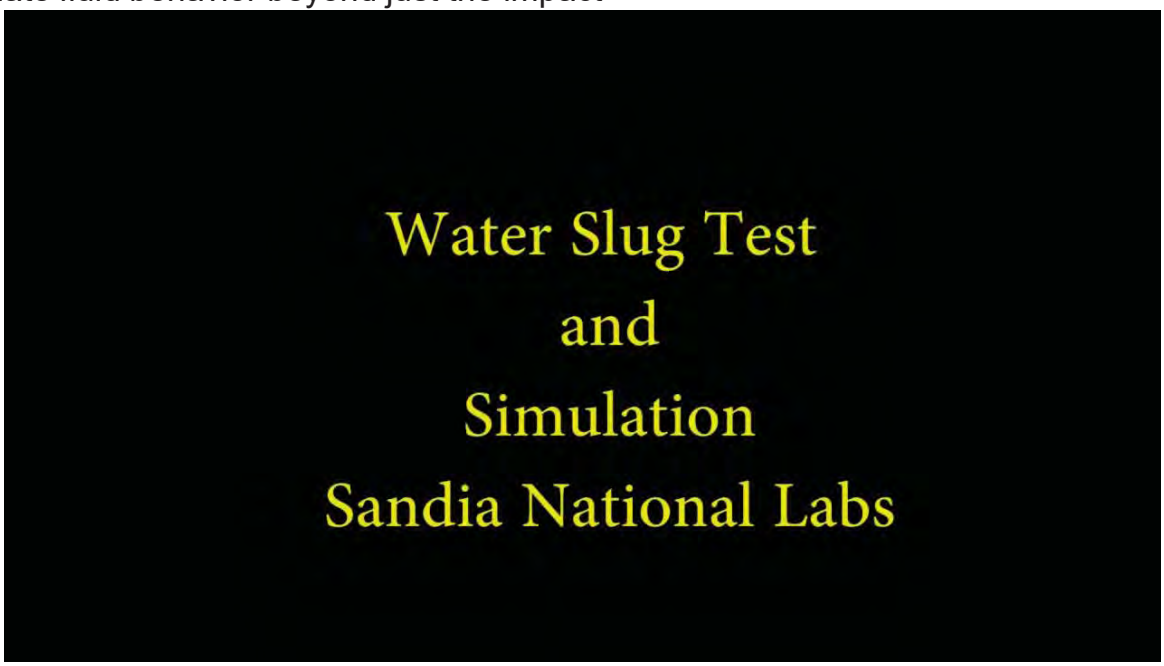

Brown, A.L., G.J. Wagner, and K.E. Metzinger, "Impact, Fire and Fluid Spread Code Coupling for Complex Transportation Accident Environment Simulation," *Journal of Thermal Science and Engineering Applications*, Vol. 4, No. 2, pp. 021004-1 to 021004-10, June 2012.

Fireball Simulations

- Follow-on work has demonstrated that predictions can be made with impacting fuels, resulting in fireball formation

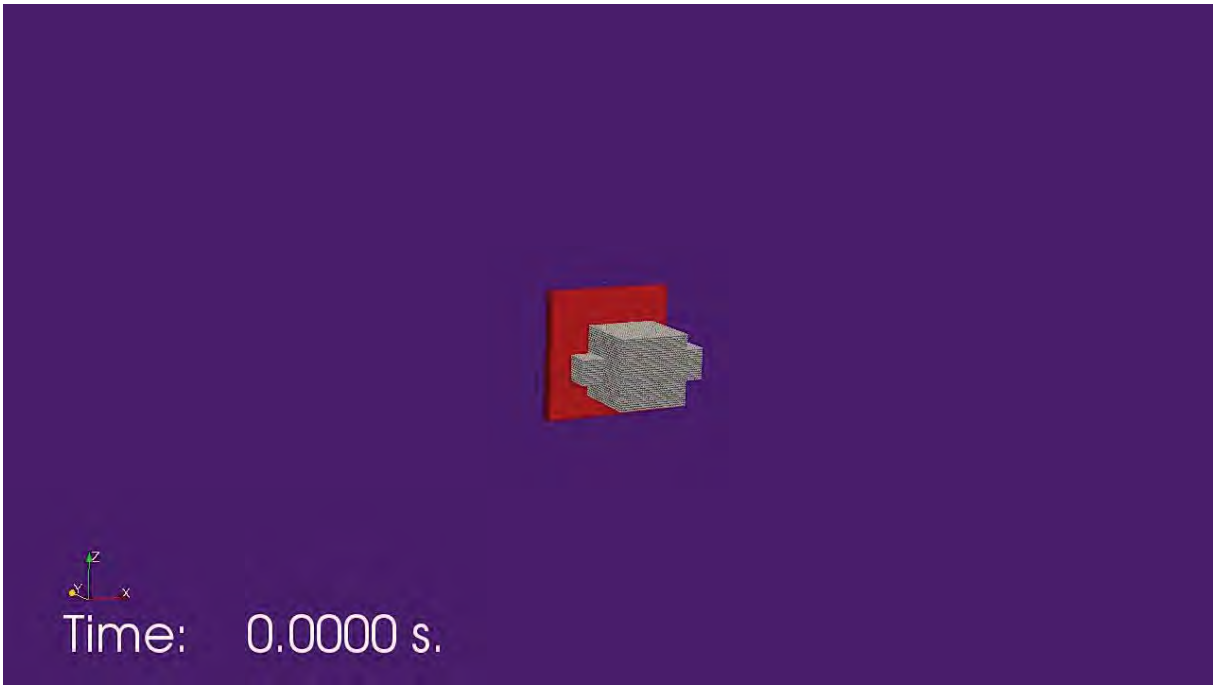

Presto/Fuego Coupling Strategy

- SPH mass/momentum conserved in a transfer between the two codes
- Mass is transferred according to an algorithm that uses a critical dimensionless particle separation distance (B_{crit}) to define transfer times:

$$B = \frac{CharacteristicSeparationDistance}{CharacteristicDropLength}$$

- All liquid mass is assumed to be spherical drops until transfer to CFD code
- Drops subsequently are predicted to distort and break-up according to the Taylor Analogy Break-up (TAB) model
- Lagrangian/Eulerian coupling employed for evaporating drops

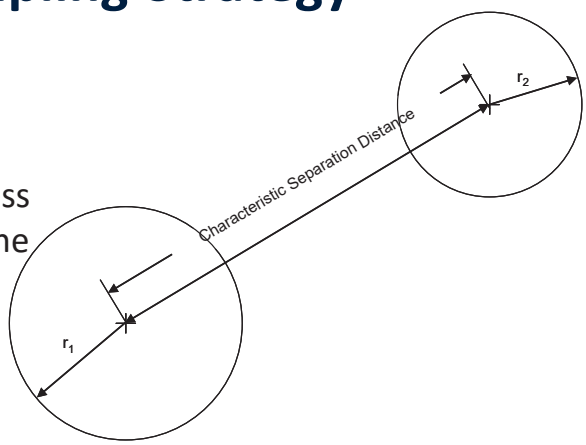

B_i assessed at each time for each particle

$$B_i = \min_{j=1\ to\ N} \left\{ \frac{\sqrt{(x_i - x_j)^2 + (y_i - y_j)^2 + (z_i - z_j)^2}}{d_i/2 + d_j/2} \right\}; i \neq j$$

Using this definition for B, reasonable B_{crit} values are between 1.0 and 1.7

Particle Force Method Description

- We start with a Lennard-Jones potential (inspired by MD):

$$U_{LJ}(r) = 4\varepsilon\left[\left(\frac{\sigma}{r}\right)^{12} - \left(\frac{\sigma}{r}\right)^{6}\right]$$

Lennard-Jones, J.E., "On the Determination of Molecular Fields," Proc. R. Soc. Lond. A, 106, 738, 463-477, (1924).

- We modify the repulsive term (the 12th power) such that the repulsion is not as non-linear:

$$U_{spring} = \frac{k}{2}(r - r_{min})^2 - \varepsilon : r < r_{min}$$

- This model form maintains a smooth function (differentiable) across the r_{min} ($r_{min} = 2^{1/6}\sigma$) threshold
- We are also modifying the particle drag term
- The need for this was motivated by the observation that some mass in the coupled methods was still in a regime where it was not dilute and dispersed, yet treated as such

Modified Potential Illustration

- A figure illustrating the modified potential shows the classical (black) and modified (red) model
- Surface tension γ relates to L-J parameters through:

$$\gamma_{LJ} = C\frac{\varepsilon}{\sigma^2}$$

- Need to tune constant C
  - Hopefully universal
- σ comes from geometry
- ε comes from C and σ
- C is dimensionless

$$C = \frac{\gamma_{LJ}\sigma^2}{\varepsilon}$$

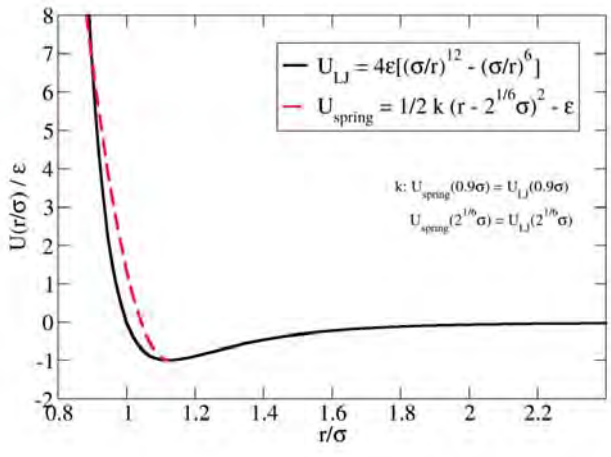

Brown, A.L., Pierce, F., (2017) "Modeling Aerodynamic Break-up of Liquid Drops in a Gas Flow with Molecular Dynamics Analogy Methods", TFESC-11710, Submitted to Proceedings of the 2nd Thermal and Fluids Engineering Conference April 2-5, 2017, Las Vegas, NV, USA.

Drag Modification

- We don't want to have to recover the shape of the liquid to recover drag; unmodified the code will over-predict the drag
- Introduce a two-component scaling factor:

$$C_{Dm} = f_S C_{Do} \qquad f_S = f_{S1} f_{S2}$$

- Define the terms numerically:

$$f_{S1} = max\left(1, \left(\frac{|k|N}{\sigma}\right)^K\right) \qquad f_{S2} = min(1, 1 + Proj)^L \qquad Proj = \hat{u} \cdot \hat{k}$$

$$\hat{k} = \frac{\vec{k}}{|k|}$$

- k is the mean connectivity vector:

$$\vec{k} = \left\{\frac{\sum_{i=1\to N}(x_o - x_i)}{N}, \frac{\sum_{i=1\to N}(y_o - y_i)}{N}, \frac{\sum_{i=1\to N}(z_o - z_i)}{N}\right\}$$

- This work is still in progress (hasn't been tuned)

Lennard-Jones Model Verification

- Red drops are non-interacting
- Others interact with like colored drops, rebound on surface impact
- This is an evaporating, low gravity test scenario

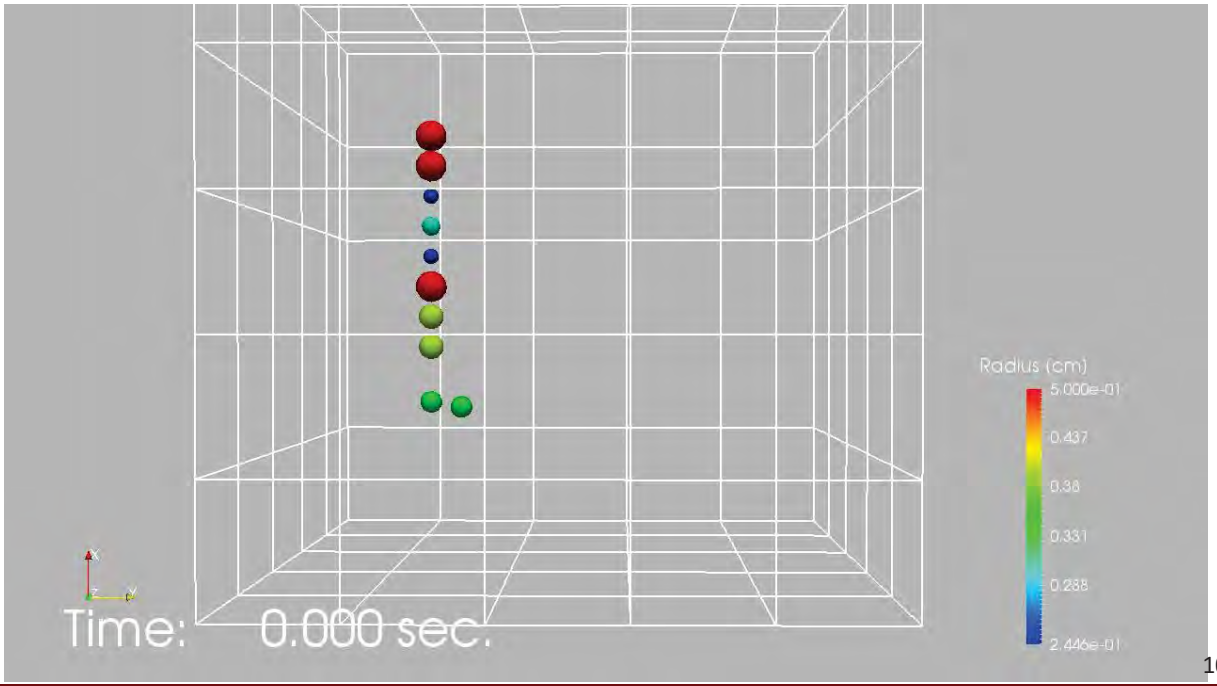

Model Validation Problem

- Data suggests a critical Weber number of 9-12
- We want to match the data as best as possible

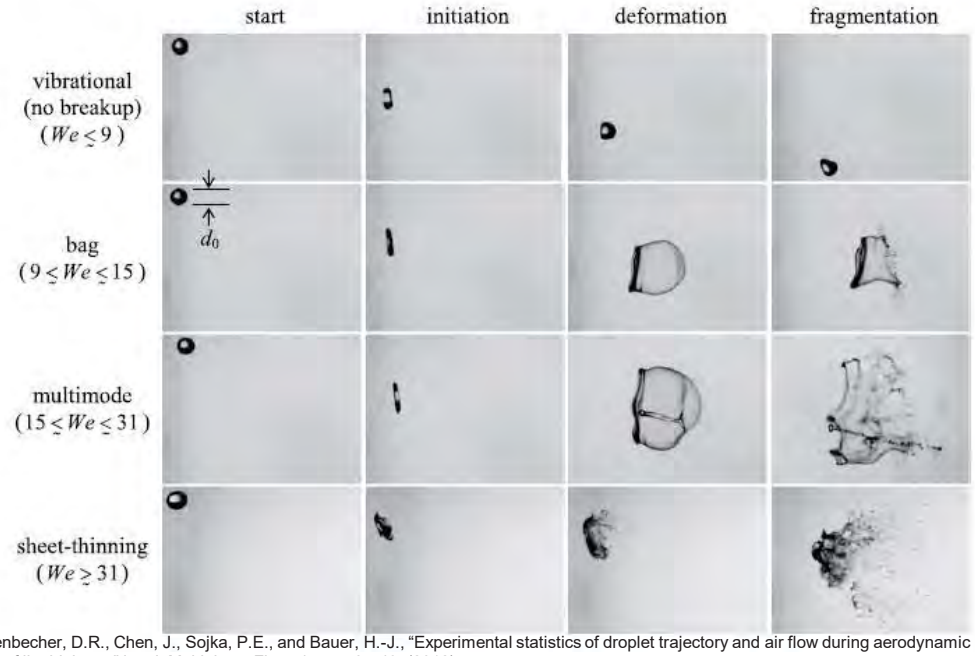

Flock, A.K., Guildenbecher, D.R., Chen, J., Sojka, P.E., and Bauer, H.-J., "Experimental statistics of droplet trajectory and air flow during aerodynamic fragmentation of liquid drops," Int. J. Multiphase Flow, 47, pp. 37-49, (2012).

Preliminary Validation Results

- We = 1, 5, 11, 20, 55 (blue to red) C=200
- Nozzle velocity = 3, 6, 9, 12, 20 (blue to red)

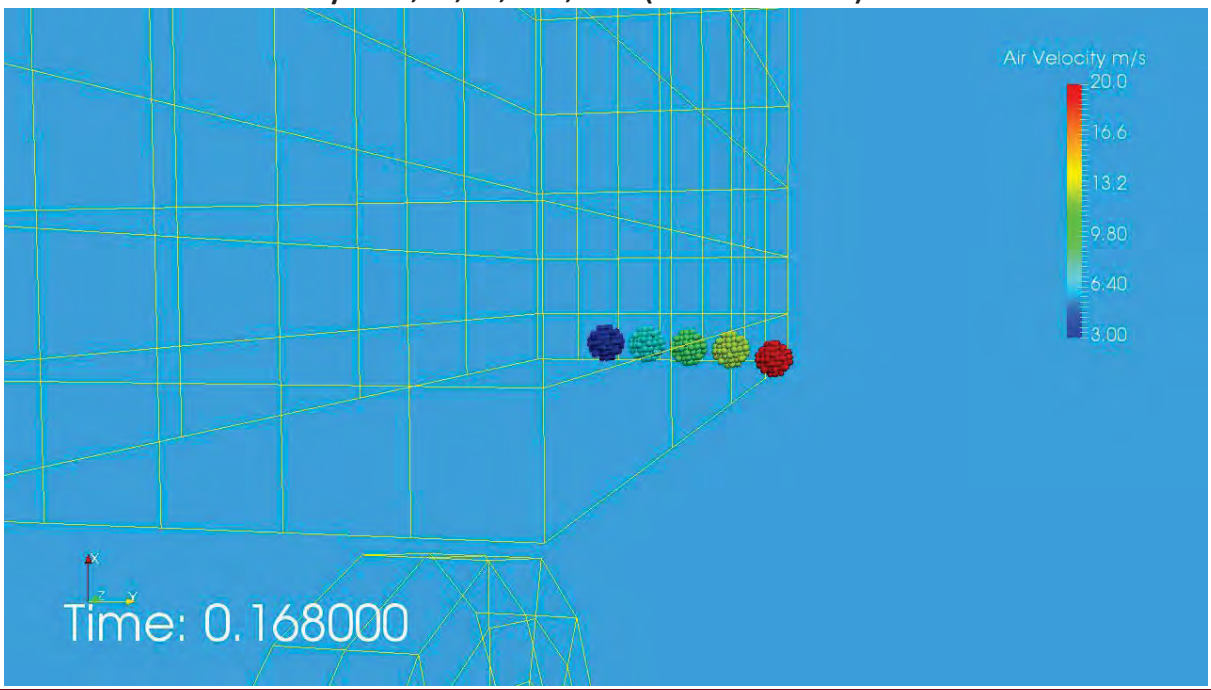

TAB model for drop break-up

- We = 1, 5, 11, 20, 55 (blue to red)
- Nozzle velocity = 3, 6, 9, 12, 20 (blue to red)

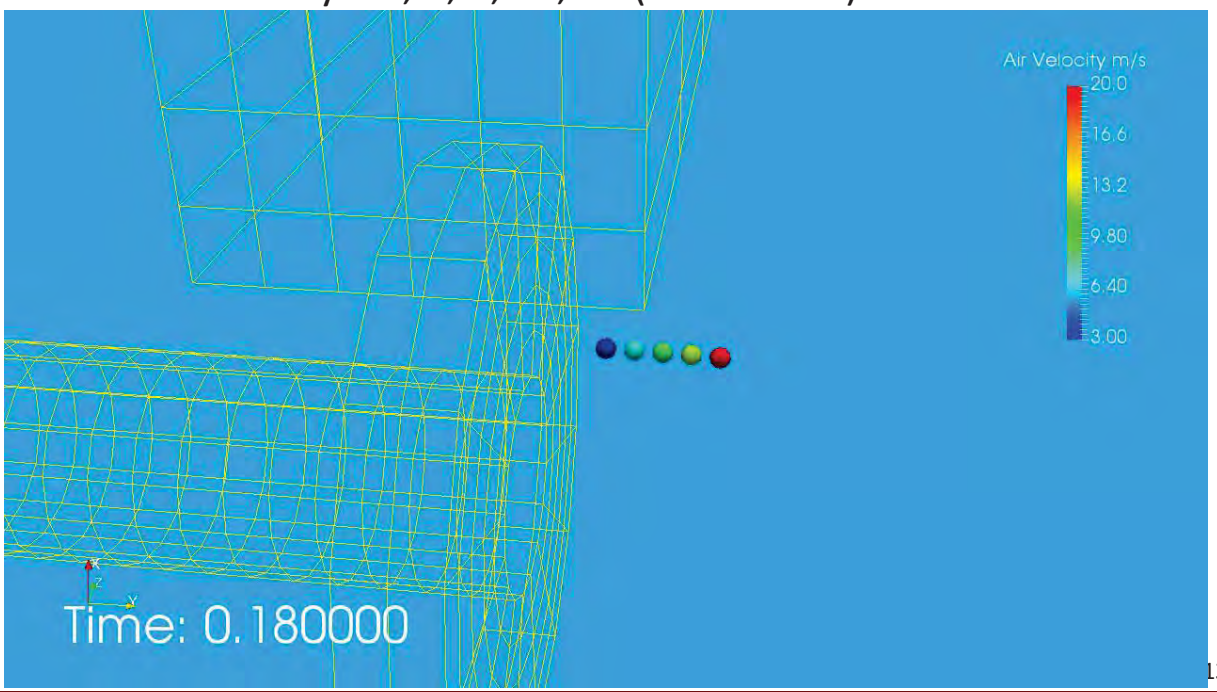

Part 2: Liquid Pool Fire Modeling

Mixed JetA-Composite Fire Test-9/14

Calorimeters

Heat Flux Gages

Thermocouple Rake in Pool

Wind

Test Arrangement

Composite Rubble Fire Test

Assembly Time Lapse

9/4/14

Test Video

What do the results mean?

- A fire resulting from an aircraft crash can last an extraordinary length of time (hours to days) because of the reacting rubble
- It is possible to have a low-level burn with a significant increase in temperatures at later times
- Fibers may continue to react with no flaming present if there is sufficient material (i.e. at this scale)
- The epoxy never appeared to be a significant or distinguishing factor in this test as a fuel, is thought to be mostly consumed early in the burn
- Total composite mass loss is still not resolved for an unmitigated fire scenario, longer-term data would be helpful
  - Likely to exhibit significantly higher mass loss

Modeling this Test

- The significance of this problem is high for people who deal with transportation safety
  - Slow heat scenario
  - Can be challenging
- We generally lack the ability to model this scenario with existing tools
  - SIERRA/Aria does level-sets, not ideal in this regime
- I have not encountered a capability in any code for liquid soaked solid fuel fires
- We have performed some rubble soaked fuel tests in the past, but never had a scenario where the 'rubble' could also react
- An external proposal was funded to model this type of event (NSR&D)

Existing PIRT

- We previously have described generically what is needed to model complex pool fire scenarios

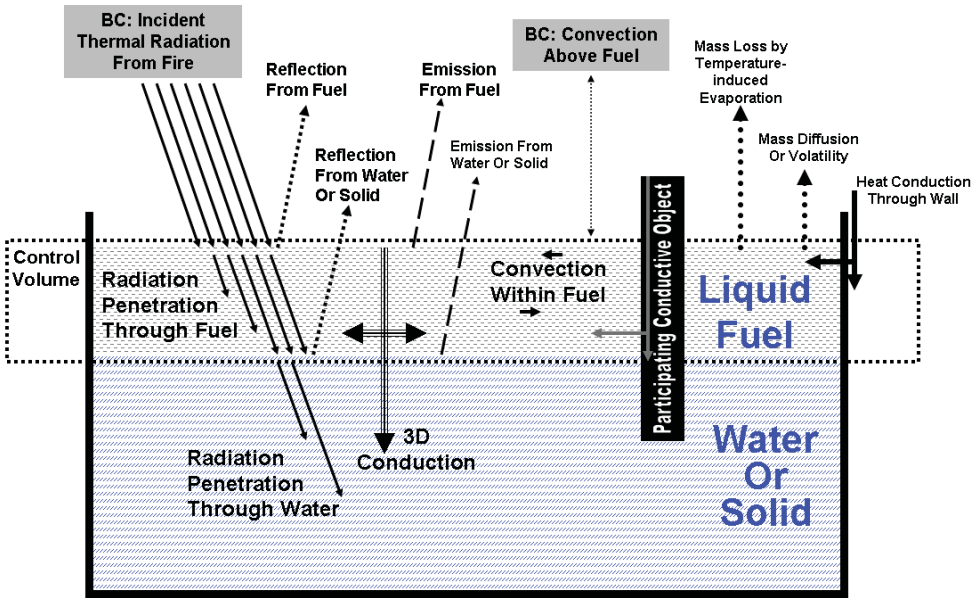

Brown, A.L., Gill, W., and Lopez, C, "Predictive evolution of fuel from a liquid pool fire: phenomenology identification and ranking exercise," Proceedings of the ASME International Mechanical Engineering Congress & Exposition, November 5-10, 2006, Chicago, IL, USA, IMECE2006-15157

Approach

- Implement a volume of fluid capability in SIERRA/Fuego to model the receding fuel layer
  - Surface tension model for Marangoni forces: $\tau_{mar} = -\nabla_s \sigma$
  - Evaporation dynamics at the interface
- Abstract the existing solid fuel modeling capabilities to predict the reactions in a rubble fuel bed
  - We leveraged this component of development to incorporate the CPD model for percolation theory based reaction kinetics
- Link the capabilities in Sandia's SIERRA/Fluid Mechanics code Fuego that has participating media radiation capability and solid reacting materials

Sources for models:
Brackbill, J.U., D. B. Kothe, and C. Zemach, "A Continuum Method for Modeling Surface Tension," Journal of Computational Physics, 100, 335-354, 1992.
Hardt, S., and F. Wondra, "Evaporation model for interfacial flows based on a continuum-field representation of the source terms," Journal of Computational Physics, 227, 5871-5895, 2008.

Preliminary Verification Results

- A basic VOF has been implemented and verified (see video)
- Currently, we are working on modeling the surface forces and radiation interaction with the surface

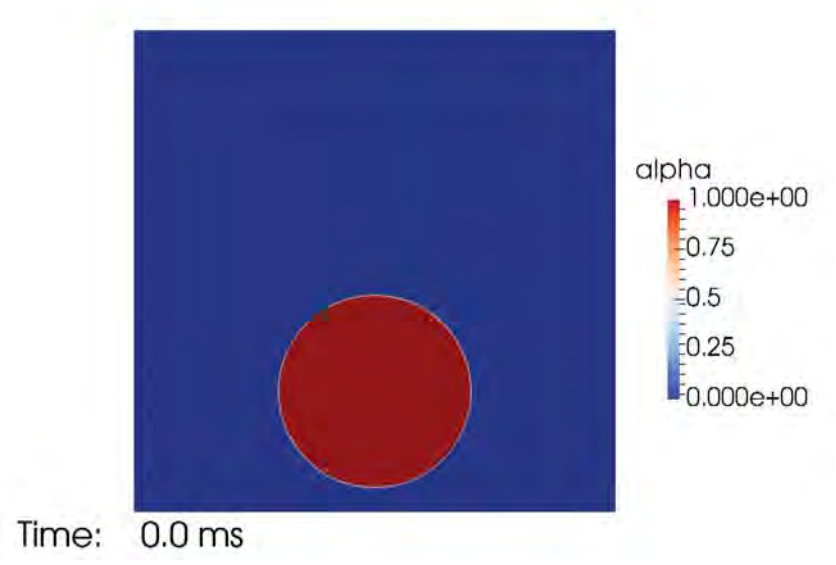

Validation Plan

- A recent dataset exists where flow is measured in a pool fire
- They show mixing at the top, stratification of temperature for a methanol pool fire

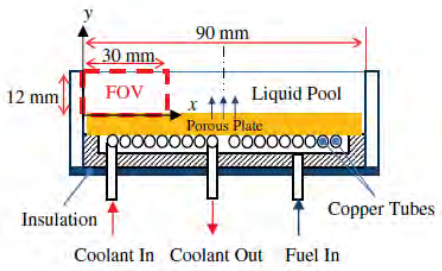

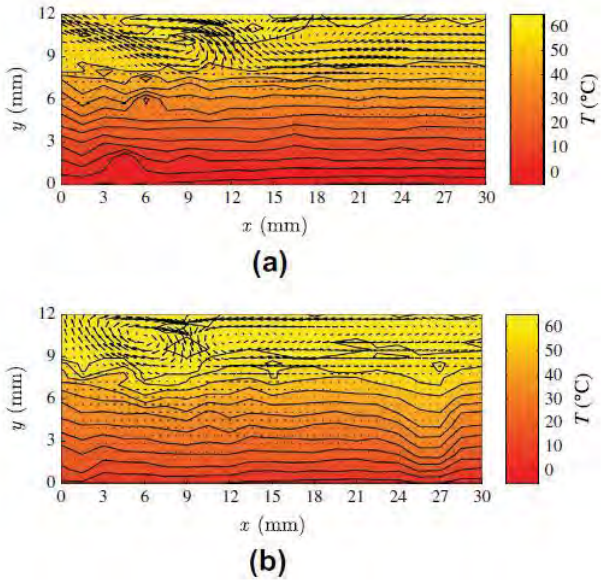

Vali, A., Nobes, D.S., and Kostiuk, L.W., "Transport phenomena within the liquid phase of a laboratory-scale circular methanol pool fire," Combustion and Flame, 161, pp. 1076-1084, 2014.

Summary

- We have two applications right now actively developing unique multi-phase engineering models
  - A particle method for simulating drop break-up, shows promise
  - A VOF method for simulating fuel fires with solid fuel mixed in
- The MD inspired particle interaction method appears to be able to model the critical break-up of drops
  - Parameter tuning and model assessment is in progress
- A VOF method is being developed for modeling the pool dynamics in a mixed pool fire including solid fuel
  - Basic VOF is implemented, need radiation coupling, evaporation, and surface tension model

Acknowledgements

- The test team including contributions from Brandon Servantes Sylvia Gomez-Vasquez, Travis Fitch, Randy Foster, Chuck Hanks, Jerry Koenig, William Dixon, Richard Simpson, Donald Mcmanaway, Deven Codding, Paul Codding, Steve Chandler, KD Pass, Craig Dickensheets, Ron Pederson, Jeff Kokos, Jim Nakos, and Randy Watkins.
- Major contributors to the code efforts including David Glaze, Stefan Domino, Flint Pierce, John Hewson, David Noble, Sam Subia, Amanda Dodd, Rekha Rao, Vern Nicolette, Anay Luketa, Sheldon Tieszen, Tyler Voskuilen
- VOF model implementation: Tyler Voskuilen
- LJ model implementation: Flint Pierce

Extra Viewgraphs

Preliminary Validation Results

- We = 1, 5, 11, 20, 55 (blue to red) C=200
- Nozzle velocity = 3, 6, 9, 12, 20 (blue to red)

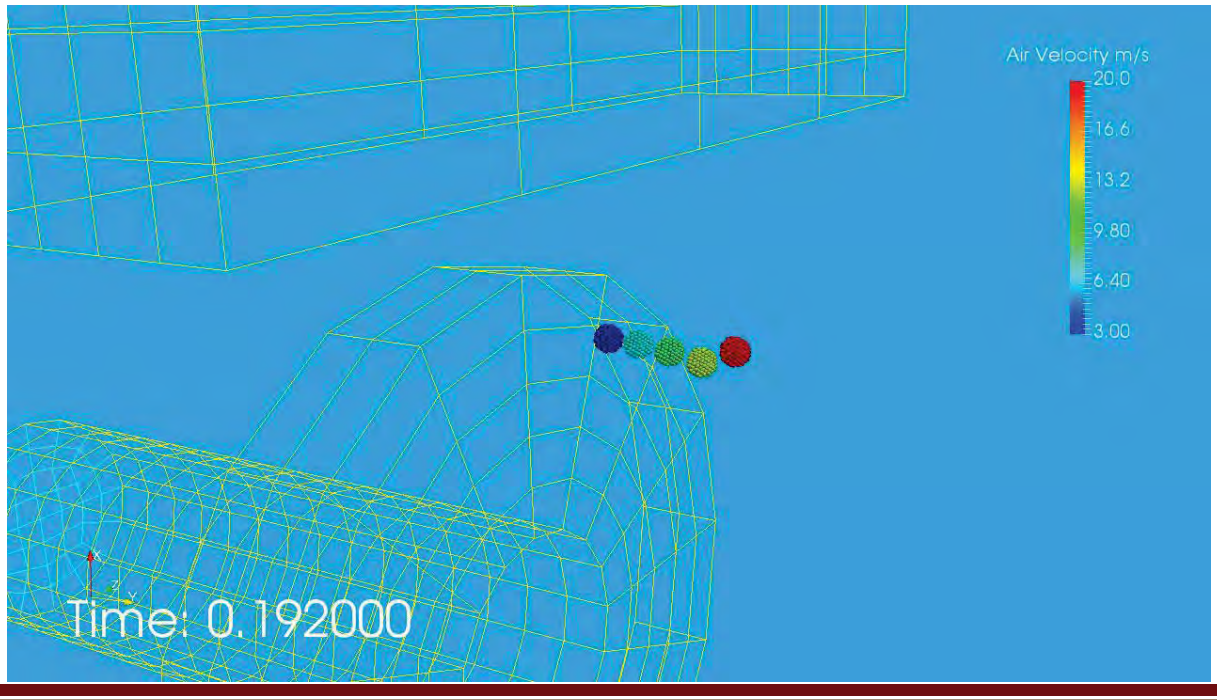

Existing Capabilities

Sandia develops the open source SIERRA mechanics. Fluid mechanics tools exist in this framework.

- The non-open source **Fuego** tool is primarily used for low-Mach number reacting flow problems and particle transport.
- **Aria** does heat transport and low-Reynolds number multi-phase transport and reaction
- **Aero** does shock, ablation, and high-Mach number simulations
- **Nalu** is a basic open source N-S flow code for testing new algorithms

Capabilities potentially relevant to the composite fire scenario include:

- Adaptive boundary level-set method for multiphase flows (Aria)
- Particle combustion model (Fuego)
- 1-D solid reacting boundary condition model (Fuego)
- 1-D liquid pool model (Fuego)
- 3-D solid reacting material model (Fuego/Aria)

Level-set methods

- CDFEM methods were recently implemented in Aria for resolving level-set multi-fluid interfaces
- The below video exhibits a 2-D prediction of a boiling drop rupturing on the surface of a liquid

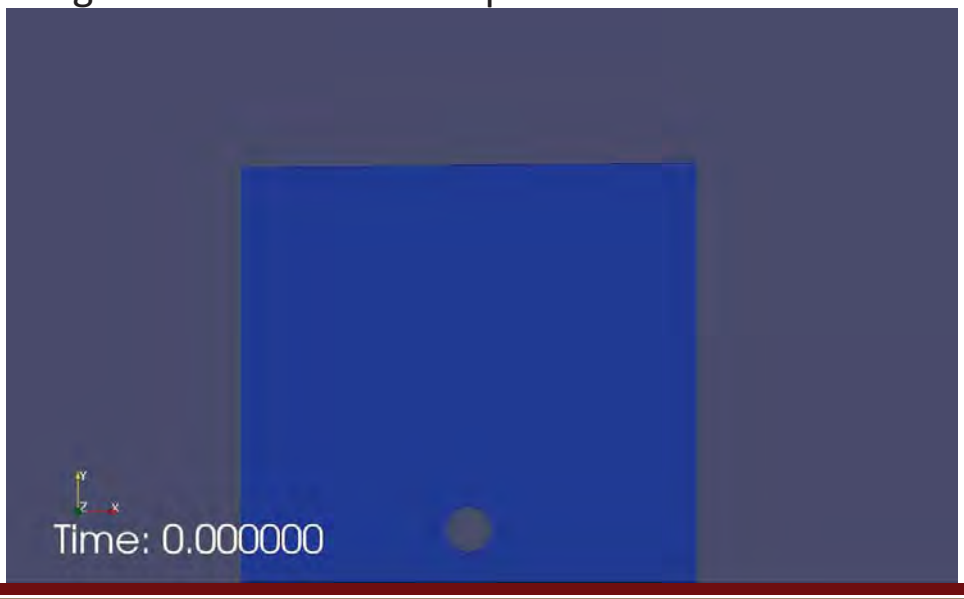

General Approach Schematic

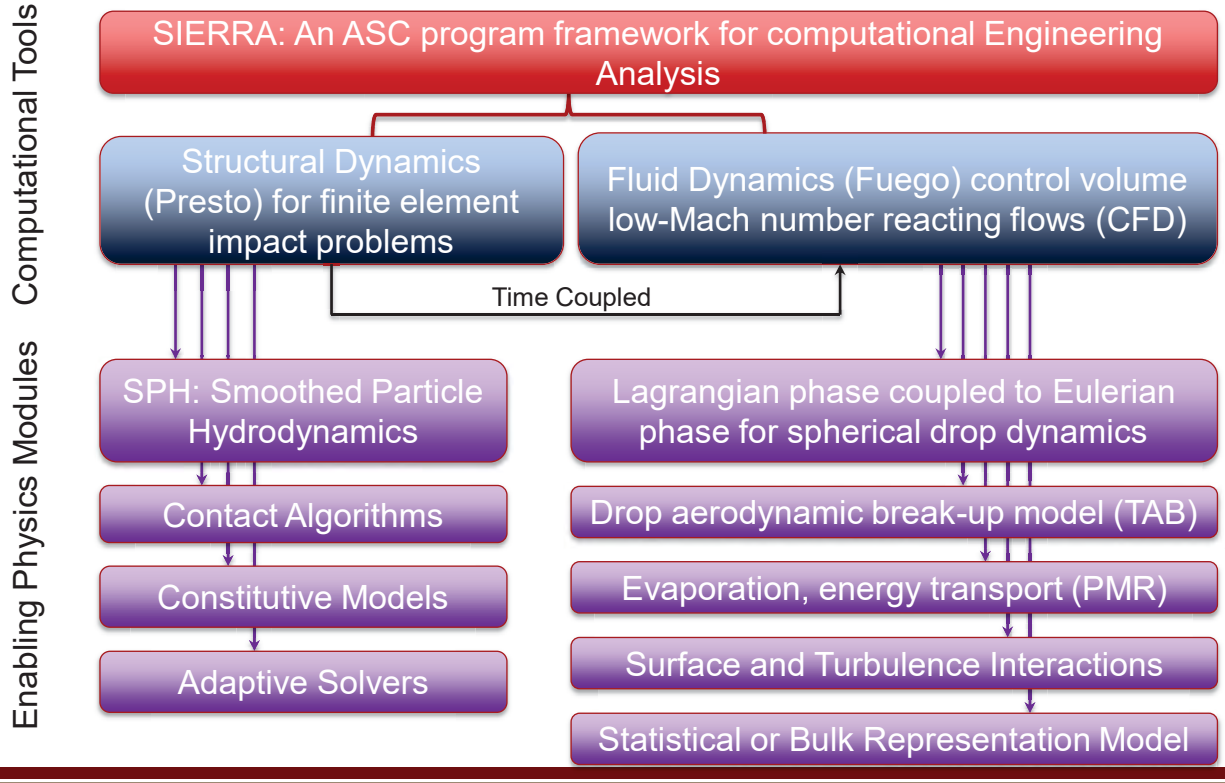

Taylor Analogy Break-up (TAB) Model

- Originally by O'Rourke and Amsden (1987)
- Approximates the drop as a damped oscillator, formulated as a second-order differential equation, with y as a deformation parameter:

$$m_d \frac{d^2 y}{dt^2} = \underbrace{m_d \frac{C_F}{C_b} \frac{\rho_g}{\rho_l} \frac{|u_d - u_g|^2}{r^2}}_{\text{Aerodynamic Forcing}} - \underbrace{m_d \frac{C_k \sigma}{\rho_l r^3} y}_{\text{Surface Energy Damping}} - \underbrace{m_d \frac{C_d \mu_l}{\rho_l r^2} \frac{dy}{dt}}_{\text{Viscous Damping}}$$

Simplified Schematic

Harmonic Deformations Forced by Velocity Differential

Critical Deformation (y=1)

New Drop(s)

- Discretized solution for y is:

$$y(t+\Delta t) = \frac{We}{C} + \left\{ \left(y(t) - \frac{We}{C} \right) \cos(\omega \Delta t) + \frac{1}{\omega} \left(\dot{y}(t) + \frac{y(t) - We/C}{\tau_b} \right) \sin(\omega \Delta t) \right\} \exp(-\Delta t / \tau_b)$$

$$\dot{y}(t+\Delta t) = \frac{\frac{We}{C} - y(t)}{\tau_b} + \left\{ \frac{1}{\omega} \left(\dot{y}(t) - \frac{y(t) - We/C}{\tau_b} \right) \cos(\omega \Delta t) - \left(y(t) - We/C \right) \sin(\omega \Delta t) \right\} \omega \exp(-\Delta t / \tau_b)$$

$$\omega = \sqrt{\frac{8 C_k \mu}{\rho_l d_p^3} - \frac{1}{\tau_b^2}}$$ Oscillation Frequency

$$\tau_b = \frac{1}{2} \frac{\rho_l d_p^2}{C_d \mu_l}$$ Viscous Damping Time

$$We = \frac{\rho_l d_p (u_p - u_g)^2}{\sigma}$$ Weber Number

- New drop diameters can be calculated:

$$d(t+\Delta t) = d(t) / \left[1 + \frac{C_k K}{20} + \frac{\rho_l d_p(t)^3}{8\sigma} \frac{6K - 5}{120} \dot{y}(t)^2 \right]$$

- We modified the algorithm to limit break-up for new particles

Particle Combustion Model

- Primarily used in the past for two projects:
  - Wildland fire predictions for idealized trees
  - Aluminized propellant reactions

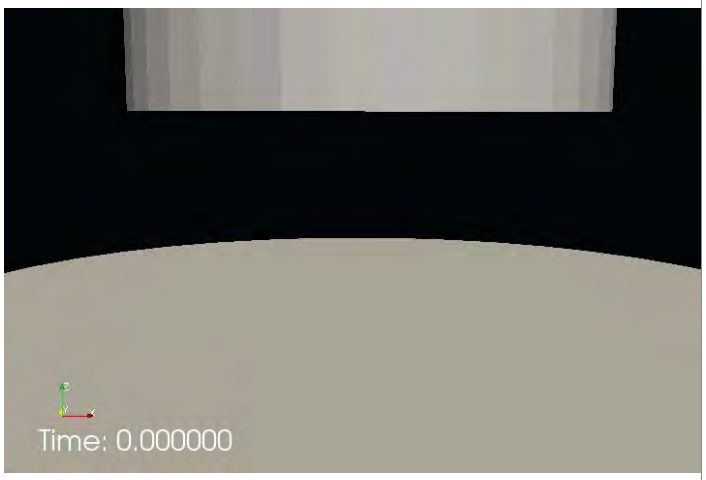

1-D Solid Reacting Boundary Condition

- Recent work demonstrates the verification of the method and compares to data in the context of a sensitivity analysis:

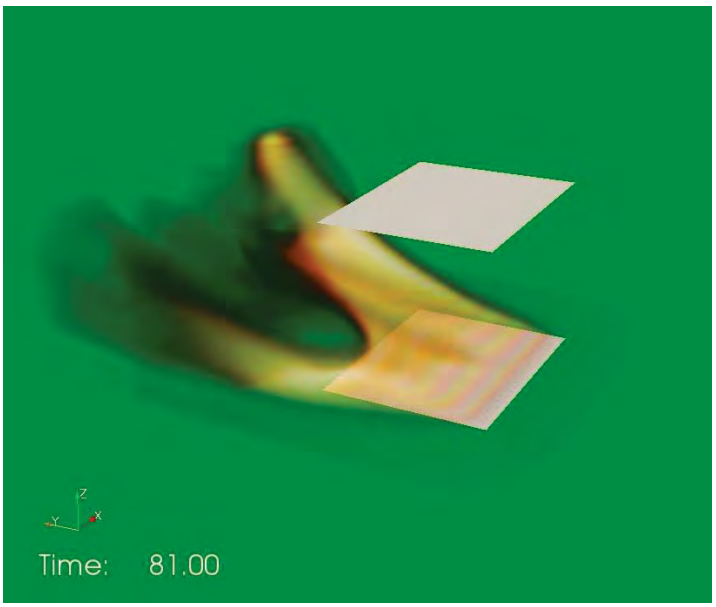

1-D Liquid Pool Model

- Historical model for predicting the burn rate for pool fires given heat transport from the flames (based on legacy SINTEF codes)

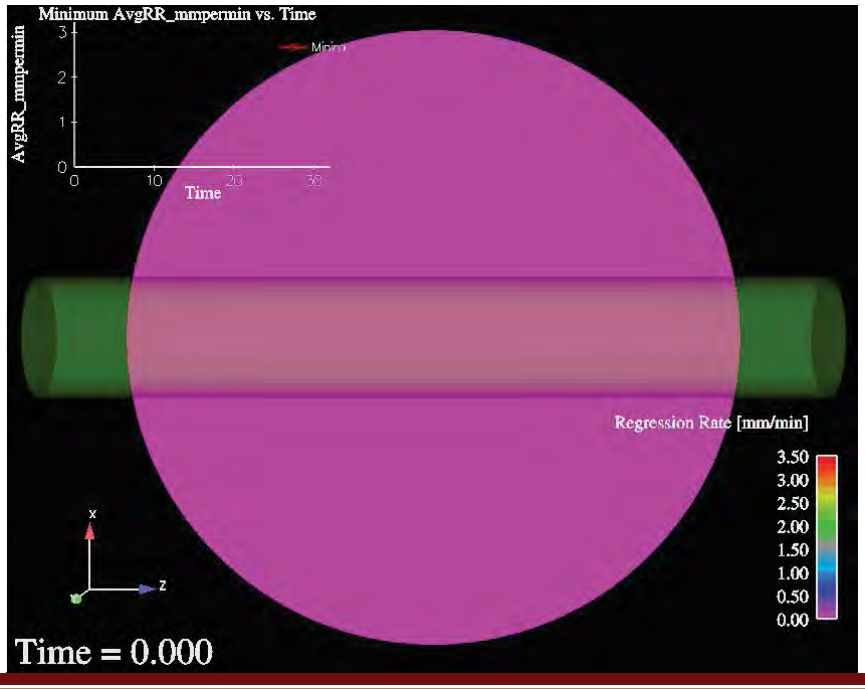

3-D Solid Reacting Material Model

- New model includes porous transport, charring reactions, oxidative reactions.

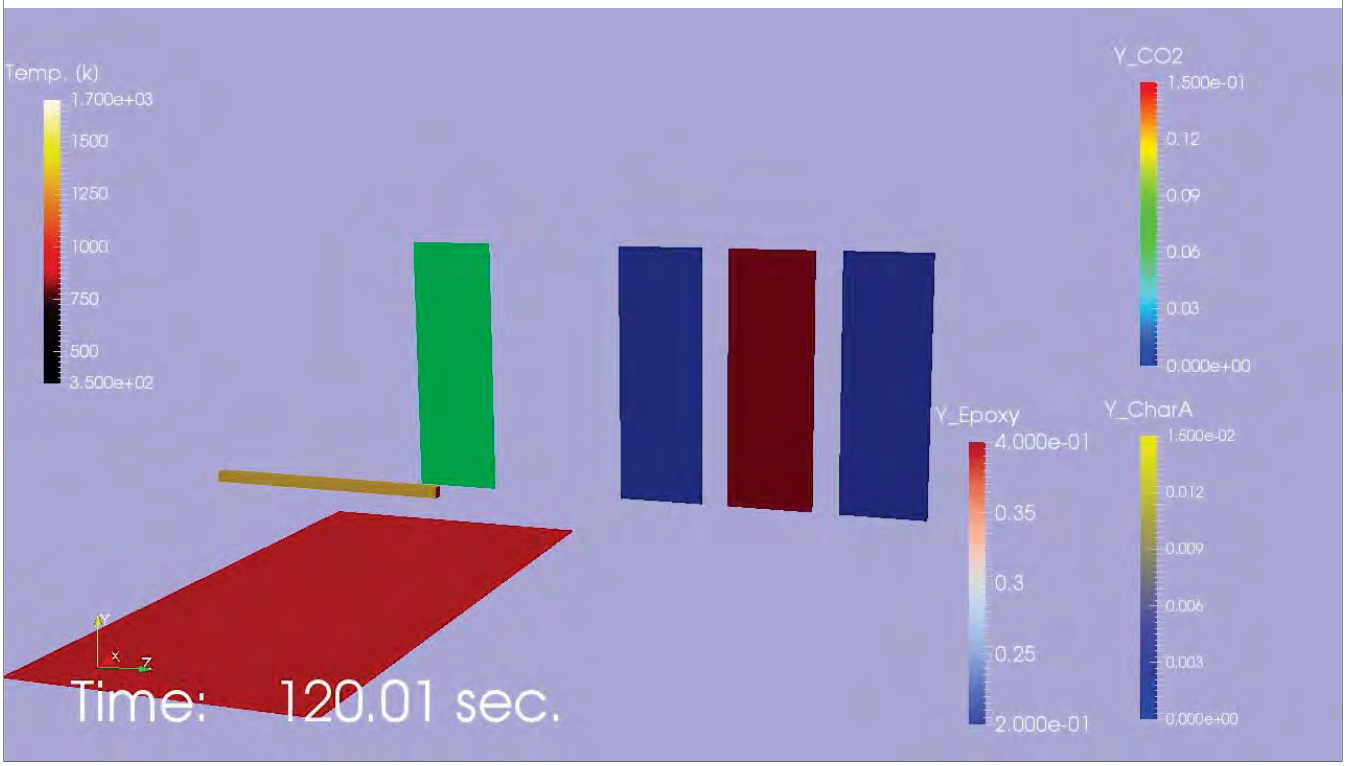

Final Injection Illustration

- The last injection is populated with pairs in many cases (e.g. detonation inside tank scenario below)

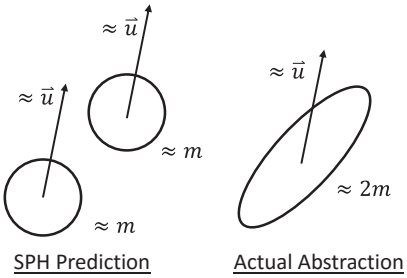

SPH Prediction Actual Abstraction

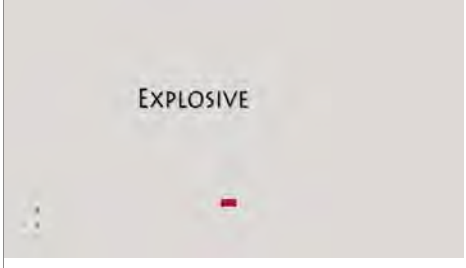

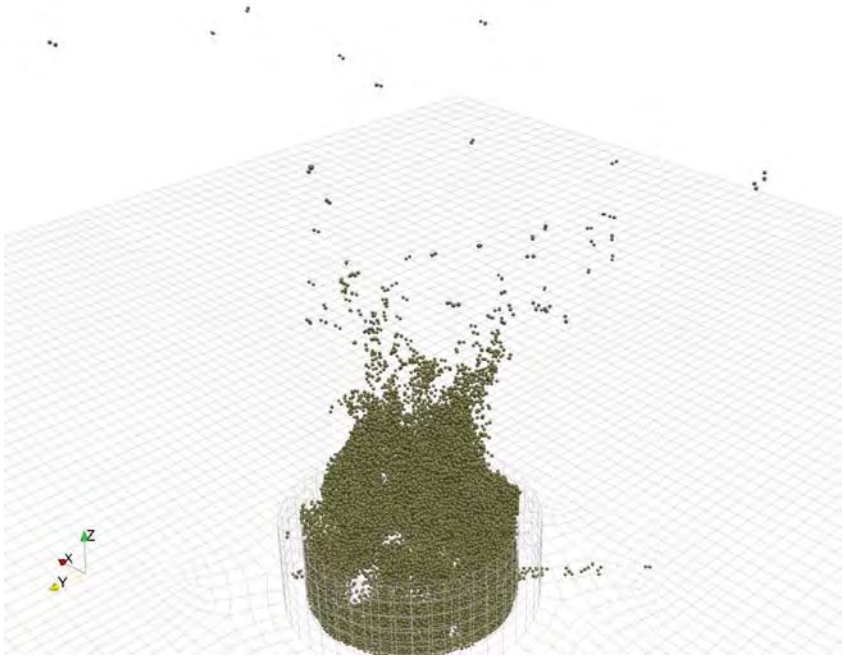

Final Injection Illustration

- Linear systems are also found in some scenarios (Detonation Outside Tank Scenario)

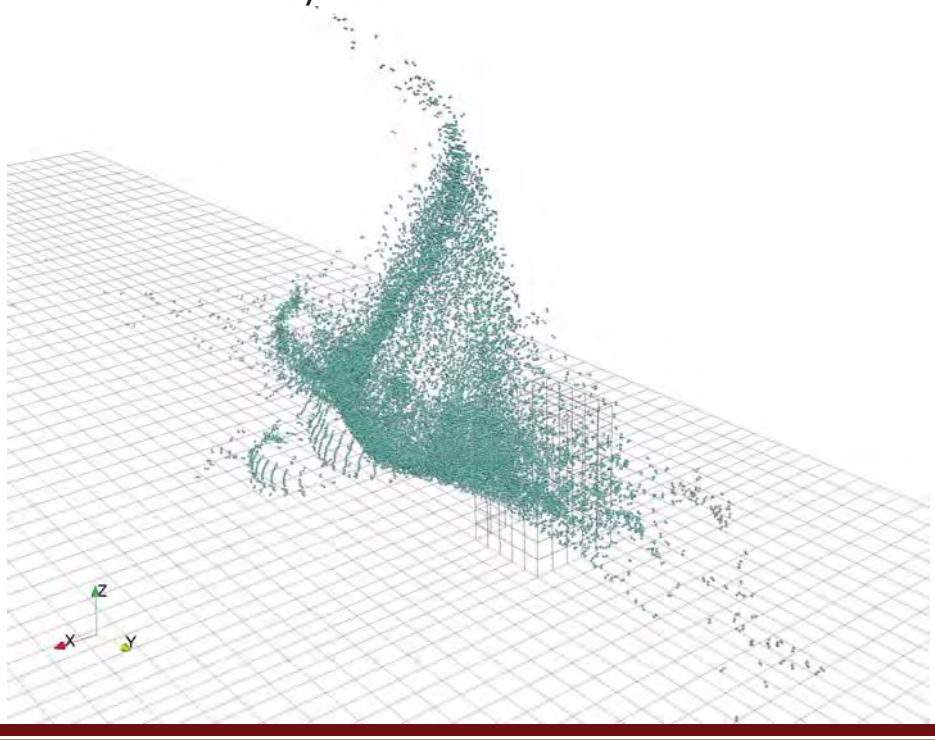

Numeric Model

- Introduce a dimensionless energy with a critical value E_{crit} for defining transfer

$$E_{dim} = SE/KE$$

$$SE = \sigma A = \sigma h \pi D_e$$

$$KE = (1/2)m\left|\vec{U}\right|^2$$

Injection Criteria
Single Particle Criterion:
$B_{i,min} > B_{crit}$
Particle Pair Criterion:
$E_{dim} > E_{crit}$

$$h = [(x_1 - x_2)^2 + (y_1 - y_2)^2 + (z_1 - z_2)^2]^{1/2}$$

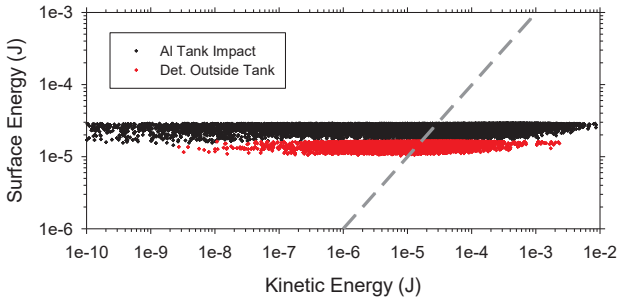

$$D_e = 2\sqrt{(4/3)h(r_1^3 + r_2^3)}$$

$$m = \rho V = (4/3)\pi\rho(r_1^3 + r_2^3)$$

$$\left|\vec{U}\right| = [(u_1 - u_2)^2 + (v_1 - v_2)^2 + (w_1 - w_2)^2]^{1/2}$$

- A reasonable E_{crit} value is 1.0 (or close)
- Particle pairs are combined if the system satisfies E_{crit} parameter

CARBON CAPTURE MULTIDISCIPLINARY SIMULATION CENTER

this talk
1. our application: power generation from coal
2. our predictive challenge: what is good enough?

Friday
3. particle dynamics: resolving particle location & rxn.
4. eulerian polydispersity

electric power generation

318GW U.S.A.coal

world coal

	January 2016 (MW)		Change since January 2015 (MW)		
	Announced + Pre-permit + Permitted	Construction	Announced + Pre-permit + Permitted	Construction	Newly Operating
East Asia	546,867	221,010	35,366	82,093	68,515
South Asia	253,009	76,595	-67,292	7,124	18,670
SE Asia	115,400	26,055	20,470	-2,879	10,099
Middle East and North Africa	9,688	2,036	4,960	0	0
Southern Africa	22,800	9,043	1,438	-1,085	1,545
Other Africa	10,665	0	-830	-600	0
Latin America	7,753	2,702	891	-573	935
US/Canada	2,860	600	-1,525	-830	618
Eurasia	16,370	1,700	2,930	-990	1,376
EU28	11,816	8,655	-8,448	-4,112	5,006
Non-EU Europe (incl Turkey)	75,253	3,265	3,843	-2,070	1,207

352GW coal under construction

compiled from EIA & endcoal.org

benefits of (A)USC (oxy-)coal combustion

technology	superheater temperature (°C)	carbon intensity (tonne CO_2/MWh)	efficiency
avg. of existing U.S. units	540	0.95	32%
current technology	600	0.79	40%
USC	700	0.73	44%
AUSC	760	0.67	48%
AUSC w CCUS (oxy-coal)	760	0.07	42%

CARBON CAPTURE MULTIDISCIPLINARY SIMULATION CENTER

CARBON CAPTURE MULTIDISCIPLINARY SIMULATION CENTER

usc coal boiler

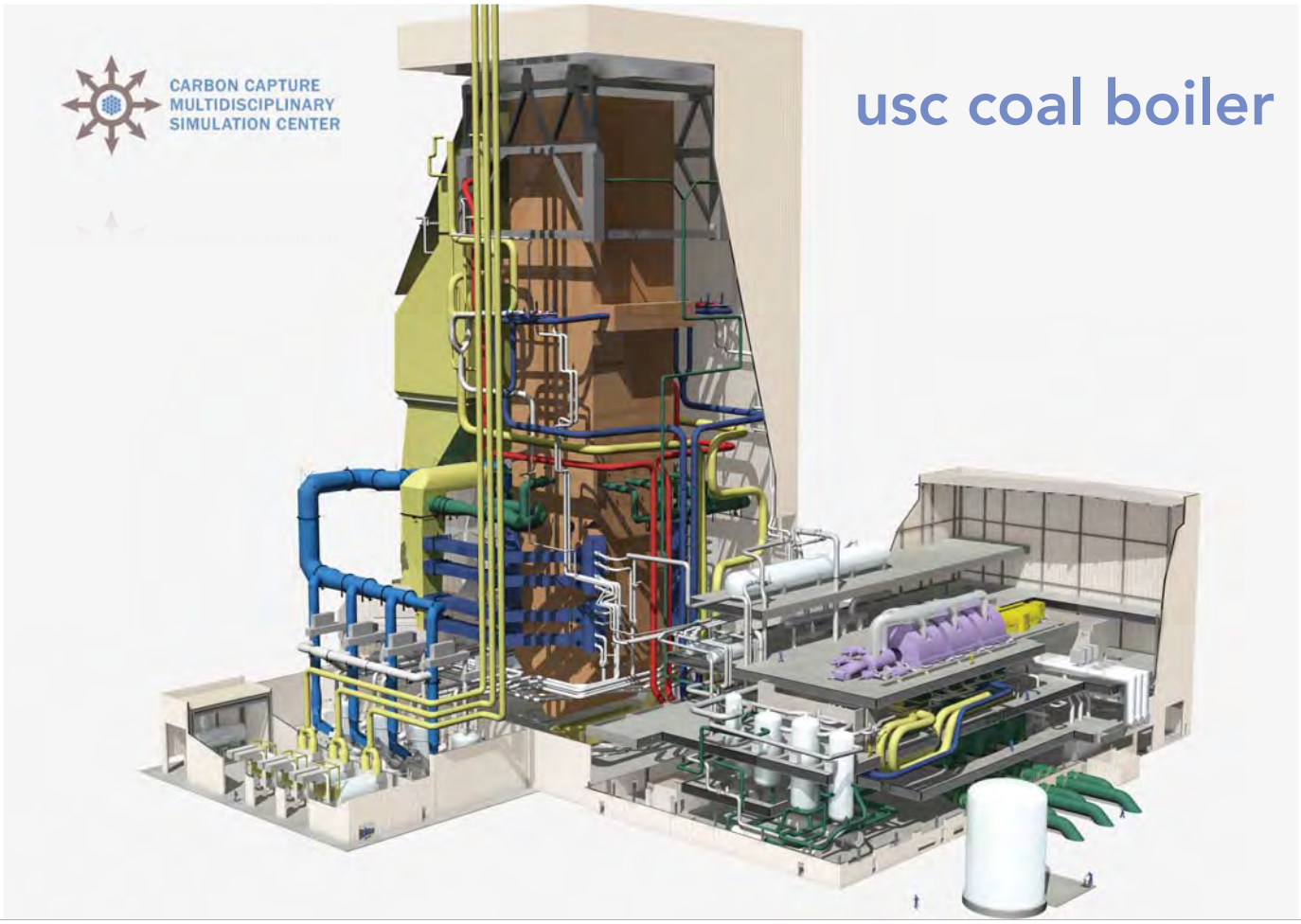

CARBON CAPTURE
MULTIDISCIPLINARY
SIMULATION CENTER

usc coal boiler

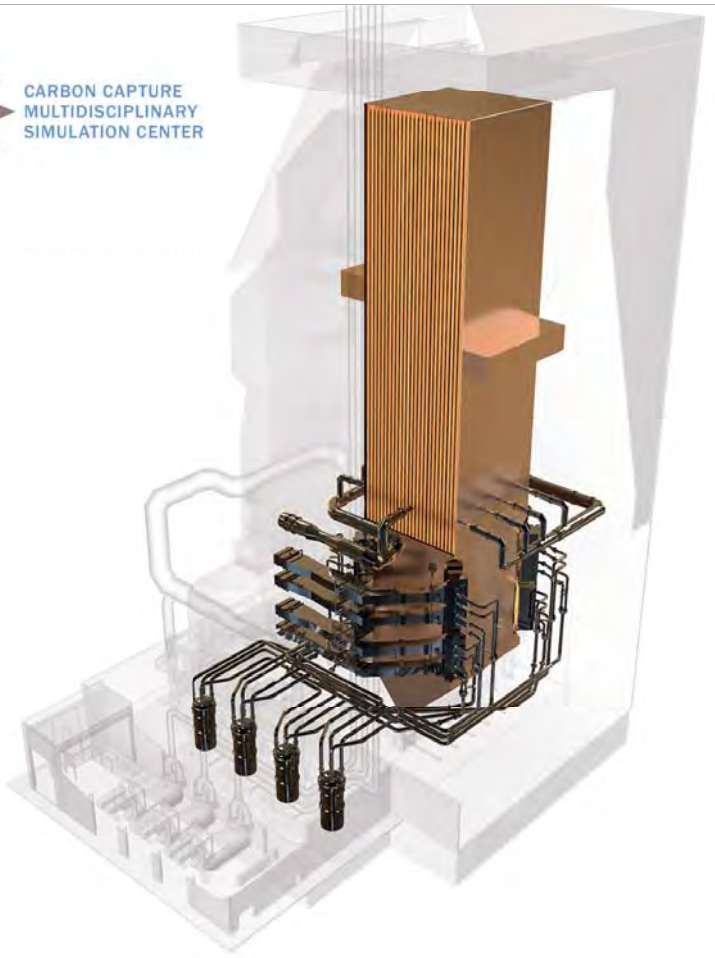

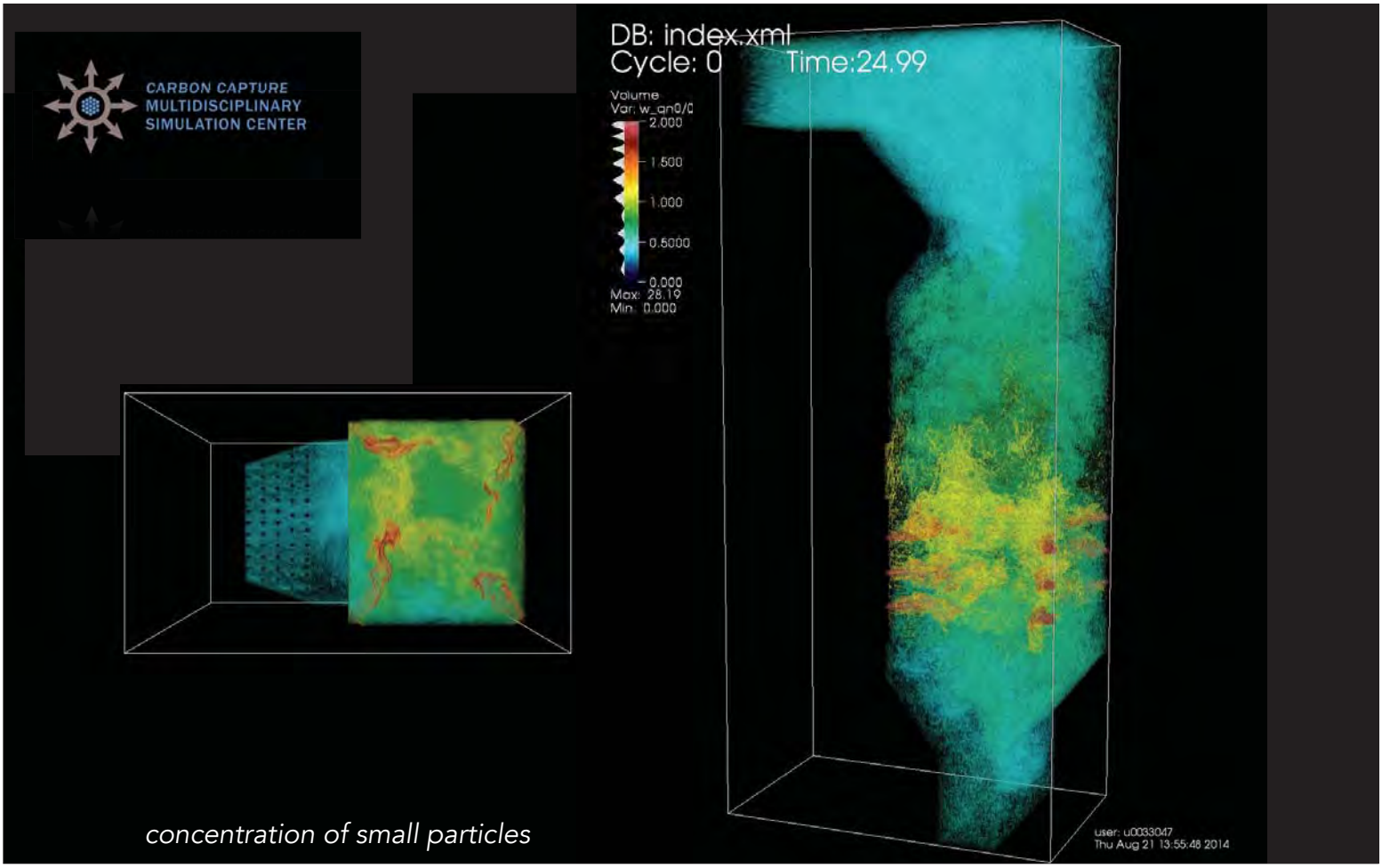

concentration of small particles

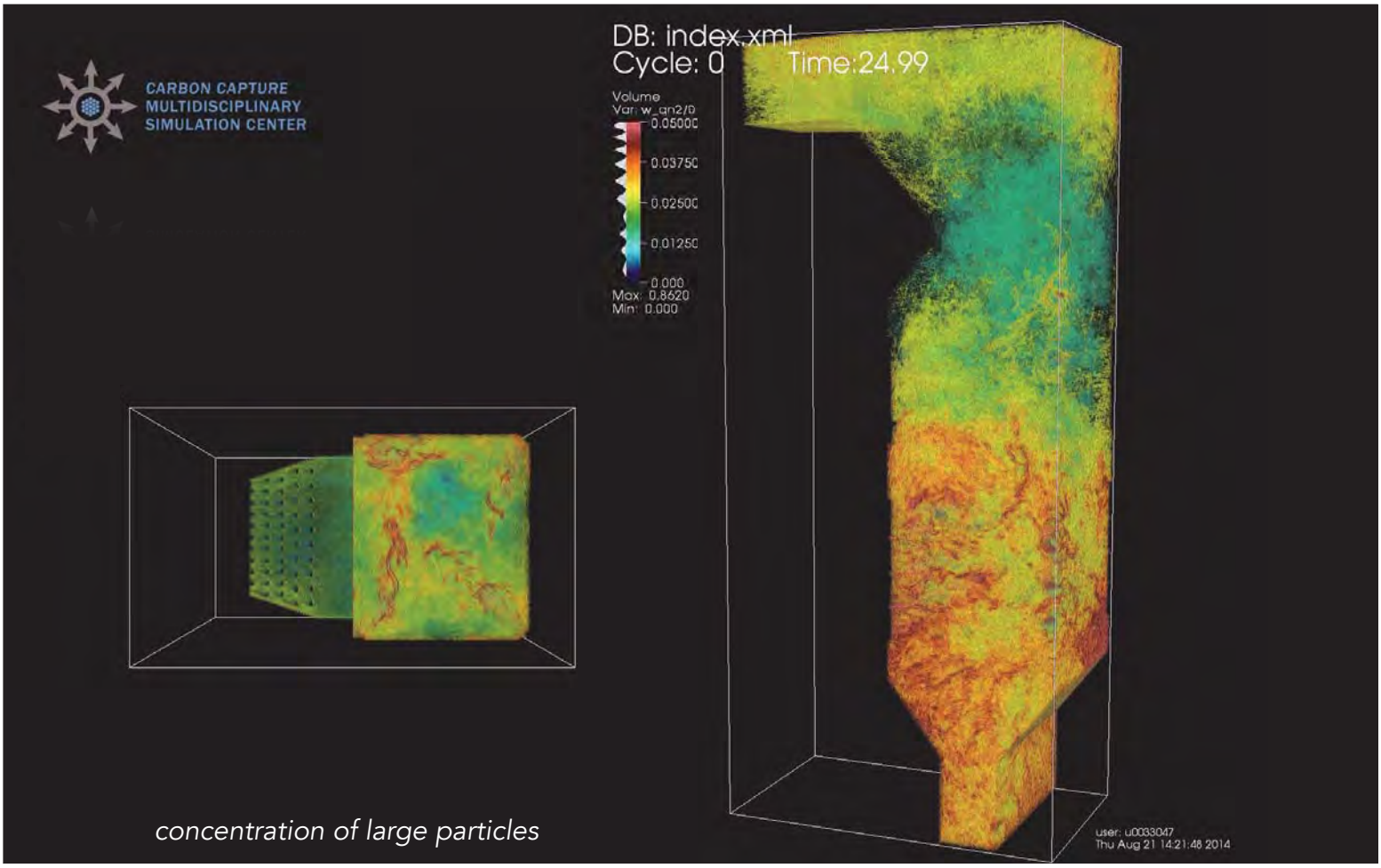

concentration of large particles

particle transformations

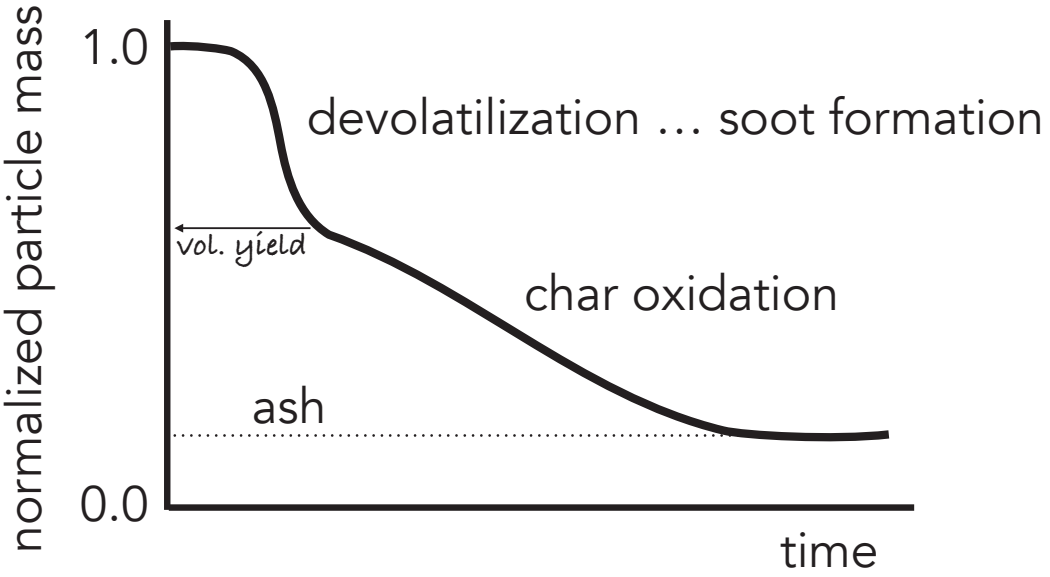

CARBON CAPTURE
MULTIDISCIPLINARY
SIMULATION CENTER

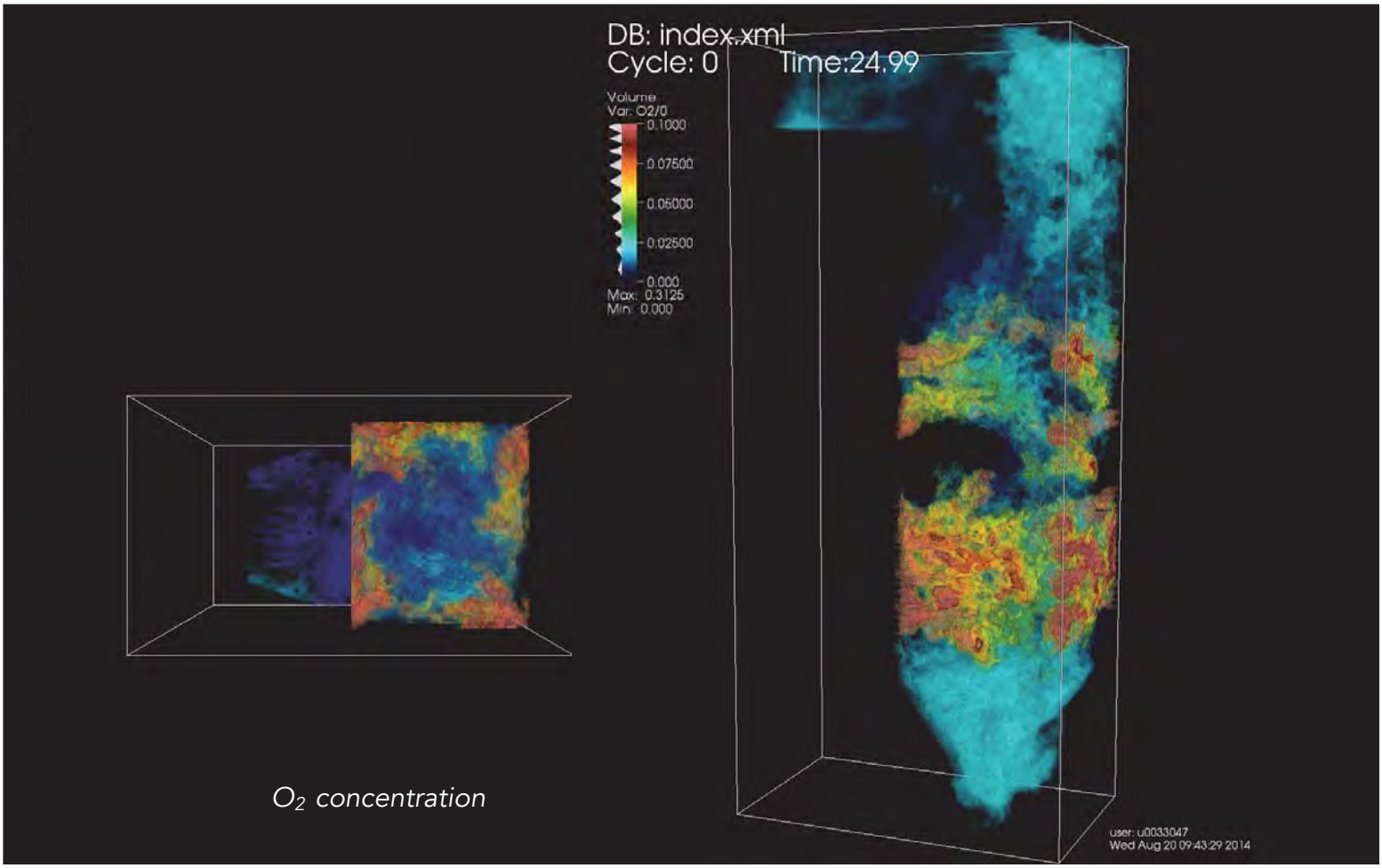

O_2 concentration

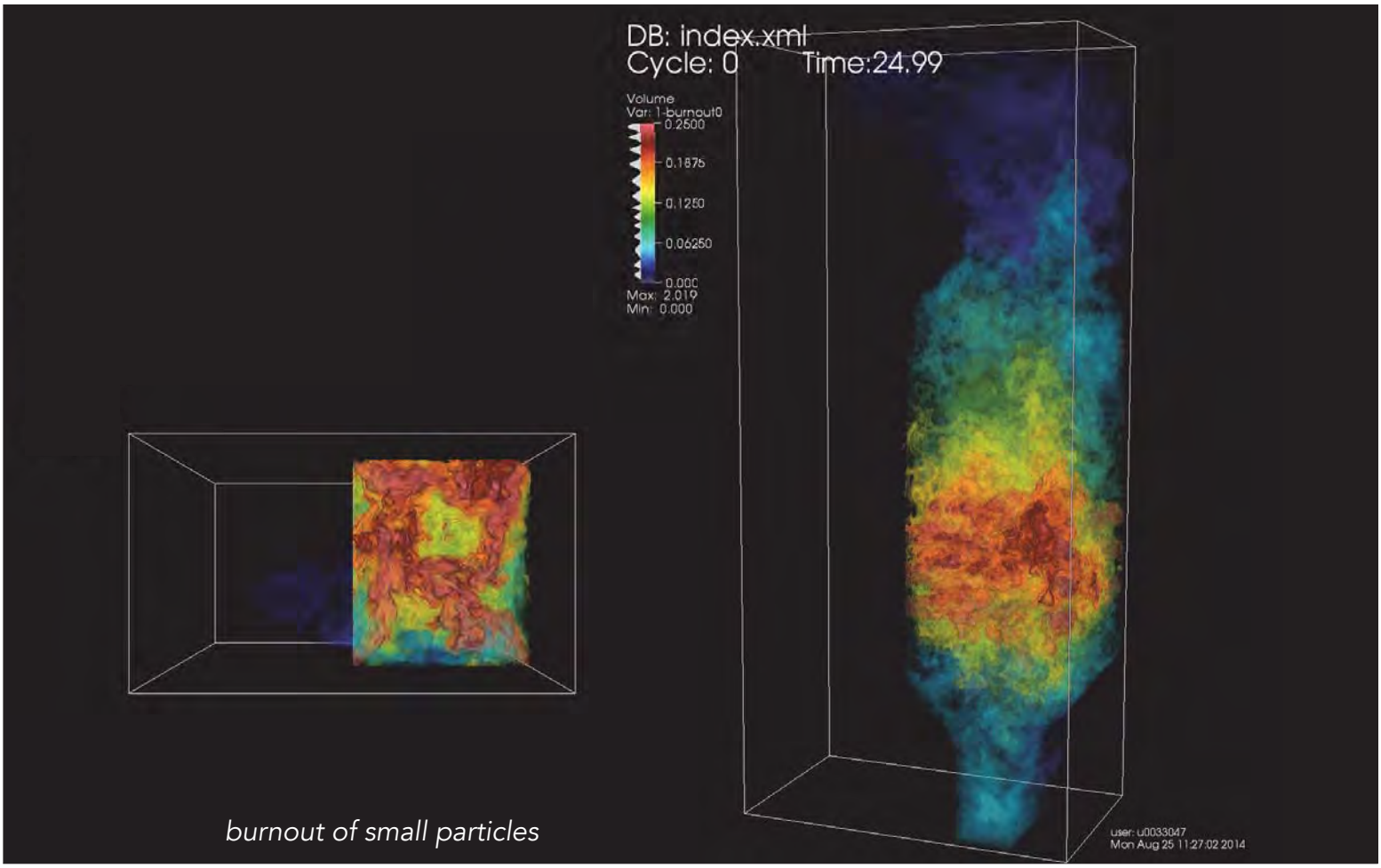

burnout of small particles

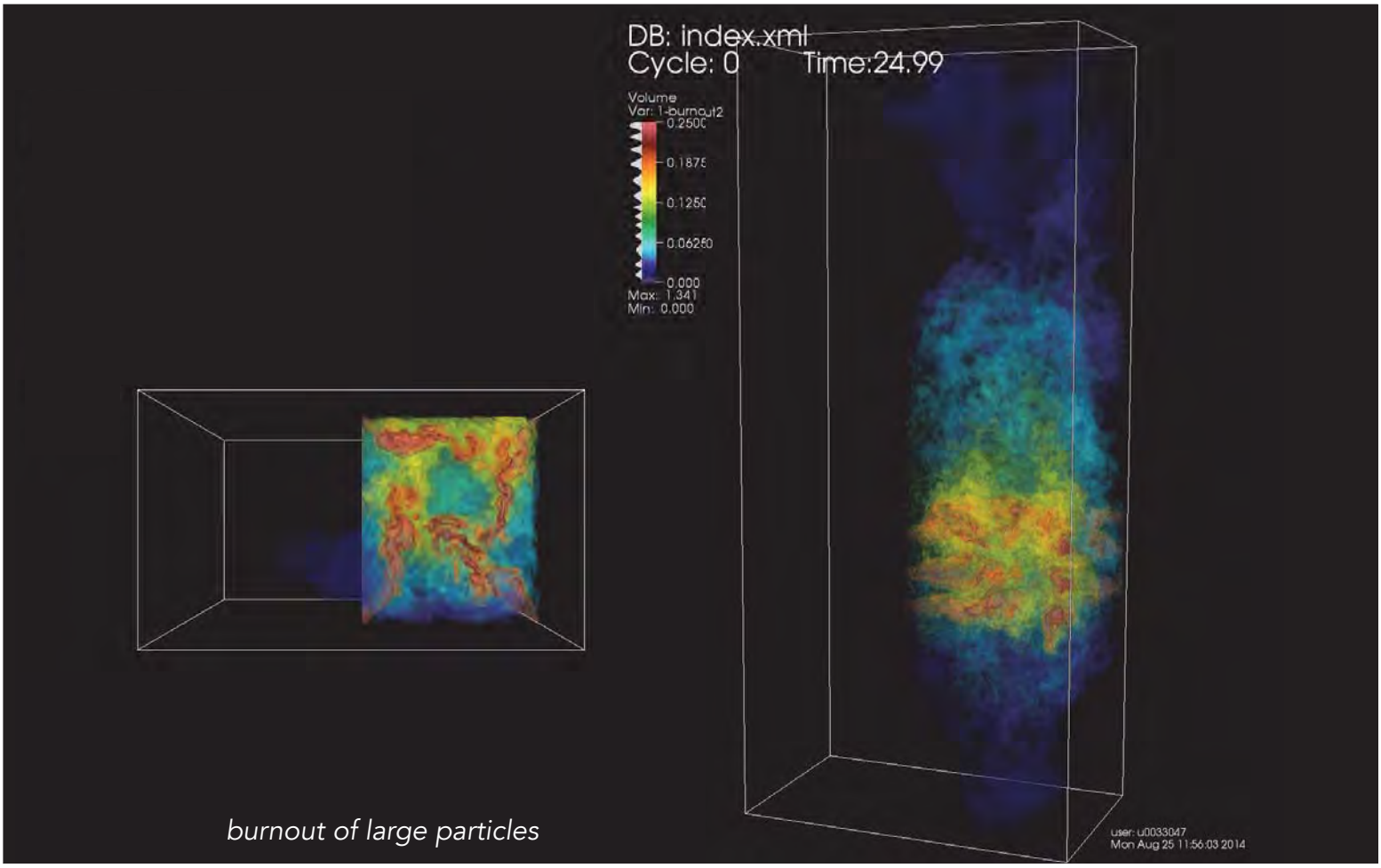

burnout of large particles

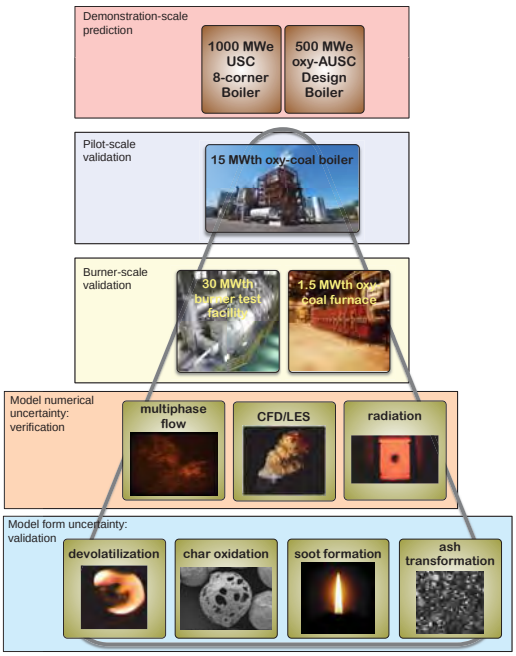

scale

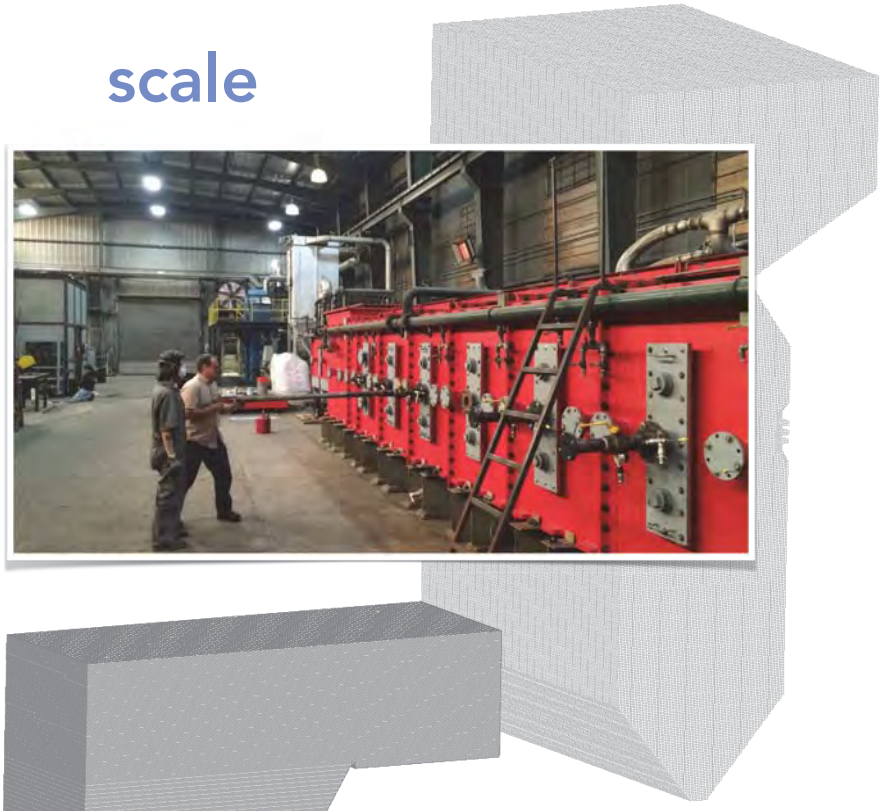

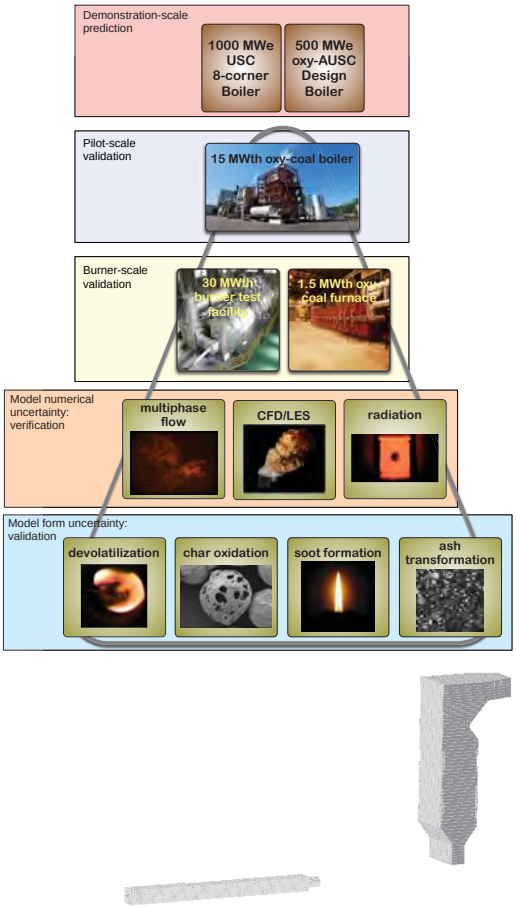

scale

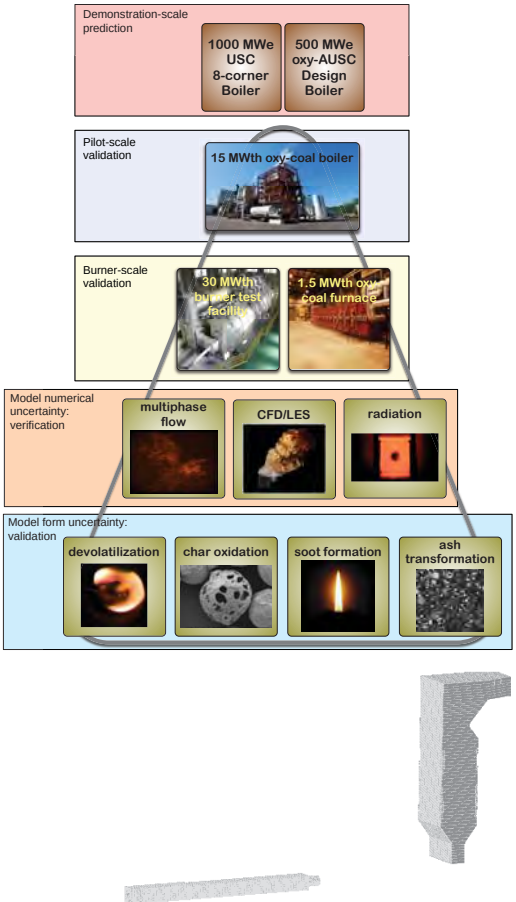

scale

CARBON CAPTURE MULTIDISCIPLINARY SIMULATION CENTER

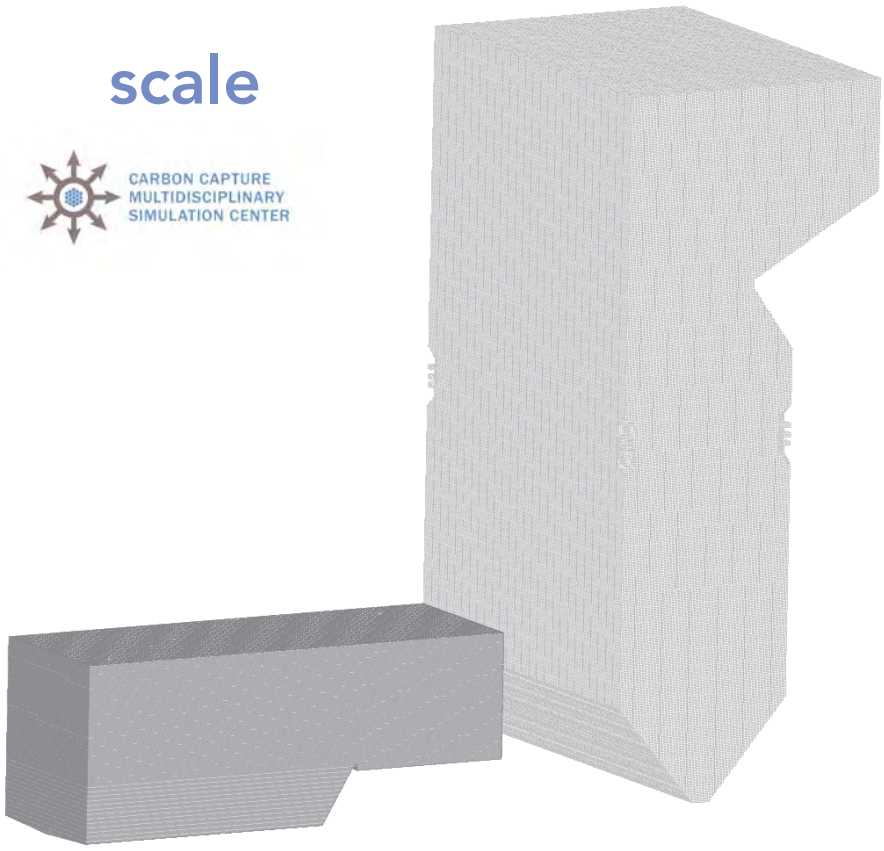

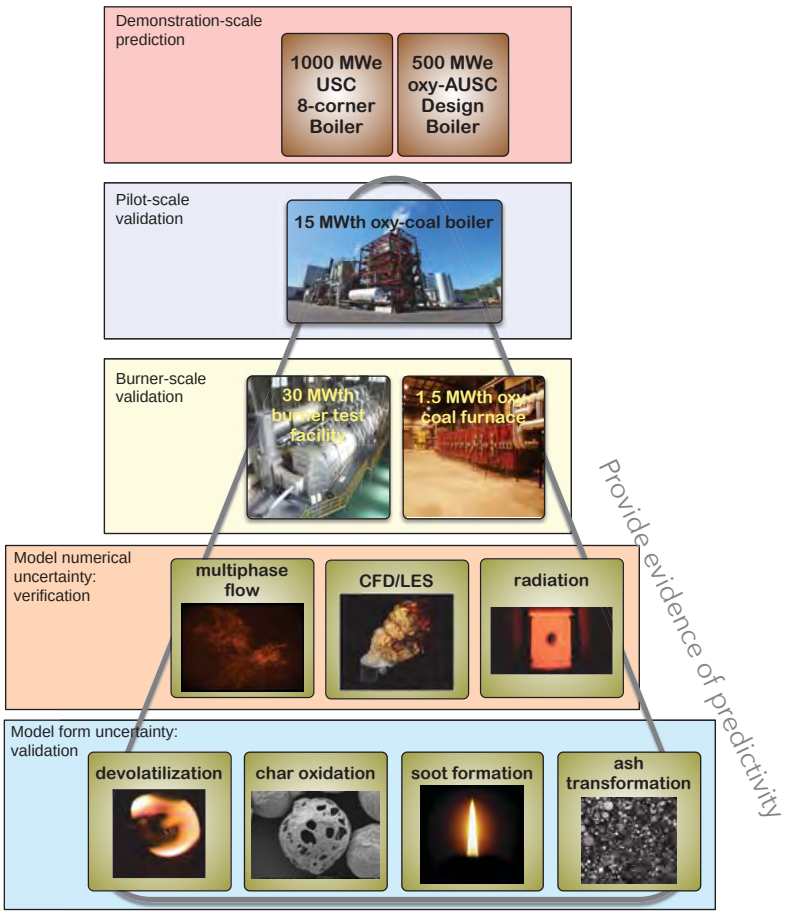

objective
predictivity

CARBON CAPTURE MULTIDISCIPLINARY SIMULATION CENTER

- PSAAPii:
  - *demonstrate positive societal impact of extreme computing*
  - *accelerate the deployment of a new technology: high efficiency carbon capture for pulverized-coal power generation (AUSC oxy-coal)*
  - *optimize state-of-the-art coal boilers for evolving energy market demands*
- GE:
  - *Model Form Uncertainty*
  - *Validation/UQ*
    - *expt. & sim. obtain predictivity*

$$y_e = y_m(x) + \epsilon + b$$

evidence: $|\mathbb{E}(b)| \leq \sigma_e \quad \forall e$

$$|\overline{y_m(\mathbf{x})} - \overline{y_e}| \leq \sigma_e$$

predictive objective:

σ_{y_p}

- find σ_{x_m} for each brick to meet predictive objective: σ_{y_p}
- find corresponding $\mathbb{E}(x|y_e)$, $\mathrm{Var}(x|y_e)$
- find model form that is 'good enough'
- this is an inverse problem
- focus on intended use

- top-down UQ methodology:
  - *given prediction constraint* σ_{y_p}
  - *do inverse problem on prediction to find* σ_{x_m}
  - *for each brick:*
    - *given* σ_{x_m} *, do forward problem to find* σ_{min}
    - *if* $\sigma_{y_e} >$ σ_{min} *: inadequate experiment*
    - *do inverse problem to find* $\mathbb{E}(x|y_e)$, $\mathrm{Var}(x|y_e)$
  - *update model form until* $\sqrt{\mathrm{Var}(x|y_e)} < \sigma_{x_m}$ for each $e \in \mathcal{E}$

CARBON CAPTURE MULTIDISCIPLINARY SIMULATION CENTER

σ_{y_p}

$T_{midwall} \leq 870 \pm 15K$

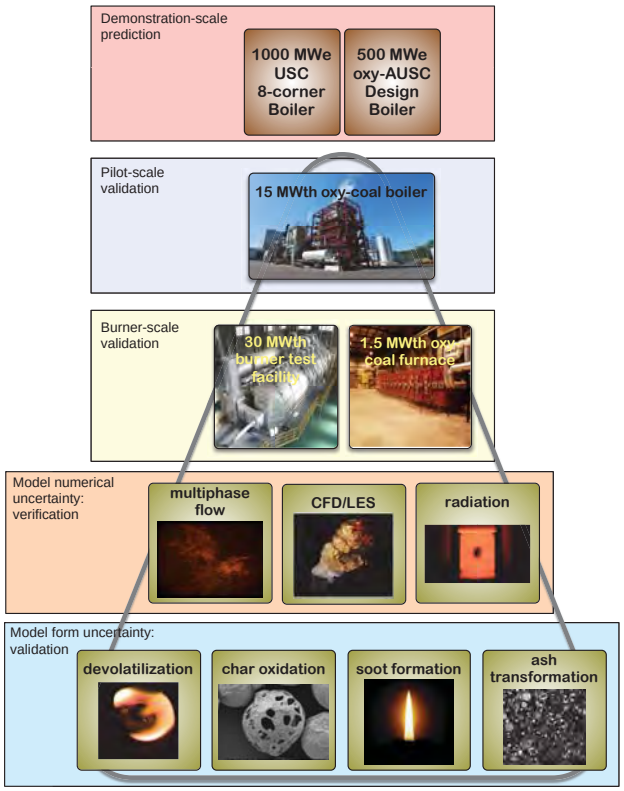

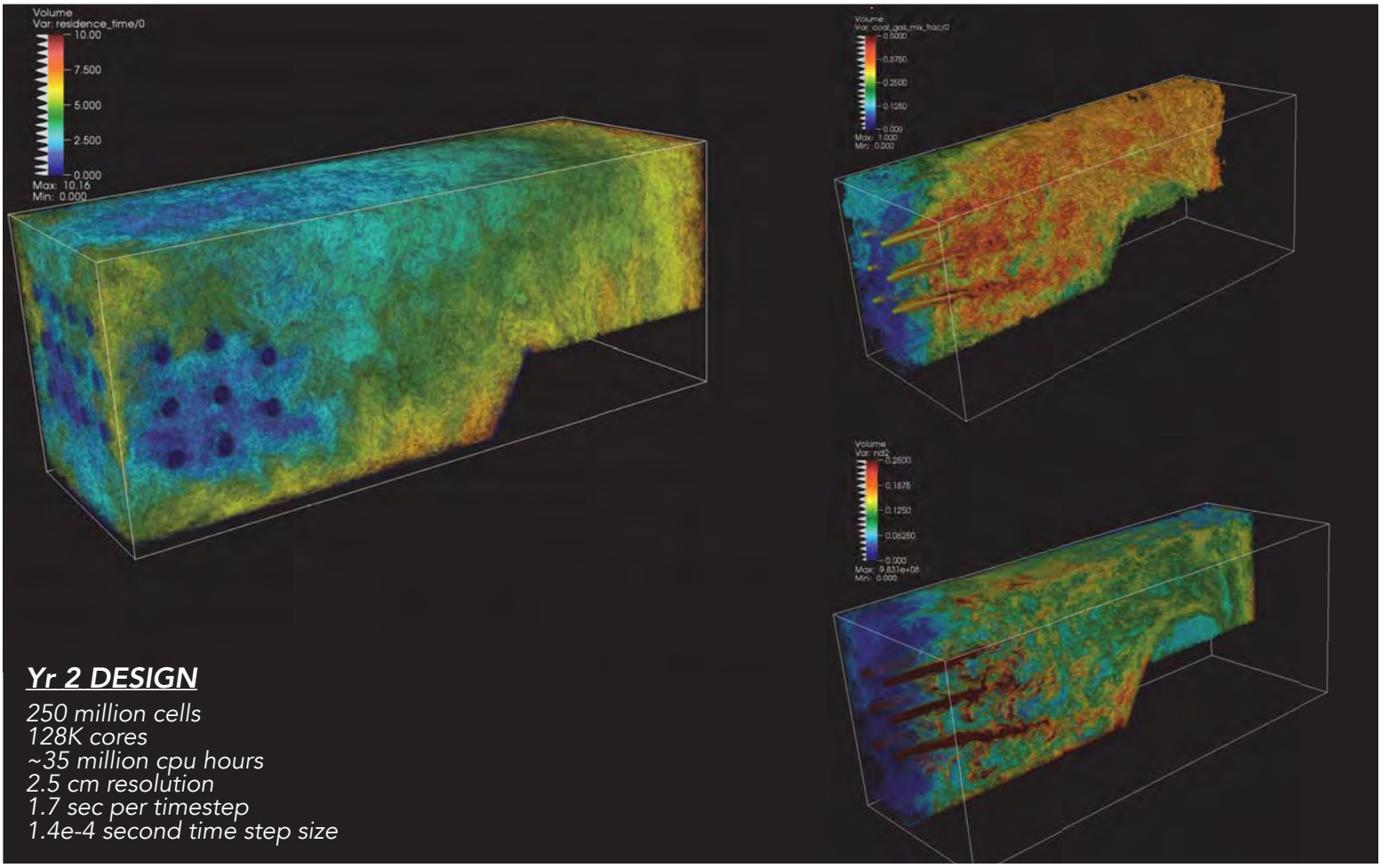

Yr 2 DESIGN

250 million cells
128K cores
~35 million cpu hours
2.5 cm resolution
1.7 sec per timestep
1.4e-4 second time step size

8-Corner Boiler

- *GE/Alstom power "flagship" boiler*
- *USC*
- *1090 MW ~ 1 million U.S. homes*
- *~430 inlets*
- *height: ~65m*
- *cross section: ~35m x 15m*
- *feed: 130 kg/s of coal (100 train cars of coal per day)*
- *O_2 from 1000 kg/s of air*
- *division panels, platens, super-heaters and re-heater tubing ~210 miles of piping*
- *walls, and tubing made of 11 different metals with varying thickness*

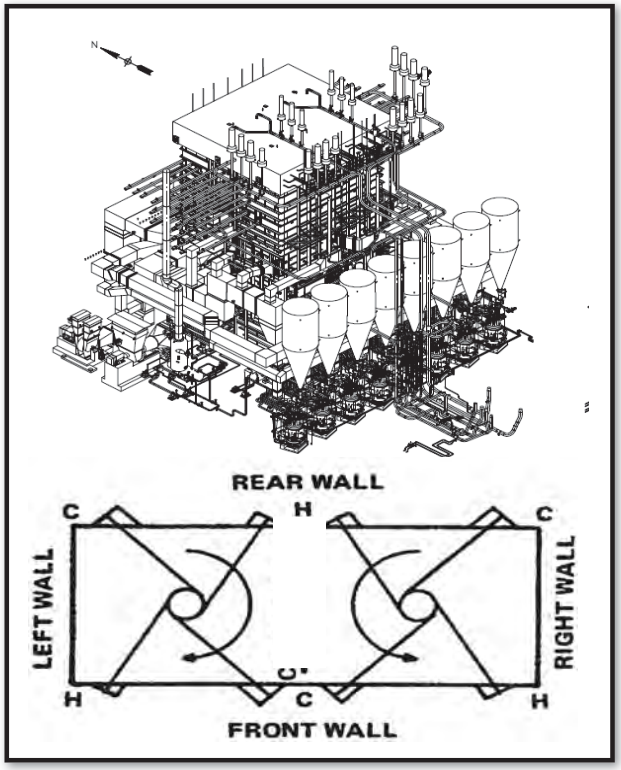

CARBON CAPTURE
MULTIDISCIPLINARY
SIMULATION CENTER

8 corner geometry

computational scale

- 2016 INCITE Award
  - 350 million core hours
  - 4 simulations
- each simulation:
  - 256,000 cores
  - 23days on MIRA
  - 8 days on TITAN
- resolution:
  - 2.5 cm^3
  - 2 billion cells

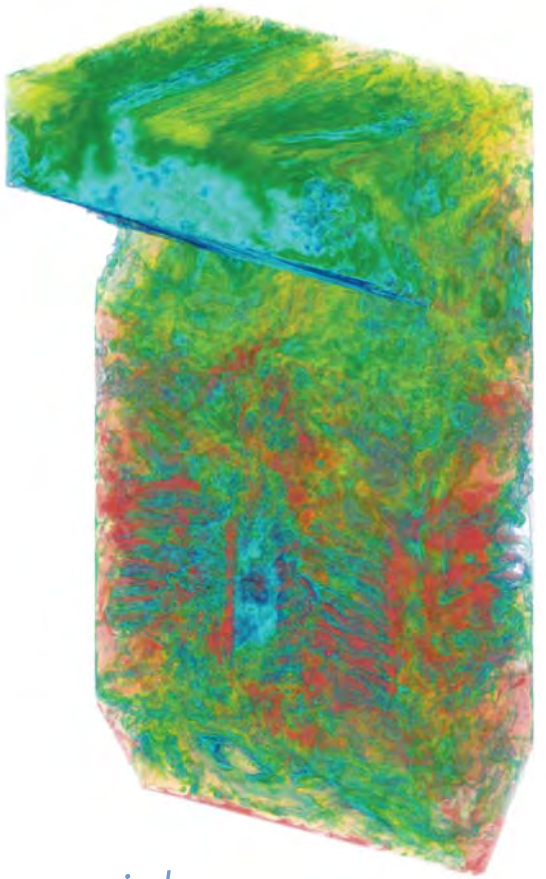

large particles

computational scale

- 2016 INCITE Award
  - 350 million core hours
  - 4 simulations
- each simulation:
  - 256,000 cores
  - 23days on MIRA
  - 8 days on TITAN
- resolution:
  - 2.5 cm^3
  - 2 billion cells

CCMT

Overview of Multiphase Flow Physics & Challenges at CCMT

S. Balachandar

UF UNIVERSITY of FLORIDA

Demonstration Experiment Configuration

From
David Frost

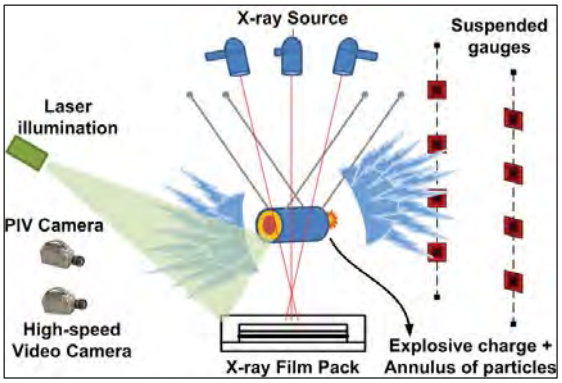

Sequence of Events

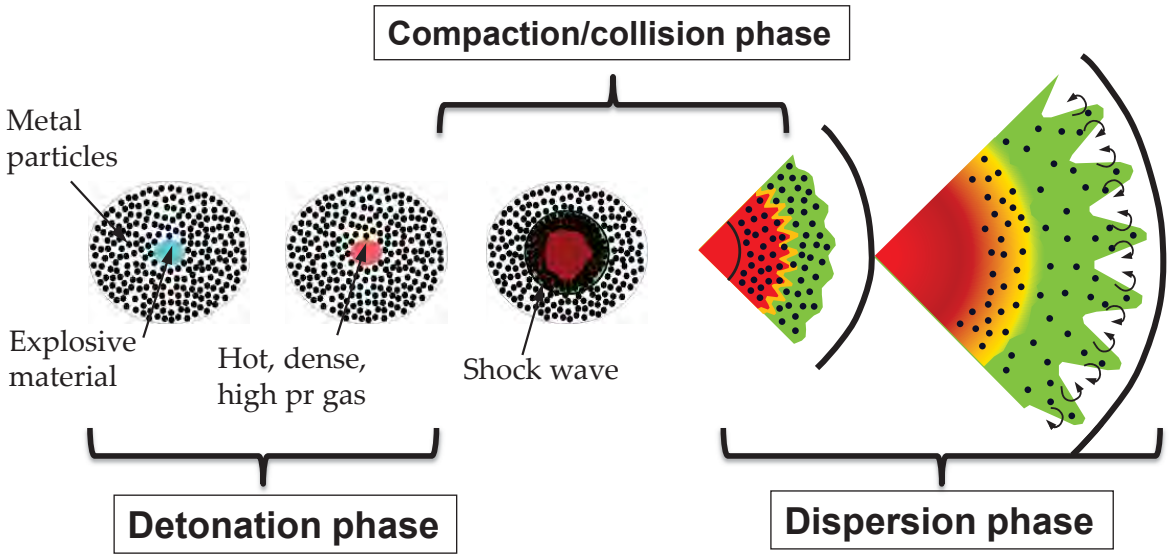

Physical Models – Sources of Errors & Uncertainties

T8:Deformation model

T4: Collision model
T5:Compaction model

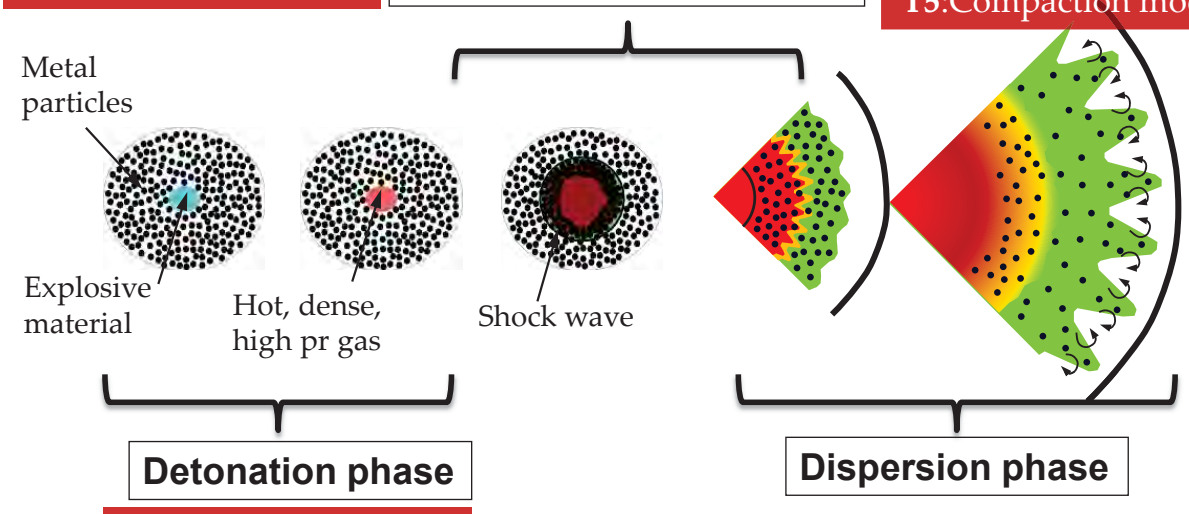

T1:Detonation model

T2: Multiphase turbulence model
T3:Thermodynamic & transport model
T6: Point particle force model
T7: Point particle heat transfer model

Multiscale Integration Strategy

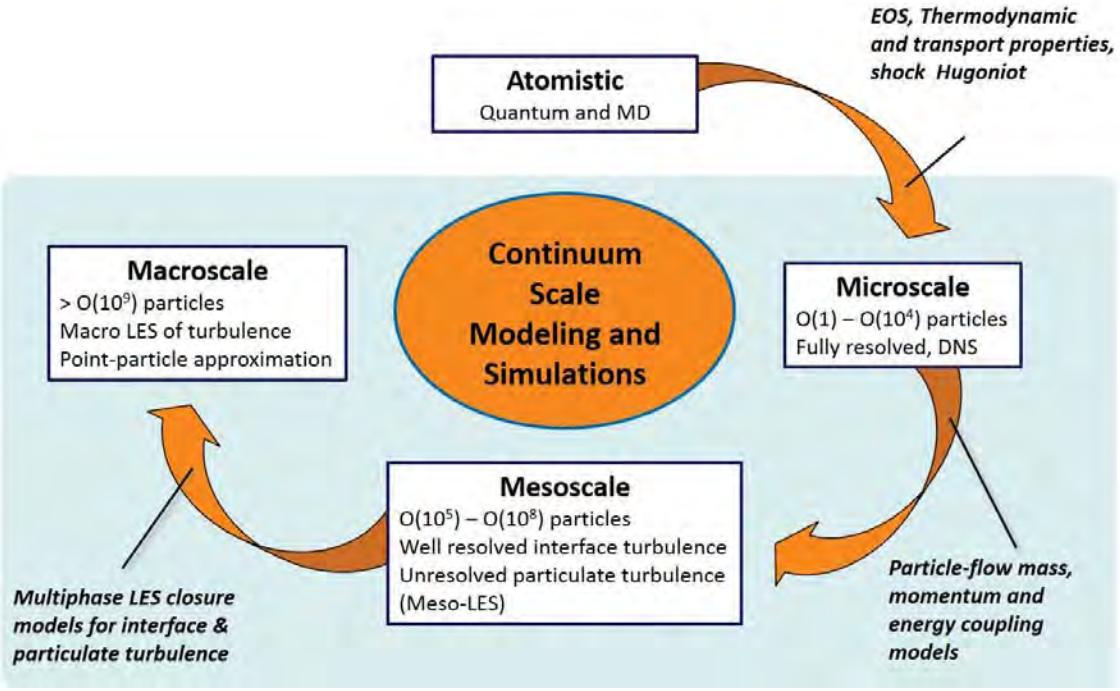

Uncertainty Budget – Overall Plan

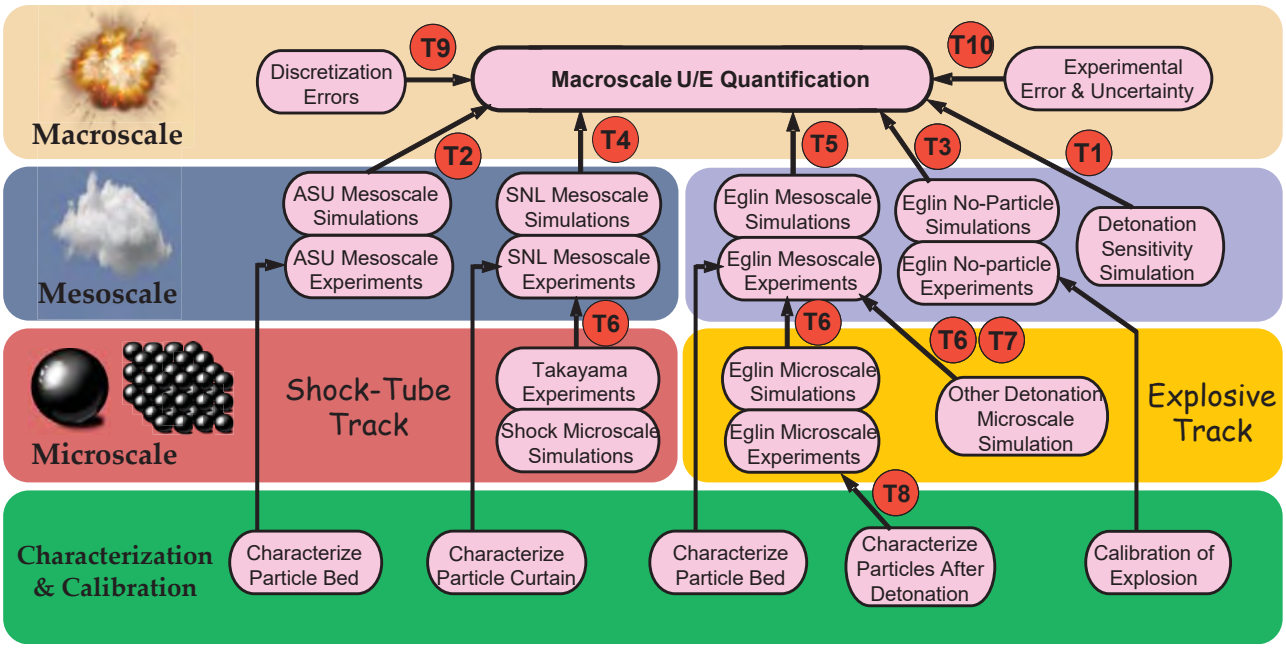

- Integrates all the center activities
- Uncertainty reduction through iterative improvement

T1 to T9: Influence on Macro Simulation

- Gas equations

$$\frac{\partial \mathbf{U}_g}{\partial t} = \mathbf{G}_{inv} + \boldsymbol{G}_{vis} + \boldsymbol{G}_{turb} + \mathbf{f}_{gp} + \mathbf{f}_{ext}$$

$$\mathbf{U}_g = \begin{Bmatrix} \alpha_g \rho_g \\ \alpha_g \rho_g \boldsymbol{u}_g \\ \alpha_g \rho_g E_g \end{Bmatrix}$$

Fluxes (T3)

Turbulence LES closure (T2)

Point particle coupling (T6, T7) (1)

Detonation source (T1)

- i^{th} Particle equations

$$\frac{d\mathbf{U}_{p,i}}{dt} = \mathbf{f}_{pp} - \mathbf{f}_{gp,i}$$

$$\mathbf{U}_p = \begin{Bmatrix} \rho_p \\ \rho_p \boldsymbol{u}_p \\ \rho_p E_p \end{Bmatrix}$$

(3) T9: Numerical errors

Collision & Compaction Model (T4, T5) (2)

Point-Particle Coupling Models

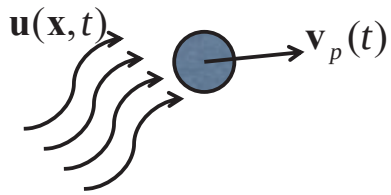

Commonly used models are based on:

- Uniform flow
- Quasi-steady flow
- Isolated particles
- Low Mach number, modest Reynolds number

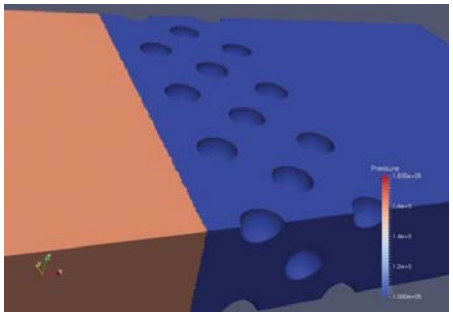

But the actual conditions are:

- Strong non-uniform
- Highly unsteady
- Very large Mach and Reynolds numbers
- Particle-Particle interaction
  - Fluid-mediated
  - Direct collision

Faxén Theorem (1924)

- Stokes flow (Re = 0 limit)

$$\text{Stokes Drag} = 3\pi\,\mu\,d\,u$$

Undisturbed flow at the particle

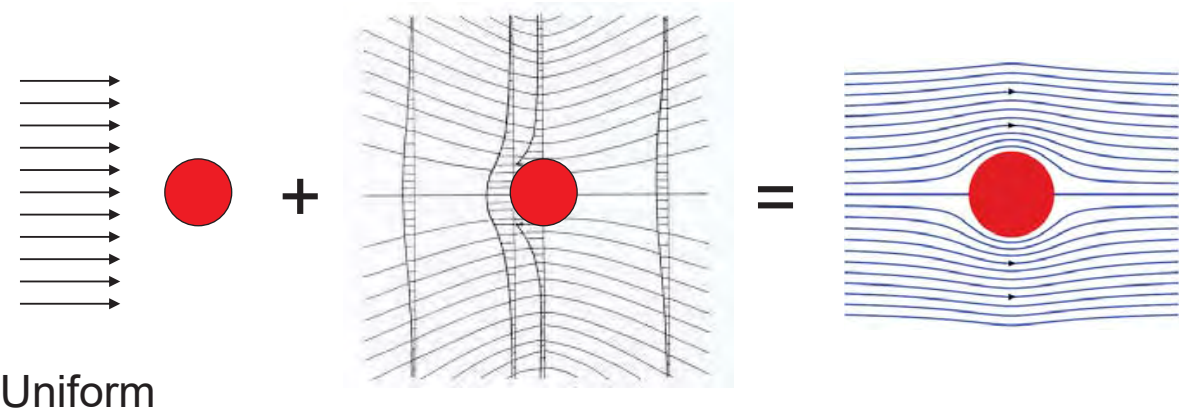

Uniform Undisturbed Ambient flow | Perturbation | Stokes flow

$$\text{Faxén Theorem:}\quad \text{Drag} = 3\pi\,\mu\,d\,\bar{u}^{S}$$

Undisturbed flow

Why We Need Faxén Theorem

- Shock-particle interaction

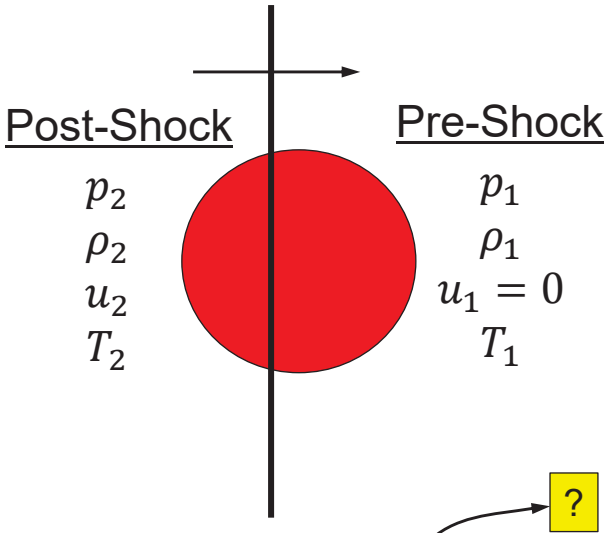

$$\text{drag} = 3\pi\,\mu\,d\,u$$

?

- Flow-mediated particle-particle interaction

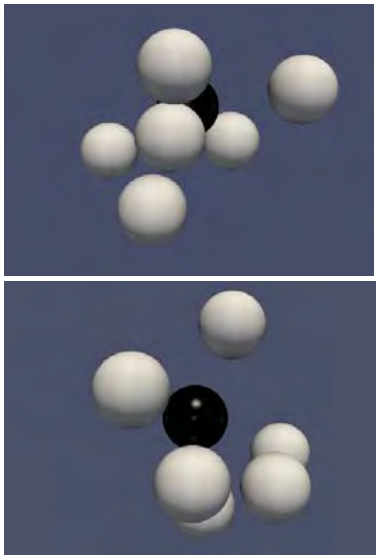

A generalized Faxén Theorem is needed at finite Re, Ma

Generalized Faxén Theorem

- Expressed in terms of undisturbed flow seen by the particle
  - Can be any spatially varying flow (shock thickness << d)
  - Can be rapidly varying flow
- Framework applies for force, heat transfer, pressure, volume, etc.

$$m_p \frac{d\mathbf{v}_p}{dt} = F_{gp,i} = \mathbb{V}\,\overline{\rho \frac{D\mathbf{u}}{Dt}}^{V} + 3\pi\mu d\,\overline{\mathbf{u}}^{S} + \mathbb{V}\int_{-\infty}^{t}\left(K_i + K_{vV}\right)\left(\frac{D\overline{\rho\mathbf{u}_r}^{S}}{Dt}\right)d\xi + \mathbb{V}\int_{-\infty}^{t} K_{vS}\left(\frac{D\overline{\rho\mathbf{u}}^{S}}{Dt}\right)d\xi$$

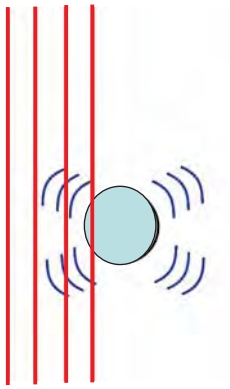

CCMT

Point-Particle Models for Single Particle

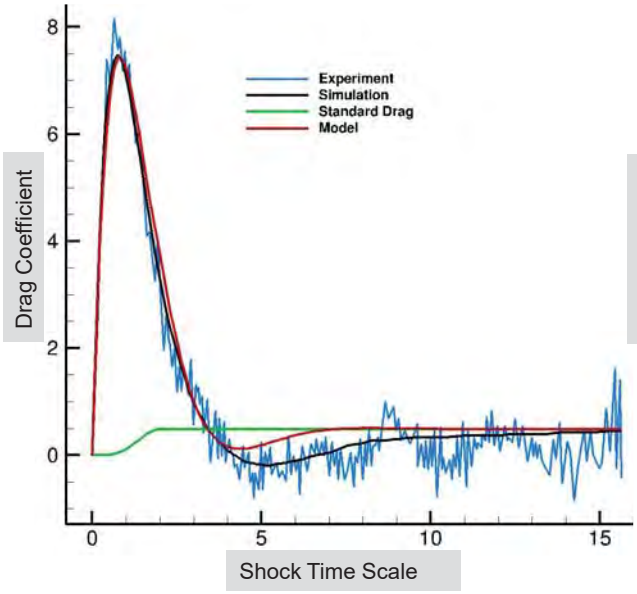

- Air Shock over a Particle ($M_s = 1.22$) (viscous simulation)

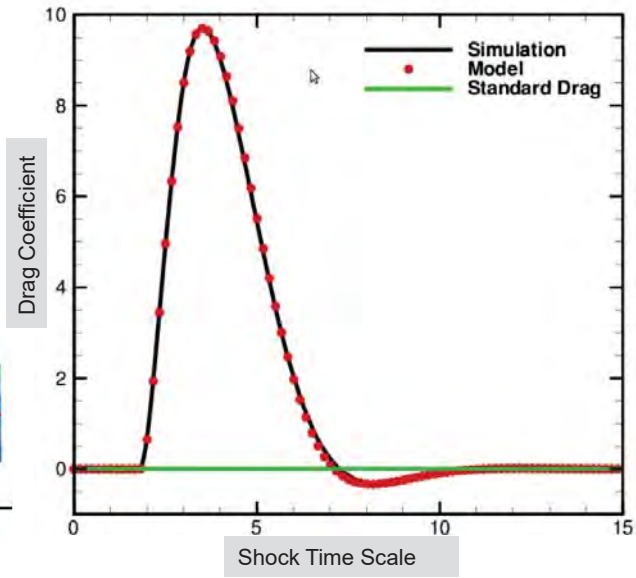

- Fan-Particle Interaction ($M_s = 1.22$) (inviscid simulation)

CCMT

Micro-Macro Integration Strategy

- The best single particle point-particle (PP) force model
- Beyond force model (single particle)
  - Particle pressure, volume and shape
  - Particle temperature
- Beyond single particle (PIEP Model)
  - Systematic inclusion of neighbor effects
    - Microscale velocity fluctuations
    - For inter-particle collisions, Reynolds stress closure, etc.

PIEP Model vs DNS (drag)

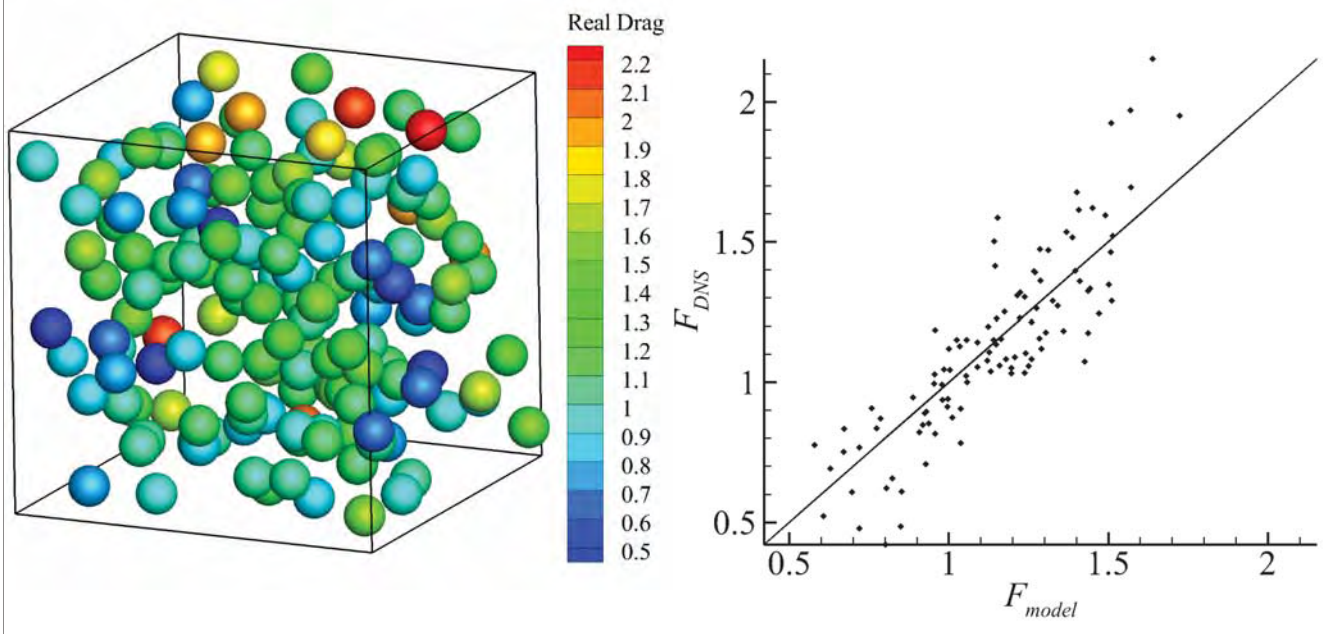

$$F_{model} = \langle F \rangle + F_{PIEP}$$

Shock-Induced Compressions and Deformation

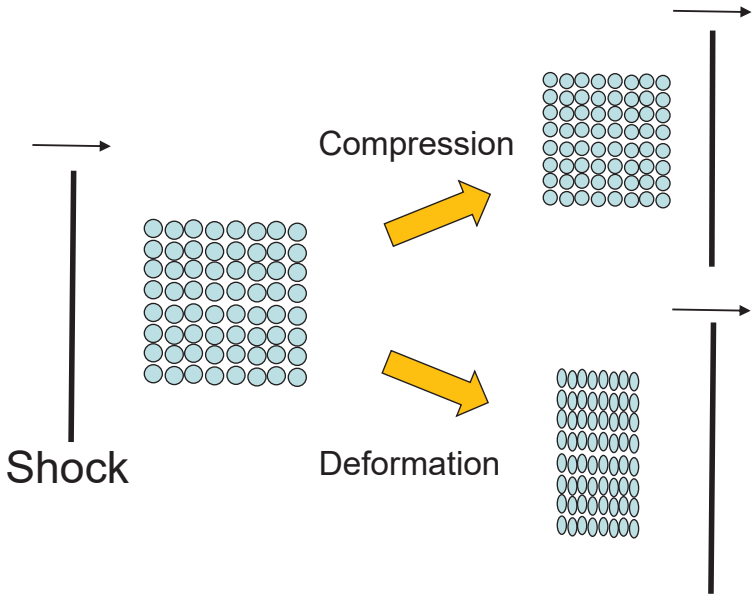

- Particle-particle-contact (PPC) drives a faster shock through the bed
- Gas-pressure and PPC-forces contribute to compression & deformation
- Both compression & deformation contribute to volume fraction evolution (or compaction)

Compaction Model

- Compaction equation (Dense limit: Baer-Nunziato model)

$$\frac{\partial \alpha_p}{\partial t} + \boldsymbol{u}_i \cdot \nabla \alpha_p = \frac{1}{\mu}(p_p - p_g)$$

- Volume fraction equation (Dilute incompressible limit)

$$\frac{\partial \alpha_p}{\partial t} + \nabla \cdot (\boldsymbol{u}_p \alpha_p) = 0$$

- Questions:
  - Can we obtain Compaction Equation from first principle?
  - How to smoothly transition from one limit to the other?
  - What is the appropriate interfacial velocity, $\boldsymbol{u}_i$?
  - How do we implement compaction in Euler-Lagrange framework?

Compaction Phase Model

- Compaction equation (Dense limit: Baer-Nunziato model)

$$\frac{\partial \alpha_p}{\partial t} + \boldsymbol{u}_i \cdot \nabla \alpha_p = \frac{1}{\mu}(p_p - p_g)$$

- Volume fraction equation (Dilute incompressible limit)

$$\frac{\partial \alpha_p}{\partial t} + \nabla \cdot (\boldsymbol{u}_p \alpha_p) = 0$$

- Pressure evolution equation (like BBO or MRG eqn):

$$\frac{dp_p}{dt} = -\frac{1}{\tilde{\mu}}(p_p - p_g) + \frac{dp_g}{dt} + \cdots$$

- Equations for particle volume or density can be derived
- Accounts for ONLY gas-induced compression effect

Pressure Evolution Equation

- 0.2 GPa NM shock over a deformable Al Particle

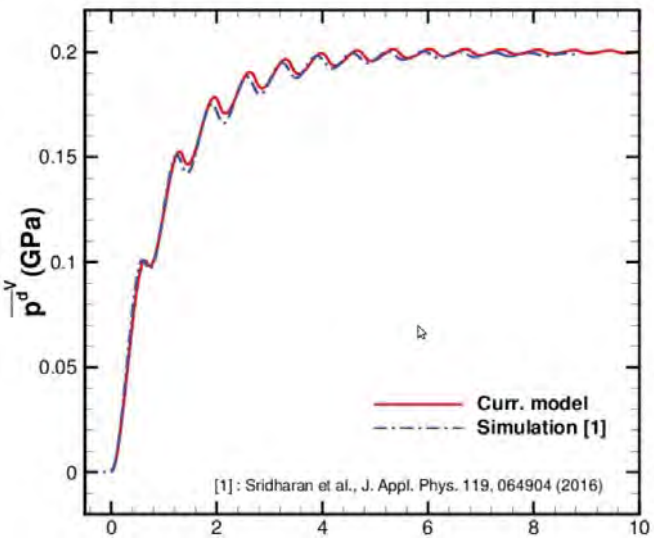

Mean pressure evolution

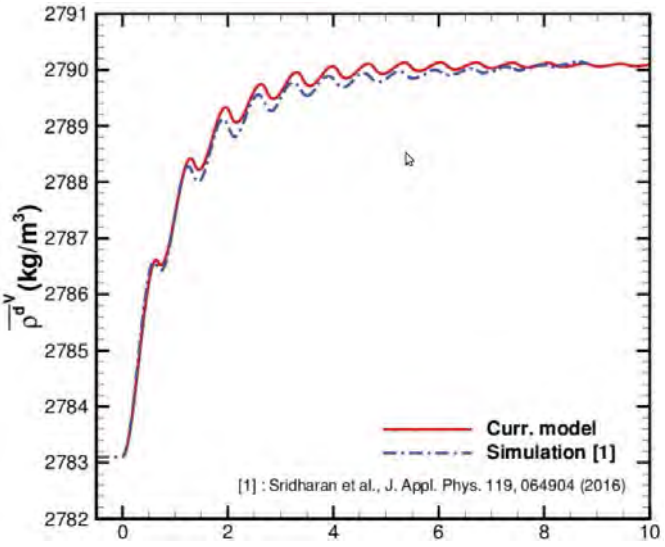

Particle density evolution

Need to include PPC-force and deformation effects

Euler-Lagrange Implementation of Compaction

- Key question: How do you allow shock waves faster than particle velocity to propagate by inter-particle contact?
- Answer: Introduce particle-contact pressure; Eigen-decompose the Lagrangian particle equations of motion

$$\frac{du_{p,i}}{dt} = -\frac{p_p}{2\alpha_p\rho_p}\left[\left.\frac{\partial\alpha_p}{\partial x}\right|_R + \left.\frac{\partial\alpha_p}{\partial x}\right|_L\right] + \frac{a_p}{2}\left[\left.\frac{\partial u_p}{\partial x}\right|_R - \left.\frac{\partial u_p}{\partial x}\right|_L\right]$$
$$-\frac{1}{2\rho_p}\left[\left.\frac{\partial p_p}{\partial x}\right|_R + \left.\frac{\partial p_p}{\partial x}\right|_L\right]$$
$$+ \text{gas forces}$$

- Particle pressure takes care of collisional forces as well

Euler-Lagrange Implementation of Compaction

- Key question: How do you allow shock waves faster than particle velocity to propagate by inter-particle contact?
- Answer: Introduce particle-contact pressure; Eigen-decompose the Lagrangian particle equations of motion

$$\frac{du_{p,i}}{dt} = -\frac{p_p}{2\alpha_p\rho_p}\left[\left.\frac{\partial\alpha_p}{\partial x}\right|_R + \left.\frac{\partial\alpha_p}{\partial x}\right|_L\right] + \frac{a_p}{2}\left[\left.\frac{\partial u_p}{\partial x}\right|_R - \left.\frac{\partial u_p}{\partial x}\right|_L\right]$$
$$-\frac{1}{2\rho_p}\left[\left.\frac{\partial p_p}{\partial x}\right|_R + \left.\frac{\partial p_p}{\partial x}\right|_L\right]$$
$$+ \text{gas forces}$$

- Particle-contact pressure takes care of collisional forces as well

Particle Diffusion

- Propagating particle fronts tend to diffuse
  - The diffusion coefficient can be quite large
  - Depends on volume fraction
- Diffusion is due to correlated velocity fluctuation
  - Collision-induced velocity fluctuation
  - Gas-mediated particle-particle interaction
  - Also due to number density fluctuation
- Can be modeled as diffusional velocity

$$-\mathfrak{D}\frac{\nabla\alpha_p}{\alpha_p}$$

where

$$\mathfrak{D} \sim 7.3\, d_p\, |\boldsymbol{u}_r|\, f(\alpha_p)$$

Segre *et al.*, Nature, 2001
Yu *et al.*, JGR, 2014

Numerical Challenges

- Rigorous convergence of Euler-Lagrange simulations is elusive
- Grid size = O(particle size) is problematic
- Grid to particle interpolation is not a problem
  - Higher order accuracy can be achieved
- Particle to grid injection or projection is problematic
  - Higher order accuracy is not easy
  - Is it a stochastic or a deterministic particle
- Particle number density naturally forms cell-to-cell fluctuation
  - How to obtain reasonable smooth particle volume fraction
  - How many particles per cell is optimal?
  - Dynamic load balancing

CCMT

Do you have any questions?

UF UNIVERSITY of FLORIDA

NNSA

UF UNIVERSITY of FLORIDA

Sources of Errors & Uncertainties

- T1: Detonation modeling
- T2: Multiphase turbulence modeling
- T3: Thermodynamics & transport properties

(2)
- T4: Particle-particle collision modeling
- T5: Compaction modeling (dense-to-dilute transition)

(1)
- T6: Point-particle force modeling
- T7: Point-particle thermal modeling

- T8: Particle deformation and other complex physics

(3)
- T9: Discretization and numerical approximation errors

- T10: Experimental and measurement errors & uncertainties

Advance state-of-the-art in multiphase numerics and point-particle models

Equations and Closures for Deformation and Flow of Continuous and Disperse Materials

Duan Z. Zhang

Fluid Dynamics and Solid Mechanics Group
T-3, Theoretical Division
Los Alamos National Laboratory
Los Alamos, New Mexico, USA

Oct. 6 - 7, 2016 , St. Petersburg, FL 33716

Transitions between Continuous and Disperse Phases

Transitions between disperse and continuous states are common phenomena. Often these transitions occur in the presence of other materials, such as air or water.

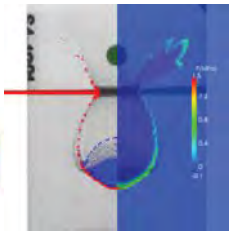

Disperse to continuous Continuous to disperse

How to build a numerical tool to model these transition process?

Two issues: model equations and numerical methods.

Zhang & Jayaraman, (2013), Int. J. Multiphase Flow. **56** pp 149 - 159.

Long et al. (2016) Comput. Methods Appl. Mech. Engrg. **300** pp 611-627.

Averaging Methods

Most of these processes are stochastic and multiscale. **Volume averaging** method are often used.

- What is the size of the representative volume element (RVE)? Does such a size exist?
- Does the RVE size change with time (because of e.g. crack growth or reduction of particles sizes due to burning)?
- How to related the closure quantities to physics at lower length and time scales? (A lot of "effective" quantities are used).

Ensemble averaging methods have been used to derive the averaged equations.

- No need for RVE.
- More directly related to physics at lower length and time scales. Less human interpretation of physics.

Ensemble Phase Average

For phase i, let C_i be the phase indicator function:

$$C_i(\mathbf{x}, t, R) = \begin{cases} 1 & \text{if } \mathbf{x} \in \text{phase } i \text{ in realization } R \\ 0 & \text{otherwise} \end{cases}$$

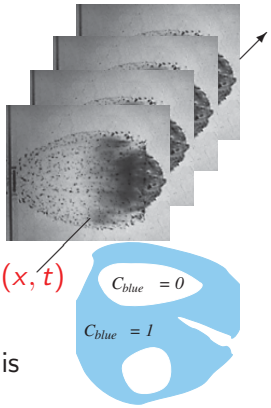

Let $\mathcal{P}$ be the probability measure for realizations.

$$\text{Volume fraction:} \quad \theta_i(\mathbf{x}, t) = \int C_i(\mathbf{x}, t) d\mathcal{P}$$

For any quantity q_i pertaining to phase i, its average is

$$\langle q_i \rangle(\mathbf{x}, t) = \frac{1}{\theta_i(\mathbf{x}, t)} \int q_i(\mathbf{x}, t, R) C_i(\mathbf{x}, t, R) d\mathcal{P}, \quad \nabla \langle q_i \rangle \neq \langle \nabla q_i \rangle$$

With this average we have the general transport equation:

$$\frac{\partial}{\partial t}(\theta_i \langle q_i \rangle) + \nabla \cdot (\theta_i \langle \mathbf{v}_i q_i \rangle) = \theta_i \left\langle \frac{\partial q_i}{\partial t} + \nabla \cdot (\mathbf{v}_i q_i) \right\rangle + \int \dot{C}_i q_i d\mathcal{P}.$$

Zhang, et al. (2007) Int. J. Multiphase Flow **33** pp 86 – 100

Kinematics

$$q_i = 1: \quad \frac{\partial \theta_i}{\partial t} + \nabla \cdot (\theta_i \langle \mathbf{v}_i \rangle) = \theta_i \langle \nabla \cdot \mathbf{v}_i \rangle + \int \dot{C}_i d\mathcal{P}.$$

$$q_i = \rho_i^0: \quad \frac{\partial}{\partial t}(\theta_i \langle \rho_i^0 \rangle) + \nabla \cdot (\theta_i \langle \mathbf{v}_i \rho_i^0 \rangle) = \int \dot{C}_i \rho_i^0 d\mathcal{P}.$$

Using $\widetilde{\mathbf{v}}_i = \langle \mathbf{v}_i \rangle + \langle \mathbf{v}_i' \rho_i^{0\prime} \rangle / \langle \rho_i^0 \rangle$, we define $d/dt = \partial/\partial t + \widetilde{\mathbf{v}}_i \cdot \nabla$.
Without phase change,

$$\frac{d\theta_i}{dt} = \theta_i(\langle \nabla \cdot \mathbf{v}_i \rangle - \nabla \cdot \langle \mathbf{v}_i \rangle) = -\int (\mathbf{v}_i - \langle \mathbf{v}_i \rangle) \cdot \nabla C_i d\mathcal{P},$$

$$\frac{d\langle \rho_i^0 \rangle}{dt} = -\langle \rho_i^0 \rangle \langle \nabla \cdot \mathbf{v}_i \rangle.$$

For a solid material, such as metal, let $\theta_v = 1 - \theta_s$ be the porosity

$$\nabla \cdot \langle \mathbf{v}_s \rangle = \underbrace{-\frac{1}{\rho_s^0}\frac{d\rho_s^0}{dt}}_{\text{elastic}} + \underbrace{\frac{1}{1-\theta_v}\frac{d\theta_v}{dt}}_{\text{plastic}}.$$

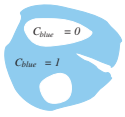

The elastic part causes density and pressure changes. The plastic part is associated with void growth — essential part of the tension plasticity (TEPLA) model for ductile metals.

Momentum Equation

With $q_i = \rho_i^0 \mathbf{v}_i$ in the transport equation, after some manipulations we have the momentum equation:

$$\theta_i \langle \rho_i^0 \rangle \frac{d\widetilde{\mathbf{u}}_i}{dt} = \theta_i \nabla \cdot \boldsymbol{\sigma}_{Ai} + \nabla \cdot \boxed{[\theta_i(\langle \boldsymbol{\sigma}_i \rangle - \boldsymbol{\sigma}_{Ai})]} + \nabla \cdot (\theta_i \boldsymbol{\sigma}_i^{Re}) + \mathbf{f}_i.$$

$$\mathbf{f}_i = -\int (\boldsymbol{\sigma}_i - \boldsymbol{\sigma}_{Ai}) \cdot \nabla C_i d\mathcal{P},$$

where $\mathbf{f}_i$ is the interfacial force, and $\boldsymbol{\sigma}_{Ai}$ is an auxiliary stress.
Different fields or authors use different auxiliary stresses:

- For Rayleigh-Taylor mixing, $\boldsymbol{\sigma}_{Ai} = \mathbf{0}$
- For soil mechanics or flows in porous media, $\boldsymbol{\sigma}_{Ai} = -\langle p_i \rangle \mathbf{I}$.
- For most disperse multiphase flows, $\boldsymbol{\sigma}_{Ai} = \langle \boldsymbol{\sigma}_{fluid} \rangle$.

All choices are legitimate as long as they are consistent in all the places. However, this consistence is never considered in current models.

Glimm et al., (1999) J. Fluid Mech. **378** pp 119-143.
Saltz et al., (2000) Phys. Fluid. **12**(10), pp 2461-2477.
Hassanizadeh & Gray, (1993) Water Resour. Res., **29**(10), 3389 – 3405.

Stresses in Solid

Let $\boldsymbol{\sigma}_{Ai} = -\langle p_i \rangle \mathbf{I}$. Using $\sigma_{sij} = \partial_k(r_i \sigma_{skj}) - r_i \partial_k \sigma_{skj}$, we have

$$\theta_s \langle \boldsymbol{\sigma}_s \rangle = \sum_{g=1}^{N} P_g(\mathbf{x}, t) \left\langle \int_{S_{gf}+S_{gg}} \mathbf{r}\mathbf{n} \cdot \boldsymbol{\sigma}_s dS \right\rangle_g + O(\ell^2/L^2),$$

S_{gf}: grain-fluid interface.
S_{gg}: the grain-grain contact surface. On S_{gg}, $\mathbf{n} \cdot \boldsymbol{\sigma}_s dS = \mathbf{f}_{gg'}$.

For isotropic grain structures, on S_{gf}, $\mathbf{n} \cdot \boldsymbol{\sigma}_s = -\langle p_f \rangle \mathbf{n}$,

$$\sum_{g=1}^{N} P_g(\mathbf{x}, t) \left\langle \int_{S_{gf}} \mathbf{r}\mathbf{n} dS \right\rangle_g = \alpha \theta_s \mathbf{I}.$$

$$\theta_s \langle \boldsymbol{\sigma}_s \rangle = \boxed{\sum_{g=1}^{N} P_g(\mathbf{x}, t) \sum_{g'=1}^{N} \mathbf{r}\mathbf{f}_{gg'}} - \alpha \theta_s \langle p_f \rangle \mathbf{I}.$$

Skeleton stress $\boldsymbol{\sigma}_{sk}$

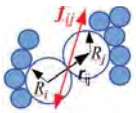

$\theta_i(\langle \boldsymbol{\sigma}_i \rangle - \boldsymbol{\sigma}_{Ai}) = \boldsymbol{\sigma}_{sk} + (1-\alpha)\theta_s \langle p_f \rangle \mathbf{I}$, — a common stress in soil mechanics.

Scale Separation and Closures

Small particle approximation

$$\mathbf{f}_c(\mathbf{x}, t) = -\int (\boldsymbol{\sigma}_c - \langle \boldsymbol{\sigma}_c \rangle) \cdot \nabla C_c d\mathcal{P},$$

$$\mathbf{f}_d(\mathbf{x}, t) = n(\mathbf{x}, t) \int (\langle \boldsymbol{\sigma}_c \rangle_1 - \langle \boldsymbol{\sigma}_c \rangle) \cdot \mathbf{n} dS,$$

$$\mathbf{T}_c(\mathbf{x}, t) = n \int \mathbf{n} \cdot (\langle \boldsymbol{\sigma}_c \rangle_1 - \langle \boldsymbol{\sigma}_c \rangle) \mathbf{n} dS,$$

$$\mathbf{f}_c = -\mathbf{f}_d + \nabla \cdot (\theta_d \mathbf{T}_c)$$

The small particle approximation provides an example of the capability or easiness of using the ensemble phase averaging method to connect macroscopic closures to interactions at lower scales.

For dilute Stokes flow:

$$\mathbf{f}_d = \frac{9}{2a^2} \mu_c (\widetilde{\mathbf{v}}_d - \widetilde{\mathbf{v}}_c) + \frac{3}{4} \mu_c \nabla^2 \widetilde{\mathbf{v}}_c$$

$$\mathbf{T}_c = 3\mu_c \dot{\varepsilon}_c, \quad \dot{\varepsilon}_c = \frac{\dot{\varepsilon}_m}{1 - \theta_d}$$

The **mixture** stress:

$$\langle \boldsymbol{\sigma}_c \rangle + \theta_d \mathbf{T} = 2\mu_c \left(1 + \frac{5}{2}\theta_d\right) \dot{\varepsilon}_m$$

For dilute potential flow:

$$\mathbf{f}_d = \frac{\langle \rho_c \rangle}{2} \left[\frac{d\widetilde{\mathbf{v}}_c}{dt} - \frac{d\widetilde{\mathbf{v}}_d}{dt} + \frac{\nabla \cdot (\theta_d \langle \mathbf{v}'_d \mathbf{v}'_d \rangle)}{\theta_d} \right]$$

$$\mathbf{T} \propto (\widetilde{\mathbf{v}}_d - \widetilde{\mathbf{v}}_c)^2.$$

Zhang and Prosperetti, (1994) J. Fluid Mech. **267**, pp 185
Irving and Kirkwood, (1950) J. Chem. Phys. 18, pp 817
Zhang and Prosperetti, (1997) Int. J. Multiphase Flow. **23**, pp 425
Zhang et. al (2002) PRE. **66**, pp 051806

Commonly Used Models

$$\theta_i \langle \rho_i^0 \rangle \frac{d\widetilde{\mathbf{u}}_i}{dt} = \theta_i \nabla \cdot \boldsymbol{\sigma}_{Ai} + \nabla \cdot [\theta_i (\langle \boldsymbol{\sigma}_i \rangle - \boldsymbol{\sigma}_{Ai})] + \nabla \cdot (\theta_i \boldsymbol{\sigma}_i^{Re}) + \mathbf{f}_i.$$

$$\mathbf{f}_i = -\int (\boldsymbol{\sigma}_i - \boldsymbol{\sigma}_{Ai}) \cdot \nabla C_i d\mathcal{P},$$

Theoretically $\boldsymbol{\sigma}_{Ai}$ needs to be consistent in these equations. In typical engineering calculation we use

$$\mathbf{f}_d = -\mathbf{f}_c = \text{drag} + \text{added mass force} + \text{Basset force}, \quad \mathbf{T} = \mathbf{0}$$

each of these forces are modeled separately, without consideration of $\boldsymbol{\sigma}_{Ai}$. The stress difference $\langle \boldsymbol{\sigma}_i \rangle - \boldsymbol{\sigma}_{Ai}$ is often ignored.

Unanswered questions:

- Are these forces independent? For instance, why added mass is independent of viscosity? How about buoyancy?
- How $\mathbf{T}$ affects the solution?
- $\boldsymbol{\sigma}_{Ai} = -p_c \mathbf{I}$ or $\langle \boldsymbol{\sigma}_c \rangle$? (e.g. viscous effects?)
- Should the effective or normal viscosity be used in $\langle \boldsymbol{\sigma}_c \rangle$?

Some Possible "Low Hanging Fruits"

Most, if not all, the models for phase interaction forces are for incompressible flows, in which any perturbation affects the entire domain.

- For many high speed cases we need to study effect of compressibility to drag, added mass, and Basset force.

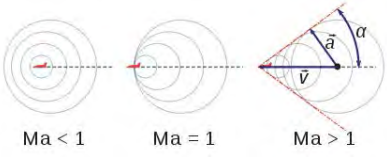

- To understand effective properties (e.g. effective viscosities) we can calculate closures, such as $\mathbf{T}$, by numerically simulating particle suspensions. Complex mesh may be needed around particles, or the material point method can be used.
- In fluid mixing problems, we need to investigate effects of pseudo turbulence at low particle Reynolds numbers introduced by random particle arrangements.

Concluding Remarks

- Currently models for multiphase flows, granular flows, porous media flows, and material failure and pulverization are developed independently. Relations among these models and their validities in more general situations need to be examined.
- The ensemble phase averaging method could be used to study the connections, validities and possible modifications of these models.
- The method provides a bridge between the macroscopic closures and the lower length and time scale physics.
- With today's computing technology (both numerical method and hardware), it is now feasible to calculate many of the closures from the ensemble phase averaging method.

3-Phase Model of Explosion Fields

A. Kuhl, J. Bell[1], V. Beckner[1] & D. Grote

Lawrence Livermore National Laboratory

CCMT-Multiphase Flow Deep Dive

October 6-7, 2016
St. Petersburg, FL

LLNL-PRES-703462
This work was performed under the auspices of the U.S. Department of Energy by Lawrence Livermore National Laboratory under Contract DE-AC52-07NA27344. Lawrence Livermore National Security, LLC

[1] Lawrence Berkeley Lab

Overview— *3 Phase Model*

GAS PHASE: compressible 2-phase Navier-Stokes equations

PARTICLE PHASE: dilute heterogeneous continuum model

FRAGMENT PHASE: Discrete Lagragian Particles (DLP) model

NUMERICAL METHODS

- Unsplit high-order Godunov schemes on uniform meshes
- Adaptive Mesh Refinement (AMR) to follow turbulent mixing
- Complete EOS based on tabulated Cheetah values

3-Phase Model

1. GAS PHASE: conservation laws of 2-phase compressible Navier-Stokes equations

Mass $\partial_t \rho + \nabla \cdot \rho \mathbf{u} = 0$

Momentum: $\partial_t \rho \mathbf{u} + \nabla \cdot \left(\rho \mathbf{u}\mathbf{u} + p\right) = \nabla \cdot 2\mu e_{ij} + \nabla \lambda e_{ii} - D_p - D_F$

Energy: $\partial_t \rho E + \nabla \cdot \left(\rho E \mathbf{u} + p\mathbf{u}\right) = \nabla \cdot \mathbf{u} 2\mu e_{ij} + \nabla \mathbf{u} \lambda e_{ii} + \nabla \cdot (\kappa / c_p)\nabla h - (Q_p + Q_F) - (D_p + D_F) \cdot \mathbf{u}$

Products: $\partial_t \rho Y_D + \nabla \cdot \left(\rho Y_D \mathbf{u}\right) = \nabla \cdot \left(\rho D_D \nabla Y_D\right)$

EOS: $p, T, \Gamma = f_i(\rho, u, Y_D)$ (Cheetah code)

Transport: $\mu, \lambda, \kappa, D = g_i(\rho, u, Y_D)$ & $Le = 1$ (Cheetah code)

Combustion:

(i) *Quadratic Model:* frozen Fuel & Air with Products at thermodynamic equilibrium $(300\ K < T < 4,000\ K)$

(ii) *Cheetah:* based on Thermodynamic equilibrium of Detonation Products-Air mixture $(300\ K < T < 15,000\ K)$

Quadratic Model

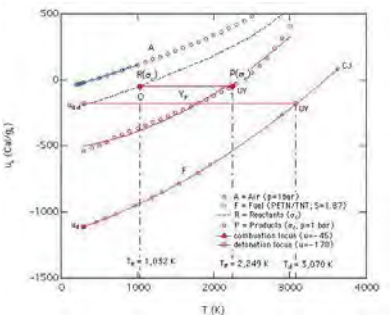

Equilibrium Model

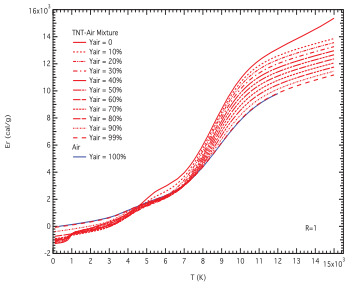

Numerical Method:

- Unsplit high-order Godunov method for hyperbolic terms (Bell, Colella, Trangenstein, 1989)
- 2nd order Runge-Kutta method for viscous terms

3-Phase Model—*continued*

2. PARTICLE PHASE—conservation laws of a dilute heterogeneous continuum

Mass: $\partial_t \sigma + \nabla \cdot \sigma \mathbf{v} = 0$

Momentum: $\partial_t \sigma \mathbf{v} + \nabla \cdot \sigma \mathbf{v}\mathbf{v} = D_p$

Energy: $\partial_t \sigma E_s + \nabla \cdot \sigma E_s \mathbf{v} = Q_p + D_p \cdot \mathbf{v}$

Drag: $D_p = (1/8)\pi d^2 \rho (\mathbf{u} - \mathbf{v})|\mathbf{u} - \mathbf{v}|C_D$

Heat Transfer: $Q_p = \pi d \mu C_p \Pr^{-1}(T - T_p)Nu$

where $C_D = 0.48 + 28\,\mathrm{Re}^{-0.85}$ & $Nu = 2 + 0.6\,\Pr^{1/3}\,\mathrm{Re}^{1/2}$

Carbon Particles in Detonation Products

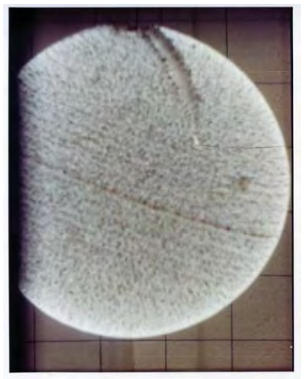

DND (Detonation Nano Diamond) Comp B

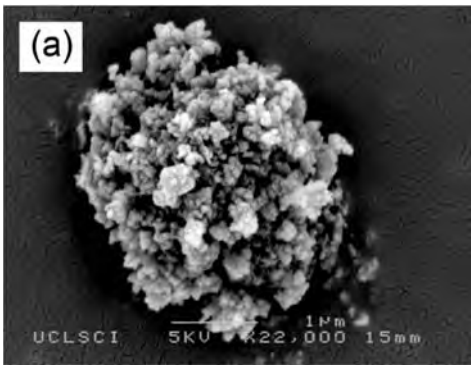

Numerical Method: 2nd order Godunov method for dilute particle systems (Collins et al., 1994)

3-Phase Model—*concluded*

3. FRAGMENT PHASE: *Discrete-Lagrangian-Particles (DLP) model*

Position: $\dot{\mathbf{x}}_i = \mathbf{v}_i(\mathbf{x}_i)$ for all particles i

Velocity: $m_i\dot{\mathbf{v}}_i = D_F(\mathbf{x}_i) + \mathbf{g}$ for all particles i

Energy: $m_i\dot{e}_i = Q_F(\mathbf{x}_i)$ for all particles i (where $e_i = c_s T_i$)

Mass: $\dot{m}_i = -\dot{s}_i(\mathbf{x}_i)$ for all particles i

Drag: $D_F = (1/8)\pi d^2 \rho(\mathbf{u}-\mathbf{v})|\mathbf{u}-\mathbf{v}|C_D$ where $C_D = 0.48 + 28\,\mathrm{Re}^{-0.85}$

Heat Transfer: $Q_F = \pi d \mu C_p \,\mathrm{Pr}^{-1}(T - T_p)Nu$ where $Nu = 2 + 0.6\,\mathrm{Pr}^{1/3}\,\mathrm{Re}^{1/2}$

Combustion Model: combustion of fragment wake with air

Air: $\partial_t \rho Y_A + \nabla\cdot(\rho Y_A \mathbf{u}) = -\alpha\dot{s}_i$

Fuel: $\partial_t \rho Y_F + \nabla\cdot(\rho Y_F \mathbf{u}) = -\dot{s}_i$

Products: $\partial_t \rho Y_P + \nabla\cdot(\rho Y_P \mathbf{u}) = (1+\alpha)\dot{s}_i$

Burning Rate: $\dot{s}_i = s d_i^2$

Numerical Method:

- 2nd order Runge-Kutta method
- fully (2-way) coupled to the fluid dynamics at all AMR levels

Numerical Methods

- High-order Godunov method for the hyperbolic terms: PPM (Colella & Glaz, 1985; Colella & Woodward, 1984; Bell, Colella & Trangenstein, 1989)
- A 2nd order explicit Rung-Kutta method for the viscous terms
- A 2nd order Godunov method for the particle phase (Collins et al., 1994)
- Adaptive Mesh Refinement (AMR) to resolve steep gradients (Bell, Berger, Saltzman, Welcome, 1994)

Conservation laws of compressible Navier-Stokes equations

Mass $\partial_t \rho + \nabla \cdot \rho \mathbf{u} = 0$

Momentum: $\partial_t \rho \mathbf{u} + \nabla \cdot \left(\rho \mathbf{u}\mathbf{u} + p\right) = \nabla \cdot 2\mu e_{ij} + \nabla \lambda e_{ii}$

Energy: $\partial_t \rho E_T + \nabla \cdot \left(\rho E_T \mathbf{u} + p\mathbf{u}\right) = \nabla \cdot \mathbf{u} 2\mu e_{ij} + \nabla \mathbf{u} \lambda e_{ii} + \nabla \cdot (\kappa / c_p) \nabla h$

Products: $\partial_t \rho Y_D + \nabla \cdot \left(\rho Y_D \mathbf{u}\right) = \nabla \cdot \left(\rho \tilde{D}_D \nabla Y_D\right)$

General Form: $\boxed{\partial_t U + \nabla \cdot W(U) = \nabla \cdot \mathcal{D}}$

where $U = \begin{Bmatrix} \rho \\ \rho \mathbf{u} \\ \rho E_T \\ \rho Y_D \end{Bmatrix}$ $W(U) = \begin{Bmatrix} \rho \mathbf{u} \\ \rho \mathbf{u}\mathbf{u} + p \\ \rho E_T \mathbf{u} + p\mathbf{u} \\ \rho Y_D \end{Bmatrix}$ $\mathcal{D} = \begin{Bmatrix} 0 \\ 2\mu e_{ij} + \lambda e_{ii} \\ \mathbf{u} 2\mu e_{ij} + \mathbf{u} \lambda e_{ii} + \kappa / c_p \nabla h \\ \rho \tilde{D}_D \nabla Y_D \end{Bmatrix}$

SOLUTION

Hyperbolic Terms: $\partial_t U + \nabla \cdot W(U) = 0$

Predictor: $\tilde{U}_{ijk}^{n+1} = U_{ijk}^{n} - \Delta t \left[W_{i+1/2,jk}^{n+1/2} - W_{i-1/2,jk}^{n+1/2}\right] / \Delta x - \Delta t \left[W_{i,j+1/2,k}^{n+1/2} - W_{i,j-1/2,k}^{n+1/2}\right] / \Delta y - \Delta t \left[W_{ij,k+1/2}^{n+1/2} - W_{ij,k-1/2}^{n+1/2}\right] / \Delta z$

Diffusion: $\partial_t U = \nabla \cdot \mathcal{D}$

Corrector: $U_{ijk}^{n+1} = \tilde{U}_{ijk}^{n+1} + \Delta t * \left(\nabla \cdot \mathcal{D}\right)_{ijk}^{n+1/2}$

Initial Conditions*

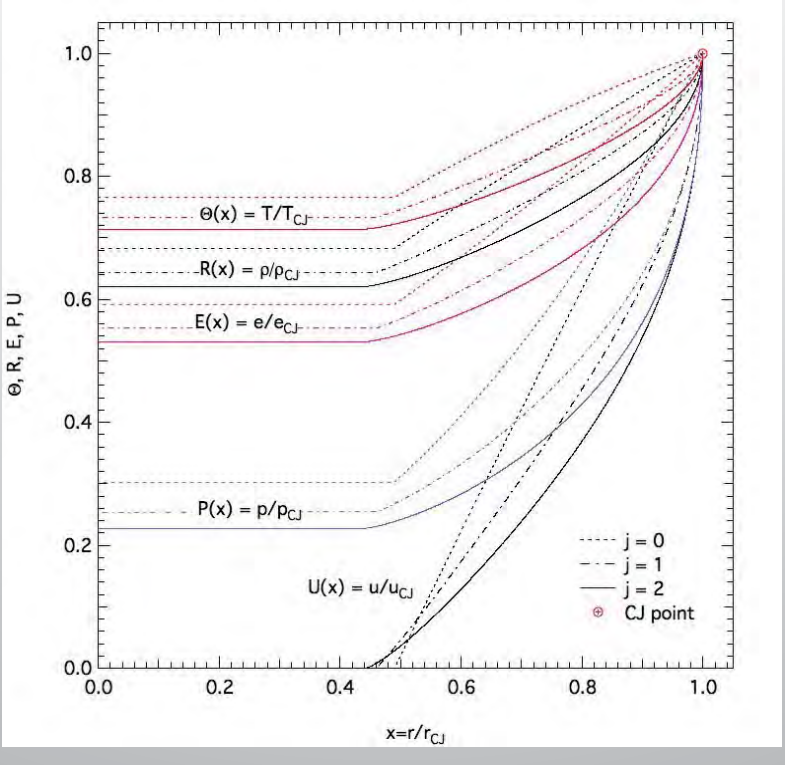

* A. Kuhl, On the Structure of Self-Similar Detonation Waves in TNT Charges, *Combustion, Explosion and Shock Waves*, 2015 **51** (1) pp. 72-79

Initial Conditions

TNT Charge Mass
* 1-g
* 1-kg
* 1-T

Mesh Size:
$\Delta r = 1 \mu m$

TABLE 2. CJ and UV states for TNT ($\rho_0 = 1.654\ g/cc$)

Variable	*CJ State*	*UV State*
$p(kbar)$	197.59759	90.13
$\rho(g/cm^3)$	2.1616	1.654
$e(cal/g)$*	1,352.46	1,064.8
$u(cal/g)$	273.16	-66.5
$T(K)$	3,237.875	2,866.9
$s(cal/g-K)$	1.58447	1.623
$\mathbf{u}_r(km/s)$	1.68595	0
$W(km/s)$	7.18	0
$a(km/s)$	5.4939	4.0593
$\Gamma = W_{CJ}/\mathbf{u}_{r,CJ} - 1$	3.2586	—

* $e \equiv u + 1{,}131$

Temperature Profiles at 2 μs

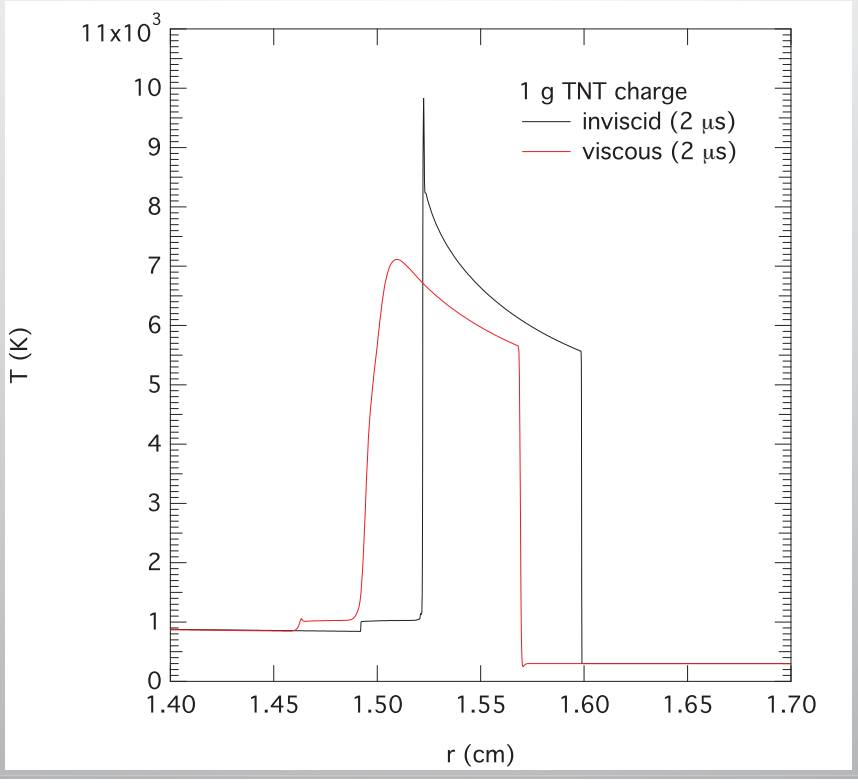

Temperature Profiles for 3 Models

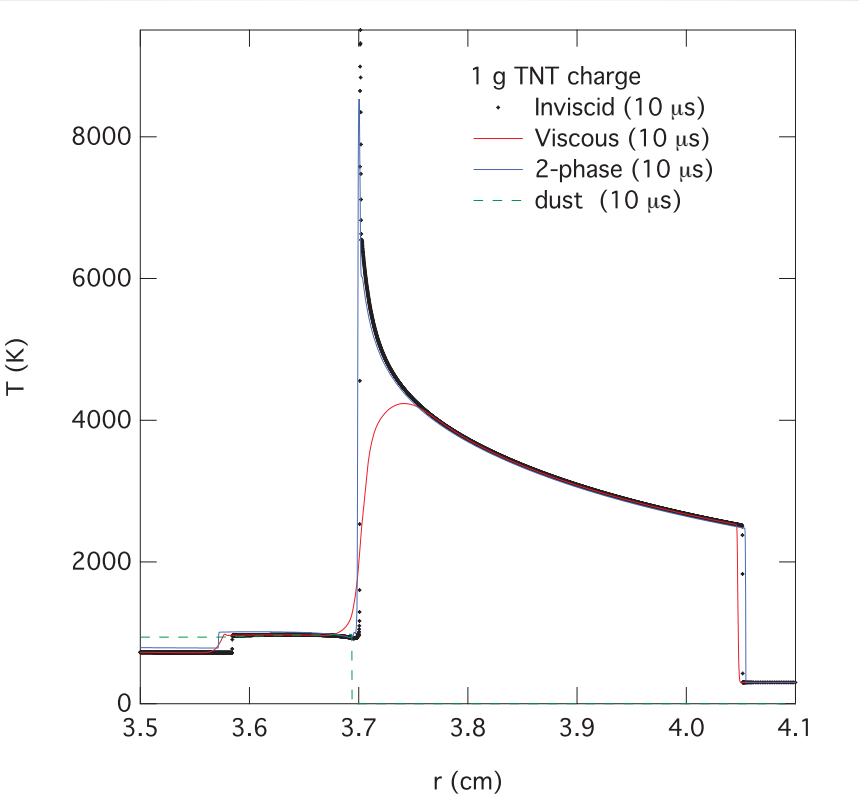

Density Field for the 3 Models

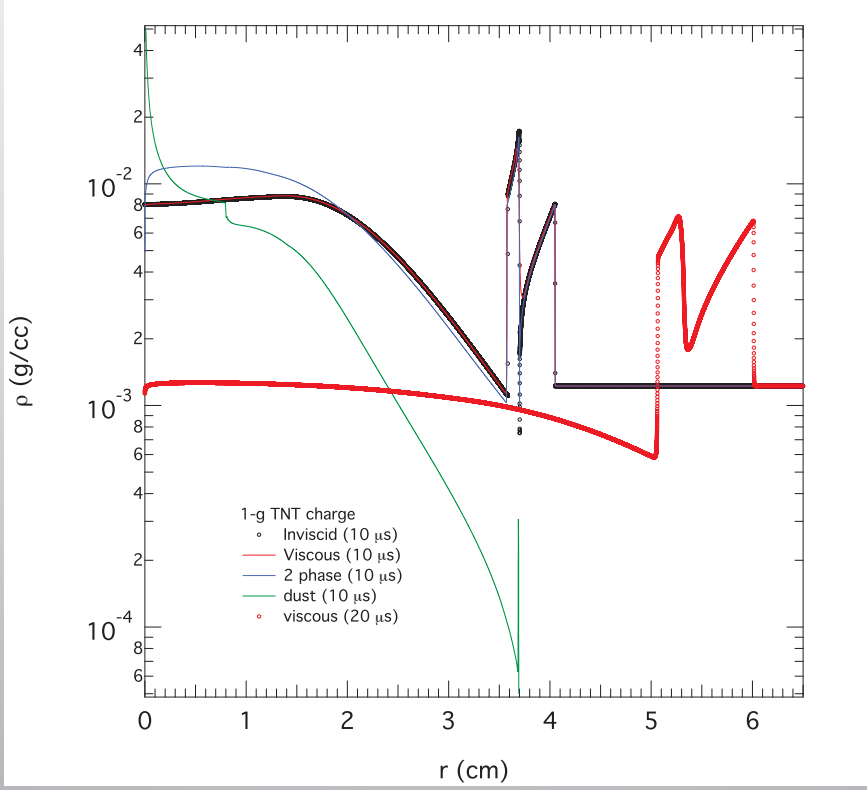

Pressure Field for the 3 Models

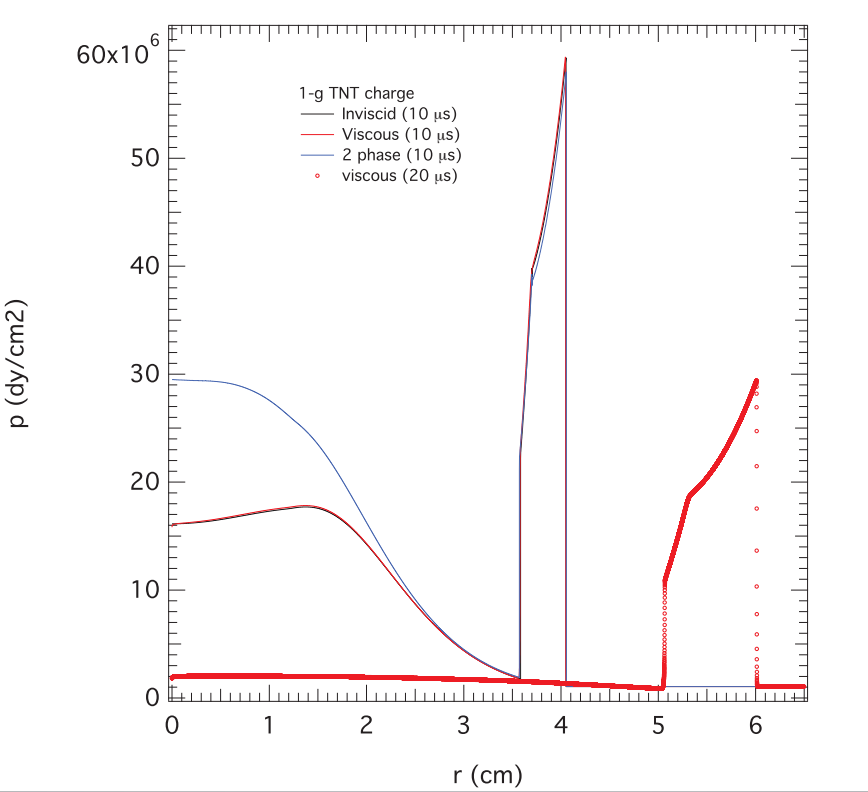

Velocity Field for the 3 Models

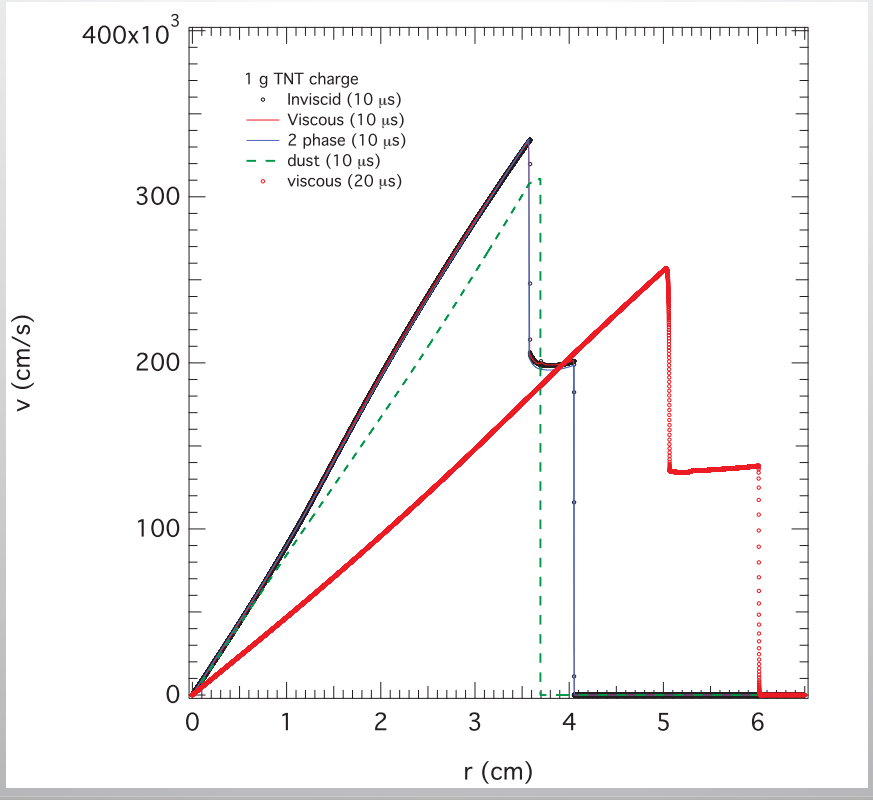

DP-Air Interface for the 3 Models

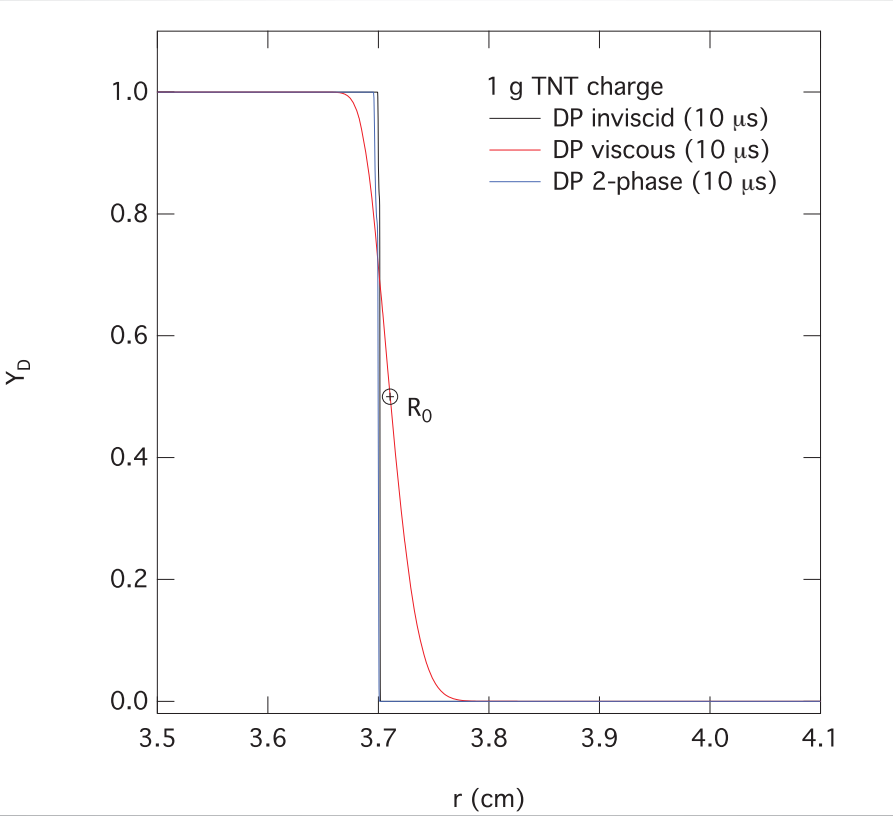

Mixing Layer Growth

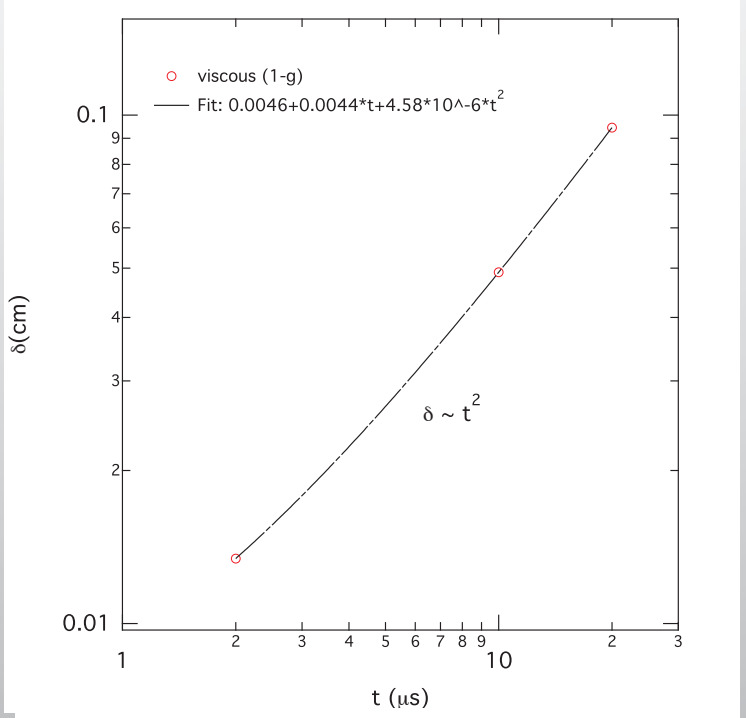

$\delta \sim t^2$: at $t = 0.63\,\mu s$

$N_\delta = 144\ cells\ \ for\ 1g\ \&\ N_\delta = 164\ cells\ \ for\ 1kg$

Similarity Solution

Conservation Law: $\partial_t \rho Y_D + \nabla \cdot (\rho Y_D \mathbf{u}) = \nabla \cdot (\rho D_D \nabla Y_D)$

Hyperbolic: $\partial_t \rho Y_D + \nabla \cdot (\rho Y_D \mathbf{u}) = 0$ $\quad (\rho \tilde{Y}_D)_i^{n+1} = (\rho Y_D)_i^n - \Delta t \left[F_{i+1/2}^{n+1/2} - F_{i-1/2}^{n+1/2} \right]$

Diffusion: $\partial_t (\rho Y_D) = \nabla (\rho D_D \nabla Y_D)$ $\quad (\rho Y_D)_i^{n+1} = (\rho \tilde{Y}_D)_i^{n+1} + \Delta t \left[\nabla \cdot \rho D_D \nabla Y_D \right]_i^{n+1/2}$

Model Law: $\partial_t Y_D = D_0 \nabla^2 Y_D$

Similarity Variable: $\xi = r / \delta$

Mixing Layer Width: $\delta \equiv Y_{10\%} - Y_{90\%} = at^2$

where inteface: $R_0(t) \equiv r @ Y_{50\%}$ is advected with the flow; $\xi_0 \equiv R_0 / \delta$

Similarity Solution: $\boxed{Y_D = f(\xi) = \frac{1}{2}\left[1 + erfc(\xi - \xi_0)\right]}$

Temperature Profiles—*viscous vs inviscid*

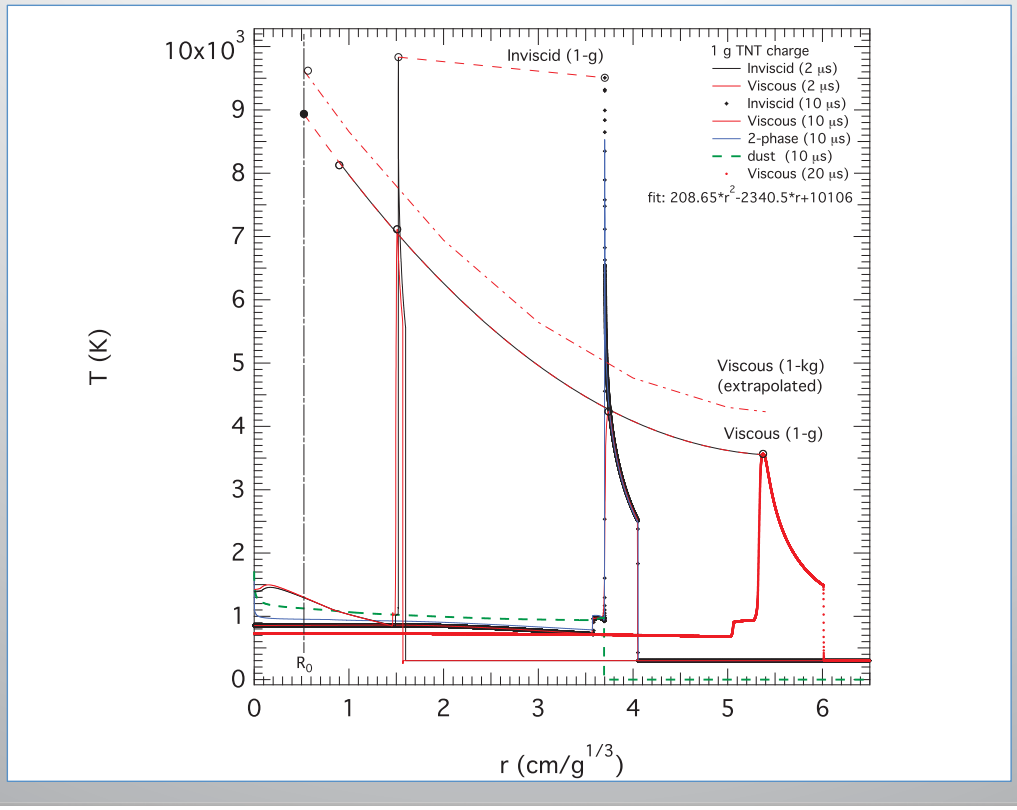

SUMMARY

1. **Mass Diffusivity**—causes DP to diffuse ~ t^2 ; the profile $Y_D(r)$—> $erfc(\xi - \xi_0)$

2. **Thermal Diffusivity**—causes heat to diffuse, lowering the temperature at the DP-air interface from 9 -10,000 K to 4 - 7,000 K

3. **Viscosity**—causes shocks to thicken to 100's of cells—but does not change the shock jump conditions

4. The **2-Phase Model** preserves the identity of the carbon particles (i.e., protects them from combustion with air) so that the evolution of the particle phase can be followed throughout the explosion field

5. **Scaling Laws:**
   - The diffusion layer δ grows as t^2 —independent of the explosion scale
   - The inviscid blast wave time and length scale as $t / kg^{1/3}$ and $r / kg^{1/3}$
   - The diffusion effects in the blast wave scale with *Re* & *Pe* numbers
   - As the explosion scale gets larger, the diffusion effects decrease

CONCLUSIONS

1. The **Complete Model** in 1D spherical coordinates (page 6) is recommended:
   - Inviscid terms — accurately model the underlying compressible flow
   - Viscous terms — diffuse the species and temperature
   - 2-phase terms — follow the carbon particle dynamics

2. The **Complete Model** must be used at early times ($t \le 20\ \mu s / kg^{1/3}$) to capture all physical effects.

3. This 1D solution can be used to initialize the 3D AMR multi-phase code to compute the evolution of turbulent mixing and combustion in the fireball.

Temperature field showing transition to turbulent combustion at 20 μs/g$^{1/3}$

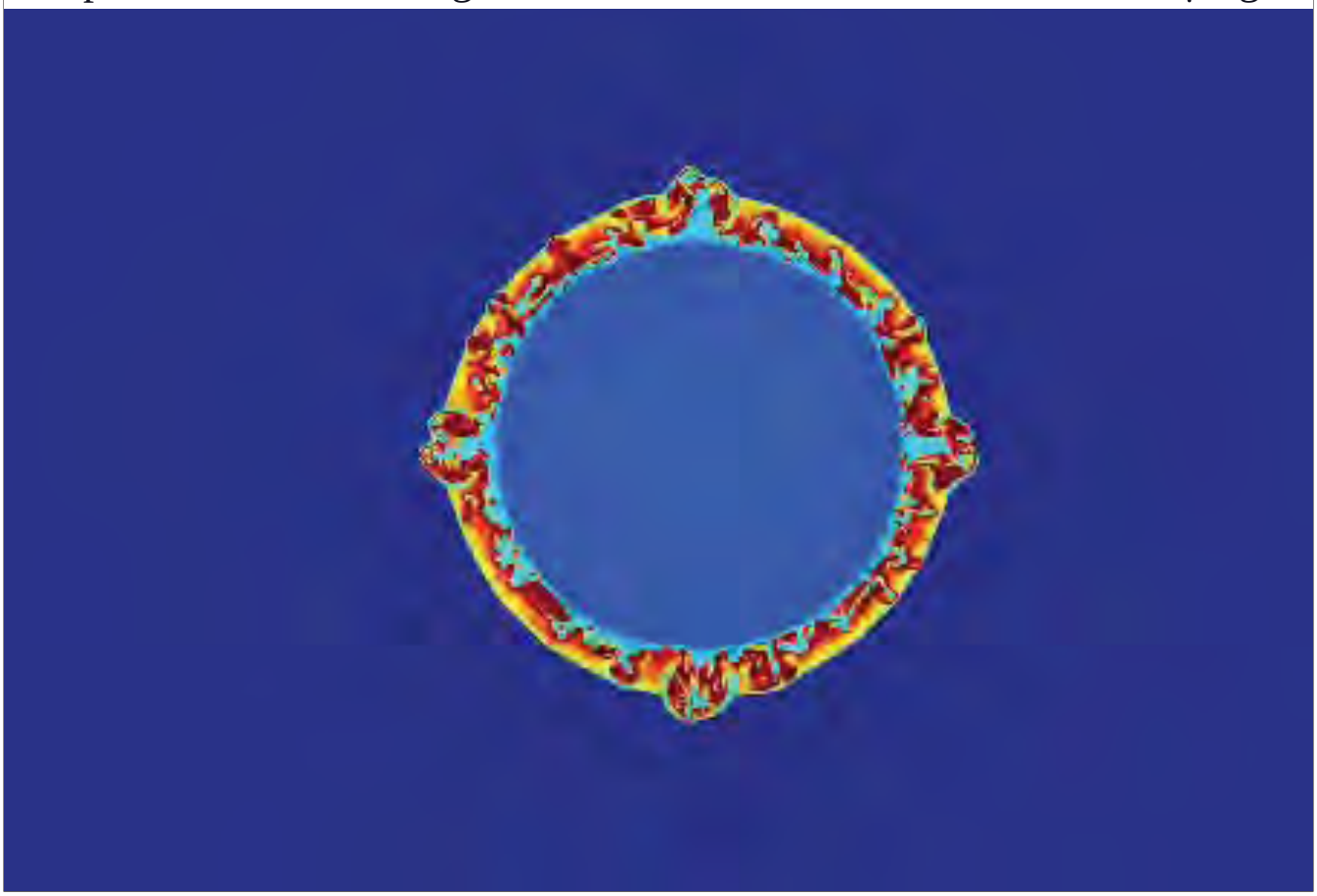

Lawrence Livermore National Laboratory

Physical Mechanisms of Optical Emissions

$t = 0$
8-lb LX-10 charge

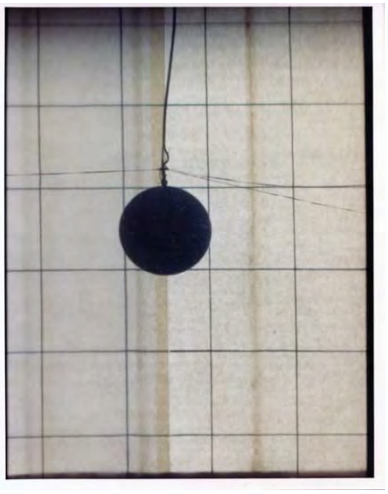

$t = 2.47\ \mu s$
air-shock emissions

$t = 49.4\ \mu s$
DP gas emissions

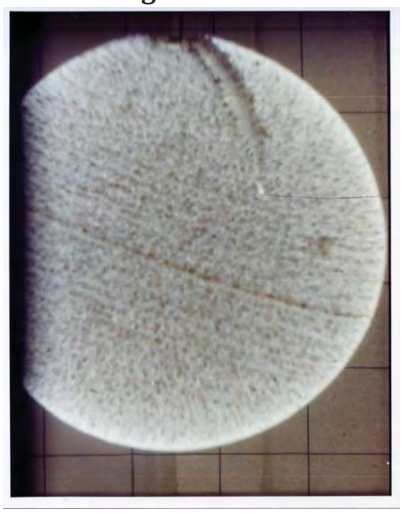

Sectioned View of LX-10 Fireball @ 49 μs

Exceptional service in the national interest

Sandia National Laboratories

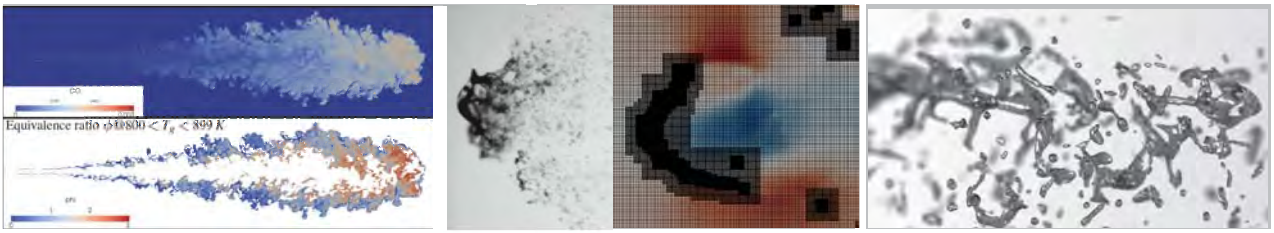

Multiphase Flow Simulation Strategies at the CRF

Marco Arienti, F. Doisneau, J. Oefelein

Sandia National Laboratories, California

U.S. DEPARTMENT OF ENERGY | NNSA

Sandia National Laboratories is a multi-program laboratory managed and operated by Sandia Corporation, a wholly owned subsidiary of Lockheed Martin Corporation, for the U.S. Department of Energy's National Nuclear Security Administration under contract DE-AC04-94AL85000. SAND NO. 2011-XXXXP

Presentation layout

Sandia National Laboratories

- From injector to spray flames
  - One-fluid formulation with interface capturing
  - Demonstration: Spray A
  - A new Eulerian Multi-Fluid approach for dense sprays
  - Continuation: spray flame auto-ignition
- Molten metal and drop fragmentation
  - *A priori* test for molten aluminum in crossflow
  - The opportunity of new experimental diagnostics/data

FROM INJECTOR TO SPRAY FLAMES

Spray A and the Engine Combustion Network (ECN)

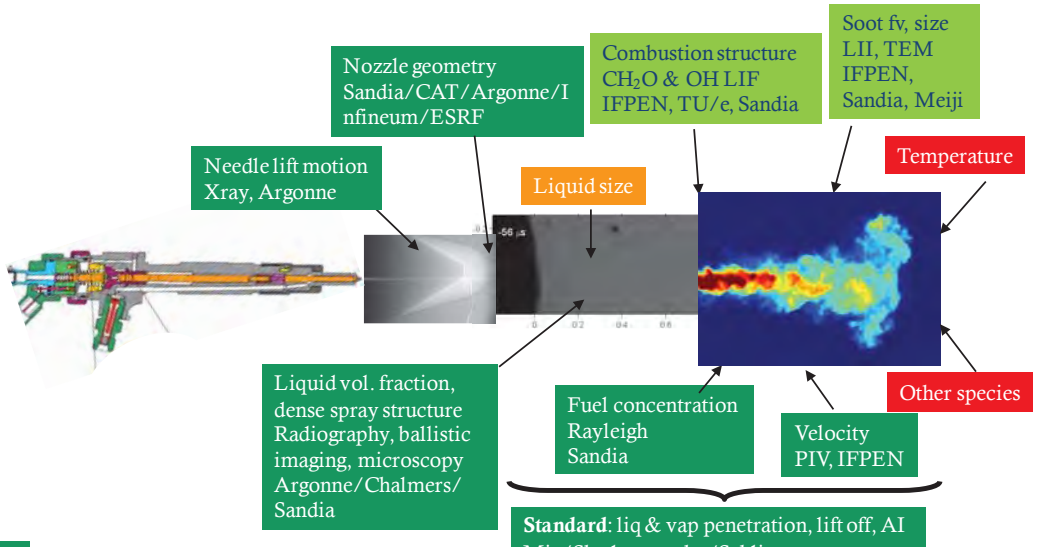

Parallel multiphase solver (CLSVOF) + adaptive mesh refinement for primary atomization

Sandia National Laboratories

Florida State University

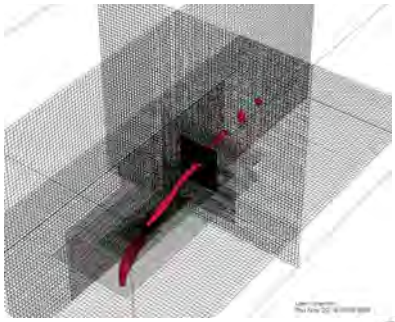

Block-structured adaptive mesh refinement (John Bell)

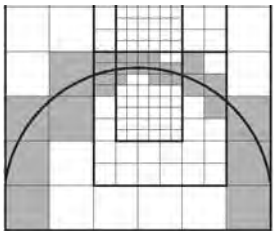

$$\frac{\partial(\mathbf{u}\rho)}{\partial t} + \nabla\cdot(\mathbf{u}\otimes\mathbf{u}\rho + pI) = \nabla\cdot\tau + \rho\mathbf{g} - \sum_{m=1}^{M}\gamma_m\kappa_m\nabla H(\phi_m)$$

Solved in the variables:

$(\rho, \rho\mathbf{u}, E)^m$, F^m, $\mathbf{x}_c{}^m$, ϕ^m

for each phase/material:

$m = 1 \ldots M$

$$\rho = \sum_{m=1}^{M}\rho_m H(\phi_m) \quad H(\phi) = \begin{cases} 1 & \phi \geq 0 \\ 0 & \text{otherwise} \end{cases}$$

$$\tau = \sum_{m=1}^{M}\tau_m H(\phi_m) \quad \tau_m = 2\mu_m\left(D - \frac{\mathrm{TR}(D)\mathcal{I}}{3}\right) \quad D = \frac{\nabla\mathbf{u} + \nabla\mathbf{u}^T}{2}$$

New feature: The moment of fluid (MOF)[1] method

Sandia National Laboratories

- MOF tracks volume fractions through advection, but also uses the centroid of a material region $\mathbf{x}_{ref} = \mathbf{x}_c{}^m$ in determining the orientation of the interface

$$(\mathbf{n}, b) = \arg\min_{|F_{ref} - F_{act}(\mathbf{n},b)|=0} ||\mathbf{x}_{ref} - \mathbf{x}_{act}(\mathbf{n}, b)||_2$$

$$\mathbf{n}\cdot(\mathbf{x} - \mathbf{x}_{i,j}) + b = 0 \qquad \mathbf{n} = \begin{pmatrix} sin(\Phi)cos(\Theta) \\ sin(\Phi)sin(\Theta) \\ cos(\Phi) \end{pmatrix}$$

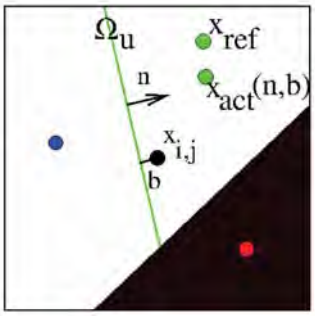

- The interface is chosen as the piece-wise linear reconstruction that contains the volume fraction and **minimizes the variation** in centroid position

[1] V. Dyadechko M. Shashkov LA-UR-05-7571 (2007)

New feature:
Moving boundaries with non-conformal mesh

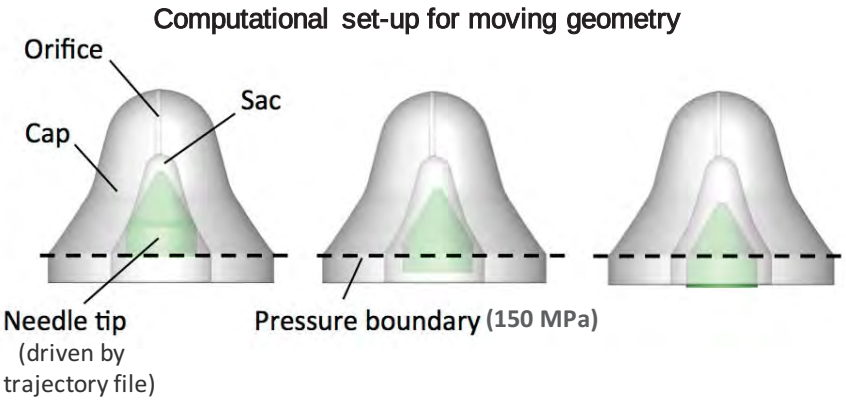

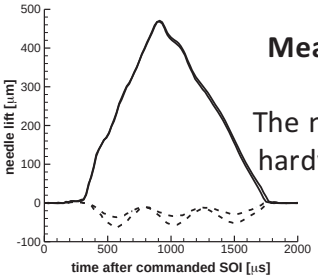

Measured needle's trajectory:
The needle' wobble is hardware-dependent

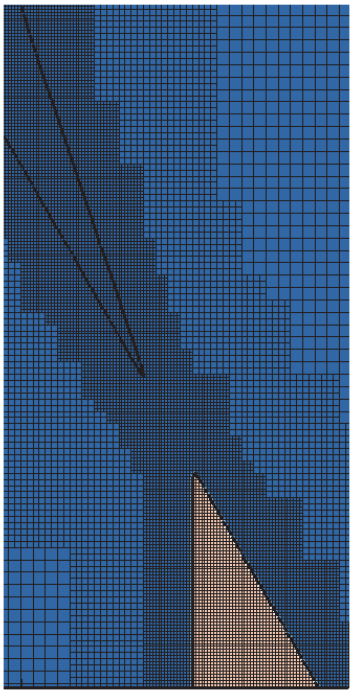

Open needle: jet tip structure

No "mushroom" jet tip because of asymmetric internal flow

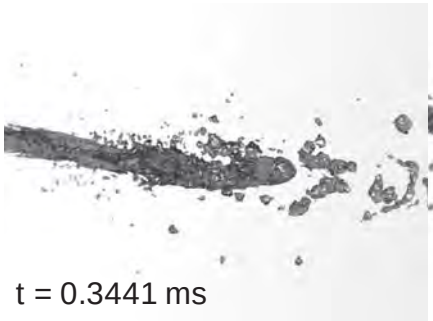
t = 0.3441 ms

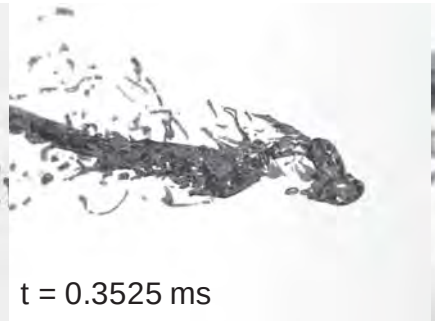
t = 0.3525 ms

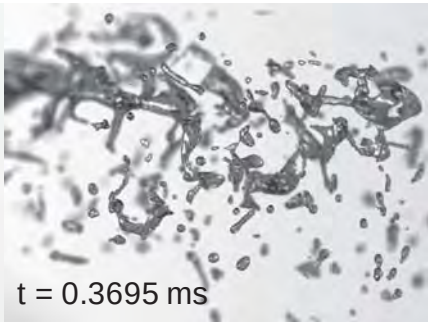
t = 0.3695 ms


t = 0.3710 ms

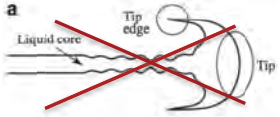

Δx = 3.32 μm; 20 x 20 x 170 d_0

Challenge: grid convergence

Same simulation repeated at twice the grid resolution: is the size distribution converging?

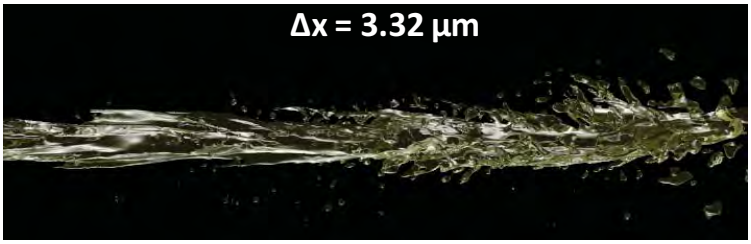

Snapshots of the jet at t_{ASOI} = 6 µs

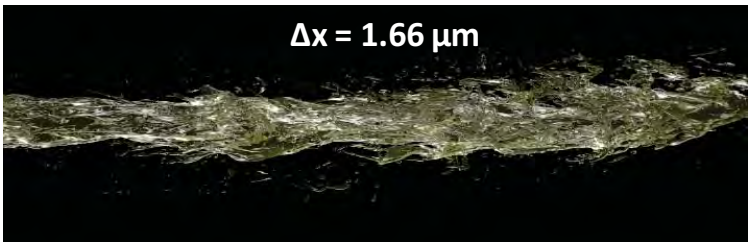

Equivalent diameter distribution

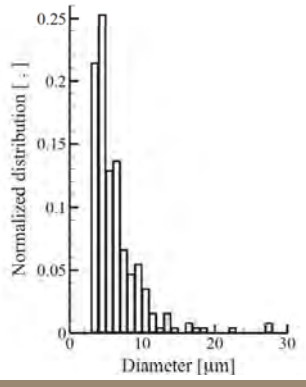

The limits of the DNS framework

Inherently under-resolved + very high cost for a very small time-step

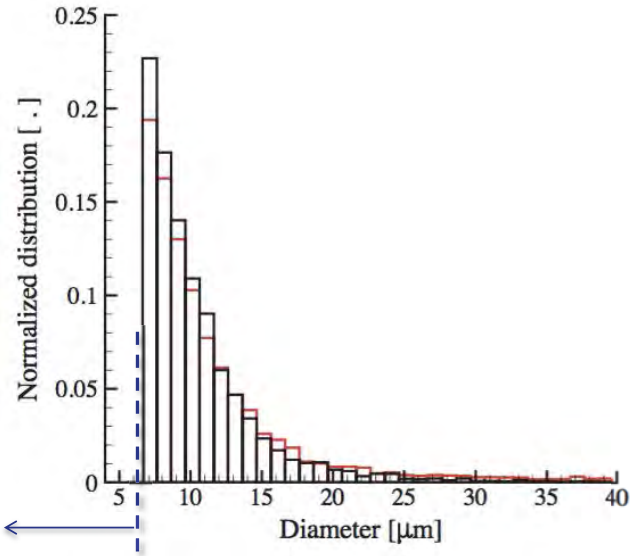

Truncated for $D_p < 2\Delta x$

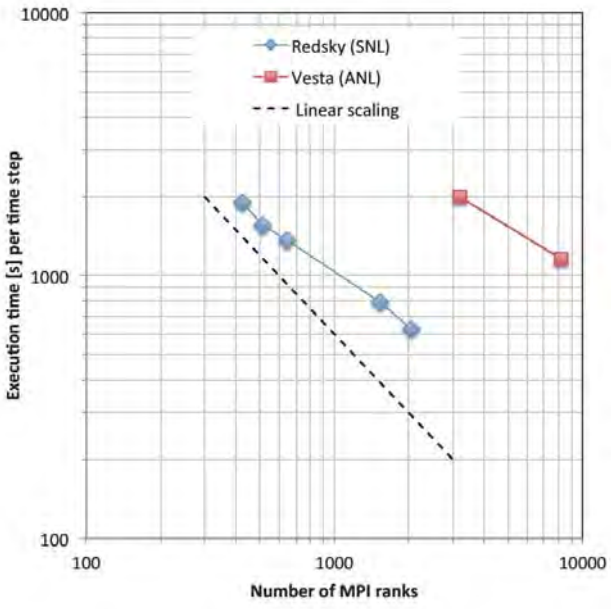

LES framework: RAPTOR

Single-fluid, diffuse interface approach applied to super-critical flow

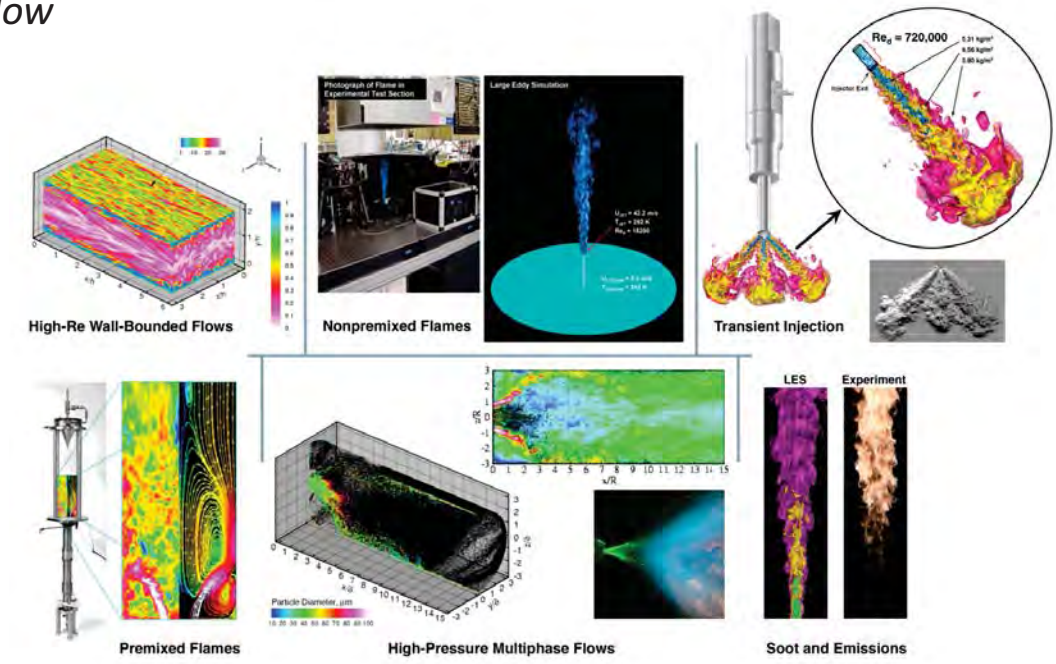

A new coupling approach from kinetic modeling: the Eulerian Multi-Fluid (EMF)

- Number density function (NDF): $dN = f(t; \mathbf{x}; \mathbf{c}, \theta, r)\, d\mathbf{x}\, d\mathbf{c}\, dr\, d\theta$
- NDF satisfies a Boltzmann-like PDE [Williams, 1958]:

$$\begin{cases} \text{Multicomponent Navier-Stokes + spray source terms} \\ \partial_t f + \partial_{\boldsymbol{x}} \boldsymbol{c} f + \partial_{\boldsymbol{c}} \mathbf{F} f + \partial_\theta \mathrm{H} f + \partial_r \mathrm{E} f = \mathrm{B} + \mathrm{C}, \end{cases}$$

- Multiple section can accommodate a given spray distribution:

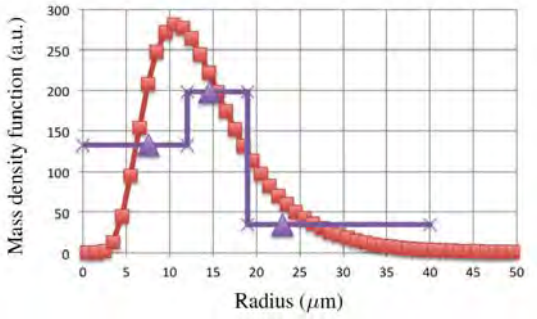

A semi-Lagrangian transport scheme

Information localized at cell nodes – good for coupling/easier load balancing

$$\begin{cases} \partial_t n_k + \partial_{\boldsymbol{x}} n_k \boldsymbol{u}_k = 0 \\ \partial_t m_k + \partial_{\boldsymbol{x}} m_k \boldsymbol{u}_k = 0 \\ \partial_t m_k \boldsymbol{u}_k + \partial_{\boldsymbol{x}} m_k \boldsymbol{u}_k \otimes \boldsymbol{u}_k = 0 \\ \partial_t m_k h_k + \partial_{\boldsymbol{x}} m_k h_k \boldsymbol{u}_k = 0 \end{cases}$$

Eulerian (coupling)

Scattering (from fixed locations)

$$\begin{pmatrix} n_k \\ m_k \\ m_k \boldsymbol{u}_k \\ m_k \phi_k \end{pmatrix} (t, \boldsymbol{x}_i) \rightarrow \begin{pmatrix} \boldsymbol{x}_p \\ n_p \\ m_p \\ \boldsymbol{u}_p \\ \phi_p \end{pmatrix} (t)$$

Lagrangian transport

$$\boldsymbol{x}_p^{n+1} = \boldsymbol{x}_p^n + \boldsymbol{u}_p^n \Delta t$$

Projection on the grid

Conservative
Positivity-preserving
Realizable whatever moments

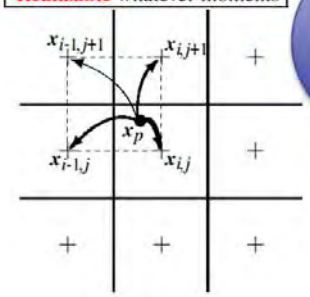

No expensive flux calculations

EMF vs Lagrangian

Example with 1-way coupling test

Mass concentration (EMF)

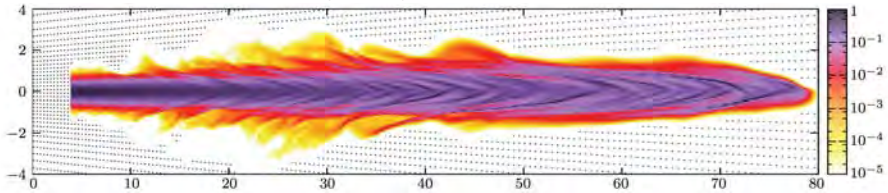

Mass concentration (Lagrangian)

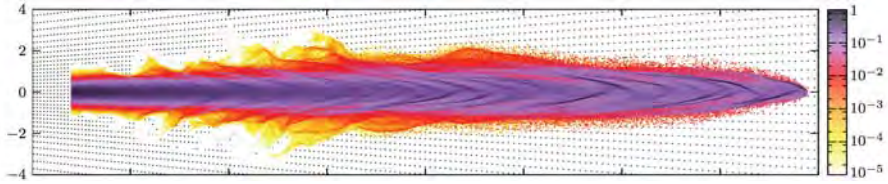

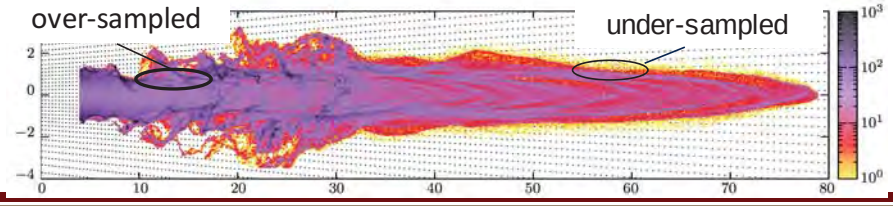

Number of Lagrangian parcels

Comparison: EMF vs CLSVOF

Test on momentum-coupling algorithm in a supersonic, laminar injection test case at high mass-loading conditions

RAPTOR + EMF
$\Delta x = 12.5\ \mu m$
$\Delta t = 8$ ns

CLSVOF
$\Delta x = 13.3\ \mu m$
$\Delta t \sim 6$ ns

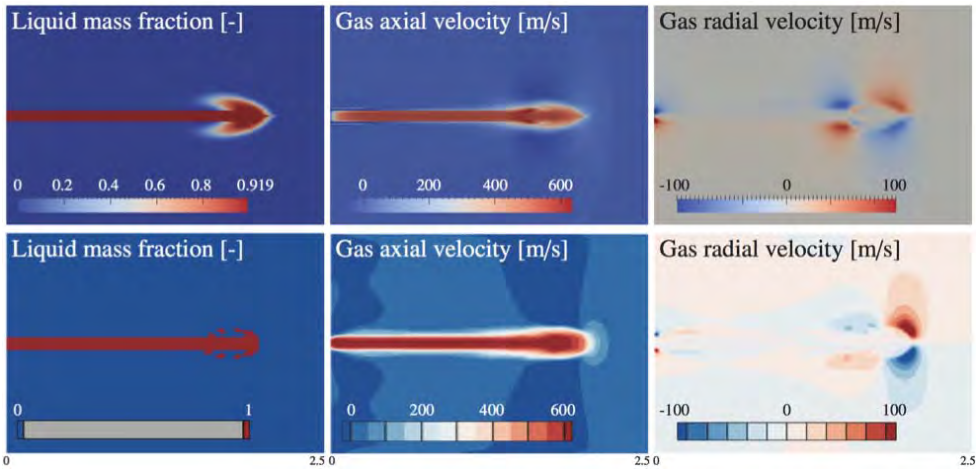

Density overshoot results from pressure-less assumption

Good agreement on jet tip trajectory

Good agreement on gas entrainment

Spray A flame autoignition

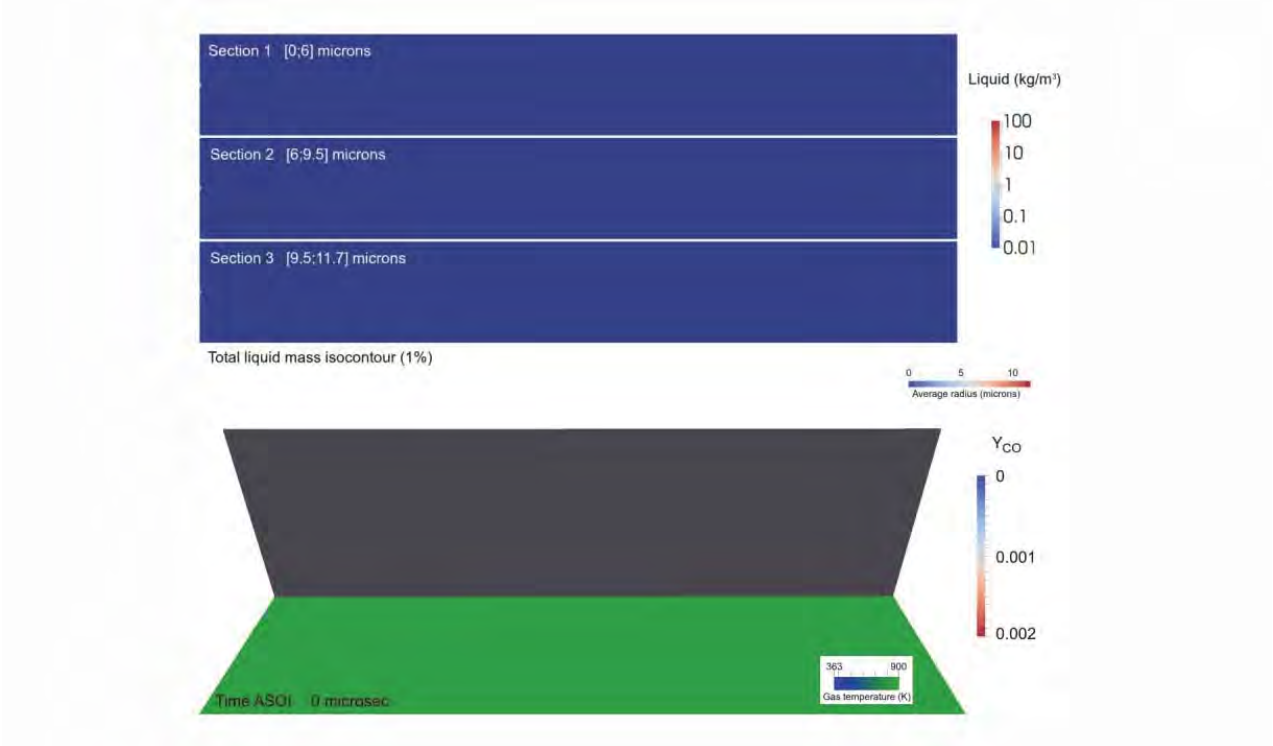

EMF issues and continuing work

- Density overshoot, no surface tension
  - Add inter-particle interaction in the Forward Lagrangian step?

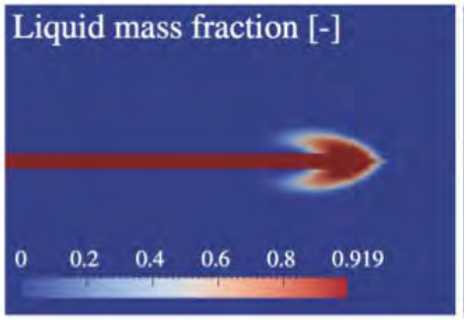

- Inclusion of collision, coalescence, and break-up models in the transition from dense to dilute spray

- What to do to prime the near field with spray data?

MOLTEN METAL DROP FRAGMENTATION

Morphology and fragmentation of molten metal

- Motivation: rocket failures can lead to propellant fires
  - Sandia Laboratories is interested in predicting the response of objects in this environment
- A new technology for validation: Digital in-line holography (DIH)

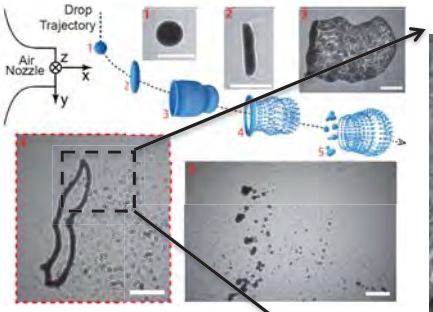

digital holograms of the breakup of an ethanol drop in an air-stream (Gao, Guildenbecher et al 2013, *Opt. Lett.*)

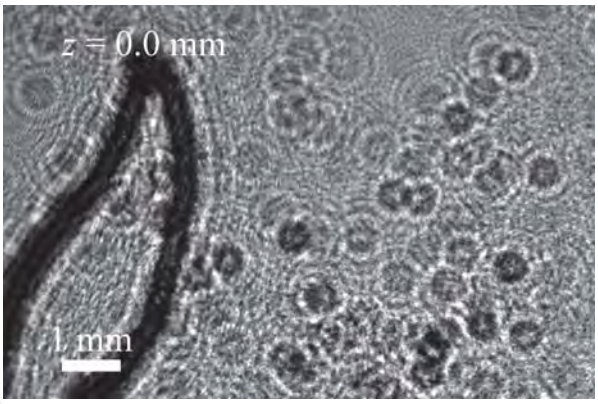

Reconstructed amplitude throughout depth, *z*

Computational set-up for 2D drop in crossflow

$$We_g = \frac{\rho_g U_g^2 d_0}{\sigma}$$ (at post-shock condition)

Water @ 300 K, d_0 = 1 mm

(Tait liquid, σ = 0.072 N/m, ρ = 1000 kg/m^3, Oh = 0.0030)

Uniform crossflow:
P.G.
We_g = 106
U_g = 77.3 m/s
M = 1.14

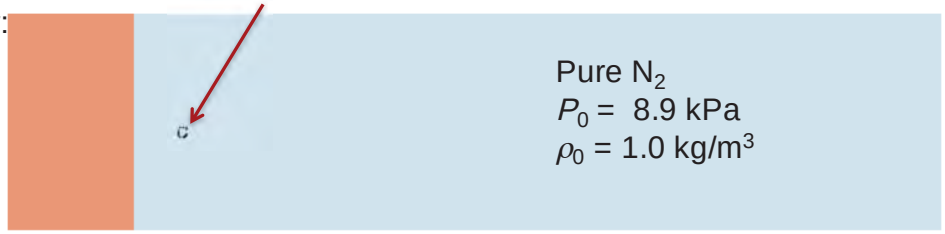

Aluminum @ 1200 K, d_0 = 1 mm

(Tait liquid, σ = 1.1 N/m, ρ = 2300 kg/m^3, Oh = 0.00022)

Uniform crossflow:
P.G.
We_g = 174
U_g = 302 m/s
M = 1.64

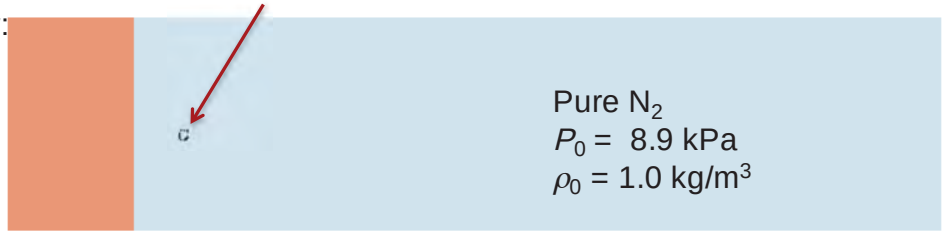

Water cross-section

U_g = 77 m/s
M = 1.14
We_g = 106

Aluminum cross-section

U_g = 302 m/s
M = 1.64
We_g = 174

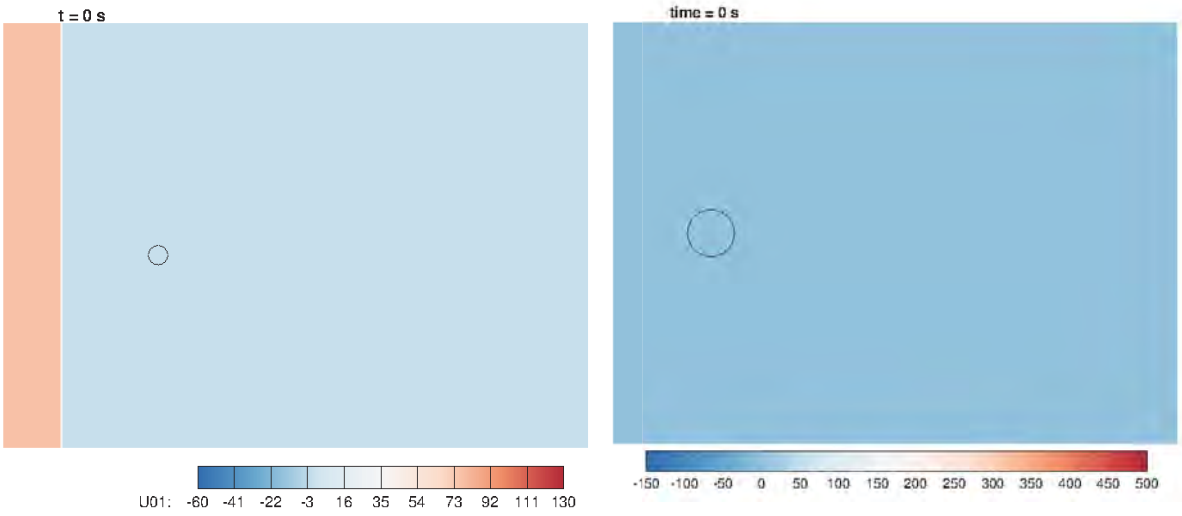

Path Forward

Continue investigation of break-up morphology for materials

We_g = 6.7	We_g = 106	We_g = 174
Oh = 0.00022	Oh = 0.0030	Oh = 0.0022
Re_g = 5,200	Re_g = 5,200	Re_g = 20,000

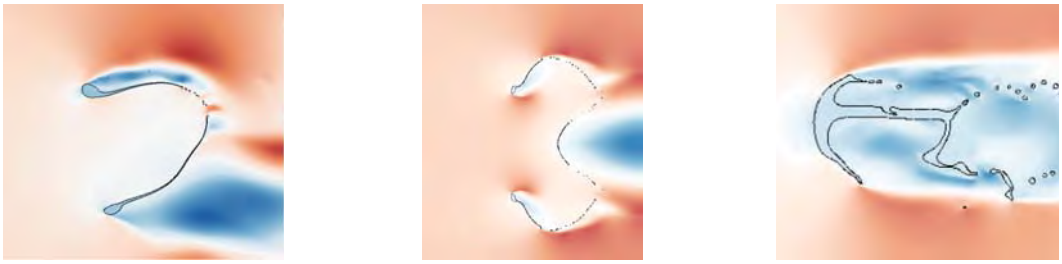

- The state of the "skin" of aluminum oxide is difficult to predict; models relies on sparse data
- Switch to galinstan (non toxic alloy, in liquid phase at room conditions) and 3D

Cross-flow of molten metal alloy (galinstan)

Shock tube tests isolate the effects of large surface tension and density ratio

Thank you!

The support by Sandia National Laboratories via the Laboratory Directed Research and Development program is gratefully acknowledged. Sandia National Laboratories is a multi-program laboratory managed and operated by Sandia Corporation, a wholly owned subsidiary of Lockheed Martin Corporation, for the U. S. Department of Energy's National Nuclear Security Administration under contract DE-AC04-94AL85000.

BACKUP

II. Extension to compressible flow

1 Advect and update volume fractions and moments for each material, *m*

II. Extension to compressible flow

6 Solve for P^{n+1}

[1] $$P^{n+1} - \rho^{n+1}\left(c^2\right)^a \Delta t^2 \nabla \cdot \left(\frac{\nabla P^{n+1}}{\rho^{n+1}}\right) = p^a - \rho^{n+1}\left(c^2\right)^a \Delta t \nabla \cdot \mathbf{u}^a$$

using the mass-weighted interpolation

$$\mathbf{u}^a_{i+1/2} = \frac{\mathbf{u}^a_i \rho_{i,R} \left|\Omega_{i,R}\right| + \mathbf{u}^a_i \rho_{i+1,L} \left|\Omega_{i+1,L}\right|}{\rho_{i+1/2} \left|\Omega_{1+1/2}\right|}$$

$$\rho_{i+1/2} = \frac{\rho_{i,R} \left|\Omega_{i,R}\right| + \rho_{i+1,L} \left|\Omega_{i+1,L}\right|}{\left|\Omega_{1+1/2}\right|}$$

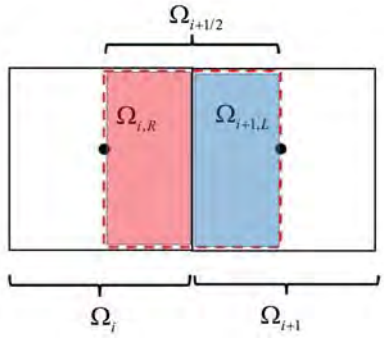

Note: the standard incompressible pressure projection method is asymptotically preserved in the limit of infinite sound speed. Each material can be treated as compressible or incompressible

[1] N. Kwatra, J. Su, J.T. Grétarsson, R. Fedkiw, J. Comput. Phys. (2009)

Single phase test: shock tube

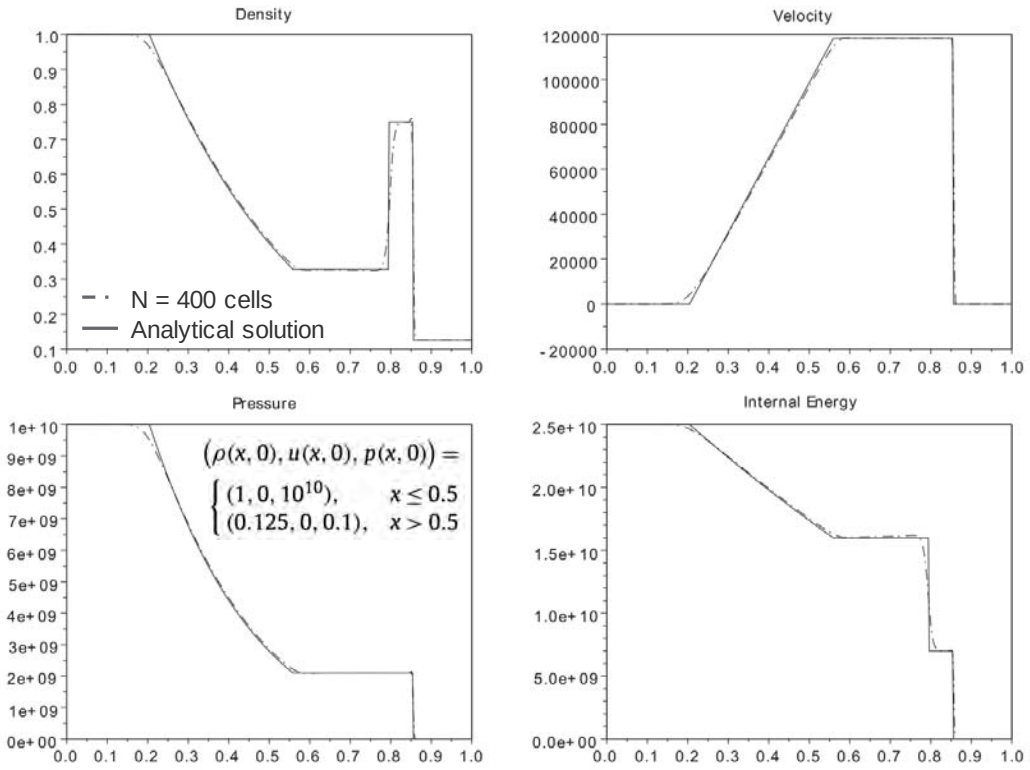

Mass conservation properties

AMR maintains mass variation under control, but this becomes increasingly challenging with increasing crossflow velocity

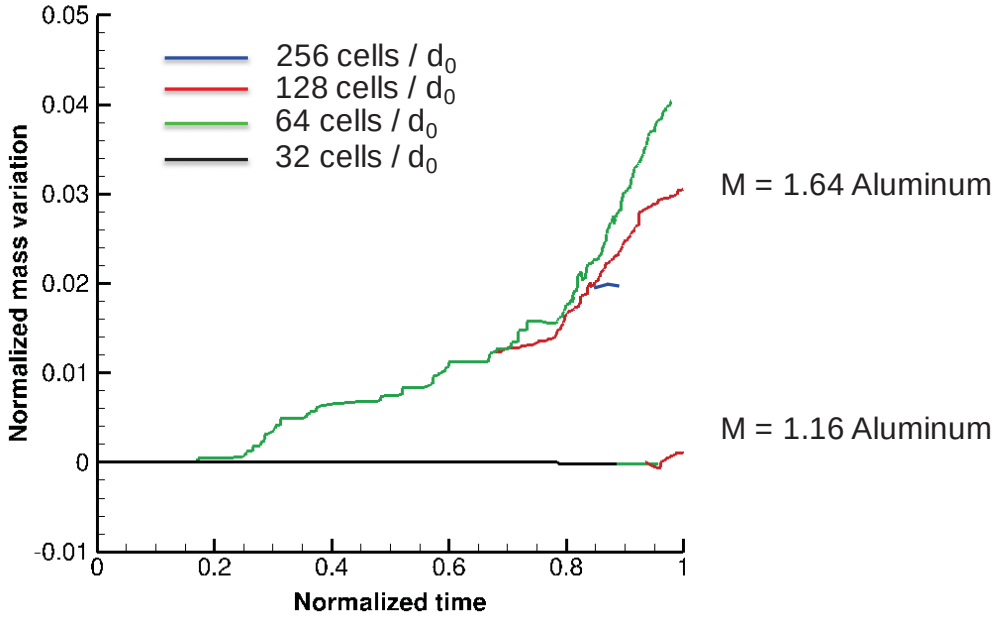

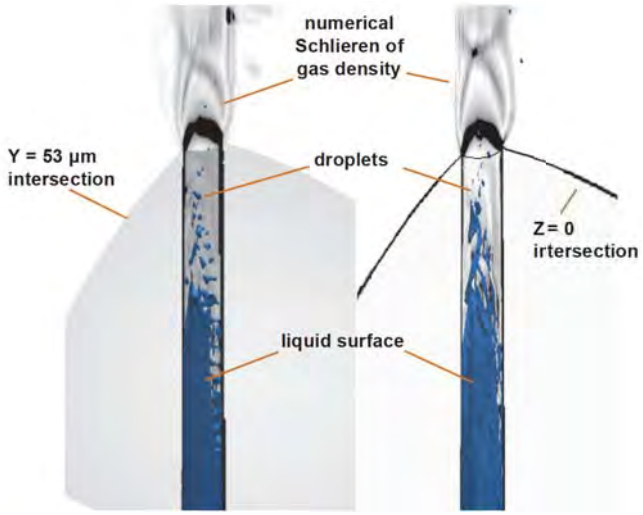

Directionally split advection for 2D/3D

Eulerian-Implicit/Lagrangian-Explicit (EI-LE)

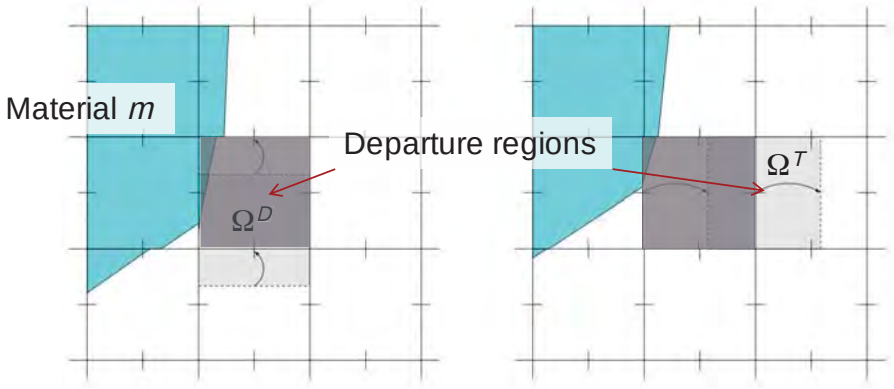

First sweep: back-tracing Eulerian Implicit

Second sweep: forward-tracing Lagrangian Explicit

Interface reconstruction

X(*EI*)➔ *Y*(*LE*)➔ *Z*(*EI*)
➔ *Z*(*LE*)➔ *Y*(*EI*)➔ *X*(*LE*)

$$\Omega^D_{i,j} = \left[y_{j-1/2} - \Delta t\, v_{j-1/2},\ y_{j+1/2} - \Delta t\, v_{j+1/2} \right] \qquad \Omega^T_{i,j} = \left[x_{i-1/2} + \Delta t\, u_{i-1/2},\ x_{i+1/2} + \Delta t\, u_{i+1/2} \right]$$

Jemison, Sussman and Arienti, J. Comp. Physics 2013

A "genealogy" of multiphase models

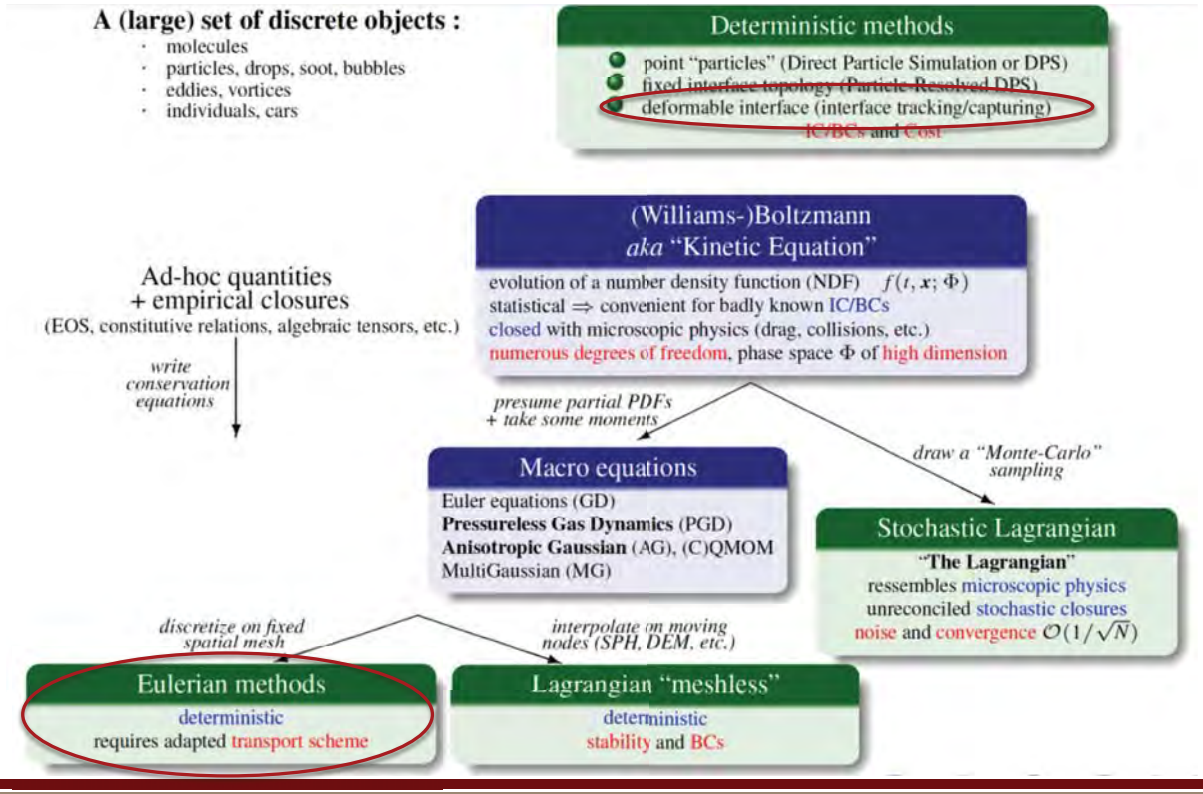

PSAAP II
Particle-laden Turbulence in a Radiation Environment

Point-particle modeling for two-way-coupled problems:

Challenges, verification, and physics-based improvements

Jeremy Horwitz, Ali Mani
Mohammad Mehrabadi, Shankar Subramaniam

Multiphase Physics Deep-Dive

October 6-7, 2016

Acknowledgements: NSF, DOE

Outline

- Modeling and Numerical Challenges
- Origin of the point-particle equations
- Verification ($\tilde{u}$-undisturbed fluid velocity)
  - Settling particle
  - Consequences for energetics
- What is the appropriate drag force model?
  - Finite Reynolds number effects
- Application to turbulent flow

Challenges

- Parameter Space: $\left(\frac{d_p}{\eta}, Re_p, St_\eta, \frac{\rho_p}{\rho_f}, \Phi_m, \Phi_v, Fr \ldots\right)$
- Polydispersity/Shape Anisotropy
- Lack of Continuum
  - Euler-Lagrange (point-particle) model
  - Data transfer
  - Interpretation of particle statistics
- Particle Equation of Motion
  - Analytical and empirical correlations
- Verification (Two-way coupled)
  - Particle settling velocity/conversion of potential to kinetic energy
- Validation
  - Comparison with Fully Resolved Simulation/Experiment

Challenges

- Parameter Space: $\left(\frac{d_p}{\eta}, Re_p, St_\eta, \frac{\rho_p}{\rho_f}, \Phi_m, \Phi_v, Fr \ldots\right)$
- Polydispersity/Shape Anisotropy
- Lack of Continuum
  - Euler-Lagrange (point-particle) model
  - Data transfer
  - Interpretation of particle statistics
- Particle Equation of Motion
  - Analytical and empirical correlations
- Verification (Two-way coupled)
  - Particle Settling velocity/Conversion of potential to kinetic energy
- Validation
  - Comparison with Fully Resolved Simulation/Experiment

Point-Particle origins

Anderson & Jackson (1967), more recently in Capecelatro & Desjardins (2012):

-Explicit filtering of fluid equations

$$\frac{\partial}{\partial t}\bar{\rho}_f \breve{u}_i + \frac{\partial}{\partial x_j}\bar{\rho}_f \breve{u}_i \breve{u}_j = -\frac{\partial \bar{p}}{\partial x_i} + \frac{\partial \bar{\tau}_{ij}}{\partial x_j} + \frac{\partial \breve{R}_{ij}}{\partial x_j} + \bar{F}_{g,i} - \frac{1}{V}\sum_k^{N_p} F_d^k \, \bar{P}\{\delta(x_i - x_i^k)\}$$

-volume fraction effects explicitly accounted for

Saffman (1973) "Point-Particle equations"

-Represent particles by a truncated multipole expansion

$$\frac{\partial}{\partial t}\rho_f u_i + \frac{\partial}{\partial x_j}\rho_f u_j u_i = -\frac{\partial p}{\partial x_i} + \mu\frac{\partial^2 u_i}{\partial x_j \partial x_j} + F_{g,i} - \frac{1}{V}\sum_k^{N_p} F_d^k \, P\{\delta(x_i - x_i^k)\}$$

-volume fraction effects neglected, suitable for dilute flows

Particle Equations

For each of N_p particles:

$$\frac{dx_p}{dt} = \mathrm{v}_p$$

$$m_p \frac{d\mathrm{v}_p}{dt} = (\rho_p - \rho_f)g + \int_S \sigma_{ij} n_j dS$$

Stokes (1850), Boussinesque (1885), Basset (1888), Faxen (1926), Stimson & Jeffrey (1926), Schiller & Nauman (193?), Oseen (1910), Proudman & Pearson (1957), Saffman (1965), Goldman, Cox, Brenner, (1967), Batchelor (1972), Batchelor & Green (1972), Maxey & Riley (1982), Lovelanti & Brady (1993), Mei (1994), Parmar, Haselbacher, Balachandar (2012)

Maxey-Riley Equation $(Re_p \ll 1)$:

$$m_p \frac{d\mathrm{v}_p}{dt} = (\rho_p - \rho_f)g + m_f \frac{D\tilde{u}_p}{Dt} - \frac{1}{2}m_f \frac{d}{dt}\left[\mathrm{v}_p - \tilde{u}_p - \frac{1}{10}a^2\nabla^2\tilde{u}_p\right] - 6\pi a\mu\left(\mathrm{v}_p - \tilde{u}_p - \frac{1}{6}a^2\nabla^2\tilde{u}_p\right)$$

gravity — Fluid accel. — Added Mass — Stokes Drag

$$-6\pi a^2\mu\int_0^t \frac{\frac{d}{d\tau}\left[\mathrm{v}_p - \tilde{u}_p - \frac{1}{6}a^2\nabla^2\tilde{u}_p\right]d\tau}{[\pi\nu(t-\tau)]^{1/2}}$$

History

"Undisturbed" Fluid Velocity

Stokes drag

$$F_d = 3\pi\mu d_p\left(\tilde{u}_p - \mathrm{v}_p\right)$$

Parameter Space:

$$\left(\frac{d_p}{\eta} \leq 1, Re_p \leq 1, \frac{\rho_p}{\rho_f} \gg 1, \Phi_v \ll 1\right)$$

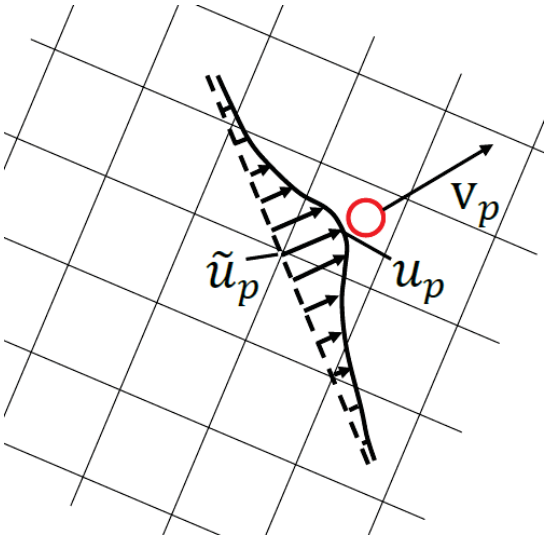

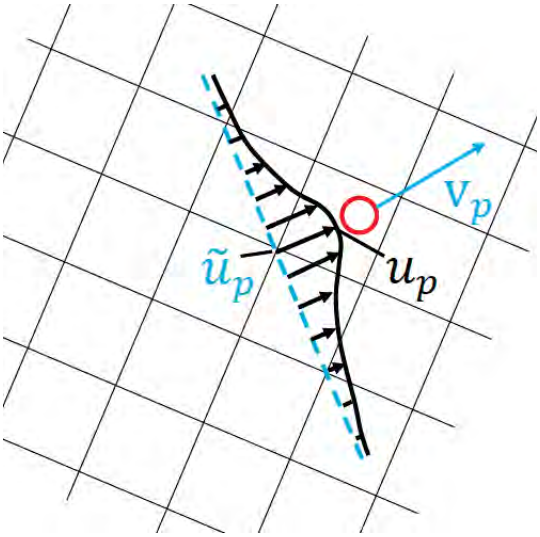
v_p
$\tilde{u}_p$
u_p

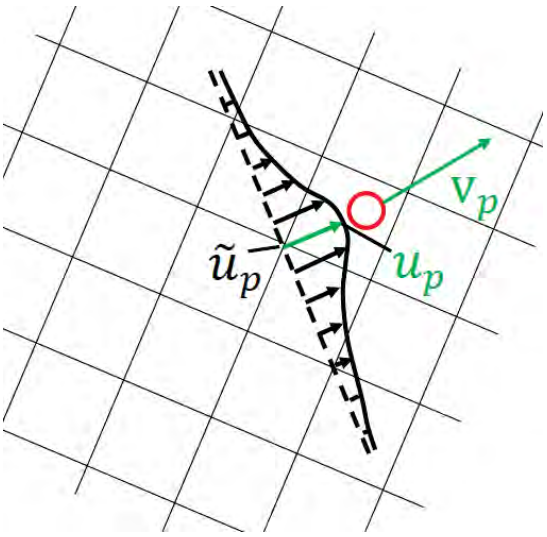
v_p
$\tilde{u}_p$
u_p

Proposed Correction method

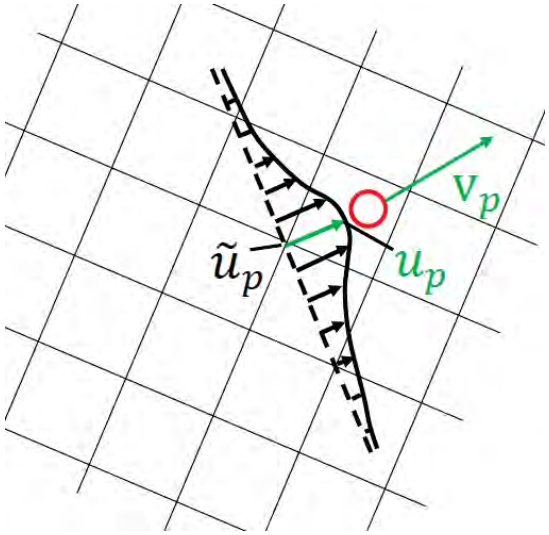

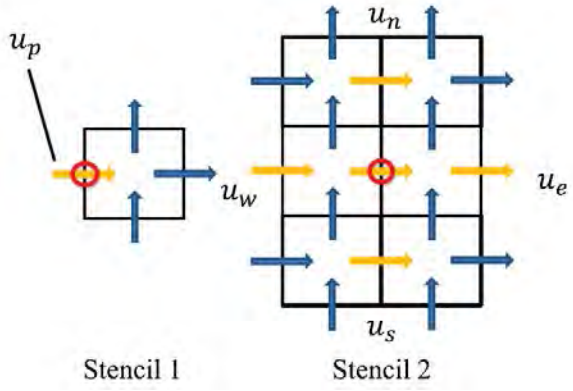

- Stencil 1: $\tilde{u}_p \approx u_p$
- Stencil 2: $\tilde{\boldsymbol{u}}_{\boldsymbol{p}} \approx \boldsymbol{u_p} + \boldsymbol{C dx^2 \nabla^2 u_p}$

$$= (1 - 4C) \times u_p + C \times (u_n + u_s + u_e + u_w)$$

- Conservative
- Has been extended to general particle location in three dimensions

Horwitz J.A.K., Mani A., JCP, (2016)

Settling velocity

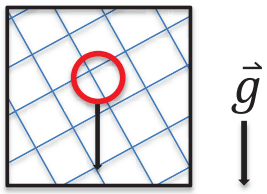

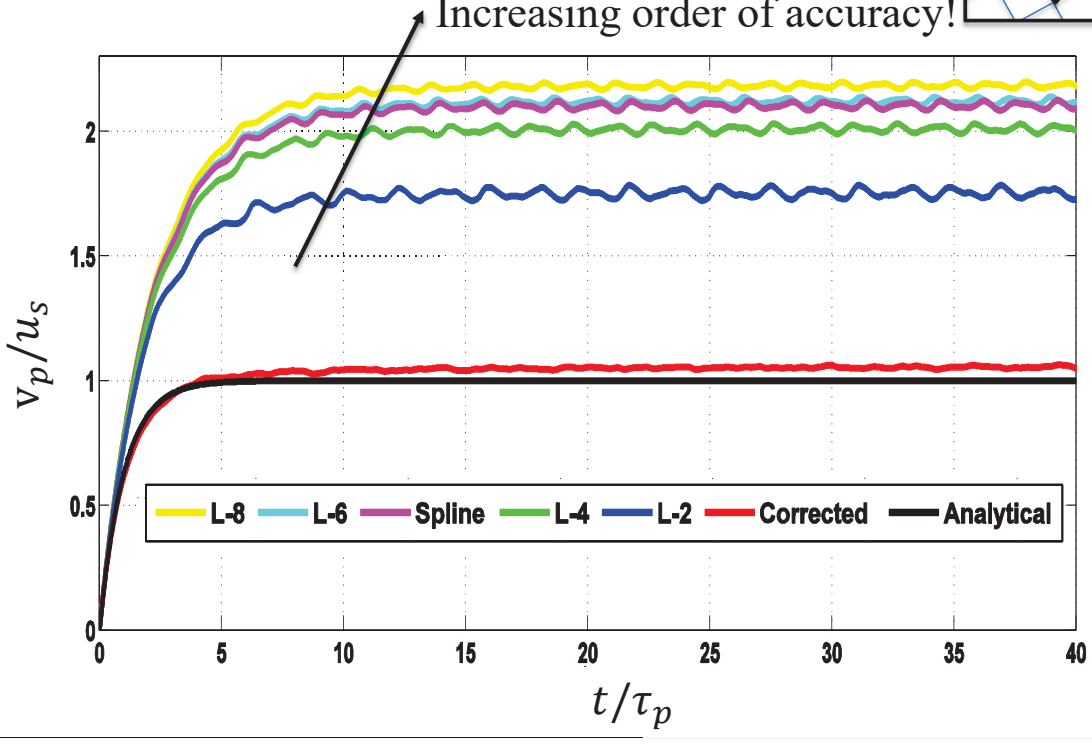

C-refinement

Layer 1

C_{141}	C_{241}	C_{341}	C_{441}
0.340	0.384	0.423	0.440
C_{131}	C_{231}	C_{331}	C_{431}
0.320	0.360	0.397	0.413
C_{121}	C_{221}	C_{321}	C_{421}
0.281	0.315	0.346	0.359
C_{111}	C_{211}	C_{311}	C_{411}
0.248	0.275	0.300	0.312

Layer 2

C_{142}	C_{242}	C_{342}	C_{442}
0.402	0.457	0.506	0.527
C_{132}	C_{232}	C_{332}	C_{432}
0.376	0.426	0.472	0.491
C_{122}	C_{222}	C_{322}	C_{422}
0.325	0.366	0.404	0.420
C_{112}	C_{212}	C_{312}	C_{412}
0.281	0.315	0.346	0.359

Layer 3

C_{143}	C_{243}	C_{343}	C_{443}
0.478	0.545	0.604	0.629
C_{133}	C_{233}	C_{333}	C_{433}
0.443	0.504	0.559	0.582
C_{123}	C_{223}	C_{323}	C_{423}
0.376	0.426	0.472	0.491
C_{113}	C_{213}	C_{313}	C_{413}
0.320	0.360	0.397	0.413

Layer 4

C_{144}	C_{244}	C_{344}	C_{444}
0.518	0.591	0.655	0.681
C_{134}	C_{234}	C_{334}	C_{434}
0.478	0.545	0.604	0.629
C_{124}	C_{224}	C_{324}	C_{424}
0.402	0.457	0.506	0.527
C_{114}	C_{214}	C_{314}	C_{414}
0.340	0.384	0.423	0.440

Table B.1: Numerical values of C field coefficients for third level of fineness.

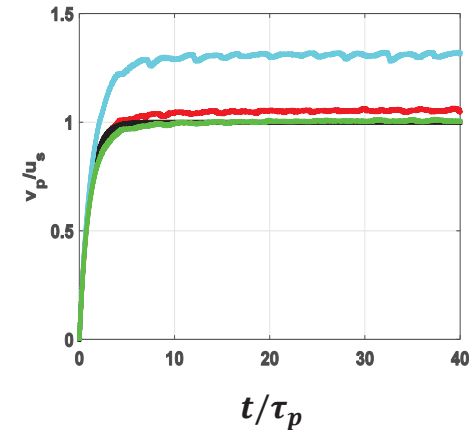

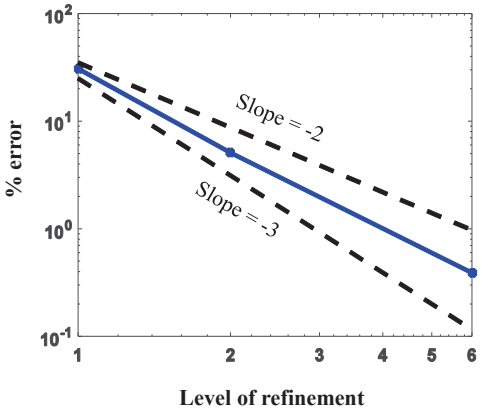

Energetics

(1) $\frac{dv_i}{dt} = (\tilde{u}_i - v_i)/\tau_p + (1 - \rho_f/\rho_p)g_i$ **Particle Momentum**

(2) $\frac{dk_p}{dt} = m_p v_i\,(\tilde{u}_i - v_i)/\tau_p + m_p(1 - \rho_f/\rho_p)g_i v_i$ **Particle Kinetic Energy**

(3) $\frac{\partial}{\partial t}\rho_f u_i + \frac{\partial}{\partial x_j}\rho_f u_j u_i = -\frac{\partial p}{\partial x_i} + \mu\frac{\partial^2 u_i}{\partial x_j \partial x_j} + F_{g,i} - \frac{1}{V}\sum_k^{N_p} F_d^k\, P\{\delta(x_i - x_i^k)\}$ **Fluid Momentum**

(4) $\frac{dk_f}{dt} = W_v - \epsilon_{pp}$ **Fluid Kinetic Energy**

(5) $W_v = \int \mu u_i \frac{\partial^2 u_i}{\partial x_j \partial x_j} dV = \int \left[\mu \nabla^2 k - \epsilon + \mu \frac{\partial u_i}{\partial x_j}\frac{\partial u_j}{\partial x_i}\right] dV$ **Viscous dissipation**

(6) $\epsilon_{pp} = \int \frac{1}{V_{cell}} u_i F_{d,i}\, P\{\delta(x_i - x_i')\} dV = u_i m_p\,(\tilde{u}_i - v_i)/\tau_p$ **Additional dissipation**

Energetics

(1) $\frac{dv_i}{dt} = (\tilde{u}_i - v_i)/\tau_p + (1 - \rho_f/\rho_p)g_i$ **Particle Momentum**

(2) $\frac{dk_p}{dt} = m_p v_i\ (\tilde{u}_i - v_i)/\tau_p + m_p(1 - \rho_f/\rho_p)g_i v_i$ **Particle Kinetic Energy**

(3) $\frac{\partial}{\partial t}\rho_f u_i + \frac{\partial}{\partial x_j}\rho_f u_j u_i = -\frac{\partial p}{\partial x_i} + \mu\frac{\partial^2 u_i}{\partial x_j \partial x_j} + F_{g,i} - \frac{1}{V}\sum_k^{N_p} F_d^k\ P\{\delta(x_i - x_i^k)\}$ **Fluid Momentum**

(4) $\frac{dk_f}{dt} = W_v - \epsilon_{pp}$ **Fluid Kinetic Energy**

(5) $W_v = \int \mu u_i \frac{\partial^2 u_i}{\partial x_j \partial x_j} dV = \int \left[\mu \nabla^2 k - \epsilon + \mu \frac{\partial u_i}{\partial x_j}\frac{\partial u_j}{\partial x_i}\right] dV$ **Viscous dissipation**

(6) $\epsilon_{pp} = \int \frac{1}{V_{cell}} u_i F_{d,i}\ P\{\delta(x_i - x_i')\} dV = u_i m_p\ (\tilde{u}_i - v_i)/\tau_p$ **Additional dissipation**

(7) $\frac{dk_f}{dt} + \frac{dk_p}{dt} = \underbrace{m_p \frac{(v_i - u_i)(\tilde{u}_i - v_i)}{\tau_p} + W_v}_{\text{Heat generation}} + \underbrace{m_p(1 - \rho_f/\rho_p)g_i v_i}_{\text{Work In}}$ **Total Energy equation**

Change in KE

Energetics

$(\tilde{u} \to 0)$: $Q_g = -m_p \frac{v_p^2}{\tau_p} = -3\pi\mu d_p v_p^2$

(7) $\frac{dk_f}{dt} + \frac{dk_p}{dt} = \underbrace{m_p \frac{(v_i - u_i)(\tilde{u}_i - v_i)}{\tau_p} + W_v}_{\text{Heat generation}} + \underbrace{m_p(1 - \rho_f/\rho_p)g_i v_i}_{\text{Work In}}$ **Total Energy equation**

Change in KE

What has been achieved...

Developed two-way coupling correction for point-particles

-Stokes limit

-provided an interpretation of dissipation, how to post-process

-predicting $\tilde{u}$ implies correct work rate

-applicable to 2nd order finite difference, uniform grid

-dilute gas-solid flows

Still requiring more exploration...

-Non-uniform grid (channel flow)

-Finite Reynolds number

-Heat transfer

-Extension to full Maxey Riley equation, Saffman Lift, etc.

-Turbulent flows

-Multiple particle interaction (Stimson & Jeffrey 1926 and Batchelor & Green 1972)

What has been achieved...

Developed two-way coupling correction for point-particles

-Stokes limit

-provided an interpretation of dissipation, how to post-process

-predicting $\tilde{u}$ implies correct work rate

-applicable to 2nd order finite difference, uniform grid

-dilute gas-solid flows

Still requiring more exploration...

-Non-uniform grid (channel flow)

-Finite Reynolds number

-Heat transfer

-Extension to full Maxey Riley equation, Saffman Lift, etc.

-Turbulent flows

-Multiple particle interaction (Stimson & Jeffrey 1926 and Batchelor & Green 1972)

Nonlinear Drag

$$F_d = 3\pi\mu d_p\left(\tilde{u} - \mathrm{v_p}\right)\left(1 + 0.15Re_p^{0.687}\right), \qquad Re_p < 800, [+5\%, -4\%]$$

(*Clift et al.* 1978)

(a) $Re_p = 0.1$ (b) $Re_p = 1$ (c) $Re_p = 10$

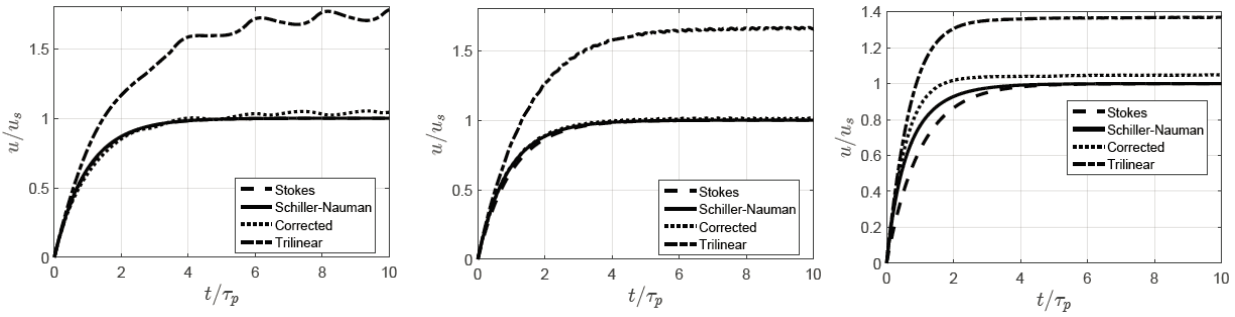

$$Re_p = \left|\tilde{u} - \mathrm{v}_p\right| d_p/\nu$$

Application to Turbulent Flow

Particle-Resolved Simulations (Tennetti et al. 2010)

Fluid:

-Spatial: Pseudo-spectral solver

-Time-stepping: Adams-Bashforth (convective), Crank-Nicholson (Viscous)

-Immersed Boundary (satisfy no-slip/no-penetration)

-$N^3 = 1152^3$

Particles:

-Force found by integrating the stress over particle surface

-Elastic soft-sphere collisions (no contribution to energetics) (Cundall & Strack 1979)

Point-particle Simulations (Pouransari et al. 2015)

-Spatial: 2nd order staggered finite difference

-Time-stepping: RK4

-point (compact-support) forces

-$N^3 = 96^3$

Particles:

-Force model (Stokes and Schiller) (Horwitz & Mani 2016 a, b)

-collisions neglected

$$\Phi_m = 1.8, \phi_v = 0.001, \frac{d_p}{\eta} = 1, \frac{\rho_p}{\rho_f} = 1800, R_{\lambda,o} \approx 27, N_p = 1689$$

M. Mehrabadi, J. Horwitz, S. Subramaniam, A. Mani, (in prep.)

Fluid Dissipation

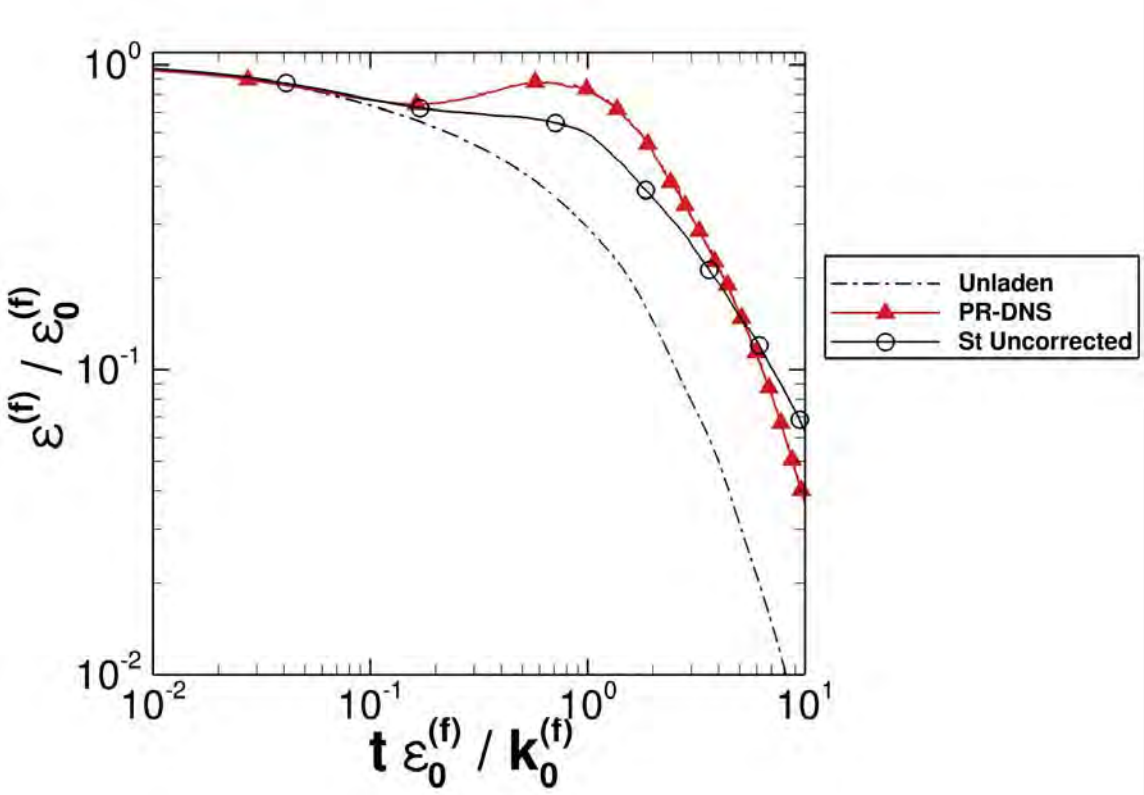

Fluid Dissipation

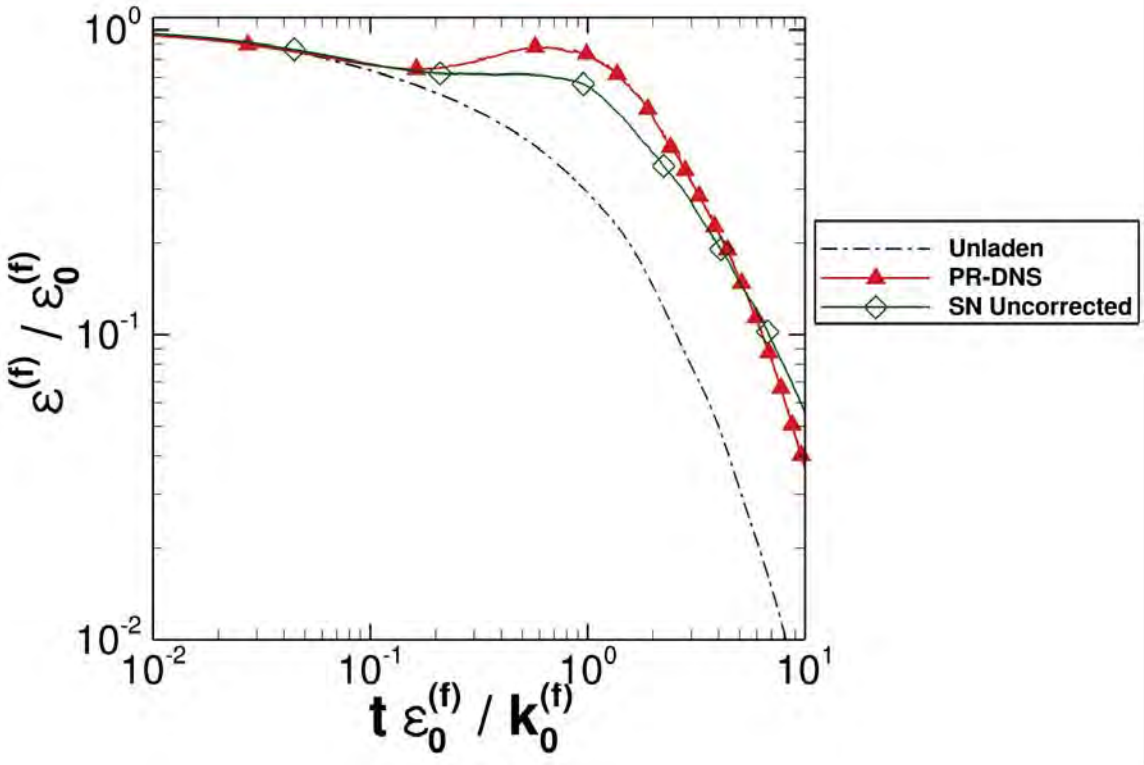

Fluid Dissipation

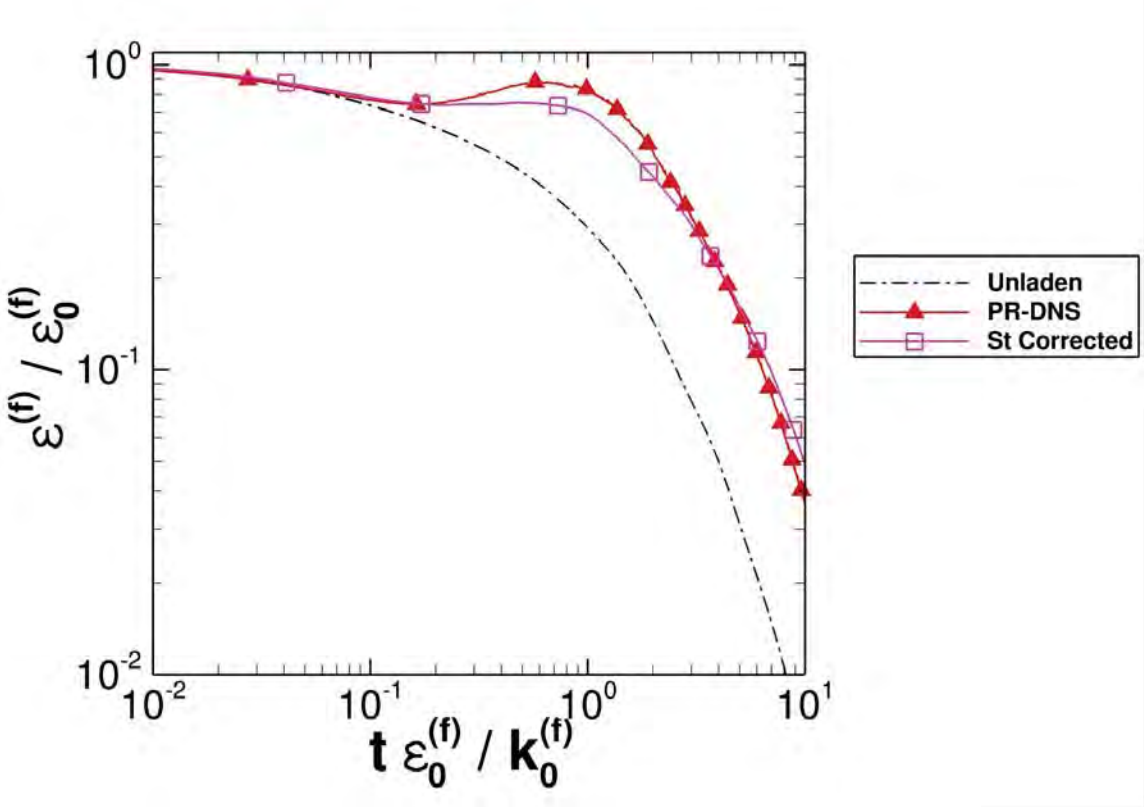

Fluid Dissipation

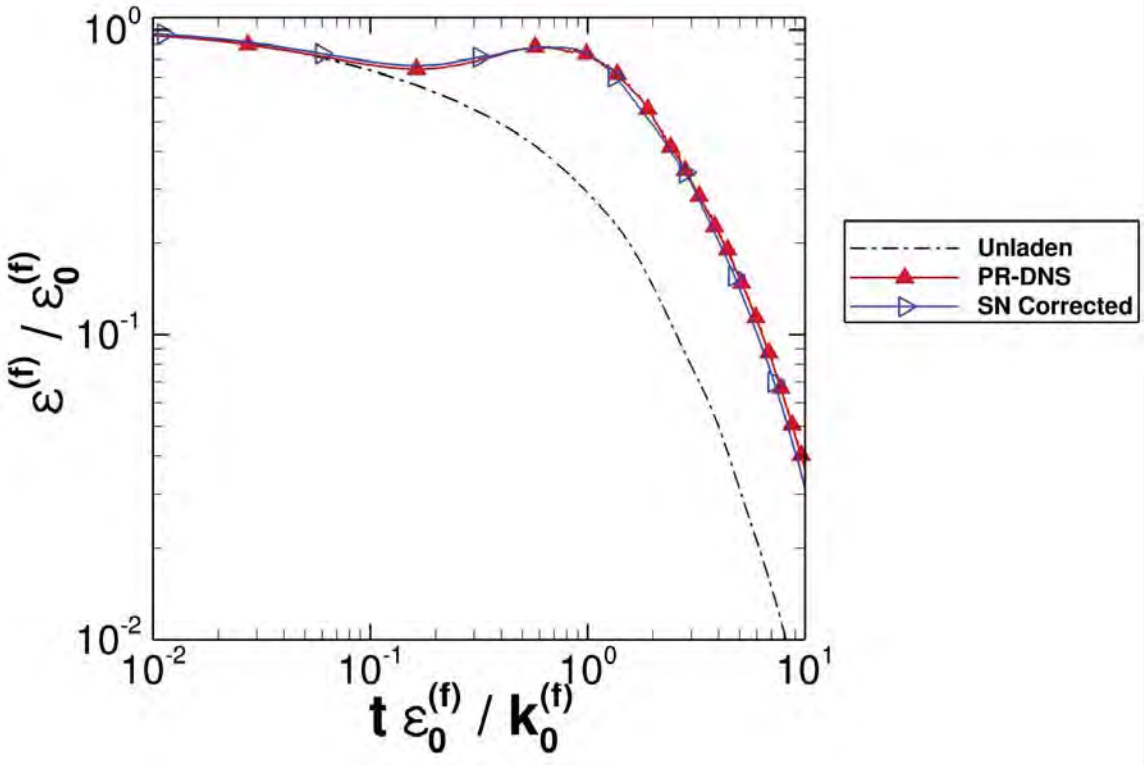

Fluid Dissipation

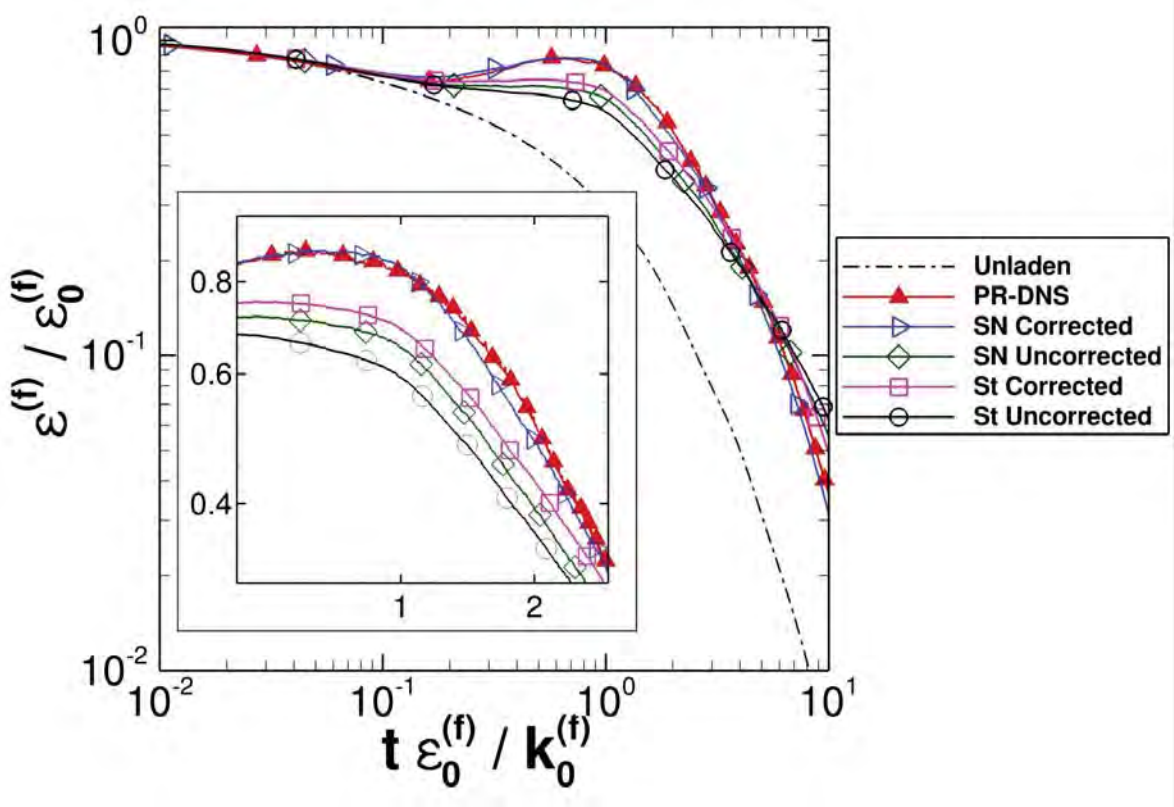

$Stokes\ Uncorrected \rightarrow Schiller - Nauman\ Uncorrected \rightarrow$
$Stokes\ Corrected \rightarrow Schiller - Nauman\ Corrected \rightarrow Particle - Resolved$

What has been achieved...

Developed two-way coupling correction for point-particles

- -Stokes limit
- -provided an interpretation of dissipation, how to post-process
- -predicting $\tilde{u}$ implies correct work rate
- -applicable to 2nd order finite difference, uniform grid
- -dilute gas-solid flows

Still requiring more exploration...

- -Non-uniform grid (channel flow)
- -Finite Reynolds number
- -Heat transfer
- -Extension to full Maxey Riley equation, Saffman Lift, etc.
- -Turbulent flows
- -Multiple particle interaction (Stimson & Jeffrey 1926 and Batchelor & Green 1972)

Questions?

Quantifying and Modeling the Force Variation within Random Arrays of Spheres

G. Akiki, T. L. Jackson and S. Balachandar
Center for Compressible Multiphase Turbulence
University of Florida

Multiphase Physics Deep-Dive Meeting
St. Petersburg, Florida, Oct. 6-7, 2016

Center *for* Compressible Multiphase Turbulence
HERBERT WERTHEIM COLLEGE *of* ENGINEERING

Extended Point-Particle Model

Point-Particle Model

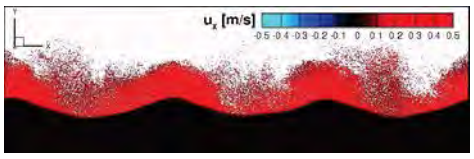

Copyright Justin Finn, 2016. All Rights Reserved

Closure Models obtained at the microscale:
- ✓ Mean cell velocity
- ✓ Mean cell volume fraction

→ Mean drag model: $F(\phi, Re)$

- Exact location of particles ?

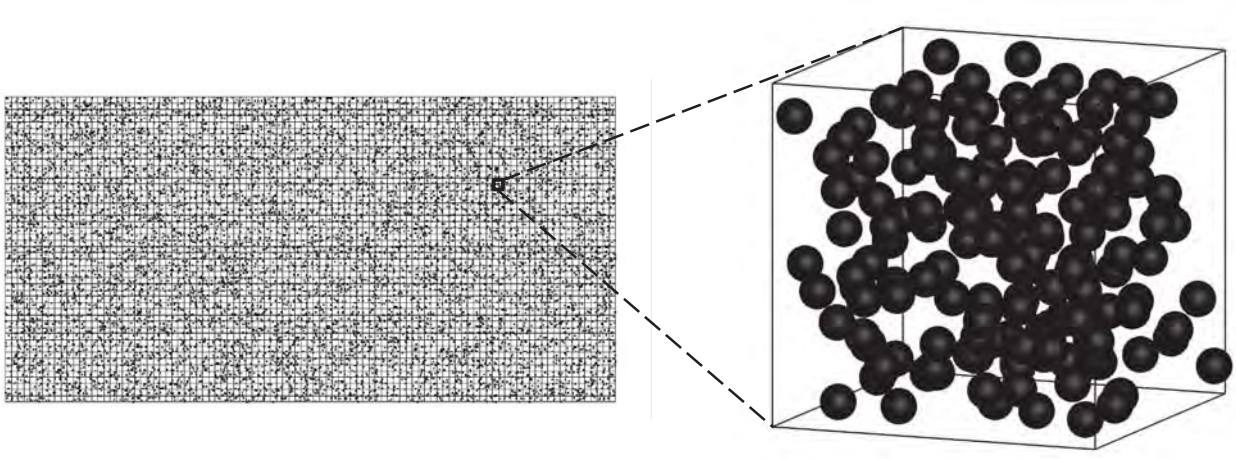

Questions to Investigate

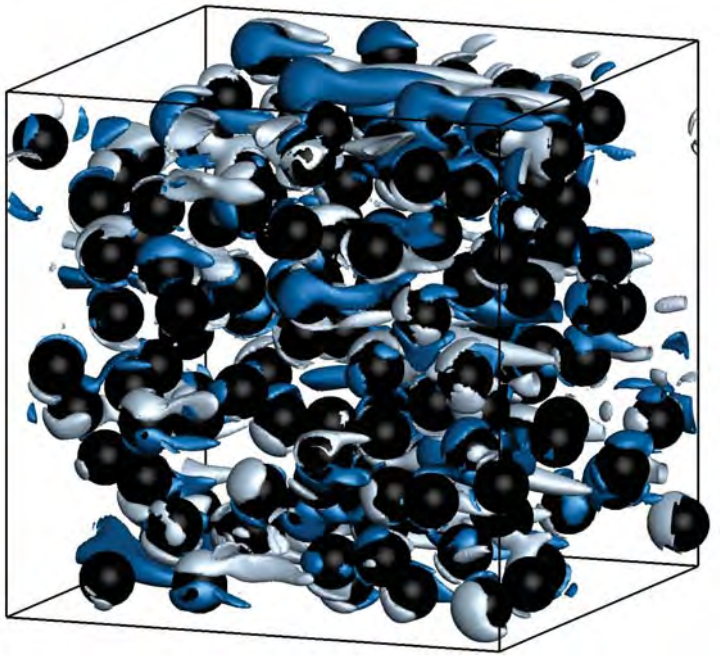

- How good are the current mean drag models?
- How significant is the variation of the forces from one particle to another within the same array?
- How significant are lateral forces?
- What governs those variations?
- Can we model it?

Outline

- Motivation
- Variation of Hydrodynamic Forces in Arrays of Spheres
- Pairwise Interaction Extended Point-particle (PIEP) Model
- PIEP Model in Sedimentation Problem
- Summary and Future Work

Outline

- Motivation
- Variation of Hydrodynamic Forces in Arrays of Spheres
- Pairwise Interaction Extended Point-particle (PIEP) Model
- PIEP Model in Sedimentation Problem
- Summary and Future Work

Force Variations

- Fully-Resolved DNS simulations of fixed random arrays

$0.1 \le \phi \le 0.45$

$2 \le Re \le 620$

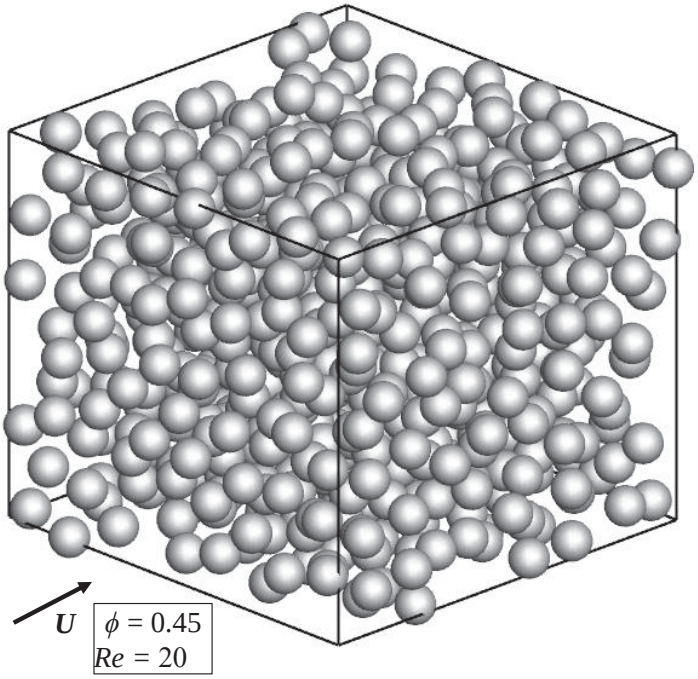

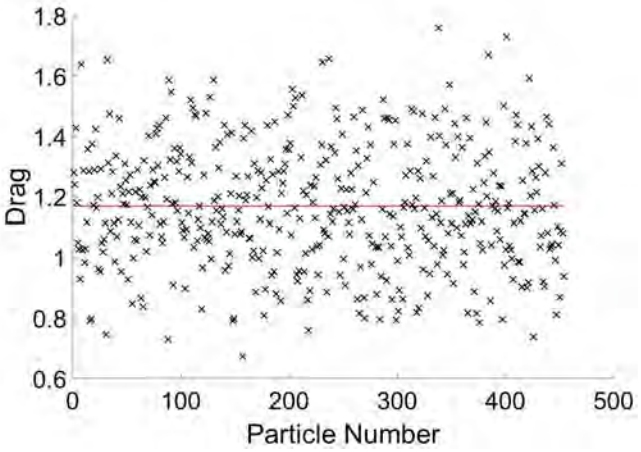

Quantifying Drag Variations

Case	*Mean Drag* F_d	σ	σ/F_d	*Skewness*	*Kurtosis*
$\phi = 0.1$, $Re = 170$	4.69	1.26	26.95%	-0.07	3.25
$\phi = 0.2$, $Re = 87$	2.48	0.61	24.71%	-0.17	2.94
$\phi = 0.4$, $Re = 20$	1.17	0.20	17.31%	0.22	2.81

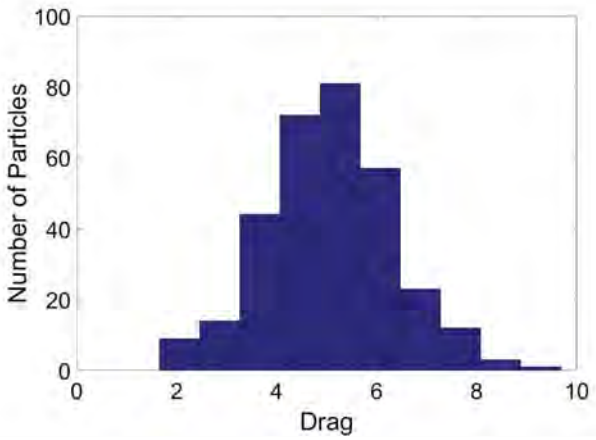

- Normal Distribution for all cases
- Standard deviation/mean drag decreases with volume fraction.
- Standard deviation/mean drag is mildly affected by *Re*.

Quantifying Lift Variations

Case	*Mean Lift*	σ	σ/F_d	*Skewness*	*Kurtosis*
$\phi = 0.1$, $Re = 170$	-8.4×10^{-4}	0.66	14.15%	0.21	3.84
$\phi = 0.2$, $Re = 87$	2.2×10^{-3}	0.33	13.19%	-0.02	3.60
$\phi = 0.4$, $Re = 20$	3.9×10^{-3}	0.18	15.16%	-0.02	3.59

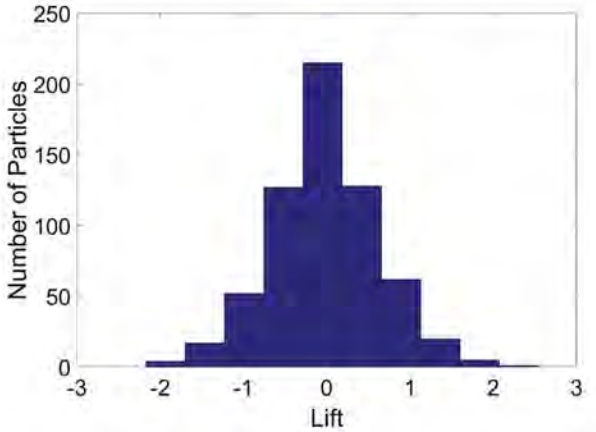

- Slightly higher Kurtosis, but still closer to normal distribution.
- Standard deviation/mean drag does not significantly vary with volume fraction nor *Re*

Outline

- Motivation
- Variation of Hydrodynamic Forces in Arrays of Spheres
- Pairwise Interaction Extended Point-particle (PIEP) Model
- PIEP Model in Sedimentation Problem
- Summary and Future Work

Goal of Model

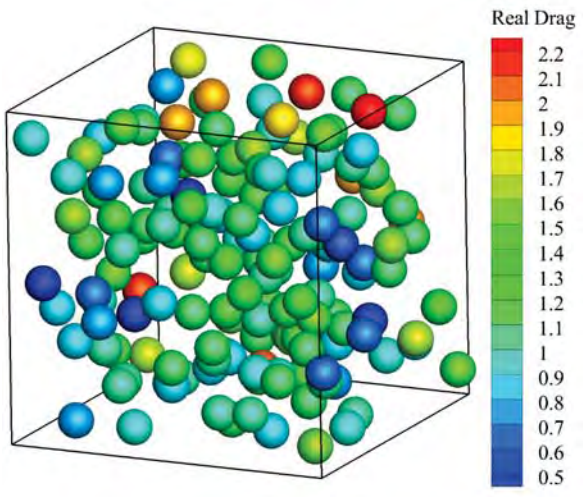

$$R^2 = 1 - \frac{\sum_{n=1}^{N_p}\left[F_{DNS}(n) - F_{PI}(n)\right]^2}{\sum_{n=1}^{N_p}\left[F_{DNS}(n) - \langle F_{DNS}\rangle\right]^2}$$

$R^2 = 1.00$

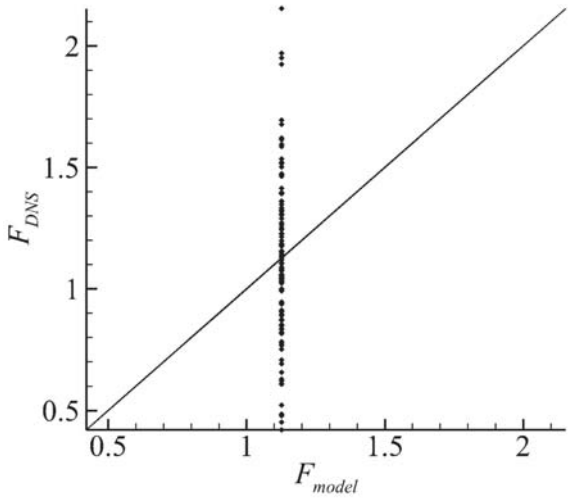

If the model is a fully-resolved DNS simulation!

Pairwise Interaction

Force on a single sphere in a steady non-uniform flow at finite *Re*:

$$\boldsymbol{F} = 3\pi\mu d\boldsymbol{u}_{un}(1+0.15Re^{0.687}) + m_f(1+C_m)\frac{D\boldsymbol{u}_{un}}{Dt} + m_f C_{IL}\boldsymbol{u}_{un}\times\boldsymbol{\omega}_{un}$$

F_{QS} F_{II} F_{RI}

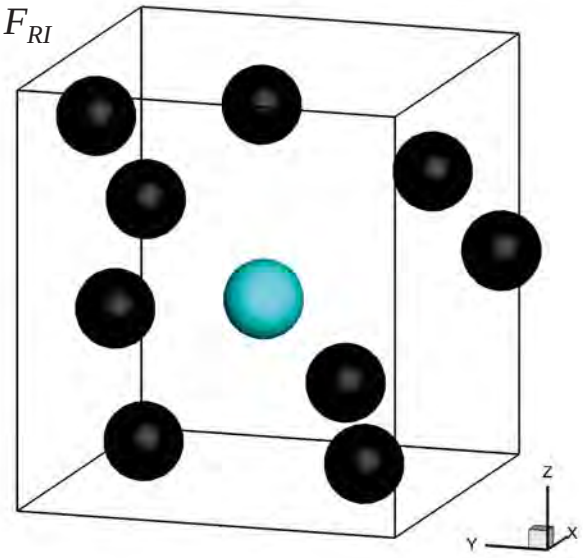

Undisturbed Velocity:

$$\boldsymbol{u}_{un,i}(\boldsymbol{x}_i) = \boldsymbol{u}_{macro}(\boldsymbol{x}_i) + \tilde{\boldsymbol{u}}_{\forall N\to i}(\boldsymbol{x}_i)$$

Pairwise Interaction assumption:

$$\boldsymbol{u}_{un,i}(\boldsymbol{x}_i) \approx \boldsymbol{u}_{macro}(\boldsymbol{x}_i) + \sum_{j=1}^{N-1}\tilde{\boldsymbol{u}}_{j\to i}(\boldsymbol{x}_i)$$

Extended Point-Particle Model

Effect on Neighbor

$$\boldsymbol{F}_{QS} = 3\pi\mu\overline{\left(\boldsymbol{u}_{un}(\boldsymbol{x})\right)}^{S} d\left[1+0.15\left(Re\right)^{0.687}\right]$$

$$\boldsymbol{F}_{II} = (1+C_m)\rho\iiint_{|\boldsymbol{x}-\boldsymbol{x}_i|\le d/2}\frac{D\boldsymbol{u}_{un}(\boldsymbol{x})}{D\hat{t}}d\boldsymbol{x}$$

$$\boldsymbol{F}_{RI} \approx C_{IL}\rho\iiint_{|\boldsymbol{x}-\boldsymbol{x}_i|\le d/2}\left[\boldsymbol{u}_{un}(\boldsymbol{x})\times\boldsymbol{\omega}_{un}(\boldsymbol{x})\right]d\boldsymbol{x}$$

We use the Generalized Faxén's theorem to account for non-uniformity.

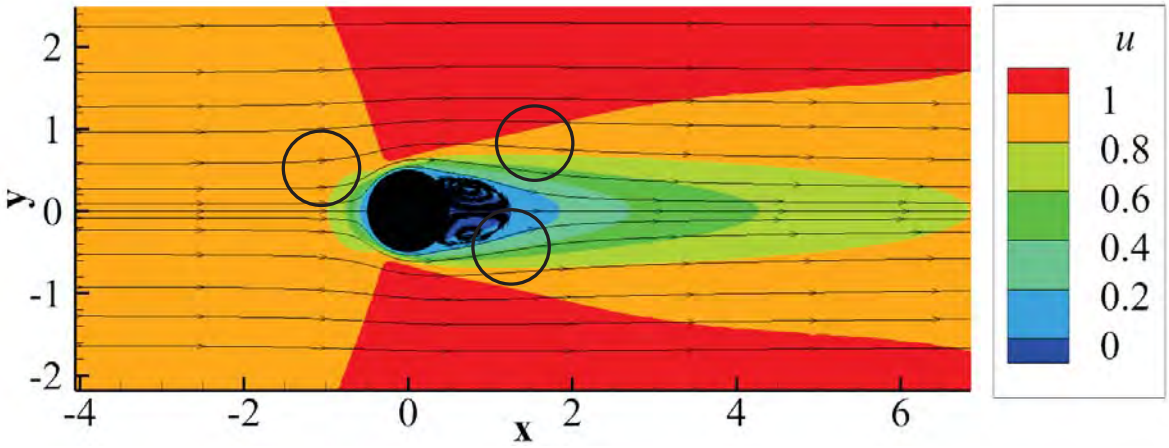

Irrotational Inviscid Force Mappings

$$\boldsymbol{F}_{II} = (1+C_m)\rho \iint_{|\boldsymbol{x}-\boldsymbol{x}_i|=d/2} \left[\boldsymbol{\tau} - p\boldsymbol{I}(\boldsymbol{x})\right].\boldsymbol{n}dA$$

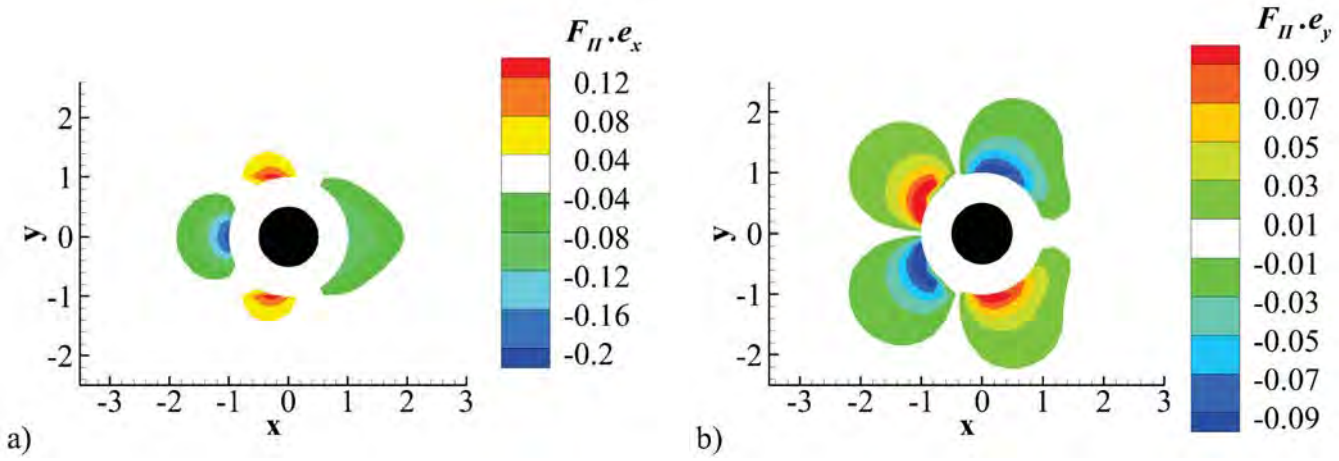

Streamwise Force

Lateral Force

Pairwise Interaction Extended Point-Particle (PIEP) Model

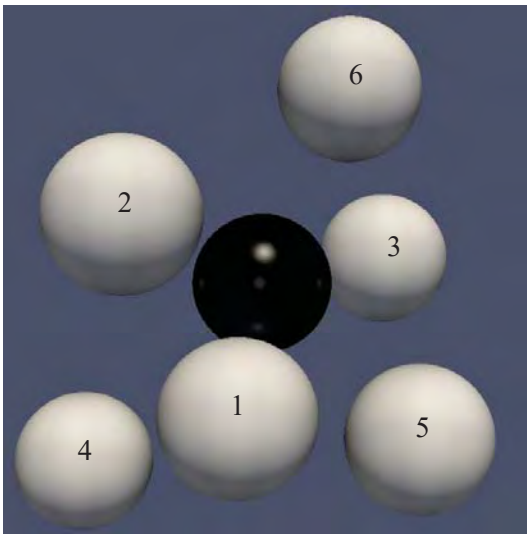

$$\boldsymbol{F}_{QS,PI}(i) = \frac{3\pi}{Re}\left[\{1,0\} + \sum_{j=1}^{P}\overline{\left(\boldsymbol{u}_{un}(\boldsymbol{x}_i - \boldsymbol{x}_j)\right)}_{map}^{S} - \{1,0\}\right]\left[1+0.15\left(Re_{surf}(i)\right)^{0.687}\right]$$

$$\boldsymbol{F}_{II,PI}(i) = \sum_{j=1}^{P}\boldsymbol{F}_{II,map}(\boldsymbol{x}_i - \boldsymbol{x}_j)$$

$$\boldsymbol{F}_{RI,PI}(i) = \sum_{j=1}^{P}\boldsymbol{F}_{RI,map}(\boldsymbol{x}_i - \boldsymbol{x}_j)$$

$$\boxed{\boldsymbol{F}_{PIEP} = \boldsymbol{F}_{QS,PI} + \boldsymbol{F}_{II,PI} + \boldsymbol{F}_{RI,PI}}$$

PIEP vs DNS for drag

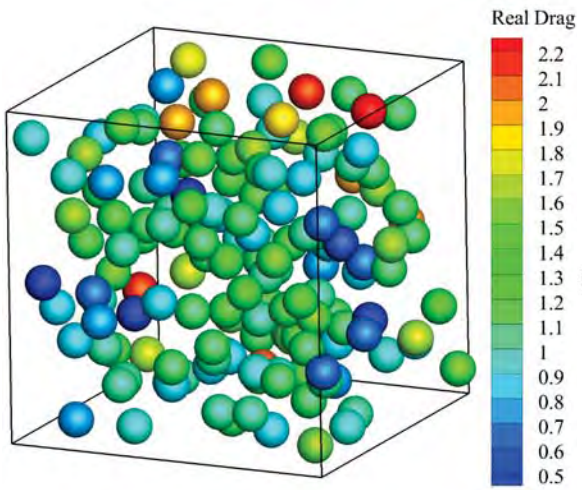

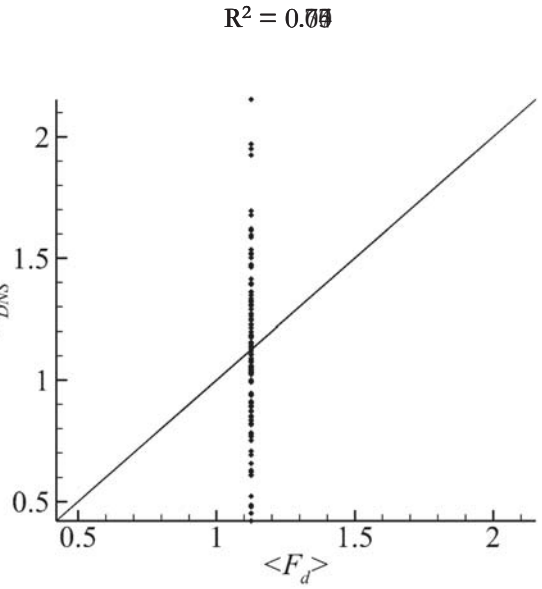

With Quasi-Steady, Inviscid and Rotation Correction

PIEP Using Limited Neighbors

P is the number of neighbors included in the model

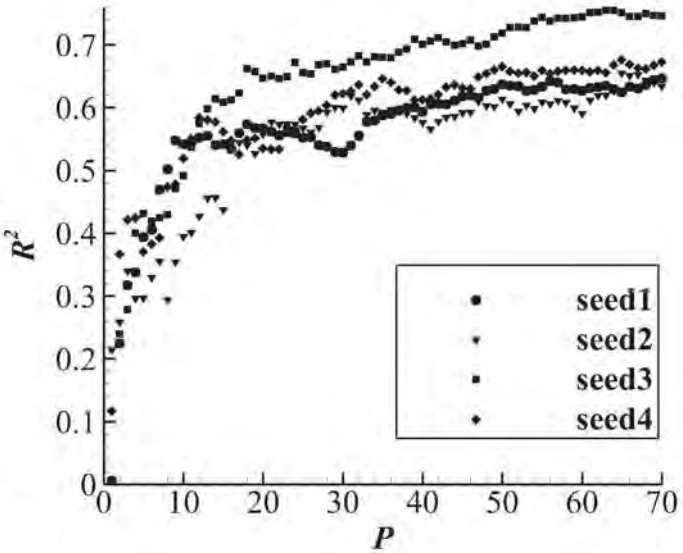

$\phi = 0.1$ $Re = 38$

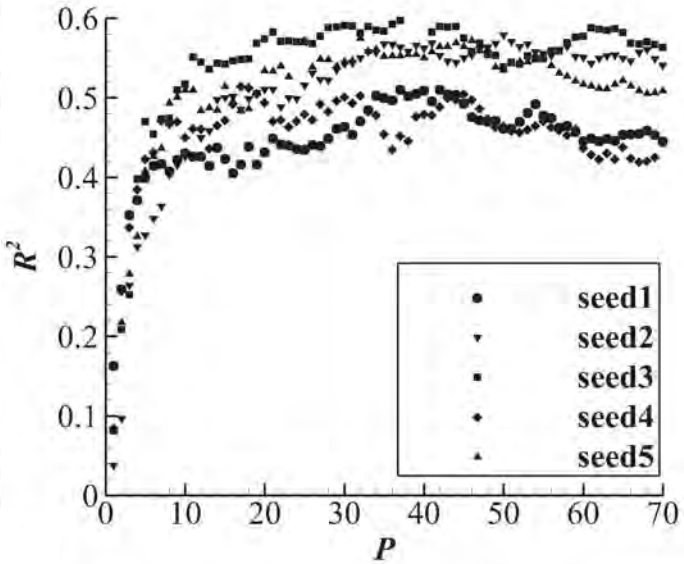

$\phi = 0.2$ $Re = 16$

PIEP vs DNS for lift

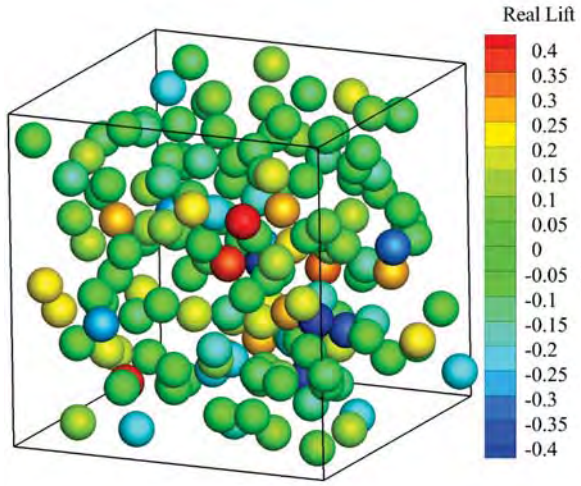

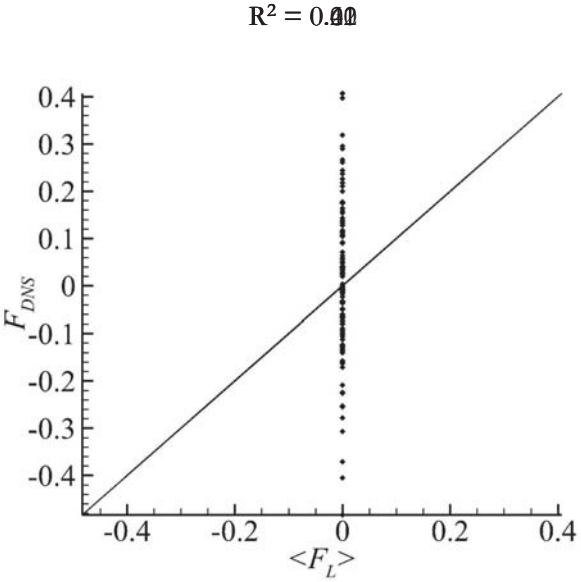

With Quasi-Steady, Inviscid, and Rotational Lift Correction

PIEP Using Limited Neighbors (lift)

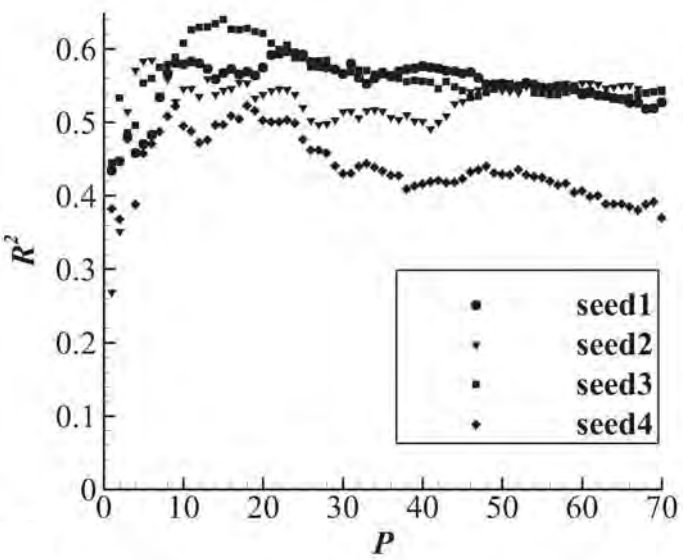

$\phi = 0.1$ $Re = 38$

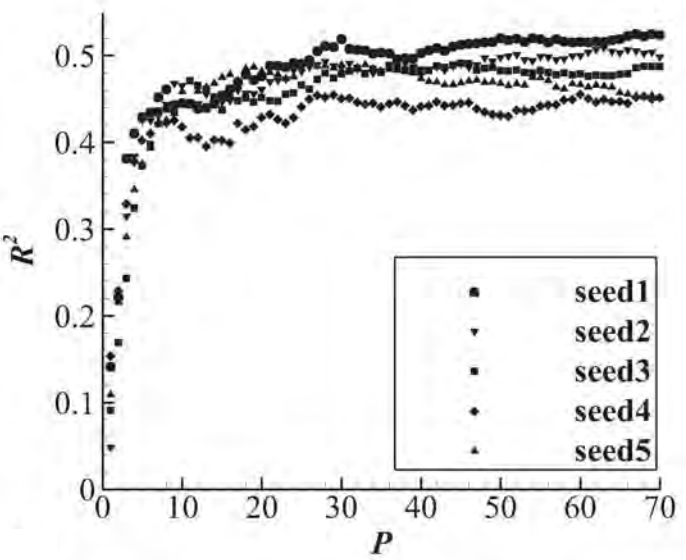

$\phi = 0.2$ $Re = 16$

Outline

- Motivation
- Variation of Hydrodynamic Forces in Arrays of Spheres
- Pairwise Interaction Extended Point-particle (PIEP) Model
- PIEP Model in Sedimentation Problem
- Summary and Future Work

Using PIEP for Sedimentation

Drafting-Kissing-Tumbling test case

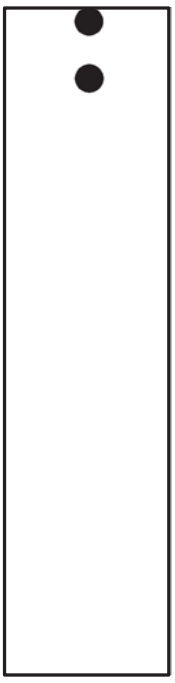

Equations of Motion:

$$\begin{cases} \dfrac{d\tilde{\boldsymbol{x}}_i}{d\tilde{t}} = \tilde{\boldsymbol{v}}_i \\ \tilde{m}_i \dfrac{d\tilde{\boldsymbol{v}}_i}{d\tilde{t}} = (\tilde{m}_i - \tilde{m}_{fi})\,\tilde{\boldsymbol{g}} + \tilde{\boldsymbol{F}}_{hyd,i} + \tilde{\boldsymbol{F}}_{lu,i} + \tilde{\boldsymbol{F}}_{col,i} \\ \tilde{I}_i \dfrac{d\tilde{\boldsymbol{\Omega}}_i}{d\tilde{t}} = \tilde{\boldsymbol{T}}_{hyd,i} + \tilde{\boldsymbol{T}}_{lu,i} + \tilde{\boldsymbol{T}}_{col,i} \end{cases}$$

F_{hyd} is obtained using PIEP to account for the position of the second sphere.

DEM w/ Standard Drag Model

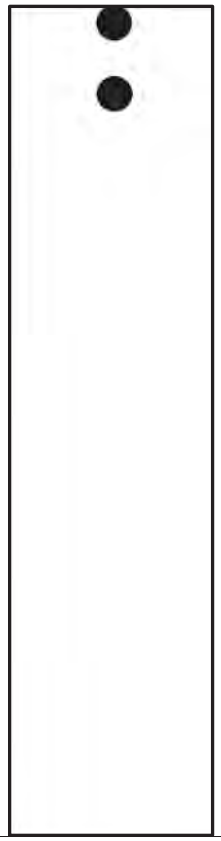

DEM w/ PIEP Model

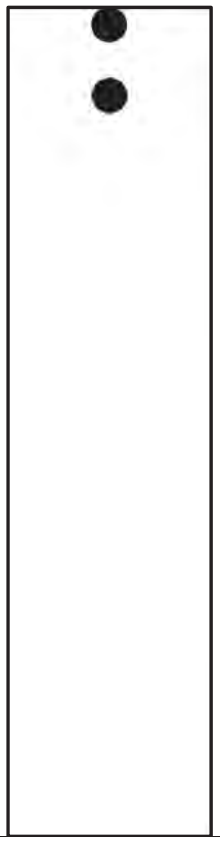

DNS

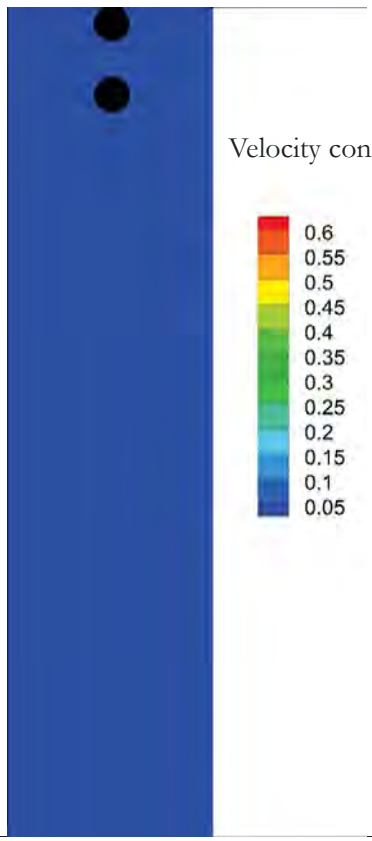

Vertical Velocity Comparison

Velocity of Trailing Sphere

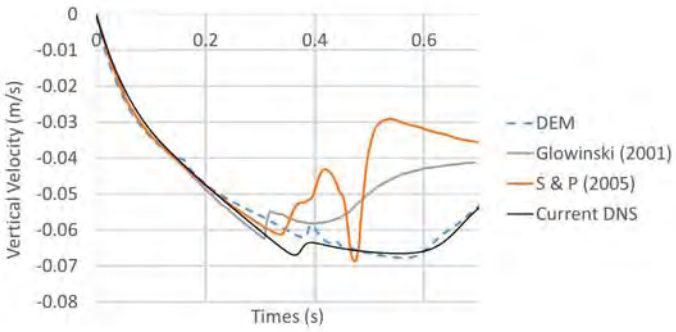

Velocity of Leading Sphere

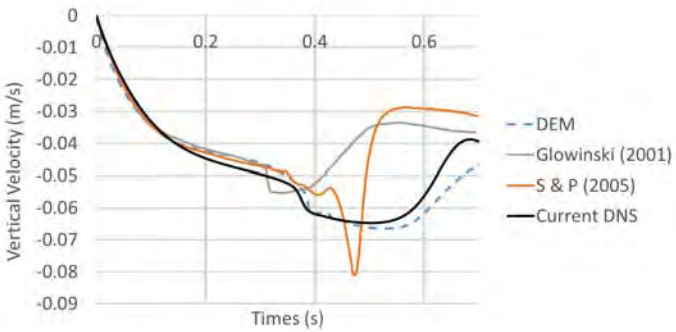

Parameters:

$\frac{\rho_p}{\rho_f} = 1.14$

$\nu = 1 \times 10^{-6}\ \mathrm{m^2/s}$

$d = 1/600\ \mathrm{m}$

$Re_{p(\max)} \simeq 112$

Other studies running the same case using DNS:

- Glowsinki, JCP 2001
- Sharma & Patankar, JCP 2005


DEM w/ PIEP model
Z (unitless)
Y (unitless)
X (unitless)

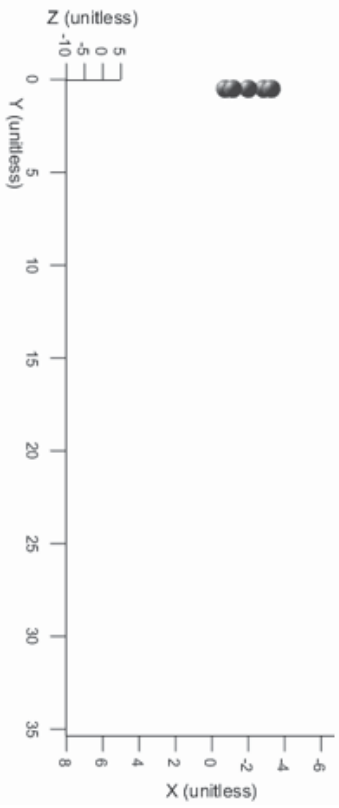
DNS
Z (unitless)
Y (unitless)
X (unitless)

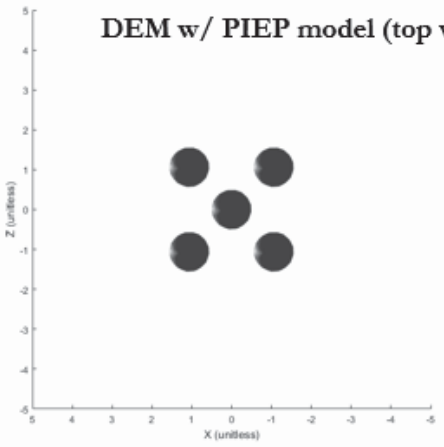
DEM w/ PIEP model (top view)
Z (unitless)
X (unitless)

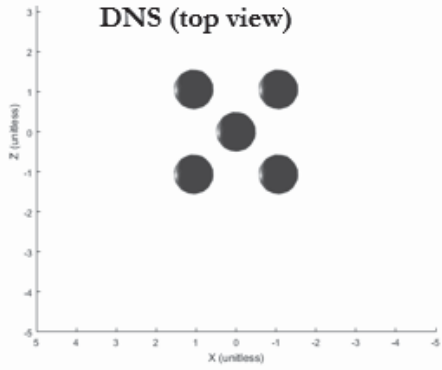
DNS (top view)
Z (unitless)
X (unitless)

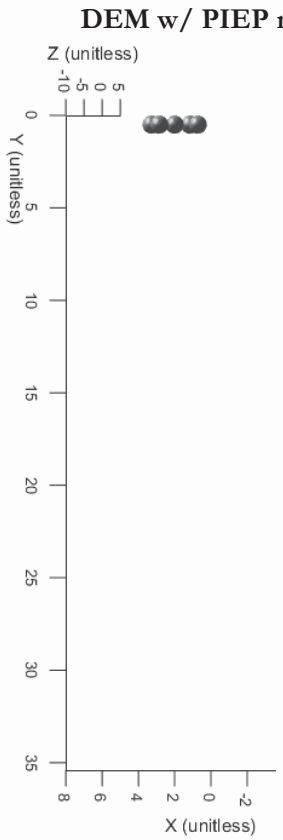
DEM w/ PIEP model
Z (unitless)
Y (unitless)
X (unitless)

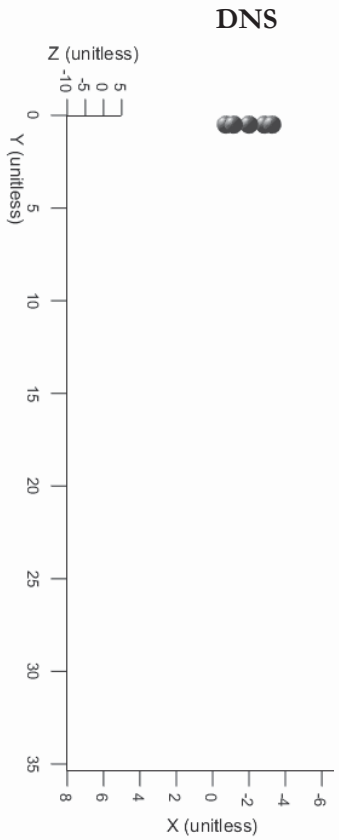
DNS
Z (unitless)
Y (unitless)
X (unitless)

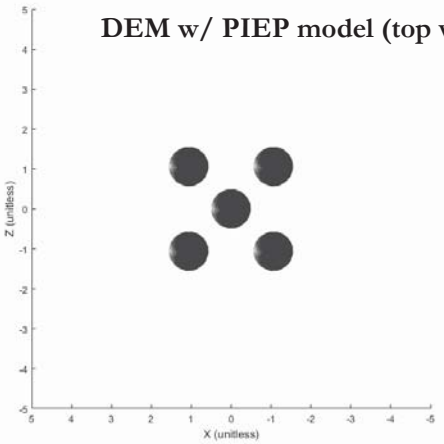
DEM w/ PIEP model (top view)
Z (unitless)
X (unitless)

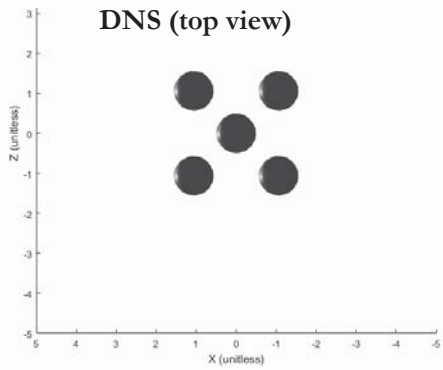
DNS (top view)
Z (unitless)
X (unitless)

Velocity Comparison

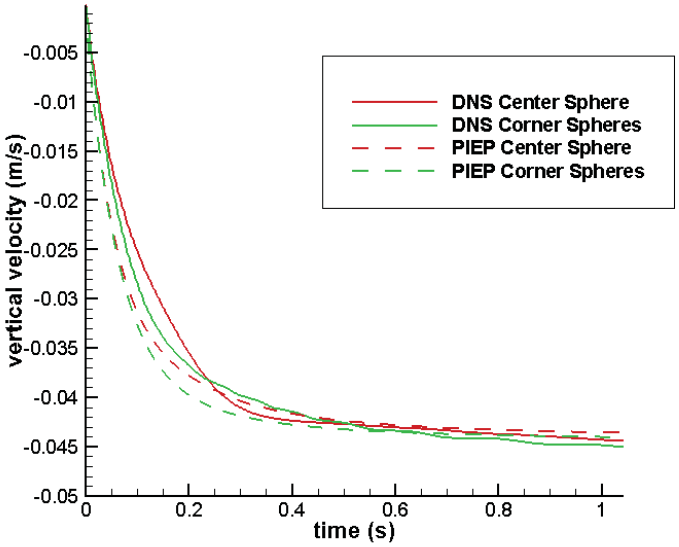

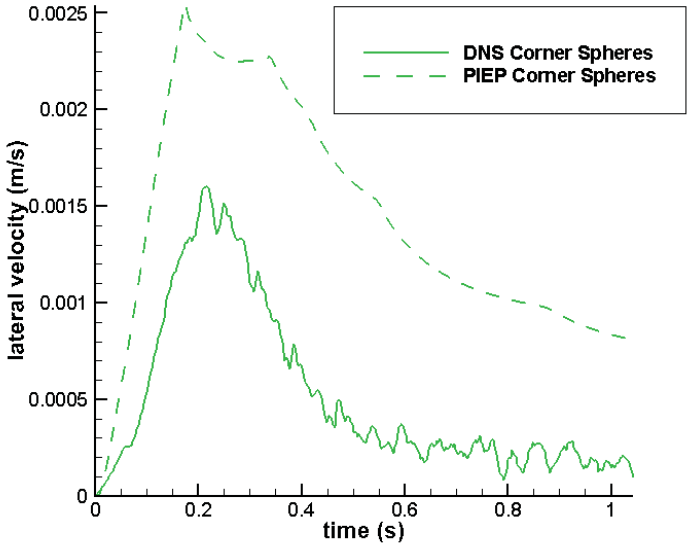

Summary and Future Work

- Quantification of the force variations inside arrays of spherical particles.
- Quantified the drag and lateral force variations within random arrays of spheres.
  - Standard deviation of the drag distribution is very significant with respect to the mean (~17%-27%) and decreases with the volume fraction.
  - Standard deviation of the lateral force distribution is approximately 14% of the mean drag.
- We developed a model (PIEP) which can approximate the drag and lateral force on each particle using the relative locations of few neighboring particles.

Future Work:

- Implementing PIEP model in Eulerian-Lagrangian simulations and compare statistics with classical point-particle models.
- Using PIEP model to explore sedimentation problems with a large number of particles.

Acknowledgment

This work was supported by the U.S. Department of Energy, National Nuclear Security Administration, Advanced Simulation and Computing Program, as a Cooperative Agreement to the University of Florida under the Predictive Science Academic Alliance Program, under Contract No. DE-NA0002378.

This work was done in part at Los Alamos National Lab, during a visit hosted by Dr. Marianne Francois.

Thank you
Questions?

Recent insights on turbulence modeling of strongly-coupled particle-laden flows

Multiphase Physics Deep-Dive

Jesse Capecelatro[1,2]

[1]*Department of Mechanical Engineering, University of Michigan*

[2]*Cetner for Exascale Simulation of Plasma Coupled Combustion (XPACC), University of Illinois*

XPACC @ Illinois

- Positions
  - postdoc (2014—2015)
  - research scientist (2015—2016)

- Advisors: Jonathan Freund, Daniel Bodony

Center for Exascale Simulation of Plasma-Coupled Combustion

XPACC @ Illinois: Overarching problem

- **Combustion** is our energy workhorse and will remain so in the foreseeable future
- Truly **predictive** simulations will accelerate fundamental advances in the use of **plasmas** to advance combustion technology

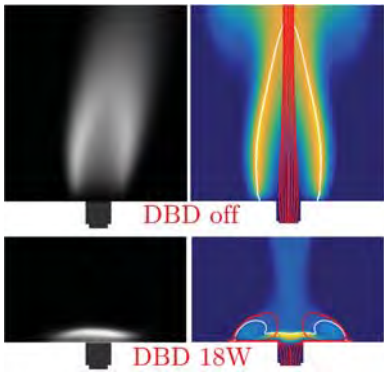

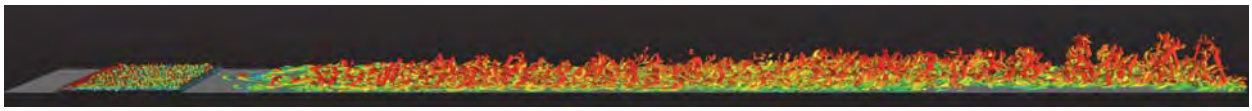

- **The** computer science **advances that enable such** massive-scale **predictive simulations will have impact across engineering and science**

Center for Exascale Simulation of Plasma-Coupled Combustion

XPACC @ Illinois: Target application

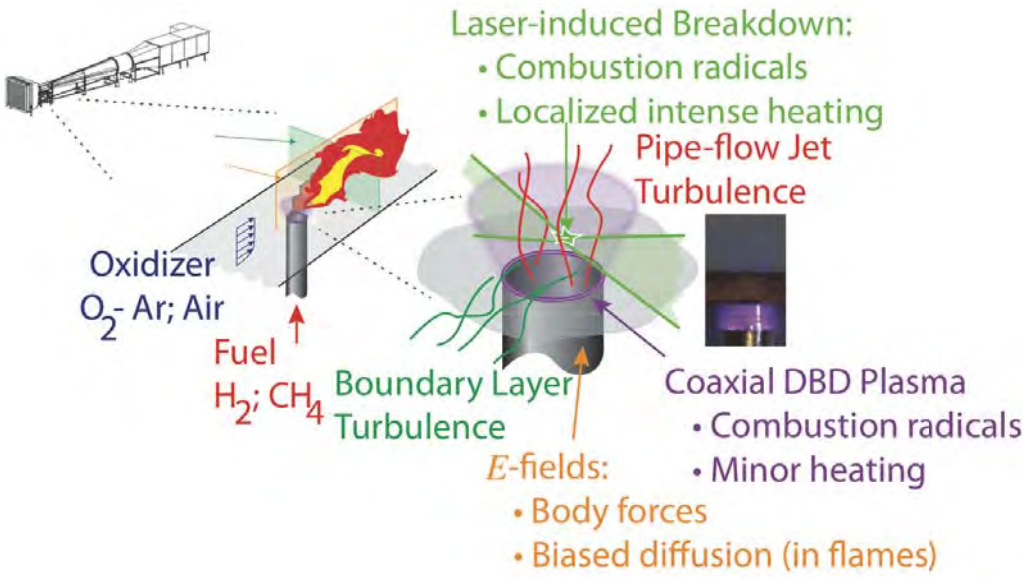

- Predict the ignition threshold of a jet in crossflow via thermal discharge and dieletric-barrier-discharge (DBD) plasmas
- Canonical combustion flow with new 'knobs' for mediating ignition

Center for Exascale Simulation of Plasma-Coupled Combustion

Particle work in XPACC

- No physical particles, per se
- Developing an integrated particle-based discretization for plasma kinetics (PIC)
- Two research projects
  - Adjoint-based sensitivity of PIC methods
  - High-order/high-resolution scalable PIC
- Contact jbfreund@illinois.edu for more info

On to Predictive Modeling of Turbulent Particle-Laden flows

Collaborators:
- Olivier Desjardins, Cornell University
- Rodney Fox, Iowa State University

Multi-scale nature of strongly-coupled gas-solid flows

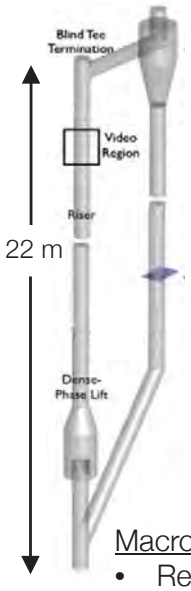

Macroscale
- Reactor geometry: O(10) m
- Number of particles: O(10^9)

Multi-scale nature of strongly-coupled gas-solid flows

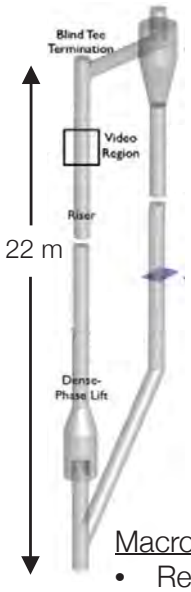

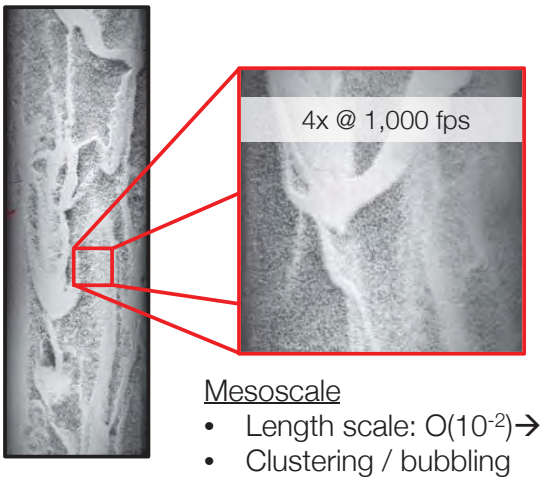

Mesoscale
- Length scale: O(10^{-2})→ O(10) m
- Clustering / bubbling
- Turbulence modulation

Macroscale
- Reactor geometry: O(10) m
- Number of particles: O(10^9)

High-speed imaging courtesy of F. Shaffer & B. Gopalan
D.O.E. National Energy Technology Lab

Multi-scale nature of strongly-coupled gas-solid flows

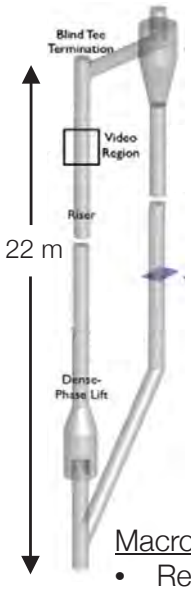

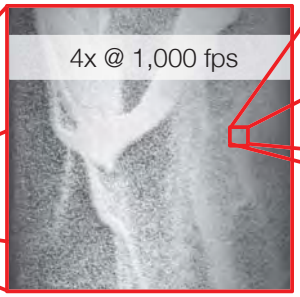

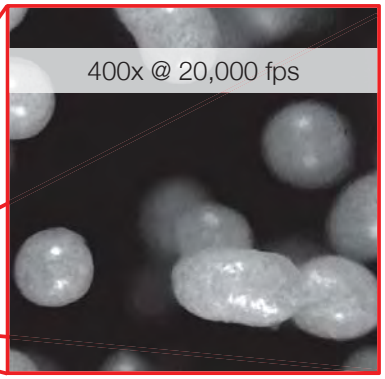

Microscale
- Particle diameter: O(10^{-6}) m
- Wakes
- Collisions
- Surface reactions
- Phase change

Mesoscale
- Length scale: O(10^{-2})→ O(10) m
- Clustering / bubbling
- Turbulence modulation

Macroscale
- Reactor geometry: O(10) m
- Number of particles: O(10^{9})

Microscale physics impact macroscale quantities of interest!

High-speed imaging courtesy of F. Shaffer & B. Gopalan
D.O.E. National Energy Technology Lab

Introduction | Modeling Aspects | VF-EL Framework | Results & Discussion | Conclusions
Multi-scale nature of strongly-coupled gas-solid flows

- Key objectives
  1. Develop accurate and tractable methods that capture detailed mesoscale features
  2. Extract useful data from simulations to inform reduced-order model closure
  3. Develop a predictive turbulence model valid across granular regimes

MichiganEngineering
Multiphase Physics Deep-Dive | 10

Towards a macroscopic turbulence model[1]

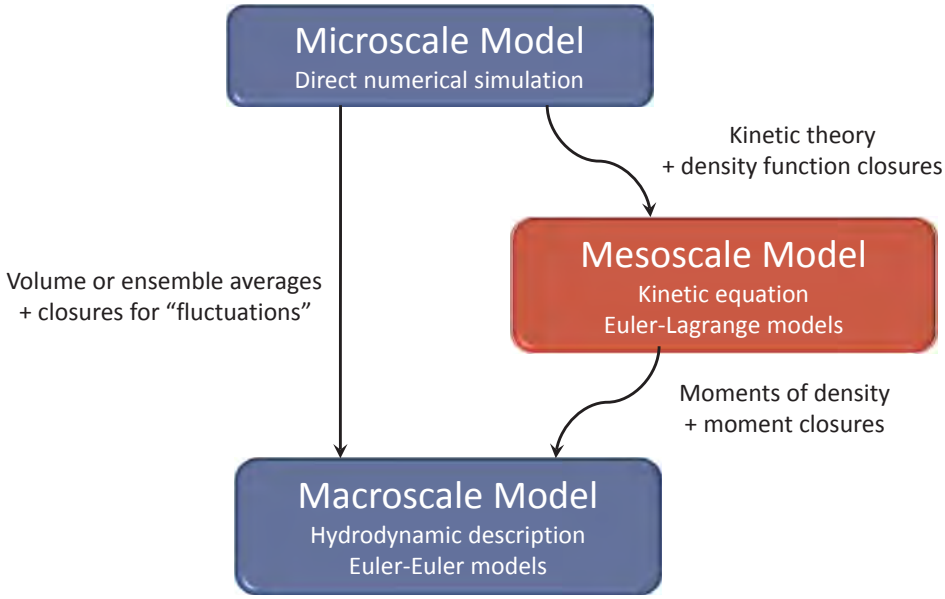

Mesoscale model incorporated more microscale physics in closures!

1. R.O. Fox (2012), *Annu. Rev. Fluid Mech.*

Correlated vs. uncorrelated granular energy

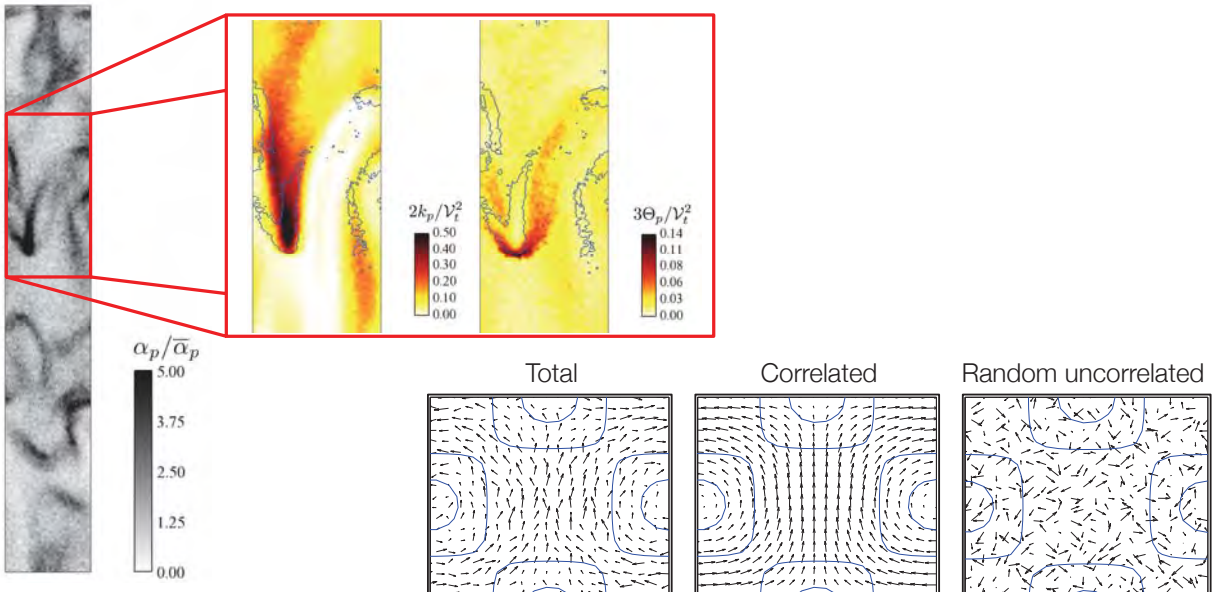

- Velocity partitioned into *correlated* and *uncorrelated* contributions

$$v_p^{(i)}(t) = u_p[x_p^{(i)}(t), t] + \delta v_p^{(i)}(t)$$

$$\kappa_p = k_p + \frac{3}{2}\langle\Theta\rangle_p$$

Correlated vs. uncorrelated granular energy

Accurately separating the two contributions is crucial for turbulence modeling!

Particle turbulent kinetic energy
- Dissipation of k_p enters as source term for $\langle\Theta\rangle_p$

Granular temperature
- Needed for computing particle pressure and viscosity
- Failure to separate leads to gross over-prediction in collision rate

$$\kappa_p = k_p + \frac{3}{2}\langle\Theta\rangle_p$$

Exact Reynolds-average equations[1]

- Homogeneous gravity-driven flow: Fluid-phase Reynolds stress

$$\frac{1}{2}\frac{\partial\langle u'''^2_{f,1}\rangle_f}{\partial t} = \frac{1}{\rho_f}\left(\left\langle p_f\frac{\partial u'''_{f,1}}{\partial x_1}\right\rangle - \left\langle \sigma_{f,1i}\frac{\partial u'''_{f,1}}{\partial x_i}\right\rangle\right) \quad PS/VD$$

$$+ \frac{\varphi}{\tau_p}\left(\langle u'''_{f,1}u''_{p,1}\rangle_p - \langle u'''^2_{f,1}\rangle_p\right) \quad DE$$

$$+ \frac{\varphi}{\tau_p}\langle u'''_{f,1}\rangle_p\langle u_{p,1}\rangle_p \quad DP$$

$$+ \frac{\varphi}{\rho_p}\left(\left\langle u'''_{f,1}\frac{\partial p'_f}{\partial x_1}\right\rangle_p - \left\langle u'''_{f,1}\frac{\partial \sigma'_{f,1i}}{\partial x_i}\right\rangle_p\right) \quad PE/VE$$

  - Fluid-phase TKE is generated by the drag production (*DP*) term, as opposed to in single-phase turbulence where it is produced by mean velocity gradients.
  - Fluid velocity *seen by the particles*: $\langle u_f\rangle_p = \langle\alpha_p u_f\rangle/\langle\alpha_p\rangle$
  - Because clusters arise spontaneously in CIT, and are negatively correlated with the fluid velocity $\langle u_f\rangle_f = \langle\alpha_f u_f\rangle/\langle\alpha_f\rangle \neq \langle u_f\rangle_p$

1. J. Capecelatro, O . Desjardins, R.O. Fox (Under review), *J. Fluid Mech.*

Exact Reynolds-average equations[1]

- PA particle-phase Reynolds stress

Turbulent dissipation of k_p

$$\frac{1}{2}\frac{\partial \langle u''^2_{p,1}\rangle_p}{\partial t} = \left\langle \Theta \frac{\partial u''_{p,1}}{\partial x_1} \right\rangle_p - \left\langle \sigma_{p,1i} \frac{\partial u''_{p,1}}{\partial x_i} \right\rangle_p \qquad PS/VD$$

$$+ \frac{1}{\tau_p}\left(\langle u'''_{f,1} u''_{p,1}\rangle_p - \langle u''^2_{p,1}\rangle_p\right) \qquad DE$$

$$+ \frac{1}{\rho_p}\left(\left\langle u''_{p,1}\frac{\partial \sigma'_{f,1i}}{\partial x_i}\right\rangle_p - \left\langle u''_{p,1}\frac{\partial p'_f}{\partial x_1}\right\rangle_p\right) \qquad VE/PE$$

- Particle-phase stress tensor:

Production of $\langle\theta\rangle_p$

$$\frac{1}{2}\frac{\partial \langle P_{11}\rangle_p}{\partial t} = -\left\langle \Theta \frac{\partial u''_{p,1}}{\partial x_1} \right\rangle_p + \left\langle \sigma_{p,1i} \frac{\partial u''_{p,1}}{\partial x_i} \right\rangle_p \qquad PS/VD$$

$$- \frac{1}{\tau_p}\langle P_{11}\rangle_p \qquad DE$$

$$+ \frac{6}{\sqrt{\pi} d_p}\langle \alpha_p \Theta^{1/2}\left(\Delta^\star_{11} - P_{11}\right)\rangle_p \qquad CD$$

Collisional equilibrium[2]

$$\Delta^\star_{11} = \frac{1}{4}(1+\mathrm{e})^2\,\Theta + \frac{1}{4}(1-\mathrm{e})^2\,P_{11}$$

1. J. Capecelatro, O . Desjardins, R.O. Fox (Under review), *J. Fluid Mech.*
2. A. Passalacqua et al. (2011), *Comm in Comp. Phys.*

Volume-Filtered Euler-Lagrange Framework

Volume-filtered Description

- Objective: formulate equations for fluid-particle flows that allow $\Delta x > d_p$
- Introduce a local volume filter based on convolution product with kernel[1] $G(r)$
  - Accurate solution requires $\Delta x \ll \delta_f$
- Define local volume fraction

$$\alpha_f(\boldsymbol{x}, t) = \int_{V_f} G(|\boldsymbol{x} - \boldsymbol{y}|) d\boldsymbol{y}$$

- Define a filtered variable $\overline{a}$ from a point variable a

$$\alpha_f \overline{a}(\boldsymbol{x}, t) = \int_{V_f} a(\boldsymbol{y}, t) G(|\boldsymbol{x} - \boldsymbol{y}|) d\boldsymbol{y} \qquad a = \overline{a} + a'$$

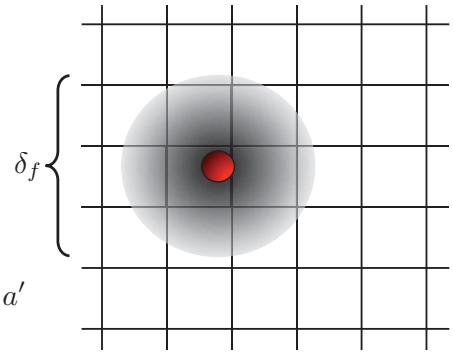

- Closure for sub-filter terms depend on choice of δ_f

[1] Anderson & Jackson (1967)

Volume-filtered Description

- What is an appropriate choice for δ_f?

$$\int_{V_f} \nabla \cdot \boldsymbol{\tau} G(|\boldsymbol{x} - \boldsymbol{y}|) d\boldsymbol{y} = \nabla \cdot (\alpha_f \overline{\boldsymbol{\tau}}) - \sum_{i=1}^{N_p} \int_{S_p} \boldsymbol{n} \cdot \boldsymbol{\tau} G(|\boldsymbol{x} - \boldsymbol{y}|) d\boldsymbol{y}$$

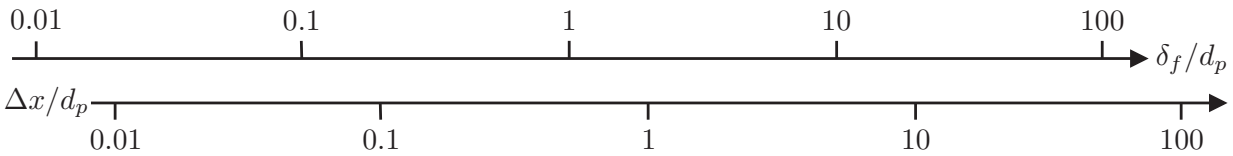

Particle-resolved DNS | *Partially resolved* | Point particle

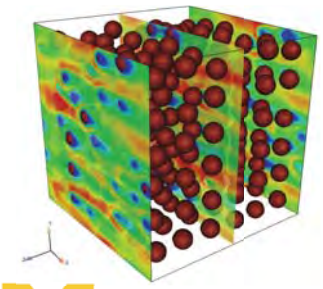

Relevant to strongly-coupled flows

Requires an efficient implementation to distribute data to the mesh

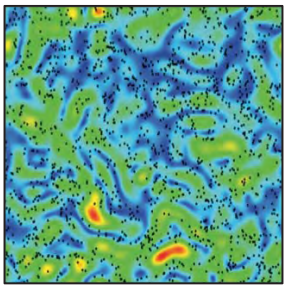

Volume-filtered Description

- What is an appropriate choice for δ_f?

$$\int_{V_f} \nabla \cdot \boldsymbol{\tau} G(|\boldsymbol{x}-\boldsymbol{y}|) d\boldsymbol{y} = \nabla \cdot (\alpha_f \overline{\boldsymbol{\tau}}) - \sum_{i=1}^{N_p} \int_{S_p} \boldsymbol{n} \cdot \boldsymbol{\tau} G(|\boldsymbol{x}-\boldsymbol{y}|) d\boldsymbol{y}$$

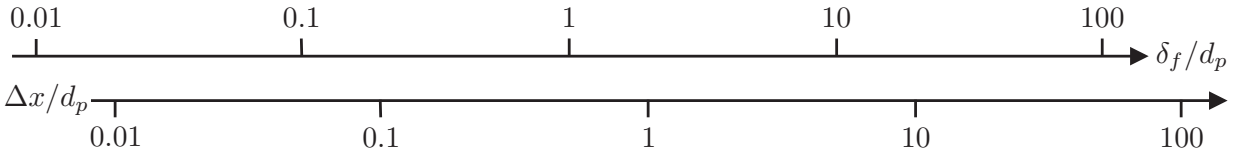

Particle-resolved DNS | *Partially resolved* | Point particle

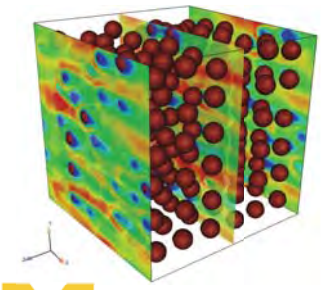

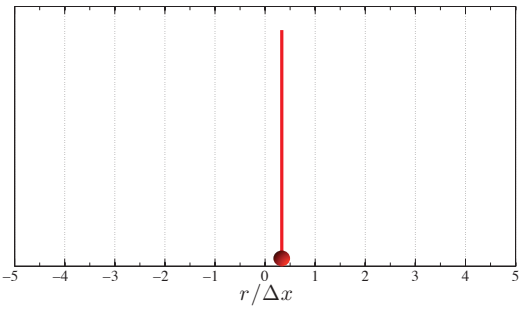

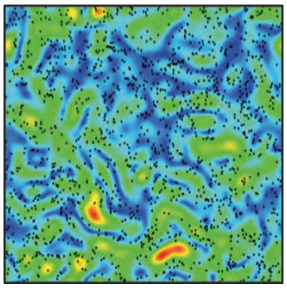

Volume-filtered Description

- What is an appropriate choice for δ_f?

$$\int_{V_f} \nabla \cdot \boldsymbol{\tau} G(|\boldsymbol{x}-\boldsymbol{y}|) d\boldsymbol{y} = \nabla \cdot (\alpha_f \overline{\boldsymbol{\tau}}) - \sum_{i=1}^{N_p} \int_{S_p} \boldsymbol{n} \cdot \boldsymbol{\tau} G(|\boldsymbol{x}-\boldsymbol{y}|) d\boldsymbol{y}$$

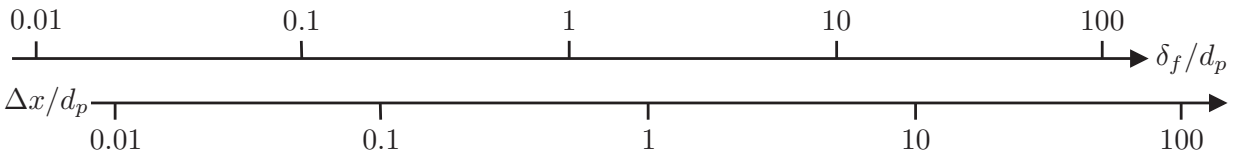

Particle-resolved DNS | *Partially resolved* | Point particle

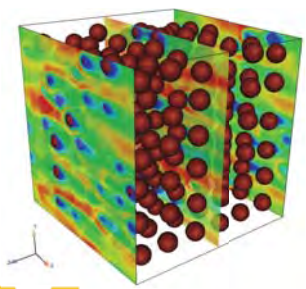

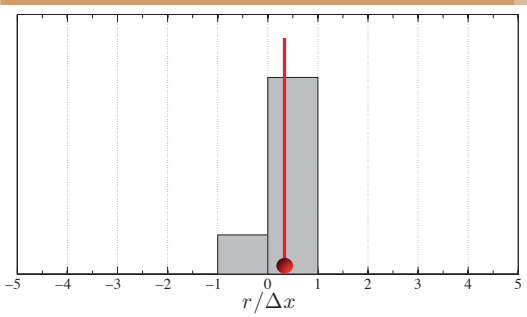

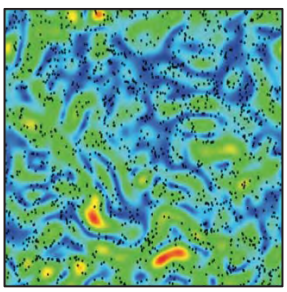

Volume-filtered Description

- What is an appropriate choice for δ_f?

$$\int_{V_f} \nabla \cdot \boldsymbol{\tau} G(|\boldsymbol{x}-\boldsymbol{y}|) d\boldsymbol{y} = \nabla \cdot (\alpha_f \overline{\boldsymbol{\tau}}) - \sum_{i=1}^{N_p} \int_{S_p} \boldsymbol{n} \cdot \boldsymbol{\tau} G(|\boldsymbol{x}-\boldsymbol{y}|) d\boldsymbol{y}$$

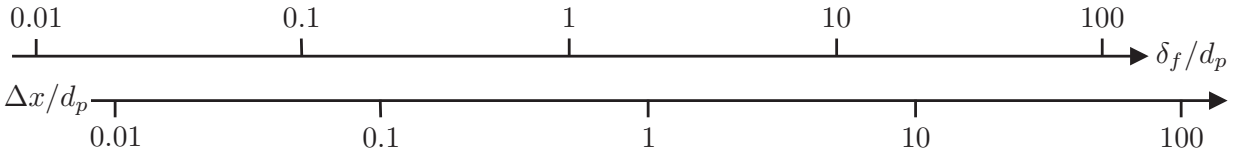

Particle-resolved DNS | *Partially resolved* | Point particle

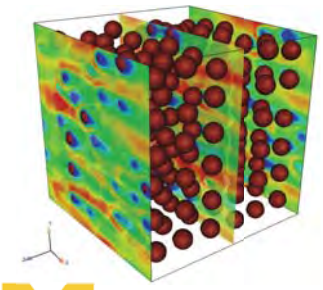

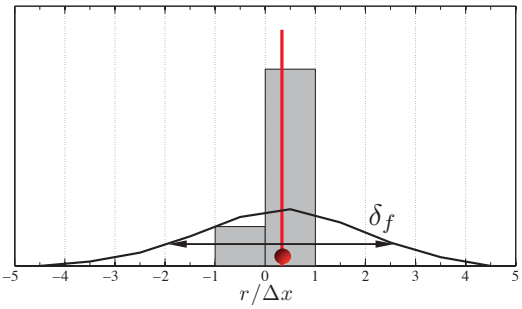

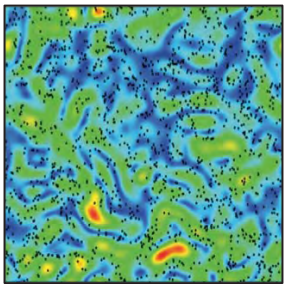

Filter width δ_f is independent of the mesh size[1]

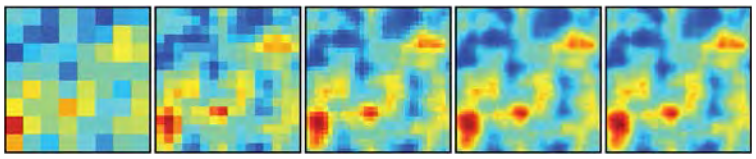

$\Delta x = 4d_p$ $\Delta x = 2d_p$ $\Delta x = d_p$ $\Delta x = d_p/2$ $\Delta x = d_p/4$

Error

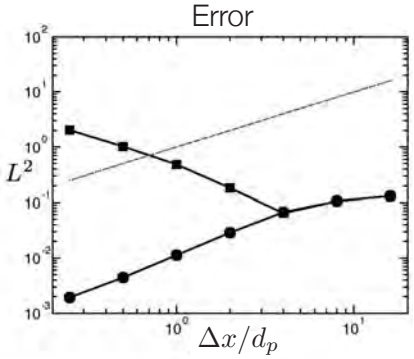

1st-order (--)
Single-step (■)
Two-step (●)

1. J. Capecelatro and O. Desjardins (2013), *J. Comp. Phys.*

Volume-filtered equations of motion

- Implemented in a low Mach, variable density solver[1]

$$\frac{\partial \alpha_f \rho_f}{\partial t} + \nabla \cdot (\alpha_f \rho_f \overline{\boldsymbol{u}}_f) = 0$$

$$\frac{\partial \alpha_f \rho_f \overline{\boldsymbol{u}}_f}{\partial t} + \nabla \cdot (\alpha_f \rho_f \overline{\boldsymbol{u}}_f \otimes \overline{\boldsymbol{u}}_f) = \nabla \cdot \overline{\boldsymbol{\tau}} - \rho_p \alpha_p \overline{\boldsymbol{\mathcal{A}}} + \alpha_f \rho_f \boldsymbol{g}$$

$$\overline{\boldsymbol{\tau}} = -\overline{p}\boldsymbol{I} + (\mu + \mu^*)\left[\nabla \overline{\boldsymbol{u}}_f + \nabla \overline{\boldsymbol{u}}_f^{\mathsf{T}} - \frac{2}{3}(\nabla \cdot \overline{\boldsymbol{u}}_f)\boldsymbol{I}\right]$$

- Lagrangian particle tracking[2]

$$\frac{d\boldsymbol{x}_p^{(i)}}{dt} = \boldsymbol{v}_p^{(i)}$$

$$\frac{d\boldsymbol{v}_p^{(i)}}{dt} = \boldsymbol{\mathcal{A}}^{(i)} + \boldsymbol{F}_c^{(i)} + \boldsymbol{g}$$

$$I_p \frac{d\omega_p}{dt} = \sum_j \frac{d_p}{2} \boldsymbol{n} \times f_{t,i \to i}^{\text{col}}$$

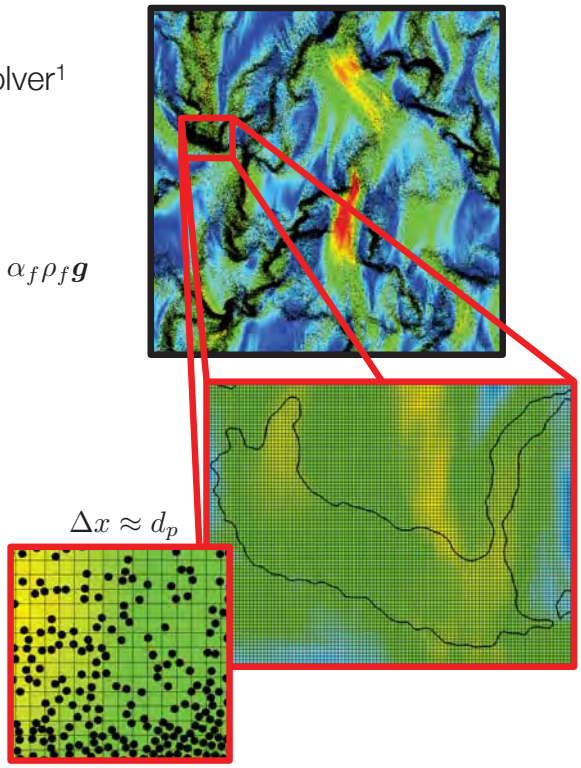

1. O. Desjardins, G. Blanquart, G. Balarac, H. Pitsch (2008), *J. Comp. Phys.*
2. J. Capecelatro and O. Desjardins (2013), *J. Comp. Phys.*

Fully-developed CIT configuration[1]

	Physical parameters			
d_p	Particle diameter	0.09 mm		
ρ_p	Particle density	1000 kg m^{-3}		
ρ_f	Fluid density	1 kg m^{-3}		
ν_f	Fluid kinematic viscosity	1.8×10^{-5} m^2 s^{-1}		
e	Coefficient of restitution	0.9		
N_p	Number of particles	55×10^6		
	Non-dimensional parameters			
$\langle \alpha_p \rangle$	Mean particle volume fraction	0.01		
φ	Mean mass loading	10.1		
Re_p	Particle Reynolds number	0.25	0.5	1.0
Re_f	Fluid Reynolds number	3.5	13.9	55.5
$L_x/\mathcal{L}$	Normalized domain length	256	128	64
	Dimensional parameters			
τ_p	Drag time	0.025 s		
$\mathcal{V}$	Cluster velocity	0.05	0.10	0.20 m s^{-1}
$\mathcal{L}$	Cluster length	1.25	2.50	5.00 mm

Table 1: Fluid-particle parameters used in CIT simulations.

Mesh: $2048 \times 512 \times 512$ $(3584 d_p \times 896 d_p \times 896 d_p)$
Particles: $N_p = 55 \times 10^6$

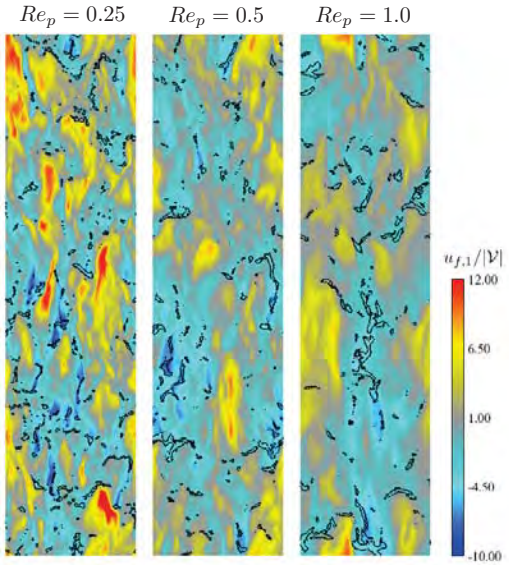

1. J. Capecelatro, O. Desjardins, R.O. Fox (2015) *J. Fluid Mech.*

Extracting multiphase statistics[1]

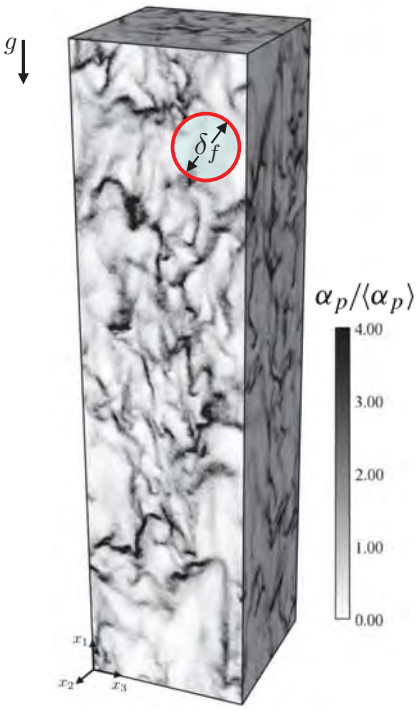

- How to extract statistics from Euler-Lagrange data?

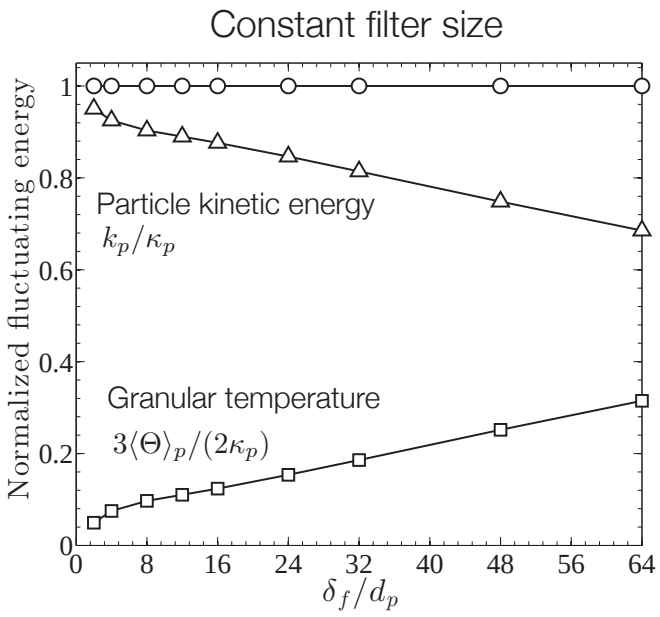

1. J. Capecelatro *et al.* (2014), *J. Fluid Mech.*

Extracting multiphase statistics[1]

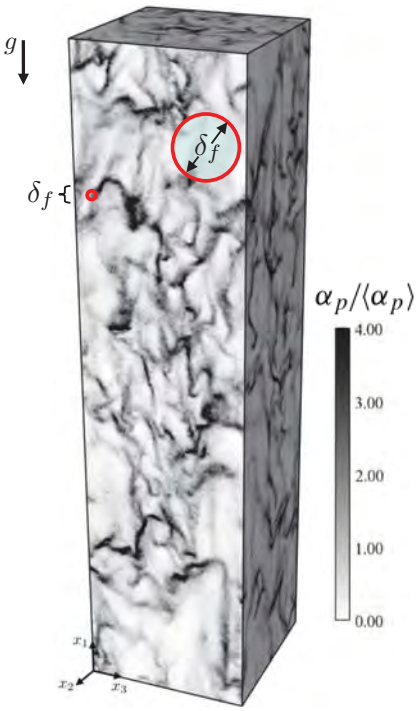

- How to extract statistics from Euler-Lagrange data?

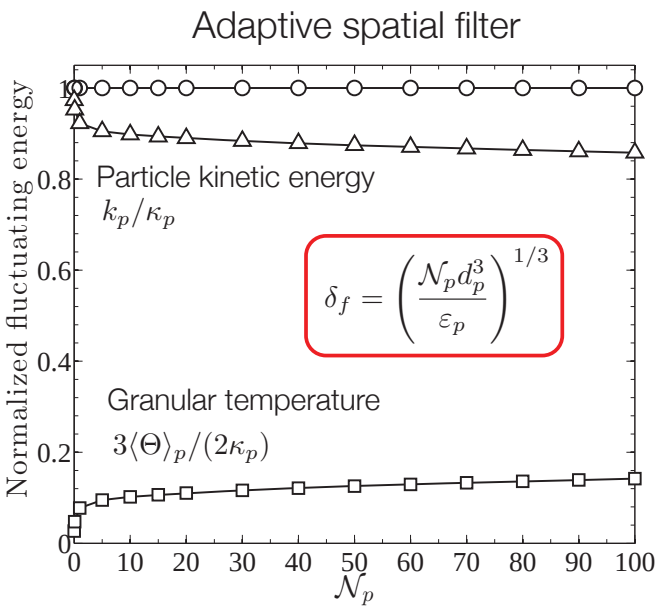

1. J. Capecelatro *et al.* (2014), *J. Fluid Mech.*

Local instantaneous granular temperature (2D example)

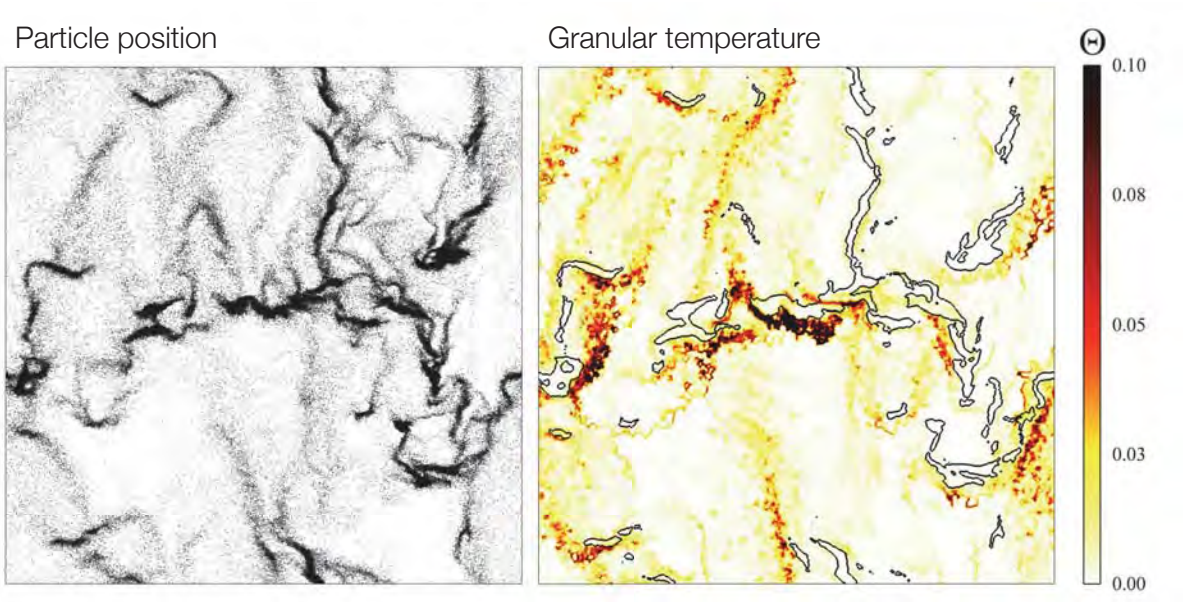

- Minimum agitation within clusters
- Maximum granular temperature located at the upstream boundary of clusters

Results & Discussion

Particle behavior in homogeneous CIT

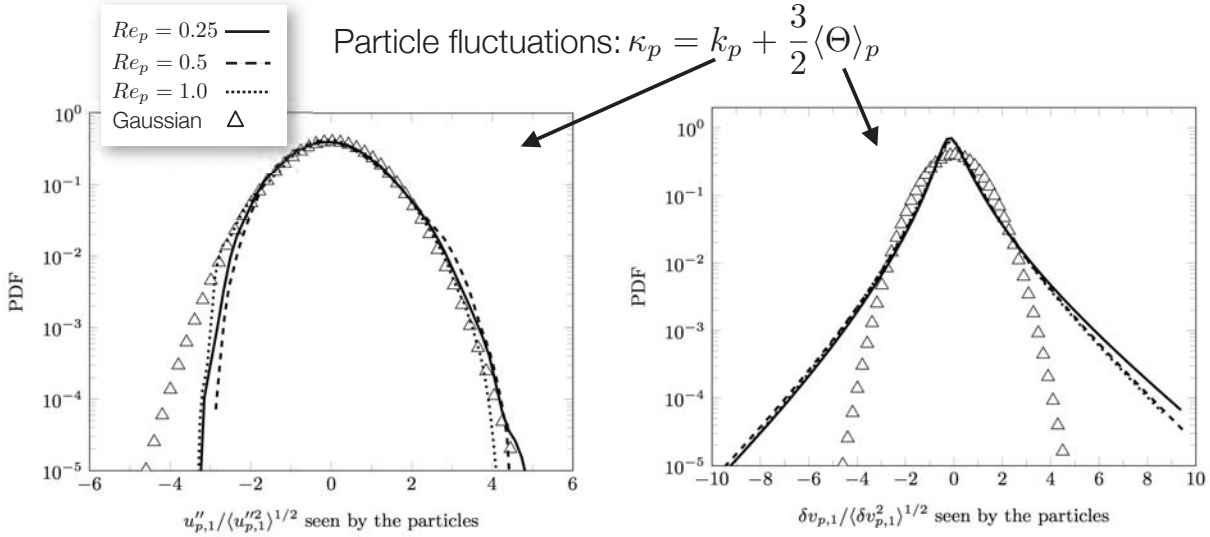

- Spatially-correlated and uncorrelated velocity behave fundamentally different!

CIT in wall-bounded flows[1]

- Two-step filter permits grid stretching near the wall

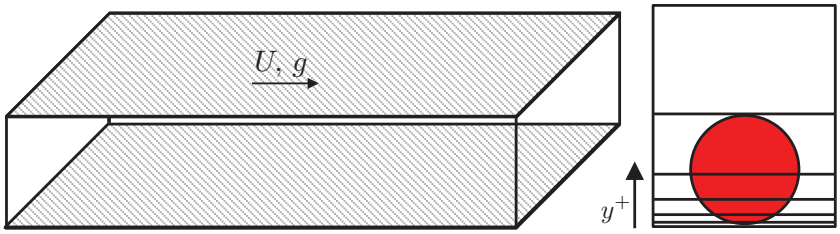

Physical parameters

d_p	Particle diameter	0.20	mm
ρ_p	Particle density	2000	kg/m^3
ρ_g	Gas density	1	kg/m^3
ν_g	Gas kinematic viscosity	1.8×10^{-5}	m^2/s
W	Channel width	0.05	m
g	Gravity magnitude	3.645	m/s^2
$\mathcal{V}_t$	Terminal velocity	0.9	m/s
$\mathcal{L}$	Cluster length	0.22	m

Non-dimensional parameters

$\overline{\alpha}_p$	Average particle volume fraction	0.01
$\overline{\varphi}$	Average mass loading	20.2
e, e_w	Coefficient of restitution	0.9
Re_p	Particle Reynolds number	10
Re_g	Fluid Reynolds number	11,000
Re_W	Channel Reynolds number	2500

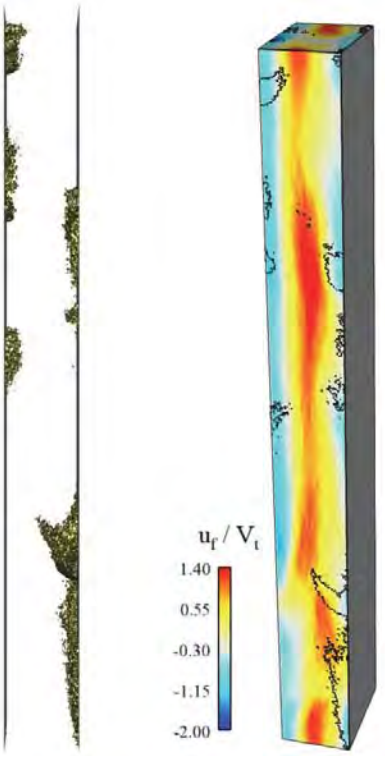

1. J. Capecelatro *et al.* (2016), *Phys. Fluids.*

Considerations for turbulence modeling

- Decomposition of correlated / uncorrelated components is needed to get BC correct

Correlated (particle TKE)

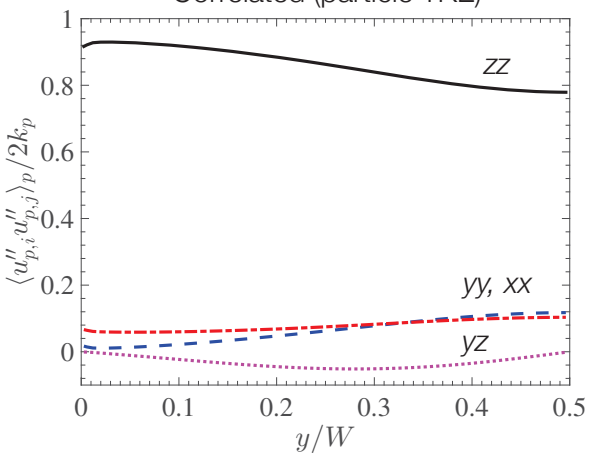

Uncorrelated (granular temperature)

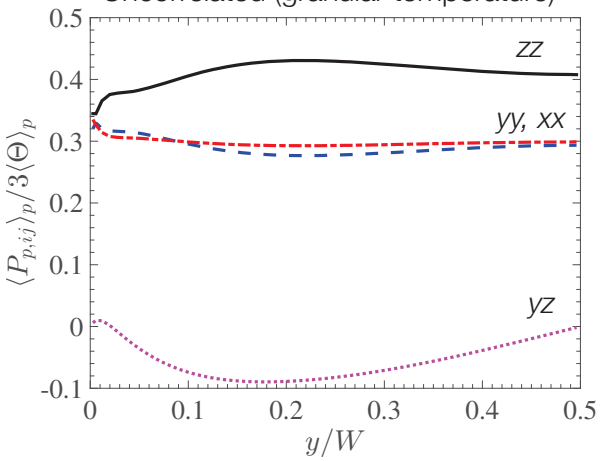

- Boundary conditions for components $\kappa_p = k_p + \frac{3}{2}\langle \Theta \rangle_p$
  - Wall-normal correlated energy: $k_p = 0$
  - Wall-normal uncorrelated energy: $\langle \Theta \rangle_p \neq 0$

Summary & conclusions (numerics)

- Volume-filtered Euler-Lagrange approach is an efficient method to handle large number of particles without requiring $\Delta x \gg d_p$

- Microscale models (e.g., drag) are agnostic to volume filter
  - If $\delta_f / d_p \ll 1$: drag entirely accounted for in resolved flow
  - If $\delta_f / d_p \gg 1$: model must account for entire drag contribution

Logical solution: develop closure models that are a function of δ_f / d_p

$$\frac{du_p}{dt} = \frac{F}{\tau_p}\left(u_f - u_p\right), \quad F = F\left(\mathrm{Re}_p, \alpha_p, \delta_f / d_p\right)$$

Summary & conclusions (modeling)

- In high mass loading flows, turbulence arises mainly due to CIT (drag production)
- TKE is produced by fluid velocity fluctuations seen by the particles
- Partitioning the granular energy into spatially correlated (particle-phase TKE) and uncorrelated (granular temperature) components is crucial
- Predictive models need to account for anisotropy in wall-bounded flows
- How best to incorporate effects of heat transfer and chemical kinetics in a reduce-order model for strongly-coupled flows?

Looking forward: from prediction to design

- Up to this point we have focused on *predictive* models in order to compute a *quantity of interest* $\mathcal{J} = \mathcal{J}(\boldsymbol{Q}, \boldsymbol{f})$
  - $\boldsymbol{Q}$: flow solution, *e.g.* $\boldsymbol{Q} = [\alpha_f,\ \rho_f, \boldsymbol{u}_f,\ \ldots]^\mathsf{T}$
  - $\boldsymbol{f}$: design / modeling parameters
- We want to *optimize* $\mathcal{J}$ or measure its *sensitivity*
  - Find optimal reactor geometry to maximize $\mathcal{J}$
  - Determine which modeling parameters $\mathcal{J}$ is most sensitive to
- Brute force: guess $\boldsymbol{f}$, calculate $\boldsymbol{Q}$, calculate $\mathcal{J}$, repeat,…
  - ~~Option *a*: hire a graduate student to do this~~
  - Option *b*: formulate a variational problem constrained by the governing equations

    → Adjoint system that provides sensitivity without requiring repeated solutions

$$\mathcal{J} = \int_{t_1}^{t_2} \int_{\Omega} T(\boldsymbol{x}, t)\ d\boldsymbol{x}\ dt$$

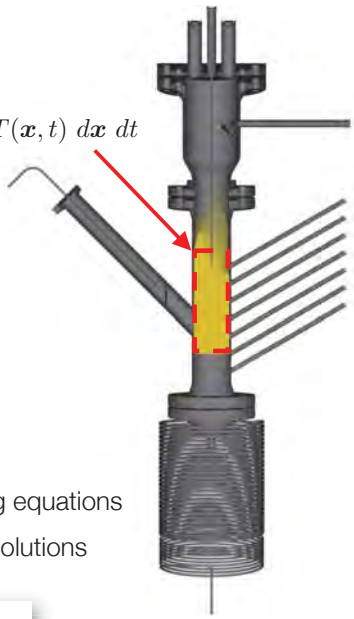

$$\frac{\delta \mathcal{J}}{\delta \boldsymbol{f}} = \int_{\Omega} \int_{t_1}^{t_2} \boldsymbol{Q}^\dagger \frac{\partial \mathcal{N}}{\partial \boldsymbol{f}} d\boldsymbol{x}\, dt \qquad -\frac{\partial \boldsymbol{Q}^\dagger}{\partial t} = \mathcal{R}^\dagger \left[\boldsymbol{Q},\ \boldsymbol{Q}^\dagger\right](\boldsymbol{x},\ t)$$

Adjoint-based methods can accelerate the design of multiphase systems!

Questions?

Backup slides

Exact Reynolds-average equations[1]

- Homogeneous gravity-driven flow: Fluid-phase Reynolds stress

$$\frac{1}{2}\frac{\partial\langle u_{f,1}'''^2\rangle_f}{\partial t} = \frac{1}{\rho_f}\left(\left\langle p_f\frac{\partial u_{f,1}'''}{\partial x_1}\right\rangle - \left\langle \sigma_{f,1i}\frac{\partial u_{f,1}'''}{\partial x_i}\right\rangle\right) \quad PS/VD$$

$$+ \frac{\varphi}{\tau_p}\left(\langle u_{f,1}''' u_{p,1}''\rangle_p - \langle u_{f,1}'''^2\rangle_p\right) \quad DE$$

$$+ \frac{\varphi}{\tau_p}\langle u_{f,1}'''\rangle_p\langle u_{p,1}\rangle_p \quad DP$$

$$+ \frac{\varphi}{\rho_p}\left(\left\langle u_{f,1}'''\frac{\partial p_f'}{\partial x_1}\right\rangle_p - \left\langle u_{f,1}'''\frac{\partial \sigma_{f,1i}'}{\partial x_i}\right\rangle_p\right) \quad PE/VE$$

  - Fluid-phase TKE is generated by the drag production (*DP*) term, as opposed to in single-phase turbulence where it is produced by mean velocity gradients.
  - Fluid velocity *seen by the particles*: $\langle u_f\rangle_p = \langle\alpha_p u_f\rangle/\langle\alpha_p\rangle$
  - Because clusters arise spontaneously in CIT, and are negatively correlated with the fluid velocity $\langle u_f\rangle_f = \langle\alpha_f u_f\rangle/\langle\alpha_f\rangle \neq \langle u_f\rangle_p$

1. J. Capecelatro, O . Desjardins, R.O. Fox (Under review), *J. Fluid Mech.*

Exact Reynolds-average equations[1]

- PA particle-phase Reynolds stress

Turbulent dissipation of k_p

$$\frac{1}{2}\frac{\partial\langle u_{p,1}''^2\rangle_p}{\partial t} = \left\langle\Theta\frac{\partial u_{p,1}''}{\partial x_1}\right\rangle_p - \left\langle\sigma_{p,1i}\frac{\partial u_{p,1}''}{\partial x_i}\right\rangle_p \quad PS/VD$$

$$+ \frac{1}{\tau_p}\left(\langle u_{f,1}''' u_{p,1}''\rangle_p - \langle u_{p,1}''^2\rangle_p\right) \quad DE$$

$$+ \frac{1}{\rho_p}\left(\left\langle u_{p,1}''\frac{\partial\sigma_{f,1i}'}{\partial x_i}\right\rangle_p - \left\langle u_{p,1}''\frac{\partial p_f'}{\partial x_1}\right\rangle_p\right) \quad VE/PE$$

- Particle-phase stress tensor:

Production of $\langle\theta\rangle_p$

$$\frac{1}{2}\frac{\partial\langle P_{11}\rangle_p}{\partial t} = -\left\langle\Theta\frac{\partial u_{p,1}''}{\partial x_1}\right\rangle_p + \left\langle\sigma_{p,1i}\frac{\partial u_{p,1}''}{\partial x_i}\right\rangle_p \quad PS/VD$$

$$- \frac{1}{\tau_p}\langle P_{11}\rangle_p \quad DE$$

$$+ \frac{6}{\sqrt{\pi}d_p}\langle\alpha_p\Theta^{1/2}\left(\Delta_{11}^\star - P_{11}\right)\rangle_p \quad CD$$

Collisional equilibrium[2]

$$\Delta_{11}^\star = \frac{1}{4}\left(1+\mathrm{e}\right)^2\Theta + \frac{1}{4}\left(1-\mathrm{e}\right)^2 P_{11}$$

1. J. Capecelatro, O . Desjardins, R.O. Fox (Under review), *J. Fluid Mech.*
2. A. Passalacqua et al. (2011), *Comm in Comp. Phys.*

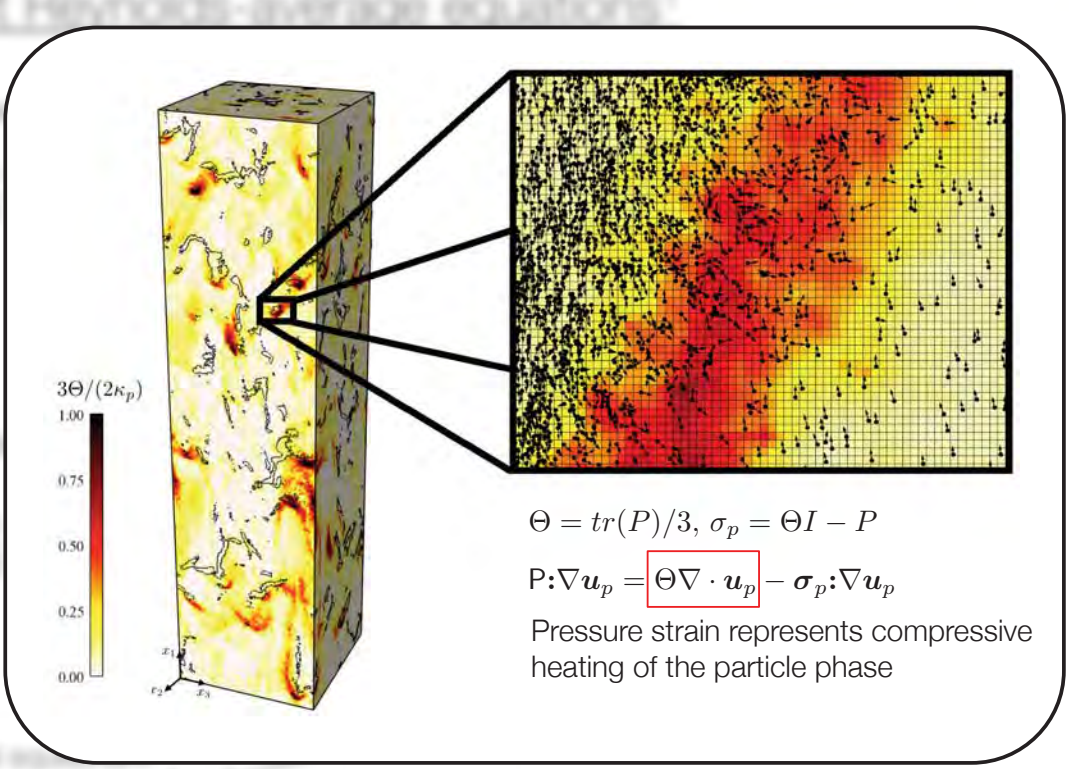

$\Theta = tr(P)/3,\ \sigma_p = \Theta I - P$

$\mathsf{P}{:}\nabla \boldsymbol{u}_p = \Theta \nabla \cdot \boldsymbol{u}_p - \boldsymbol{\sigma}_p{:}\nabla \boldsymbol{u}_p$

Pressure strain represents compressive heating of the particle phase

Validating the adaptive filter[1]

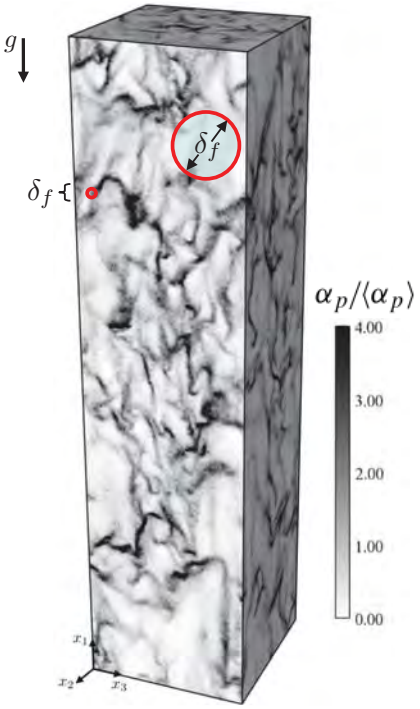

- Verification of the proposed filter
  - Lagrangian data projected to Eulerian mesh via

$$\alpha_p \widetilde{A}(\boldsymbol{x}, t) = \sum_{i=1}^{N_p} A^{(i)}(t) G(|\boldsymbol{x} - \boldsymbol{x}_p^{(i)}|) V_p$$

  - Filter kernel G will sample $\mathcal{N}_p$ particles with $\delta_f = \left(\dfrac{\mathcal{N}_p d_p^3}{\alpha_p} \right)^{1/3}$
  - Comparison with Lagrangian two-point velocity correlations

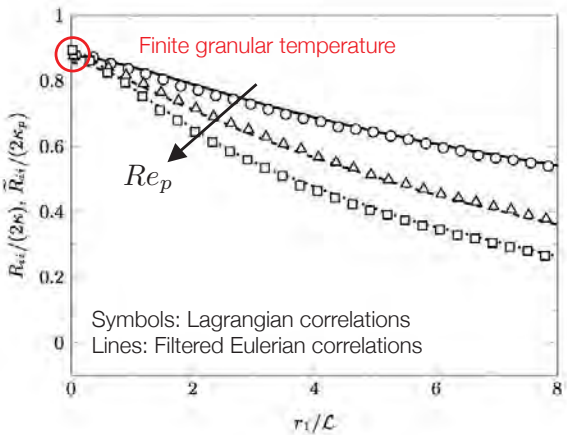

1. J. Capecelatro *et al.* (2014), *J. Fluid Mech.*

CCMT

Microscale Simulations Of Shock-Particle Interactions

T.L. Jackson
Center for Compressible Multiphase Flow
University of Florida

G. Akiki, S. Balachandar, Y. Mehta, C. Moore,
C. Neal, B. Osborne, P. Sridharan, S. Thakur
J. Zhang (FIT)

UF UNIVERSITY of FLORIDA

Goals

- Advance modeling to next generation point-particle force and temperature models for meso/macroscale simulations that take into account neighboring particles
- Perform DNS simulations of shock propagating over a random pack of particles in air

Frost et al. 2012

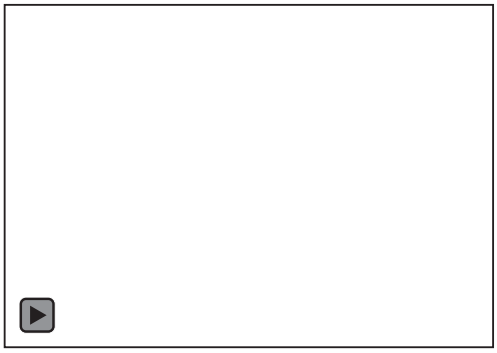

Time Scale Analysis

- Shock-particle $\tau = d_p/u_s$
- Acoustic $\tau_a = d_p/c$
- Inviscid $\tau_i = d_p/u_{ps}$
- Viscous diffusional $\tau_v = \delta_v^2/\nu_m$
- Particle motion $\tau_p = \rho_p\, d_p^2/18\mu_m$

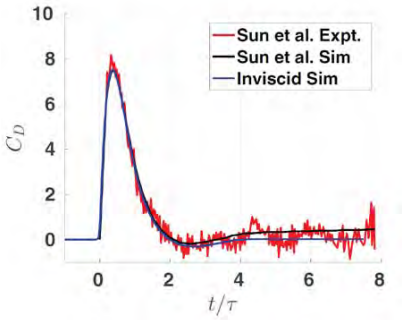

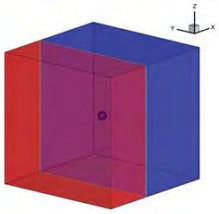

- Ratios: $\frac{\tau_p}{\tau} \sim \frac{\rho_p}{\rho_m} Re \sim 10^4$ $\frac{\tau_v}{\tau} = \frac{u_s}{u_{ps}} \sim 2$

- Inviscid simulations will accurately capture peak and short time evolution of force

Previous Results (2014-2015)

Single Particle

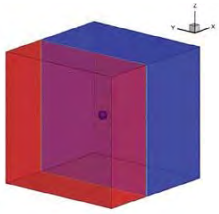

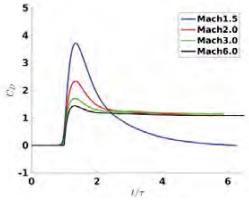

1-D Array

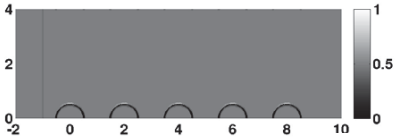

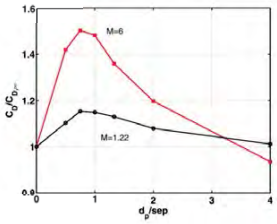

Transverse Array

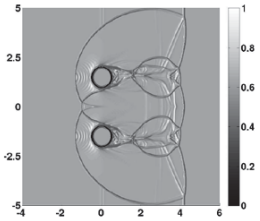

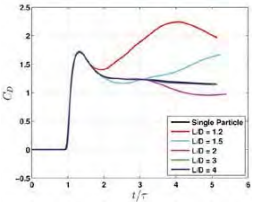

Deformable Particle (NM/Al)

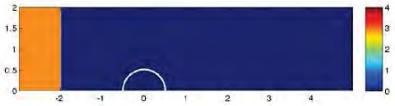

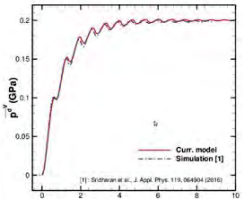

Microscale Simulations

- Shock propagation over a FCC array of spheres

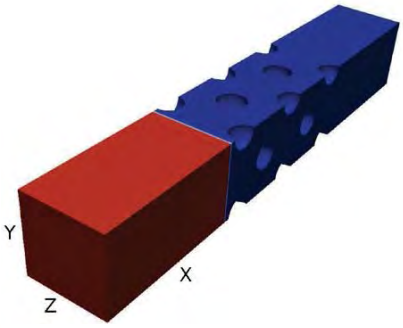

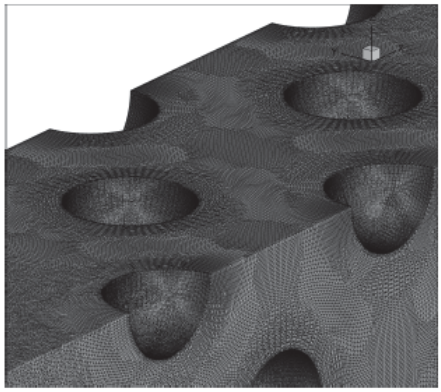

Resolution ~ 30M Cells

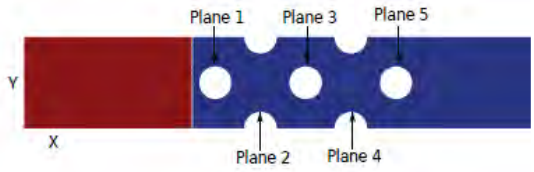

	$\varphi = 10\%$	$\varphi = 20\%$	$\varphi = 30\%$	$\varphi = 40\%$
$M_s = 1.5$	RUN1	RUN5	RUN9	RUN13
$M_s = 2.0$	RUN2	RUN6	RUN10	RUN14
$M_s = 3.0$	RUN3	RUN7	RUN11	RUN15
$M_s = 6.0$	RUN4	RUN8	RUN12	RUN16

CCMT

Shock Interaction with FCC Array of Particles

$\varphi = 10\%$
$M_s = 1.5$

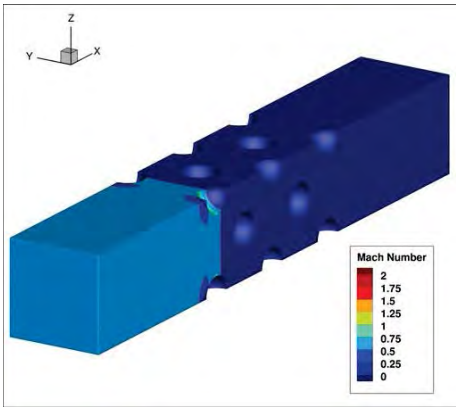

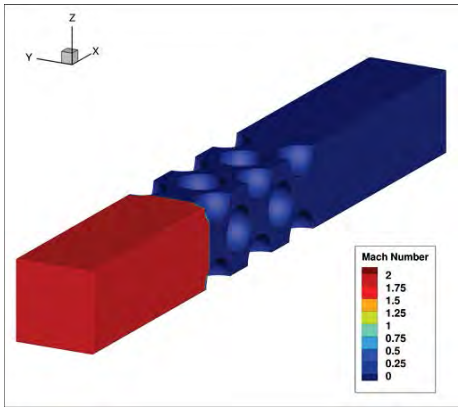

$\varphi = 40\%$
$M_s = 6.0$

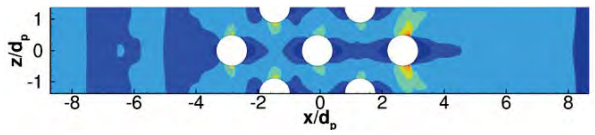

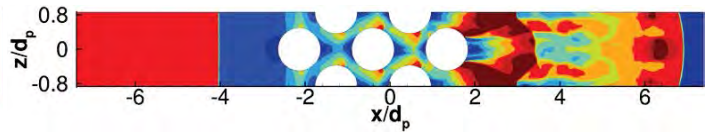

- Even for structured array, ensuing flow is quite complicated
- There is a strong effect of the particles on the flow

CCMT

FCC - Effect of Volume-fraction; $M_s = 1.5$

$\varphi = 10\%$

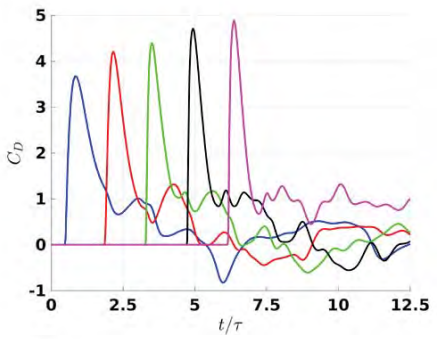

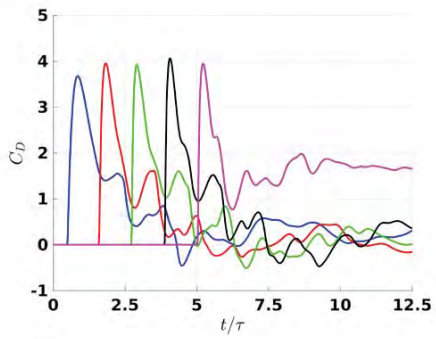

$\varphi = 20\%$

$\varphi = 30\%$

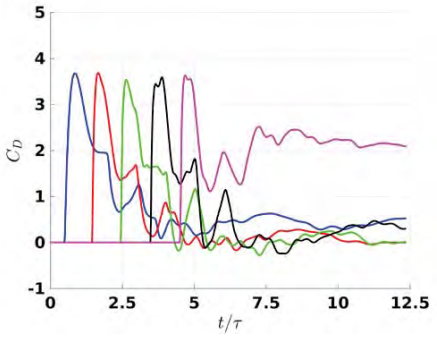

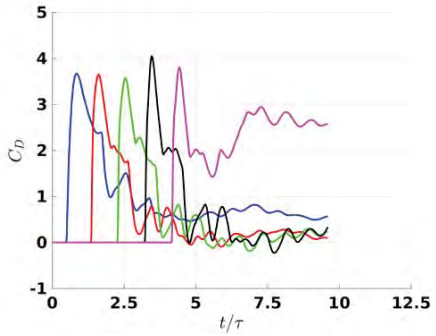

$\varphi = 40\%$

- At higher volume fractions the last plane of particles will move faster, resulting in curtain spreading

FCC - Effect of Mach number; $\varphi = 10\%$

$M_s = 1.5$

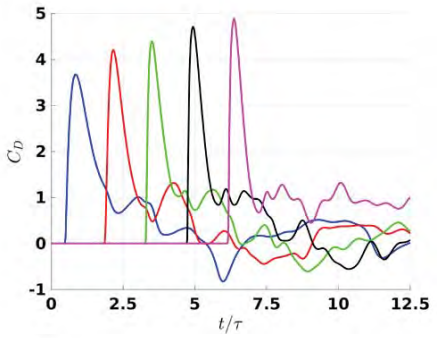

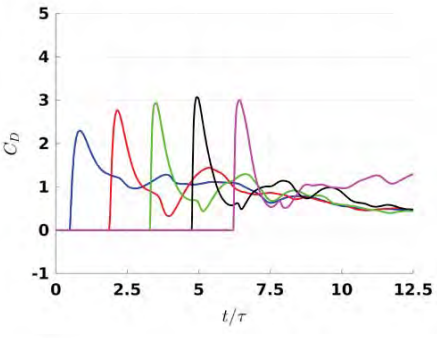

$M_s = 2.0$

$M_s = 3.0$

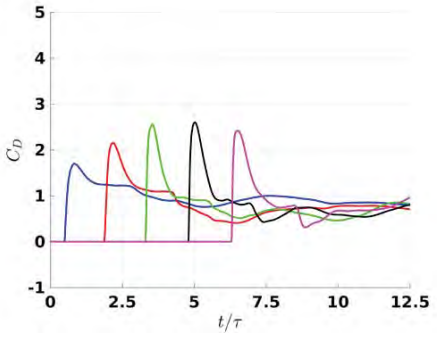

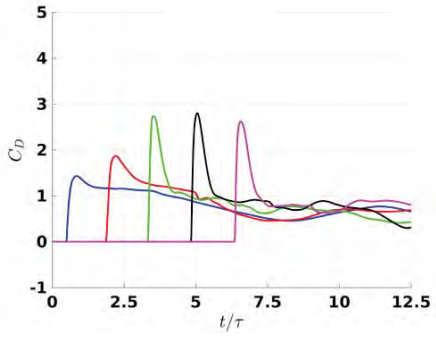

$M_s = 6.0$

- There is a high variability for peak forces and no clear pattern

Multi-Particle Microscale Simulations

- Simulation of random cluster of particles to extract force history information
- Extracted information is compared with current models to establish areas that need model enhancement
- In collaboration with K. Salari

Mach 3 shock over 200 particles

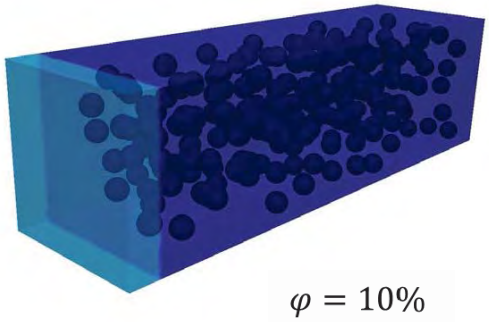

$\varphi = 10\%$

Force histories of 20 particles

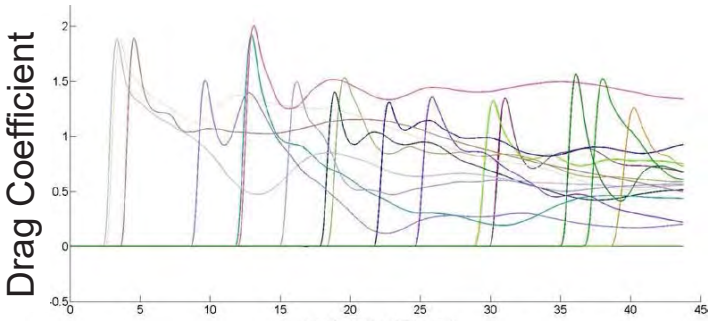

- Current point-particle models do not capture these large particle-to-particle variations

Random Pack of Particles; $M_s = 3.0$

$\phi = 10\%$

$\phi = 15\%$

$\phi = 20\%$

$\phi = 25\%$

- Mach 3.0 shock traveling through the particle beds for different volume fractions

Streamwise Drag; $M_s = 3.0$

$\varphi = 10\%$

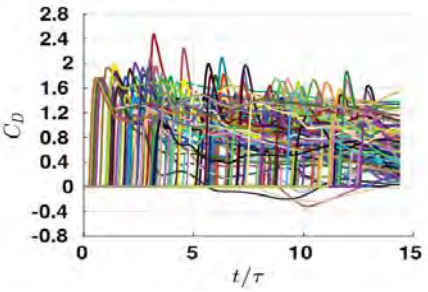

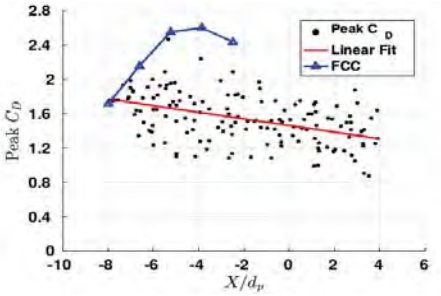

$\varphi = 20\%$

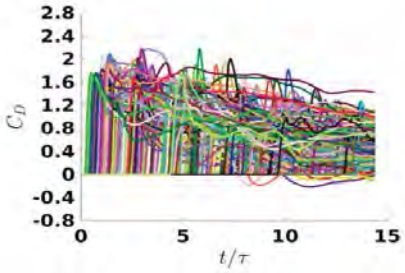

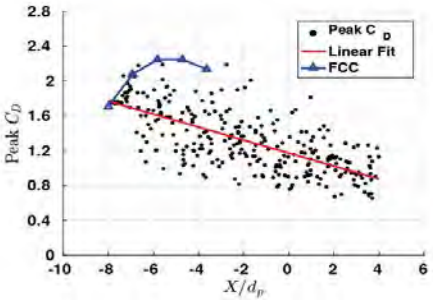

- There is a high variability for the peak drag and a clear downward trend
- Variability in peak drag force is not captured by the current models

CCMT

Streamwise Drag; $M_s = 3.0$; $\varphi = 15\%$

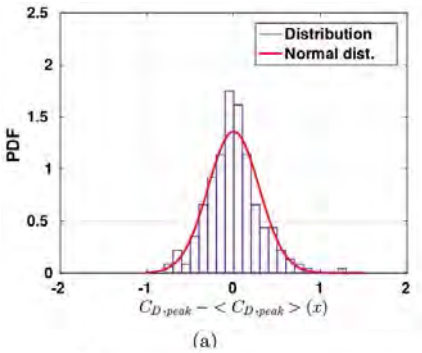

(a)

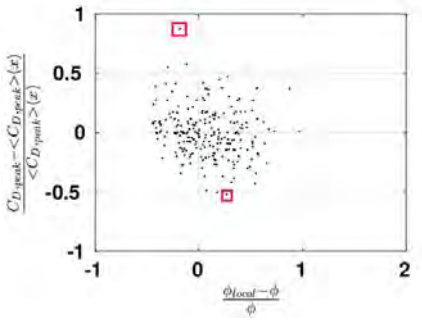

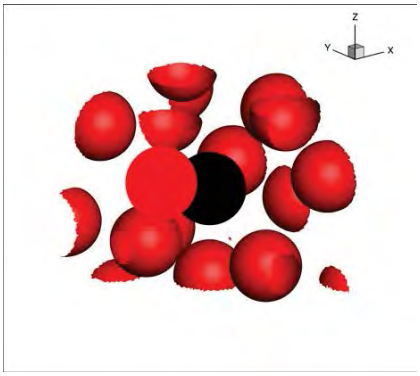

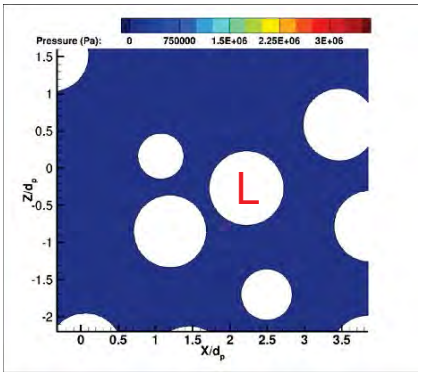

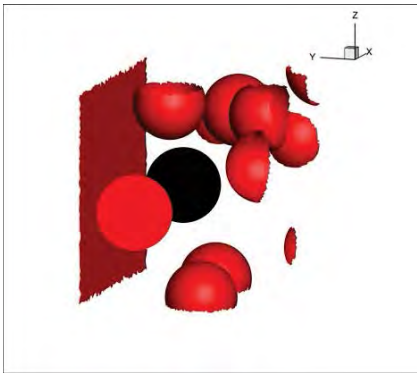

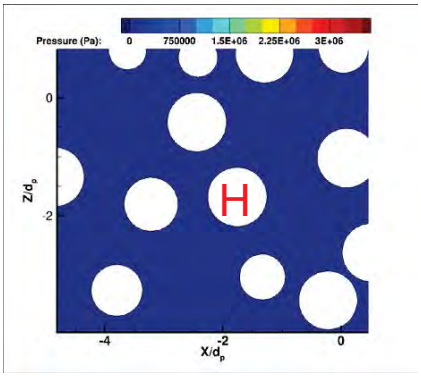

CCMT

Lateral Forces; ϕ = 25%; $M_s = 3.0$

- Lateral forces are same order as streamwise drag
- Show similar trend
- Current models ignore lateral forces

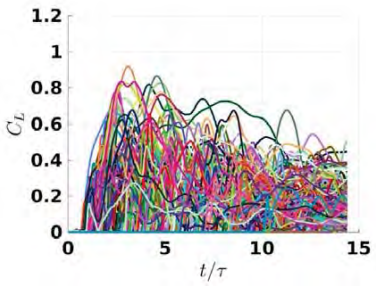

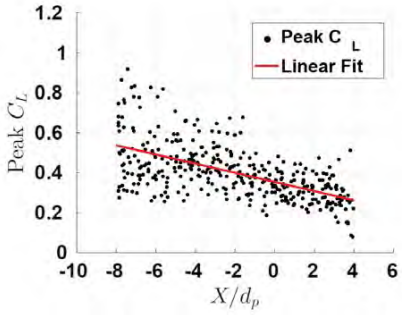

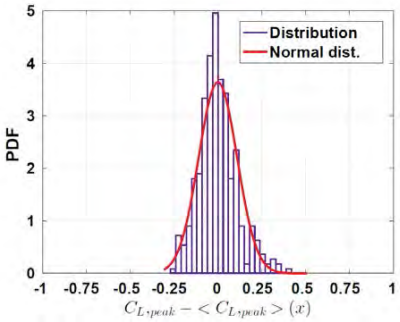

Fluctuations (Pseudo-turb); ϕ = 25%; $M_s = 3.0$

$$u = \langle u \rangle(x,t) + u'(x,y,z,t) \qquad \langle F \rangle(x,t) = \frac{1}{A_{slice}} \int_{y_1}^{y_2} \int_{z_1}^{z_2} F(x,y,z,t)\, dydz$$

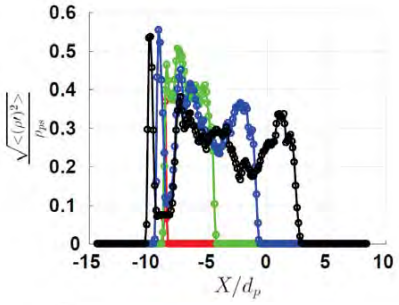

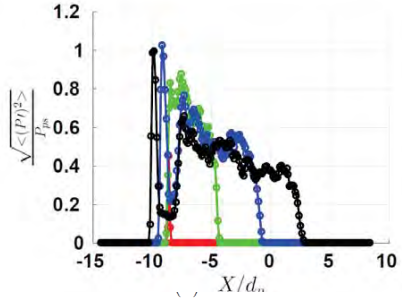

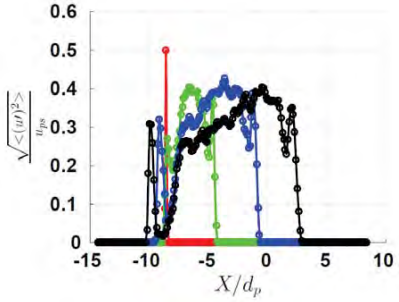

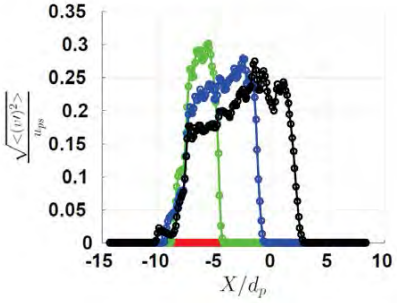

Point-Particle Model Development

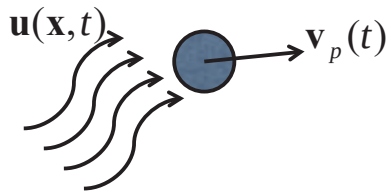

Commonly used models are based on:

- Uniform flow
- Quasi-steady flow
- Isolated particles
- Low Mach number, modest Reynolds number

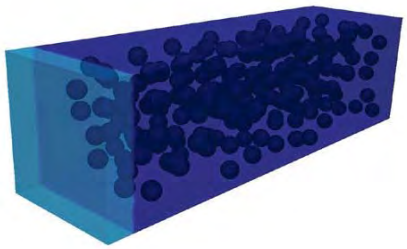

But reality:

- Highly unsteady and spatially non-uniform flow
- Large Mach and Reynolds numbers
- Closely clustered particles
- Particles can deforms
- Real gas & turbulence effects

Physics-Based Modeling

- Isolated particle
  - Rigorous point-particle formulation with empirical extension to finite Re and Mach condition
- Particle-particle interaction (current status)
  - Simple volume fraction correction to point-particle model for predicting average behavior
- Particle-particle interaction (New Development)
  - A novel Pairwise-Interaction Extended Point-particle (PIEP) model for predicting average & fluctuation behavior

Isolated Particle – Model Validation

Experiments by Tanno et al (2003) at Tohoku, Japan

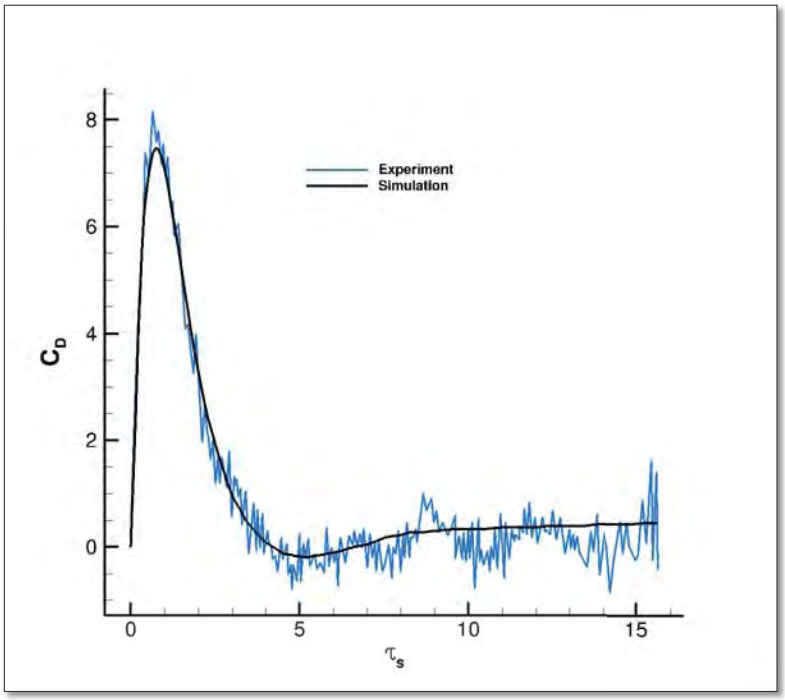

Data:
Sun et al. (2005)

$M_s = 1.22$

$d = 8\,\mathrm{mm}$

Isolated Particle – Model Validation

Experiments by Tanno et al (2003) at Tohoku, Japan

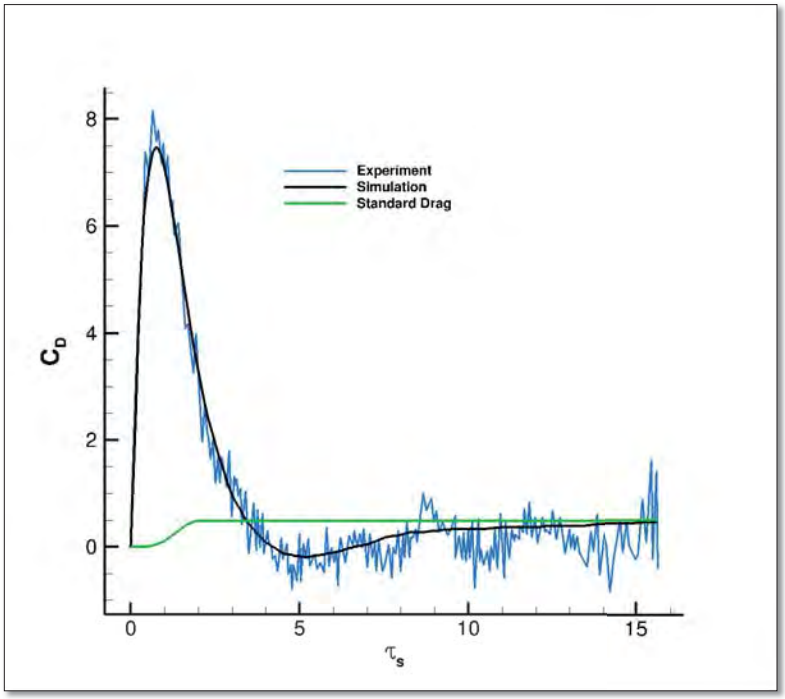

Data:
Sun et al. (2005)

$M_s = 1.22$

$d = 8\,\mathrm{mm}$

Isolated Particle – Model Validation

Experiments by Tanno et al (2003) at Tohoku, Japan

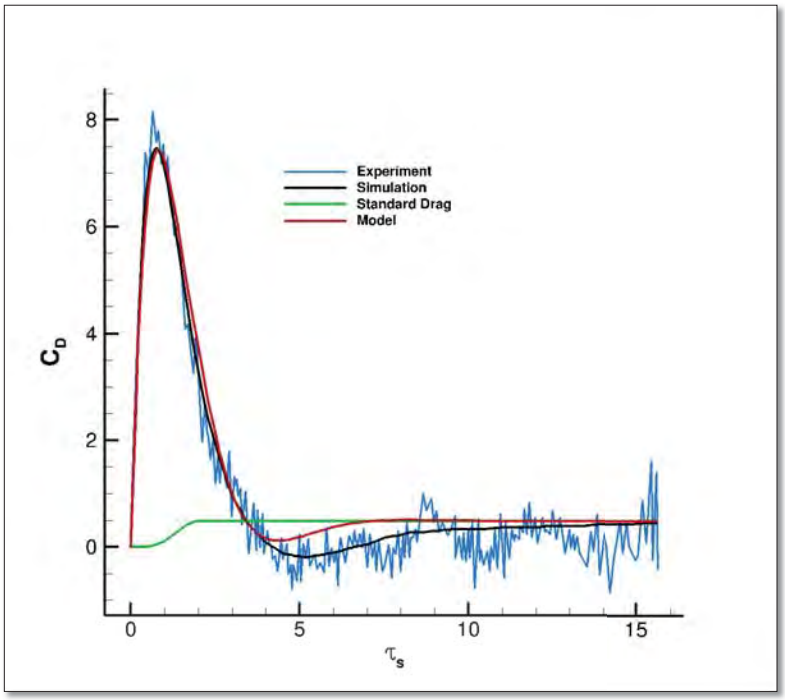

Data:
Sun et al. (2005)

$M_s = 1.22$

$d = 8\,\mathrm{mm}$

We have a very good model for a single particle

PIEP – Streamwise Force

- Shock interaction with transverse array of particles

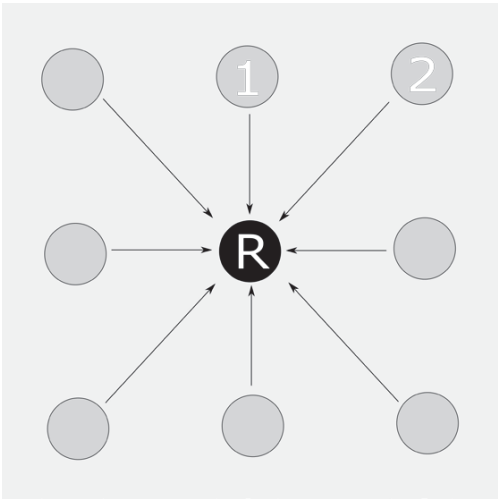

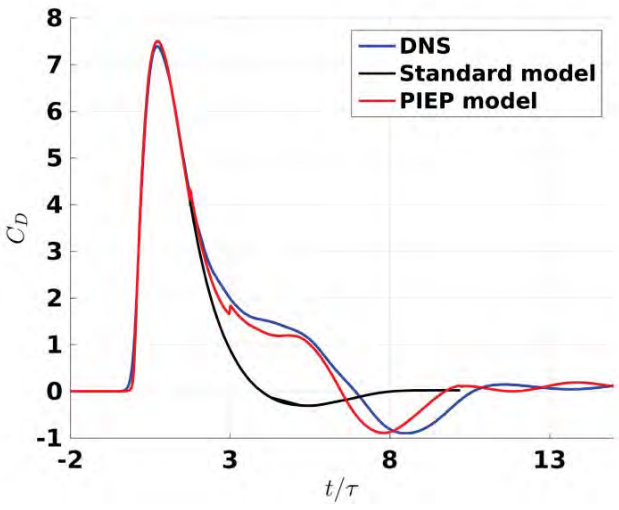

- Force found by superposition
- $\mathrm{Force}_{\mathrm{part-R}} = \mathrm{Force}_{\mathrm{shock}} + 4 * \mathrm{Force\_diff}_{\mathrm{part-1}} + 4 * \mathrm{Force\_diff}_{\mathrm{part-2}}$

PIEP – Streamwise Force

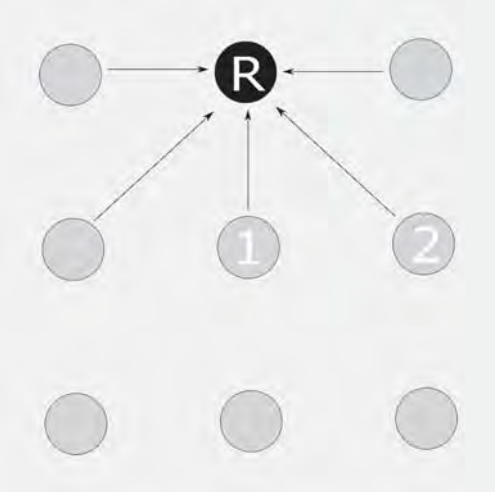

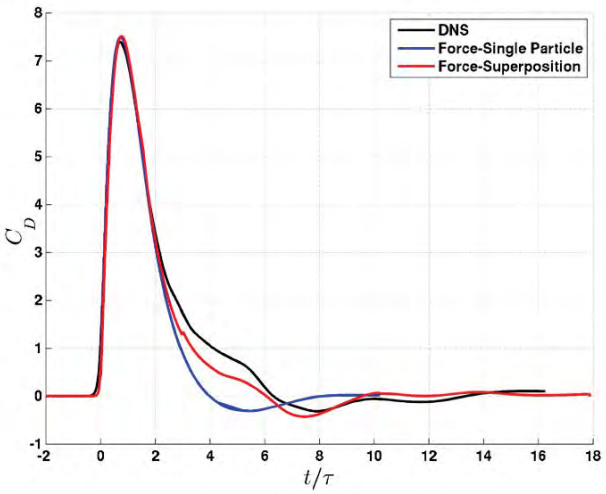

- $\text{Force}_{\text{part-R}} = \text{Force}_{\text{shock}} + 3 * \text{Force\_diff}_{\text{part-1}} + 2 * \text{Force\_diff}_{\text{part-2}}$

PIEP – Streamwise Force

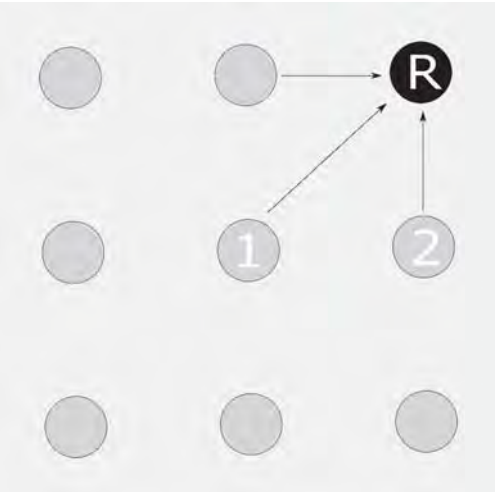

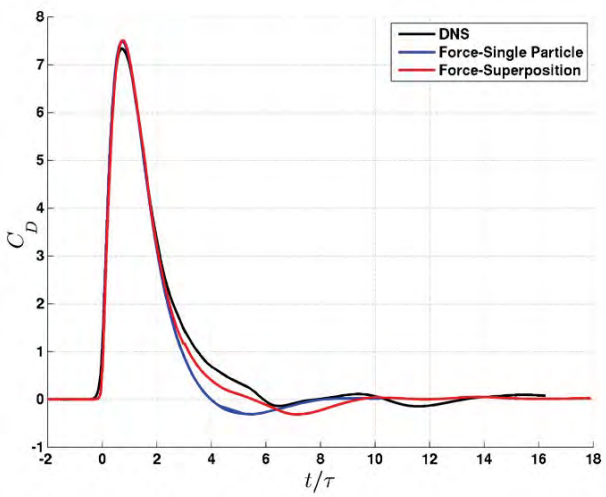

- $\text{Force}_{\text{part-R}} = \text{Force}_{\text{shock}} + 2 * \text{Force\_diff}_{\text{part-1}} + 1 * \text{Force\_diff}_{\text{part-2}}$

PIEP - Transverse Force

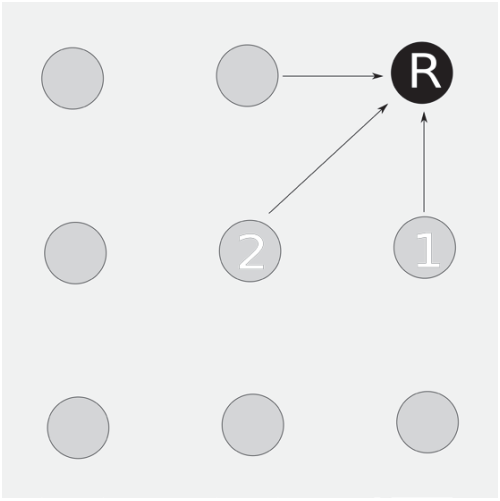

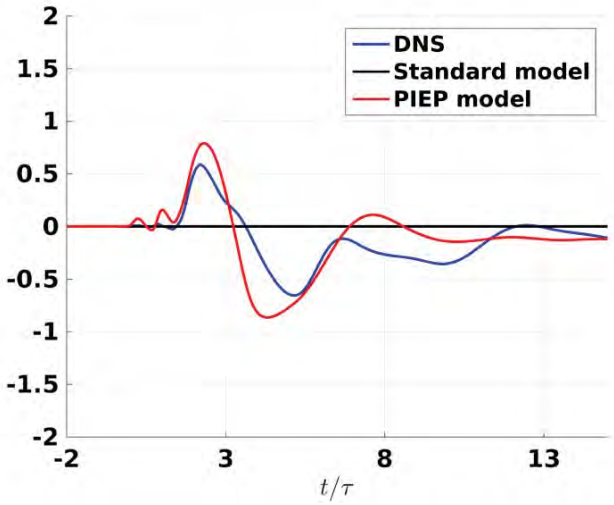

- $\text{Force}_{\text{part}-\text{R}} = 2 * \text{Force\_diff}_{\text{part}-1} + 1 * \text{Force\_diff}_{\text{part}-2}$

Outstanding Challenges

- Simulations with a large cluster of moving particles
  - Dynamic gridding (immersed boundary method?)
  - How to handle particle-particle interaction?
- Simulations of detonation-induced particle deformation
  - Numerical issue of particle mass preservation
  - Material modeling and EOS
- Upscaling of the microscale results
  - Point-particle force model (effect bow shock & wave drag)
  - Heat transfer model, deformation model, etc
  - PIEP model extension to compressible flows and testing

Journal Publications (2015-2016)

- Sridharan, P., Jackson, T.L., Zhang, J. and Balachandar, S. (2015). Shock interaction with 1-D array of particles in air. ***Journal of Applied Physics***, Vol. 117, 075902.
- Sridharan, P., Jackson, T.L., Zhang, J., Balachandar, S., and Thakur, S. (2016). Shock interaction with deformable particles using a constrained interface reinitialization scheme. ***Journal of Applied Physics***, Vol. 119, 064904, 18 pages.
- Mehta, Y., Jackson, T. L., Zhang, J., & Balachandar, S. (2016). Numerical investigation of shock interaction with one-dimensional transverse array of particles in air. ***Journal of Applied Physics***, *119*(10), 104901.
- Akiki, G., Jackson, T.L., & Balachandar, S. (2016). Force variation within arrays of mono-disperse spherical particles. ***Physical Review Fluids***, 1, 044202.
- Mehta, Y., Neal, C., Jackson, T.L., Balachandar, S., Thakur, S. (2016). Shock interaction with three-dimensional face centered cubic array of particles in air. ***Physical Review Fluids***, 1, 054202.
- Annamalai, S., Balachandar, S. Sridharan, P. and Jackson, T.L. (2016). A pressure evolution equation for the particulate phase in inhomogeneous compressible disperse multiphase flows. ***Physical Review Fluids***, (submitted).
- Akiki, G., Jackson, T.L., & Balachandar, S. (2016). PIEP model for a random array of monodisperse spheres. *Journal of Fluid Mechanics*, under review.
- Neal, C., Mehta, Y., Salari, K., Jackson, T.L., Balachandar, S., Thakur, S. (2016). Shock propagation in air over a random bed of spherical particles. (in preparation).

CCMT

Do you have any questions?

CARBON CAPTURE MULTIDISCIPLINARY SIMULATION CENTER

Particle dynamics: coal-specific modeling

Sean T. Smith
University of Utah,
Particle Deep Dive
St. Petersburg, FL – Friday, 7th of Oct, 2016

ALSTOM · Institute for Clean and Secure Energy, The University of Utah · SCI www.sci.utah.edu · Berkeley · BYU Brigham Young University · NNSA National Nuclear Security Administration

Coal: properties

- Context: pulverized coal
- SG ≈ 1 ($\rho \approx 1000$ kg/m^3)
- Dp ~ 10–200 μm
  Poly-disperse: Rosin-Rammler
- **~10% ash**
  Si, Al, Fe oxides
  ~90% organic
  C: 75%, O: 9%, H: 5%,
  S: 1%, trace N & Hg
- Multiple coal types (rank)

D_p ~ 10–200 μm

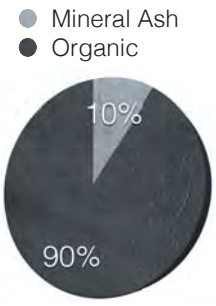

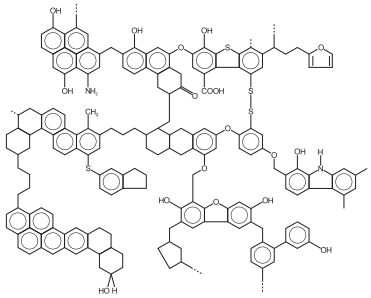

CARBON CAPTURE MULTIDISCIPLINARY SIMULATION CENTER

Coal: processes

- **Heat transfer**
  primarily: radiation (Mie)
- **Devolatilization**
  metaplast, network breakdown, VLE & swelling
  $\tau_{devol} \approx 10$ ms
- **Char oxidation**
  diffusion, reactions, porosity & friability
  $\tau_{char\ ox} \approx 1$ sec.
- **Drag**
  turbulence, blowing, slip
  broad range on *St*
- **Thermophoresis**
  and deposition (at cold walls)

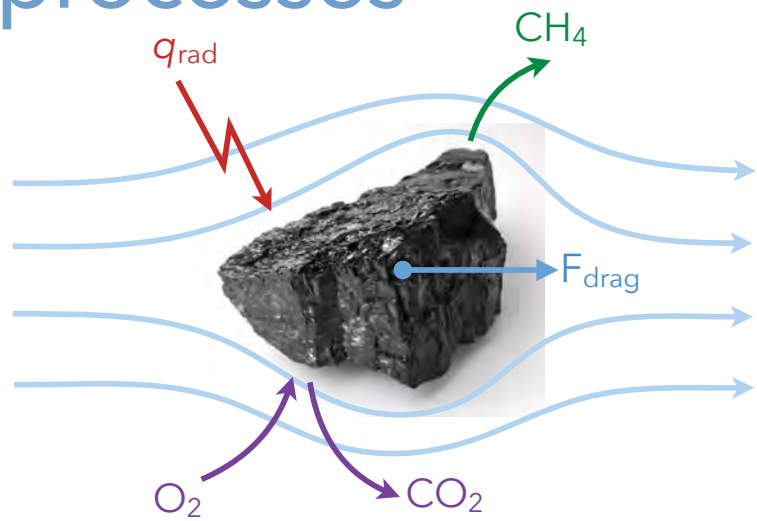

CARBON CAPTURE MULTIDISCIPLINARY SIMULATION CENTER

Coal: processes

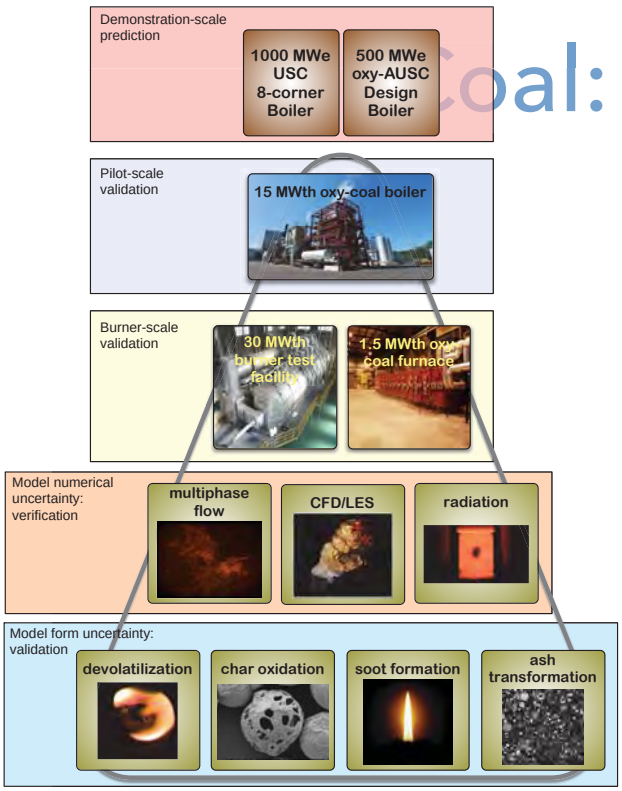

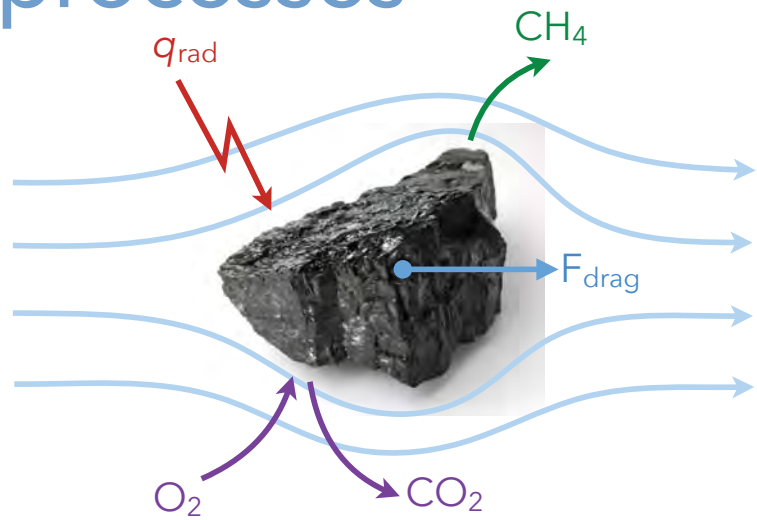

CARBON CAPTURE MULTIDISCIPLINARY SIMULATION CENTER

oal: processes

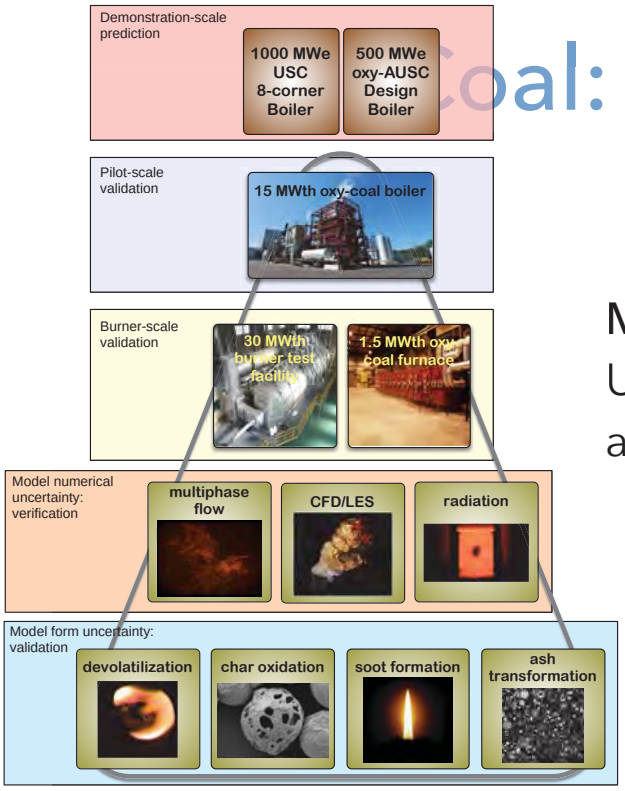

Modeling:

Use the model that has been made as simple as possible, but no simpler

CARBON CAPTURE MULTIDISCIPLINARY SIMULATION CENTER

Devolatilization – model form

- Detailed approach: CPD
  - historical gold standard
  - very good at rates (not ultimate yield)
  - computationally demanding
- Timescale analysis
- BT model *(1st order w/ yield):*

$$\frac{\mathrm{d}V}{\mathrm{d}t} = A \exp\left(\frac{-E_\mathrm{a}}{RT}\right) \max\left(V_\mathrm{ult.}(T) - V,\, 0\right)$$

$$V_\mathrm{ult.}(T) = 1 - \exp\left(\frac{-T}{B}\right)$$

Biagini, E., and Tognotti, L., 2014. ***Fuel Process. Technol.***, 126, pp. 513-520.

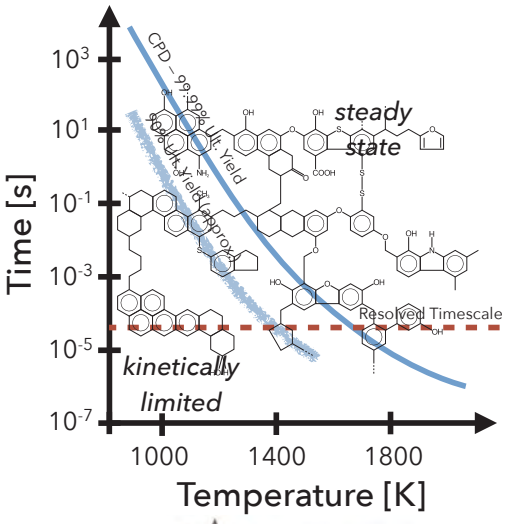

CARBON CAPTURE MULTIDISCIPLINARY SIMULATION CENTER

Devolatilization – Yield

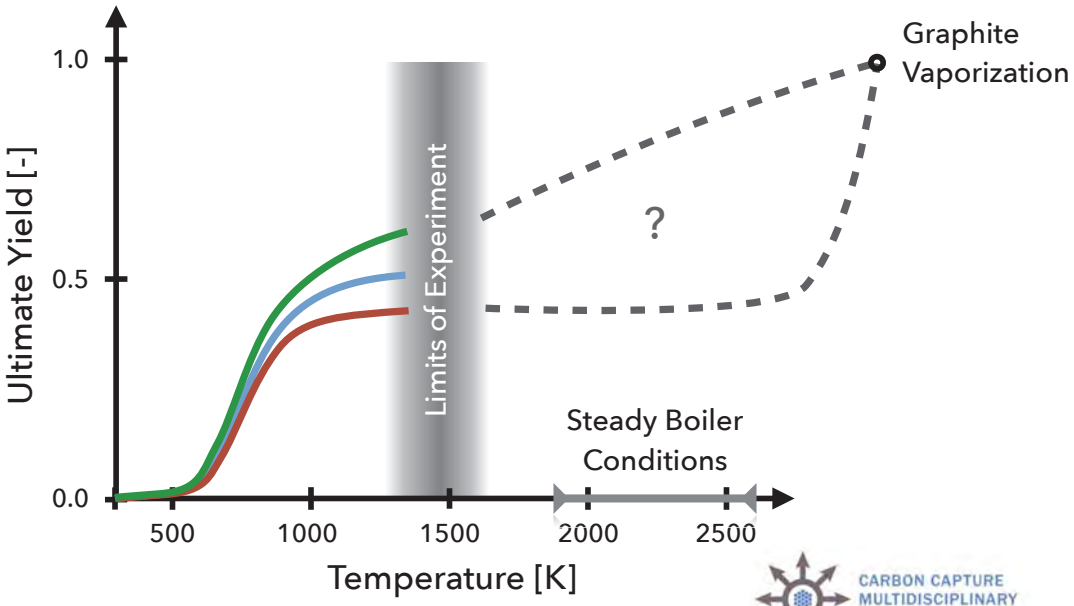

CARBON CAPTURE MULTIDISCIPLINARY SIMULATION CENTER

Devolatilization – Yield

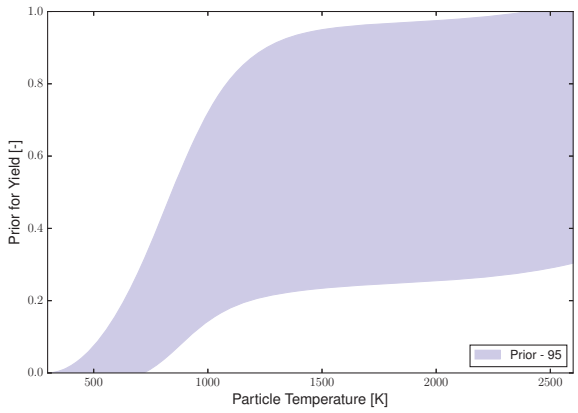

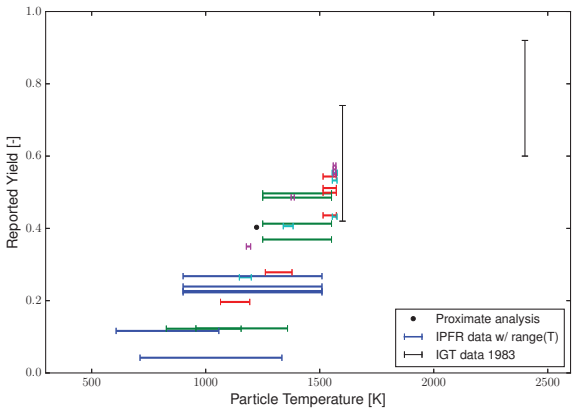

CARBON CAPTURE MULTIDISCIPLINARY SIMULATION CENTER

Devolatilization – Yield

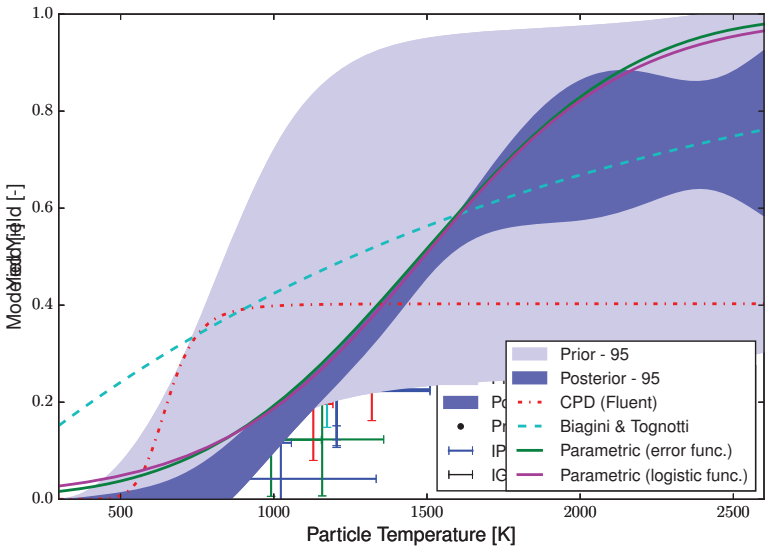

CARBON CAPTURE MULTIDISCIPLINARY SIMULATION CENTER

Char oxidation – model form

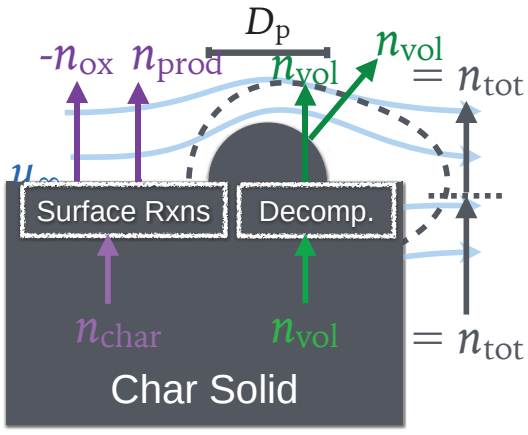

- **Coupled problem**:
  mass transfer & surface reactions
- **Mass transfer**:
  convection – mass transfer coefficient,
  blowing – penetration theory,
  multi-component – (diagonal) Fickian assumption,
  reaction appears as a boundary condition.
- **Surface Reactions**:
  rate laws – Arrhenius (for oxidation & gasification),
  important to match fluxes,
  mass transfer provides gas composition.

CARBON CAPTURE MULTIDISCIPLINARY SIMULATION CENTER

Particle Transport

- **Particle size vs. grid**:
  200 μm (largest) vs. 2 cm (smallest)
- **Volume fraction**:
  low (< 0.001)
- **Reynolds number**:
  very low (~10)
- **Surface blowing** (due to chemical reactions):
  modeling – drag correlations w/ penetration theory
- **Knudsen number**:
  slip regime – for only the smallest particles
  (Young, *Aerosol Sci. & Tech*. **2011**)

CARBON CAPTURE MULTIDISCIPLINARY SIMULATION CENTER

Particles & Turbulence

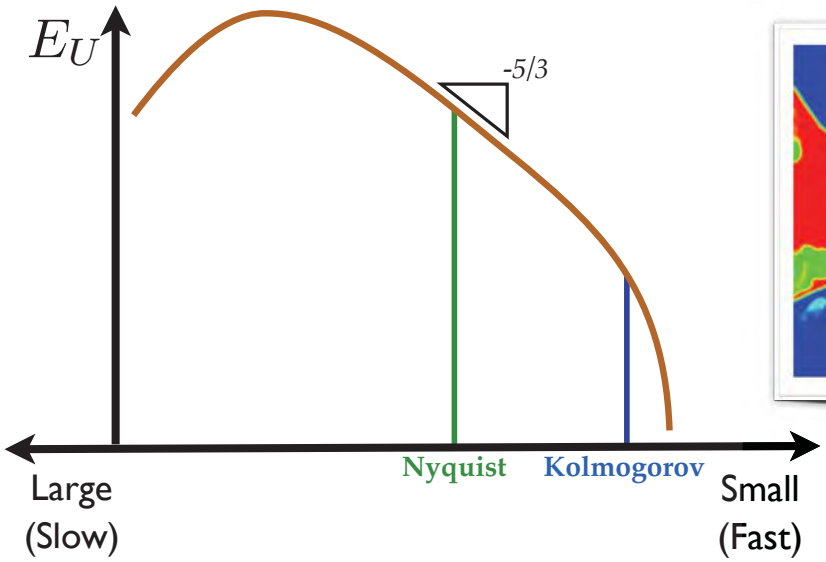

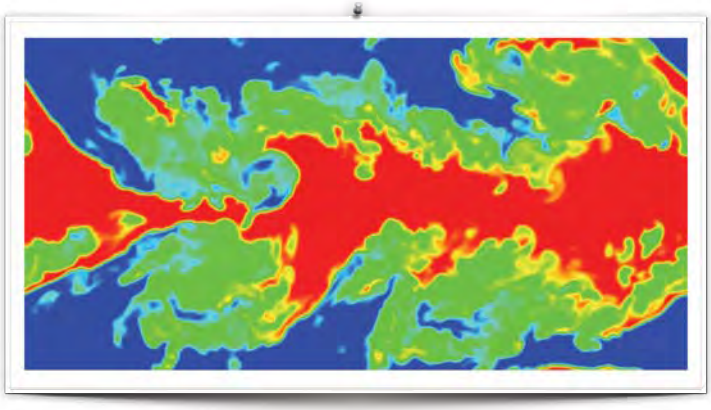

CARBON CAPTURE MULTIDISCIPLINARY SIMULATION CENTER

Particle Time Scales

$$St = \frac{\text{particle relaxation time}}{\text{fluid acceleration time}}$$

Fixed particle size, multiple eddy sizes:

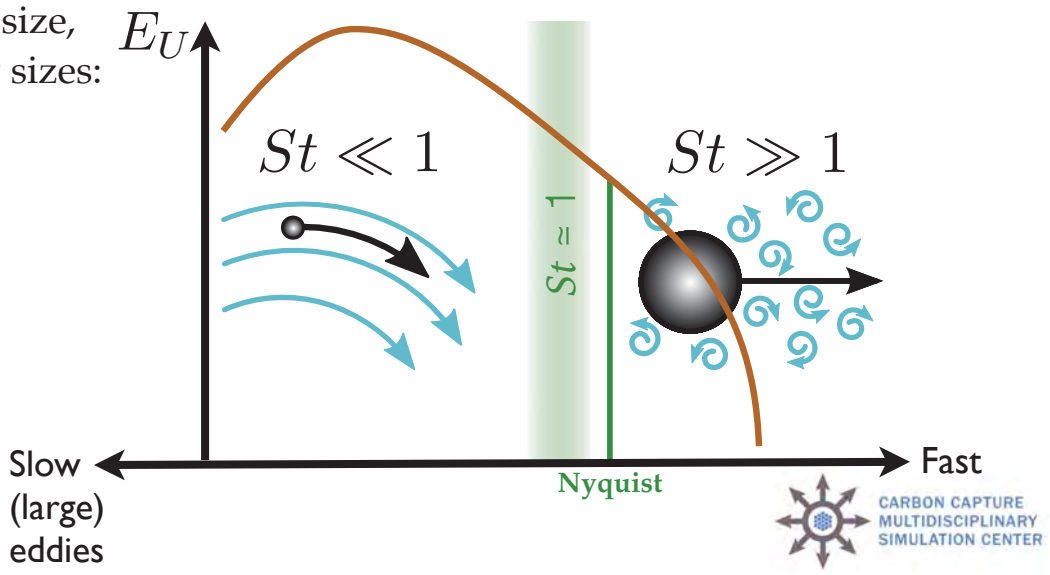

CARBON CAPTURE MULTIDISCIPLINARY SIMULATION CENTER

Particle Modeling Regimes

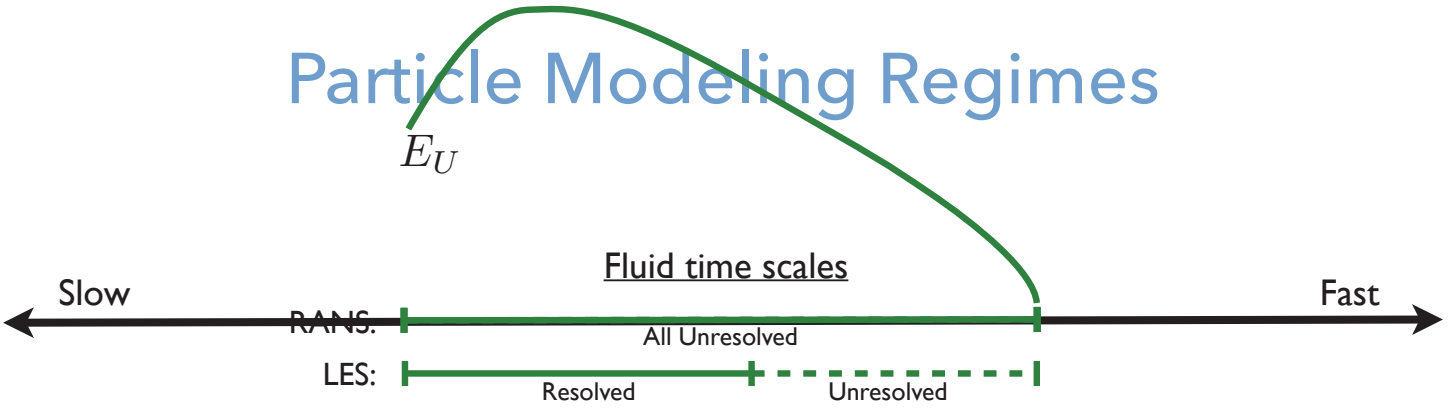

Multiple particle time Scales

Modeling approach: time-scale separation

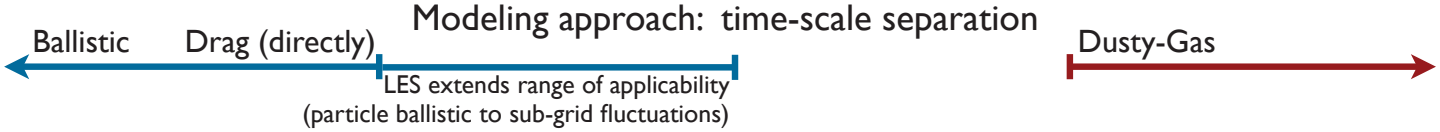

Modeling the overlap with fluid time-scales

CARBON CAPTURE MULTIDISCIPLINARY SIMULATION CENTER

Mixing & Reaction Modeling Regimes

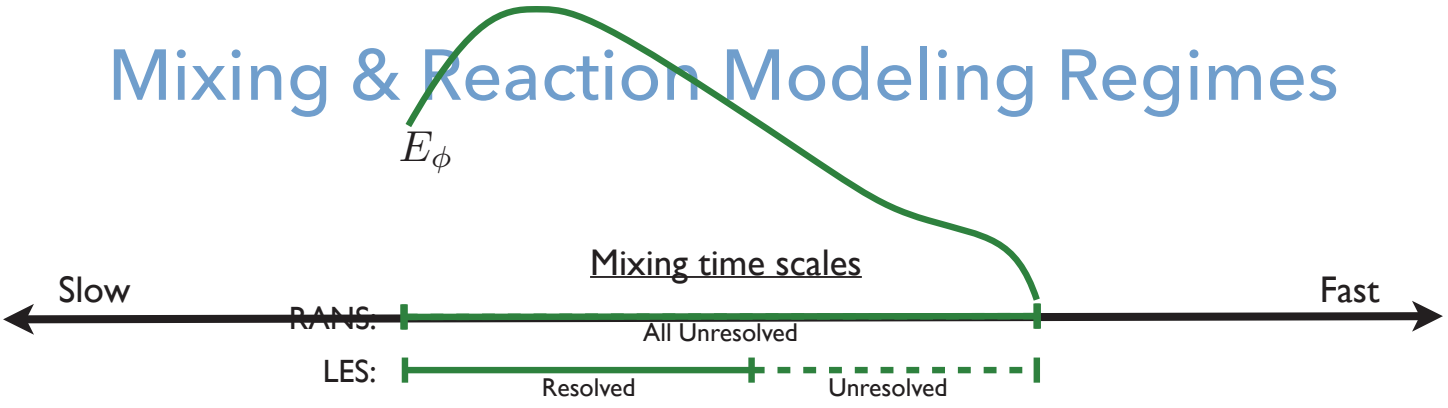

Multiple reaction time scales

Modeling approach: time-scale separation

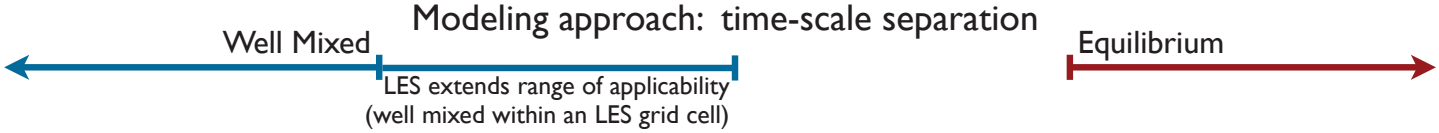

Modeling the overlap with mixing time-scales

CARBON CAPTURE MULTIDISCIPLINARY SIMULATION CENTER

CCMT

Microscale Modeling based on Generalized Faxén's Theorem

Subramanian Annamalai

Dept. of Mechanical & Aerospace Eng.

University of Florida, Gainesville

Contact: **Subramanian Annamalai** | subbu.ase@gmail.com

UF UNIVERSITY of FLORIDA

Explosive Particle Dispersal

Radius-Time Schematic

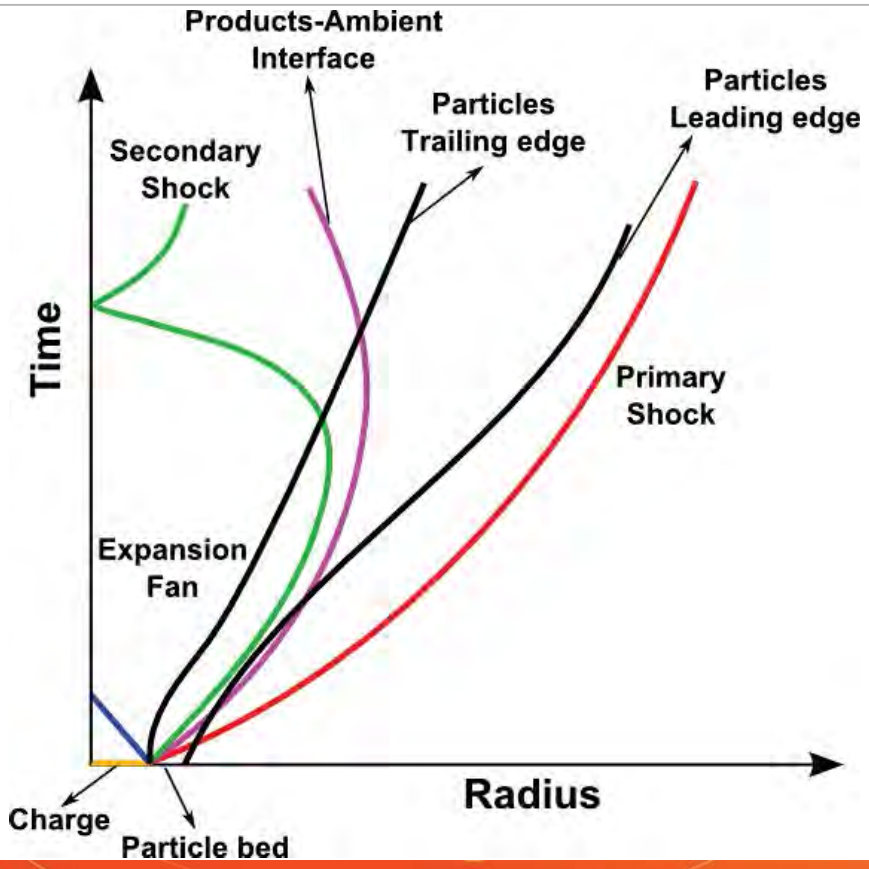

CCMT

Force Modeling: Microscale vs Macroscale

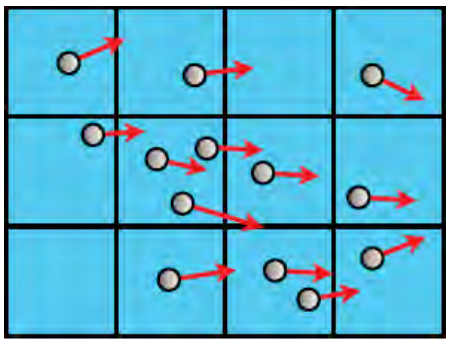

$$m_{p_i}\frac{\mathrm{d}\mathbf{v}_i}{\mathrm{d}t} = \mathbf{F}_i(t)\ ,$$

$$\frac{\partial(\rho\phi\mathbf{u})}{\partial t} + \boldsymbol{\nabla}\cdot(\rho\phi\mathbf{u}\mathbf{u}) + \boldsymbol{\nabla}p = -\frac{1}{V}\sum_{i=1}^{\mathrm{nPcls}}\mathbf{F}_i(t)\ .$$

Detailed flow analysis over each particle → MICRO

Model forces as source terms in the gas momentum equation → MACRO

CCMT

Force Components

$$\mathbf{F}_i = \mathbf{F}_{qs} + \mathbf{F}_{iu} + \mathbf{F}_{sg} + \mathbf{F}_{vu}$$

Viscous | Inviscid | Viscous

Steady | Unsteady

$\mathbf{F}_{qs}$: Quasi-Steady

Considered with appropriate correction factors

$\mathbf{F}_{iu}$: Inviscid Unsteady

$\mathbf{F}_{sg}$: Stress Gradient

$\mathbf{F}_{vu}$: Viscous Unsteady

Generally ignored in literature

Additional physics involved

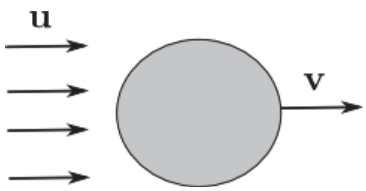

Steady + Inhomogeneous

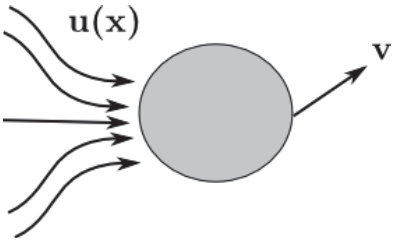

Stokes drag: $6\pi\mu R(\mathbf{u} - \mathbf{v})$

$\mathbf{F}_{qs}$: Quasi-Steady

Faxén's law: $6\pi\mu R(\overline{\mathbf{u}}^S - \mathbf{v})$

$$\overline{()}^S = \frac{1}{S^p}\int_{S^p} () \, \mathrm{d}S$$

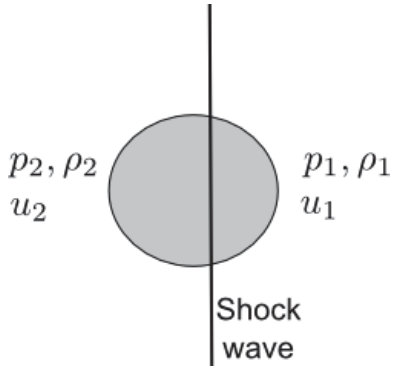

- Unsteadiness
- Compressibility
- Inhomogeneity
- Highly space and time dependent

Acoustic analogy & scalar potential

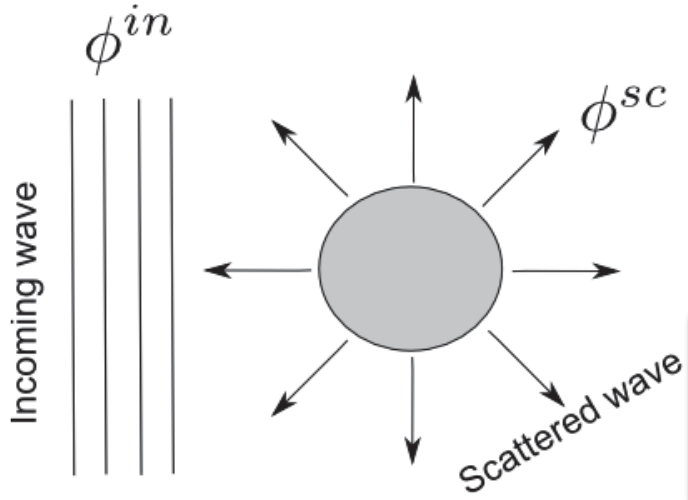

$$\mathbf{u} = \mathrm{e}^{-\mathrm{i}(kz-\omega t)}\mathbf{e_z}$$

Incoming acoustic wave of a given frequency and wavenumber

Quiescent flow-field

Acoustic theory (Scalar potential)

Inviscid Limit

$$\mathbf{u} = \nabla\phi$$
$$\phi = \phi^{\mathrm{in}} + \phi^{\mathrm{sc}}$$

Linearized Euler

We have extended this analysis to viscous regime

Inviscid force expression

$$\phi^{\mathrm{in}} = \sum_{n=0}^{\infty} C_n(2n+1)(-\mathrm{i})^n j_n(kr)P_n(\cos\theta)\mathrm{e}^{\mathrm{i}\omega t}$$

$$\phi^{\mathrm{sc}} = \sum_{n=0}^{\infty} C_n(2n+1)(-\mathrm{i})^n S_n h_n(kr)P_n(\cos\theta)\mathrm{e}^{\mathrm{i}\omega t}$$

Rigid Particle: $\mathbf{u}\cdot\mathbf{n} = 0 \;\; (u_r = 0)$

$$\mathbf{F}_{\mathrm{inv}} = \int_{V^p} \boldsymbol{\nabla}\cdot\boldsymbol{\sigma}_{\mathrm{inv}}\,\mathrm{d}V = -\int_{S^p} p\,\mathbf{n}\,\mathrm{d}S$$

$$\mathbf{F}_{\mathrm{inv}}(t) = \mathbf{F}_{sg}(t) + \mathbf{F}_{iu}(t)$$

$$\mathbf{F}_{sg}(t) = \tfrac{4}{3}\pi R^3 \rho \overline{\frac{\mathrm{D}\mathbf{u}}{\mathrm{D}t}}^{V}$$

$$\mathbf{F}_{iu}(t) = 4\pi R^3 \int_{\tilde{\xi}=-\infty}^{\tilde{t}} K_{iu}(\tilde{t}-\tilde{\xi})\left[\frac{\partial}{\partial t}\overline{(\rho\mathbf{u}_r)}^{S}\right]_{\tilde{t}=\tilde{\xi}} \mathrm{d}\tilde{\xi}\,.$$

Expansion fan over the particle

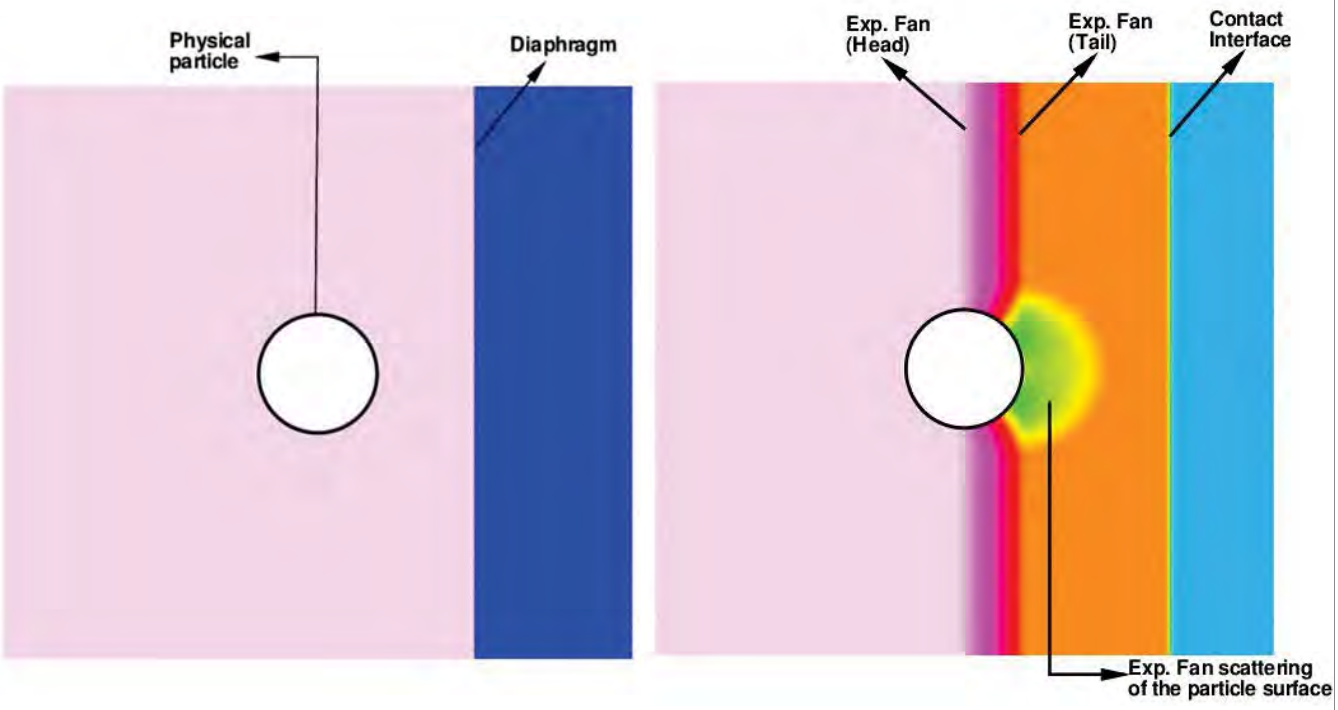

$t = 0$

$t = 0.3$ ms

CCMT

1d Shock Tube : Isolated Particle

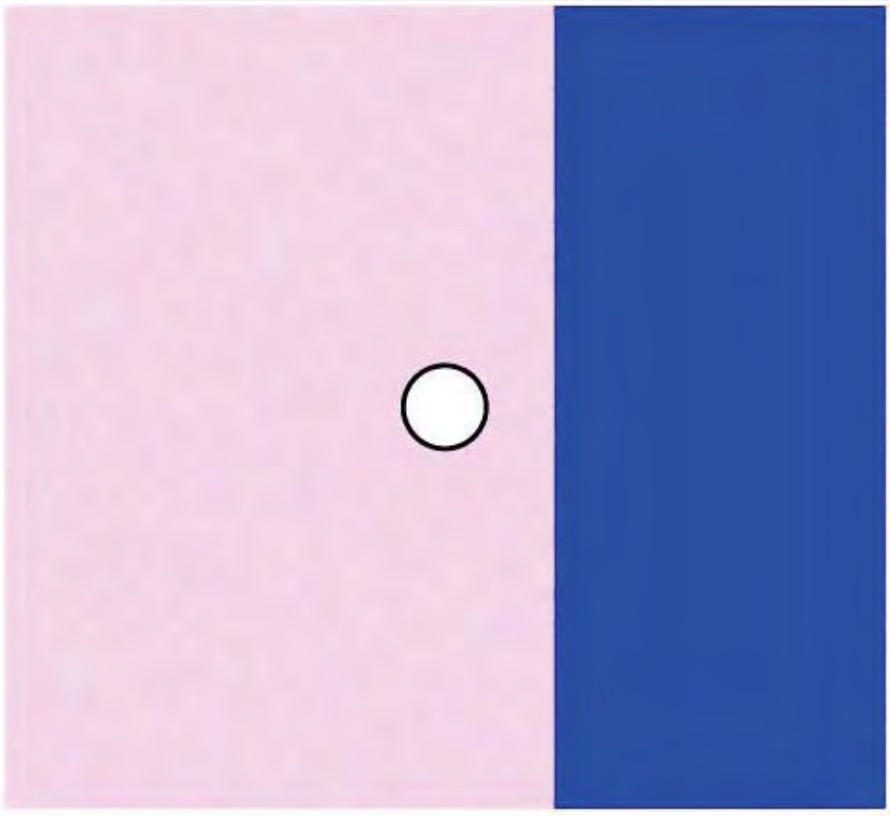

Highly resolved axisymmetric flow over a sphere (5 mil. grid cells)

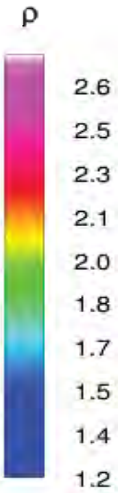

CCMT

Expansion fan over the particle

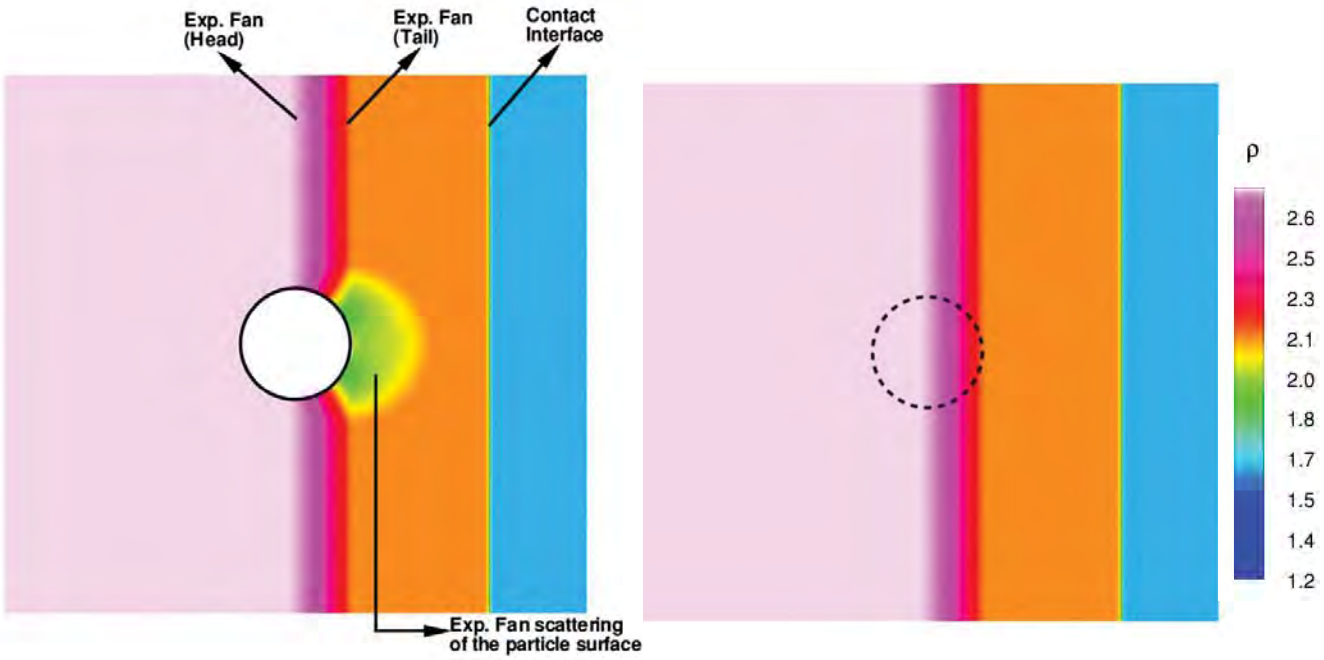

$$\mathbf{F}_{\text{inv}}(t) = \tfrac{4}{3}\pi R^3 \rho \overline{\frac{\mathrm{D}\mathbf{u}}{\mathrm{D}t}}^{V} + 4\pi R^3 \int_{\tilde{\xi}=-\infty}^{\tilde{t}} K_{iu}(\tilde{t}-\tilde{\xi}) \left[\frac{\partial}{\partial t} \overline{(\rho \mathbf{u}_r)}^{S} \right]_{\tilde{t}=\tilde{\xi}} \mathrm{d}\tilde{\xi} \, .$$

CCMT

Weak expansion fan

$$\mathbf{F}_{\text{inv}}(t) = \tfrac{4}{3}\pi R^3 \rho \overline{\frac{\mathrm{D}\mathbf{u}}{\mathrm{D}t}}^{V} + 4\pi R^3 \int_{\tilde{\xi}=-\infty}^{\tilde{t}} K_{iu}(\tilde{t}-\tilde{\xi}) \left[\frac{\partial}{\partial t} \overline{(\rho \mathbf{u}_r)}^{S} \right]_{\tilde{t}=\tilde{\xi}} \mathrm{d}\tilde{\xi} \, .$$

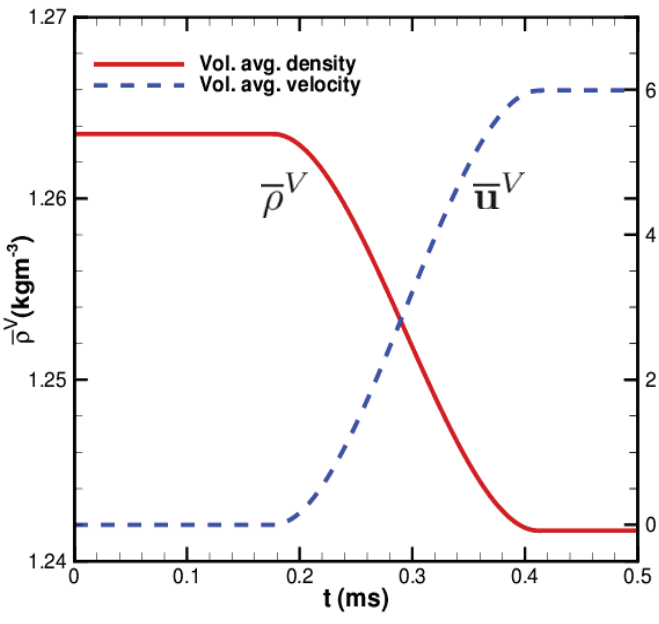

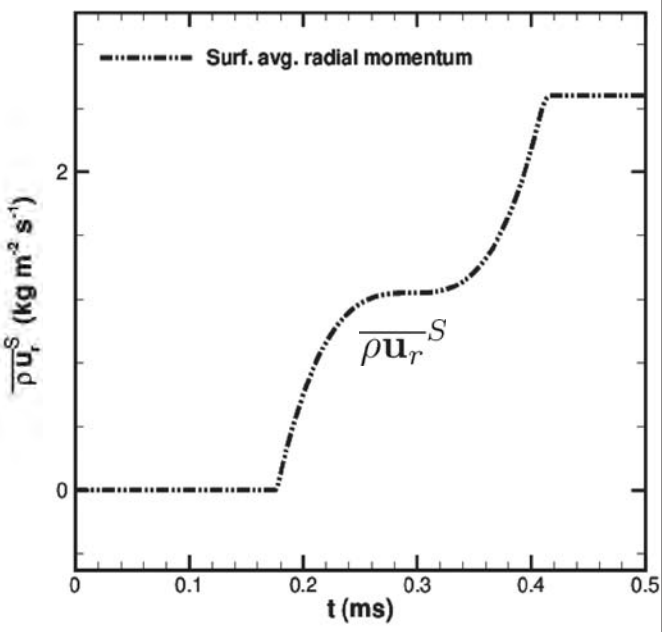

CCMT

Weak expansion fan

$$\mathbf{F}_{\text{inv}}(t) = \tfrac{4}{3}\pi R^3 \rho \overline{\frac{\mathrm{D}\mathbf{u}}{\mathrm{D}t}}^{V} + 4\pi R^3 \int_{\tilde{\xi}=-\infty}^{\tilde{t}} K_{iu}(\tilde{t}-\tilde{\xi}) \left[\frac{\partial}{\partial t} \overline{(\rho \mathbf{u}_r)}^{S} \right]_{\tilde{t}=\tilde{\xi}} \mathrm{d}\tilde{\xi} \, .$$

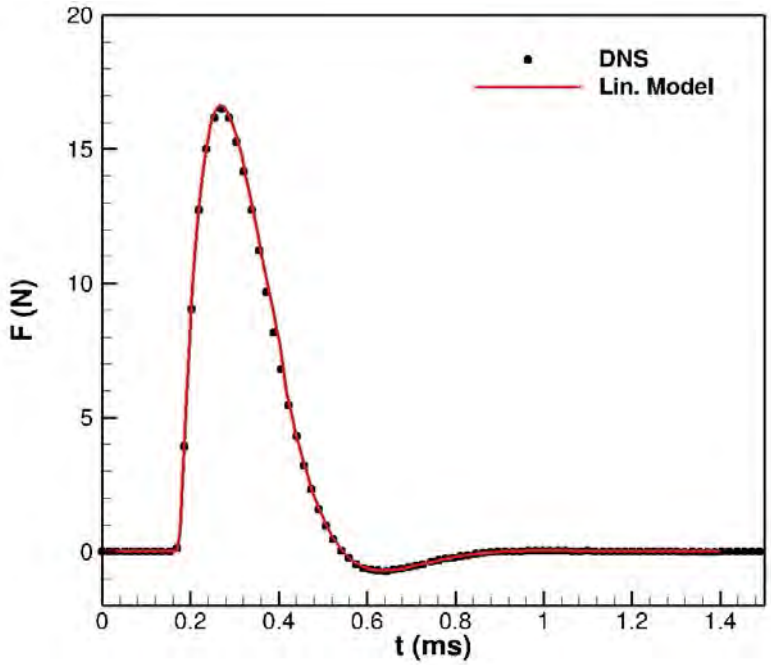

Averaged undisturbed flow properties

Local time derivative

Initial Pressure Ratio = 1.05

Shock Mach number = 1.01

CCMT

Strong expansion fan

$$\mathbf{F}_{\text{inv}}(t) = \tfrac{4}{3}\pi R^3 \rho \overline{\frac{\mathrm{D}\mathbf{u}}{\mathrm{D}t}}^{V} + 4\pi R^3 \int_{\tilde{\xi}=-\infty}^{\tilde{t}} K_{iu}(\tilde{t}-\tilde{\xi}) \left[\overline{\frac{\mathrm{D}}{\mathrm{D}t}} \overline{(\rho \mathbf{u}_r)}^{S} \right]_{\tilde{t}=\tilde{\xi}} \mathrm{d}\tilde{\xi} \, .$$

Exp. fan first interacts w/ particle

$t = 0.174$ ms

$\frac{\delta_1}{R} = 0.6$

Exp. fan last interacts w/ particle

$t = 0.672$ ms

$\frac{\delta_1}{R} = 2.25$

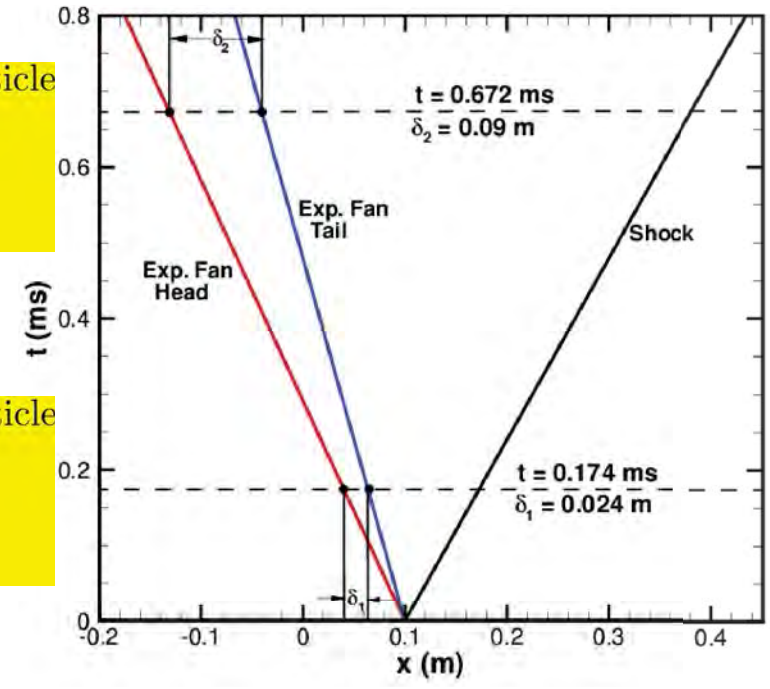

CCMT

Strong expansion fan

$$\mathbf{F}_{\text{inv}}(t) = \tfrac{4}{3}\pi R^3 \rho \overline{\frac{\mathrm{D}\mathbf{u}}{\mathrm{D}t}}^{V} + 4\pi R^3 \int_{\tilde{\xi}=-\infty}^{\tilde{t}} K_{iu}(\tilde{t}-\tilde{\xi}) \left[\overline{\frac{\mathrm{D}}{\mathrm{D}t}(\rho \mathbf{u}_r)}^{S} \right]_{\tilde{t}=\tilde{\xi}} \mathrm{d}\tilde{\xi} \, .$$

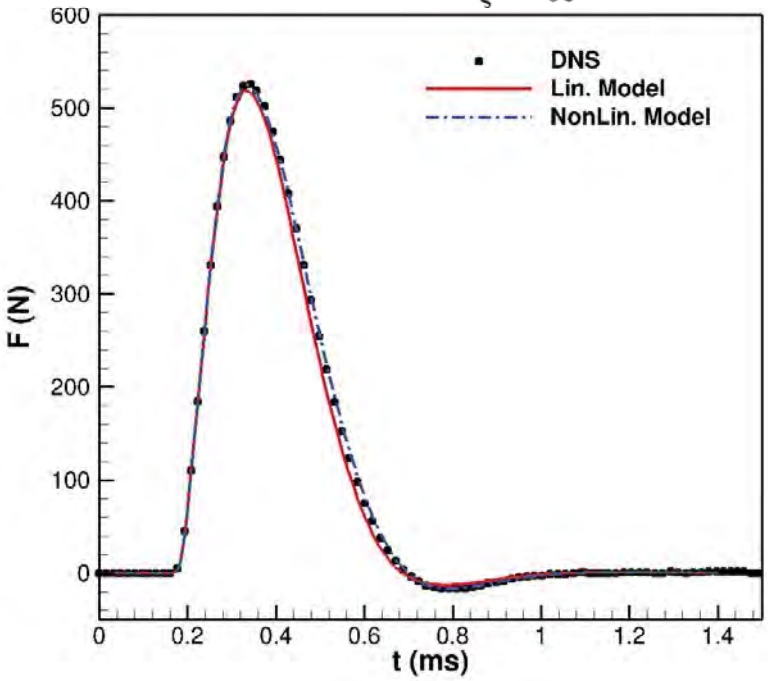

$$K_{iu} = \mathrm{e}^{-(\tilde{t}-\tilde{\xi})} \cos(\tilde{t}-\tilde{\xi})$$

Substantial time derivative

Initial pressure ratio = 2.5

Shock Mach number = 1.22

Weak & Strong normal shock

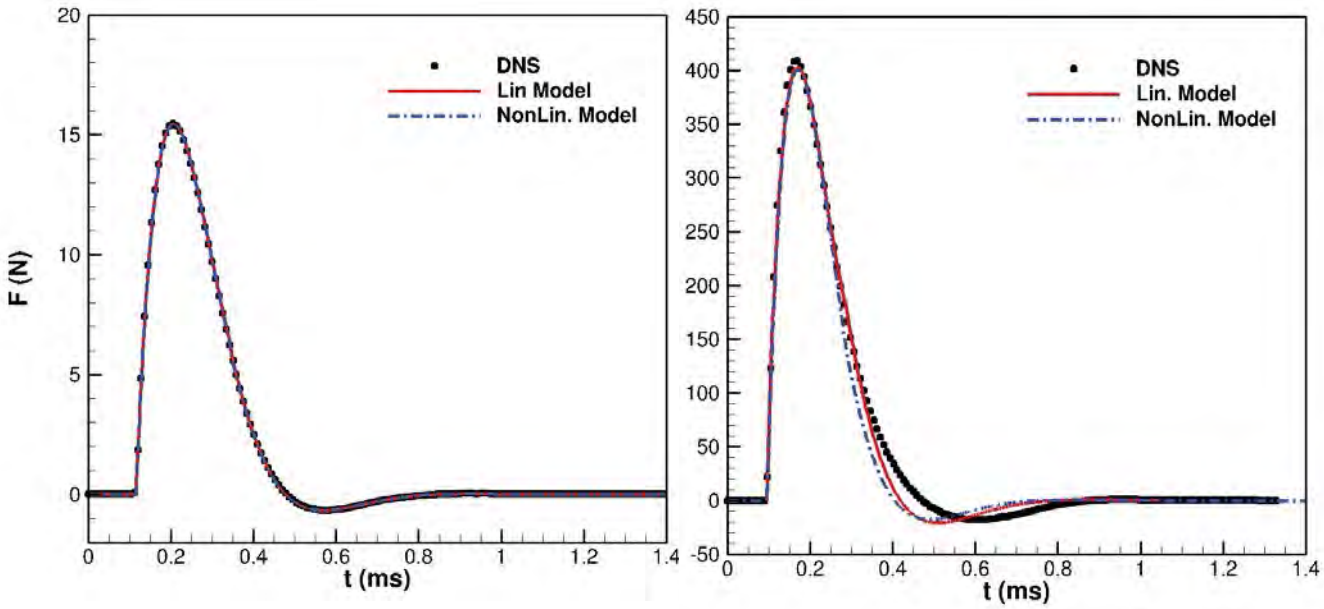

Weak Shock (M_s= 1.01)

Strong Shock (M_s= 1.22)

Expansion fan – Multi-particle system

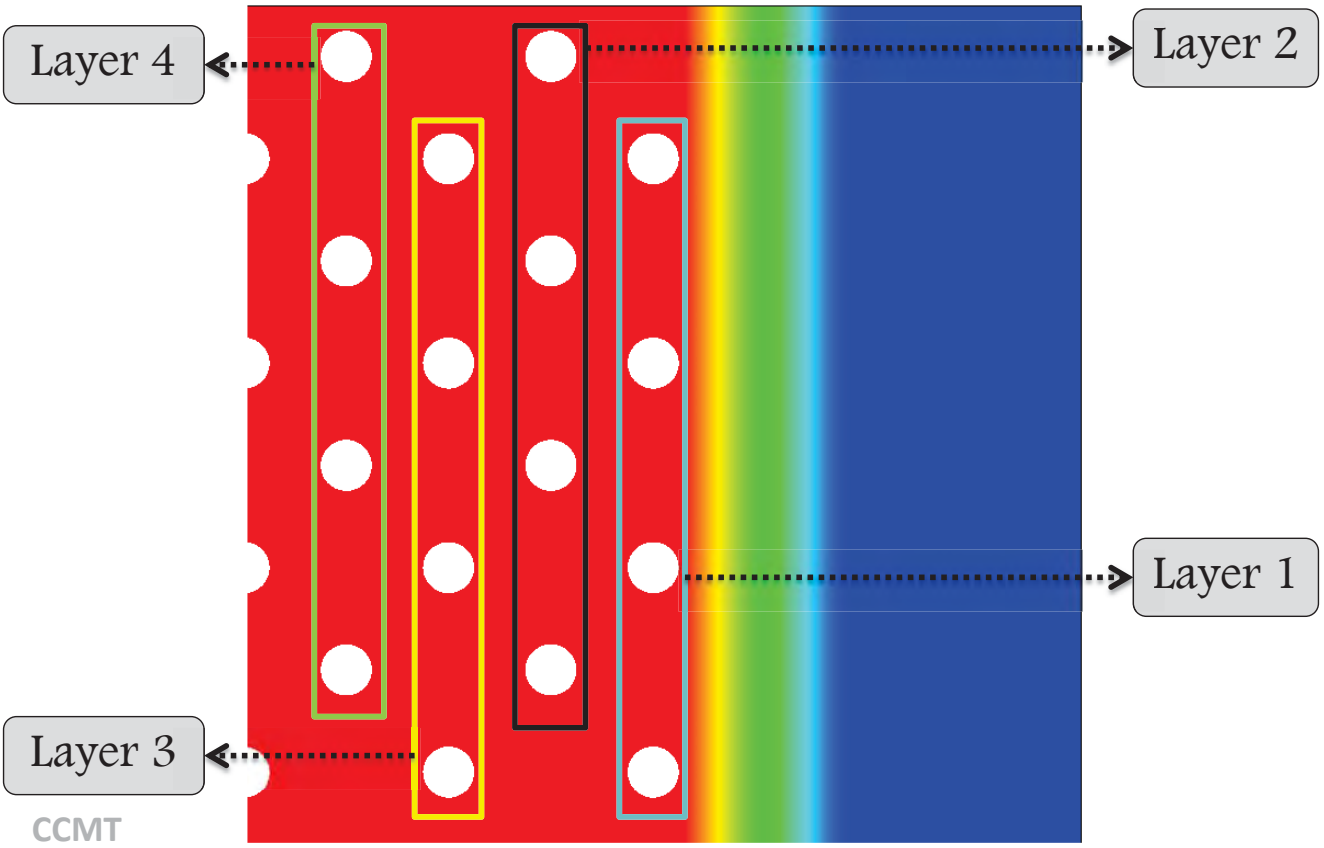

CCMT

Expansion fan – Multi-particle system

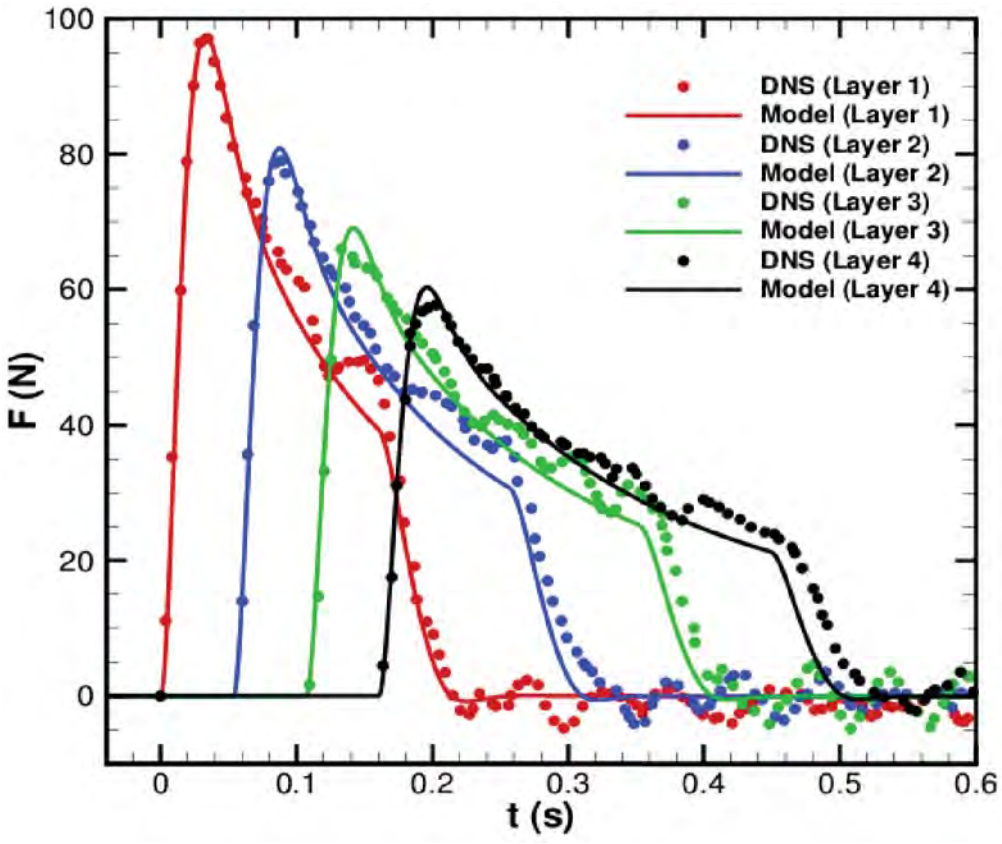

CCMT

Pressure evolution inside the particle

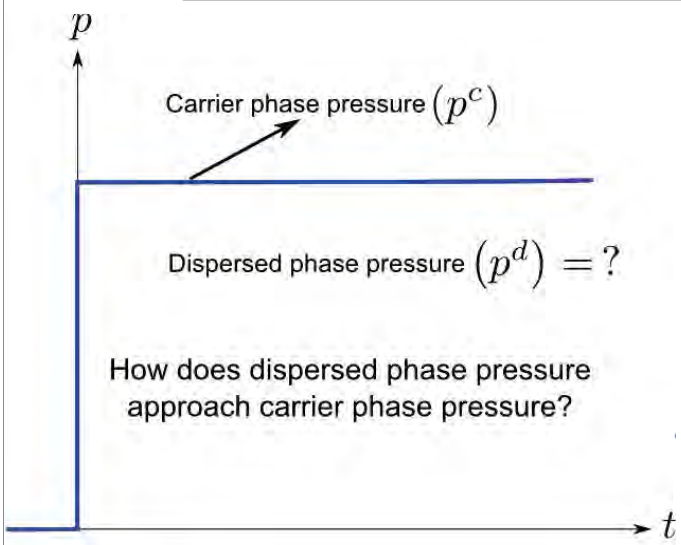

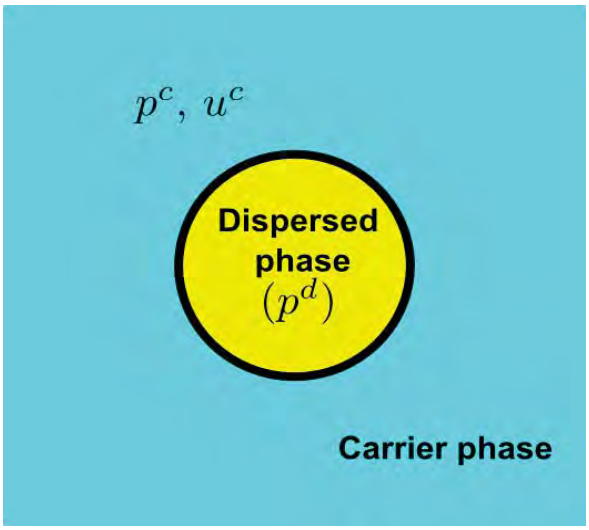

$$\frac{\mathrm{d}\mathbf{u}^d}{\mathrm{d}t} = \frac{\mathbf{u}^c - \mathbf{u}^d}{\tau_{pV}}$$

$$\tau_{pV} = \frac{(2\tilde{\rho}+1)R_0^2}{9\nu^c \Phi_V}$$

Momentum balance

Stokes drag

$$\frac{\mathrm{d}p^d}{\mathrm{d}t} = ?$$

$$\tau_{pP} = ?$$

Pressure equilibration equation

CCMT

Pressure Equilibration Equation

The volume-averaged particle phase pressure expressed purely in terms of "undisturbed" time-variation of the carrier phase properties is given as below:

Response to unit-step change in ambient pressure

Response to unit-step change in ambient radial momentum

$$\overline{p^d}^V(t) - \overline{p_0^d}^V = \frac{R_0}{a_0^c}\int_{\tilde{\xi}=-\infty}^{\tilde{t}} K_p(\tilde{t}-\tilde{\xi})\left.\frac{\mathrm{d}}{\mathrm{d}t}\overline{p^c}^S\right|_{\tilde{t}=\tilde{\xi}} \mathrm{d}\tilde{\xi} + R_0\int_{\tilde{\xi}=-\infty}^{\tilde{t}} K_w(\tilde{t}-\tilde{\xi})\left.\frac{\mathrm{d}}{\mathrm{d}t}\overline{(\rho u_r)^c}^S\right|_{\tilde{t}=\tilde{\xi}} \mathrm{d}\tilde{\xi}$$

Change in particle pressure (volume averaged)

Time-varying ambient pressure (surface averaged)

Time-varying ambient radial momentum (surface averaged)

R_0 : Mean particle radius, a_0^c : Ambient speed of sound

$K_p,\ K_w = f(\tilde{\rho}, \tilde{a})$ where $\tilde{\rho}$: density ratio, $\tilde{a}$: Speed of sound ratio

CCMT

Pressure Evolution: Shock Ma = 1.11

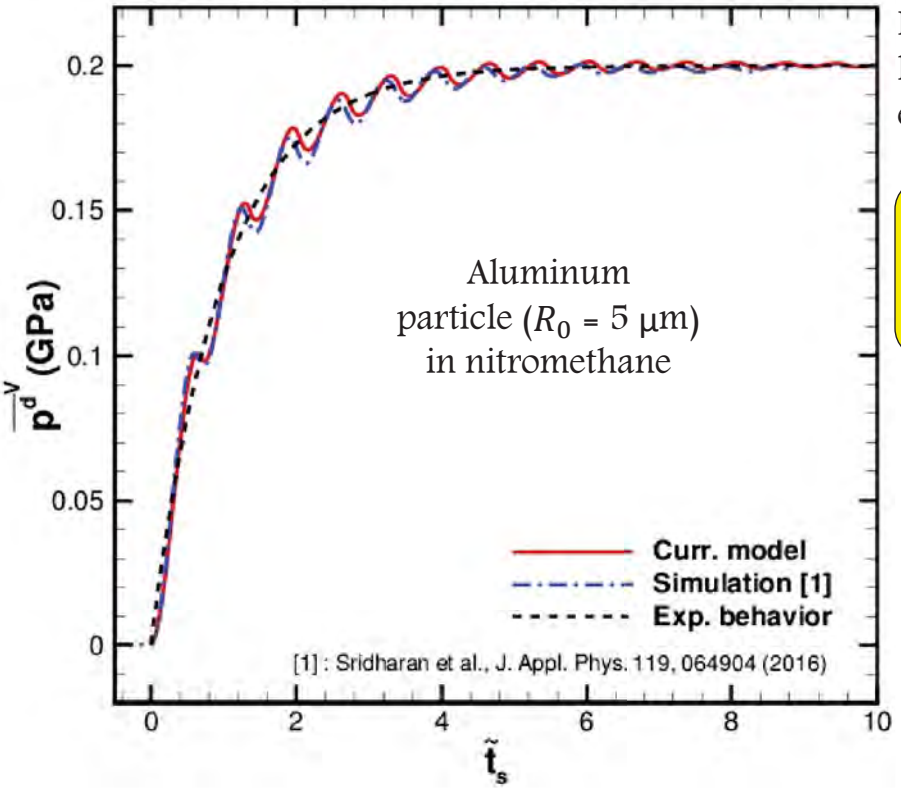

Exp. behavior (black-dash line) analogous to particle equation of motion:

$$\frac{\mathrm{d}\overline{p^d}^V}{\mathrm{d}t} = \frac{p^c_{\text{final}} - \overline{p^d}^V}{\tau_{pP}}$$

$\tau_{pP} = R_0/u_s$ is the particle time-scale

Similar agreements also observed for higher Mach numbers and particles with larger radii.

Pressure kernels

$$\overline{p^d}^V(t) - \overline{p_0^d}^V = \frac{R_0}{a_0^c}\int_{\tilde{\xi}=-\infty}^{\tilde{t}} K_p(\tilde{t}-\tilde{\xi})\,\frac{\mathrm{d}}{\mathrm{d}t}\overline{p^c}^S\Big|_{\tilde{t}=\tilde{\xi}}\,\mathrm{d}\tilde{\xi} + R_0\int_{\tilde{\xi}=-\infty}^{\tilde{t}} K_w(\tilde{t}-\tilde{\xi})\,\frac{\mathrm{d}}{\mathrm{d}t}\overline{(\rho u_r)^c}^S\Big|_{\tilde{t}=\tilde{\xi}}\,\mathrm{d}\tilde{\xi}$$

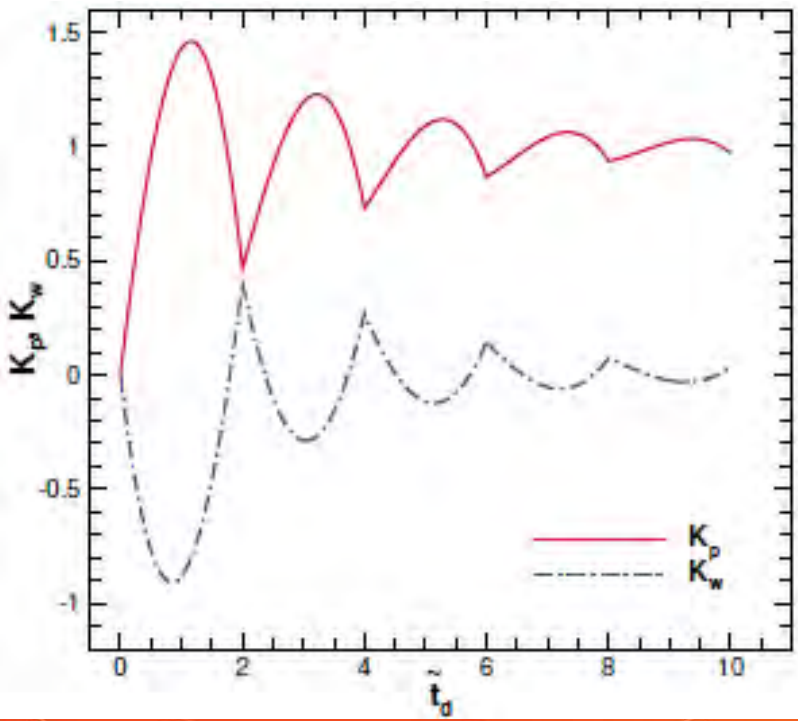

Density Evolution: Shock Ma = 1.11

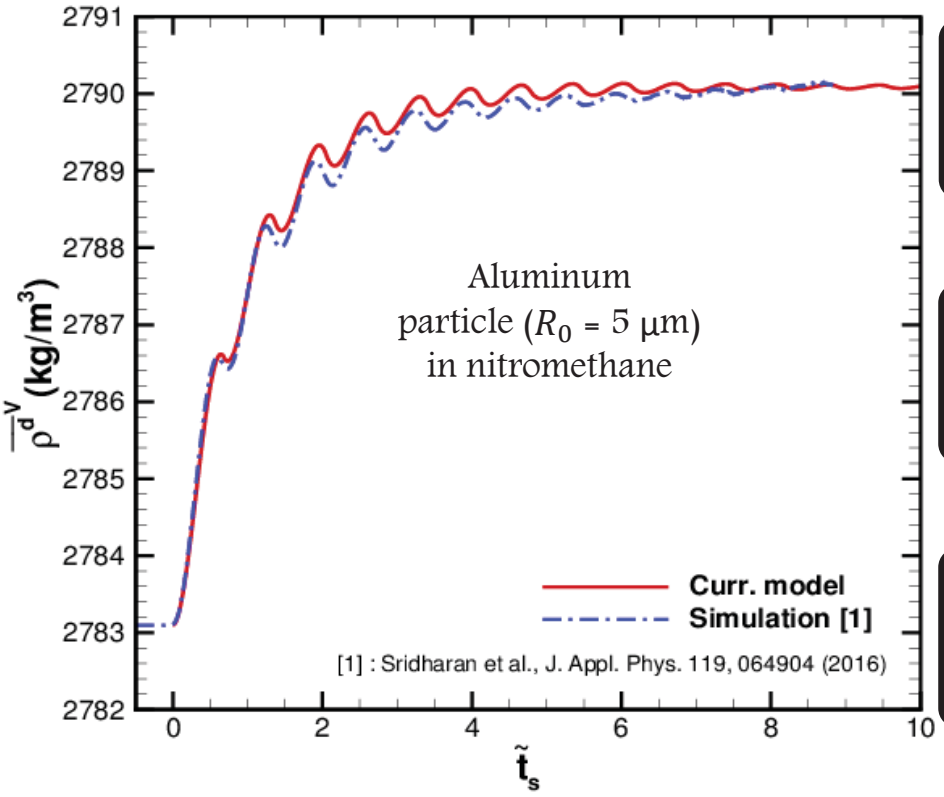

Density evolution

↓

Specific volume time history

↓

Equation for volume fraction evolution

CCMT

Future work & Challenges

- Application of the generalized Faxén theorem when there is a random cloud of particles.
- How does one handle particle compaction especially when a strong blast wave rams on a close-packed particle bed?
- A similar pressure model allowing for particle deformation.
- While we have a state of the art hydrodynamic force model (gas-particle interaction), a model for particle-particle interaction in highly compressible and unsteady environments is still in its primitive stages.

CCMT

Any Questions

LA-UR-16-27657

Modeling of Ejecta Particles in the FLAG Continuum Mechanics Code

Alan K. Harrison
Lagrangian Codes Group (XCP-1)
Computational Physics Division

Multiphase Physics Deep-Dive
St. Petersburg, Florida
October 7, 2016

Operated by Los Alamos National Security, LLC for the U.S. Department of Energy's NNSA

Motivation: Ejecta and modeling ejecta experiments

- Extreme shock loading may cause damage and failure at material free surfaces, producing particulate fragmentation known as ejecta.
- Theories, experiments, and modeling involve a wide range of solid and fluid mechanics at relevant spatial and temporal scales.

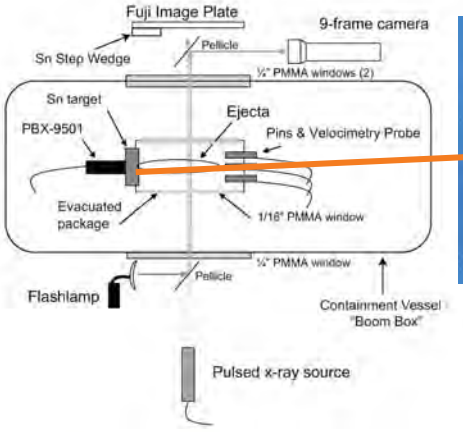

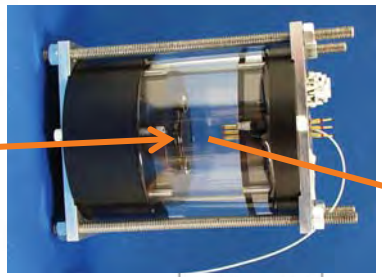

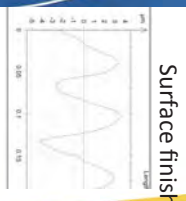

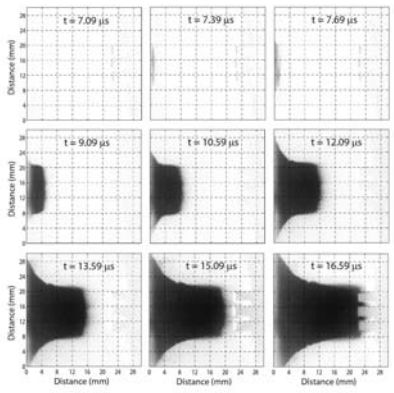

See many experimental papers by W. T. Buttler, R. T. Olson, M. B. Zellner and coworkers

Operated by Los Alamos National Security, LLC for the U.S. Department of Energy's NNSA

The FLAG hydrocode is our testbed to simulate the experiment.

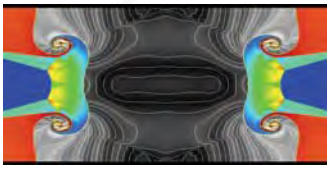

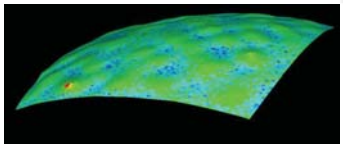

High strain rates

Strength, damage, failure

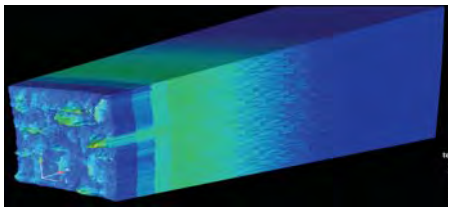

Compressibility

Mixtures

Impact/contact

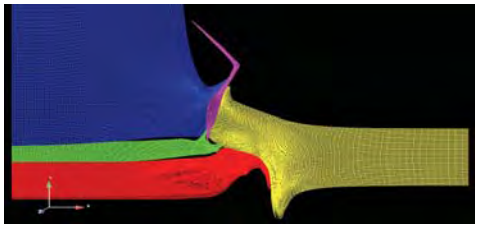

1, 2, 3D
Lagrange/ALE hydro
Fully unstructured meshes
(arbitrary polygons/polyhedra

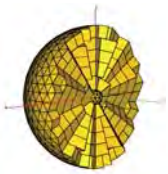

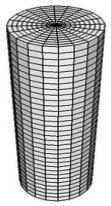

Operated by Los Alamos National Security, LLC for the U.S. Department of Energy's NNSA

A particle-in-cell formulation is used to model ejecta in FLAG.

- (Super) particles represent packets of multiple physical particles.
  - Tracking individual physical particles is expensive, so allowing computational particles to represent "many" reduces cost. The tradeoff is the statistical resolution.
- While FLAG hydro advances the continuum equations of motion, a distinct solver is implemented to advance particle equations of motion.
  - Positions and velocities in space and time
  - Positions relative to the hydrodynamics mesh
- Particle-fluid coupling involves
  - Summing/averaging particle quantities over zones (to an "ejecta phase")
  - Interpolating continuum information from mesh zones and points to particles
- How is the formulation integrated with FLAG hydro?
  1. Predictor step for continuum momentum and energy
  2. Corrector step for continuum momentum and energy
  3. Ejecta tracking and transport*
  4. Ejecta sourcing (for launch next cycle)*

*Including momentum/energy exchange with continuum

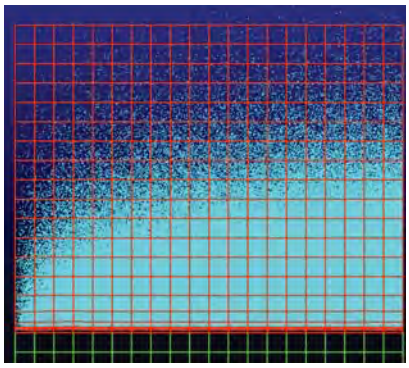

Andrews, M.J. and O'Rourke, P.J. : MP-PIC

Operated by Los Alamos National Security, LLC for the U.S. Department of Energy's NNSA

An ejecta calculation begins with a shock passing through the source metal

Calculation and slide by I. Tregillis

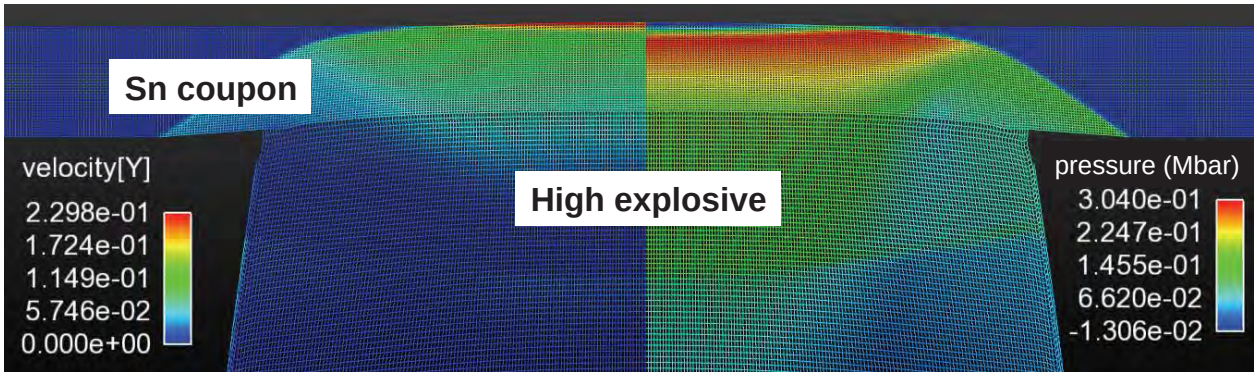

Operated by Los Alamos National Security, LLC for the U.S. Department of Energy's NNSA

The calculation tracks ejecta within or/and beyond the problem mesh

When the surface doesn't refreeze, ejecta production in the calculation can persist indefinitely.

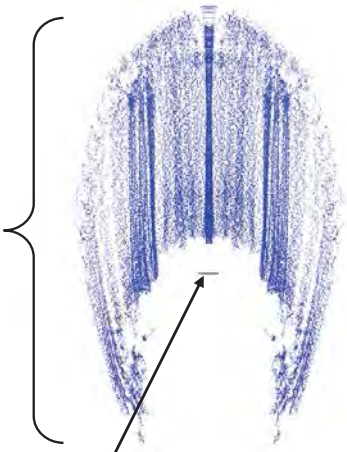

Calculation and slide by I. Tregillis

Size & location of central $LiNbO_3$ piezo head for this shot

Melt state of Sn coupon:
Melted
Solid

Operated by Los Alamos National Security, LLC for the U.S. Department of Energy's NNSA

The ejecta package includes pieces corresponding to different stages of ejecta development

- The source package determines *whether/when* to produce ejecta, the *production rate*, and the *initial conditions* (size and velocity distributions) of the particles produced
  - The production decision is based on shock detection and surface properties
  - The Richtmyer-Meshkov Instability (RMI) source model predicts
    - the production rate, and
    - initial particle sizes and velocities
- Other packages account for particle-gas forces during the transport phase
  - drag
  - buoyant force
  - effective force field in dense particle clouds
- Other packages account for various types of particle transformations
  - heat flux
  - mass flux (evaporation)
  - particle breakup
  - collisions

Operated by Los Alamos National Security, LLC for the U.S. Department of Energy's NNSA

Shock detection and characterization depend on acceleration and melt state of the metal surface

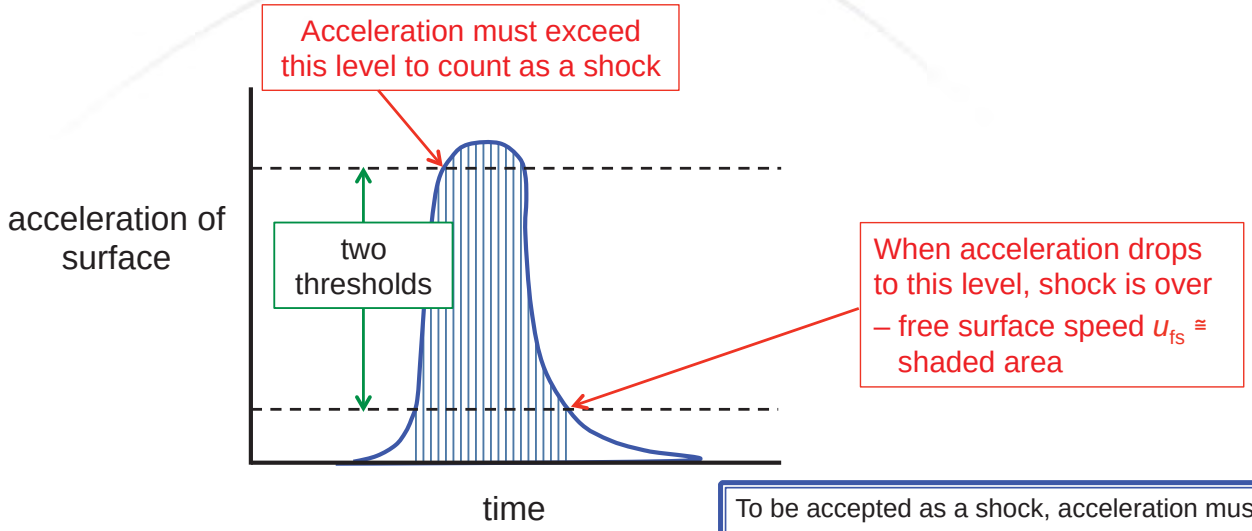

To be accepted as a shock, acceleration must
(1) start below lower threshold
(2) exceed upper threshold
(3) drop below lower threshold
and surface must be melted at time (3)

Operated by Los Alamos National Security, LLC for the U.S. Department of Energy's NNSA

Under conditions known to produce ejecta, proton radiography shows the spikes and bubble of RM instability

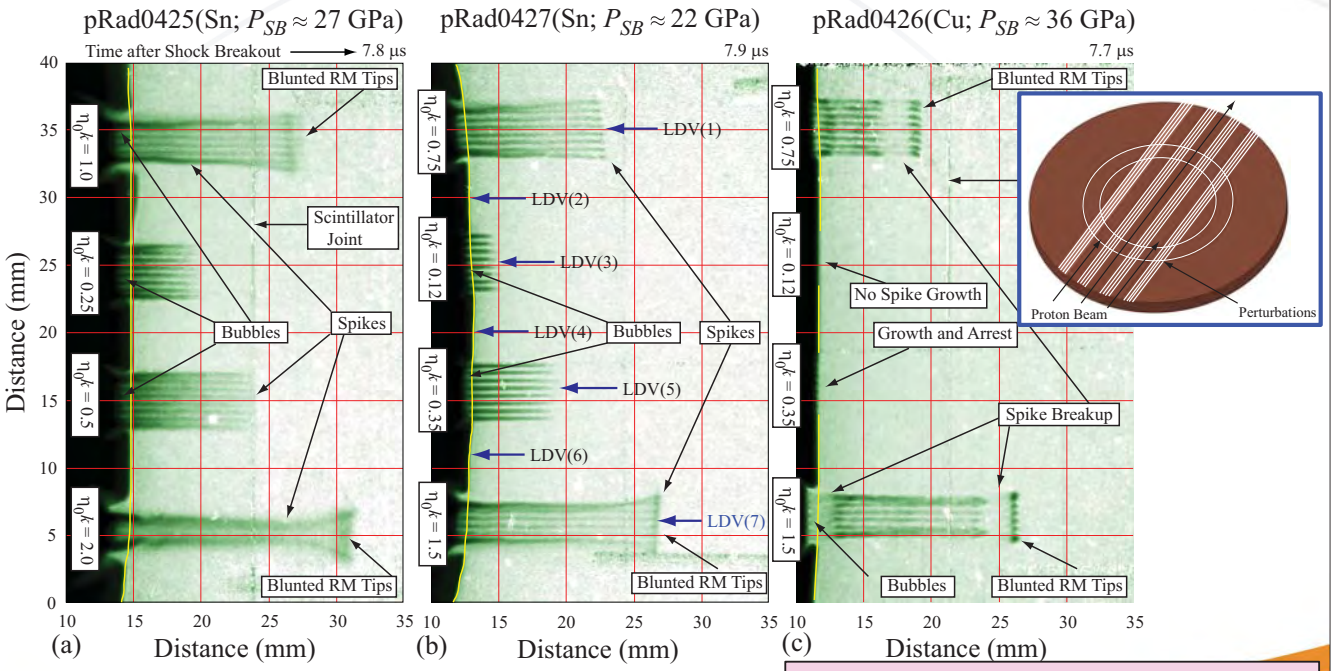

W. T. Buttler, D. M. Oró, D. L. Preston, K. O. Mikaelian, F. J. Cherne, R. S. Hixson, F. G. Mariam, C. Morris, J. B. Stone, G. Terrones and D. Tupa, Journal of Fluid Mechanics **703**(July 2012):60-84
DOI: 10.1017/jfm.2012.190, Published online: 13 June 2012

Ejecta particles are droplets broken off spike tips

Buttler *et al.* (2012) analysis of spike and bubble growth rates (based on earlier work by Mikaelian):

$$\dot{\eta}^b(t) = \frac{2\dot{\eta}_0^b}{2 + 3\dot{\eta}_0^b kt} \qquad \dot{\eta}^s(t) \simeq \sqrt{3}\,\dot{\eta}_0^s$$

with initial rates

$$\dot{\eta}_0^{b,s} = \pm F_l F_{nl}^{b,s} a u_{fs}$$

where

$$a = \eta_0 k = \frac{2\pi\eta_0}{\lambda} \qquad F_l = 1 - \frac{u_{fs}}{2u_{sh}}$$

$$F_{nl}^b = \frac{1}{1+\frac{a}{6}} \qquad F_{nl}^s = \frac{1}{1+\frac{a^2}{4}}$$

u_{sh} = shock velocity

u_{fs} = free surface velocity

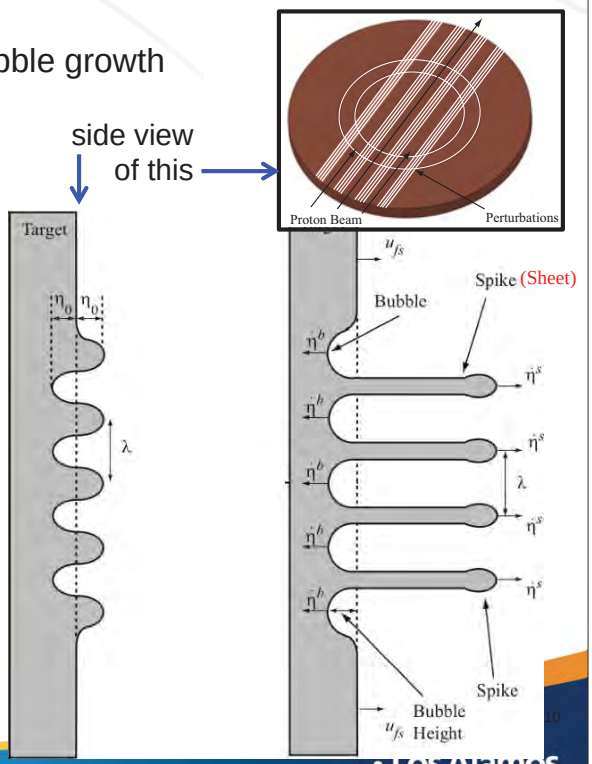

We have implemented a force-field model due to particle-particle interactions

$$F_i^{pp} = -\frac{V_i^p}{\phi_i^p}\nabla\tau_{pp,i}$$

$$\tau_{pp,i} = \frac{P_s\left(\phi_i^p\right)^\beta}{\phi_c^p - \phi_i^p}$$

- This code capability does not actually predict individual collisions, but it is intended to account for their effect.
- The model is simple and designed for dense-particle flows, so it will tend to spread out particles even if they are stationary.
- Predicting individual collisions is much more expensive (future work), so a model of this type is welcome.

Operated by Los Alamos National Security, LLC for the U.S. Department of Energy's NNSA

We have implemented a model of heat flux between particles and gas

- Convective heat transfer

  $$\dot{Q}_c = \mathrm{Nu}\,\pi D k_c\left(T_s - T_c\right)$$

  where T_s is the particle surface temperature and T_c is the gas temperature, and we use the Ranz-Marshall correlation for Nusselt number:

  $$\mathrm{Nu} = 2 + 0.6\,\mathrm{Re}^{1/2}\,\mathrm{Pr}^{1/3}$$

- This capability should be important in predicting the temperature history of ejecta particles, which is needed for proper prediction of their evaporation (next slide)
- Reference for this model and mass flux model (next slide): C. T. Crowe, J. D. Schwarzkopf, M. Sommerfeld and Y. Tsuji, *Multiphase Flows with Droplets and Particles*, 2nd ed. (CRC Press: Boca Raton, 2012).

Operated by Los Alamos National Security, LLC for the U.S. Department of Energy's NNSA

We have implemented a model of mass flux between particles and gas (evaporation)

- Evaporation

$$\dot{m} = \mathrm{Sh}\,\pi D \rho_c D_v \left(\omega_\infty - \omega_s\right)$$

where ω_∞ is the mass fraction for the evaporated phase in the free stream and ω_s is the surface concentration of the evaporated phase. We use the Ranz-Marshall correlation for Sherwood number:

$$\mathrm{Sh} = 2 + 0.6\,\mathrm{Re}^{1/2}\,\mathrm{Sc}^{1/3}$$

This mass flux also carries energy with it:

$$\dot{Q}_m = \frac{\mathrm{Sh}}{2}\frac{12 k_c}{c_d \rho_d D^2}\frac{\mathrm{Pr}}{\mathrm{Sc}}\frac{h_l}{c_p}\left(\omega_\infty - \omega_s\right)$$

- As a particle loses matter from its surface, the code tracks its decrease in mass and diameter
- When its mass drops to zero it is deleted from the calculation
- This model relies on predicting the metal vapor pressure at the surface of a particle, which depends on knowing its thermodynamic state

Operated by Los Alamos National Security, LLC for the U.S. Department of Energy's NNSA

We model oscillations in a liquid droplet as a damped driven harmonic oscillator—an analogy

- Experimental evidence suggests that ejecta are liquid drops, not solid particles
- Accordingly, we have implemented a drop breakup model—the Taylor Analogy Breakup (TAB) model—in FLAG.

- We model an ejecta particle as a liquid drop
  - with radius r, density ρ_l, viscosity μ_l, surface tension σ
  - moving through a gas of density ρ_g
  - with relative velocity u

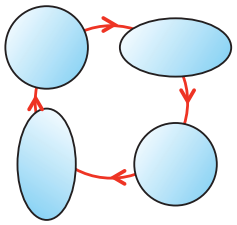

- The displacement x of the droplet's equator from its equilibrium position satisfies the differential equation

$$m\ddot{x} = F - kx - d\dot{x}$$

in which aerodynamics, surface tension and droplet viscosity provide the force terms:

$$\frac{F}{m} = C_F \frac{\rho_g u^2}{\rho_l r} \qquad \frac{k}{m} = C_k \frac{\sigma}{\rho_l r^3} \qquad \frac{d}{m} = C_d \frac{\mu_l}{\rho_l r^2}$$

- We evaluate the exact solution to the ODE and test for the breakup condition $x = C_b r$.

Operated by Los Alamos National Security, LLC for the U.S. Department of Energy's NNSA

When a particle breaks up we must model the daughter droplets

- Daughter droplets acquire a new velocity increment perpendicular to the original velocity vector

$$C_v = 1 \qquad \text{(default } C_v = 1\text{)}$$

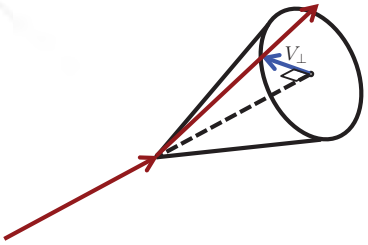

- An energy conservation argument determines the Sauter mean radius $r_{32} \equiv \langle r^3 \rangle / \langle r^2 \rangle$ of the expected distribution of daughter droplet radii:

$$r_{32} = r\left[1 + \frac{2K}{5} + \left(\frac{K}{20} - \frac{1}{24}\right)\frac{\rho_l r \dot{x}^2}{C_b^2}\right]^{-1} \qquad \text{(default } K = 10/3\text{)}$$

  - It suffices to create a single daughter, with the direction of $V_\perp$ sampled from [0,2π], and radius sampled from the indicated size distribution
  - We must rescale the number of physical particles in the daughter packet

$$N^{\text{new}} = N\left(\frac{r}{r^{\text{new}}}\right)^3$$

Operated by Los Alamos National Security, LLC for the U.S. Department of Energy's NNSA

The TAB-SHEET and TAB-LIG models account for breakup of spikes to droplets

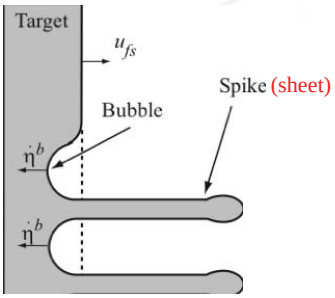

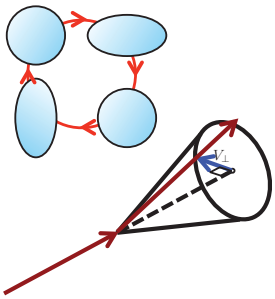

RMI source model: production of sheets → TAB-SHEET model: sheets tear into ligaments → TAB-LIG model: ligaments break up into droplets → TAB model: droplets break up into smaller droplets

These models are mathematically similar to the original TAB model; only the coefficients in the ODE are different.

Operated by Los Alamos National Security, LLC for the U.S. Department of Energy's NNSA

Acknowledgments

- The code development work reported here was done in partnership with J. Fung, N. Denissen and other code developers on the FLAG code team
- We have benefitted from collaborations with LANL research teams in experimental, model development and V&V areas
- This work was supported by the Advanced Simulation and Computing Program (ASC) of the National Nuclear Security Administration (NNSA) of the U. S. Department of Energy.

Los Alamos National Laboratory, an affirmative action/equal opportunity employer, is operated by Los Alamos National Security, LLC, for the National Nuclear Security Administration of the U.S. Department of Energy under contract DE-AC52-06NA25396.

References

- Andrews, M. J. and D. L. Preston, “TAB Models for Liquid Sheet and Ligament Breakup,” Los Alamos National Laboratory, Los Alamos, NM, Report no. LA-UR-14-26937 (2014).
- Buttler, W. T., D. M. Oró, D. L. Preston, K. O., Mikaelian, F. J. Cherne, R. S. Hixson, F. G. Mariam, C. Morris, J. B. Stone, G. Terrones, and D. Tupa, “Unstable Richtmyer-Meshkov Growth in Solid and Liquid Metals in Vacuum,” *J. Fluid Mech.* **703**:60-84 (2012).
- Crowe, C. T., J. D. Schwarzkopf, M. Sommerfeld and Y. Tsuji, *Multiphase Flows with Droplets and Particles*, 2nd ed. (CRC Press: Boca Raton, 2012), 60-62, 103-105.
- Fung, J., A. K. Harrison, S. Chitanvis, and J. Margulies, “Ejecta Source and Transport Modeling in the FLAG Hydrocode,” *Computers & Fluids* **83**:177-186 (2013).
- Ling, Y., J. L. Wagner, S. J. Beresh, S. P. Kearney, and S. Balachandar, “Interaction of a planar shock wave with a dense particle curtain: Modeling and experiments.” *Physics of Fluids* **24**:113301 (2012).
- O’Rourke, P. J. and A. A. Amsden, “The TAB Method for Numerical Calculation of Spray Droplet Breakup.” Los Alamos National Laboratory, Los Alamos, NM, Report no. LA-UR-87-2105-Rev (1987).
- Zellner, M. B., W. V. McNeil, J. E. Hammerberg, R. S. Hixson, A. W. Obst, R. T. Olson, J. R. Payton, P. A. Rigg, N. Routley, G. D. Stevens, W. D. Turley, L. Veeser, and W. T. Buttler, “Probing the Underlying Physics of Ejecta Production from Shocked Sn Samples,” *J. Appl. Phys.* **103**:123502 (2008).

Summary and invitation

- We have developed a particle-in-cell capability to model mass ejection and transport (ejecta) in a Lagrange/ALE continuum dynamics code.
- We are building models of ejecta phenomena including production, transport through gases, evaporation and breakup. The models are at various levels of fidelity and maturity.
- We invite collaboration with experts in relevant phenomena—theory, experiment, simulation and modeling.
- Contact us (Alan K. Harrison or Marianne M. Francois) if you are interested.

NNSA National Nuclear Security Administration
Operated by Los Alamos National Security, LLC for the U.S. Department of Energy's NNSA
Los Alamos NATIONAL LABORATORY EST. 1943

Backup slides

NNSA National Nuclear Security Administration
Operated by Los Alamos National Security, LLC for the U.S. Department of Energy's NNSA
Los Alamos NATIONAL LABORATORY EST. 1943

Initial mesh

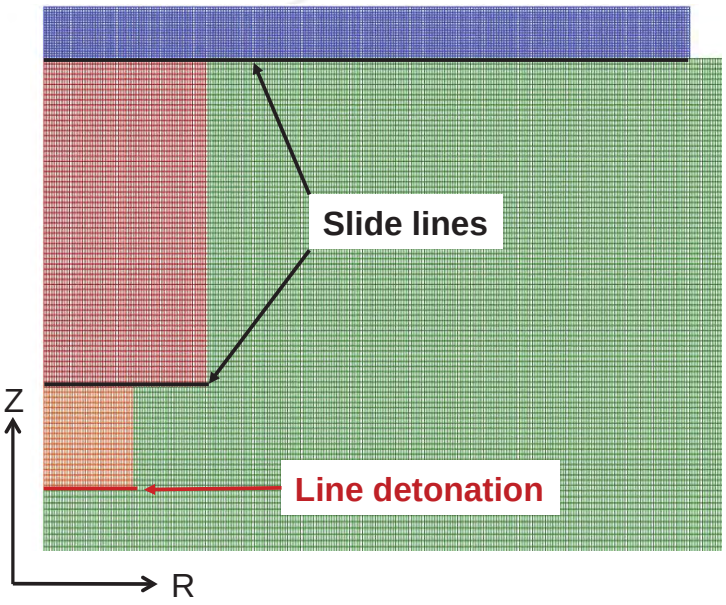

- **Initial zone size in the coupon: Δz = Δr = 100, 50, 25 μm**
- **Zone sizes in the HE & sheath blocks are impedance matched in Δz via $\sqrt{\rho_1/\rho_2}$.**
- **All boundaries are free except the z-axis, where radial forces and velocities are set to 0.**
- **There is no mesh above the coupon surface. Ejecta package tracks the particles through vacuum.**
- **All mesh hydro is frozen after ejecta are launched to sidestep mesh tangling issues.**

Calculation and slide by I. Tregillis

Operated by Los Alamos National Security, LLC for the U.S. Department of Energy's NNSA

High explosive drive produces a "triangle wave" velocity front

Calculation and slide by I. Tregillis

0.852 μs

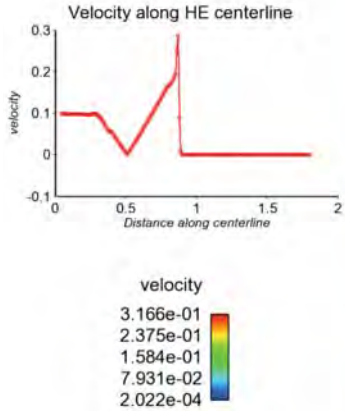

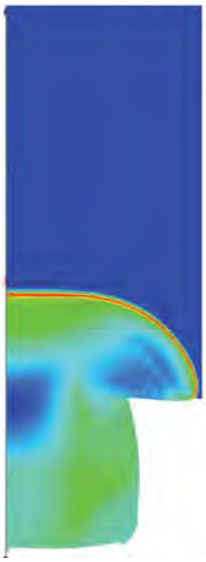

1.876 μs

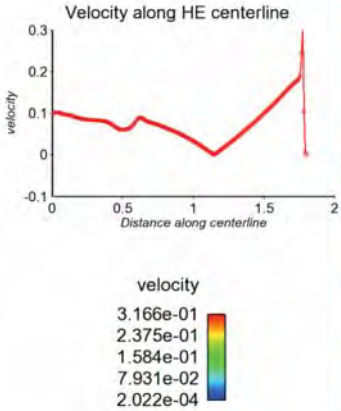

Δz = Δr = 50 μm in coupon

Operated by Los Alamos National Security, LLC for the U.S. Department of Energy's NNSA

Ejecta production rate (volume/area/time) is inferred from equality of spike and bubble volumes

$\chi_{s,b}$ = spike, bubble area fractions

$\chi_s + \chi_b = 1$

Spikes and bubbles must have equal growth rates:

$$\dot{\Delta} = \chi_s |\dot{\eta}_s| = \chi_b \dot{\eta}_b$$

Eliminate $\chi_{s,b}$ from equations:

$$\frac{1}{\dot{\Delta}} = \frac{1}{\dot{\eta}_b} + \frac{1}{|\dot{\eta}_s|}$$

Integrate $\dot{\Delta}$ over one cycle from t_f to t_i (measured from shock breakout time):

$$\Delta = \frac{2}{3k} \ln \frac{t_f + t_0}{t_i + t_0} \qquad t_0 = \frac{\frac{1}{F_{nl}^b} + \frac{1}{\sqrt{3} F_{nl}^s}}{\frac{3}{2} ka F_l u_{fs}}$$

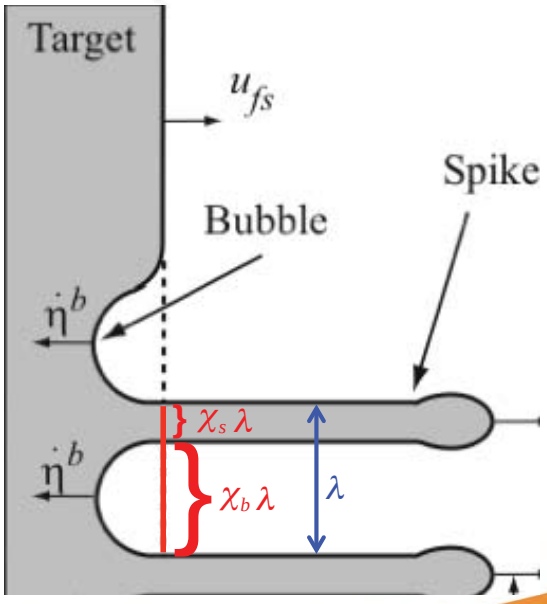

Operated by Los Alamos National Security, LLC for the U.S. Department of Energy's NNSA

Solution of the damped driven harmonic oscillator

- Suppose the droplet breaks up when $x = C_b r$, and define $y = \frac{x}{C_b r}$. Then the solution of the ODE is

$$y(t) = C_0 \mathrm{We} + e^{-t/t_d} \left\{ (y_0 - C_0 \mathrm{We}) \cos \omega t + \frac{1}{\omega} \left[\dot{y}_0 + \frac{1}{t_d} (y_0 - C_0 \mathrm{We}) \right] \sin \omega t \right\}$$

in which

$$C_0 = \frac{C_F}{C_b C_k} \qquad \mathrm{We} = \frac{\rho_g u^2 r}{\sigma}$$

$$\frac{1}{t_d} = \frac{C_d}{2} \frac{\mu_l}{\rho_l r^2} \qquad \omega^2 = C_k \frac{\sigma}{\rho_l r^3} - \frac{1}{t_d^2} \qquad (\omega^2 < 0 \text{ only for very small drops})$$

- Default coefficient values are based on experiments and modeling hypotheses:

$$C_k = 8 \qquad C_d = 5 \qquad C_b = \frac{1}{2} \qquad C_F = \frac{1}{3} \qquad C_0 = \frac{1}{12} = \frac{1}{2\,\mathrm{We}_{\mathrm{crit}}}$$

- At every cycle, for each particle, FLAG updates y and $\dot{y}$ and checks for the breakup condition $|y| = 1$.

Operated by Los Alamos National Security, LLC for the U.S. Department of Energy's NNSA

Finite-size particles in homogeneous-isotropic turbulence

Clustering and preferential concentration

Markus Uhlmann[1] and Agathe Chouippe

Institute for Hydromechanics
Karlsruhe Institute of Technology, Germany

October 2016

[1]currently on leave at CCMT, U. Florida

Finite-size particles interacting with turbulence

(Nishino & Matsushita, ICMF 2004)

www.usclaimexpert.com

- mobility
- collective effects
- ~~gravity~~

Applications

- meteorology, chemical engineering, . . .

Open questions

- settling velocity, cluster formation
- influence of/on turbulence

$\rho_p/\rho_f = 1.5$, $\Phi_s = 0.005$

ambient settling

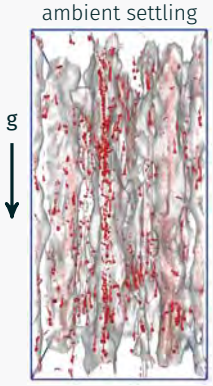

MU & Doychev (JFM 2014)

hom.-isotropic turbulence

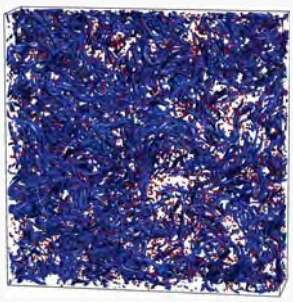

- present work
- Homann & Bec (2010)
- Cisse et al. (2013)
- Ten Cate et al. (2004)
- Yeo et al. (2010)
- Fiabane et al. (2012)

settling & turbulence

Chouippe & MU (ETC 2015)

Immersed boundary method

Principle

- fixed Cartesian grid, uniform
- no-slip condition at interface imposed via body force
- smooth interpolation through regularized δ function

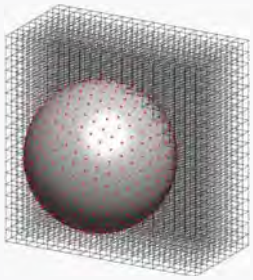

MU, *J. Comput. Phys.* (2005)

Rigid body motion

- translational & angular particle motion
- dilute $\rightarrow$ simple repulsion model (Glowinski 1999)

Forcing statistically stationary turbulence

Random forcing (Eswaran & Pope 1988)

- momentum source in low-wavenumber band
- Uhlenbeck-Ornstein processes per Fourier mode

Present implementation

- avoids use of FFT
- validated against single-phase data
- stable procedure in presence of particles (Lundgren's 2003 linear forcing is not)

→ allows long-time integration

Chouippe & MU (PoF 2015)

Two-phase flow parameter values

		cases	
		D5	D11
diameter/Kolmogorov-length ratio	D/η	5.5	11.0
Reynolds number	Re_λ	125	140
density ratio	ρ_p/ρ_f	1.5	
solid volume fraction	Φ_s	0.005	
Stokes number (Kolmogorov)	St_η	2.4	10.7
Stokes number (large-eddy)	St_L	0.05	0.29
number of particles	N_p	20026	2540

Energy spectrum and length scales

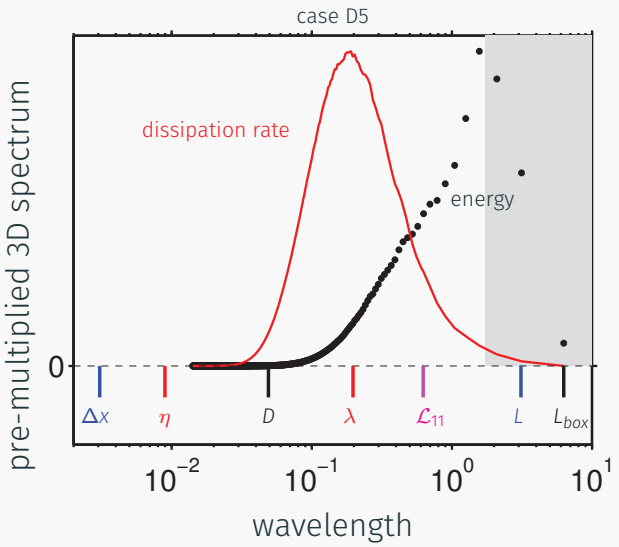

$$L_{box}/\mathcal{L}_{11} = 10$$
$$L_{box}/D = 128$$
$$\eta/\Delta x = 3$$
$$D/\Delta x = 16$$

Kinetic energy budget

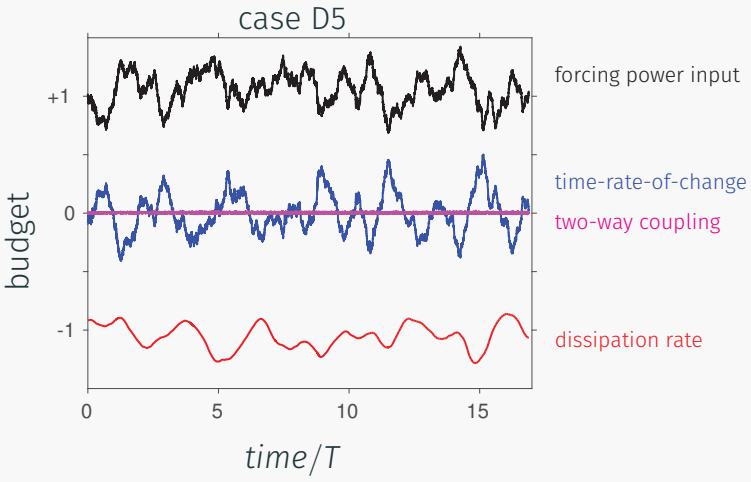

$$\frac{\mathrm{d}}{\mathrm{d}t}\langle E_k\rangle_\Omega = \langle \mathbf{u}\cdot\mathbf{f}^{(t)}\rangle_\Omega + \langle \mathbf{u}\cdot\mathbf{f}^{(ibm)}\rangle_\Omega - \varepsilon_\Omega$$

Fluid-particle relative velocity

shell-averaged relative velocity

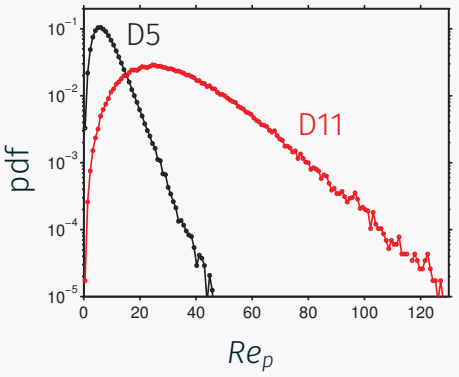

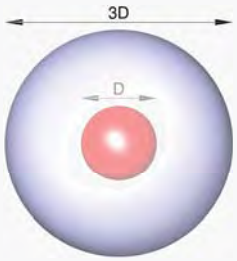

$$\mathbf{u}_f^{\mathcal{S}} = \frac{1}{A_{\mathcal{S}}} \int_{\mathcal{S}} \mathbf{u}_f(\mathbf{x}, t) \mathrm{d}A$$

$$u_{rel} = |\mathbf{u}_p - \mathbf{u}_f^{\mathcal{S}}|$$

$$Re_p = u_{rel} D/\nu$$

Spatial particle arrangement – clustering

Voronoï tesselation analysis

2D example

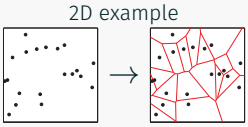

normalized Voronoï cell volumes

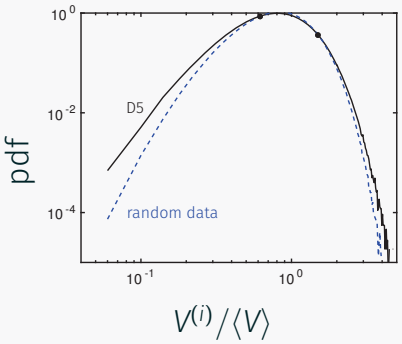

standard-deviation of V

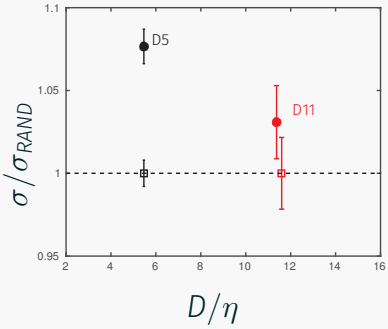

Relation between particles and coherent vortices

Coherent vortex extraction

- q-criterion (Hunt et al. 1989)
- iso-surfaces: 1.5·std-dev

case D5

Relation between particles and coherent vortices

Coherent vortex extraction

- q-criterion (Hunt et al. 1989)
- iso-surfaces: 1.5·std-dev

case D5

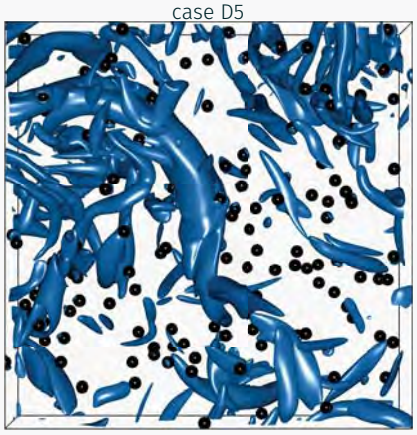

(zoom)

Relation between particles and coherent vortices

Coherent vortex extraction

- q-criterion (Hunt et al. 1989)
- iso-surfaces: 1.5·std-dev
- volume statistics (Moisy, Jiménez 2004)

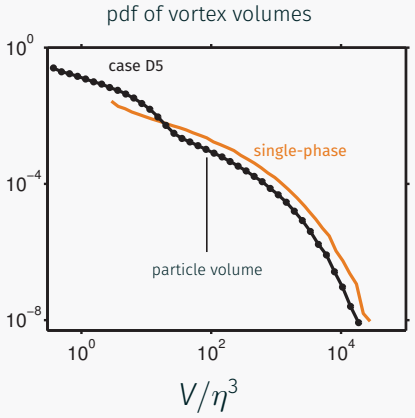

Relation between particles and coherent vortices

Coherent vortex extraction

- q-criterion (Hunt et al. 1989)
- iso-surfaces: 1.5·std-dev
- volume statistics (Moisy, Jiménez 2004)
- preferential locations

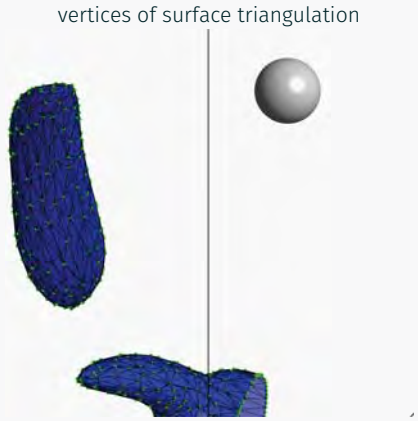

Relation between particles and coherent vortices

Coherent vortex extraction

- q-criterion (Hunt et al. 1989)
- iso-surfaces: 1.5·std-dev
- volume statistics (Moisy, Jiménez 2004)
- preferential locations

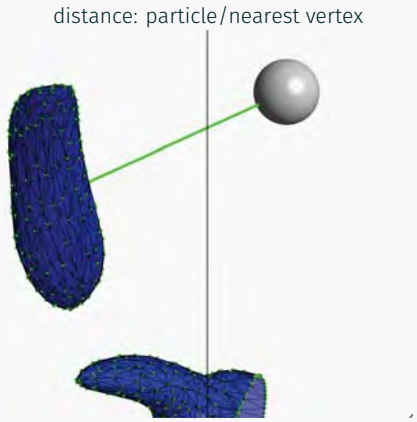

Relation between particles and coherent vortices

Coherent vortex extraction

- q-criterion (Hunt et al. 1989)
- iso-surfaces: 1.5·std-dev
- volume statistics (Moisy, Jiménez 2004)
- preferential locations

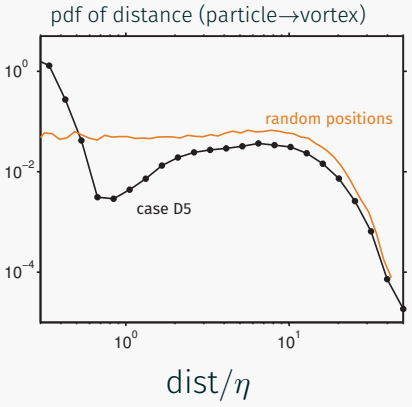

Relation between particles and coherent vortices

Coherent vortex extraction

- q-criterion (Hunt et al. 1989)
- iso-surfaces: 1.5·std-dev
- volume statistics (Moisy, Jiménez 2004)
- preferential locations excluding small vortices ($V \leq V_p$)

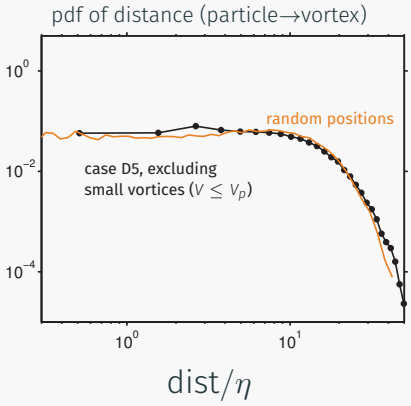

The role of the fluid acceleration field

Goto, Vassilicos (2008)

- point-particles
- 'sticky' points: $\mathbf{e}_1 \cdot \mathbf{a}_f = 0$ and $\lambda_1 > 0$

$\rightarrow$ particles converge

Finite-size particles?

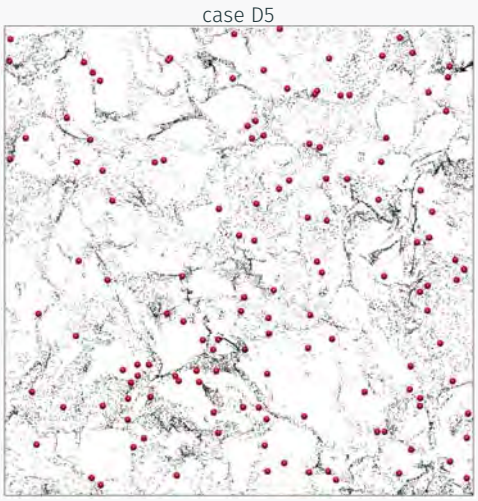

(slice: $380\eta \times 380\eta \times 15\eta$)

λ_1 largest eigenvalue of $\nabla \mathbf{a}_f + (\nabla \mathbf{a}_f)^T$; eigenvector $\mathbf{e}_1$

Spatial distribution of ‘sticky points’

- ‘sticky points’ exhibit strong clustering

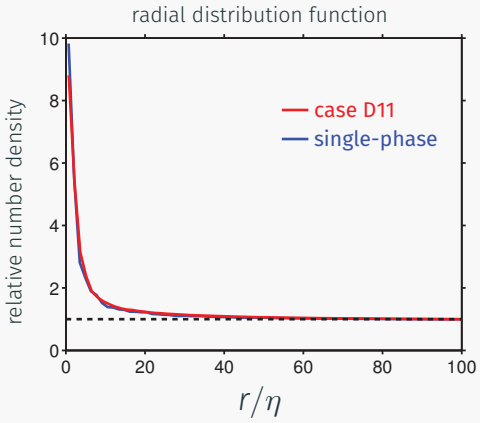

→ no apparent modification when adding particles

Particle-conditioned distribution of ‘sticky points’

- probability of finding a ‘sticky point’ at distance *r* from particle surface

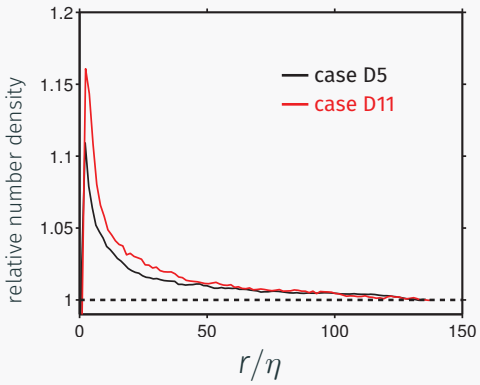

→ increased probability near particles

Particle acceleration statistics

- normalized pdf matches fit of Qureshi et al. (2007)

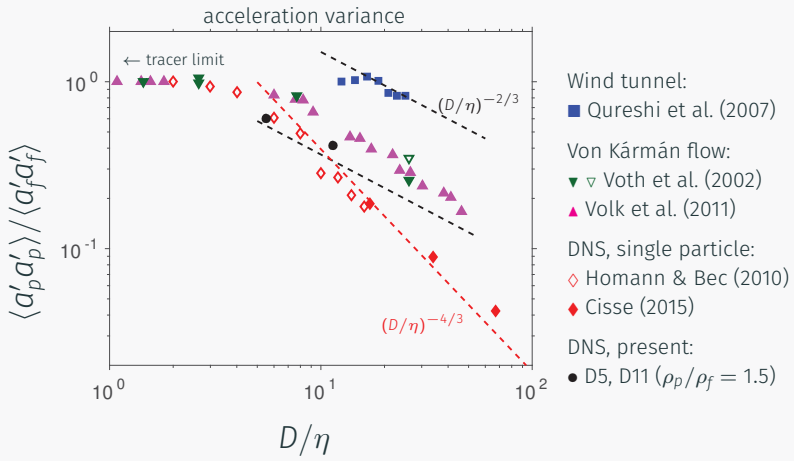

Conclusions so far

Moderately dense particles in hom-iso turbulence

- acceleration variance: similar trend as density matched
- 'clustering' detected, intensity decreases with D
- no significant preferential concentration w.r.t. vortex
- significant spatial correlation with 'sticky points' (Goto & Vassilicos 2008)

Challenges

Relevance of numerical simulations:

- large-scale DNS can provide high-fidelity data
- the cost: € 0.03/core-hour
- next generation “heroic” simulation: dilute, 10^6 parts.

Challenges

Relevance of numerical simulations:

- large-scale DNS can provide high-fidelity data
- the cost: € 0.03/core-hour
- next generation “heroic” simulation: dilute, 10^6 parts.

Current bottleneck: “après-simulation”

- data transfer & long time storage
- visualization & exploring the data
- making data available to the community

More challenges

Going from data $\rightarrow$ physics

- understanding: requires widening the parameter range
- scaling laws

More challenges

Going from data $\rightarrow$ physics

- understanding: requires widening the parameter range
- scaling laws

Going from physics $\rightarrow$ models

- teaching point-particle models about collective effects

Acknowledgements

A. Chouippe and M. Uhlmann. Forcing homogeneous turbulence in DNS of particulate flow with interface resolution and gravity. *Phys. Fluids*, 27(12):123301, 2015. doi: 10.1063/1.4936274.

M. Cisse. *Suspensions turbulentes de particules de tailles finies: dynamique, modifications de l'écoulement et effets collectifs*. PhD thesis, Université de Nice-Sophia Antipolis, 2015. *(in French)*.

V. Eswaran and S.B. Pope. An examination of forcing in direct numerical simulations of turbulence. *Comput. Fluids*, 16(3):257–278, 1988.

L. Fiabane, R. Zimmermann, R. Volk, J.-F. Pinton, and M. Bourgoin. Clustering of finite-size particles in turbulence. *Phys. Rev. E*, 86(035301(R)), 2012.

R. Glowinski, T.-W. Pan, T.I. Hesla, and D.D. Joseph. A distributed Lagrange multiplier/fictitious domain method for particulate flows. *Int. J. Multiphase Flow*, 25:755–794, 1999.

S. Goto and J.C. Vassilicos. Sweep-stick mechanism of heavy particle clustering in fluid turbulence. *Phys. Rev. Lett.*, 100(5):054503, 2008.

H. Homann and J. Bec. Finite-size effects in the dynamics of neutrally buoyant particles in turbulent flow. *J. Fluid Mech.*, 651:81–91, 2010.

F. Lucci, A. Ferrante, and S. Elghobashi. Modulation of isotropic turbulence by particles of Taylor length-scale size. *J. Fluid Mech.*, 650:5–55, 2010.

F. Lucci, A. Ferrante, and S. Elghobashi. Is Stokes number an appropriate indicator for turbulence modulation by particles of Taylor length-scale size. *Phys. Fluids*, 23: 025101, 2011.

T.S. Lundgren. Linearly forced isotropic turbulence. In *Annual Research Briefs*, pages 461–473. (Center for Turbulence Research, Stanford), 2003.

F. Moisy and J. Jiménez. Geometry and clustering of intense structures in isotropic turbulence. *J. Fluid Mech.*, 513:111–133, 2004.

K. Nishino and H. Matsushita. Columnar particle accumulation in homogeneous turbulence. In Y. Matsumoto, K. Hishida, A. Tomiyama, K. Mishima, and S. Hosokawa, editors, *Proc. ICMF 2004 (5th Int. Conf. Multiphase Flow)*, Yokohama, Japan, 2004.

C. Rosales and C. Meneveau. Linear forcing in numerical simulations of isotropic turbulence: Physical space implementations and convergence properties. *Phys. Fluids*, 17:095106, 2005.

A. Ten Cate, J.J. Derksen, L.M. Portella, and H.E. Van Den Akker. Fully resolved simulations of colliding monodisperse spheres in forced isotropic turbulence. *J. Fluid Mech.*, 519:233–271, 2004.

M. Uhlmann. An immersed boundary method with direct forcing for the simulation of particulate flows. *J. Comput. Phys.*, 209(2):448–476, 2005. doi: 10.1016/j.jcp.2005.03.017.

M. Uhlmann and A. Chouippe. Clustering and preferential concentration of finite-size particles in forced homogeneous-isotropic turbulence. *submitted to J. Fluid Mech.*, 2016.

K. Yeo, S. Dong, E. Climent, and M.R. Maxey. Modulation of homogeneous turbulence seeded with finite size bubbles or particles. *Int. J. Multiphase Flow*, 36(3):221–233, 2010.

Long time history of unsteady drag on shock accelerated micro-particles

Ankur Deep Bordoloi
Adam Martinez
Kathy Prestridge

Operated by Los Alamos National Security, LLC for the U.S. Department of Energy's NNSA

Multiphase flows in high-speed are extremely complex

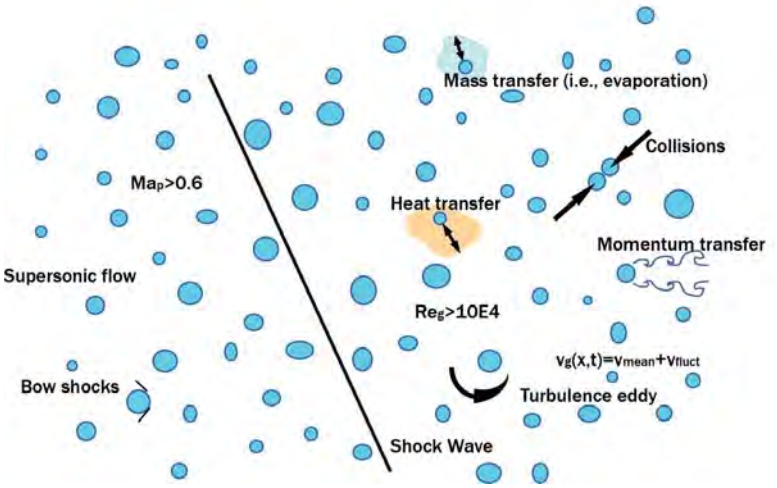

- ❑ Mass exchange
- ❑ Momentum transfer
- ❑ Evaporation
- ❑ Collision
- ❑ Deformation & breakup
- ❑ Turbulence modulation

Experimental envelop is designed to simplify the problem

- Drag measurement
- Solid spherical particles (no deformation/breakup)
- Low volume fraction

Previous models describe unsteady forces on a stationary particle only over a short time scale

$$F(t) = F_{qs}(t) + F_{iu}(t) + F_{vu}(t) + F_{l}(t) + F_{bg}(t)$$

- $F_{qs}(t)$: quasi-steady
- $F_{iu}(t)$: inviscid unsteady (added mass) (pressure gradient)
- $F_{vu}(t)$: viscous unsteady (Basset history)
- $F_{l}(t)$: lift
- $F_{bg}(t)$: buoyancy/ gravity

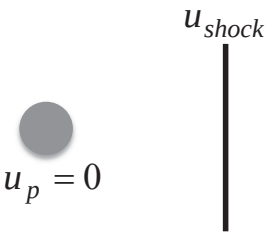

$O(d_p/u_{shock})$

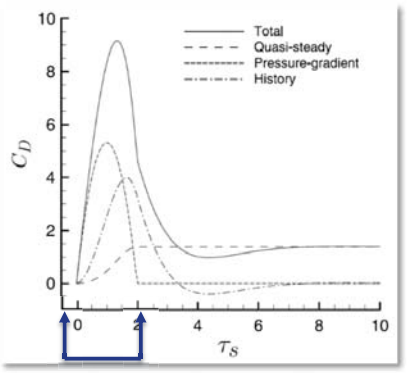

(Parmar & Balachandar, 2008)

Objectives

- Estimate unsteady drag on shock accelerated particle
- Drag history over longer time period, $1000 \times O(d_p/U_{shock})$

The horizontal shock-tube facility is capable of repeatable multi-frame particle & shock tracking

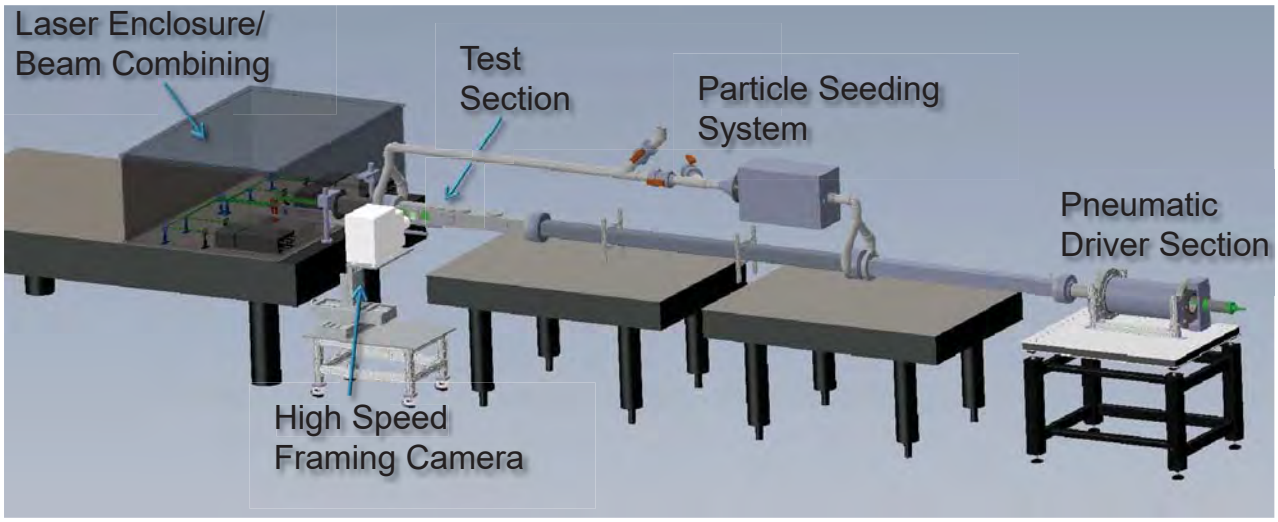

Camera:
5 ns min exposure duration
7 million fps over 8 frames

8 independent frames and 532 nm laser pulses

High resolution imaging allows precise tracking of particle

Spatial resolution: 2.14 μm/pixel

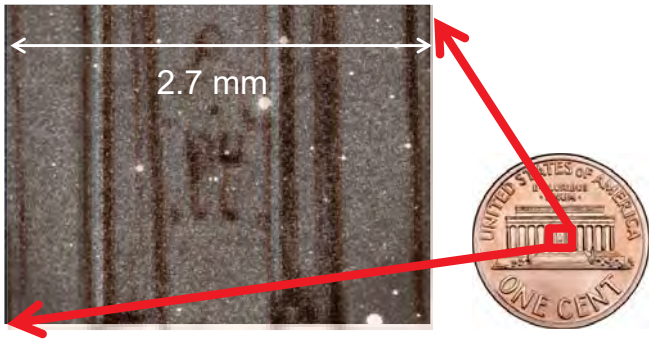

A shadowgraph system lets us measure the shock location more precisely than with pressure transducers

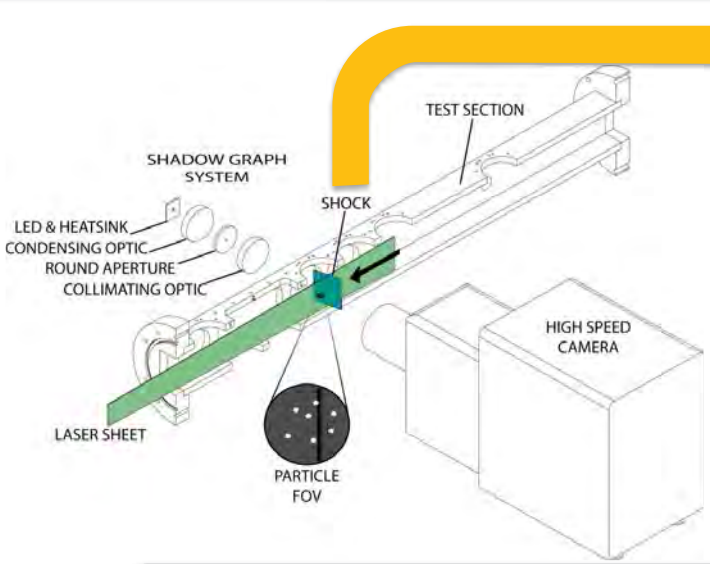

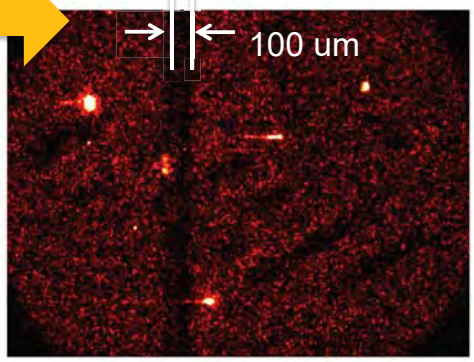

$$t_0 = t_{shock} - \frac{\Delta x_{shock-particle}}{u_{shock}}$$

- Simultaneous imaging of shock and particle
- Shock detection on multiple frames
- Better estimates of t = 0

Heavy, microscopic particles show polydispersed size distribution

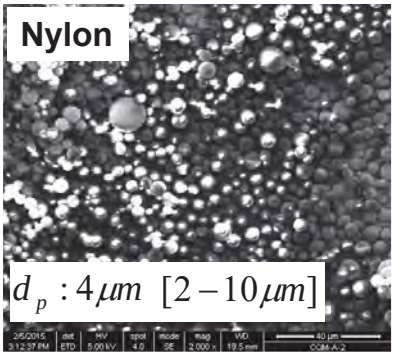

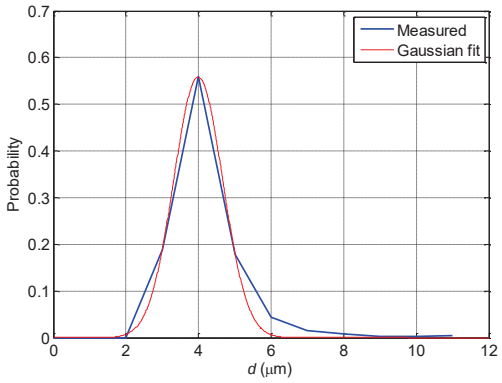

Manufacturer:
mean: 4 μm
std dev: 1.5 μm

Measured:
mean: 4 μm
std dev: 1 μm

Incident Mach number:	**M = 1.2, 1.3, 1.4, 1.5**
Particle Mach number:	**$M_{p,0}$ = 0.1, 0.3, 0.5, 0.7**
Particle Reynolds number:	**$Re_{p,0}$ = 25, 35, 55, 72**
Gas phase velocity:	**u_{f2} = 109-246 m/s**
Particle Volume Fraction:	**C ≈ 1e-7**

Drag is estimated based on piecewise curve fitting of experimental data on force equation

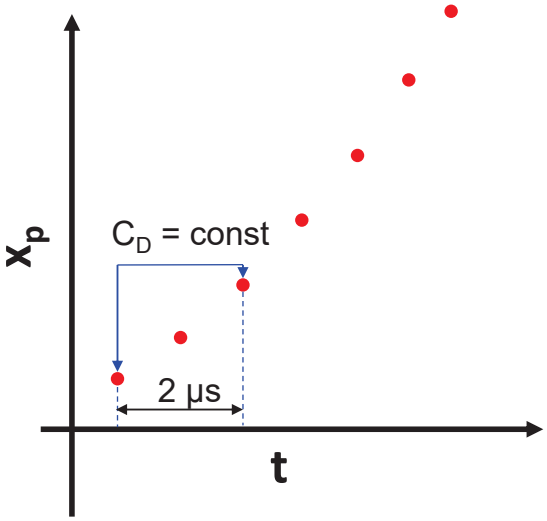

$$\frac{du_p}{dt} = \frac{3\rho_2\left(u_{f2}-u_p\right)^2}{4\rho_p d_p} C_D$$

$$u_p = \frac{u_f^2 At}{1+u_f At}; \qquad A = \frac{3\rho_2 C_D}{4\rho_p d_p}$$

$$x_p = u_2 t - \frac{\log(Au_2 t+1)}{A} + x_0$$

5th order Taylor Expansion

$$x_p = u_2(t-t_0) - \frac{\log(Au_2(t-t_0)+1)}{A} + x_0 + TSE$$

3 fitting parameters: x_0, t_0, A

$$C_D = \frac{4\rho_p d_p A}{3\rho_2}$$

Example showing piecewise fit on particle location, and estimated velocity, acceleration and unsteady drag

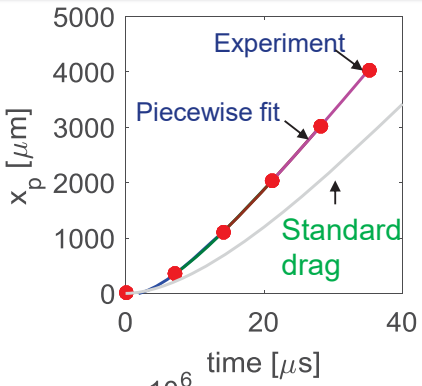

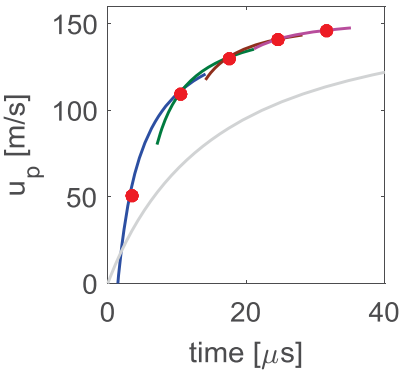

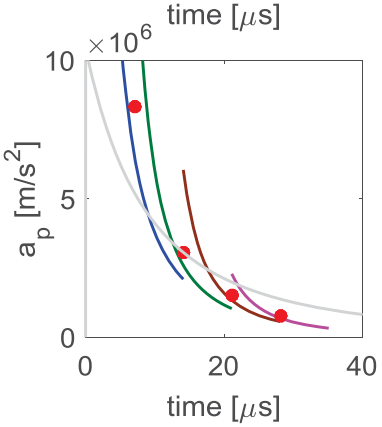

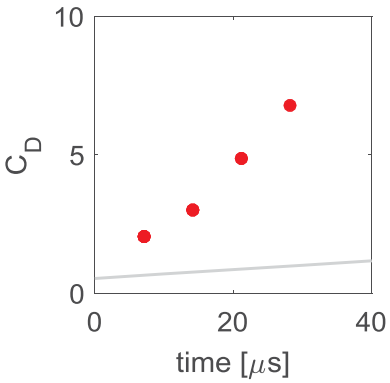

Due to diameter distribution particles accelerate at different rates

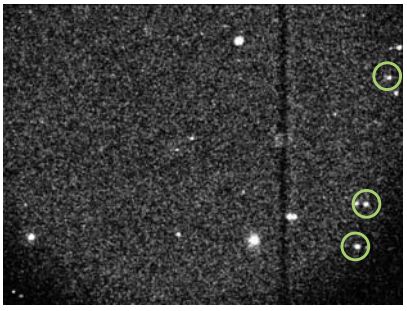

$\times O(50)$

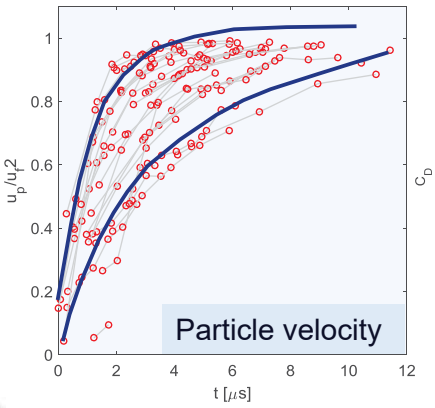

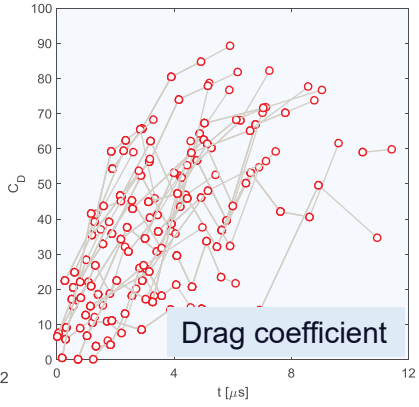

Diameter distribution

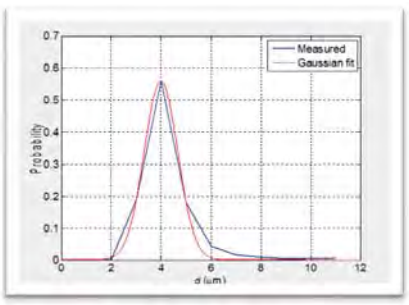

- Drag increases dramatically at later post-shock times
- The increase rate of C_D is sensitive to particle size

Particle velocity (u_p) asymptotically catches up with the post-shock fluid velocity (u_{f2})

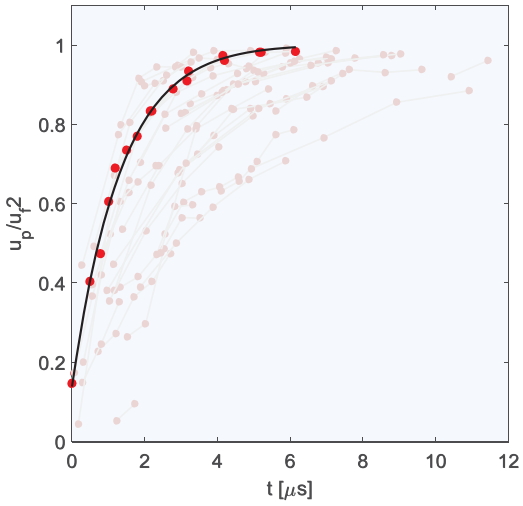

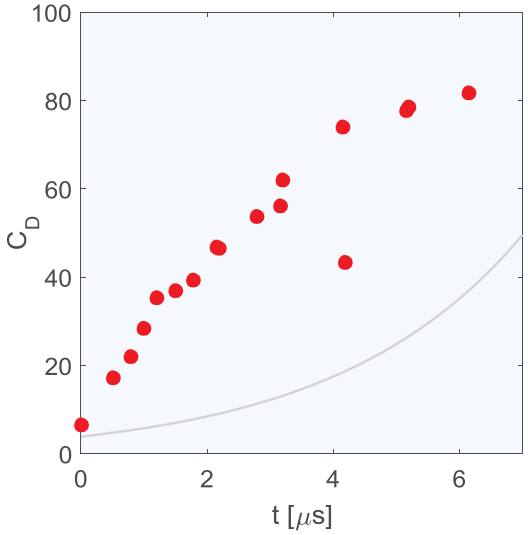

- The maximum drag is order of magnitude higher than earlier predictions

Why is measured drag higher than earlier predictions?

Quasisteady drag force

(Parmar et al. PRL, 2011)

$$\mathrm{Re} = \frac{V d_p}{\nu} = 53 \qquad Kn' = \frac{M}{\mathrm{Re}} = 0.02$$

$$C_{D,qs} = \frac{24}{\mathrm{Re}}(1 + 0.15\,\mathrm{Re}^{0.687}) + 0.42\left(1 + \frac{42500}{\mathrm{Re}^{1.16}}\right)^{-1}$$

Continuum is valid; no compressibility effect on quasisteady force

Unsteady drag force

Acoustic time scale, $\tau = \frac{c_0 t}{d_p}$

Convective time scale, $\tau_c = \frac{Vt}{d_p}$

- $F_{iu}(t)$ acts on a very short acoustic time scale (validated for static particle, Parmar 2009)
- Basset history kernel in $F_{vu}(t)$ is valid only for $\tau_c << 1/\mathrm{Re}$ (Mei and Adrian, 2009)

Earlier model captures drag at earlier times for stationary particle

$$F(t) = F_{qs}(t) + F_{iu}(t) + F_{vu}(t)$$

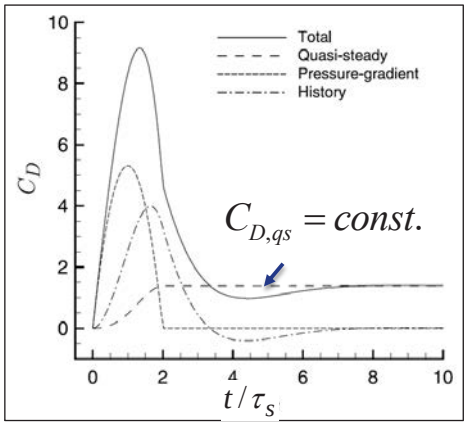

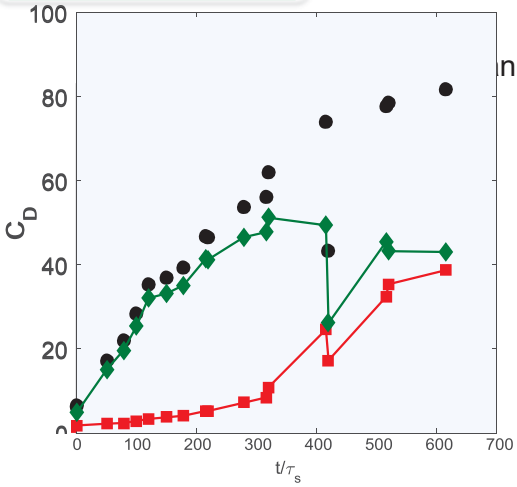

ndar, 2008)

$$\tau_s = d_p / u_{shock}$$

$$\tau_s = 0.01 \mu s$$

$$C_{D,qs} = \frac{24}{\mathrm{Re}}(1 + 0.15\,\mathrm{Re}^{0.687}) + 0.42\left(1 + \frac{42500}{\mathrm{Re}^{1.16}}\right)^{-1}$$

Los Alamos National Laboratory

Earlier model captures drag at earlier times for stationary particle

$$F(t) = F_{qs}(t) + F_{iu}(t) + F_{vu}(t)$$

- Consistent with Parmar model at acoustic time scale, $\tau_s \cup 10$ 2008)
- We expect late time CD to be contributed by $F_{qs}(t)$
- Large contribution from unsteady forces in intermediate time
- $F_{vu}(t)$ is not modeled by Basset history forces

$$\tau_s = d_p / u_{shock}$$

$$\tau_s = 0.01 \mu s$$

$$C_{D,qs} = \frac{24}{\mathrm{Re}}(1 + 0.15\,\mathrm{Re}^{0.687}) + 0.42\left(1 + \frac{42500}{\mathrm{Re}^{1.16}}\right)^{-1}$$

LA-UR-16-27836

Non-linear effects should dominate in the high drag regime

Nonlinear effects dominate when $\tau_c >> 1/\mathrm{Re}$

Basset history kernel is valid only when $\tau_c << 1/\mathrm{Re}$

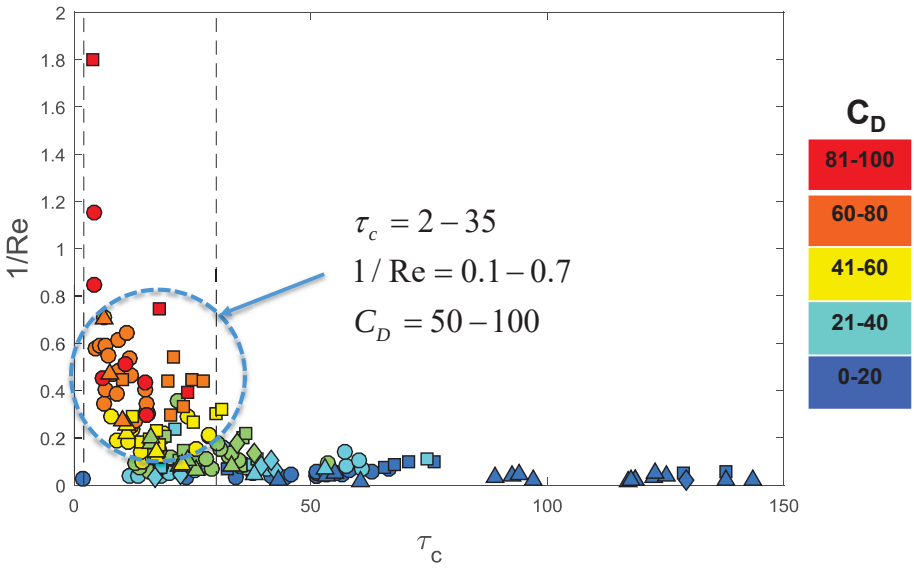

Drag acts differently on shock accelerated particles

Standard particle drag

$u_p = 0$ $\qquad$ $u_p = const.$

C_D decelerates particle

Shock accelerated particle drag

u_{shock}

$u_p = 0$ $\qquad$ $u_{f2} \approx 200 m/s$

$u_p \approx 0 - 200 m/s$

C_D accelerates particle

A time scale t^* is chosen based on particle slip velocity

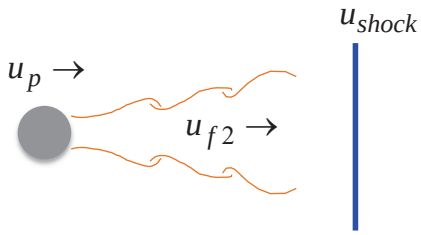

$$t^* = \frac{d_{p,mean}}{|u_{f2} - u_p|}$$

$$t^* \rightarrow \infty \Rightarrow u_p \rightarrow u_{f2}$$

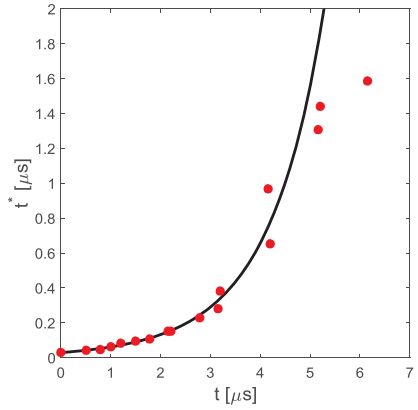

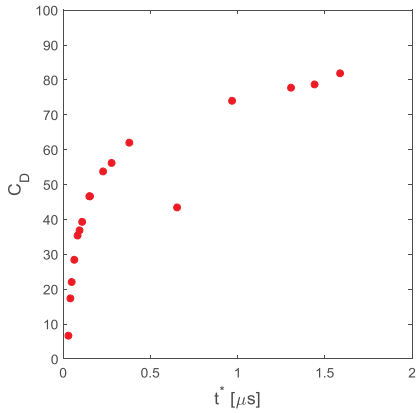

C_D increases with particle velocity following a power law relation with t^*

□ M = 1.2 ◇ M = 1.4
○ M = 1.3 △ M = 1.5

$$C_D = 140.6 - 68t^{*-1/5}$$

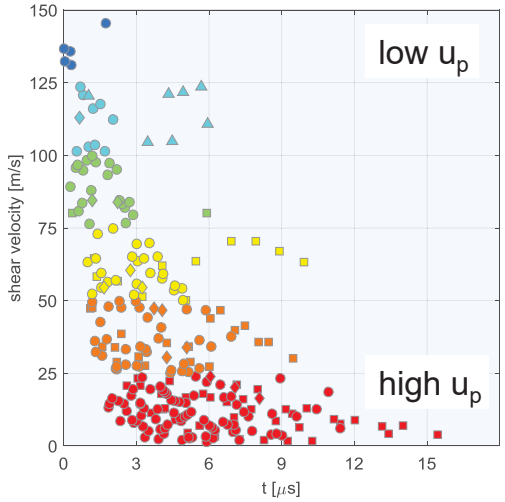

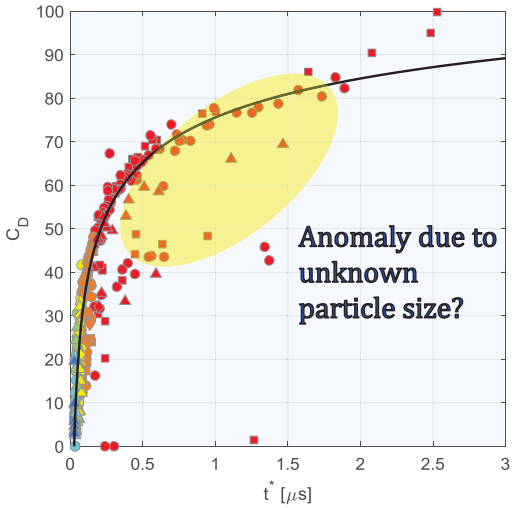

- Shows a power-law fit to C_D when t* is used
- C_D vs t^* is less sensitive to incident Mach number

Diagnostic improvement

Dynamic particle sizing using PDPA technique

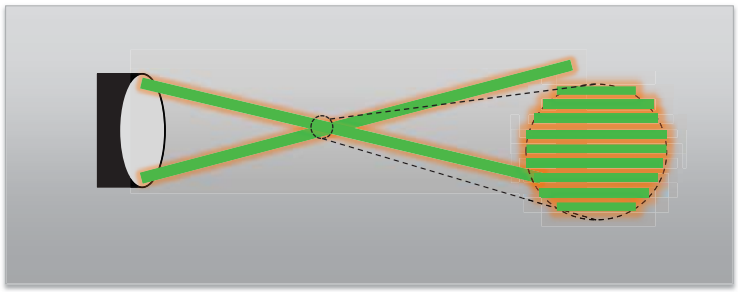

PDPA is capable of simultaneously measuring particle size and velocity

Work in progress..

Improve C_D measurement

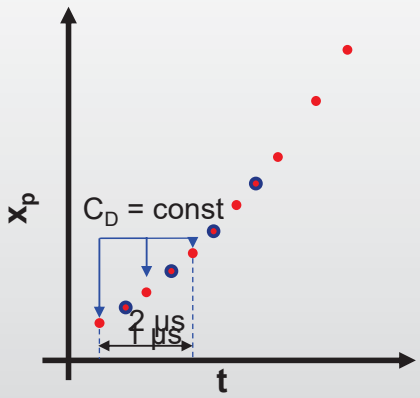

Smaller inter-frame Δt to obtain a better piecewise fit

- Predictor/corrector: Predict a relationship between C_D and t* and correct the piecewise fit
- Noise reduction: Apply Kalman filter

Open for discussion

- Drag is order of magnitude larger in the long time range
- Previous models and simulations are limited to short time
- The nonlinearity of flow contributes to large drag
- Drag follows a power law relationship with slip velocity time scale
- Drag is highly sensitive to particle size
- Mach number effects are small on C_D

PSAAP II
Particle-laden Turbulence in a Radiation Environment

Including Real Experimental Effects in Validation of Numerical Models for Confined Particle-Laden Flows

Laura Villafañe, Andrew Banko, Mahdi Esmaily,
Chris Elkins, Ali Mani, John Eaton

Multiphase Physics Deep-Dive

October 6-7, 2016

Outline

- Concept
- Experimental/simulation overview
- Ideal vs. real
- Influence of real experimental effects for data comparison
  - ✓ Particle concentration distributions
  - ✓ 2D preferential concentration statistics
  - ✓ Particle velocities

Turbulence-Particle-Radiation Interaction

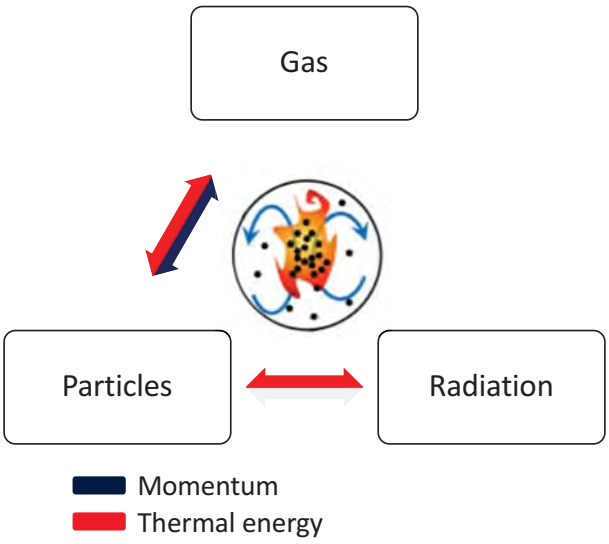

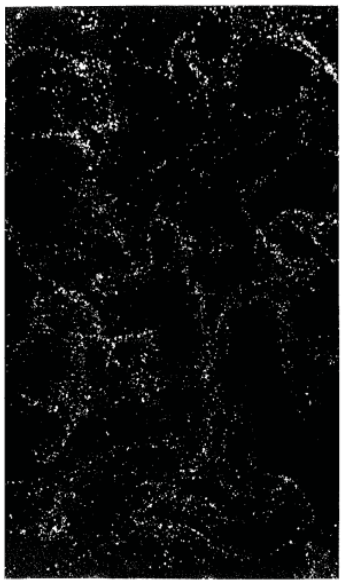

Channel Flow Experiment

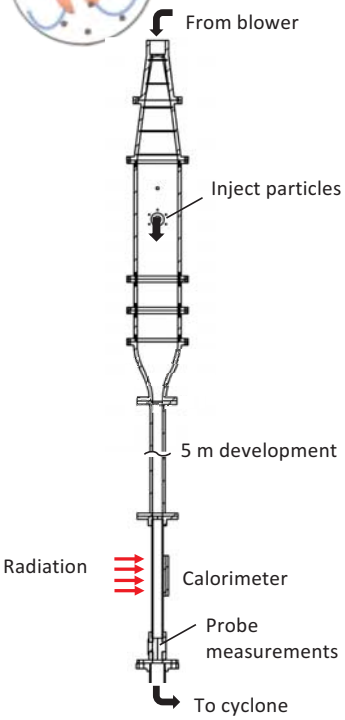

- Fully developed, vertical, turbulent channel flow of air
- Laden with small Nickel particles
- Optical and probe-based measurements

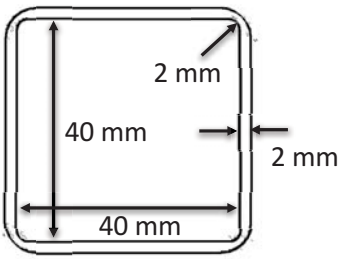

Parameters

- Nickel particles:

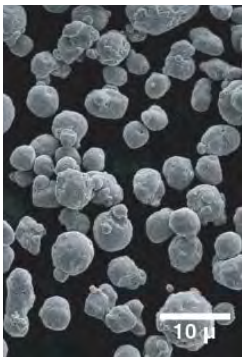

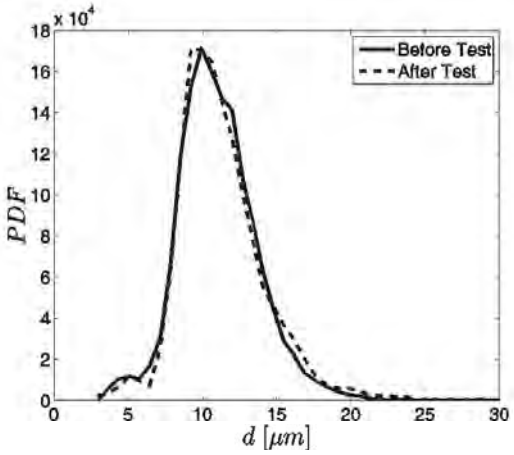

- Flow conditions:

Re_H	St_η	d_p/η	MLR	φ_V
10,000	5	0.11	0.01-0.1	10^{-6}-10^{-5}
20,000	12	0.17	0.01-0.1	10^{-6}-10^{-5}
40,000	31	0.27	0.01-0.1	10^{-6}-10^{-5}

Experimental Techniques

Particle phase

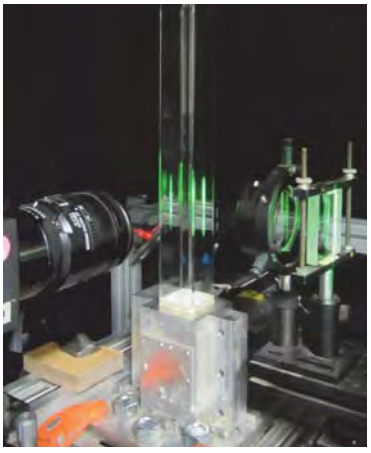

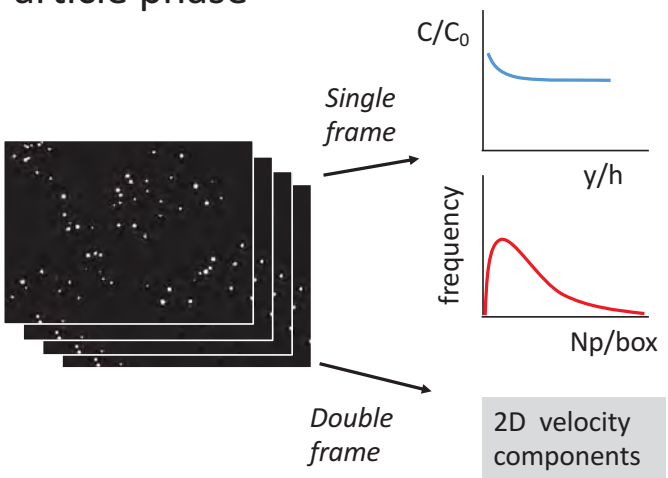

Laser Thickness (mm)	0.5-1.6
FOV (mm)	≤ 35

Overview of the DNS

Governing equations:

$$\frac{\partial}{\partial t}\rho + \nabla \cdot (\rho \boldsymbol{u}) = 0$$

$$\frac{\partial}{\partial t}(\rho \boldsymbol{u}) + \nabla \cdot (\rho \boldsymbol{u} \otimes \boldsymbol{u}) = \nabla \cdot \boldsymbol{T} + \rho \boldsymbol{g}$$

$$\boldsymbol{T} = -p\boldsymbol{I} + \mu\left(\nabla \boldsymbol{u} + (\nabla \boldsymbol{u})^{\mathrm{T}} - \frac{2}{3}\nabla \cdot u\boldsymbol{I}\right)$$

$$\dot{\boldsymbol{x}}_p = \boldsymbol{u}_p$$

$$m_p \dot{\boldsymbol{u}}_p = \boldsymbol{g} - \boldsymbol{f}_p$$

$$\boldsymbol{f}_p = m_p \tau_p^{-1}(\boldsymbol{u}_p - \boldsymbol{u})$$

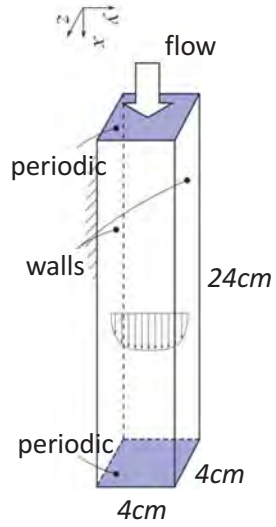

- Point particle
- Hard collision model, k=1 (p-p,p-wall)

$Re = 10000, 20000$
$U_{bulk} = 3.93\ m/s, 7.86\ m/s$
$D_p \epsilon\ [4,16]\mu m$

Ideal vs. Real

Ideal	Real
Planar laser illumination, point measuremements	Finite thickness Gaussian profile laser, volume average, particle overlap
Collimated scattered light from 2D plane	Diffraction and aberrations, no particle size information
Square channel, near wall optical access	Duct with real corners, reflections
Infinite number of sampling particles	Finite number of particles

Particle Concentration Distribution

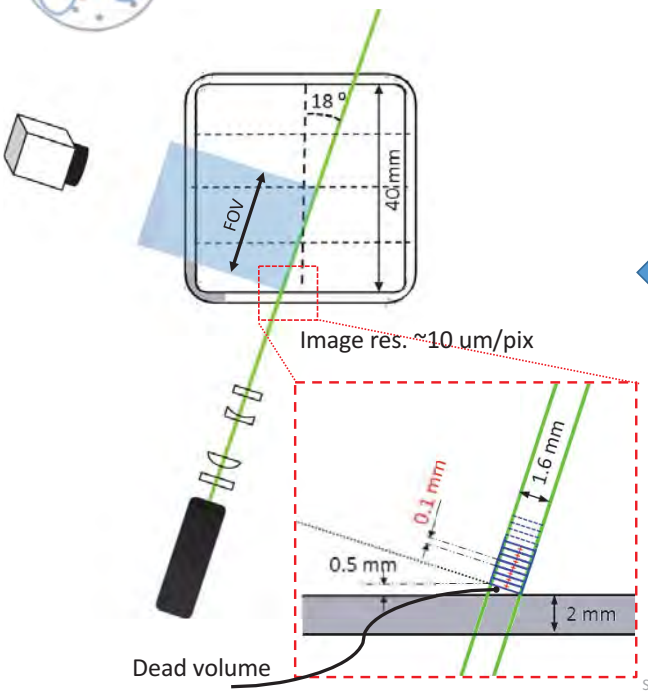

Numerical data processing

-Traditional:

-Experimental like:

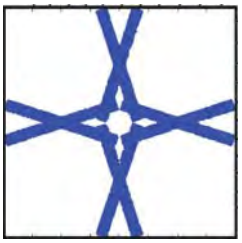

Re	10k	Re 20k
y^+ resol.~	8-10	16-20

Particle Concentration Distribution

Experiments vs DNS

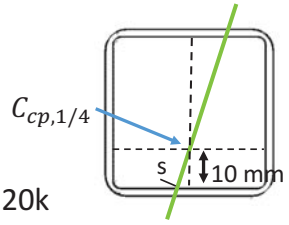

Re 10k

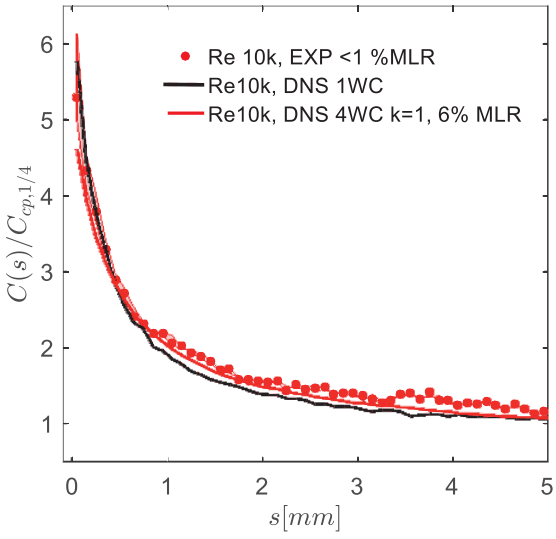

Re 20k

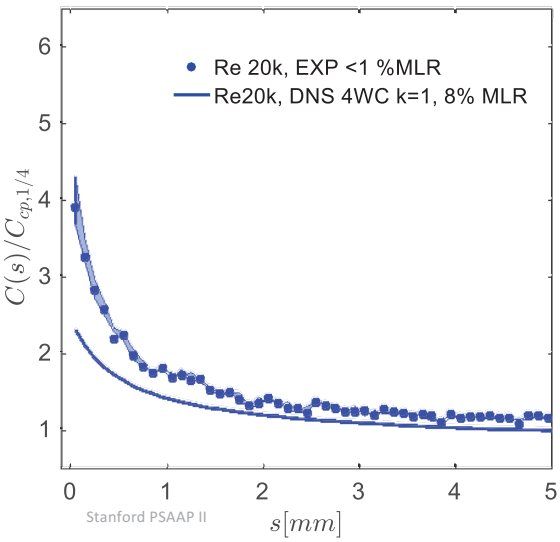

Preferential Concentration: Box Counting

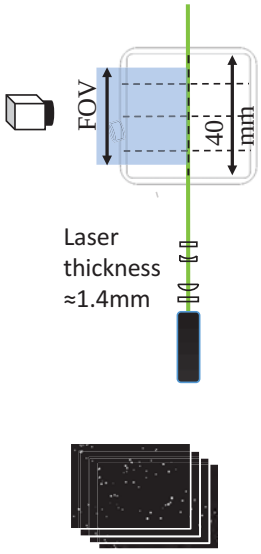

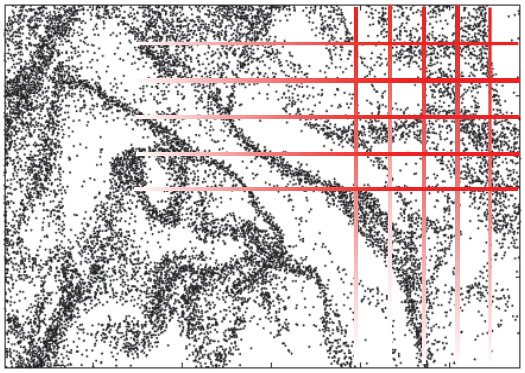

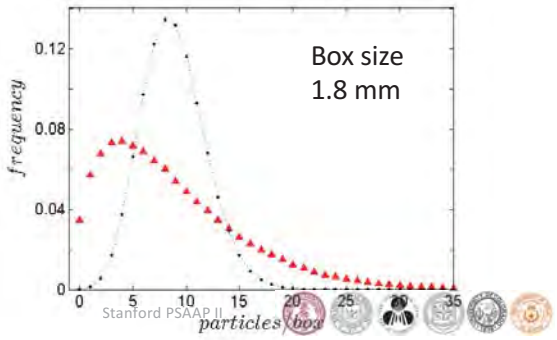

Stanford PSAAP II

$$\left(\frac{\sigma}{\lambda}\right)_c = \sqrt{\frac{\sigma_s^2 - \lambda_s}{\lambda_s^2}} \xrightarrow{\lambda_s \to \infty} \frac{\sigma_s}{\lambda_s}$$

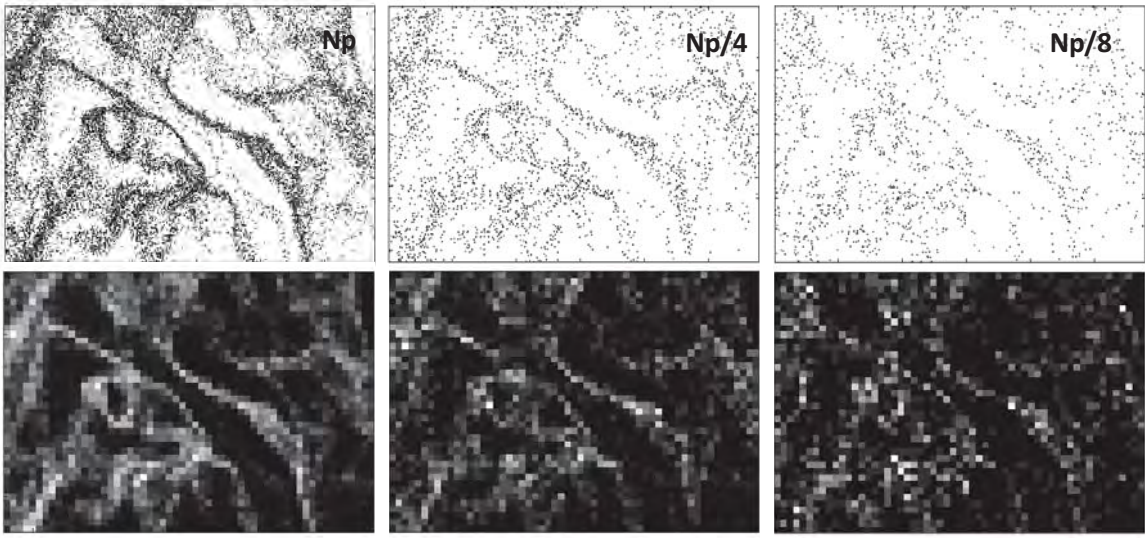

	Np	Np/2	Np/4	Np/8
σ_s/λ_s	0.9	1.0	1.2	1.4
$(\sigma/\lambda)_c$	0.8	0.8	0.8	0.8

Preferential Concentration:

Preferential Concentration: *Laser thickness*

DNS , Re= 10k, different thickness

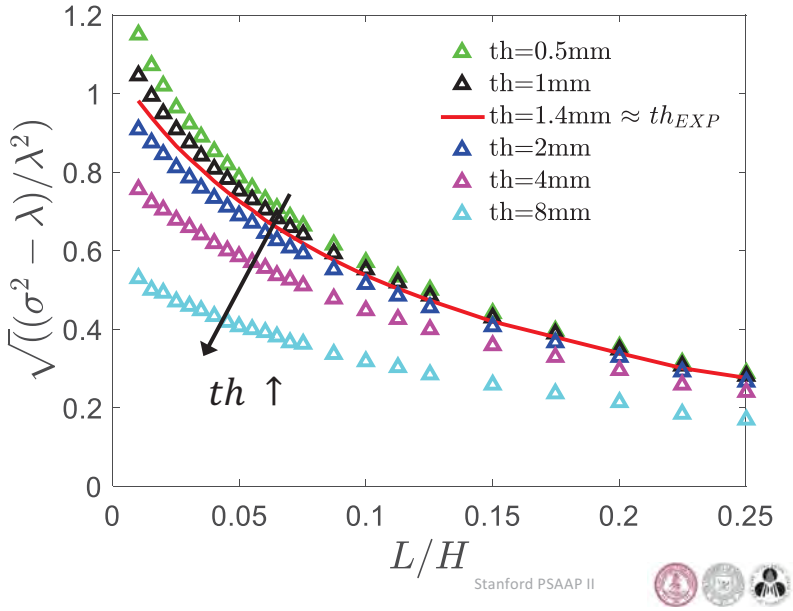

Preferential Concentration

EXP-DNS Comparison

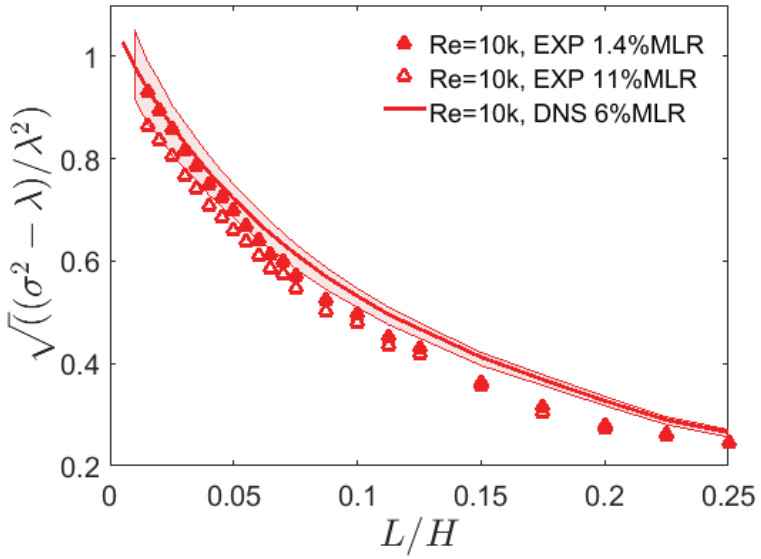

Preferential Concentration: *Stokes number*

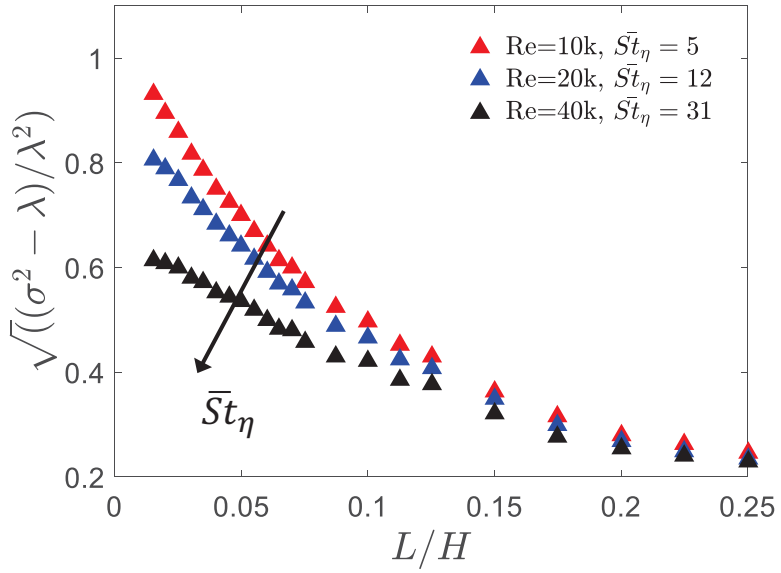

Effect of polydispersity

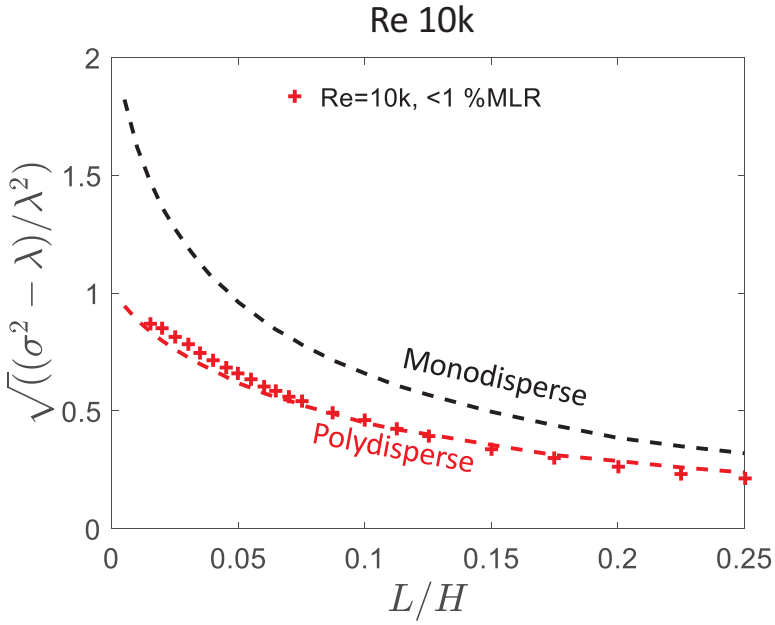

Preferential Concentration

Cluster/Void Identification

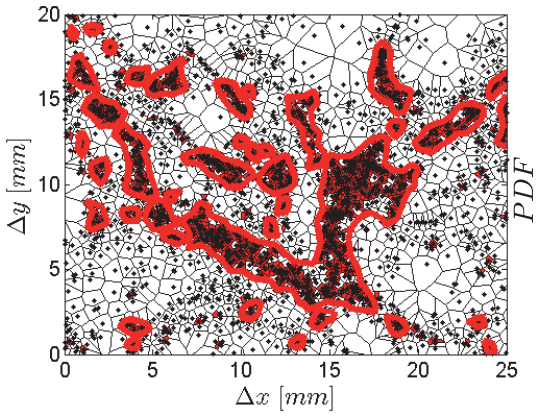

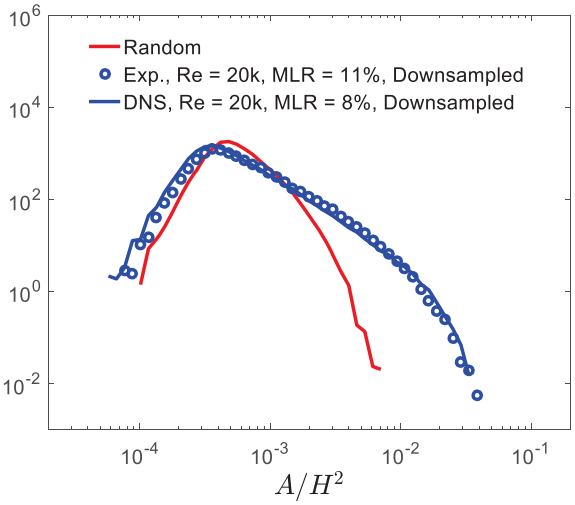

Particle Velocities

Experiments

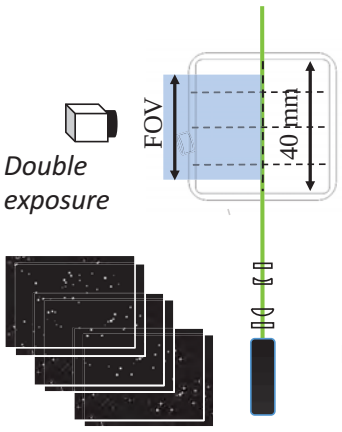

PIV-Interrogation windows:
$0.5x0.5mm^2$

Mean and fluctuating particle velocity

DNS

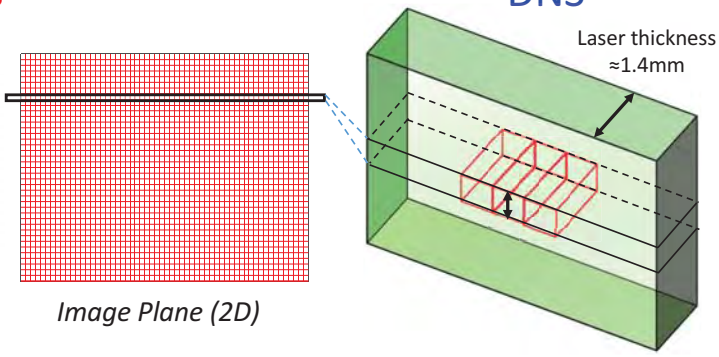

DNS-Interrogation volumes:
$0.5x0.5x1.4mm^3$

Projected 2-D Velocity field

Eulerian & Lagrangian mean and fluctuating particle velocity

Conclusions & Challenges

- Particle phase statistics are volumetric measurements. Comparison between cases requires integration in equivalent volumetric units.
- Statistics of preferential concentration are affected by finite number of particles. Limit of increasing Np challenging both in exp. & simulations

- Agreement was achieved between DNS and experiments in terms of particle clustering at the center of the duct when including real effects.

- Measuring near wall concentration data remains a challenge.
- Careful comparison of particle velocity statistics. PTV processing techniques are being implemented. Processing of DNS particle velocities by class.
- Experimental particle velocities at high MLR?

Meso-Scale Simulations of Shock-Particle Interactions

F. Najjar

Mulitphase Deepdive Workshop

Tampa, FL

October 6-7, 2016

LLNL-PRES-702745

This work was performed under the auspices of the U.S. Department of Energy by Lawrence Livermore National Laboratory under contract DE-AC52-07NA27344. Lawrence Livermore National Security, LLC

Lawrence Livermore National Laboratory

This talk discusses hydrodynamic simulations to investigate Shock-Particle Interactions

- Introduction & Goals
- Multiphase Simulations:
  - Shock-Particle interactions EM
  - Meso-scale Simulations of particle clusters with shock waves
- Summary & Future Work

Our goal is to understand using computational tools the formation of coherent clusters of particles or jet-like particle structures during MBX detonation

Particle jetting

Is a common feature of explosive dispersal of solid particles or liquids:

- Jets influence:
  - particle-gas mixing/burning
  - blast wave propagation
- Many possible instability mechanisms

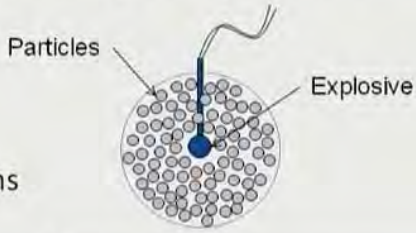

Spherical dispersal of sand particles

Frost et al.

Complex mechanisms of Shock-Particle Interaction (SPI) are summarized

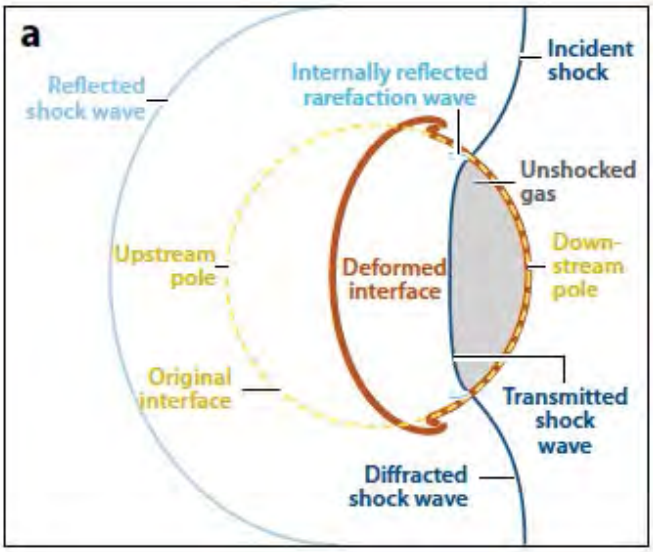

Acoustic Impedance: $\mathcal{R}=\rho c$

Positive Impendance: $\delta\mathcal{R}>0$

(Rajan et al., Ann. Rev Fluid Mech, 2011)

LLNL Hydrodynamics Code is used and is based on Arbitrary Lagrange-Eulerian approach

- Perform high-resolution multiphysics simulations for SPI problems
- Why Hydrodynamics Code?
  - Multiphysics coupled code using Operator-Split Method
  - Extensive suite of EOS models
  - Massively parallel on HPC platforms
- Hydro code is based on Lagrange+Remap steps

$$\frac{D\phi}{Dt} + \vec{u}\cdot\vec{\nabla}\phi = F$$

$$\frac{D\phi}{Dt} = F \qquad \vec{u}\cdot\vec{\nabla}\phi = 0$$

Lagrange **Advection**

ALE3D results compare quite well with Sun's experiments and numerical results by Sun et al & Jackson et al.

2-D Axisymetric Simulations

- Particle size (d) 80mm; P=1.53MPa; Ma=1.22

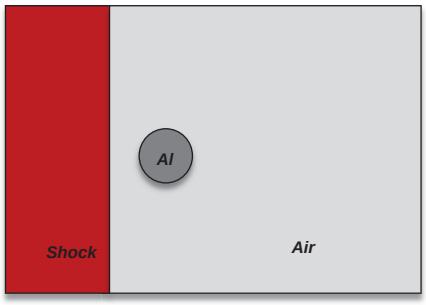

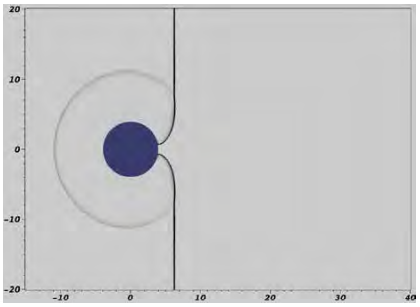

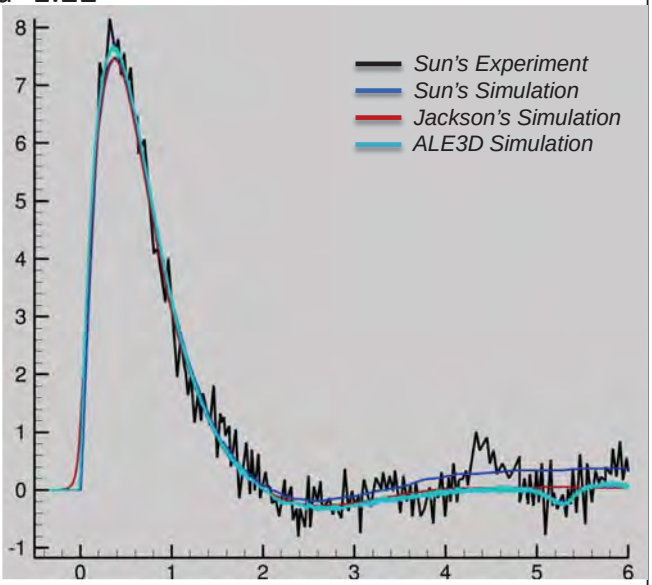

Sun et al., SW 14 (2004)
Jackson et al., JAP 117, (2015)

Wagner's shock tube experiments provide data for Steel particles accelerated in shock-induced flows

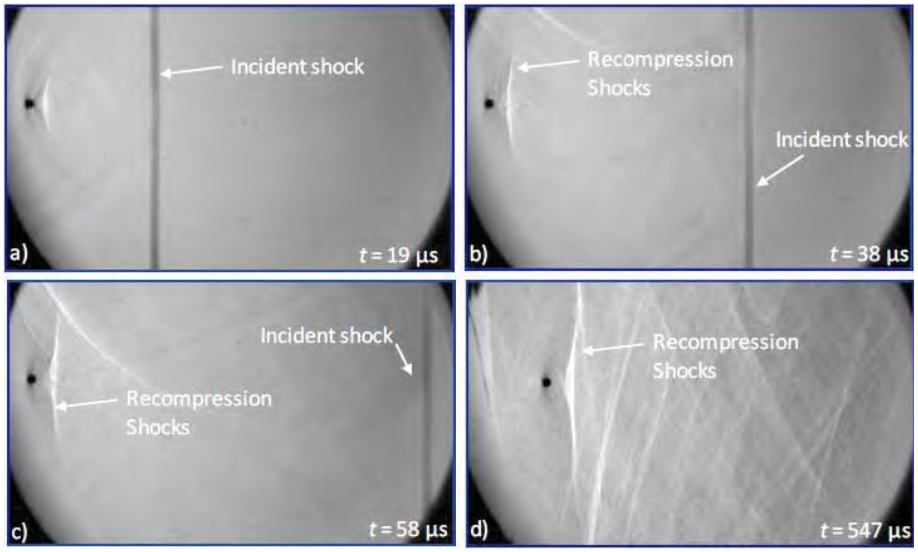

Wagner et al. SW (2012)

The 1-mm steel particle is predicted in the current simulations to speed up at a lower rate than Wagner's experiments

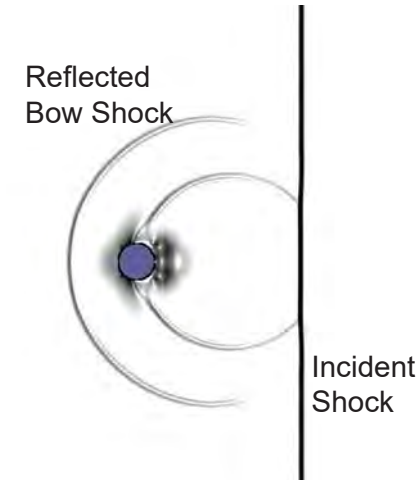

Numerical Schlieren

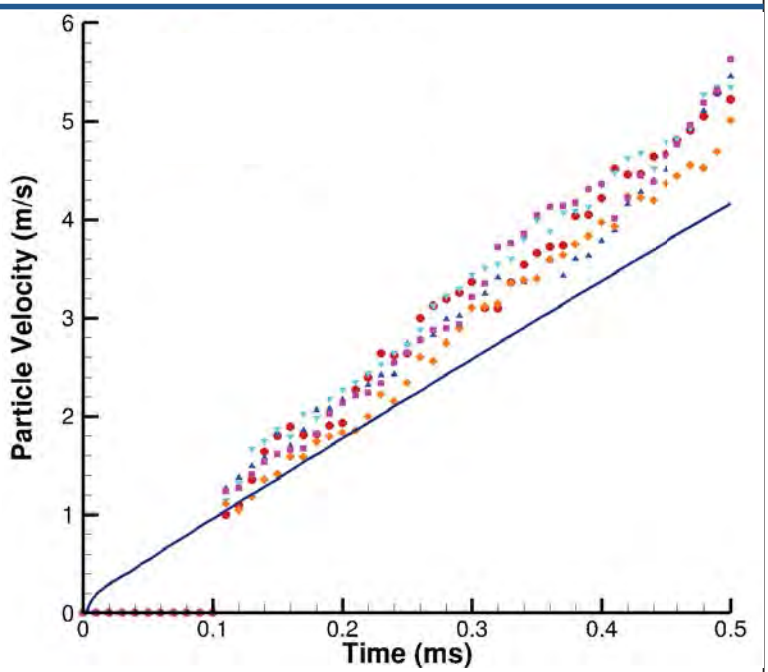

We are collaborating with Dr. Wagner at SNL to identify key differences

Symbols: Experiments
Line: Hydro Code

Meso-scale simulations of multi-particle pack are studied to investigate 3D effects and particle-particle interactions

- N-particle pack of Aluminum particles in 3D volume
  - d_p=1mm
  - ϕ=0.1 (N=20), 0.2 (N=40), & 0.3 (N=60)
  - Shock: M=1.5
  - Mesh Resolution = 4.5M zones
- Individual particle positions, velocities and accelerations are tracked in time using an Embedded Grid Method.

Compaction phase is observed followed by an expansion phase

M=1.5, φ=0.1

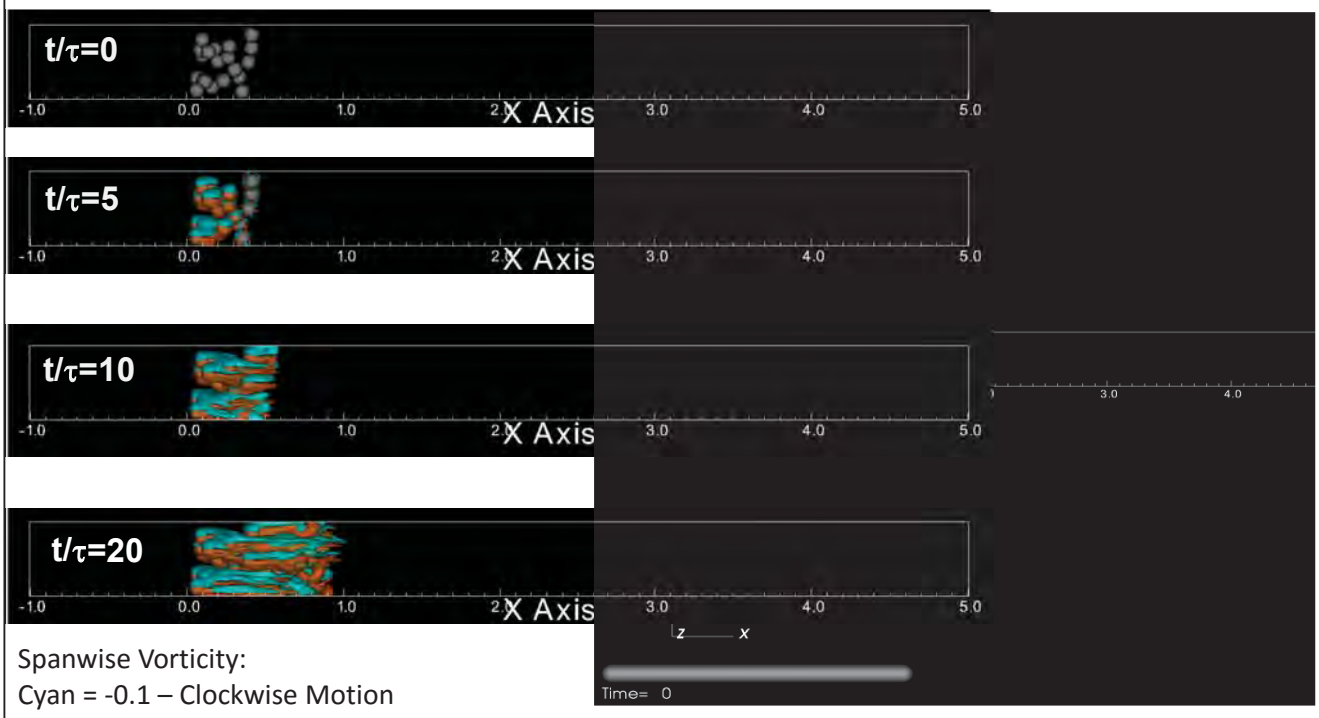

Spanwise Vorticity:
Cyan = -0.1 – Clockwise Motion
Orange = +0.1 – Counterclockwise Motion

Mesh resolution study shows that 16 zones across each particle are sufficient to capture the SPI dynamics

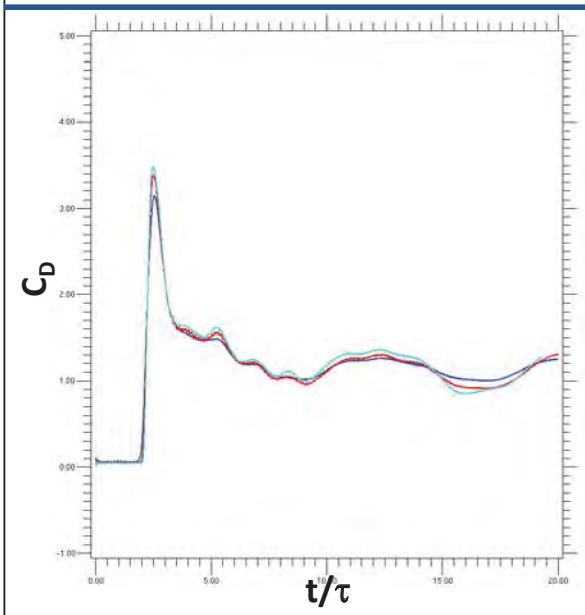

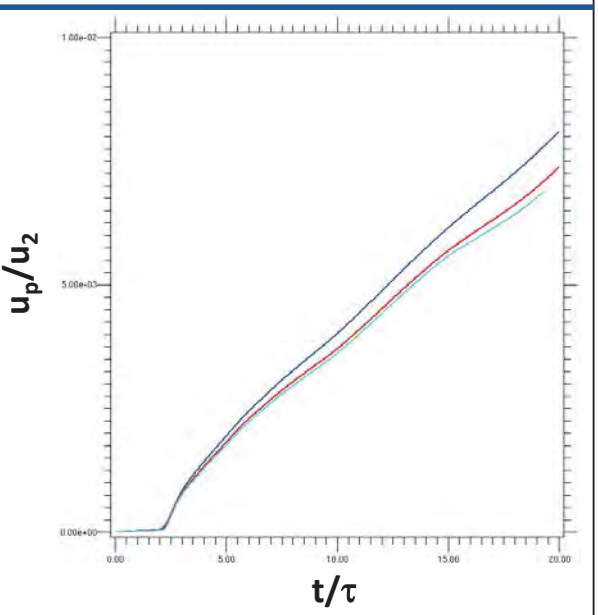

Particle 19 is located at front
Blue: Mesh=1.3M zones
Red: Mesh = 4.5M zones
Cyan: Mesh=10.8M zones

M=1.5,
ϕ=0.1

The maximum in drag coefficient reaches ~3.5 and steady state values range from ~0 to ~1.4 for the 20-particle cluster

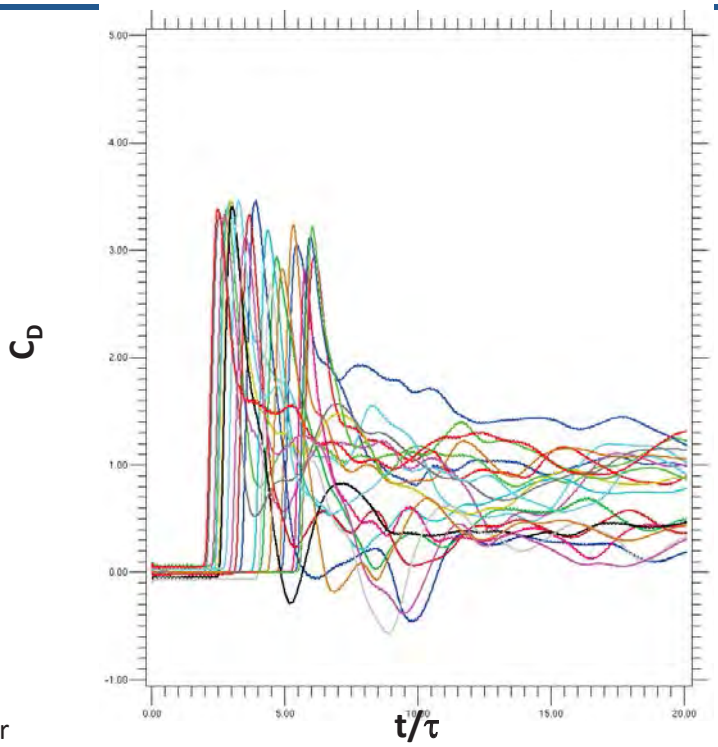

All particles in cluster

M=1.5,
ϕ=0.1

Particles at 3 key locations are identified and their time history behavior is tracked, showing slow velocity and minimal motion

Drag | Position, (x-x0)/d | x-Velocity, u_p/u_2

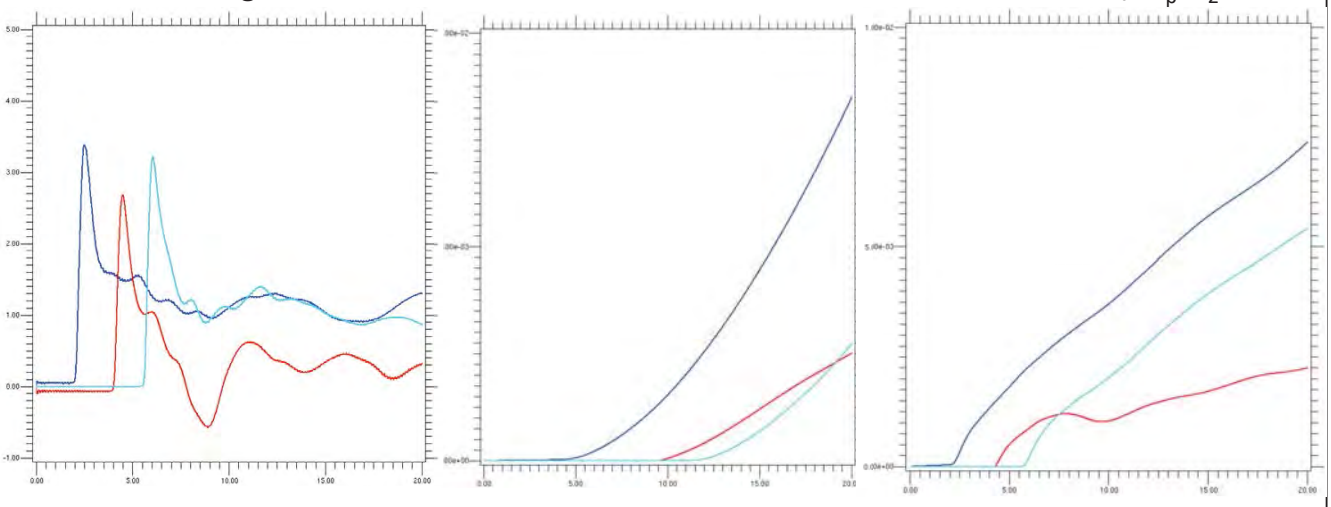

t/τ

Particle 19: Front-Blue
Particle 14: Middle-Red
Particle 17: Back-Cyan

M=1.5,
ϕ=0.1

Drag, Position & Velocity at M=1.5: long time span-t/τ=45

Drag | Position, (x-x0)/d | x-Velocity, u_p/u_2

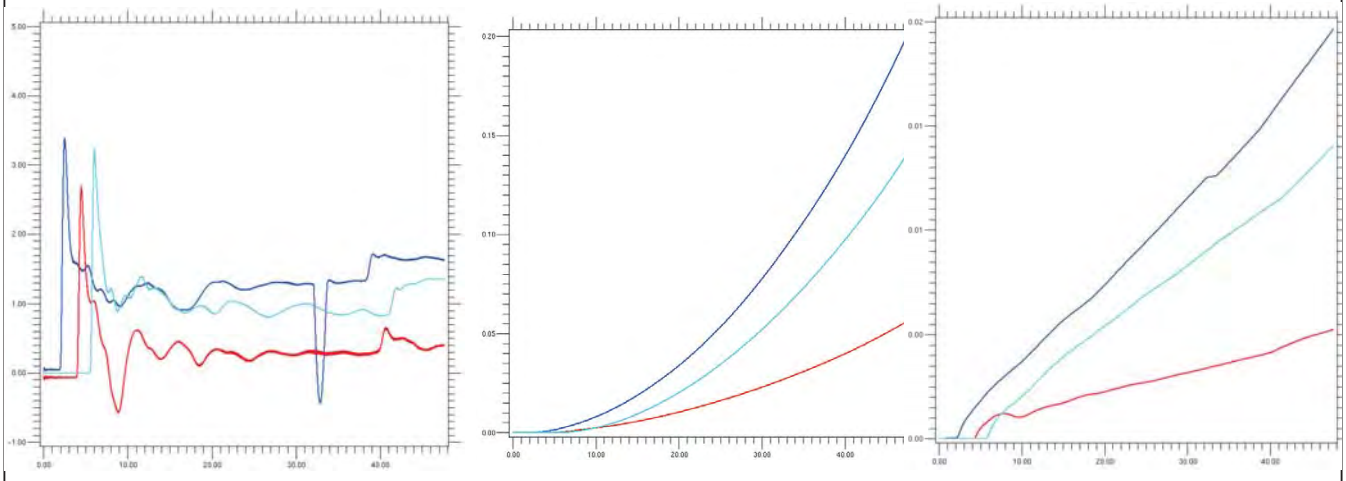

t/τ

ϕ=0.1

Particles 19, 14, & 17 are located at front (blue), middle (red) and back (cyan) of pack.

3D computations performed with varying volume fractions of 0.1, 0.2 & 0.3 to evaluate its effects on cluster dynamics

ϕ=0.1: Np=20

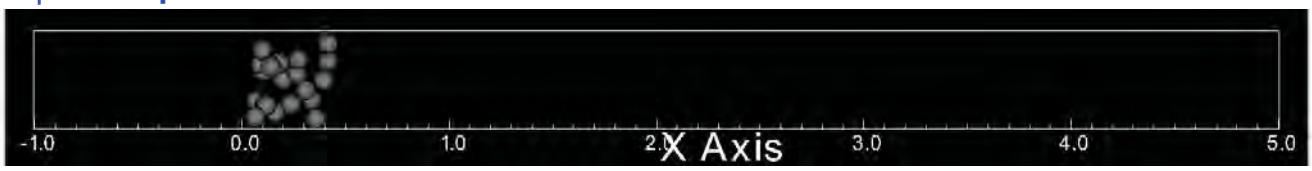

ϕ=0.2: Np=40

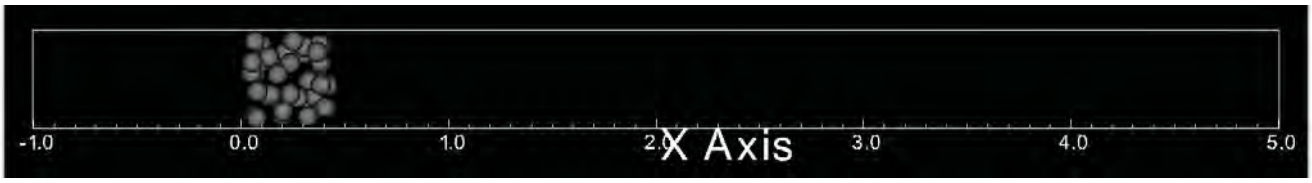

ϕ=0.3: Np=60

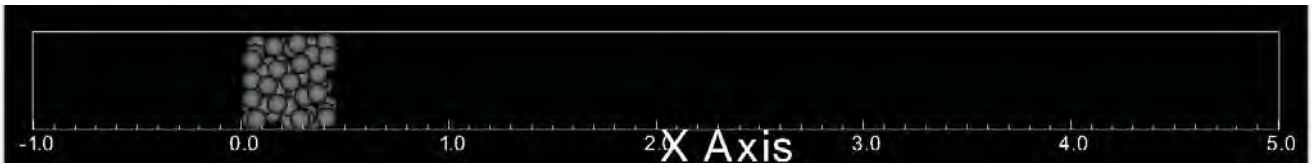

With increasing volume fraction, flow field in the cluster breaks down into smaller scales

ϕ=0.1

ϕ=0.2

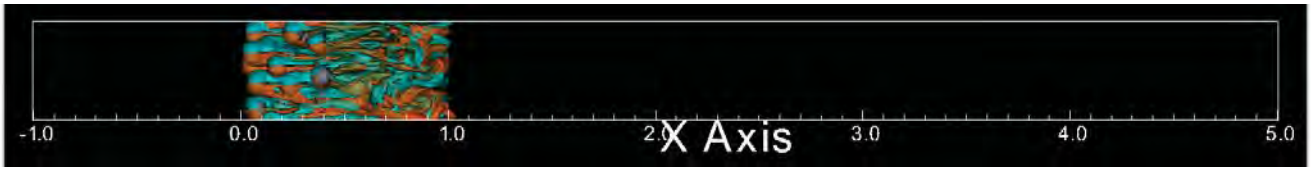

ϕ=0.3

t/τ ~20

With increasing volume fraction, collision events between particles in the pack occur more frequently and earlier in time

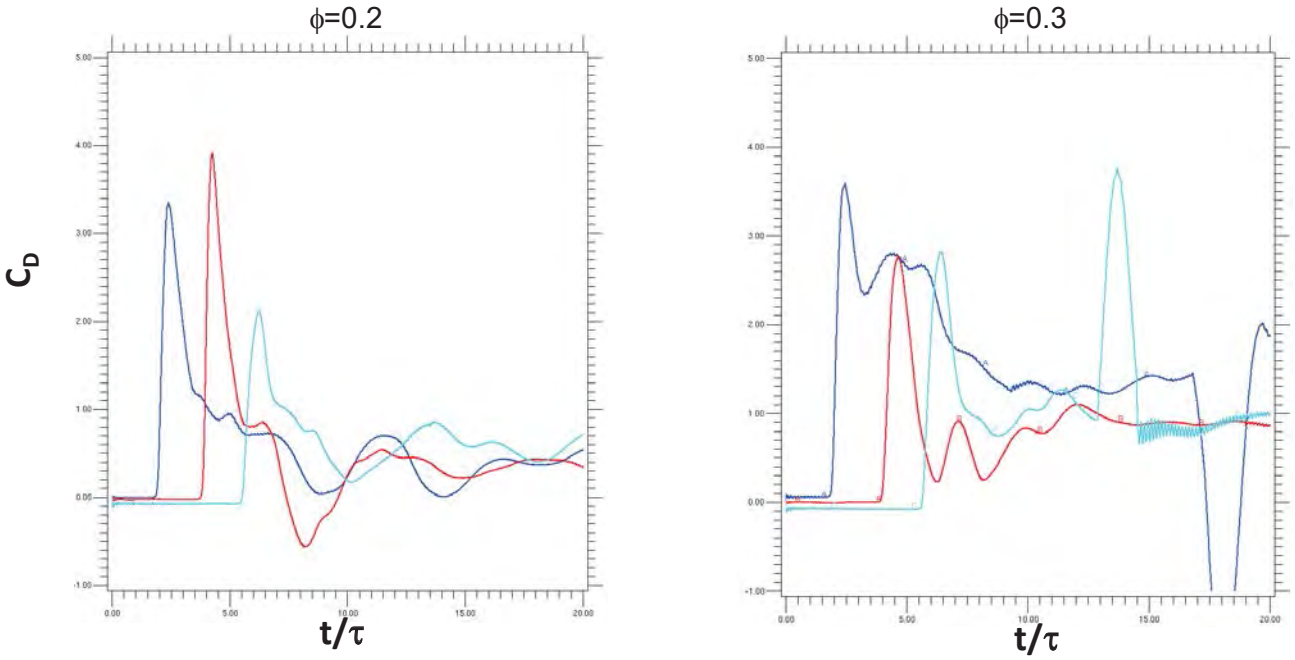

Particles are located at: front (blue), middle (red) and back (cyan) of pack.

As volume fraction increases, particles in the cluster are able to move farther compared to low volume fraction case. Hence an assumption of "frozen" pack no longer holds for higher volume fraction

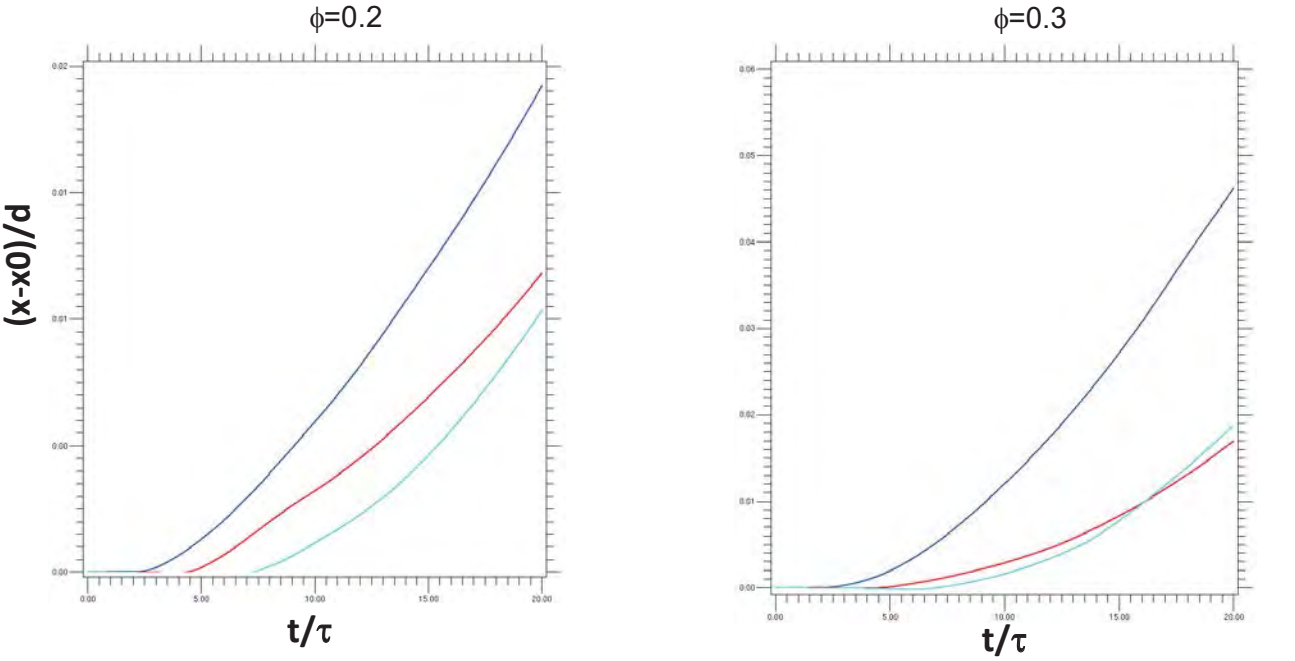

Particle locations are at front (blue), middle (red) and back (cyan) of pack.

With higher volume fraction, particle velocities in the cluster increase due to the complex wake dynamics

ϕ=0.2

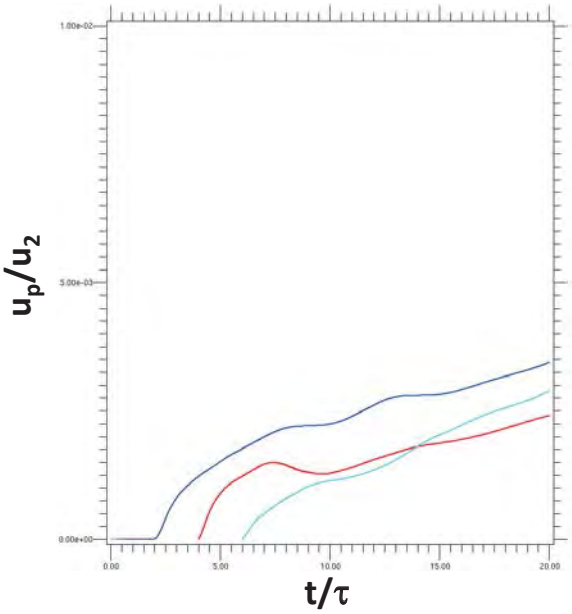

ϕ=0.3

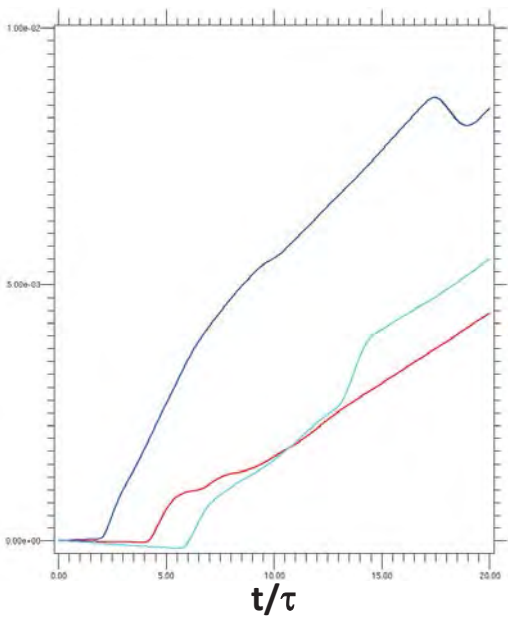

Particle locations are at front (blue), middle (red) and back (cyan) of pack.

Effects of shock strength are also studied to understand pack dynamics-t/τ~20

M=1.5

M=3.0

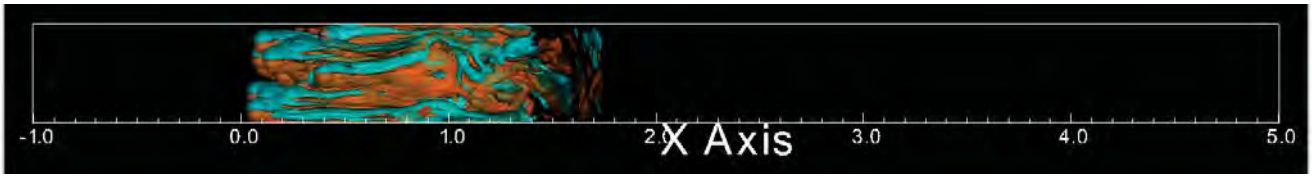

ϕ=0.1

With increasing Mach number, the particle moves and accelerates faster. Hence, an assumption of "frozen" pack no longer holds for higher Mach number

Drag | Position, (x-x0)/d | x-Velocity, u_p/u_2

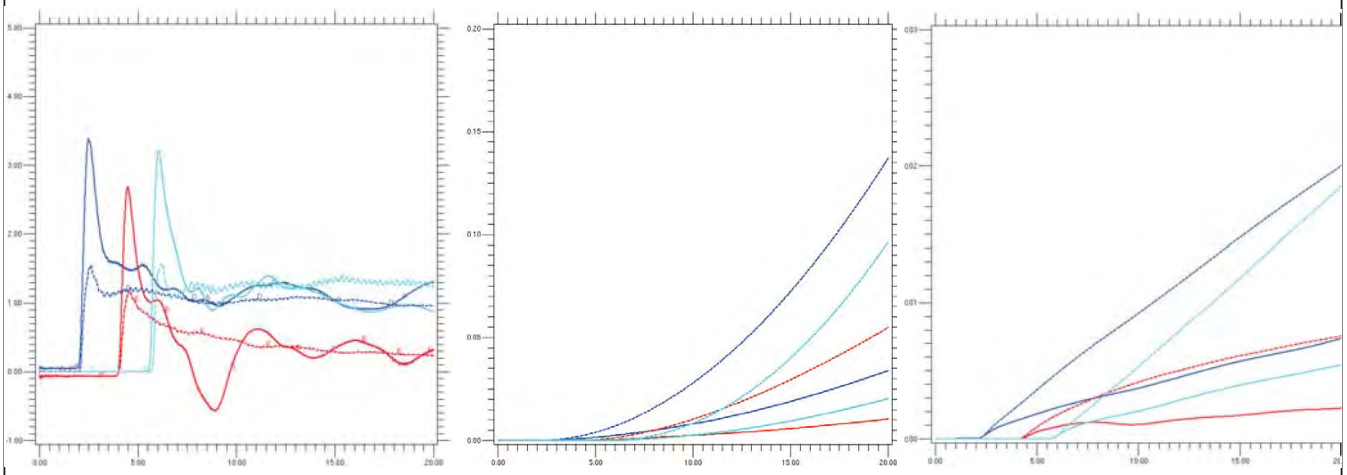

t/τ

Particles 19, 14, & 17 are located at front (blue), middle (red) and back (cyan) of pack.
Solid: M=1.5; Dashed: M=3.0

ϕ=0.1

Drag, Position & Velocity at M=3: long time span-t/τ=45

Drag | Position, (x-x0)/d | x-Velocity, u_p/u_2

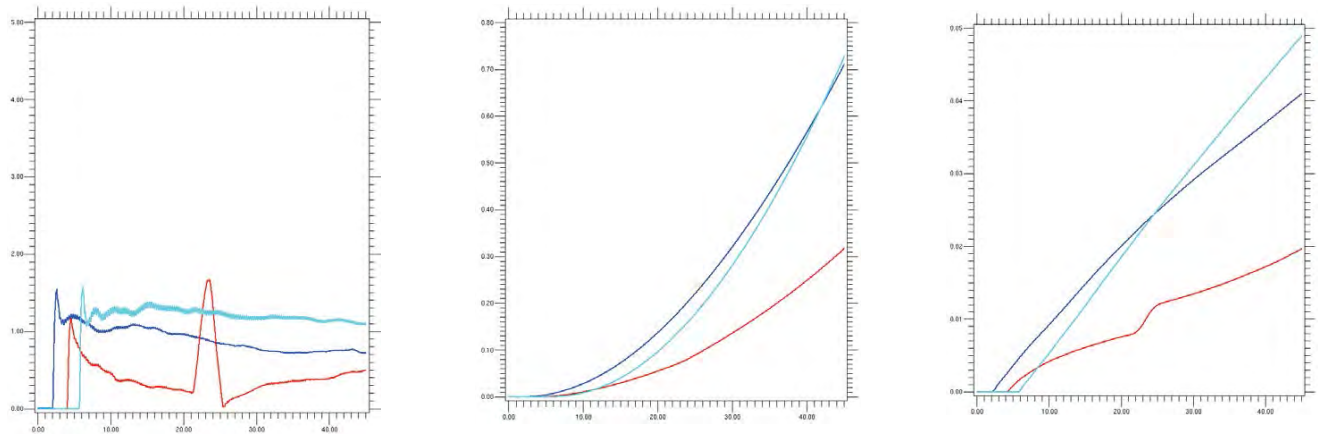

t/τ

ϕ=0.1

Particles 19, 14, & 17 are located at front (blue), middle (red) and back (cyan) of pack.

Drag, Position & Velocity at M=3: long time span-t/τ=200

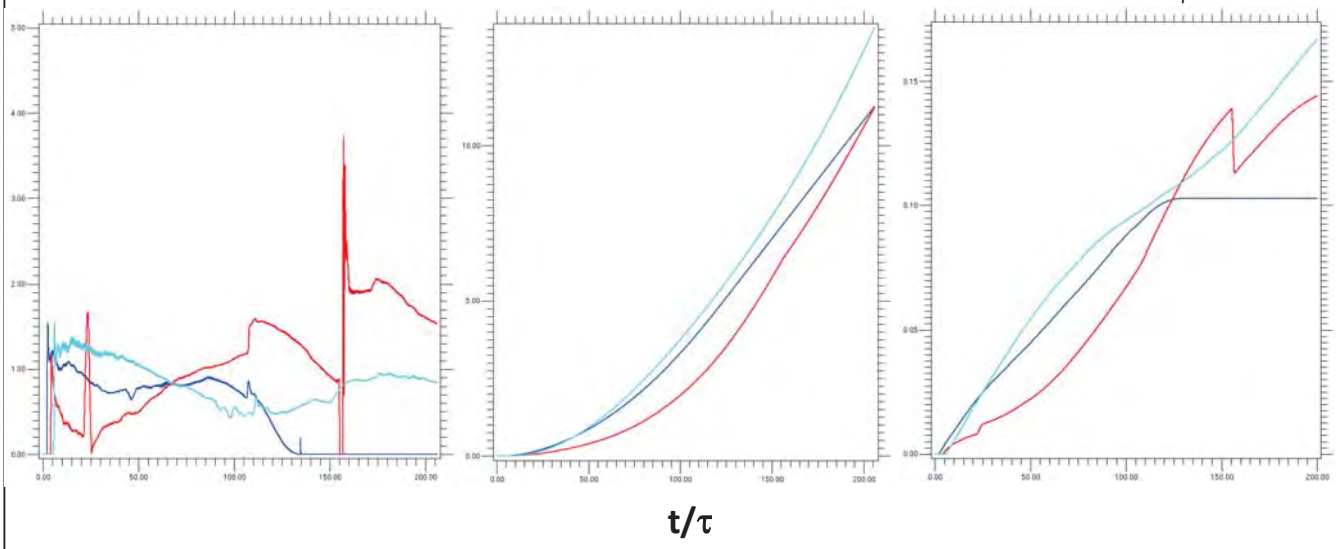

ϕ=0.1

Particles 19, 14, & 17 are located at front (blue), middle (red) and back (cyan) of pack.

Summary & Future Work

- Multiphase computations provide a powerful tool to study complex effects that are challenging to measure experimentally
- SPI mechanisms are validated using available experimental data
- Meso-scale simulations of shock-particle clusters are investigated for various volume fractions and shock strength & highlight the complex interactions
- Future work:
  - Perform 3D simulations of shock-particle cluster with larger particle count ~10^3-10^4
  - Create advanced drag models based on meso-scale simulations
  - Understand clustering mechanisms in MBX systems

Thank you for listening

Questions?

Fady Najjar, Ph.D.

Physics Design Division

LLNL

Email: najjar2@llnl.gov

Lawrence Livermore National Laboratory

The shear layers break up faster when the viscous effects are active as the

Inviscid

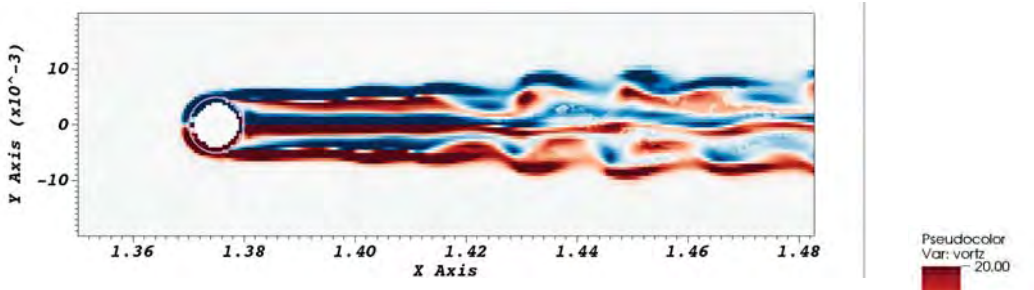

Viscous

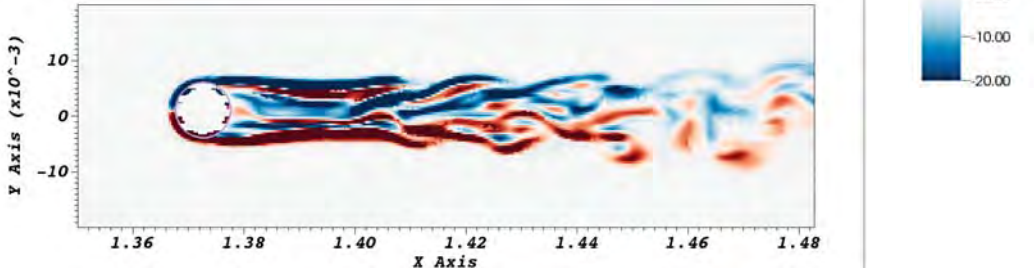

Z-vorticity at t=4μs

W-Particle has moved to x~1.37cm

Minimal differences in particle position and its speed are observed with and without viscous effects

Position

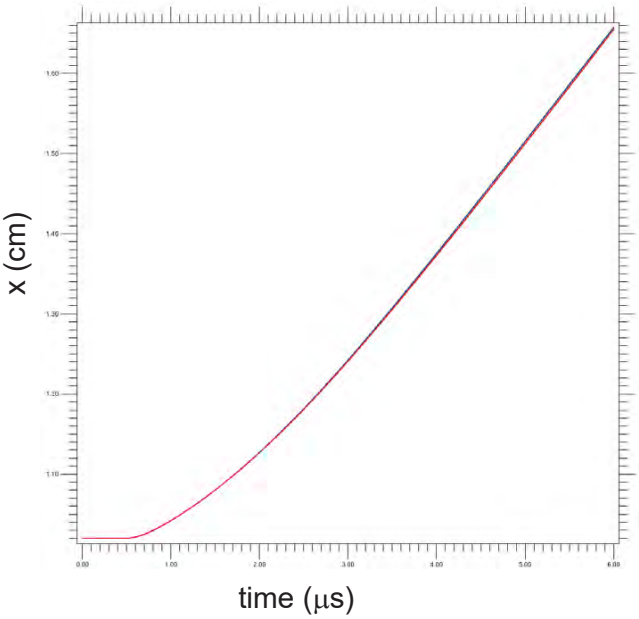

Speed

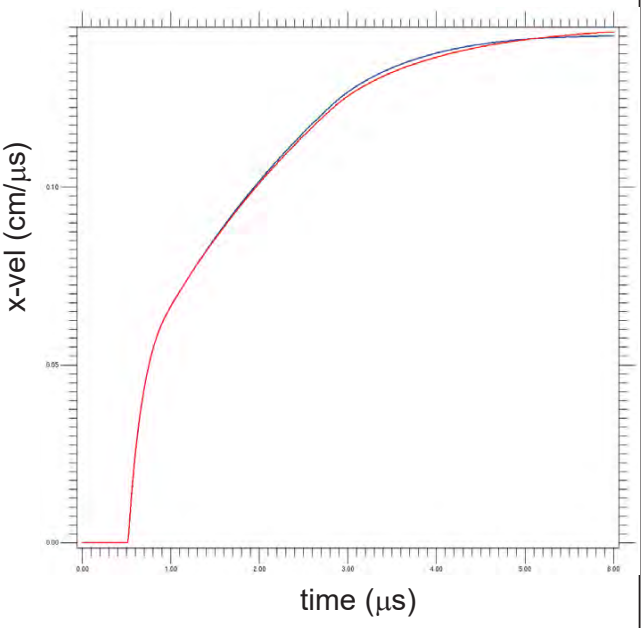

Blue Line: Inviscid
Red Line: Viscous

Particle "Coasting" speed is = 0.14 cm/μs

Minimal difference in its acceleration is observed with and without viscous effects

Acceleration

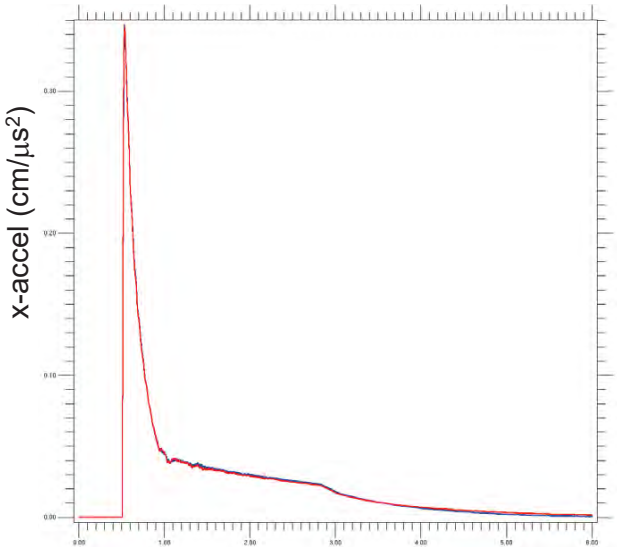

X-Force on Particle

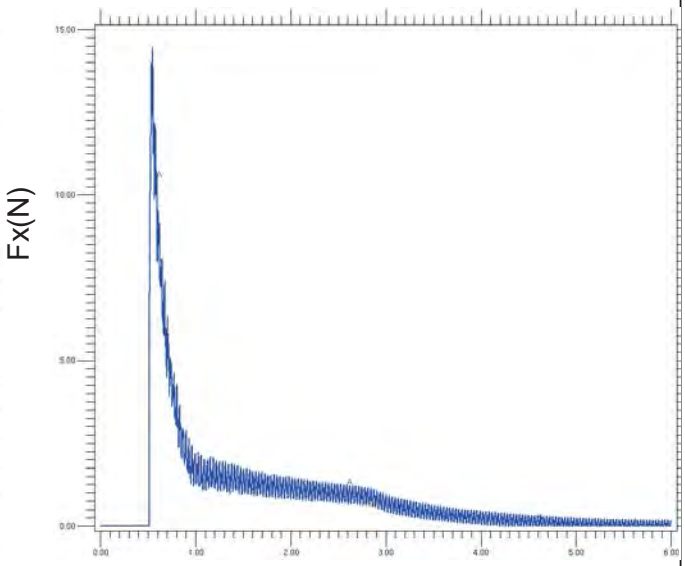

Blue Line: Inviscid
Red Line: Viscous

A systematic study of turbophoresis

four-way-coupled simulation of Stokesian particles in channel flow

Mahdi Esmaily
Ali Mani

Stanford University

Deep Dive
Oct. 6-7, 2016

Outline

- Challenges
- Objectives
- Short notes on
  - Boundary conditions for particles
  - Computing near-wall statistics
- Systematic study of particles in the viscous layer
  - Effect of flow Reynolds number, Stokes number, density ratio, volume fraction, and restitution coefficient
  - Concentration and velocity statistics
- Open questions

Challenges

- Particle-flow interaction
  - Finite Reynolds number effects: Particle resolved vs. unresolved Lagrangian/Eulerian
  - Point-particle assumption: Stokes drag, history terms, added mass, pressure gradient, ...
  - Two-way-coupling effects: disturbed vs. undisturbed velocity
  - Boundary conditions for particles
- Particle-wall interaction
  - Restitution coefficient
  - Wall roughness
  - Wall vibration
  - Electrostatistic, Saffman lift, and thermophoretic forces
- Particle-particle interaction
  - Restitution coefficient
  - Polydispersity
  - Particle shape effects

Objectives

- Targeting regimes with:
  - Low mass loading ratio (no two-way-coupling)
  - Small spherical particles (no finite Reynolds number effects)
  - High particle to fluid density ratio (Only linear Stokes drag)
  - Absence of body force
  - Mono-dispersed distribution
  - Smooth walls with no vibration
  - Absence of electorstatic, thermophoretic, and Saffman lift forces
- Systematically investigating the effect of:
  - Flow Reynolds number : Re
  - Particle Stokes number (particle-to-fluid density ratio) : St+
  - Particle size (relative to the viscous length scale) : Dp+
  - Restitution coefficient (particle-particle ≡ particle-wall) : k
  - Volume fraction (one-way-coupled and one-way-coupled+collision) : Φ

Boundary conditions for particles

- Periodic boundary condition can be considered as a substitute for a long (case-dependent) inflow-outflow boundary condition
- Flow-based streamwise computational period is also sufficient for particles

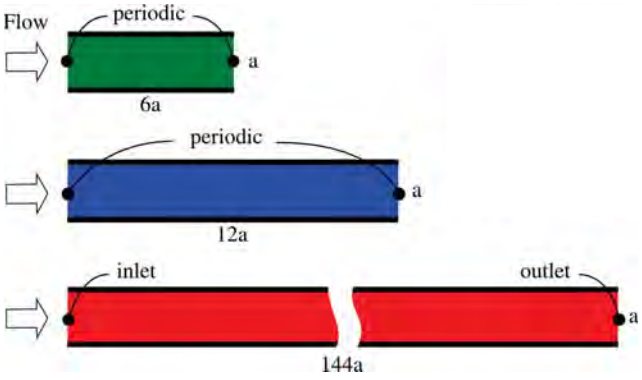

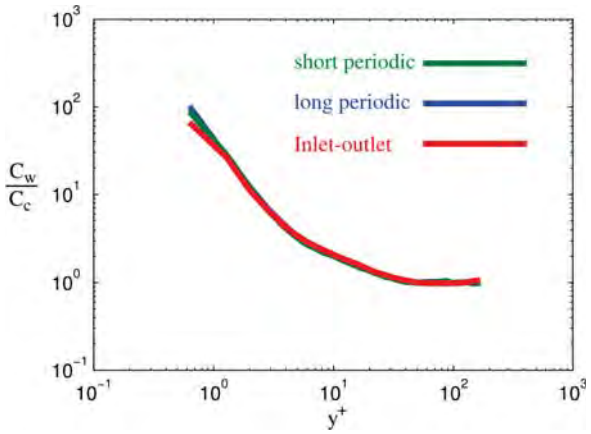

Re_B 5,200 St^+ 4.3

Computing number density

- It is important to adjust the position of the first control-volume for Lagrangian-to-Eulerian mapping based on the particle diameter

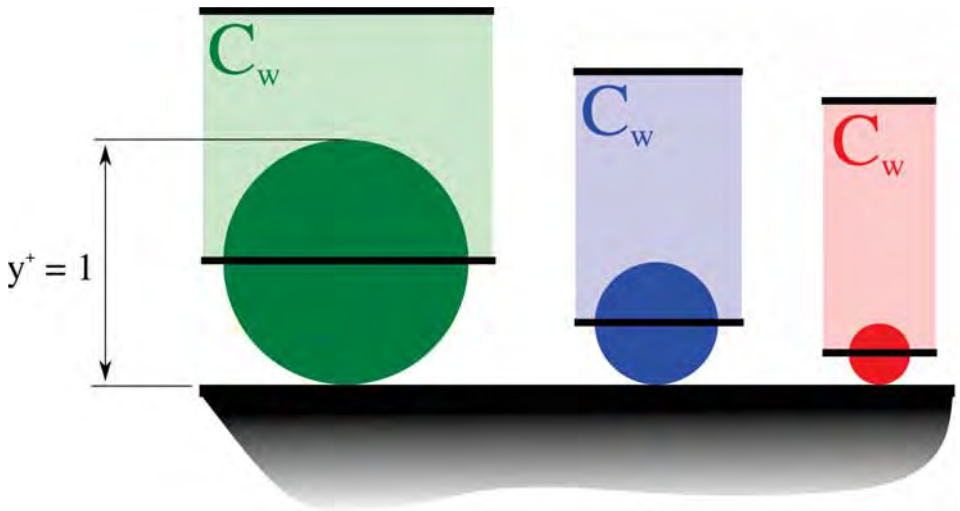

Problem setup

- Turbulent channel flow
  - Reynolds number (based on the channel half height and friction velocity): **178 (KMM) and 356**
  - Grid size in wall unit: 5.8 x 0.41-5.7 x 4.4
- Particle to fluid density ratio:
  - 18, 36, 72, ... , 18432 (i.e. 11 classes **18x2^(0:10)**)
- Particle diameter in wall unit:
  - **Dp+ = 1/4** : St+ = 1/16, ... , 64
  - **Dp+ = 1/2** : St+ = 1/4, ... , 256
  - **Dp+ = 1** : St+ = 1, ..., 1024
- Restitution coefficient:
  - **k = 0.0, 0.25, 0.5, 0.75, 1.0**
- Volume fraction:
  - **Φ = 0 (one-way-coupled)** : Np = 10^5
  - **Φ = {1/16, 1/4, ..., 16}x10^-5**: Np = 800 – 2x10^5 (**8X** for higher Re), MLR = 4x10^-5 – 10^-2
- In total
  - **55** classes of particles in the one-way-coupled simulations at each Reynolds
  - **15** classes of particles in the four-way-coupled simulations at each Reynolds

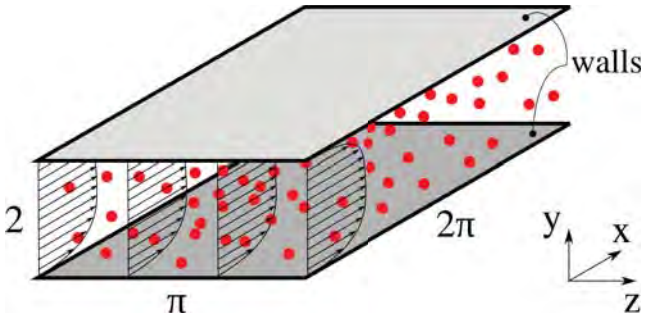

Time convergence

Re = 180

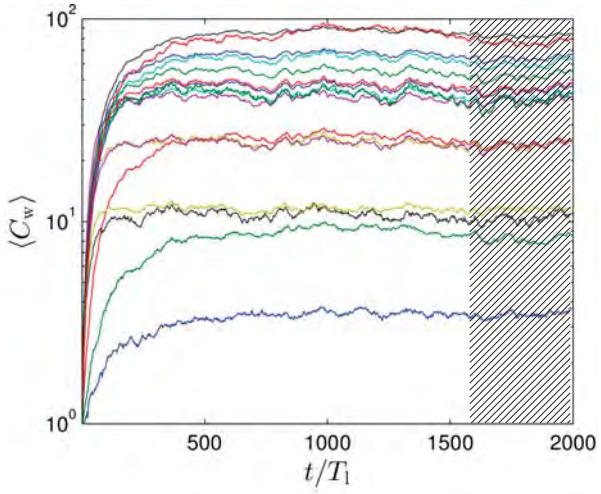

Re = 360

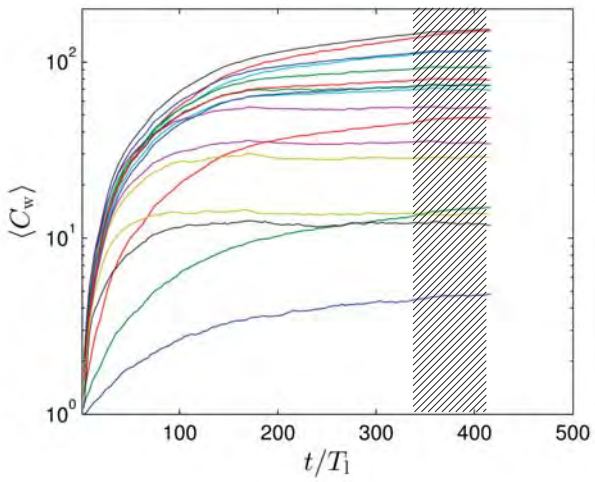

- Only simulations with collisions will be presented

Does particle number density follow a power law in the viscous-layer?

Individual curves must be constant if the **power-law** holds

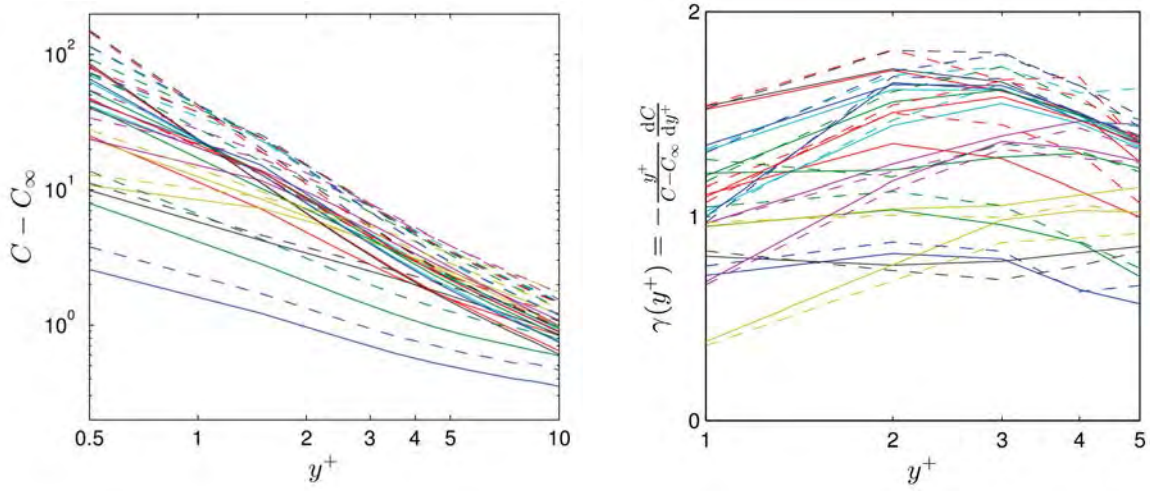

- It appears so, however, higher resolution is required before drawing any conclusion

Effect of St (number density)

- Dp+ = 1/2, k = 1, Φ = 10^-5
- Adopting γ for analysis of the near-wall number density allows for a collapse with respect to Re
- Highest concentration is observed at St+ = O(10)
- Trends are expected to change at lower k

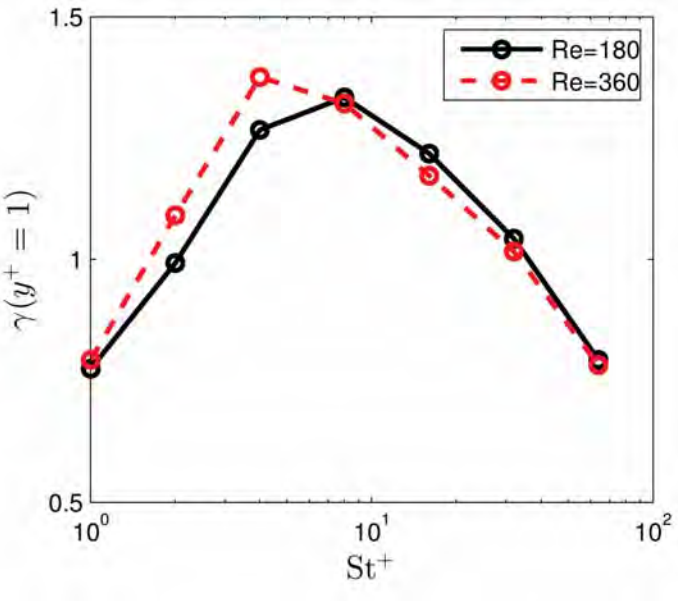

Effect of Stokes number (velocity)

- Dp+ = 1/2, k = 1, Φ = 10^-5
- Near-wall velocities in wall-units are independent of Re
- At higher St+, particles are faster than the flow in the viscous-layer
- Despite strong turbophoresis, the bulk velocity of particles is similar to the gas at high St+

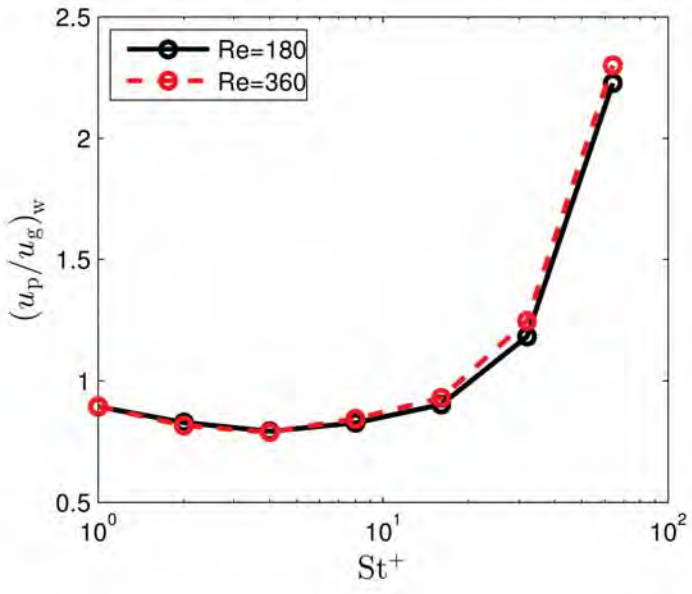

Effect of particle size

- St+ = 8, k = 1, Φ = 10^-5
- Density and number of particles are adjusted to keep St+ and Φ constant
- The effect of particle size on γ is an order of magnitude less than St+
- Particle size has a larger effect when Φ is smaller

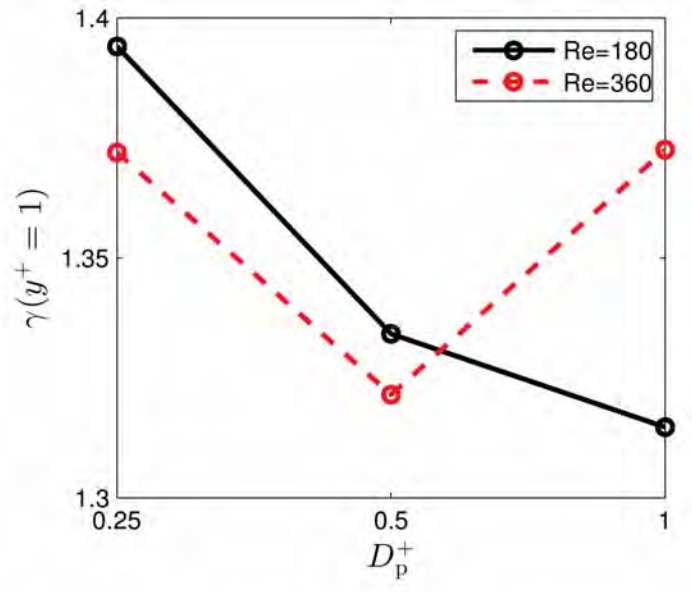

Effect of volume fraction

- Dp+ = 1/2, St+ = 8, k = 1
- γ appears to be linearly proportional to log(Φ)
- Normalized near wall concentration decreases significantly as Φ increases
- The normalized near-wall number density decrease approximately proportional to Φ^{-1/3}

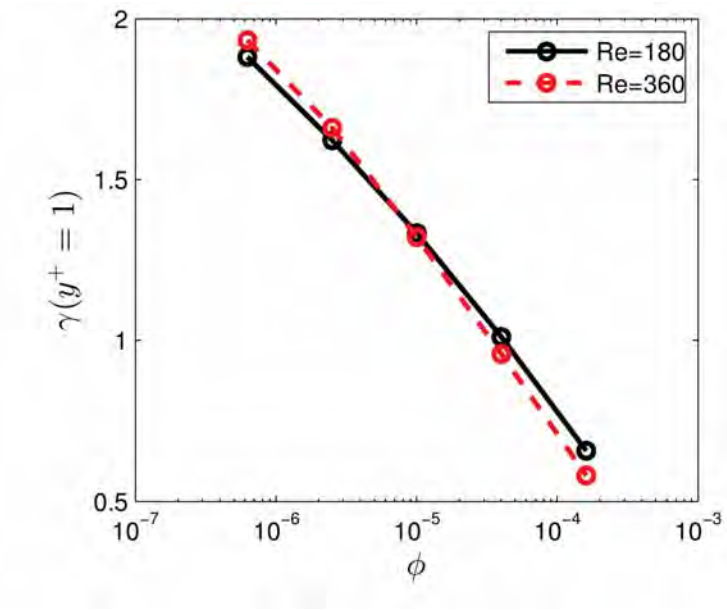

Effect of restitution coefficient

- Dp+ = 1/2, St+ = 8, Φ = 10^-5
- Same restitution coefficient is employed for the particle-particle as the particle-wall collisions
- The restitution coefficient changes the near-wall number density at most by a factor of two

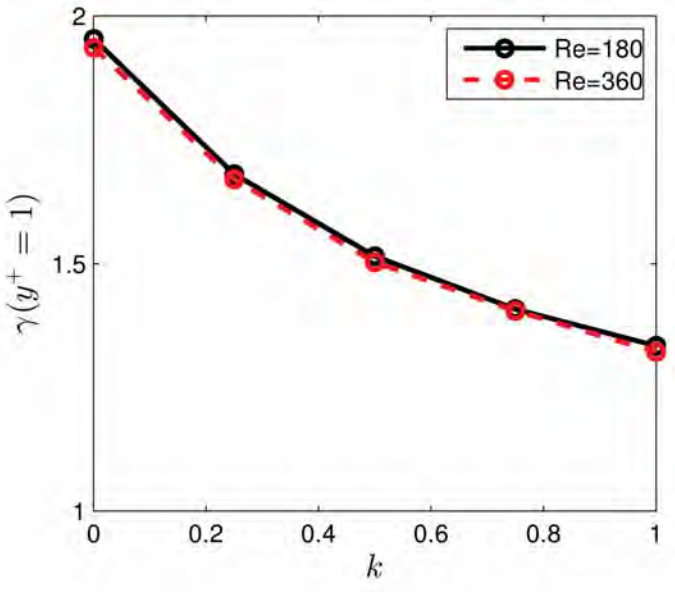

Conclusions

- The power-law exponent (γ) appears to be independent of Re as oppose to near-wall number density that varies depending on the size of the depletion region (i.e. Re)
- γ is most sensitive to the Stokes number
- The particle size is of minimal importance in the investigated regime
- The volume fraction influence on γ appears to be log-linear
- The restitution coefficient changes near-wall number density at most by a factor two in the investigated regime
- Particles can be faster than the flow in the viscous-layer at higher Φ or St+

Open questions

- Is a collision model with a single restitution coefficient an accurate model?
- How does restitution coefficient vary versus St+, Dp+, ... ?
- How polydispersity changes the observed trends?
- What is the development length for different St+, ...?
- Are there simple universal laws for predicting near-wall behavior of particles?

Acknowledgment and discussion

PSAAP II

U.S. DEPARTMENT OF ENERGY

Stanford University

Bayesian Analysis as an Aid to Improving Multiphase Modeling

Balu Nadiga, LANL

October 7, 2016

Context: Consortium for Advanced Simulation of Light Water Reactors

www.casl.gov

Aim: Develop a virtual reactor testbed to improve the performance of currently operating light water reactors
A Specific Thermohydraulic Problem: Predictive modeling of Departure from Nucleate Boiling/Critical Heat Flux

Departure from Nucleate Boiling/Critical Heat Flux

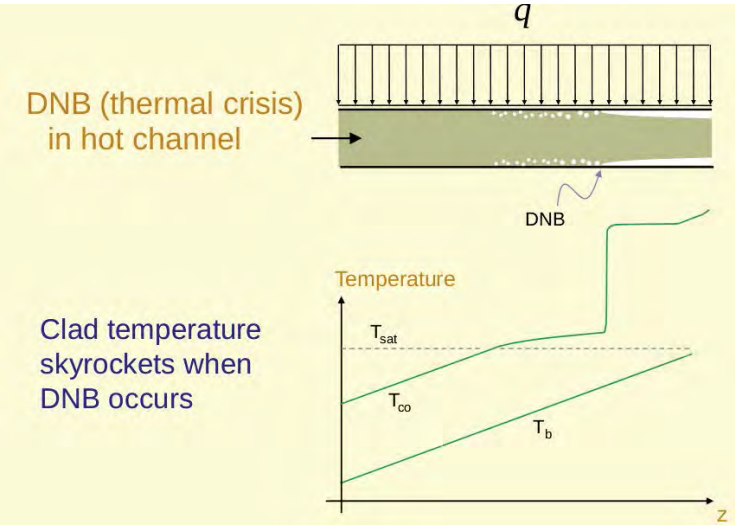

Departure from Nucleate Boiling/Critical Heat Flux

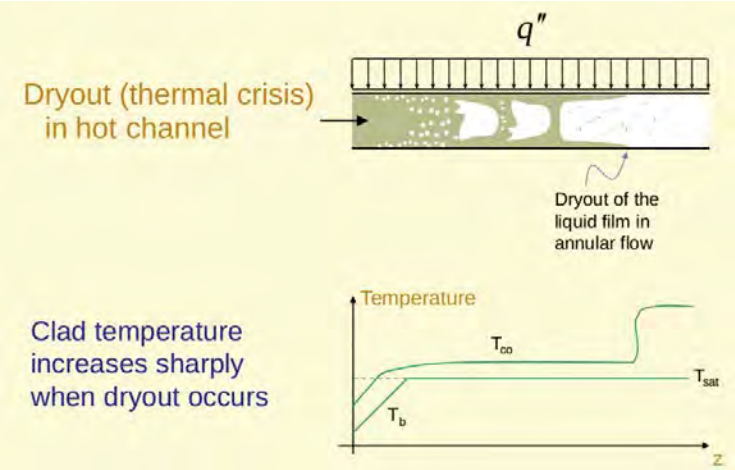

Complex ≫≫≫ Simple

Fuel Assembly ≫ Rod Bundle ≫ Heated Pipe ≫ Adiabatic Bubbly Flow

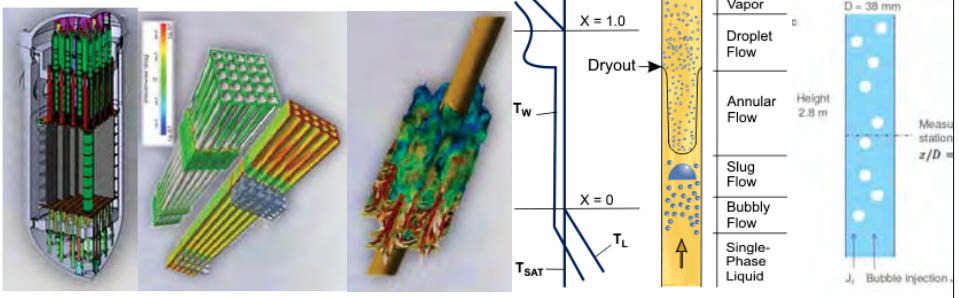

Complex ≫≫≫ Simple

- Upward bubbly flow in a pipe. **Steady**, **axissymmetric** and **turbulent** flow without phase change
  $Re \sim 50000$
- **48 flow conditions**
  - liquid superficial velocity J_f
  - gas superficial velocity J_g
- Measuring station z/D=36. **Radial profiles**:
  - Axial velocity
  - Velocity fluctuations
  - Void fraction

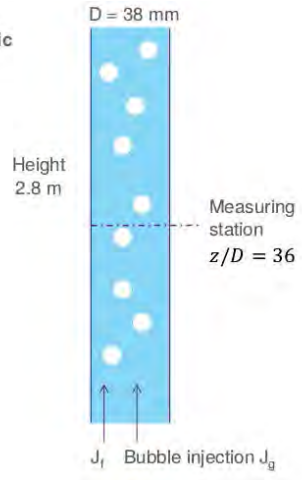

Liu-Bankoff Experiments

Complex ≫≫≫ Simple

- Upward bubbly flow in a pipe. **Steady**, **axissymmetric** flow without phase change
- Fluid = aqueous solution + glycerine
- **Low Reynolds number**: 875 – 1860
- **9 experiments**
- Measuring station at the top. **Radial profiles**:
  - Liquid velocity and velocity fluctuations
  - Void fraction

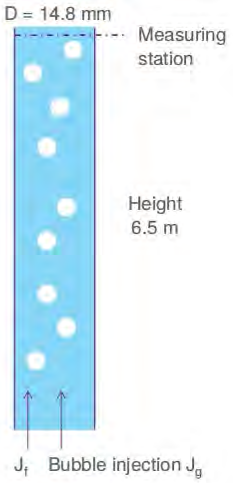

Nakaryakov Experiments

Void Fraction Predictions

2013 – GEN-I

- Drag: Tomiyama
- Lift: C_L=0.03
- Wall Lub.: Antal

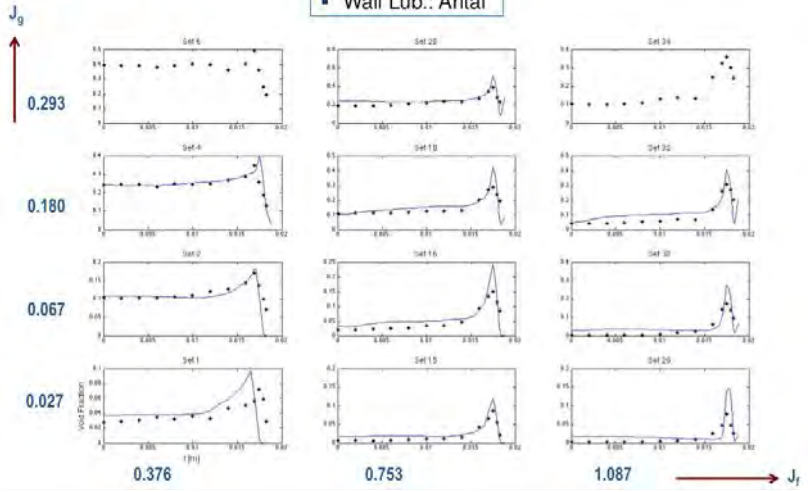

Sugrue-Baglietto

Void Fraction Predictions
Sensitivities example

- Drag: Tomiyama
- Lift: CL=0.03
- Wall Lub.: Antal
- Simple Turb. Dispersion (Tchen)

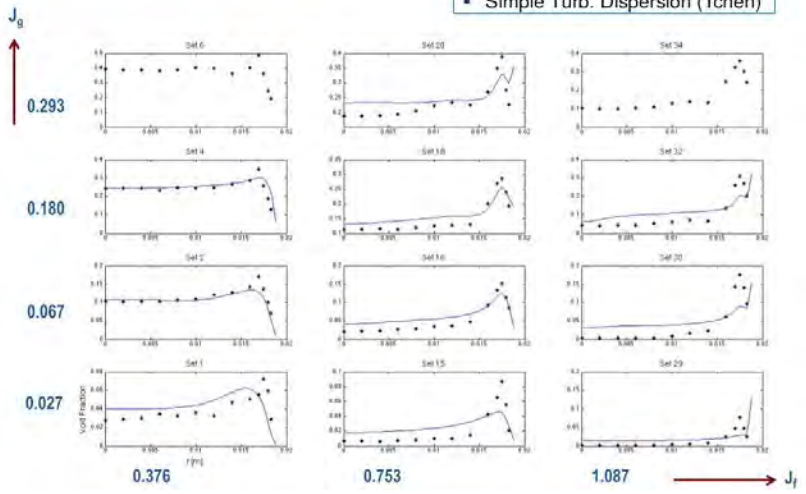

Void Fraction Predictions
Sensitivities example

- Drag: Tomiyama
- Lift: CL=0.03
- Wall Lub.: Antal
- Turb. Dispersion
- Virtual Mass

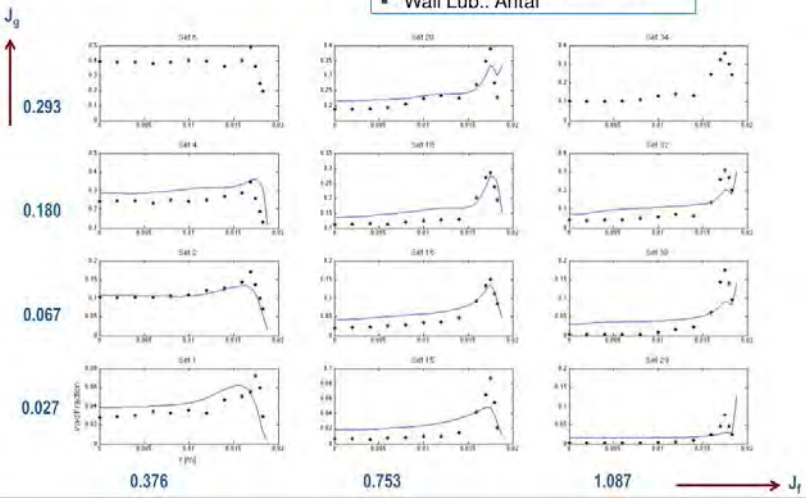

Can Bayesian Analysis Be Used to Improve Modeling?

- Single phase turbulence closures are robust
- Not the case with multiphase closures
  - Equation for void fraction can be highly nonlinear and very sensitive to parameter values
  - Parameterization of different processes can have unintended interactions
- How can they be made more robust?
  - Better Analysis of (almost) Direct Numerical Simulations, Experiments

Summary

- There is (almost) DNS capability
- There are multiple parameterizations of multiphase phenomena (drag, lift, turbulent dispersion, …)
- Modern UQ, ML, and Bayesian analysis techniques can be used to integrate DNS/Experiments with multiphase phenomenology to make RANS models (ensemble averaged Eulerian Dispersed-Multiphase) more robust
  - Discrepancy model, Representation error
  - Hierarchical model

Approach *not unlike* top-down VUQ approach that Phil Smilth talked about

Ensemble-Averaged Dispersed Eulerian Multiphase —Two Fluid—Approach Considered and Thought Sufficient—No Particle-Flow Interaction!

$$
\begin{aligned}
\frac{\partial \hat{\rho}_k}{\partial t} + \boldsymbol{\nabla} \cdot (\hat{\rho}_k \tilde{\mathbf{v}}_k) &= \Gamma_k \\
\frac{\partial \hat{\rho}_k \tilde{\mathbf{v}}_k}{\partial t} + \boldsymbol{\nabla} \cdot (\hat{\rho}_k \tilde{\mathbf{v}}_k \tilde{\mathbf{v}}_k) &= -\alpha_k \boldsymbol{\nabla} p_k + \nabla \cdot (\alpha_k \boldsymbol{\tau}_k) \\
&\quad + \Gamma_k \tilde{\mathbf{v}}_k + \mathbf{M}_k + \hat{\rho}_k \mathbf{f} \\
\frac{\partial \hat{\rho}_k \tilde{e}_k}{\partial t} + \boldsymbol{\nabla} \cdot (p + \hat{\rho}_k \tilde{e}_k \tilde{\mathbf{v}}_k) &= -\nabla \cdot (\alpha_k \mathbf{q}_k) + \alpha_k Q_k + \\
&\quad \alpha_k \mathbf{T}_k : \nabla \cdot \tilde{\mathbf{v}}_k + e_k \Gamma_k \\
\frac{\partial \alpha_k}{\partial t} + \tilde{\mathbf{v}}_k \cdot \boldsymbol{\nabla} \alpha_k &= \mathcal{V}_k \\
\bar{\rho}_k &= \bar{\rho}_k(p_k, \tilde{T}_k)
\end{aligned}
$$

$$
(\hat{\rho}_k = \alpha_k \bar{\rho}_k, \quad \tilde{\mathbf{v}}_k = \overline{\mathcal{X}_k \rho \mathbf{v}} / \overline{\mathcal{X}_k \rho}, \quad \tilde{e}_k = \overline{\mathcal{X}_k \rho e} / \overline{\mathcal{X}_k \rho})
$$

Sensitivity Analysis

Non-Intrusive Sensitivity Analysis w/ Starccm+ & Dakota Sampling Study Using Hundreds of Starccm+ Simulations

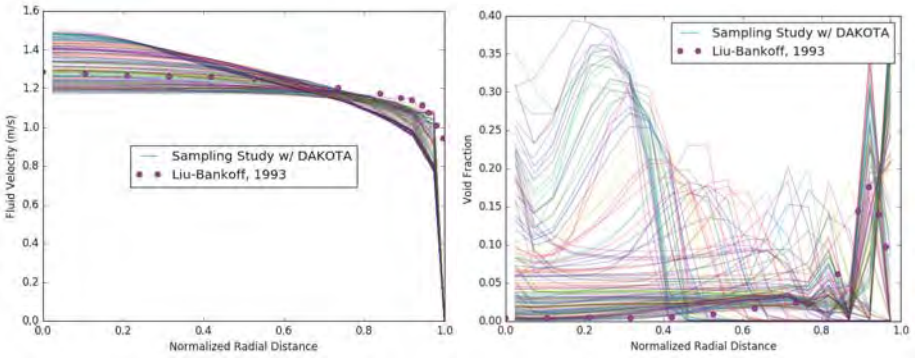

Void fraction behavior is more sensitive than fluid-velocity behavior

Simple and Rank Correlations

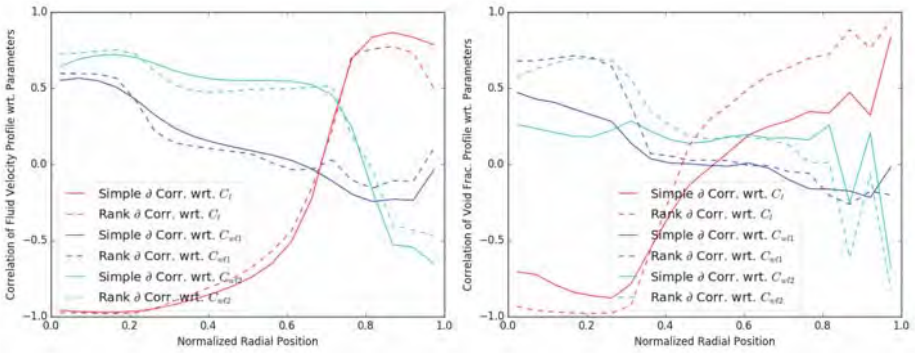

Larger differences between simple and rank correlations for void fraction indicates a higher degree of nonlinearity in the relationship between the void fraction profile and the multiphase closure parameters

Polynomial Chaos Expansion Based Sensitivity

Even though wall lubrication is active only near the wall,
it has an effect on the the velocity and void frac. profiles everywhere

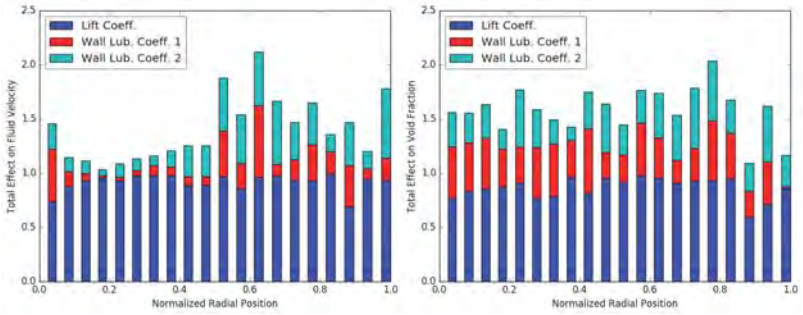

Total Effect

Polynomial Chaos Expansion Based Sensitivity

Even though wall lubrication is active only near the wall,
it has an effect on the the velocity and void frac. profiles everywhere

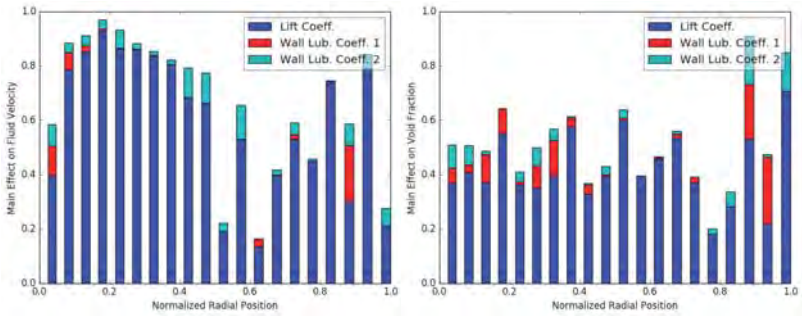

Main Effect

Polynomial Chaos Expansion Based Sensitivity

Even though wall lubrication is active only near the wall,
it has an effect on the the velocity and void frac. profiles everywhere

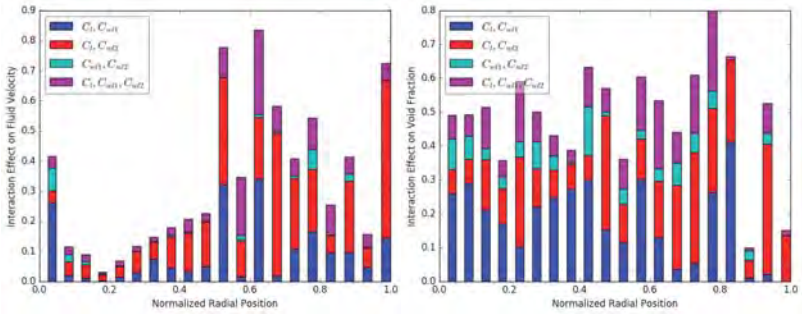

Interaction Effect

Starccm+ Parameter Optimization with Dakota

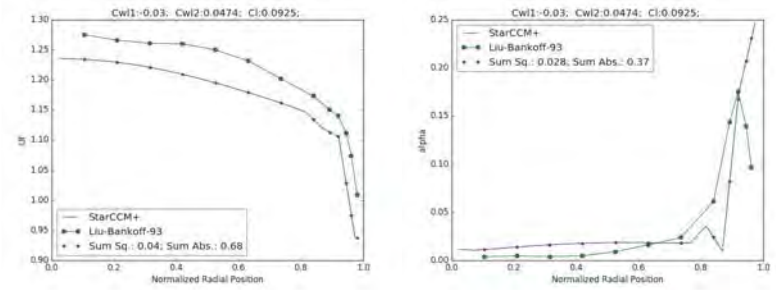

Least squares fit

Starccm+ Parameter Optimization with Dakota

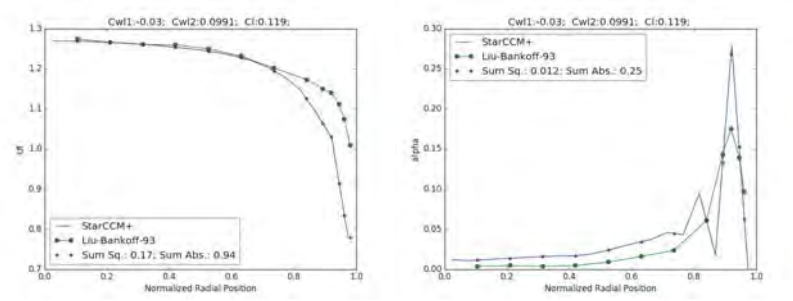

L1 norm produces a better fit of the void fraction profile

Bayesian Analysis

Experiments of Nakaryakov et al., 1986

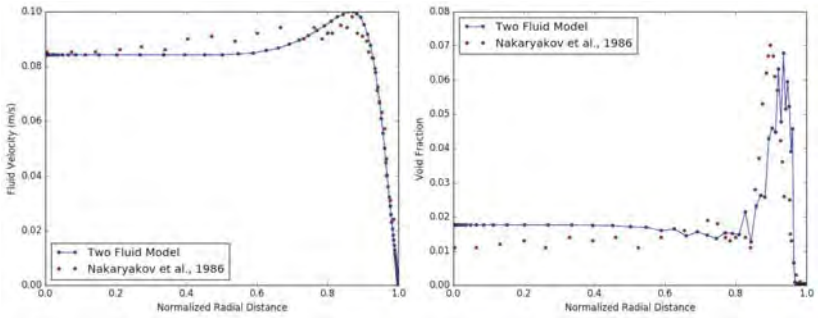

An example model solution using lift, drag, and wall lubrication
Nakaryakov et al., 1986; Antal, Lahey, Flaherty, 1991

Bayes. Analysis can Provide Insights into Model Behavior

However, converged statistics may be difficult to obtain with STARCCM+. Here the same parameterizations as in the STARCCM+ studies are used in a Bayesian calibration study

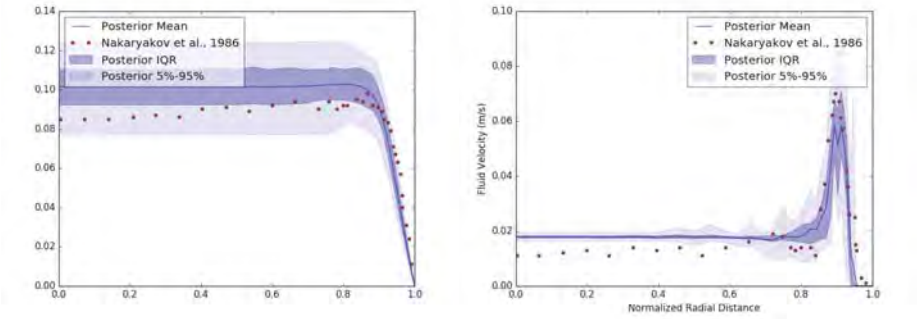

Nakaryakov et al., 1986; Antal, Lahey, Flaherty, 1991

Bayes. Analysis can Provide Insights into Model Behavior

However, converged statistics may be difficult to obtain with STARCCM+. Here the same parameterizations as in the STARCCM+ studies are used in a Bayesian calibration study

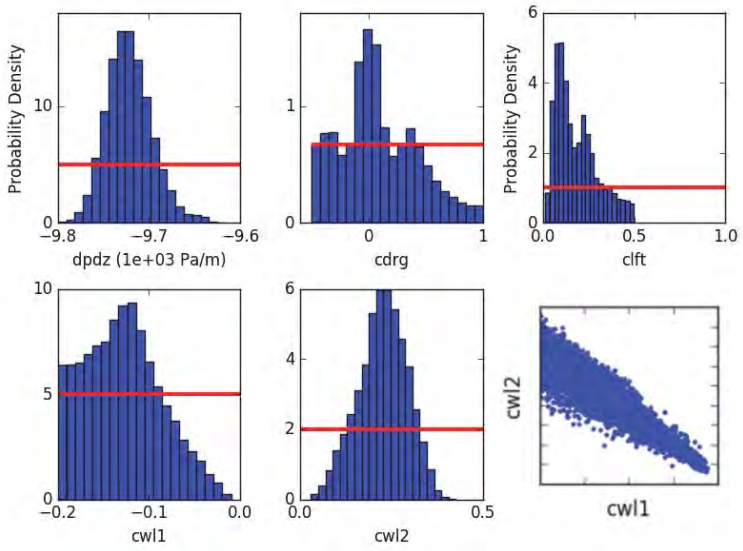

Bayes. Analysis can Provide Insights into Model Behavior

However, converged statistics may be difficult to obtain with STARCCM+. Here the same parameterizations as in the STARCCM+ studies are used in a Bayesian calibration study

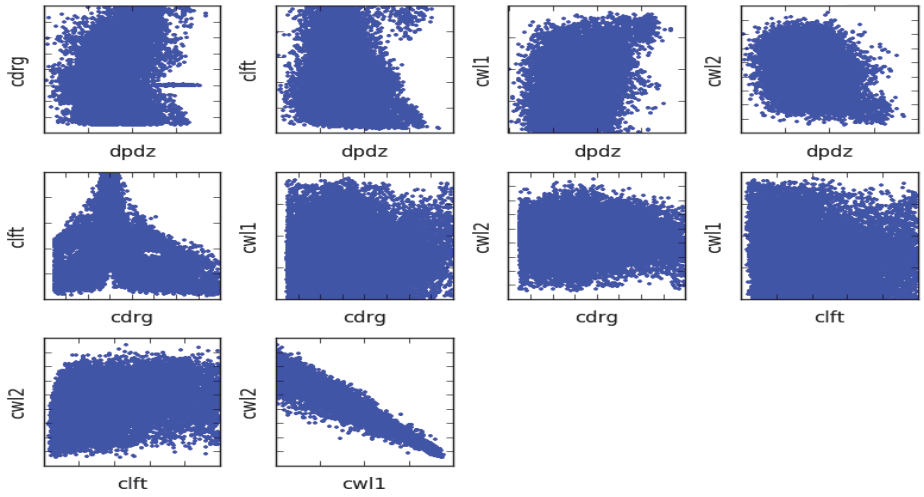

Pairwise correlations between parameters

Looking Forward
Towards Making Multiphase Modeling Robust

- There is (almost) DNS capability
- There are multiple parameterizations of multiphase phenomena (drag, lift, turbulent dispersion, …)
- Modern UQ, ML, and Bayesian analysis techniques can be used to integrate DNS/Experiments with multiphase phenomenology to make RANS models (ensemble averaged Eulerian Dispersed-Multiphase) more robust
  - Discrepancy model, Representation error
  - Hierarchical model

Approach *not unlike* top-down VUQ approach
that Phil Smilth talked about

Eulerian Models and Polydispersity Treatment for Dilute Gas-Particles Flows

John Milo Parra-Alvarez (Speaker)
Phil Smith
Sean Smith

October 6th -7th 2016

THE INSTITUTE FOR CLEAN AND SECURE ENERGY
AT THE UNIVERSITY OF UTAH

Overview

- Motivation
- Eulerian Moment-Based Methods
- Polydispersity treatment of multiphase flows
  - Size-conditioned moment method
  - Size-reconstructed moment method
- Applications

THE UNIVERSITY OF UTAH

Motivation

Industrial Applications

Chemical Looping Processes

http://www.netl.doe.gov/research/coal/energy-systems/advanced-combustion/prototype

Oxy-Coal combustion

And many more:

- Catalytic combustion
- Fluidization technologies
- Coal gasification
- Pneumatic transport
- Drying
- plasma arc coating
- Aerosol transport
- …

THE INSTITUTE FOR CLEAN AND SECURE ENERGY
AT THE UNIVERSITY OF UTAH

Motivation

Multiscale Phenomena

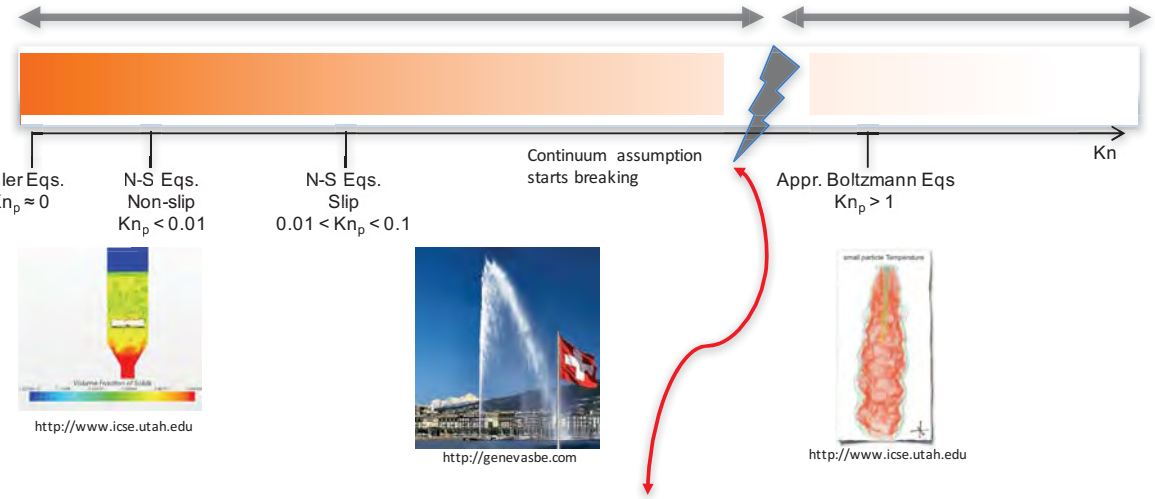

More complex modeling approaches are necessary to describe non-equilibrium phenomena in particulate flows

Eulerian moment-based methods

The mathematical model

$$\mathfrak{F} = \mathfrak{F}(\mathbf{x}, \mathbf{v}, \boldsymbol{\theta}, \xi)$$

$$\frac{\partial \mathfrak{F}}{\partial t} + \underbrace{\nabla_{\mathbf{x}} \cdot (\mathbf{v}\mathfrak{F})}_{\text{(i)}} + \underbrace{\nabla_{\xi} \cdot (\mathbf{G}(\xi, \boldsymbol{\theta}, \mathbf{v})\mathfrak{F})}_{\text{(ii)}} + \underbrace{\nabla_{\theta} \cdot (\mathbf{H}(\xi, \boldsymbol{\theta}, \mathbf{v})\mathfrak{F})}_{\text{(iii)}} + \underbrace{\nabla_{\mathbf{v}} \cdot (\mathbf{F}(\boldsymbol{\xi}, \mathbf{v})\mathfrak{F})}_{\text{(iv)}} = \underbrace{\mathbb{C}[f, f]}_{\text{(v)}}$$

(i) Advection in physical space
(ii) Advection in size space
(iii) Advection in scalar space
(iv) Advection in velocity space
(v) Particle-particle interactions

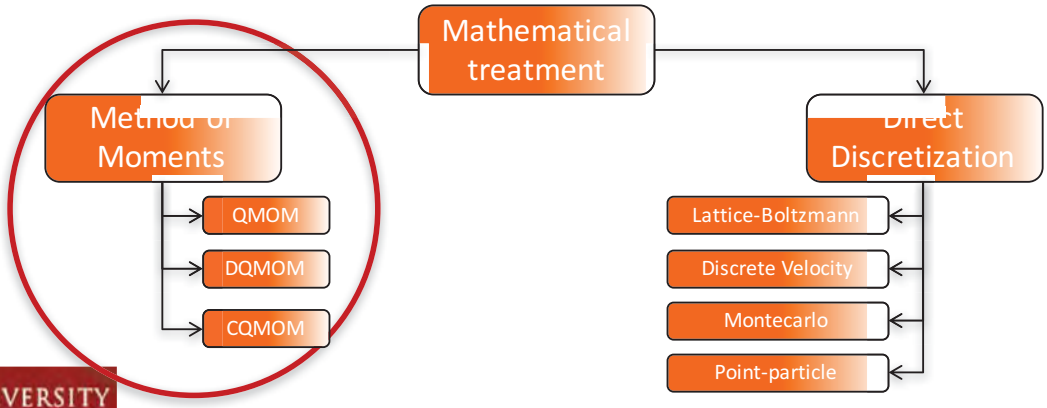

THE UNIVERSITY OF UTAH

THE INSTITUTE FOR CLEAN AND SECURE ENERGY
AT THE UNIVERSITY OF UTAH

Polydispersity treatment - DQCMOM

Size-conditioned moment method

THE UNIVERSITY OF UTAH

Polydispersity treatment - DQCMOM

Joint NDF Approximation

$$\frac{\partial \mathfrak{F}}{\partial t} + \nabla_{\mathbf{x}} \cdot (\mathbf{v}\mathfrak{F}) = \underbrace{-\nabla_{\xi} \cdot (\mathbf{G}(\xi, \boldsymbol{\theta}, \mathbf{v})\mathfrak{F}) - \nabla_{\theta} \cdot (\mathbf{H}(\xi, \boldsymbol{\theta}, \mathbf{v})\mathfrak{F}) - \nabla_{\mathbf{v}} \cdot (\mathbf{F}(\boldsymbol{\xi}, \mathbf{v})\mathfrak{F}) + \mathbb{C}[f, f]}_{\mathfrak{S}(\xi, \boldsymbol{\theta}, \mathbf{v})}$$

$$\mathfrak{F}(\mathbf{x}, \mathbf{v}, \boldsymbol{\theta}, \xi) = \mathfrak{g}(\xi)\mathfrak{f}(\boldsymbol{\theta}|\xi)\mathfrak{F}(\mathbf{v}|\xi, \boldsymbol{\theta}) \approx \sum_{\alpha=1}^{N_s} w_\alpha g(\xi, \xi_\alpha) f(\boldsymbol{\theta}, \boldsymbol{\theta}_\alpha|\xi_\alpha)\mathfrak{F}(\mathbf{v}|\xi_\alpha, \boldsymbol{\theta}_\alpha) \approx \sum_{\alpha=1}^{N_s} w_\alpha g(\xi, \xi_\alpha) f(\boldsymbol{\theta}, \boldsymbol{\theta}_\alpha)\mathfrak{F}(\mathbf{v}|\xi_\alpha)$$

$$\sum_{\alpha=1}^{N_s} w_\alpha \mathfrak{g}(\boldsymbol{\xi}, \boldsymbol{\xi}_\alpha)\mathfrak{f}(\boldsymbol{\theta}, \boldsymbol{\theta}_\alpha)\Big[\frac{\partial}{\partial t}(\mathfrak{F}(\mathbf{v}|\boldsymbol{\xi}_\alpha)) + \nabla_{\mathrm{x}} \cdot (\mathbf{v}\mathfrak{F}(\mathbf{v}|\boldsymbol{\xi}_\alpha))\Big]$$
$$+ \sum_{\alpha=1}^{N_s} \mathfrak{F}(\mathbf{v}|\boldsymbol{\xi}_\alpha)\Big[\frac{\partial}{\partial t}(w_\alpha \mathfrak{g}(\boldsymbol{\xi}, \boldsymbol{\xi}_\alpha)\mathfrak{f}(\boldsymbol{\theta}, \boldsymbol{\theta}_\alpha)) + \nabla_{\mathrm{x}} \cdot (\mathbf{v}w_\alpha \mathfrak{g}(\boldsymbol{\xi}, \boldsymbol{\xi}_\alpha)\mathfrak{f}(\boldsymbol{\theta}, \boldsymbol{\theta}_\alpha))\Big] = \mathfrak{S}(\xi, \boldsymbol{\theta}, \mathbf{v})$$

$$\mathfrak{g}(\xi, \xi_\alpha) = \delta(\xi - \xi_\alpha)$$
$$\mathfrak{f}(\boldsymbol{\theta}, \boldsymbol{\theta}_\alpha) = \prod_{k=1}^{M} \delta(\theta_{m_k} - \theta_{m_k,\alpha})$$

$$\mathfrak{M}^{(l,M,N)} = \int_{\mathbb{R}} \int_{\mathbb{R}^m} \int_{\mathbb{R}^3} \xi^l \boldsymbol{\theta}^{(M)} \mathbf{v}^{(N)} \mathfrak{F}(\xi, \boldsymbol{\theta}, \mathbf{v}; \mathbf{x}, t) \mathrm{d}\mathbf{v}\mathrm{d}\boldsymbol{\theta}\mathrm{d}\xi$$

THE INSTITUTE FOR CLEAN AND SECURE ENERGY
AT THE UNIVERSITY OF UTAH

System of equations

$$\iiint \xi^l \boldsymbol{\theta}^{(M)} \mathbf{v}^{(N)} \sum_{\alpha=1}^{N_s} w_\alpha \delta(\xi - \xi_\alpha) \prod_{k=1}^{N_\theta} \delta(\theta_{m_k} - \theta_{m_k,\alpha})\Big[\frac{\partial}{\partial t}(\mathfrak{F}(\mathbf{v}|\boldsymbol{\xi}_\alpha)) + \nabla_{\mathrm{x}} \cdot (\mathbf{v}\mathfrak{F}(\mathbf{v}|\boldsymbol{\xi}_\alpha))\Big]\mathrm{d}\mathbf{v}\mathrm{d}\boldsymbol{\theta}\mathrm{d}\xi$$
$$+ \iiint \xi^l \boldsymbol{\theta}^{(M)} \mathbf{v}^{(N)} \sum_{\alpha=1}^{N_s} \mathfrak{F}(\mathbf{v}|\boldsymbol{\xi}_\alpha)\Big[\frac{\partial}{\partial t}(w_\alpha \mathfrak{g}(\boldsymbol{\xi}, \boldsymbol{\xi}_\alpha)\mathfrak{f}(\boldsymbol{\theta}, \boldsymbol{\theta}_\alpha)) + \nabla_{\mathrm{x}} \cdot (\mathbf{v}w_\alpha \mathfrak{g}(\boldsymbol{\xi}, \boldsymbol{\xi}_\alpha)\mathfrak{f}(\boldsymbol{\theta}, \boldsymbol{\theta}_\alpha))\Big]\mathrm{d}\mathbf{v}\mathrm{d}\boldsymbol{\theta}\mathrm{d}\xi = \overline{\mathfrak{S}}(\xi, \boldsymbol{\theta}, \mathbf{v})$$

The original NDF can be rewritten in terms of transport equations for primitive variables and conditional moments

Each set of transport equations is weighted by a matrix of coefficients of primitive variables and conditional moments

$$\left.\begin{array}{l} \mathcal{L}[\langle \mathfrak{m} \rangle_\alpha^N] \\ \mathcal{L}[w_\alpha \boldsymbol{\xi}_\alpha] \\ \mathcal{L}[w_\alpha \boldsymbol{\theta}_\alpha] \\ \mathcal{L}[w_\alpha] \end{array}\right\} \quad \mathcal{L}[\cdot] \equiv \frac{\partial}{\partial t} + \mathbf{U}\nabla_{\mathrm{x}} - \mathbf{S}$$

$$[\mathbf{A}_w]\mathcal{L}[\langle \mathfrak{m} \rangle_\alpha^N] + [\mathbf{A}_{w\theta}]\mathcal{L}[w_\alpha \boldsymbol{\xi}_\alpha] + [\mathbf{A}_{w\xi}]\mathcal{L}[w_\alpha \boldsymbol{\theta}_\alpha] + [\mathbf{A}_{\mathfrak{m}}]\mathcal{L}[w_\alpha] = \mathfrak{V}_\alpha$$

THE UNIVERSITY OF UTAH

Polydispersity treatment - DQCMOM

Matrix form, MNS and final set

Minimum norm solution for homogeneous linear systems

$$\left[\begin{array}{c|c|c|c} \mathbf{A}_w & \mathbf{A}_{w\theta} & \mathbf{A}_{w\xi} & \mathbf{A}_{\mathfrak{m}} \end{array}\right] \left[\begin{array}{c} \mathcal{L}[\langle \mathfrak{m} \rangle_\alpha^N] \\ \mathcal{L}[w_\alpha \boldsymbol{\xi}_\alpha] \\ \mathcal{L}[w_\alpha \boldsymbol{\theta}_\alpha] \\ \mathcal{L}[w_\alpha] \end{array}\right] = \left[\begin{array}{c} \mathfrak{0}_\alpha \\ \mathfrak{0}_\alpha \\ \mathfrak{0}_\alpha \\ \mathfrak{0}_\alpha \end{array}\right]$$

$$\left[\begin{array}{c} \mathcal{L}[\langle \mathfrak{m} \rangle_\alpha^N] \\ \mathcal{L}[w_\alpha \boldsymbol{\xi}_\alpha] \\ \mathcal{L}[w_\alpha \boldsymbol{\theta}_\alpha] \\ \mathcal{L}[w_\alpha] \end{array}\right] = \left[\begin{array}{c} \mathfrak{0}_\alpha \\ \mathfrak{0}_\alpha \\ \mathfrak{0}_\alpha \\ \mathfrak{0}_\alpha \end{array}\right]$$

$$\frac{\partial \langle \mathfrak{m} \rangle_\alpha^{(N)}}{\partial t} + \nabla_{\mathrm{x}} \langle \mathfrak{m} \rangle_\alpha^{(N)+1} = (N) \int_{\Omega_{\mathrm{v}}} \mathbf{v}^{(N)-1} \mathfrak{F}(\mathbf{v}|\xi_\alpha) \mathbf{F}(\xi, \mathbf{v}) \mathrm{d}\mathbf{v}$$

$$\frac{\partial w_\alpha \boldsymbol{\xi}_\alpha}{\partial t} + \mathbf{U}_\alpha^{(N)} \cdot \nabla_{\mathrm{x}} (w_\alpha \boldsymbol{\xi}_\alpha) = w_\alpha \mathbf{G}(\xi, \boldsymbol{\theta}, \mathbf{v})$$

$$\frac{\partial w_\alpha \boldsymbol{\theta}_\alpha}{\partial t} + \mathbf{U}_\alpha^{(N)} \cdot \nabla_{\mathrm{x}} (w_\alpha \boldsymbol{\theta}_\alpha) = w_\alpha \mathbf{H}(\xi, \boldsymbol{\theta}, \mathbf{v})$$

$$\frac{\partial w_\alpha}{\partial t} + \mathbf{U}_\alpha^{(N)} \cdot \nabla_{\mathrm{x}} (w_\alpha) = 0$$

THE UNIVERSITY OF UTAH

THE INSTITUTE FOR CLEAN AND SECURE ENERGY
AT THE UNIVERSITY OF UTAH

Polydispersity treatment - DQCMOM

Applications 1D packets

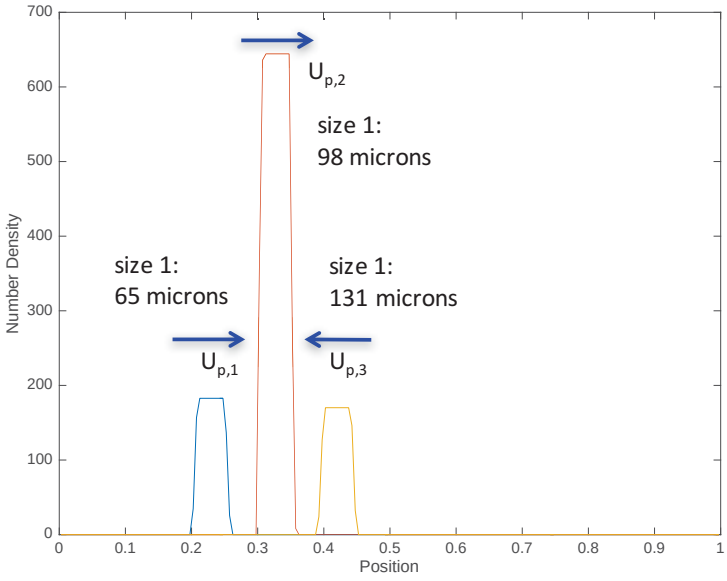

The drag force has the form:

$$\langle A \rangle_{\beta,\alpha} = \frac{m_p}{\tau_p} (|U_f - v_{\beta,\alpha}|)$$

$$\tau_p = \tau_p(\mathbb{R}\mathrm{e}_p)$$

$$\mathbb{R}\mathrm{e}_p = \frac{2|U_f - v_{\beta,\alpha}|r}{\mu_f}$$

- Three discrete sizes are considered
- Velocity moments are conditioned on these 3 sizes
- Particles move in a vacuum
- The purpose of this simple example is to capture PTC present in dilute systems

THE UNIVERSITY OF UTAH

Polydispersity treatment - DQCMOM

Applications 1D packets

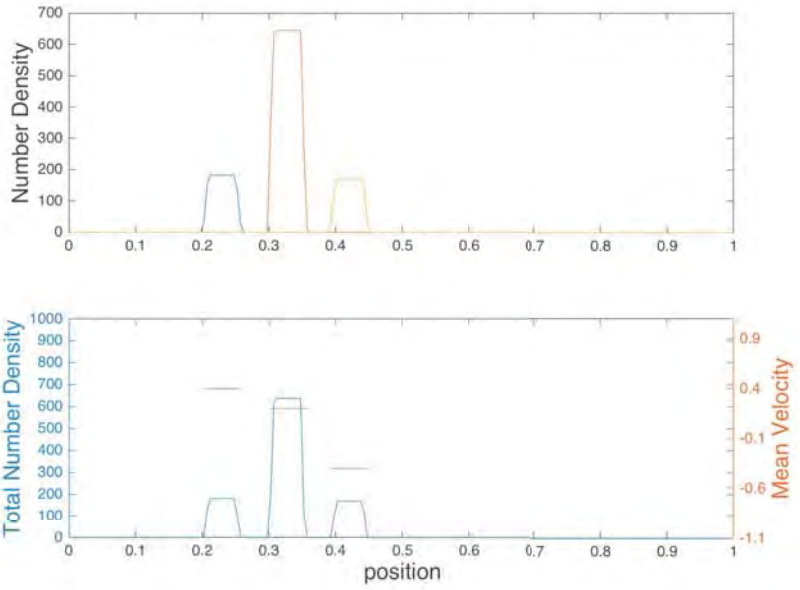

THE INSTITUTE FOR CLEAN AND SECURE ENERGY
AT THE UNIVERSITY OF UTAH

Polydispersity treatment - DQCMOM

Applications 2D Taylor vortex

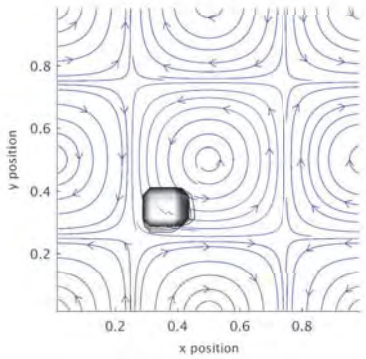

65 Microns

131 Microns

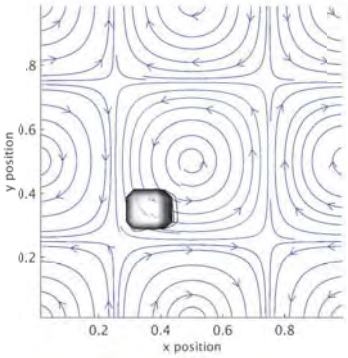

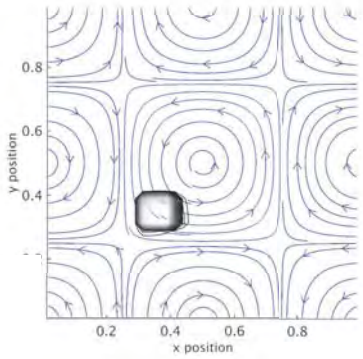

98 Microns

THE UNIVERSITY OF UTAH

Polydispersity treatment - DQCMOM

Size-reconstruted moment method

THE INSTITUTE FOR CLEAN AND SECURE ENERGY
AT THE UNIVERSITY OF UTAH

Polydispersity treatment - PMOM

Formulation

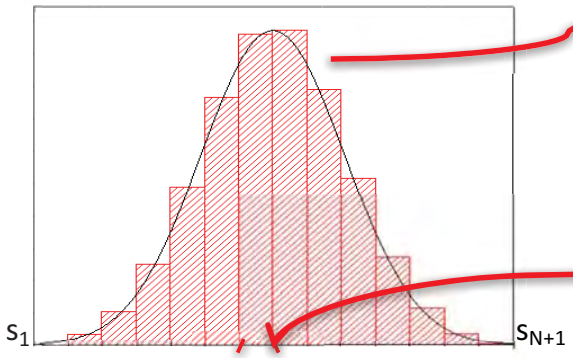

$$\frac{\partial \mathfrak{F}}{\partial t} + \nabla_{\mathbf{x}} \cdot (\mathbf{v}\mathfrak{F}) = \mathfrak{S}$$

$$\mathfrak{F}(\xi, \boldsymbol{\theta}, \mathbf{v}) = \sum_{k=1}^{N_s+1} \ell_k(\xi)\mathfrak{g}_k(\xi)\mathfrak{f}_k(\boldsymbol{\theta}, \mathbf{v}|\xi) = \sum_{k=1}^{N_s+1} \ell_k(\xi)\mathfrak{g}_k(\xi)\boldsymbol{\delta}(\boldsymbol{\theta} - \overline{\boldsymbol{\theta}}_k(\xi)) \sum_{\alpha=1}^{N_v} \mathbf{w}_{k,\alpha}\boldsymbol{\delta}(\mathbf{v} - \overline{\mathbf{U}}_{k,\alpha}(\xi))$$

$$\ell_k(\xi) = \begin{cases} 1 & \text{if } \xi \in [s_k, s_{k+1}] \\ 0 & \text{otherwise} \end{cases}$$

$$\overline{\boldsymbol{\theta}}^{(M)} = \overline{\theta}_1^{m_1}\overline{\theta}_2^{m_2}\cdots\overline{\theta}_M^{m_M}$$
$$\overline{\mathbf{U}}_{\alpha}^{(N)} = \overline{\mathrm{U}}_{x,\alpha}^{n_1}\overline{\mathrm{U}}_{y,\alpha}^{n_2}\overline{\mathrm{U}}_{z,\alpha}^{n_3}$$

$$\frac{\partial \mathfrak{M}_k^{(l,M,N)}}{\partial t} + \nabla_{\mathbf{x}} \cdot \mathfrak{M}_k^{(l,M,N+1)} = \int_{s_k}^{s_{k+1}} \int_{\Omega_\theta} \int_{\Omega_v} \xi^l \boldsymbol{\theta}^{(M)} \mathbf{v}^{(N)} \mathfrak{S}_k \mathrm{dv} \mathrm{d}\boldsymbol{\theta} \mathrm{d}\xi$$

$$\mathfrak{M}_k^{(l,M,N)} = \sum_{\alpha=1}^{N_v} \mathbf{w}_\alpha \int_{s_k}^{s_{k+1}} \xi^l \mathfrak{g}(\xi) \overline{\boldsymbol{\theta}}^{(M)} \overline{\mathbf{U}}_{\alpha}^{(N)} \mathrm{d}\xi$$

$$\mathfrak{M}^{(l,M,N)} = \sum_{k=1}^{N_s+1} \mathfrak{M}_k^{(l,M,N)}$$

$$g_k(\xi) = \sum_{j=0}^{l} C_{k,j}(\xi - s_k)^j$$

$$[\mathbf{A}] \cdot [\mathbf{C}] = [\mathbf{M}]$$

THE UNIVERSITY OF UTAH

Polydispersity treatment - PMOM

Computational loop

while t < t_f

$$\mathfrak{M}_i(t) = \mathfrak{M}^{(l,M,N)}(\mathbf{x},t)$$

$$\mathfrak{M}^{(0,0,N)} \Rightarrow [\mathbf{w}_\alpha, \overline{\mathbf{U}}_\alpha]$$
$$N = [n_1, n_2, n_3] \quad n_i = 1, \cdots, 4$$
$$\alpha = 1, 2$$

Obtain velocity via inversion

$$\mathfrak{M}^{(l,0,0)} \Rightarrow [C_{k,j}]$$
$$g_k(\xi) = \sum_{j=0}^{l} C_{k,j}(\xi - s_k)^j$$
$$k = 1, \cdots, 5; \quad l = 2$$

Obtain polynomial coefficients by solving linear system from the moments

$$\mathfrak{M}^{(0,M,0)} \Rightarrow [\boldsymbol{\theta}]$$
$$M = [m_1, m_2, \cdots, m_M]$$
$$\overline{\boldsymbol{\theta}} = [\theta_1, \cdots, \theta_M]$$

Obtain scalars by averaging each parcel

$$\mathfrak{G} = \mathfrak{G}\Big(\mathfrak{M}_l(t), \mathfrak{M}_r(t)\Big)$$

use previous values to reconstruct the numerical flux function

$$\mathfrak{M}_i(t+\Delta t) = \mathfrak{M}_i(t) - \frac{\Delta t}{|V_i|} \sum_{e \in \partial V_i} \Big[\mathfrak{G}\Big(\mathfrak{M}_{e,l}(t), \mathfrak{M}_{e,r}(t), \hat{\mathbf{n}}_e\Big) A_e\Big]$$

Advance solution

end

THE UNIVERSITY OF UTAH

THE INSTITUTE FOR CLEAN AND SECURE ENERGY
AT THE UNIVERSITY OF UTAH

Polydispersity treatment - PMOM

Reconstruction test

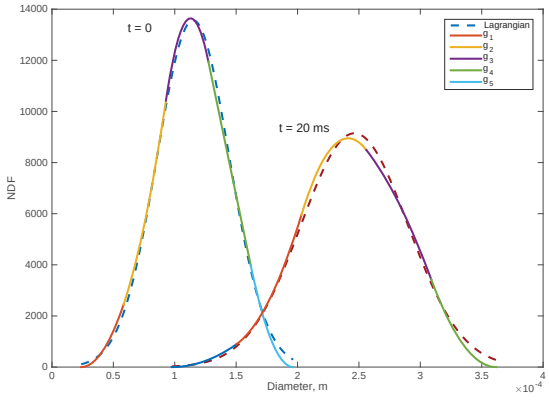

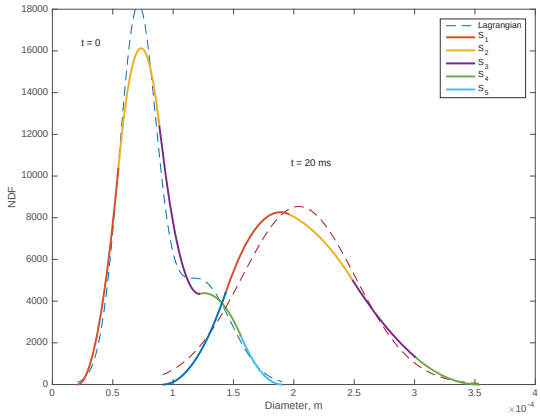

$$\frac{\mathrm{d}D_p}{\mathrm{d}t} = 0.5 * \sqrt{D_p}$$

- The size distribution is reconstructed at each time step
- 5 parcels are used
- In each parcel a second order polynomial is used

$$[\mathbf{A}] \cdot [\mathbf{C}] = [\mathbf{M}]$$

THE UNIVERSITY OF UTAH

Polydispersity treatment - PMOM

Applications 1D packets

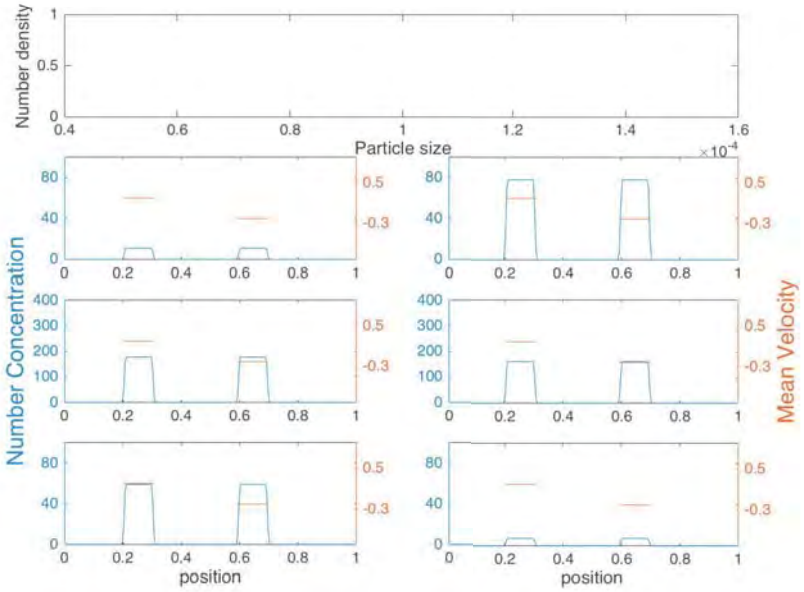

THE INSTITUTE FOR CLEAN AND SECURE ENERGY
AT THE UNIVERSITY OF UTAH

Polydispersity treatment - PMOM

Applications 2D Taylor vortex

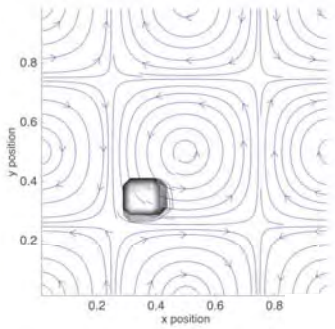

Parcel 1

Parcel 6

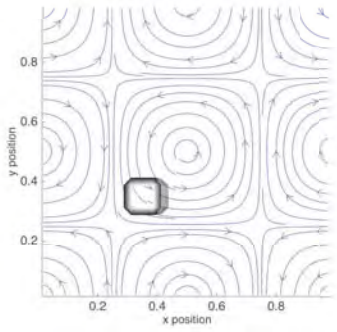

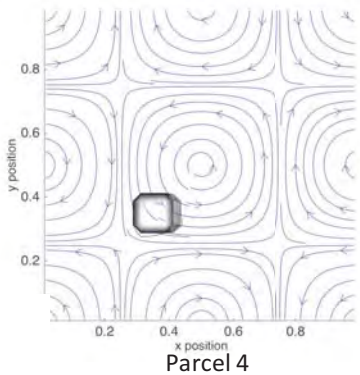

Parcel 4

THE UNIVERSITY OF UTAH

Polydispersity treatment - PMOM

Applications 2D Taylor vortex

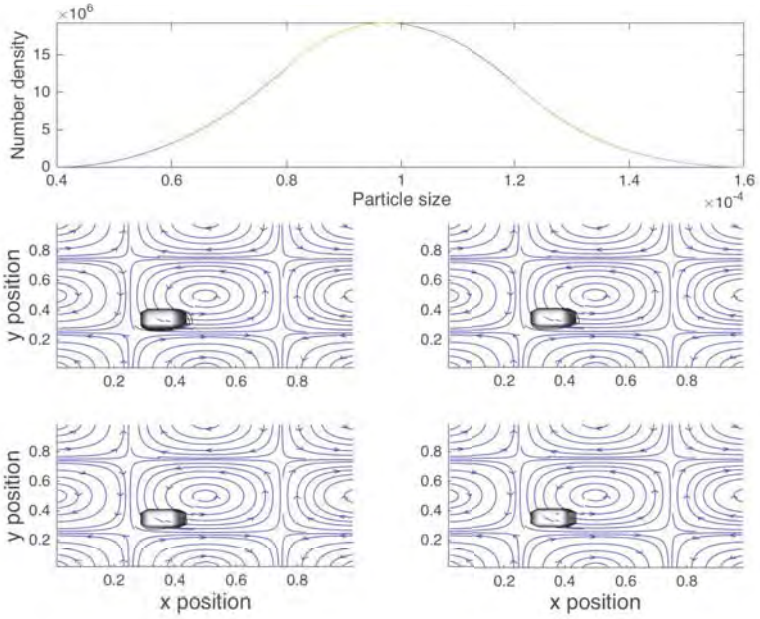

THE INSTITUTE FOR CLEAN AND SECURE ENERGY
AT THE UNIVERSITY OF UTAH

Char oxidation test

$$\frac{\partial \mathfrak{M}_k^{(l,M,T,N)}}{\partial t} + \frac{\partial \mathfrak{M}_k^{(l,M,T,N+1)}}{\partial x} =$$
$$+ M \sum_{\alpha=1}^{N_v} w_\alpha \int_{s_k}^{s_{k+1}} \xi^l \mathfrak{g}(\xi) \left(\mathrm{U}_\alpha^N(\xi) \overline{m}_p^{M-1}(\xi) \overline{\theta}^T(\xi) \mathrm{G}(\xi, \overline{m}_p(\xi), \overline{\theta}(\xi))\right) \mathrm{d}\xi$$
$$+ T \sum_{\alpha=1}^{N_v} w_\alpha \int_{s_k}^{s_{k+1}} \xi^l \mathfrak{g}(\xi) \left(\mathrm{U}_\alpha^N(\xi) \overline{m}_p^{M} \overline{\theta}^{T-1}(\xi) \mathrm{H}(\xi, \overline{m}_p(\xi), \overline{\theta}(\xi))\right) \mathrm{d}\xi$$
$$+ N \sum_{\alpha=1}^{N_v} w_\alpha \int_{s_k}^{s_{k+1}} \xi^l \mathfrak{g}(\xi) \overline{m}_p^{M} \overline{\theta}^T \mathrm{U}_\alpha^{N-1}(\xi) \frac{1}{\overline{m}_p} \mathrm{F}_\alpha(\xi, \overline{\theta}(\xi), \mathrm{U}_\alpha(\xi)) \mathrm{d}\xi$$

Moment equations for a 1D tubular reactor describing mass, temperature, size and velocity

Numerical Splitting

$$\frac{\partial \mathfrak{M}_k^{(l,M,T,N)}}{\partial t} + \frac{\partial \mathfrak{M}_k^{(l,M,T,N+1)}}{\partial x} = 0 \rightarrow \frac{\Delta t}{2}$$
$$\frac{\partial \mathrm{U}_\alpha(\xi)}{\partial t} = \frac{U_g - \mathrm{U}_\alpha(\xi)}{\tau(\xi, \mathbb{Re})} \rightarrow \Delta t$$
$$\frac{\partial \overline{m}_p}{\partial t} = \mathrm{G}(\xi, \overline{m}_p, \overline{\theta}) \rightarrow \Delta t$$
$$\frac{\partial \overline{\theta}}{\partial t} = \mathrm{H}(\xi, \overline{m}_p, \overline{\theta}) \rightarrow \Delta t$$
$$\frac{\partial \mathfrak{M}_k^{(l,N)}}{\partial t} + \frac{\partial \mathfrak{M}_k^{(l,N+1)}}{\partial x} = 0 \rightarrow \frac{\Delta t}{2}$$

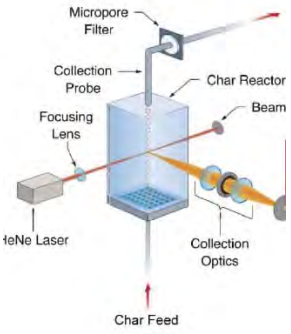

Heat and mass transfer from the particle to the gas

$$\mathrm{G}(\xi, \overline{m}_p, \overline{\theta}) = \pi \xi^2 q \mathrm{M}_c$$
$$\mathrm{H}(\xi, \overline{m}_p, \overline{\theta}) = -\frac{6\varepsilon\sigma}{\xi C_p \rho_p}(\theta^4 - T_w^4) - \frac{12\gamma}{\xi^2 C_p \rho_p}\left[\frac{\kappa/2}{\exp(\kappa/2) - 1}\right](\theta - T_g) + q\Delta h$$

THE UNIVERSITY OF UTAH

Char oxidation test

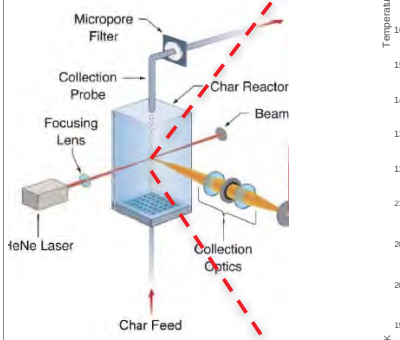

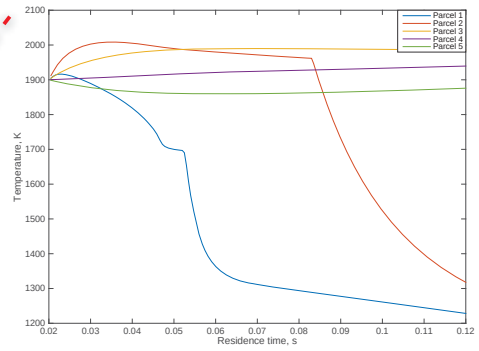

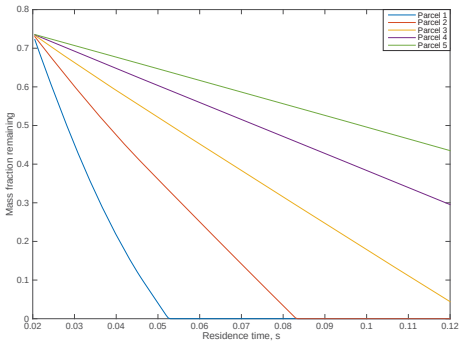

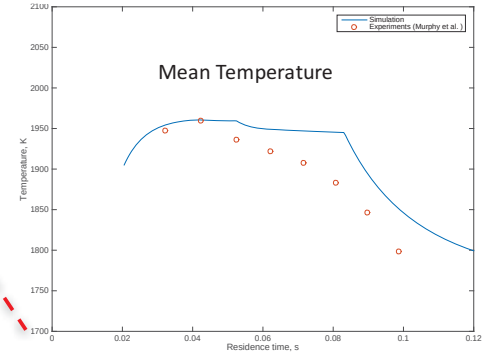

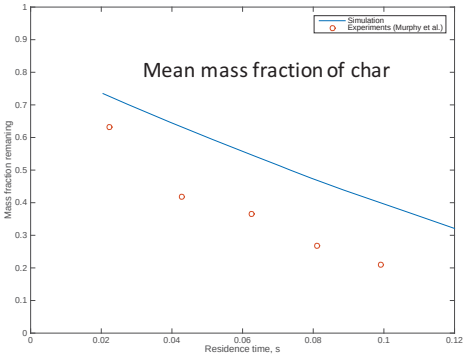

THE UNIVERSITY OF UTAH

THE INSTITUTE FOR CLEAN AND SECURE ENERGY
AT THE UNIVERSITY OF UTAH

Thank you

THE UNIVERSITY OF UTAH